Discotic Materials for Organic Electronics

Dissertation zur Erlangung des Grades

"Doktor der Naturwissenschaften"

am Fachbereich Chemie, Pharmazie und Geowissenschaften

der Johannes Gutenberg-Universität Mainz

Marcel Kastler

geboren in Weilburg

Mainz, 2006

Dekan:

1. Berichterstatter:

2. Berichterstatter:

Tag der mündlichen Prüfung:

Herrn Prof. Dr. K. Müllen,

unter dessen Anleitung ich die vorliegende Arbeit am Max-Planck Institut für Polymerforschung in Mainz in der Zeit von Dezember 2002 bis Dezember 2005 angefertigt habe, danke ich für seine wissenschaftliche und persönliche Unterstützung sowie seine ständige Diskussionsbereitschaft.

Dedicated to my parents

Contents

1 Introduction 1

1.1 Organic Electronics 1

1.2 Why Discotics? 2

1.3 Polycyclic aromatic hydrocarbons 6

1.3.1 Synthesis 7

1.3.1.1 FRIEDEL-CRAFTS-type Reactions 7

1.3.1.2 DIELS-ALDER Cycloaddition 8

1.3.1.3 Photocyclization 9

1.3.1.4 Flash Vacuum Pyrolysis (Thermolysis) 10

1.3.1.5 Extrusion of Heteroatoms 11

1.3.1.6 SCHOLL-Cyclodehydrogenation 12

1.4 Supramolecular Organization 14

1.4.1 Self-assembly 14

1.4.2 Orientation on Substrates 16

1.4.3 Characterization of the Organization 16

1.5 Processing 20

1.6 Electronic Devices 23

1.6.1 Light Emitting Diode 23

1.6.2 Photovoltaic Element 23

1.6.3 Field-Effect Transistor 25

1.7 References 26

2 Motivation and Objective 31

2.1 References 35

3 Hexa-*peri*-hexabenzocoronenes with Improved Processability 37

3.1 Synthesis 39

3.2 Self-Assembly 43

3.2.1 NMR Investigation 44

3.2.2 Electronic Spectroscopy 51
3.2.3 Conclusion 56
3.3 Processing 61
3.3.1 Solution Processing 61
3.3.2 Melt Processing 67
3.3.2.1 Morphology 67
3.3.2.2 Characterization of the molecular orientation 72
3.3.2.3 Mechanism of the Homeotropic Phase Formation 77
3.3.2.4 Zone-Crystallization 81
3.3.3 Mechanical Alignment - Structural Investigation 83
3.3.3.1 Thermal Behavior 83
3.3.3.2 Mechanically Aligned Fibers 85
3.3.3.3 Molecular Dynamics 89
3.3.3.4 Manipulation of the Superstructure 93
3.4 Charge Carrier Mobility 102
3.4.1 Pulse-Radiolysis Time-Resolved Microwave Conductivity 102
3.4.2 Life-Time of Charge Carriers 104
3.4.3 Time-of-Flight 109
3.5 Implementation in Photovoltaic Devices 115
3.6 Organization in porous materials – Pyrolysis 119
3.7 Summary 125
3.8 References 127
4 Functionalization of Hexa-*peri*-hexabenzocoronenes 135
4.1 Attachment of a Chromophore 136
4.2 a posteriori Functionalizations 144
4.2.1 Synthesis 145
4.2.2 Supramolecular Organization 148
4.3 “Tailoring” Supramolecular Properties 153
4.4 Structure-Property Relation 159

4.5 Chemical Cross-Linking of Hexa-peri-hexabenzocoronene 161
4.5.1 Fixation of supramolecular organizations 161
4.5.2 Nanostructuring 165
4.6 Summary 171
4.7 References 172
5 Polycyclic Aromatic Hydrocarbons with Different Peripheries 177
5.1 Nomenclature 177
5.2 Clar-Rule and Peripheries 180
5.3 Electronic Spectroscopy of PAHs 182
5.4 Introduction of "zigzag" Sites 187
5.4.1 Tetrabenzo[*bc,ef,hi,uv*]ovalene 188
5.4.2 Dibenzo[*hi,uv*]phenanthro-[3,4,5,6-*bcdef*]-ovalene 201
5.4.3 Diphenanthro[3,4,5,6-*uvabc*;3',4',5',6'-*efghi*]ovalene 211
5.4.4 Dibenzo[*ef,hi*]phenanthro[3,4,5,6-*u,v,a,b,c*]ovalene 218
5.4.5 Circumcoronene 221
5.5 Electronic Spectroscopy of the "zigzag" PAHs 224
5.5.1 Aromatic Core Symmetry 224
5.5.2 Self-Association in Solution 231
5.6 Supramolecular Organization 233
5.6.1 Introduction of a Novel Substitution Pattern 233
5.6.2 Self-Assembly in the Bulk Phase 235
5.6.3 Self-Assembly on Surfaces 239
5.7 Functionalization of PAHs in the Periphery 250
5.7.1 3H-Cyclopenta[*cde*]hexa-*peri*-hexabenzocoronene 251
5.7.2 Investigation of the Supramolecular Self-Organization 255
5.7.3 Functionalization 261
5.7.4 Other "Reactive" Peripheries 264
5.8 Graphite with "Defects" 268
5.8.1 Synthesis of an Extended PAH with "Hole" 268
5.8.2 Engineering of microporous organic crystals 275
5.8.3 Phase Forming Ring 277

5.8.4 Non-planar PAHs with hole 281
5.8.5 Softlanding 284
5.9 Summary 287
5.10 References 289
6 Conclusion and Outlook 299
7 Experimental Part 305
7.1 General methods 305
7.1.1 Chemicals and solvents 305
7.1.2 Chromatography 305
7.1.3 Microwave Assisted Reactions 305
7.1.4 Inert atmosphere 305
7.2 Analytical techniques 306
7.2.1 Mass spectrometry 306
7.2.2 NMR spectroscopy 306
7.2.3 Elemental Analysis 306
7.2.4 UV/vis spectroscopy 306
7.2.5 Photoluminescence spectroscopy 307
7.2.6 Differential scanning calorimetry (DSC) and thermogravimetric analysis (TGA) 307
7.2.7 Polarization microscopy 307
7.2.8 X-Ray Diffractometry 307
7.2.9 Single crystal analysis 308
7.2.10 Synchrotron experiments 308
7.2.11 Pulse-radiolysis time-resolved microwave conductivity investigation 308
7.2.12 Time-of-flight experiments 309
7.2.13 Electrochemical Characterization 309
7.2.14 Preparation of Photovoltaic Devices 310
7.3 Synthesis 311
7.3.1 4,4'-Bis(2-ethyl-hexyl)diphenylacetylene (3-11a) 311
7.3.2 Hexa-(4-(2-ethyl-hexyl-))phenylbenzene (3-12a) 311
7.3.3 2,5,8,11,14,17-Hexa(4-(2-ethyl-hexyl-)-hexa-*peri*-hexabenzocoronene (3-13a) 312
7.3.4 4,4'-Bis(2-hexyl-decyl)diphenylacetylene (3-11b) 313

7.3.5 Hexa-(4-(2-hexyl-decyl-))phenylbenzene (3-12b) 313

7.3.6 2,5,8,11,14,17-Hexa(2-hexyl-decyl)-hexa-*peri*-hexabenzocoronene (3-13b) 314

7.3.7 2-Decyl-tetradecylbromide (3-10c) 315

7.3.8 4,4'-Bis(2-decyl-tetradecyl)diphenylacetylene (3-11c) 315

7.3.9 Hexa-(4-(2-decyl-tetradecyl-))phenylbenzol (3-12c) 316

7.3.10 2,5,8,11,14,17-Hexa(2-decyl-tetradecyl)-hexa-*peri*-hexabenzocoronene (3-13c) 316

7.3.11 Bis(4,4''-dibromo-4-biphenyl)-acetylene (3-15) 317

7.3.12 Bis(4,4''-di-(2-decyl-tetradecyl)-4-biphenyl)-acetylene (3-16) 317

7.3.13 Hexa-(4-(2-decyl-tetradecyl)phenyl)phenylbenzene (3-17) 318

7.3.14 2,5,8,11,14,17-Hexa-(4-(2-decyl-tetradecyl)phenyl)-hexa-*peri*-hexabenzocoronene (3-18) 319

7.3.15 9-[5,8,11,14,17-penta(3,7-dimethyloctyl)-hexa-*peri*-hexabenzocoronen-2-yl]-N-(2,6-di-*iso*-propylphenyl)-perylene-3,4-dicarboxiimide (4-4) 320

7.3.16 4,4'-Bis(5-acetoxypentyl)diphenylacetylene (4-9) 321

7.3.17 Hexa-4-(5-acetoxypentyl)phenylbenzene (4-10) 321

7.3.18 2,5,8,11,14,17-Hexa-(5-acetoxypentyl)-hexa-*peri*-hexabenzocoronene (4-11) 322

7.3.19 2,5,8,11,14,17-Hexa-(5-hydroxypentyl)-hexa-*peri*-hexabenzocoronene (4-12) 323

7.3.20 4,4'-Bis(8-hydroxyoctyl)diphenylacetylene (4-13) 323

7.3.21 4,4'-Bis(8-acetoxyoctyl)diphenylacetylene (4-14) 324

7.3.22 Hexa-(8-acetoxyoctyl)phenylbenzene (4-15) 324

7.3.23 2,5,8,11,14,17-Hexa-(8-acetoxyoctyl)-hexa-*peri*-hexabenzocoronene (4-16) 325

7.3.24 2,5,8,11,14,17-Hexa-(8-hydroxyoctyl)-hexa-*peri*-hexabenzocoronene (4-17) 326

7.3.25 2,5,8,11,14,17-Hexa-(5-acryloxypentyl)-hexa-*peri*-hexabenzocoronene (4-18) 327

7.3.26 2,5,8,11,14,17-Hexa-(5-pent-5'-ene-oxypentyl)-hexa-*peri*-hexabenzocoronene (4-19) 328

7.3.27 2,5,8,11,14,17-Hexa-(5-pent-5'-yne-oxypentyl)-hexa-*peri*-hexabenzocoronene (4-20) 328

7.3.28 2,5,8,11,14,17-Hexa-(5-octanoyl-oxypentyl)-hexa-*peri*-hexabenzocoronene (4-21) 329

7.3.29 2,5,8,11,14,17-Hexa-(5-(2,2,3,3,4,4,5,5,6,6,7,7,8,8,8-pentadecafluoro-octanoyloxy)-oxypentyl)-hexa-*peri*-hexabenzocoronene (4-22) 330

7.3.30 2,5,8,11,14,17-Hexa-[5-(3,4,5-Trimethoxy-benzoyloxy)-pentyl]-hexa-*peri*-hexabenzocoronene (4-23) 331

7.3.31 2,5,8,11,14,17-Hexa-(5-pentafluorobenzoyloxy-pentyl)-hexa-*peri*-hexabenzocoronene (4-24) 331

7.3.32 2,5,8,11,14,17-Hexa-[5-(2-ethyl-hexanoyloxy)-pentyl]-hexa-*peri*-hexabenzocoronene (4-25) 332

7.3.33 2,5,8,11,14,17-Hexa-[5-(2-hexyl-decanoyloxy)-pentyl]-hexa-*peri*-hexabenzocoronene (4-26) 333

7.3.34 9,11-Diphenyl-cyclopenta[*e*]pyren-10-one (5-2) 333

7.3.35 9,10,11,12-Tetraphenylbenzo[*e*]pyrene (5-3) 334

7.3.36 2,7-Di-*tert*-butylpyrene-4,5-dione (5-6) 335

7.3.37 2,7-Di-*tert*-butyl-9,11-bis-(4-*tert*-butyl-phenyl)-cyclopenta[*e*]pyren-10-one (5-7) 335

7.3.38 4-Ethynyl-phenanthrene (5-21) 336

7.3.39 4-Phenyl-[1,1';4',1'']terphenyl-2'yl)-phenanthrene (5-13a) 337

7.3.40 Tetrabenzo[*bc,ef,hi,uv*]ovalene (5-4, 5-16a) 337

7.3.41 4-(4,4'',5',6'-Tetra-*t*-butyl-phenyl)-[1,1';4',1'']terphenyl-2'yl)-phenanthrene (5-13b) 338

7.3.42 8,11,14,17-Tetra(*t*-butyl)tetrabenzo[*bc,ef,hi,uv*]ovalene (5-16b) 339

7.3.43 4-(4,4'',5',6'-Tetra-*n*-dodecyl-phenyl)-[1,1';4',1'']terphenyl-2'yl)-phenanthrene (5-13c) 340

7.3.44 8,11,14,17-Tetra-*n*-dodecyl-tetrabenzo[*bc,ef,hi,uv*]ovalene (5-16c) 341

7.3.45 2-(2-Methoxyphenyl)benzaldehyde (5-28) 341

7.3.46 2-Ethynyl-2'-methoxy-biphenyl (5-29) 342

7.3.47 4-Methoxy-phenanthrene (5-30) 343

7.3.48 4-Hydroxy-phenanthrene (5-31) 343

7.3.49 1,1,2,2,3,3,4,4,4-Nonafluoro-butane-1-sulfonic acid phenanthren-4-yl ester (5-32) 344

7.3.50 4-Ethynyltrimethylsilyl-phenanthrene (5-33) 344

7.3.51 1,3-Bis(4-*t*-butyl-phenyl)-2-propanone 345

7.3.52 2,3,4,5-Tetrakis(4-*t*-butyl-phenyl)-cyclopentadienone (5-34b) 345

7.3.53 10-Phenanthren-4-yl-9,12-diphenyl-benzo[*e*]pyrene (5-35) 346

7.3.54 Dibenzo[*hi,uv*]phenanthro-(3,4,5,6-bcdef)-ovalene (5-36) 347

7.3.55 2,7-Di-*t*-butyl-9,12-bis-(4-*t*-butyl-phenyl)-10-phenanthren-4-yl-benzo[*e*]pyrene (5-37) 348

7.3.56 8,10,15,17-Tetra(*t*-butyl)-dibenzo[*hi,uv*]phenanthro-[3,4,5,6-*bcdef*]-ovalene (5-38) 349

7.3.57 9,11-Bis-(4-bromo-phenyl)-cyclopenta[*e*]pyren-10-one (5-39) 349

7.3.58 9,12-Bis-(4-bromo-phenyl)-10-phenanthren-4-yl-benzo[*e*]pyrene (5-40) 350

7.3.59 9,12-Bis-(4-*n*-dodecyl-phenyl)-10-phenanthren-4-yl-benzo[*e*]pyrene (5-41) 351

7.3.60 8,17-Di-*n*-dodecyl-dibenzo[*hi,uv*]phenanthro-[3,4,5,6-*bcdef*]-ovalene (5-42) 352

7.3.61 4,4,5,5-Tetramethyl-2-phenanthren-4-yl-[1,3,2]dioxaborolane (5-43) 352

7.3.62 1,3,5-Tris-phenanthren-4-yl-benzene (5-44) 353

7.3.63 Diphenanthro[3,4,5,6-*u,v,a,b,c*;3',4',5',6'-*e,f,g,h,i*]ovalene (5-45) 354

7.3.64 2-(Dihydroxyboryl)-N,N-diethyl-3-methoxybenzamide (5-48) 354

7.3.65 6-Methoxy-2'-methyl-biphenyl-2-carboxylic acid diethylamide (5-49) 355

7.3.66 5-Methoxy-phenanthren-9-ol (5-50) 355

7.3.67 4-Methoxy-phenanthrene-9,10-dione (5-51) 356

7.3.68 1,1,2,2,3,3,4,4,4-Nonafluoro-butane-1-sulfonic acid 9,10-di-*n*-dodecyl-phenanthren-4-yl ester (5-54) 356

7.3.69 2-(9,10-Di-*n*-dodecyl-phenanthren-4-yl)-4,4,5,5-tetramethyl-[1,3,2]dioxaborolane (5-55) 357

7.3.70 1,3,5-Tris-(9,10-bis-*n*-dodecyl-phenanthren-4-yl)-benzene and 1-Bromo-3,5-Bis-(9,10-bis-*n*-dodecyl-phenanthren-4-yl)-benzene (5-56) 358

7.3.71 5,6,11,12,17,18-Hexa-*n*-dodecyl-diphenanthro[3,4,5,6-*uvabc*;3',4',5',6'-*efghi*]ovalene (5-57) 359

7.3.72 1,3-Bis-(9,10-bis-*n*-dodecyl-phenanthren-4-yl)-5-(biphenyl-2-yl)-benzene (5-61) 360

7.3.73 5,6,17,18-Tetra-*n*-dodecyl-dibenzo[*ef,hi*]phenanthro[3,4,5,6-*u,v,a,b,c*]ovalene (5-62) 360

7.3.74 [3,5-Bis-(4-*n*-dodecyl-benzyl)-phenyl]-trimethylsilane (5-65) 361

7.3.75 1,3-Bis-(4-*n*-dodecyl-benzyl)-5-iodo-benzene (5-66) 362

7.3.76 [3,5-Bis-(4-*n*-dodecyl-benzyl)-phenylethynyl]-trimethyl-silane (5-67) 362

7.3.77 1,3-Bis-(4-*n*-dodecyl-benzyl)-5-ethynyl-benzol (5-68) 363

7.3.78 Bis(3,5-(4'-*n*-dodecyl-benzyl)-phenyl)-acetylene (5-69) 363

7.3.79 Hexa-(3,5-bis-(4-*n*-dodecylbenzyl))phenylbenzene (5-70) 364

7.3.80 Tetra-(4,4',4'',4'''-*n*-dodecyl-)phenylbenzene (5-73) 365

7.3.81 2,5,8,11-Tetra-*n*-dodecyl-hexa-*peri*-hexabenzocoronene (5-74) 365

7.3.82 4-Trimethylsilylethynyl-fluoren-9-one 366

7.3.83 4-Ethynyl-fluoren-9-one (5-77) 367

7.3.84 4-(2,3,4,5-Tetra(4-*n*-dodecylphenyl)phenyl)-fluoren-9-one (5-78) 367

7.3.85 4-(2,3,4,5-Tetra(4-*n*-dodecylphenyl)phenyl)-fluoren-9-one (5-79) 368

7.3.86 8,11,14,17-Tetra-*n*-dodecyl-3H-cyclopenta[*cde*]hexa-*peri*-hexabenzocoronene (5-80) 369

7.3.87 8,11,14,17-Tetra-*n*-dodecyl-cyclopenta[*cde*]hexa-*peri*-hexabenzocoronene-3-one (5-81) 370

7.3.88 2-Bromo-7-(2-decyl-tetradecyl)-pyrene (5-97) 370

7.3.89 Bis(7,7'-di-(2-decyl-tetradecyl)-2-pyrenyl)-acetylene (5-98) 371

7.3.90 Hexa(7-(2-decyltetradecyl)-pyren-2-yl)benzene (5-99) 372

7.3.91 1,3-Diiodo-5-(trimethylsilyl)-benzene (5-102) 372

7.3.92 3-Bromo-5-(trimethylsilyl)-phenylboronic acid (5-103) 373

7.3.93 5,3"-Dibromo-3,5',5"-tris-trimethylsilyl-[1,1';3',1"]terphenyl (5-104) 373

7.3.94 5,5',5'',5''',5'''',5''''',-Hexatrimethylsilyl-hexa-*m*-phenylene (5-105) 374

7.3.95 5,5',5'',5''',5'''',5''''',-Hexa-iodo-hexa-*m*-phenylene (5-106) 375

7.3.96 5,5',5'',5''',5'''',5''''',-Hexa-ethynyltri-*iso*-propylsilyl-cyclohexa-*m*-phenylene (5-107) 375

7.3.97 5,5',5'',5''',5'''',5''''',-Hexa-ethynyl-cyclohexa-*m*-phenylene (5-108) 376

7.3.98 5,5',5'',5''',5'''',5''''',-Hexa-((2,3,4,5-tetraphenyl)phenyl)-cyclohexa-*m*-phenylene (5-109) 377

7.3.99 5,5',5'',5''',5'''',5''''',-Hexa-phenylethynyl-cyclohexa-*m*-phenylene (5-113) 378

7.3.100 5,5',5'',5''',5'''',5''''',-Hexa-((2,3,4,5,6-pentaphenyl)phenyl)-cyclohexa-*m*-phenylene (5-114) 378

7.3.101 5,5',5'',5''',5'''',5''''',-Hexa-tetradec-1-yne-hexa-*m*-phenylene (5-115) 379

7.3.102 3,3''-Diiodo-5,5',5''-tris-trimethylsilyl-[1,1';3',1'']-terphenyl (5-121) 380

7.3.103 5,3''''-Dibromo-3,5',5'',5''',5''''-pentakis-trimethylsilyl-[1,1';3',1'';3'',1''';3''',1'''']quinquephenyl (5-122) 380

7.3.104 3''''-Brom-5-(4,4,5,5-tetramethyl-1,3,2-dioxaborolan-2-yl)-3,5',5'',5''',5''''-pentakis-trimethylsilanyl-[1,1';3',1'';3'',1''';3''',1'''']quinquephenyl (5-123) 381

7.3.105 5,5',5'',5''',5'''',5''''',5'''''',5'''''''',5''''''''',5''''''''''-Decatrimethylsilyl-cyclodeca-*m*-phenylene (5-127) 382

8 Appendix: Single Crystal Structures 383

8.1 8,11,14,17-Tetra(t-butyl)tetrabenzo[bc,ef,hi,uv]ovalene (5-16b) (crystallized with TCNQ) 383

8.2 4,4,5,5-Tetramethyl-2-phenanthren-4-yl-[1,3,2]dioxaborolane (5-43) 390

8.3 1-bromo-3,5-Bis-(9,10-bis-n-dodecyl-phenanthren-4-yl)-benzene (5-60) 392

8.4 4,5,9,10-Tetrahydro-pyrene (5-94) 395

8.5 2,7-Dibromopyrene (5-95) 397

8.6 5,5’,5’’,5’’’,5’’’’,5’’’’’-Hexatrimethylsilyl-hexa-m-phenylene (5-105) 398

8.7 5,5’,5’’,5’’’,5’’’’,5’’’’’-Hexa-ethynyltri-iso-propylsilyl-cyclohexa-m-phenylene (5-107) 401

8.8 5,5’,5’’,5’’’,5’’’’,5’’’’’-Hexa-((2,3,4,5,6-pentaphenyl)phenyl)-cyclohexa-m-phenylene (5-114) 410

8.9 5,5’,5’’,5’’’,5’’’’,5’’’’’,5’’’’’’,5’’’’’’’,5’’’’’’’’,5’’’’’’’’’-Decatrimethylsilyl-cyclodeca-m-phenylene (5-127) 418

Index of Abbreviations

2D-WAXS	two-dimensional wide-angle X-ray scattering
9-BBN	9-borabicyclononane
AcOH	acidic acid
AFM	atomic force microscopy
bd	doublet broad (NMR)
bipy	bipyridyl
bq	quartet broad (NMR)
bs	broad singlet (NMR)
bt	triplet broad (NMR)
COT	cylcoocta-1,3,5,7-tetraene
CPHBC	3H-cyclopenta[*cde*]hexa-peri-hexabenzocoronene
CPHBCCO	cyclopenta[*cde*]hexa-*peri*-hexabenzocoronene-3-one
d	doublet (NMR)
DBU	1,8-Diazabicyclo[5,4,0]undec-7-en
DCC	dicyclohexylcarbodiimide
DIBAL	di-*iso*-butylaluminiumhydrid
DMAP	N,N-dimethyl-4-aminopyridine
DMF	N,N-dimethylformamide
DPO	diphenanthro[3,4,5,6-*uvabc*;3',4',5',6'-*efghi*]ovalene
DSC	differential scanning calorimetry
EI	electron impact
Et	ethyl
FD	field desorption
FET	field-effect transistor
FFT	fast FOURIER transformation
FVP	flash vacuum pyrolyis
GPC	gel permeation chromatography
h	hour
HBC	hexa-*peri*-hexabenzocoronene
HOMO	highest occupied molecular orbital
HOPG	highly ordered pyrolytic graphite
HPLC	high performance liquid chromatography
HR-TEM	high-resolution transmission electron microscopy

^{i}Pr	*iso*-propyl
LB	LANGMUIR-BLODGETT
LC	liquid crystal
LDA	lithium di-*iso*-propylamide
LED	light emitting diode
LHDMS	lithium bis(trimethylsilyl)amide
LUMO	lowest unoccupied molecular orbital
m	multiplett (NMR)
M^{+}	molecular ion
MAS	magic angle spinning
MALDI-TOF	matrix-assisted laser desorption/ionization time-of-flight
mDBPO	dibenzo[*ef,hi*]phenanthro[3,4,5,6-*u,v,a,b,c*]ovalene
Me	methyl
min	minute
MS	mass spectrometry
Nf	nonaflate
NMR	nuclear magnetic resonance
NN	nearest neighbor
NOE	nuclear OVERHAUSER effect
NOESY	nuclear OVERHAUSER enhancement spectroscopy
OAc	acetate
oDCB	1,2-dichlorobenzene
PAH	polycyclic aromatic hydrocarbon
PAM	phenylacetylene macrocycles
pDBPO	dibenzo[*hi,uv*]phenanthro-[3,4,5,6-*bcdef*]-ovalene
pent.	pentet (NMR)
Ph	phenyl
PL	photoluminescence
PLE	photoluminescence excitation
POM	polarization optical microscopy
ppm	parts per million
PTFE	poly-tetra-fluoro-ethylene
q	quartet (NMR)
s	singlet (NMR)
SEM	scanning electron microscopy

sept.	septet (NMR)
STM	scanning tunneling microscopy
STS	scanning tunneling spectroscopy
t	triplet (NMR)
TBAF	tetra-iso-butyl ammonium fluoride
^{t}Bu	*tert*-butyl
TBO	tetrabenzo[*bc,ef,hi,uv*]ovalene
TCNQ	7,7,8,8-tetracyanoquinodimethane
TEM	transmission electron microscopy
THF	tetrahydrofuran
TGA	thermo-gravimetry analysis
TIPS	tri-*iso*-propylsilyl-
TLC	thin layer chromatography
TMS	trimethylsilyl-
TOF	time-of-flight
tt	triplet of triplets (NMR)
UV/vis	UV-visible absorption spectroscopy

1 Introduction

1.1 Organic Electronics

There is a memorable scene in “The Graduate” where Benjamin, the title character played by a young DUSTIN HOFFMAN, is given advice as he faces a career after college. He is told a single word: "plastics".

Thirty years later, the soundness of that advice is being revealed in ways undreamt of by the cinema audiences of the time, even the scientists among them. Plastic materials are now being created with increasingly useful electronic and optical properties. These developments extend the application of plastics beyond the familiar garden furniture, toys and plumbing, and into "smart" electronic devices such as identification tags, programmable credit cards and flat-panel displays.

Over the past decades, the element central to the microelectronics industry is silicon. In particular the ability to refine and produce large single crystals of ultra-high purity silicon has allowed devices to be miniaturized such that a Pentium-4 chip now contains over 40 million transistors.

The goal of all-polymer electronics has motivated an increasing number of research groups around the world for the past 20 years. These groups hope to provide plastics - which have the advantages of low-cost processing, flexibility and toughness - with the electronic properties needed for practical circuitry. In the past years, exciting new results towards this goal have been reported by independent groups. The Cambridge and Bell Labs groups have both succeeded in integrating a polymeric transistor with an organic light-emitting diode.[1,2] Organic light-emitting diodes (LEDs) are under development in many laboratories all over the world, and could be used for flat-panel displays in devices such as cellular phones, and perhaps eventually in televisions and computer screens. The active layer in an organic LED is a fluorescent organic material, either a specially designed polymer or a small dye molecule that emits light when an electrical current passes through it. Most work to date combines this organic layer with other components - such as substrates, electrodes and the encapsulation material needed to protect the device - that must be made from inorganic compounds. The ultimate aim of the new work is to produce a fully functioning display, including the driving circuitry, made almost entirely from plastic materials.

Plastic devices have real advantages: In addition to being lighter and more rugged, plastic semiconductors are have enormous potential for optoelectronic applications, and would be significantly cheaper to produce than both single crystal and amorphous silicon equivalents (Figure 1-1). Implementation of plastic semiconductors into electronic devices would reduce the weigh about a factor of 100 compared to a silicon-based cell.[3]

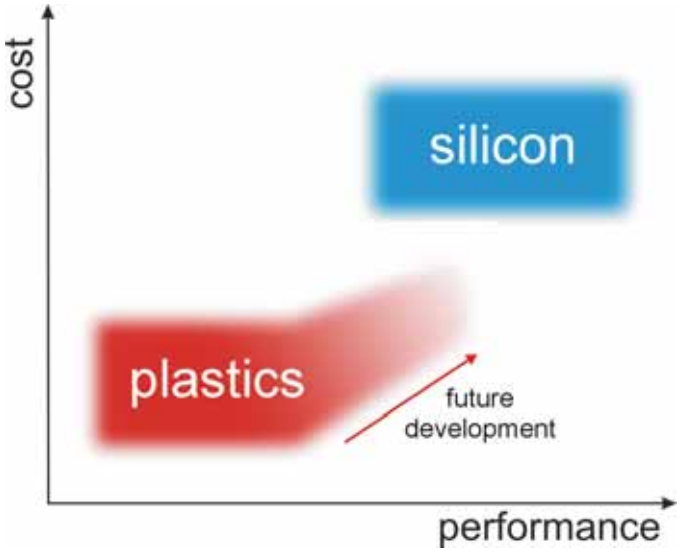

Figure 1-1: *"Silicon versus plastic electronics", performance – cost relation.*

Performance improvements, coupled with the ability to process these "active" materials at low temperatures over large areas on materials such as plastic or paper, may provide unique technologies and generate new applications and form factors to address the growing needs for pervasive computing and enhanced connectivity.

Recently, organic electronics started to make significant inroads into the commercial world, and if the field continues to progress at its current, rapid pace, electronics based on organic thin-film materials will soon become a mainstay of our technological existence. Already products based on active thin-film organic devices are in the market place, most notably the displays of several mobile electronic appliances. A recent forecast predicted an increase of this market of about 30 billion US dollars until 2015.[4] Every 18 months the charge mobility of transistors made from organic materials increases by a factor of ten.[5]

1.2 Why Discotics?

In the area of organic electronics, two distinct approaches are pursued. In the late 1970's, the three scientists HEEGER, MACDIARMID, and SHIRAKAWA demonstrated

that polymers can be made to conduct electricity by manipulating its molecular structure. The Royal Swedish Academy of Sciences decided to award the Nobel Prize in Chemistry for 2000 to these *"scientists who discovered and developed conductive polymers*". These conjugated polymers possess the inherent ability to conduct electric charges along their backbone.[6,7] Very famous examples of this class of compounds are shown in Figure 1-2.

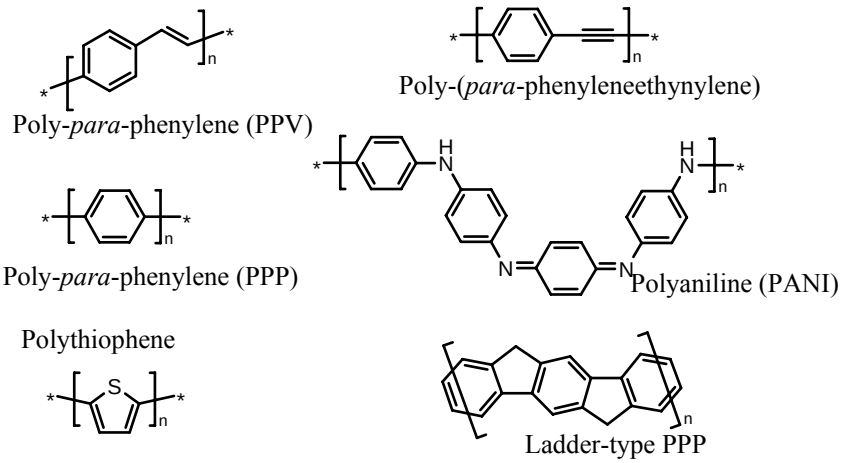

Figure 1-2: *Examples of few conjugated polymers.*

When substituted appropriately, these processable materials exhibit charge carrier mobilities in the order of 0.1 $cm^2V^{-1}s^{-1}$, such as determined for a regioregular hexyl substituted polythiophene.[1,8]

The second, much newer approach aims to exploit non-covalent interactions of small molecules to prepare large domains by spontaneous, supramolecular organization. Liquid crystalline materials possess the unique propensity to form highly organized films, which can be obtained by very cheap processing techniques from solution. Since REINITZER[9] discovered the state of liquid crystallinity in 1888, immense efforts in research and development have pushed this field and many mesophase forming classes of compounds are known. A relatively young group of thermotropic liquid crystals was discovered by CHANDRASEKHAR[10] in 1977 – the class of discotic mesogens. In many cases, these disc-like structures assemble in columnar structure due to an overlap of orbitals. What is often referred as "π- π interactions" is a result of electrostatic attractive forces between a positively charged σ-framework and the negatively charged electron cloud of neighboring units.[11] Figure 1-3 exhibits some prominent examples of discotic molecules, which form columnar superstructures due to these aromatic π- interactions.

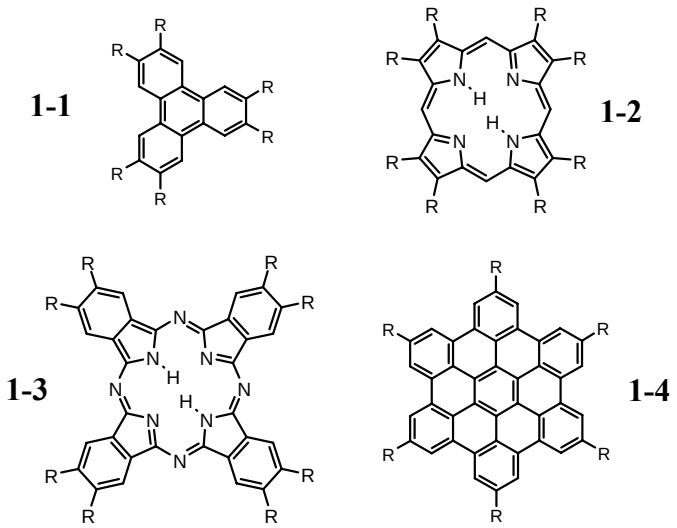

Figure 1-3: *Examples of some prominent discotic liquid crystalline materials.*

Triphenylenes **1-1**, porphyrins **1-2**, phthalocyanines **1-3**, and hexa-*peri*-hexabenzocoronenes (HBCs) **1-4** consist of a planar, rigid aromatic core which is substituted by flexible substituents in the periphery, ensuring solubility and the phase formation. The partial orbital overlap of neighboring molecules leads to the formation of charge carrier pathways. Very high intrinsic charge carrier mobilities have been determined for these discotics, which are about one order of magnitude higher than the one found for conjugated polymers.[12] A record intrinsic charge carrier mobility in excess of 1 $cm^2V^{-1}s^{-1}$ was determined for a substituted HBC derivative, which qualifies such materials for the implementation in organic electronic devices.[13] For triphenylenes **1-1**, positive and negative charge carrier mobilities for macroscopic films were determined to be in the range of 0.1 $cm^2V^{-1}s^{-1}$, which further emphasizes the potential of these discotic materials.[14-16] The size of the aromatic cores is discussed to be in close relation to the intracolumnar charge transport, which increased from 0.1 $cm^2V^{-1}s^{-1}$ for triphenylenes **1-1**[12,17] over 0.7 $cm^2V^{-1}s^{-1}$ for phthalocyanines **1-3**[18-20] up to 1.0 $cm^2V^{-1}s^{-1}$ for HBCs **1-4**. These mobility values are already in the range of amorphous silicon.[21]

Two mechanisms for the charge carrier transfer are being discussed for this group of molecules. The hopping mechanism describes a “hopping” of the charge carriers between localized states. The high mobilities found require hopping rates in excess of 10^{12} Hz. Since discotic liquid crystals contain imperfections[22], the actual required hopping rate will be probably much higher than this. The second more probable

mechanism involves the formation of conduction bands across several molecules, where the charge is delocalized, which better explains the high charge carrier mobility values.[23]

In summary, discotic materials based on extended polycyclic aromatic hydrocarbons (PAHs), such as the described examples, have performed the transition from molecule to an actual material and promise to be implemented as active component in organic devices. Bulk heterojunction photovoltaic elements have been built with phthalocyanines **1-3** and HBCs **1-4**, revealing good external quantum efficiencies up to 34%.[24-27] Furthermore, HBC derivatives have been solution-cast into films implemented in well-performing field-effect transistors (FETs).[28,29]

1.3 Polycyclic aromatic hydrocarbons

The most important and thermodynamic most stable allotrope of carbon is graphite. In this modification, every carbon atom forms σ-bonds to three neighboring atoms. This sp^2-hybridization of the carbon atoms causes the planar geometry of the uniform hexagon. The fourth valence electron is available for an additional, delocalized bond within the extended, planar sheets (Figure 1-4). The delocalization of the electrons within these layers leads to a metallic conductivity. Perpendicular to these stacked layers, graphite is an insulator. Many properties of graphite are still not completely understood. One example is its black color which is either attributed to impurities or intercalates, which cause a change of the band gap between valence and conduction band.[30]

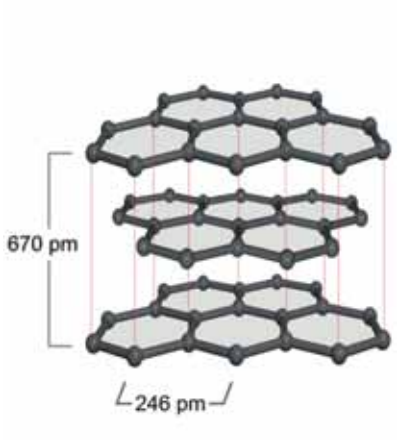

Figure 1-4: *Layer structure of graphite.*

Benzene is the simplest, aromatic compound, and consists of six sp^2-hybridized carbon atoms, which form a uniform hexagon, similar to graphite. Already discovered 1825 by M. FARADAY, the structure remained in focus for a controversial discussion over the real chemical structure.[31] The periodical composition of benzene rings in PAHs has already early sparked the interest of many theoreticians to predict the properties of the PAHs and is an ongoing field of research.[32-37] PAHs constitute an extraordinarily large and diverse class of organic molecules. The major sources of PAHs are crude oil, coal and oil shale. The PAHs can be considered as monomeric graphite molecules.

1.3.1 Synthesis

Besides the isolation of smaller PAHs from coal tar[38,39] or side-products of the catalytic hydrocracking of petroleum[40,41], the pioneers of this field R. SCHOLL[42-44], E. CLAR[30,45-49], and M. ZANDER[50-53] developed many different methodologies which allowed a whole variety of different PAHs to be specifically synthesized. The most generally useful methods for the construction of PAH ring systems are summarized in the following. While the classical synthetic methods tend to involve relatively vigorous reaction conditions, the trend in recent years is towards the development of milder methods, which proceed with greater regioselectivity and provide higher yields.

1.3.1.1 FRIEDEL-CRAFTS-type Reactions

The classic HAWORTH synthesis entails FRIEDEL-CRAFTS condensation of succinic anhydrides **1-6** with a polyarene **1-5** to from a keto-acid product, followed by reduction of the keto group and acid-catalyzed cyclization of the resulting carboxylic acid to yield a ketone product **1-9**, which can be aromatized to the corresponding PAH **1-10** (Scheme 1-1).[54,55]

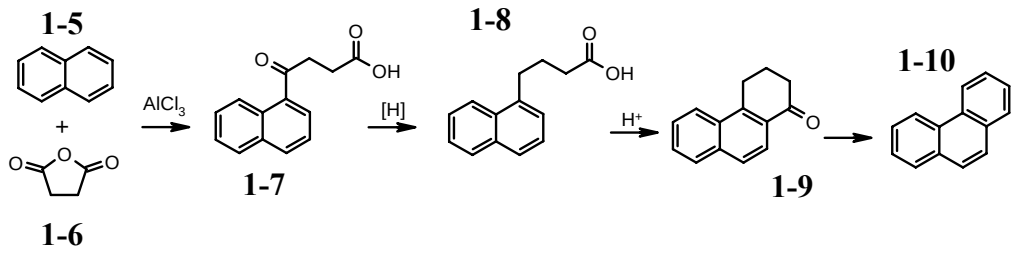

Scheme 1-1: *Example of the HARWORTH synthesis.*

The HARWORTH synthesis may be modified for the construction of larger polycyclic ring systems by the use of aromatic dibasic acid anhydrides, such as phthalic anhydride, thereby allowing fusion of two or more benzenoid rings to an existing aromatic system.

Ketones and aldehydes also serve as useful precursors for the synthesis of PAHs.

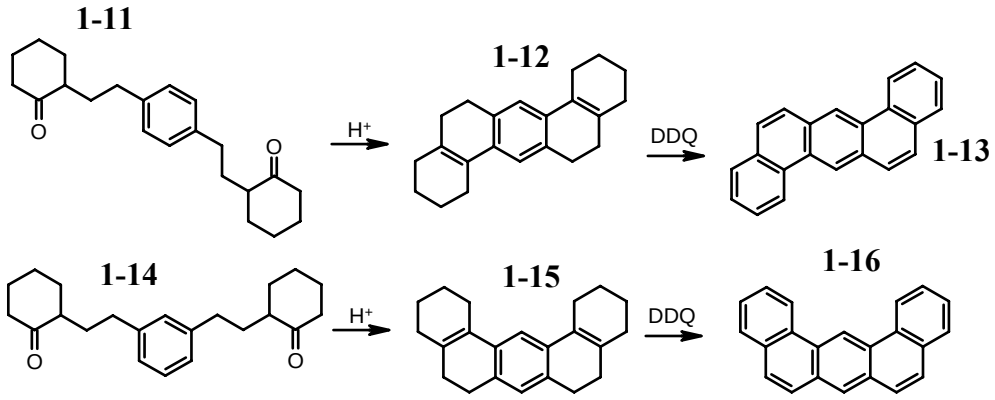

Scheme 1-2: *Acid-catalyzed cyclohehydration of diketones as an convenient synthetic access to PAHs.*

For example, acid-catalyzed cyclodehydration of the diketone **1-11** and **1-14** provides convenient synthetic access to dibenz[*a,h*]anthracene **1-13** and dibenz[*a,j*]anthracenes **1-16**, respectively (Scheme 1-2).[56] It is notable that both of these reactions occur strictly regiospecifically and that no side product could be isolated.

1.3.1.2 DIELS-ALDER Cycloaddition

Diels-Alder cycloaddition provides one of the most versatile methods for the construction of PAH ring systems. One of the numerous examples on this theme is illustrated in Scheme 1-3. Maleic anhydride and quinones, such as benzoquinone, are frequently employed as dienophiles for this purpose. The reaction of 1-vinylnaphthalene **1-17** with 1,4-benzoquinone **1-18** affords a cycloadduct that is converted directly to chrysene-1,4-dione **1-19** by dehydrogenation with excess benzoquinone. Chrysene-1,4-dione **1-19** is reduced to chrysene **1-20** by treatment with lithium aluminumhydride.[57]

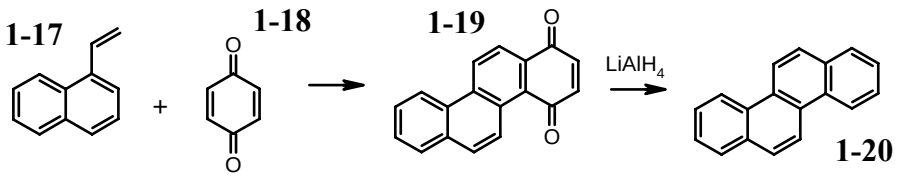

Scheme 1-3: *Example of the use of Diels-Alder cycloaddition for the construction of PAHs.*

One very elegant approach towards an extended PAH was presented by M. MÜLLER in the group of Prof. MÜLLEN, who utilized an intramolecular DIELS-ALDER reaction

to construct a suitable precursor for a 60 carbon containing, rhombus-shaped PAH **1-23**.[58]

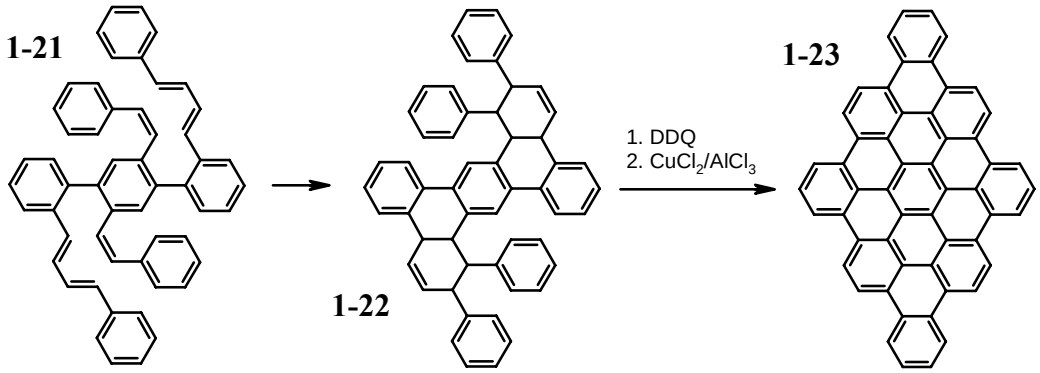

Scheme 1-4: *MÜLLER's Synthesis of the rhombus-shaped PAH*

In the phenylenevinylene-precursor **1-21**, which was obtained in seven reaction steps, both the diene- and dienophilic component are topologically arranged in a way, that the intramolecular cycloaddition reaction proceedes smoothly at a temperature of 135 °C to yield **1-22**. After a mild oxidation with 2,3-dichloro-4,5-dicyanonquinone (DDQ), the precursor was planarized to the desired molecule **1-23**.

1.3.1.3 Photocyclization

Photochemical methods first gained popularity for the synthesis of helicenes, but the method has seen increasingly wide application for the synthesis of diverse PAHs in recent years. The main limitations of the method are the need for photochemical apparatus and the restriction of scale caused by the necessity to carry out reactions in relatively dilute solutions. Most intensively investigated has been the conversion of stilbenes to phenanthrenes by irradiation with UV light in the presence of an oxidant, such as iodine or iron(III) chloride. These reactions are photochemically allowed conrotatory conversions of 1,3,5-hexatrienes to cyclohexadienenes; the oxidant serves to dehydrogenate the unstable primary dihydroaromatic products. Typical is the conversion of 2-(3,5-di-*tert*-butylstyryl)benzo[*c*]phenanthrene **1-24** to 1,3-di-tert-butylhexahelicene **1-25** (Scheme 1-5).[59] It is interesting, that cyclization occurs regiospecifically to the α-position despite the strong steric interactions in this region.

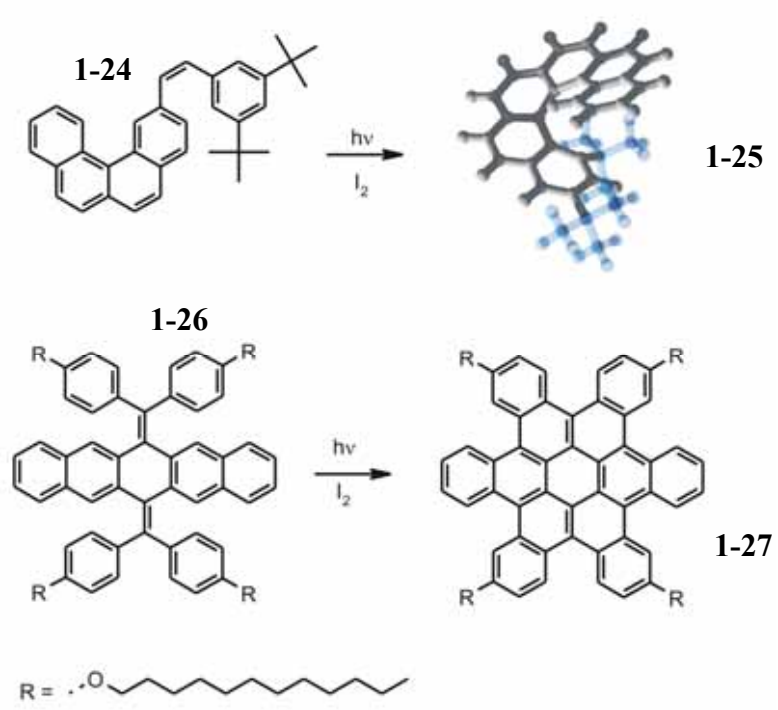

Scheme 1-5: *Photochemical cyclization as an approach to obtain PAHs.*

Very recently, S. XIAO et. al. published a novel approach towards a phase forming, distorted hexa-*cata*-hexabenzocoronone derivative **1-27**, whereby the decisive step is accomplished by the photocyclization of a adequate precursor molecule **1-26**.[60] The material revealed to form columnar liquid-crystalline phases with high charge carrier mobilities which were determined in an FET setup.

1.3.1.4 Flash Vacuum Pyrolysis (Thermolysis)

High temperature gas-phase pyrolysis with short contact time in the hot zone, resulting in electrocyclization with loss or migration of hydrogen (or hydrogen halide), is known as flash vacuum pyrolysis (FVP). The utility of FVP is illustrated by the synthesis of corannulene **1-32** in only three steps from commercially available starting materials *via* a route involving, in the key step, FVP of 7,10-(bis(1-chlorovinyl)fluoranthene **1-31** obtained from 7,10-diacetylfluoranthene **1-30** by reaction with phosphorous pentachloride (Scheme 1-6).[61,62]

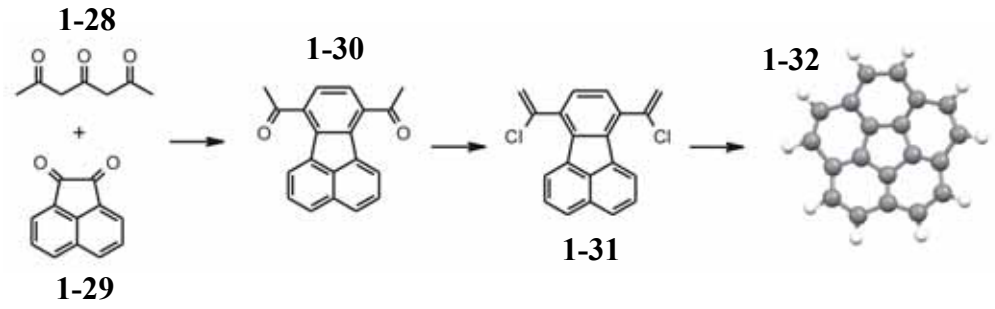

Scheme 1-6: *A short synthesis of corannulene involving in the key step cyclodehydrogenation by FVP.*

Recently, the synthesis of fullerene has been reported, whereby the key step was accomplished by FVP.[63]

1.3.1.5 Extrusion of Heteroatoms

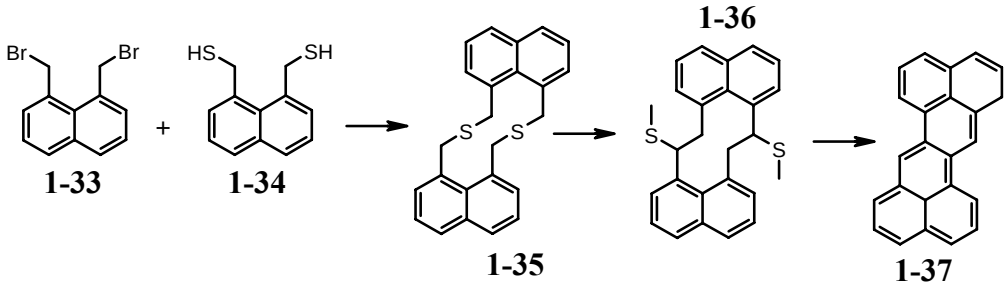

Scheme 1-7: *Synthesis of PAHs by a route that involves extrusion of sulfur.*

The best-known synthetic method that involves extrusion of sulfur is the cyclophane synthesis developed by MITCHELL and BOEKELHEIDE.[64,65] Applications of this approach to the synthesis of planar polyarenes are illustrated by the synthesis of dibenzo[*de,mn*]naphthacene (Scheme 1-7).[66]

Reaction of **1-33** with **1-34** yields the bis-sulfide **1-35**. Methylation of **1-35** followed by STEVENS rearrangement gives a mixture of isomeric sulfides, which eliminate according to HOFFMAN to yield dibenzo[*de,mn*]naphthacene **1-37**.

An outstanding preparative work in the field of PAHs consists in the synthesis of kekulene **1-40**, which has been reported by J.F. DIEDERICH and H.A. STAAB.[67-69] Key step for this challenging synthesis was the double sulfur extrusion of the dithiaphanes **1-38** to form the carbocyclic system **1-39**, which was converted to kekulene **1-40**.

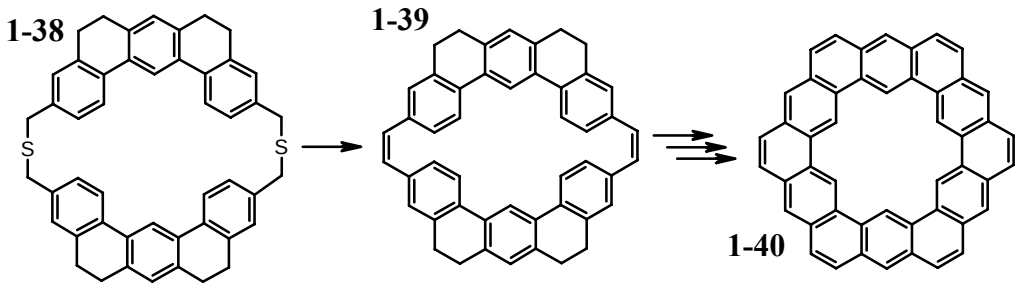

Scheme 1-8: *Synthesis of kekulene according to DIEDERICH and STAAB.*

1.3.1.6 SCHOLL-Cyclodehydrogenation

In addition to the above described methodologies, electrocyclization with loss of hydrogen may take place in the presence of LEWS acid catalysts, platinum or palladium metals, or potassium graphite. The coupling of two aromatic molecules in the presence of a LEWIS acid is called the SCHOLL reaction. Although the mechanism is speculated controversially[70], the reaction is one of the principal methods employed in the literature.

In the MÜLLEN group, this method was improved over the past decade and applied to a wide range of different oligophenylene precursors to synthesize extended PAHs.[71-73]

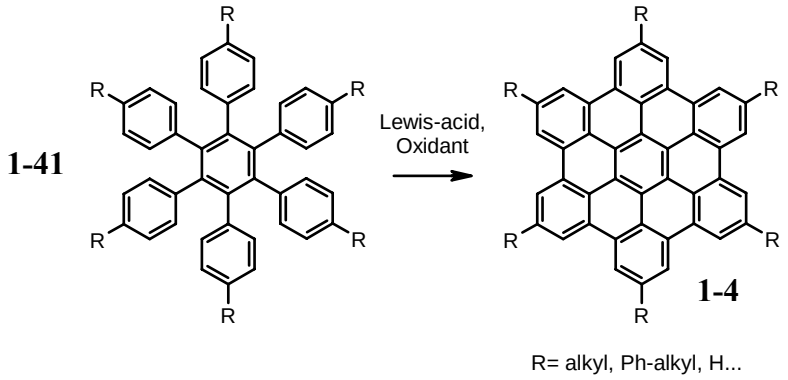

Scheme 1-9: *Cyclodehydrogenation of hexa-phenylbenzene to HBC.*

The reaction of substituted hexa-phenylbenzenes **1-41** with iron(III) chloride gives in one step the fully planarized HBC derivative **1-4**, which can be obtained on the multi-gram scale (Scheme 1-9). Since the first synthesis by P. HERWIG[74], the SCHOLL cyclodehydrogenation led to a large number of differently substituted HBC derivatives, which possess outstanding material properties.

Recently, D. WASSERFALLEN presented the synthesis of an extended, processable PAH, which contains 72 carbon atoms in the aromatic core.[75]

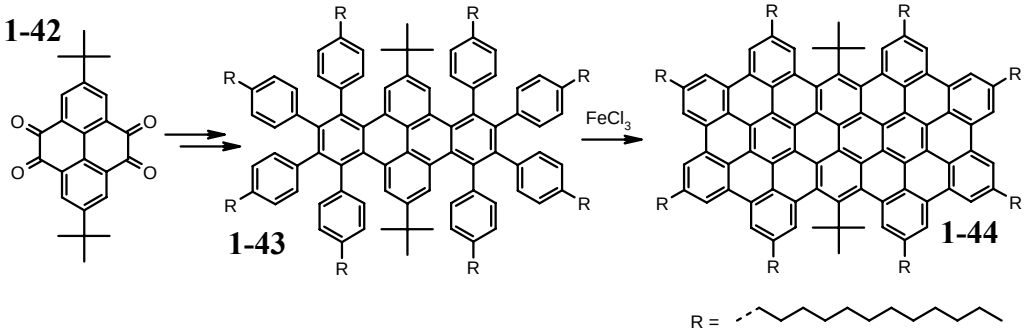

Scheme 1-10: *Synthesis of a non-planar 72 carbon containing PAH.*

Starting from the pyrenetetraone **1-42**, a suitable precursor for the SCHOLL planarization is built using the DIELS-ALDER approach (chapter 1.3.1.2). Interestingly, the treatment with iron(III) chloride yielded the fully fused PAH **1-44**, although the *tert*-butyl groups induce a strong distortion of the aromatic core. It turns out, that this is crucial to remain a reasonable solubility due to a perturbed self-aggregation.

1.4 Supramolecular Organization

Supramolecular structures emerge from spontaneous association because of non-covalent interactions. Interactions such as hydrogen bonds[76,77] or aromatic π-stacking[78] are driving forces to organize molecules into supramolecular architectures. The properties of these aggregates differ distinctly from the single molecule. HBCs belong to a group of molecules, which reveal a pronounced tendency to self-assemble both in solution and in the bulk phase.

1.4.1 Self-assembly

Self-assembly is the autonomous organization of components into patterns or structures without human intervention. Self-assembling processes are common throughout nature and technology.[79] Liquid crystalline phases are typical systems which self-assemble and form order on the microscopic scale. As a mesophase, one refers to a state, which combines properties of crystalline (optical and electric anisotropy) and of liquid phases (mobility, viscosity). The long range organization with respect to the orientation of the molecules is disturbed (Figure 1-5).

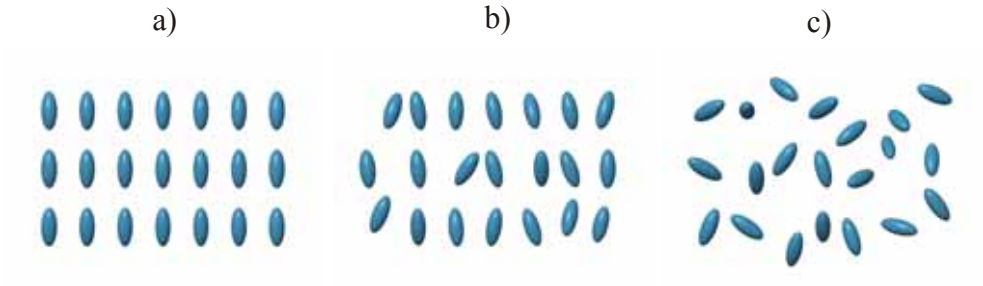

Figure 1-5: *a) crystalline, b) liquid-crystalline, and c) liquid (isotropic)*

The mesophases of disc-like molecules such as the HBC potentially can be classified into three distinct types (Figure 1-6): columnar (col), discotic-nematic (N_d), and discotic-lamellar, where the structure of the latter has not yet been elucidated.[80,81]

Figure 1-6: *Illustration of the two different mesophases of discotic liquid crystals, (A) columnar, and (B) discotic-nematic.*

The columnar phase consists of discs stacked one on top of the other to form columns, the different columns constituting a two-dimensional lattice. Several variations of the columnar structure have been identified, i.e. columns with hexagonal lattice (Col_h), rectangular lattice (Col_r), and an oblique lattice (Col_{ob}).

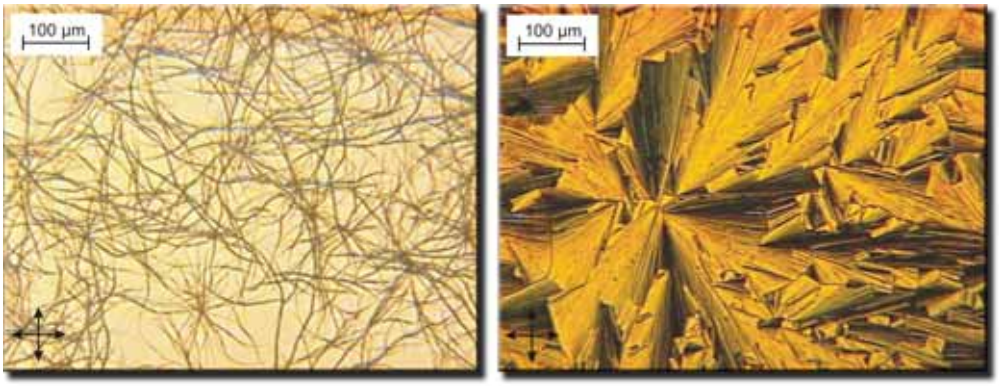

Figure 1-7: *POM images of n-dodecyl substituted HBC (A) from THF and (B) after crystallization from the melt (fast cooling).*[82]

HBC substituted with flexible alkyl chains is one representative of the group of discotics, which exhibits a very stable mesophase with a temperature broadness of often more than 200 °C. The large aromatic core establishes due to the pronounced aromatic π-stacking columnar structures, a layered structure similar to graphite. Both from solution and from the isotropic melt, which is for most of the HBC derivatives at temperatures above 400 °C, one obtains long-range organized molecules, as can be seen in the polarization optical microscopy (POM). Figure 1-7 depicts the very pronounced aggregation propensity of a hexa-fold *n*-dodecyl substituted HBC derivative both from solution-casting and from the melt. The birefringence impressively proves the long-range organization due to the π-stacking of the aromatic discs.

1.4.2 Orientation on Substrates

The implementation of discotic materials into electronic devices bears one disadvantage compared to conjugated polymers. Since the charge carriers are migrating strictly along the columns, the materials are quasi-one-dimensional nanowires.

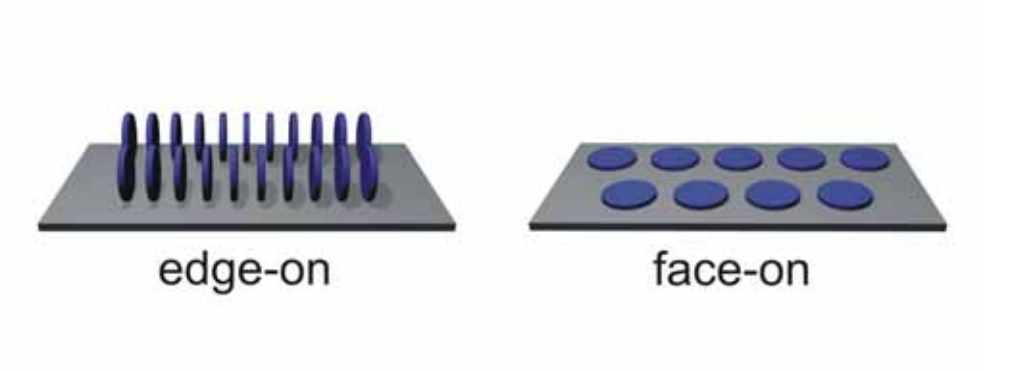

Figure 1-8: *Illustration of the two possible orientations of the disc-like molecule on a support.*

This requires therefore an organization of these pathways for electric charges with respect to substrate or device geometry. In FETs, the charges migrate between source and drain parallel to the substrate, which requires an edge-on arrangement of the molecules (Figure 1-8).[83] On the other hand, a molecular face-on orientation (Figure 1-8), which leads to the formation of a homeotropic phase, is thought to improve the efficiency of photovoltaic cells or could be interesting as hole-injection layers for organic LEDs.[84] The control of the molecular orientation and therefore the alignment of the charge carrier pathways constitute a task of major importance for material scientists, because it sensitively determines the performance of the electronic device. From solution most of the discotic materials organize in the edge-on fashion, while face-on was obtained when processed from the melt.[85] However, the mechanism of this process has not been completely understood.

1.4.3 Characterization of the Organization

Alkyl substituted HBC derivatives exhibit discotic mesophases. This has been demonstrated by POM, differential scanning calorimetry (DSC) and X-ray studies. Thermogravimetric analysis (TGA) revealed that the derivatives are stable up to temperatures of about 300 °C, at which point decomposition of the attached alkyl substituents starts. The most important information is obtained from temperature controlled two-dimensional wide-angle X-ray scattering of mechanically extruded

fibers. During the extrusion of the filament, the disc-like molecules align due to the shear forces perpendicular to the extrusion direction (Figure 1-9).[86]

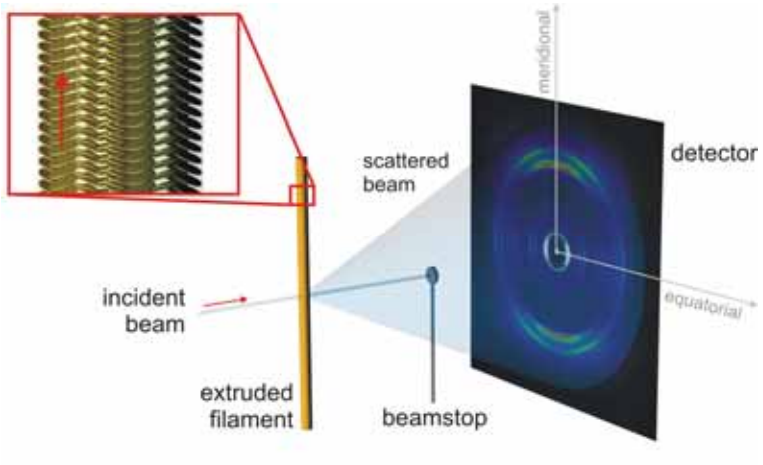

Figure 1-9: *Schematic illustration of the experimental setup of the 2D-WAXS scattering on mechanically aligned samples (inset shows the molecular organization within the fiber).*

With the incident X-ray beam orthogonal to the fiber axis, the recorded 2D-WAXS pattern reveals characteristic reflections (Figure 1-10).

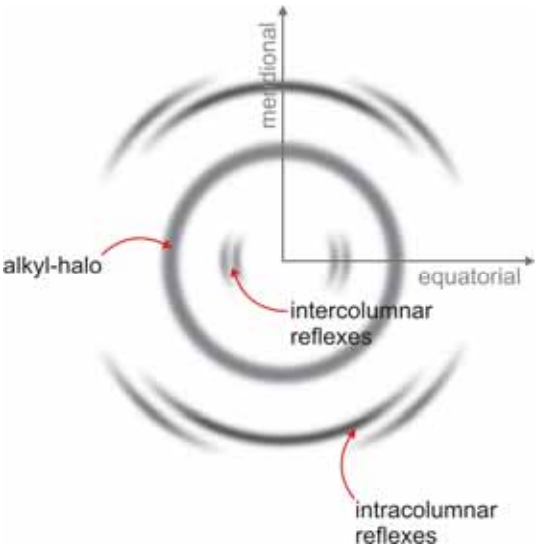

Figure 1-10: *Typical X-ray pattern obtained for extruded filaments of alkyl substituted HBCs.*

Firstly, the packing lattice of the columns, the intercolumnar correlation, are being identified by the reflexes on the equatorial plane. Furthermore, intracolumnar correlations lead to meridional reflexes, which allow even tilted columnar organizations to be identified. The stacking distance for most PAH-discotics is 3.5-3.6 Å, which is similar to graphite (3.35 Å). While these X-ray experiments elucidate the packing organization of the discotic molecules, solid-state NMR has proven to be a valuable tool to probe the molecular dynamics in these systems.[87,88] Using these

techniques, the bulk properties and the solid state characteristics of a material can be studied. In the case of typical alkyl substituted HBC derivatives, three distinct phases have been found. Both X-ray and the solid-state NMR experiment revealed a tilted columnar organization in the crystalline phase, in which the aromatic core is crystallized and positioned on fixed lattice points (Figure 1-11). The alkyl chains are not necessarily crystalline and in some cases possess a residual mobility. Entering the mesophase, a considerable increase of the molecular mobility has been found. The disc-like molecules adopt a non-tilted arrangement with respect to the columnar axis (Figure 1-11).

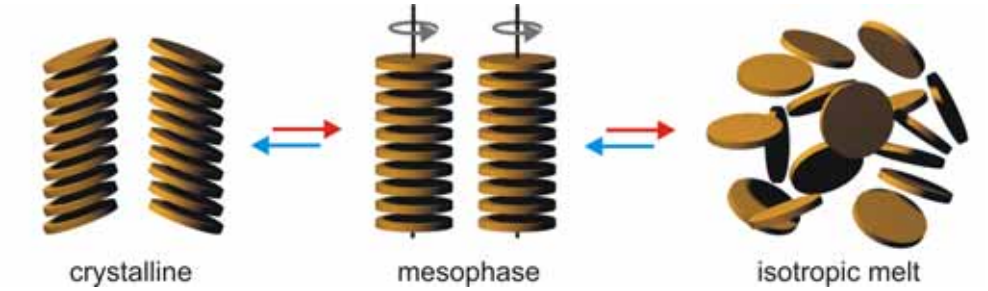

Figure 1-11: *Schematic representation of the organization within the three phases for discotic materials based on alkylated HBCs.*

At elevated temperatures, the material enters the isotropic phase, where a similar organization like in solution was determined. The aromatic discs are associating into small stacks of about 3-6 discs and the long-range organization has been lost.

In the quest for the fabrication of electronic devices based on single molecules, an important goal is the visualization and possibly the manipulation of single species. In order to explore organic surfaces on different length scales in various environments, scanning probe microscopy (STM) has played a paramount role. STM was invented in 1981 by G. BINNIG and H. ROHRER, who received the NOBEL Prize in Physics already five years later. An atomically sharp tip is moved over the surface of the material under study, and a voltage is applied between the probe and the surface. Depending on the voltage, electrons will tunnel from the tip into the surface, resulting in a weak current. Obviously, for a current to occur the substrate being scanned must be conductive. Insulators cannot be scanned through the STM.

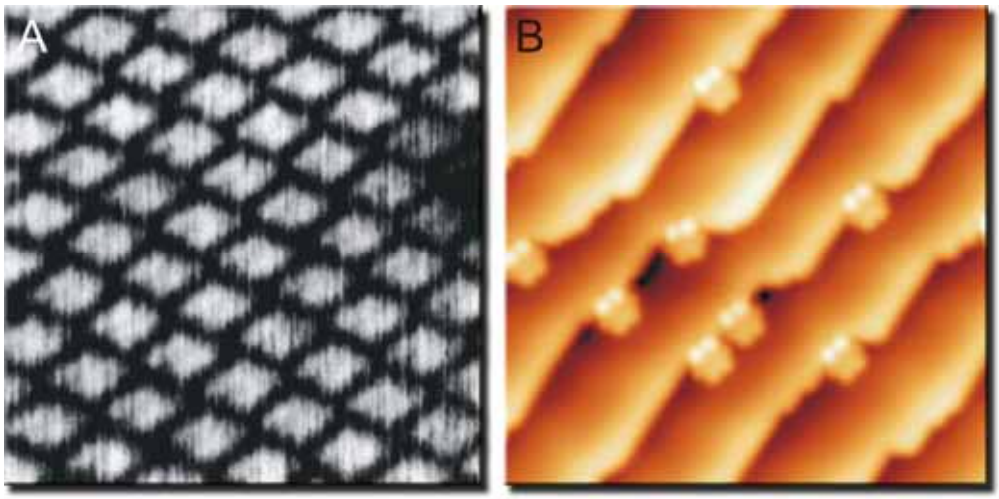

Figure 1-12: *STM image of (A) UHV deposited PAH* 1-23 *on MoS_2 and (B) UHV deposited unsubstituted HBC on Au(111) surfaces with terraces.*

Figure 1-12 depicts two STM images which have been obtained after UHV deposition of the respective PAH. As a very elegant structure proof, the rhombus-shape of the PAH **1-23** was imaged with STM. Interestingly, one obtained a well organized commensurate packing on molybdenum sulfide after ultra-high vacuum deposition (UHV) (Figure 1-12A). Recently, astonishing STM images have been recorded after the UHV of unsubstituted HBC onto gold with terraces. The interactions with this surface cause a strong distortion of the aromatic core, two benzenoid rings of the PAH are placed on top of a neighboring terrace (Figure 1-12B). Calculations are currently performed to elucidate the reason for this behavior.

1.5 Processing

The implementation of discotic materials in electronic device requires the organization of the one-dimensional charge carrier pathways to span the gap between the working electrodes of the device. Long-range and defect free alignment of the molecules determine the performance in these applications. Therefore, the processing into adequate morphologies remains a focus of research.

The fabrication of single crystals is connected to a high technical effort and only small and symmetric molecules crystallize into crystals with the required dimensions. However, the organization in crystals can be considered as almost perfect, leading to high performance values when incorporated in devices. Charge carrier mobilities determined in FETs have been found for single crystalline rubrene up to 15 $cm^2V^{-1}s^{-1}$.[89] Thin films of polycrystalline, highly ordered PAHs, obtained by the widely used vacuum deposition technique, revealed great performance values, when incorporated in organic electronic devices. Pentacene deposited by this technique exhibits one of the highest bulk charge carrier mobility.[90] Advantages for this technique is the facile control of the thickness, the refinement and therefore high purity of the material and the high order in the obtained films. As disadvantages, one has to mention the high processing costs, the large instrumentational effort and the limitation to small, mostly unsubstituted compounds.

The simple coating of a solution onto a spinning substrate is one of the most elegant ways to realize a homogenous film of a soluble, organic material. This technology is believed to have the highest potential impact on manufacturing costs of soluble organic semiconductors. Spin-coating allows homogenous films with good control of thickness to be fabricated over relatively large areas. However, this solution processing produces only morphologies with small domain sizes and no preferential organization of potential charge carrier pathways.

Recently, together with other scientists, W. PISULA developed a novel, solution-based processing technique, where molecules can be uniaxially aligned over macroscopic dimensions.[91-93] The zone-casting technique permitted thin films of *n*-dodecyl substituted HBC to be produced with a thickness of 15 nm and a single-crystalline-like order over several square centimeters. Figure 1-13 illustrates the specially constructed device, where a solution was deposited through a flat nozzle onto a

moving support, both of which were thermally stabilized. The rates of support motion and solution deposition were optimized to obtain stationary film solidification conditions. This allowed the HBC molecule to naturally self-assemble into edge-on arrange columns, uniaxially aligned to the substrate.

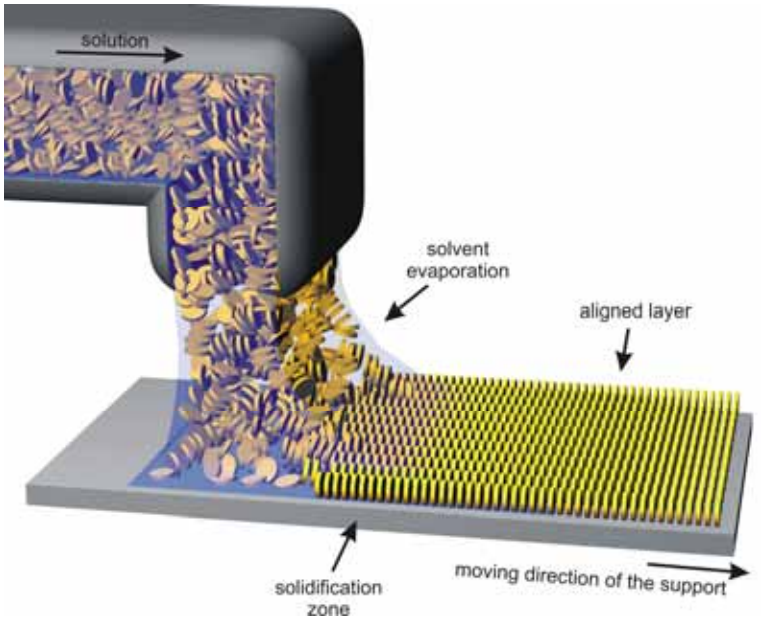

Figure 1-13: *Schematic presentation of the zone-casting process. The discs represent HBC molecules.*

The investigation of the film morphology revealed to be highly organized, as can be seen from atomic force microscopy (AFM) and high-resolution transmission electron microscopy (HR-TEM) (Figure 1-14).

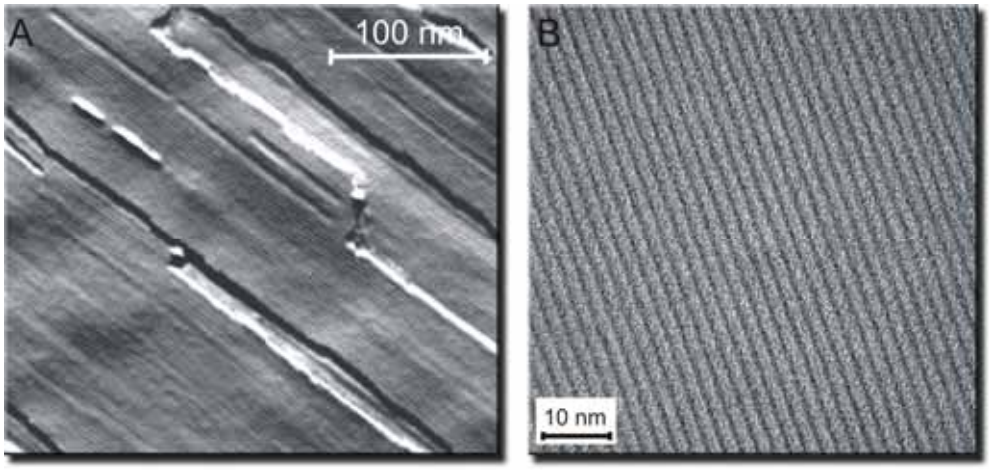

Figure 1-14: *Zone-cast film of n-dodecyl substituted HBC (A) AFM topography image and (B) HR-TEM image.*

The implementation of these films as semiconductor layer in FETs impressively emphasized the high molecular organization. Without any optimization, a charge

carrier mobility of 0.01 $cm^2V^{-1}s^{-1}$ has been determined.[28] Currently, the parameters for both the zone-casting and the implementation into the device are optimized to obtain better performing devices.

1.6 Electronic Devices

Finally, after the synthesis, the investigation of the supramolecular organization, and the successful processing into adequate morphologies, the potentially promising material can be tested as active component in an organic electronic device. One needs a clear appreciation of the material requirements of organic light emitting diodes (LED), photovoltaics and transistors in order to assess the potential of discotic liquid crystals for these devices.

1.6.1 Light Emitting Diode

Figure 1-15 shows a schematic representation of the simplest type of organic LED where light is generated by electrical excitation. A thin film of an organic emitter is sandwiched between a transparent anode and a metallic cathode, which differ in their work function. Electrons and holes, which are injected into the lowest unoccupied molecular orbital (LUMO) and highest occupied molecular orbital (HOMO), respectively, drift through the organic film under the influence of the applied electric field. The coulombic attraction between an electron and hole at the same chromophore site results in the formation of an exciton, a bound electron-hole pair, which recombines to produce luminescence.

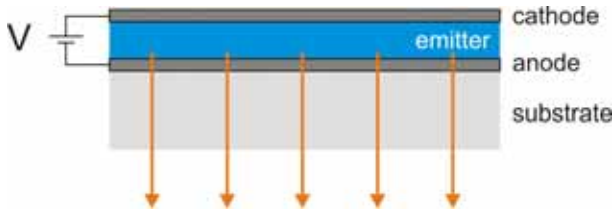

Figure 1-15: *Schematic presentation of the single layer organic light emitting diode.*

More sophisticated devices have multiple layers with the luminescent layer sandwiched between hole- and electron injection/transport layers. Examples of successfully incorporated discotics in charge transporting/compensating layers have been reported.[94] Important for a successful implementation in organic LEDs are high charge carrier mobilities and the balance between the injection of holes and electrons.

1.6.2 Photovoltaic Element

There are many recent reviews on organic photovoltaics.[95-97] The physical setup resembles the one of the LEDs (Figure 1-16). One way to obtain high efficiencies in photovoltaic devices is the blending of a donor and an acceptor component which

microscopically phase-segregate between the two working electrodes. Thereby, it is important to increase the interface between the two components.

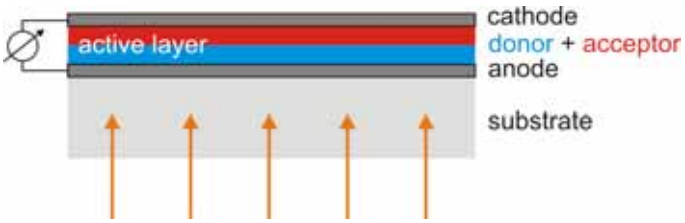

Figure 1-16: *Schematic presentation of the setup of a heterojunction photovoltaic device.*

Figure 1-17 illustrates the energy level diagram of a photovoltaic blended device under short-circuit conditions. The photovoltaic effect requires:

i) absorption of solar radiation and photogeneration of excitons

ii) polarization of the bound electron-hole pairs at the hetero-interface between donor and acceptor species

iii) charge separation, and the transport of the free charge carriers for collection at electrodes.

Each of these individual processes should be highly efficient and there should be a minimum of charge recombination.

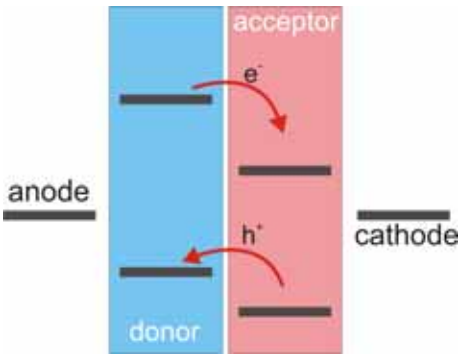

Figure 1-17: *Energy level diagram under short-circuit conditions showing charge separation and transport in a blend consisting of an electron donor and acceptor placed between a dissimilar anode and cathode, which provide an built-in field.*

Discotic materials based on HBC have together with rylene dyes as acceptor component been implemented successfully into bulk heterojunction photovoltaic elements, exhibiting excellent external quantum efficiencies of 34% under monochromatic illumination.[26,98]

1.6.3 Field-Effect Transistor

The widespread interest in organic FETs is based on their large-area coverage, structural flexibility, and low-cost processing.[83] A typical organic FET configuration is shown in Figure 1-18. For a p-type semiconductor, conduction of charge between the source and drain electrodes is governed by the gate voltage. When the gate is positive with respect to the source, the semiconductor is depleted of carriers. When the gate is biased negatively, carriers accumulate in the channel between source and drain. The drain current is then proportional to the material mobility.

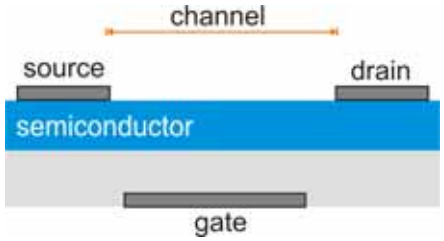

Figure 1-18: *Typical configuration of an organic FET.*

Long-range, edge-on organized discotic materials exhibit good FET performances, due to an intrinsically high charge carrier mobility.[28,60]

However, next to high charge carrier mobilities, the injection of charge carriers into a material is of major importance. Therefore, the energetic levels of HOMO and LUMO are crucial and have to be sensitively tuned by the molecular architecture. To inject positive charge carriers, the material should possess a low oxidation potential. Analogous, for efficient injections of electrons, the reduction potential should be low.

1.7 References

(1) Sirringhaus, H.; Tessler, N.; Friend, R. H. *Science* **1998**, *280*, 1741-1744.

(2) Dodabalapur, A.; Bao, Z.; Makhija, A.; Laquindanum, J. G.; Raju, V. R.; Feng, Y.; Katz, H. E.; Rogers, J. *Appl. Phys. Lett.* **1998**, *73*, 142-144.

(3) Shaw, J. M.; Seidler, P. F. *Ibm Journal of Research and Development* **2001**, *45*, 3-9.

(4) (www.idtechex.com), I. "Organic Electronics Forecasts, Players & Opportunities 2005-2025."

(5) http://www.phys.unsw.edu.au "Introduction to Organic Electronics," ScienceUNSW, 2004.

(6) Heeger, A. J. *Angew. Chem., Int. Ed.* **2001**, *40*, 2591-2611.

(7) Kertesz, M.; Choi, C. H.; Yang, S. J. *Chem. Rev.* **2005**, *105*, 3448-3481.

(8) Sirringhaus, H.; Brown, P. J.; Friend, R. H.; Nielsen, M. M.; Bechgaard, K.; Langeveld-Voss, B. M. W.; Spiering, A. J. H.; Janssen, R. A. J.; Meijer, E. W.; Herwig, P.; de Leeuw, D. M. *Nature* **1999**, *401*, 685-688.

(9) Reinitzer, F. *Monatsh. Chem.* **1888**, *9*, 421.

(10) Chandrasekhar, S.; Sadashiva, B. K.; Suresh, K. A. *Pramana* **1977**, *9*, 471-480.

(11) Hunter, C. A.; Sanders, J. K. M. *J. Am. Chem. Soc.* **1990**, *112*, 5525-5534.

(12) Warman, J. M.; de Haas, M. P.; Dicker, G.; Grozema, F. C.; Piris, J.; Debije, M. G. *Chem. Mater.* **2004**, *16*, 4600-4609.

(13) van de Craats, A. M.; Warman, J. M.; Fechtenkötter, A.; Brand, J. D.; Harbison, M. A.; Müllen, K. *Adv. Mater.* **1999**, *11*, 1469-1472.

(14) Iino, H.; Takayashiki, Y.; Hanna, J.; Bushby, R. J.; Haarer, D. *Appl. Phys. Lett.* **2005**, *87*.

(15) Simmerer, J.; Glusen, B.; Paulus, W.; Kettner, A.; Schuhmacher, P.; Adam, D.; Etzbach, K. H.; Siemensmeyer, K.; Wendorff, J. H.; Ringsdorf, H.; Haarer, D. *Adv. Mater.* **1996**, *8*, 815-&.

(16) Adam, D.; Schuhmacher, P.; Simmerer, J.; Haussling, L.; Siemensmeyer, K.; Etzbach, K. H.; Ringsdorf, H.; Haarer, D. *Nature* **1994**, *371*, 141-143.

(17) van de Craats, A. M.; Warman, J. M.; deHaas, M. P.; Adam, D.; Simmerer, J.; Haarer, D.; Schuhmacher, P. *Adv. Mater.* **1996**, *8*, 823-&.

(18) Warman, J. M.; Kroeze, J. E.; Schouten, P. G.; van de Craats, A. M. *J. Porphyrins Phthalocyanines* **2003**, *7*, 342-350.

(19) Ohta, K.; Hatsusaka, K.; Sugibayashi, M.; Ariyoshi, M.; Ban, K.; Maeda, F.; Naito, R.; Nishizawa, K.; van de Craats, A. M.; Warman, J. M. *Mol. Cryst. Liq. Cryst.* **2003**, *397*, 325-345.

(20) Schouten, P. G.; Chen, W. M.; Warman, J. M.; Dehaas, M. P.; Vanderpol, J. F.; Zwikker, J. W. *Synth. Met.* **1991**, *42*, 2665-2668.

(21) Kraft, A. *ChemPhysChem* **2001**, *2*, 163-165.

(22) Pecchia, A.; Lozman, O. R.; Movaghar, B.; Boden, N.; Bushby, R. J.; Donovan, K. J.; Kreouzis, T. *Phys. Rev. B* **2002**, *65*.

(23) Lever, L. J.; Kelsall, R. W.; Bushby, R. J. *Phys. Rev. B* **2005**, *72*.

(24) Petritsch, K.; Friend, R. H.; Lux, A.; Rozenberg, G.; Moratti, S. C.; Holmes, A. B. *Synth. Met.* **1999**, *102*, 1776-1777.

(25) Schmidt-Mende, L.; Fechtenkotter, A.; Müllen, K.; Friend, R. H.; MacKenzie, J. D. *Physica E* **2002**, *14*, 263-267.

(26) Schmidt-Mende, L.; Fechtenkotter, A.; Müllen, K.; Moons, E.; Friend, R. H.; MacKenzie, J. D. *Science* **2001**, *293*, 1119-1122.

(27) Schmidt-Mende, L.; Watson, M.; Müllen, K.; Friend, R. H. *Mol. Cryst. Liq. Cryst.* **2003**, *396*, 73-90.

(28) Pisula, W.; Menon, A.; Stepputat, M.; Lieberwirth, I.; Kolb, U.; Tracz, A.; Sirringhaus, H.; Pakula, T.; Müllen, K. *Adv. Mater.* **2005**, *17*, 684-+.

(29) van de Craats, A. M.; Stutzmann, N.; Bunk, O.; Nielsen, M. M.; Watson, M.; Müllen, K.; Chanzy, H. D.; Sirringhaus, H.; Friend, R. H. *Adv. Mater.* **2003**, *15*, 495-499.

(30) Clar, E. *The Aromatic Sextet*; Wiley: New York, 1972.

(31) Balaban, A. T.; Schleyer, P. V.; Rzepa, H. S. *Chem. Rev.* **2005**, *105*, 3436-3447.

(32) Connor, D. A.; Lin, P. P.; Herndon, W. C. *Abstracts of Papers of the American Chemical Society* **1990**, *199*, 418-ORGN.

(33) Herndon, W. C.; Connor, D. A.; Lin, P. P. *Pure Appl. Chem.* **1990**, *62*, 435-444.

(34) Herndon, W. C.; Nowak, P. C.; Connor, D. A.; Lin, P. P. *J. Am. Chem. Soc.* **1992**, *114*, 41-47.

(35) Schleyer, P. V.; Jiao, H. J.; Hommes, N.; Malkin, V. G.; Malkina, O. L. *J. Am. Chem. Soc.* **1997**, *119*, 12669-12670.

(36) Schleyer, P. V.; Kiran, B.; Simion, D. V.; Sorensen, T. S. *J. Am. Chem. Soc.* **2000**, *122*, 510-513.

(37) Zander, M. *Polycyclische Aromaten*; B. G. Teubner Verlag: Stuttgart, 1995.

(38) Lang, K. F.; Kalowy, J.; Buffleb, H. *Chem. Ber. Recl.* **1964**, *97*, 494-&.

(39) Lang, K. F.; Kalowy, J.; Buffleb, H. *Chem. Ber. Recl.* **1962**, *95*, 1052-&.

(40) Lang, K. F.; Buffleb, H.; Zander, M. *Angew. Chem., Int. Ed.* **1963**, *75*, 170-&.

(41) Lang, K. F.; Buffleb, H. *Chem. Ber. Recl.* **1962**, *95*, 1049-&.

(42) Scholl, R.; Seer, C. *Justus Liebigs Ann. Chem.* **1912**, *394*, 111-177.

(43) Scholl, R.; Seer, C. *Ber. Dtsch. Chem. Ges.* **1911**, *44*, 1233-1240.

(44) Scholl, R.; Seer, C.; Weitzenbock, R. *Ber. Dtsch. Chem. Ges.* **1910**, *43*, 2202-2209.

(45) Clar, E. *Ber. Dtsch. Chem. Ges.* **1929**, *62*, 1574-1582.

(46) Clar, E.; Wallenstein, H.; Avenarius, R. *Ber. Dtsch. Chem. Ges.* **1929**, *62*, 950-955.

(47) Clar, E.; John, F.; Hawran, B. *Ber. Dtsch. Chem. Ges.* **1929**, *62*, 940-950.

(48) Clar, E. *Ber. Dtsch. Chem. Ges.* **1929**, *62*, 350-359.

(49) Clar, E. *Polycyclic Hydrocarbons*; John Wiley and Sons: New York, 1964; Vol. 1+2.

(50) Clar, E.; Ironside, C. T.; Zander, M. *Tetrahedron* **1959**, *6*, 358-363.

(51) Clar, E.; Zander, M. *J. Chem. Soc.* **1958**, 1577-1579.

(52) Clar, E.; Zander, M. *J. Chem. Soc.* **1957**, 4616-4619.

(53) Zander, M. *Handbook of Polycyclic Aromatic Hydrocarbons*; Marcel Dekker: New York, 1983.

(54) Berliner, E. *Org. Reac.* **1949**, *5*, 229.

(55) Johnson, W. S. *Org. React.* **1944**, *5*, 114.

(56) Harvey, R. G.; Pataki, J.; Cortez, C.; Diraddo, P.; Yang, C. X. *J. Org. Chem.* **1991**, *56*, 1210-1217.

(57) Davies, W.; Porter, Q. N. *J. Chem. Soc.* **1957**, 4967-4970.

(58) Müller, M.; Kübel, C.; Müllen, K. *Chem. Eur. J.* **1998**, *4*, 2099-2109.

(59) Behm, H.; Lourens, A. F.; Beurskens, P. T.; Prinsen, W. J. C.; Hajee, C. A. J.; Laarhoven, W. H. *J. Cryst. Spec. Res.* **1988**, *18*, 465-470.

(60) Xiao, S. X.; Myers, M.; Miao, Q.; Sanaur, S.; Pang, K. L.; Steigerwald, M. L.; Nuckolls, C. *Angew. Chem., Int. Ed.* **2005**, *44*, 7390-7394.

(61) Scott, L. T.; Cheng, P. C.; Hashemi, M. M.; Bratcher, M. S.; Meyer, D. T.; Warren, H. B. *J. Am. Chem. Soc.* **1997**, *119*, 10963-10968.

(62) Scott, L. T.; Hashemi, M. M.; Meyer, D. T.; Warren, H. B. *J. Am. Chem. Soc.* **1991**, *113*, 7082-7084.

(63) Scott, L. T.; Boorum, M. M.; McMahon, B. J.; Hagen, S.; Mack, J.; Blank, J.; Wegner, H.; de Meijere, A. *Science* **2002**, *295*, 1500-1503.

(64) Mitchell, R. H.; Boekelhe.V *J. Am. Chem. Soc.* **1974**, *96*, 1547-1557.

(65) Keehn, P. M.; Rosenfeld, S. M. *Cyclophanes*; Academic Press: New York, 1983.

(66) Kemp, W.; Storie, I. T.; Tulloch, C. D. *J. Chem. Soc. -Perk. Trans. 1* **1980**, 2812-2817.

(67) Diederich, F.; Staab, H. A. *Angew. Chem., Int. Ed.* **1978**, *17*, 372-374.

(68) Krieger, C.; Diederich, F.; Schweitzer, D.; Staab, H. A. *Angew. Chem., Int. Ed.* **1979**, *18*, 699-701.

(69) Staab, H. A.; Diederich, F. *Chem. Ber. Recl.* **1983**, *116*, 3487-3503.

(70) Rempala, P.; Kroulik, J.; King, B. T. *J. Am. Chem. Soc.* **2004**, *126*, 15002-15003.

(71) Müller, M.; Kübel, C.; Morgenroth, F.; Iyer, V. S.; Müllen, K. *Carbon* **1998**, *36*, 827-831.

(72) Morgenroth, F.; Kübel, C.; Müller, M.; Wiesler, U. M.; Berresheim, A. J.; Wagner, M.; Müllen, K. *Carbon* **1998**, *36*, 833-837.

(73) Müller, M.; Iyer, V. S.; Kübel, C.; Enkelmann, V.; Müllen, K. *Angew. Chem., Int. Ed.* **1997**, *36*, 1607-1610.

(74) Stabel, A.; Herwig, P.; Müllen, K.; Rabe, J. P. *Angew. Chem., Int. Ed.* **1995**, *34*, 1609-1611.

(75) Wasserfallen, D.; Kastler, M.; Pisula, W.; Hofer, W. A.; Fogel, Y.; Wang, Z.; Müllen, K. *J. Am. Chem. Soc.* **2006**, *in press*.

(76) Brunsveld, L.; Folmer, B. J. B.; Meijer, E. W.; Sijbesma, R. P. *Chem. Rev.* **2001**, *101*, 4071-4097.

(77) Pak, C.; Lee, H. M.; Kim, J. C.; Kim, D.; Kim, K. S. *Struct. Chem.* **2005**, *16*, 187-202.

(78) Hoeben, F. J. M.; Jonkheijm, P.; Meijer, E. W.; Schenning, A. *Chem. Rev.* **2005**, *105*, 1491-1546.

(79) Whitesides, G. M.; Grzybowski, B. *Science* **2002**, *295*, 2418-2421.

(80) Dierking, I. *Textures of Liquid Crystals*; Wiley-VCH: Weinheim, 2003.

(81) Chandrasekhar, S.; Prasad, S. K. *Contemp. Phys.* **1999**, *40*, 237-245.

(82) Pisula, W., Johannes Gutenberg Universität, 2005.

(83) Dimitrakopoulos, C. D.; Malenfant, P. R. L. *Adv. Mater.* **2002**, *14*, 99-117.

(84) Stapff, I. H.; Stumpflen, V.; Wendorff, J. H.; Spohn, D. B.; Mobius, D. *Liq. Cryst.* **1997**, *23*, 613-617.

(85) Kopitzke, J.; Wendorff, J. H. *Chem. unserer Zeit* **2000**, *34*, 4-16.

(86) Pisula, W.; Tomovic, Z.; Simpson, C.; Kastler, M.; Pakula, T.; Müllen, K. *Chem. Mater.* **2005**, *17*, 4296-4303.

(87) Brown, S. P.; Schnell, I.; Brand, J. D.; Müllen, K.; Spiess, H. W. *J. Am. Chem. Soc.* **1999**, *121*, 6712-6718.

(88) Brown, S. P.; Schnell, I.; Brand, J. D.; Müllen, K.; Spiess, H. W. *Phys. Chem. Chem. Phys.* **2000**, *2*, 1735-1745.

(89) Nelson, S. F.; Lin, Y. Y.; Gundlach, D. J.; Jackson, T. N. *Appl. Phys. Lett.* **1998**, *72*, 1854-1856.

(90) Dimitrakopoulos, C. D.; Purushothaman, S.; Kymissis, J.; Callegari, A.; Shaw, J. M. *Science* **1999**, *283*, 822-824.

(91) Tang, C. B.; Tracz, A.; Kruk, M.; Zhang, R.; Smilgies, D. M.; Matyjaszewski, K.; Kowalewski, T. *J. Am. Chem. Soc.* **2005**, *127*, 6918-6919.

(92) Pisula, W.; Menon, A.; Stepputat, M.; Lieberwirth, I.; Kolb, U.; Tracz, A.; Sirringhaus, H.; Pakula, T.; Müllen, K. *Advanced Materials* **2005**, *17*, 684-+.

(93) Tracz, A.; Pakula, T.; Jeszka, J. K. *Mater. Sci. Pol.* **2004**, *22*, 415-421.

(94) Seguy, I.; Jolinat, P.; Destruel, P.; Farenc, J.; Mamy, R.; Bock, H.; Ip, J.; Nguyen, T. P. *J. Appl. Phys.* **2001**, *89*, 5442-5448.

(95) Nelson, J. *Curr. Opin. Solid State Mater. Sci.* **2002**, *6*, 87-95.

(96) Moons, E. *J. Phys - Cond. Matt.* **2002**, *14*, 12235-12260.

(97) Brabec, C. J.; Sariciftci, N. S.; Hummelen, J. C. *Adv. Funct. Mater.* **2001**, *11*, 15-26.

(98) Schmidtke, J. P.; Friend, R. H.; Kastler, M.; Müllen, K. *submitted* **2006**.

2 Motivation and Objective

Discotic liquid crystalline materials are being recognized for their potential application in organic electronic applications. Implementation of these materials into memory cards[1-3], sensors[4,5], displays[6,7] and high-resolution xerography[8] is being discussed. As anticipated from promising measurements of record charge carrier mobilities[9] along the stacked columns, formed by the disk-like molecules, the large hexa-*peri*-hexabenzocoronene (HBC) derivatives have proven successful as active component in solar-cells and organic, thin-film field effect transistors (FETs).[10,11] HBCs are larger than the widely studied triphenylenes[8,12], porphyrins[13,14], and phthalocyanines[15,16] and combine the electronic properties of semiconductors and mechanical processing properties of polymeric materials. This qualifies them as suitable for commercial applications in optoelectronic technologies where the adaptability and simplicity and low cost manufacturing make them extremely attractive.

Once a chemical substance crosses the border from being simply a new compound to the stage where its materials properties become most dominant and relevant for its application in devices, one has to think of designing the synthesis to be as easy, inexpensive and efficient as possible. Furthermore, to gain a more thorough understanding of the potential of such materials, a library of derivatives, controllable molecular and supramolecular properties are required to study the influence onto the device performance. The query for novel materials requires a very close interaction between synthesis, processing of the materials into adequate morphologies and finally the fabrication of electronic devices.

Figure 2-1: *"The interdisciplinary path" from the synthesis of novel material, over the processing into adequate morphologies to the final, successful implementation into an organic, electronic device.*

Synthetic chemists have to design materials which fulfill needs of the scientists which process the materials. This requires the tuning of solubility, melting points, nucleation and crystallization behavior. Thus researchers from all three fields must closely

interact to work on the implementation of organic semiconductors into electronic devices. The elucidation of structure-morphology relations is one important focus.

An improvement of the solubility and thus the processability is desired since most of the known HBC derivatives are sparingly soluble in organic solvents, due to the very strong aromatic π-stacking interactions. The introduction of sterically demanding substituents would modulate the intermolecular, attractive forces. Consequently, this would lead to a reduced aggregation behavior, higher solubility and even lower isotropization temperatures, highly desired for cheap processing techniques from the molten state. Better soluble materials promise furthermore a better purification during the work-up. For this purpose, alkyl chains with a branching site close to the aromatic system were chosen to be introduced into the perimeter of HBC (Figure 2-2). The chains were used as a racemic mixture to additionally hamper a crystallization of the flexible alkyl surrounding around the aromatic core.

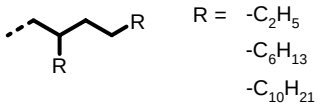

Figure 2-2: *Chosen branched alkyl substituents*

The investigation of the self-association behavior in solution of a series of HBC derivatives would give important insights to control the processing parameters (concentration, temperature, nature of solvent) from solution. To implement these discotic materials as active component into a macroscopic device, the columnar stacks have to be uniaxially, defect free aligned to allow an undisturbed charge carrier migration between the working electrodes. Thereby, different device geometries necessitate a specific macroscopic alignment of the molecules with respect to the substrate. In field-effect transistors (FETs), the charges are migrating between source and drain parallel to the substrate which requires an edge-on orientation of the columns. On the other hand, a molecular face-on orientation, which leads to the formation of a homeotropic phase is thought to improve the efficiency of photovoltaic cells or could be interesting as hole-injection layers for organic LEDs. The mechanism and the exact structural requirements for the face-on ordering are not yet understood. The synthesis of novel HBC derivatives, where the orientation of the molecule is determined and controlled by the molecular architecture, is highly desired. Since the face-on organization of HBC derivative has not yet been obtained

and the mechanism for this process has not yet been reported, novel processing techniques have to be developed and tested.

The skillful functionalization of HBCs leading to a whole variety of mono-, di- and even tri-functionalized derivatives, bearing different functional groups, has been investigated in the past. By varying appropriate parameters, an accurate control over the supramolecular ordering of the discotic molecules could be achieved. However, these concepts are synthetically challenging and require a multi-step synthesis with tedious purifications. Novel concepts to functionalize the HBC core in the periphery are required to produce homologous series of materials, which can be processed and potentially implemented in well performing devices. An *a posteriori* functionalization of a suitable "building block"- HBC would allow the nature of the flexible alkyl surrounding to be manipulated in the very last step (Figure 2-3). Different functions such as cross-linkable side groups could be introduced and the molecular order could be fixed with different external stimuli such as light or heat. The chosen reactive moiety will be hydroxyl functions, which can be converted with different carboxy derivatives, such as acid chlorides or anhydrides, to the corresponding esters in very high yields.

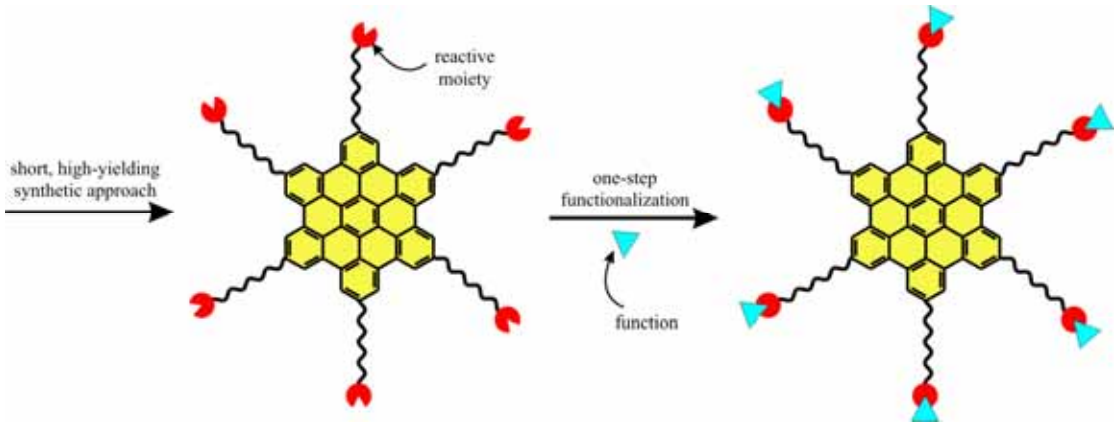

Figure 2-3: *Schematic representation of the desired a posteriori functionalization of HBC.*

Besides the necessity for an interesting material to be processable into the required morphology, properties such as a high charge carrier mobility, UV/vis absorption, or electronic character are equally important. The redox potential of a semiconductor is a crucial value which influences the charge carrier injection from the electrode, which have a specific work function. In the past, the extension of the aromatic system was a parameter which was changed to tune these molecular properties. However, this approach turned out to be chemically very challenging, *inter alia* the very pronounced

aggregation of the large π-areas reduced the solubility and therefore often hampered a successful purification. A theoretically well investigated parameter is to tune the nature of the periphery. Introducing "zigzag" edges into the all-"arm-chair" periphery of HBC, quantum chemical calculation predicted a significant influence onto the electronic behavior.

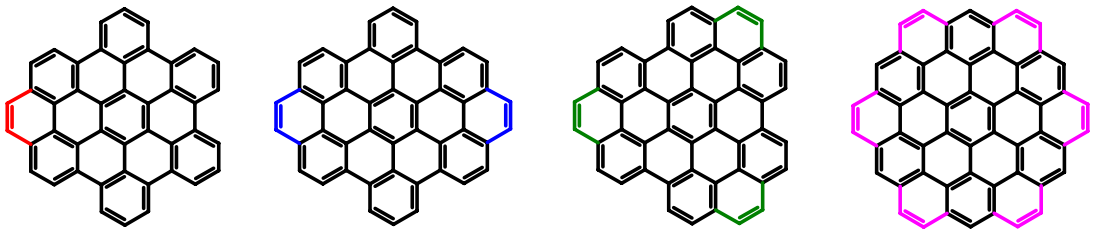

Figure 2-4: *Novel PAHs, formally derived from HBC, with partial "zigzag" peripheries.*

Furthermore, the change of the symmetry of the aromatic entity changes the number of electronic transitions and their oscillator strengths, which should give different UV/vis characteristics. The question to which extent the nature of the periphery influences the liquid crystalline behavior (i.e. stability of the aromatic stacking) has to be answered.

In summary, the development of synthetic concepts towards novel discotic materials with novel peripheries for the potential implementation in organic electronic devices, based on extended PAHs, will be presented (Figure 2-4). For selected materials, the processing conditions will be optimized and subsequently tested as active component in electronic devices, such as heterojunction photovoltaic elements. Analytical techniques such as two-dimensional wide angle X-ray scattering and solid state NMR will be used to investigate the supramolecular organization, which is correlated to the molecular architecture, to gain valuable information about structure-relationships and helps to improve the fabrication of devices. The potential of a synthesized material will be evaluated by time-of-flight and pulse-radiolysis time-resolved microwave conductivity measurements to study the macroscopic and the nanoscopic charge carrier mobility. Promising derivatives will be implemented in electronic devices such as bulk heterojunction photovoltaic devices.

2.1 References

(1) Bock, H.; Helfrich, W. *Liq. Cryst.* **1995**, *18*, 707-713.

(2) Liu, C. Y.; Pan, H. I.; Fox, M. A.; Bard, A. J. *Science* **1993**, *261*, 897-899.

(3) Scherowsky, G.; Chen, X. H. *J. Mater. Chem.* **1995**, *5*, 417-421.

(4) Clements, J.; Boden, N.; Gibson, T. D.; Chandler, R. C.; Hulbert, J. N.; Ruck-Keene, E. A. *Sensors and Actuators B-Chemical* **1998**, *47*, 37-42.

(5) Wright, J. D.; Roisin, P.; Rigby, G. P.; Nolte, R. J. M.; Cook, M. J.; Thorpe, S. C. *Sensors and Actuators B-Chemical* **1993**, *13*, 276-280.

(6) Christ, T.; Glusen, B.; Greiner, A.; Kettner, A.; Sander, R.; Stumpflen, V.; Tsukruk, V.; Wendorff, J. H. *Adv. Mater.* **1997**, *9*, 48-&.

(7) Tanaka, S.; Adachi, C.; Koyama, T.; Taniguchi, Y. *Chem. Lett.* **1998**, 975-976.

(8) Boden, N.; Bissell, R.; Clements, J.; Movaghar, B. *Curr. Sci.* **1996**, *71*, 599-601.

(9) van de Craats, A. M.; Warman, J. M.; Fechtenkötter, A.; Brand, J. D.; Harbison, M. A.; Müllen, K. *Adv. Mater.* **1999**, *11*, 1469-1472.

(10) Schmidt-Mende, L.; Fechtenkötter, A.; Müllen, K.; Friend, R. H.; MacKenzie, J. D. *Physica E* **2002**, *14*, 263-267.

(11) Pisula, W.; Menon, A.; Stepputat, M.; Lieberwirth, I.; Kolb, U.; Tracz, A.; Sirringhaus, H.; Pakula, T.; Müllen, K. *Adv. Mater.* **2005**, *17*, 684-+.

(12) Boden, N.; Bushby, R. J.; Cammidge, A. N. *Mol. Cryst. Liq. Cryst. Sci. Technol., Sect. A* **1995**, *260*, 307-&.

(13) Giroudgodquin, A. M.; Maitlis, P. M. *Angew. Chem. Int. Ed.* **1991**, *30*, 375-402.

(14) Liu, W.; Shi, T. S. *Acta Chim. Sinica* **2001**, *59*, 466-471.

(15) Stevenson, K.; Miyashita, N.; Smieja, J.; Mazur, U. *Ultramicroscopy* **2003**, *97*, 271-278.

(16) Petritsch, K.; Friend, R. H.; Lux, A.; Rozenberg, G.; Moratti, S. C.; Holmes, A. B. *Synth. Met.* **1999**, *102*, 1776-1777.

3 Hexa-*peri*-hexabenzocoronenes with Improved Processability

Hexa-*peri*-hexabenzocoronenes (HBC), as a prominent representative of discotic liquid crystals, exhibit some of the highest values for the intrinsic charge carrier mobility for mesogens, which makes them promising candidates for electronic devices[1]. Prerequisites for efficient charge carrier transport between electrodes are a high purity of the material to reduce possible trapping sites for charge carriers and a pronounced and defect-free,[2] long-range order.[3,4]

Next to adequate electronic properties, the morphology of the material is a crucial property to form distinct columnar pathways over large domains and thus closely related to the device performance. Controlling the interactions between the molecules and therefore the self-association by changing the chemical composition is the key factor tailoring the solubility and the thermal properties. The degree of self-aggregation dominates the processing from solution. Therefore, one major challenge for material science is to tune the self-association of a material because it translates into the processing behavior and furthermore into the performance of a device. Molecules with a pronounced tendency to self-associate are suitable for processing from solution, since the required pre-aggregation is given.[5] Materials with a moderate propensity to aggregate exhibit low isotropization temperatures and become available for processing from the melt.

Most of the known HBC derivatives possess isotropization temperatures that are far above the thermal decomposition threshold, which prohibits processing from the molten state.[6] The crystallization of materials from the isotropic state is an inexpensive, clean, solvent-free and even refining processing technique. In the following chapter, the synthesis of novel HBC derivatives that are decorated by six branched, space-demanding, alkyl side chains is described. The key feature of the implemented chains is the close proximity of the branching site to the aromatic core, which dramatically influences the self-organization behavior. This perfectly fulfils the demands: extraordinary long-range self-ordering, high purity and facile processing from the isotropic state because of their low isotropization temperatures.

The results in this project emerged from a fruitful collaboration. D. WASSERFALLEN supported me with the development of synthetic concepts, conduction of reactions, purifications and chemical characterizations, to obtain the target molecules in large quantities and a minimum of experimental time. This allowed the in the following described HBCs to be obtained on a multi-gram scale. W. PISULA investigated the mechanically organized materials with different X-ray experiments, recorded atomic force microscopy images and helped me to interpret the obtained results. He worked with me on the processing both from solution and melt. Furthermore, he supported me planning the experiments which we conducted at the European Synchrotron Radiation Facilities in Grenoble, France.

3.1 Synthesis

Synthetic approaches towards materials that are purposed to be implemented as active components in electronic devices have to be straightforward and accomplishable on a multi-gram scale. This is a prerequisite to providing enough material to investigate suitable processing parameters and techniques. Appropriate processing techniques are required to induce a high degree of aligned structures in the discotic material. Highly ordered surface layers of different discotics, in particular of HBC derivatives, have been previously obtained by using Langmuir-Blodgett-,[7,8] zone-casting techniques,[5,9] or solution casting onto preoriented PTFE substrates.[10-12] Long-range order achieved by the latter protocol proved to be suitable for field effect transistors (FET).

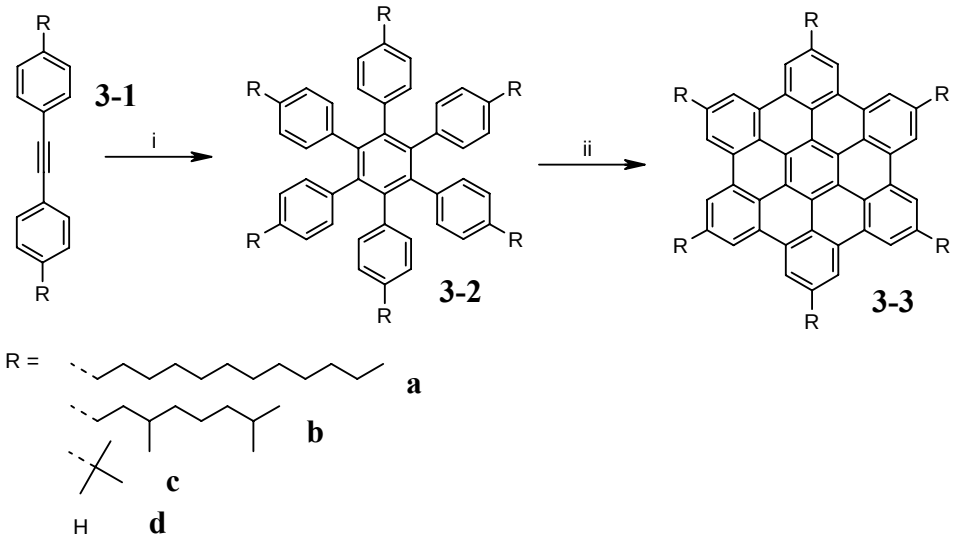

Scheme 3-1: *i) $Co_2(CO)_8$, 60-90%; ii) $FeCl_3$, 99%*

Scheme 3-1 shows the previously described,[13] straightforward synthetic route for hexafold substituted HBC derivatives. Differently prepared 4,4'-difunctionalized diphenylacetylene **3-1** derivatives were cyclotrimerized with catalytical amounts of dicobaltoctacarbonyl to the corresponding hexa-phenylbenzene **3-2**, which was subsequently planarized with iron(III) chloride to yield the discotic HBC **3-3**. This concept opened access to HBC derivative bearing i.e. dodecyl- **3-3a**[14], 3,7-dimethyloctyl- **3-3b**[13], simple *tert*-butyl groups **3-3c** or no substituents **3-3d**.

An often applied approach toward the dialkylated diphenylacetylenes **3-1** was the palladium catalyzed alkylation of 4,4'-dibromodiphenylacetylene **3-5**. This compound has been made by the bromination of commercially available stilbene **3-7**, which has been dehydrobrominated with strong base to yield **3-5** in an over all yield

of 44%.[15] A much simpler access to **3-5** was recently published, describing a one-pot synthesis of symmetrical bisarylethynes by a modification of the HAGIHARA-SONOGASHIRA cross-coupling reaction.[16] Starting from 1-bromo-4-iodo-benzene **3-4**, the cross-coupling reaction with trimethylsilylacetylene in the presence of an amidine base and a substoichiometric amount of water generated the desired compound **3-5** in high yield. This reaction improved the concept towards alkylated HBCs, since the overall yield has been increased significantly.

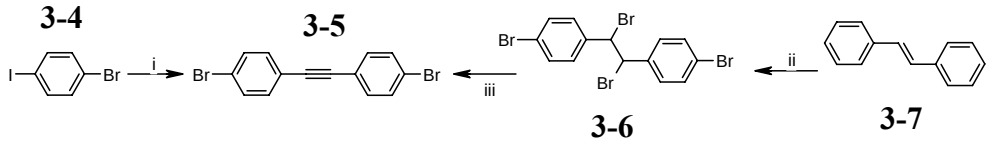

Scheme 3-2: *i) DBU, H_2O, trimethylsilylacetylene, $(PPh_3)_4Pd$, 92%; ii) Br_2, 45%; iii) KOtBu, 98%*

However, the successful synthesis of dialkylated diphenylacetylenes **3-1** using **3-5** as the starting substance revealed to be a crucial step. The palladium catalyzed NIGISHI or KUMMADA-type reactions often created a significant amount of the debrominated species **3-8** as a side product, which could not be separated by common purification techniques such as preparative column chromatography. Many attempts to suppress that problematic side-reaction have failed.

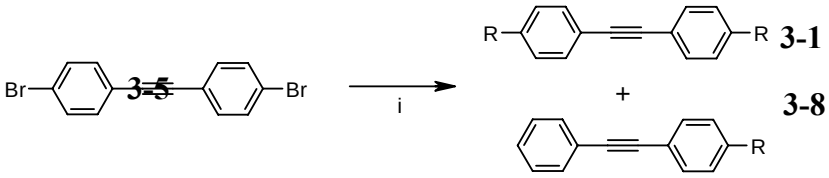

Scheme 3-3: *i) RMgBr, $Cl_2Pd(dppf)$*

Based on that knowledge, a synthetic concept towards novel HBC derivatives has been developed, bypassing possible separation problems in the diphenylacetylene synthesis. Furthermore, the very strong aromatic π-stacking of the large polycyclic aromatic hydrocarbons (PAH) was tried to be modulated by the use of sterically demanding alkyl substituents. The reduction of the intermolecular attractive forces goes hand in hand with a lowering of the melting point, enhancement of solubility and therefore a simplified purification.

Scheme 3-4 presents the synthetic concept towards a homologous series of HBC derivatives. The commercially accessible alkyl alcohols **3-9a-c** were converted in an

APPEL reaction to the corresponding alkyl bromides[17] **3-10a-c**, which have been further reacted into GRIGNARD-reagents. Interestingly, the direct metallation reaction with magnesium metal required very harsh conditions, because of the steric demand excerted from the alkyl chain. The coupling onto **3-5** utilizing a KUMADA protocol was immediately conducted.[13] The branched alkyl chains **a-c** allowed the mentioned partially debrominated side-products to be chromatographically separated. After the cyclotrimerization and the final oxidative planarization, three HBCs with branched alkyl chains were obtained in good overall yields. The three materials will be labeled in following chapters with HBC-$C_{6,2}$ **3-13a**, HBC-$C_{10,6}$ **3-13b** and HBC-$C_{14,10}$ **3-13c**.

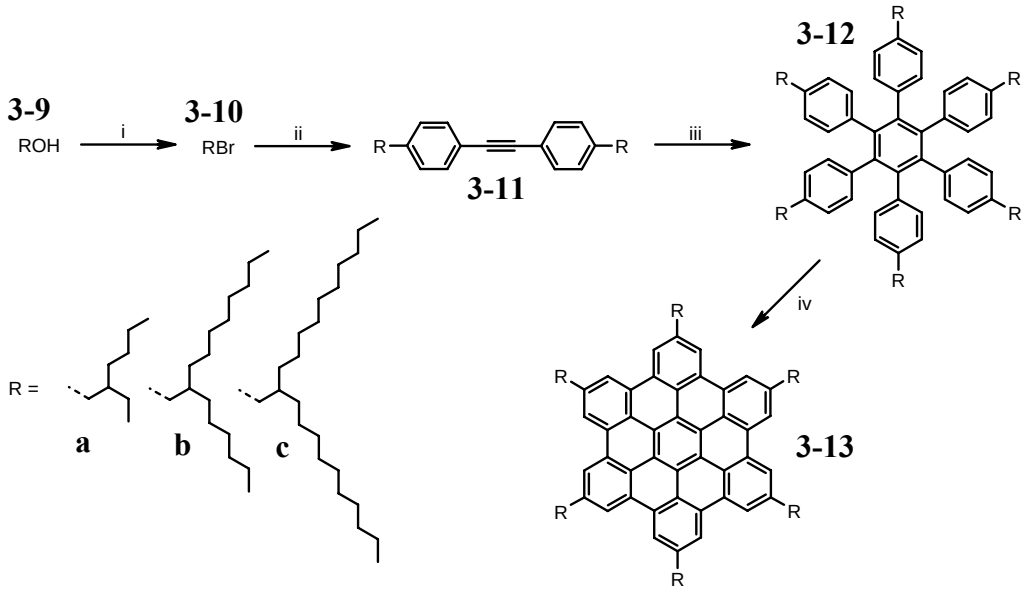

Scheme 3-4*: Synthesis of HBC with bulky, branched alkyl chains of different lengths: i) NBS, PPh_3, 80% ii)* 3-5*, Mg, $Cl_2Pd(dppf)$, 56-86% iii) $Co_2(CO)_8$, 75-93% iv) $FeCl_3$, 75-94%.*

The alkyl substituents imposed their waxy properties onto the aromatic disc, which allowed for the first time a column chromatographical purification of the PAHs to separate inorganic and organic impurities.

In contrast to the oxidative cyclodehydrogenation in other HBC cases, the branching of the alkyl chain excerted enough steric congestion to completely suppress the chlorination as a prominent side-reaction of the SCHOLL-reaction. The MALDI-TOF spectra of **3-13a-c** did not show any indication for an additional chlorine atom attached to the desired products (Figure 3-1).

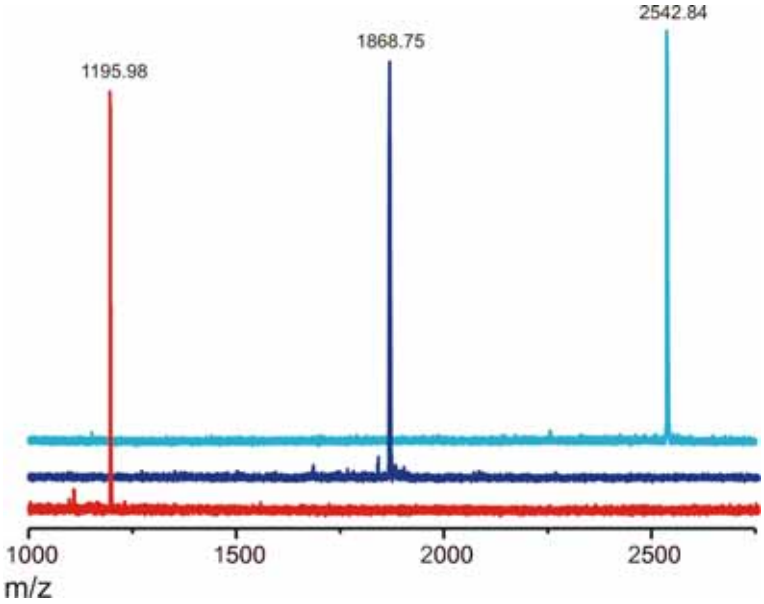

Figure 3-1: *MALDI-TOF spectra of HBC-$C_{6,2}$* **3-13a**, *HBC-$C_{10,6}$* **3-13b**, *and HBC-$C_{14,10}$* **3-13c**, *utilizing the solid state preparation and TCNQ as the matrix substance.*

In the following, the solution phase self-association of the new, highly soluble HBCs was investigated and compared to known derivatives to gain an insight into the effect of the space demand of the attached chains onto the solution organization. The propensity to self-organize translates into the processing and gives valuable information about required parameters such as nature of solvent, temperature and concentration. Furthermore, the morphology formation from solution of the HBC derivatives was investigated revealing the nucleation and growth of these materials which is important for the solution processability.

3.2 Self-Assembly

The self-association of single elements into complex, organized supramolecular structures via specific intermolecular interactions is impressively illustrated in nature, for example, by the base-pair stacking in the DNA[18] and tertiary structures of proteins. This principle transfers the intrinsic information from the molecular level onto the superstructure.[19,20] In order to exploit this concept for material science, it is important to understand the interactions between the single building blocks.[21,22] Different non-covalent interactions between the molecules play significant roles during the self-assembly. Inspired by nature, the main challenge of supramolecular chemistry is to design specific intermolecular interactions leading to the desired architectures with increased size and complexity. Different attractive intermolecular forces, such as hydrogen bonding[23-25], metal coordination, and π-stacking[26,27], can dominate individually or cooperate to establish the organization and stability of the system.[28-31]

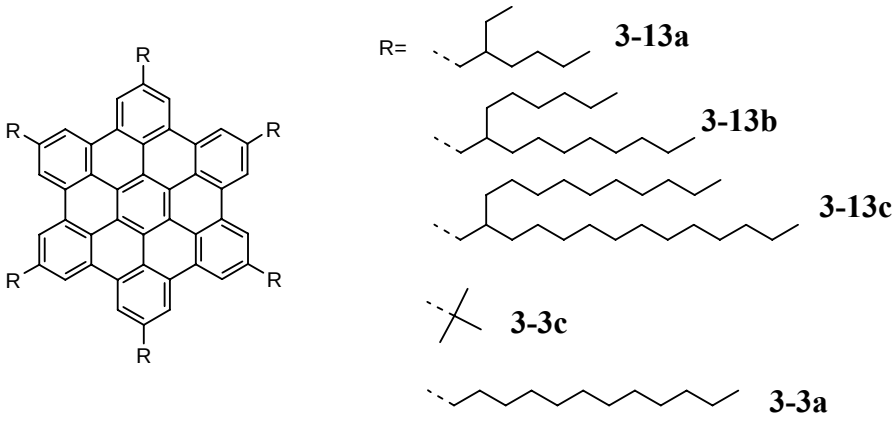

Figure 3-2: *Investigated HBC Derivatives.*

In the following, the self-association behavior of the novel HBCs **3-13a-c** will be investigated and compared to the known hexa-*t*-butyl- **3-3c** and hexa-dodecyl- HBC **3-3a** (Figure 3-2).[14]

A prominent class of such compounds utilizes aromatic stacking in order to form one-dimensional columnar rods in solution.[32] The electrostatic driving force of these aromatic interactions is the result of an attraction between the positively charged σ-framework and the negatively charged electron cloud of the neighboring units.[33] MOORE and co-workers reported the synthesis of various types of shape-persistent phenylacetylene macrocycles (PAMs).[34] They investigated the influence of substitution, temperature and solvent on the self-association behavior. The solution-

phase organization of other macrocycles[35-38], helicenes[39,40], porphyrins[41], and phthalocyanines[42-45] has been reported, too.

The aggregation properties influenced by the steric demand of the alkyl chains were analyzed using temperature and concentration dependent ^{1}H NMR, UV/vis, and photoluminescence spectroscopy in different organic solvents. These measurements included the determination of self-association constants and thermodynamic parameters.

3.2.1 NMR Investigation

The chemical shift data of NMR spectra provided insight not only into the structural arrangement, but furthermore gave information about the stacking in solution. Thus the aromatic resonance of HBC-C_{12} **3-3a** is strongly dependent on concentration, which is considered as a signature for aromatic stacking (Figure 3-3).[46]

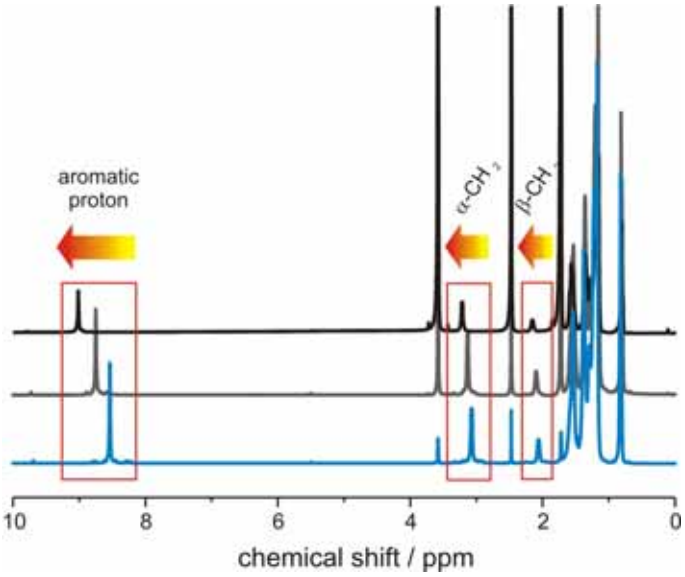

Figure 3-3: *Concentration dependent ^{1}H NMR spectra of HBC-C_{12}* **3-3a**.

The ring current magnetic anisotropy of an aromatic ring induces a resonance shifting of the nuclei of a molecule, in close vicinity to it.[46] The interacting units are usually in a slightly offset, face-to-face arrangement that leads to an upfield shifting. The chemical shift of the aromatic proton of HBC-C_{12} **3-3a** in 1,1,2,2-tetrachloroethane-d_2 at 60 °C shifted from 7.9 ppm at a concentration of 1.7×10^{-1} M to 9.0 ppm at 1.0×10^{-6} M suggesting stacking beyond dimers.[47]

Compared to other systems, such as PAMs, self-association for HBCs occurs in a concentration range, which is at least one order of magnitude lower.[48] Recording

satisfactory spectra at such low concentrations required high field instrumentation and very long experimental times. With an inverse probe head, spectra of the dilute samples were obtained after about 100 000 scans on a 500 MHz instrument.

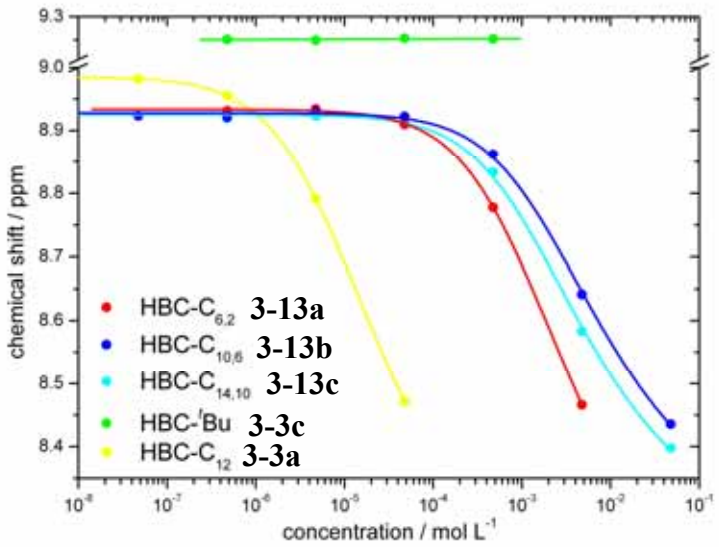

Figure 3-4: *Concentration dependent ^{1}H NMR chemical shifts, recorded in 1,1,2,2-tetrachloroethan-d^2 (30 °C, 500 MHz), fitted with the indefinite self-association model including next nearest neighbor relations.*

In 1,1,2,2-tetrachloroethane-d_2 (Figure 3-4), the aromatic resonance for HBC-C_{12} **3-3a** at 30 °C reached a plateau at a concentration lower than approximately 1x10^{-6} M, which indicated monomeric species. Compounds **3-13a-c** revealed a strong concentration dependence in the ^{1}H NMR spectra occurring at much higher values than in the case of HBC-C_{12} **3-3a**. Below 1x10^{-5} M, the three HBC derivatives with the branched alkyl chains **a-c** existed as monomers in solution. HBC-$C_{6,2}$ **3-13a** possessed the lowest solubility among the three dove-tailed HBC samples. In comparison with HBC-$C_{10,6}$ **3-13b** and HBC-$C_{14,10}$ **3-13c**, HBC-$C_{6,2}$ **3-13a** appeared to be more strongly aggregated (chemical shift at higher field at the same concentration). HBC-$C_{10,6}$ **3-13b** showed the lowest self-association in 1,1,2,2-tetrachloroethane-d_2 at 30 °C, followed by HBC-$C_{14,10}$ **3-13c** with the longest alkyl substituents, while HBC-^{t}Bu **3-3c** failed to exhibit association in solution.

Least-squares curve fitting was performed on the concentration dependent ^{1}H NMR assuming an indefinite self-association process to elucidate the stacking behavior.[46]

The association processes were thereby described as consecutive equilibrium states, where monomers were added to the existing aggregate.

Table 3-1: *Association constants for self-aggregation of the investigated HBC derivative in 1,1,2,2-tetrachloroethane-d^2 at 30 °C.*

Compound	K_a / L mol^{-1}
3-13a	13.4
3-13b	1.8
3-13c	2.9
3-3a	898

Additional parameters, such as the chemical shift of the monomer, terminal, and internal units, were required to fit the concentration dependent NMR data. The commonly used monomer-dimer model, which could be used, when association into higher aggregates was negligible, was not suitable to analyze our data. The model of indefinite self-association yielded the best curve fittings for the concentration dependent ^{1}H NMR data. Table 3-1 lists the determined association constants.

The determination of error bars was very difficult. Already in the measurement, the error of precision varied strongly upon the concentration. The signal to noise ratio for the very dilute samples is far smaller than for concentrated solutions. In the first step a nonlinear least squares fitting analysis (Levenberg-Marquardt) was performed, which led in all described examples to very good fitting results even if the region of transition was not covered with experimental data points. The precision of the fit was dependent on the starting parameters and the number of iterations. The errors we determined from the fits were small, but definitely not negligible, especially in the cases, where only few data points were recorded. The theory of the indefinite self-association model, which was applied to calculate the thermodynamic parameters, is built on assumptions (e.g. the constant chemical shifts for molecules within the columns). This led to the conclusion that the comparability between the association constants is given, but the values are not absolute. Finally, an error propagation with a weighting of the experimental errors would have to be conducted, which is

mathematically difficult. All these reasons clarify why the determinations of precise error bars were not done.

The solution aggregation of HBC-C_{12} **3-3a** was significantly more pronounced, as already evidenced by a lower solubility. At a concentration of 4.75×10^{-5} M, the average aggregate of HBC-C_{12} **3-3a** consisted of *ca.* six discs, but with a broad distribution, while the HBCs with the branched substituents existed mainly as monomers (Figure 3-5).

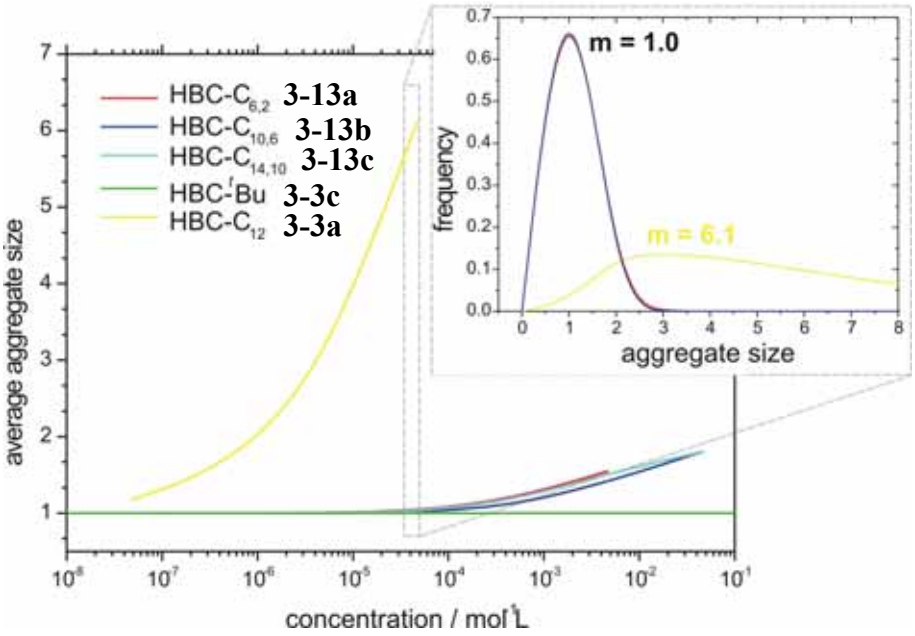

Figure 3-5: *Concentration dependent aggregation size for the investigated HBC derivatives in 1,1,2,2-tetrachloroethane-d^2 at 30 °C, inset: aggregation size distribution at a concentration of 4.75×10^{-5} M.*

Temperature dependent ^{1}H NMR spectra were also taken of the aggregating HBC-derivatives **3-3a** and **3-13a-c** at a concentration of 4.75×10^{-3} M in 1,1,2,2-tetrachloroethane-d^2. Because of its limited solubility HBC-C_{12} **3-3a** could not be measured at a temperature below 70 °C. The aggregation of all investigated structures is also strongly temperature dependent (Figure 3-6), whereby HBC-$C_{10,6}$ **3-13b** aggregated slightly stronger than HBC-$C_{14,10}$ **3-13c** above 60 °C. Above 130 °C, both derivatives existed exclusively as monomer, since the aromatic resonance reached the value of the monomer. HBC-C_{12} **3-3a** showed also the strongest aggregation at high temperatures in relation to the other examples. The chemical shift decreased by lowering the temperature as was observed for HBC-$C_{10,6}$ **3-13b** dissolved in dichloromethane-d^2.

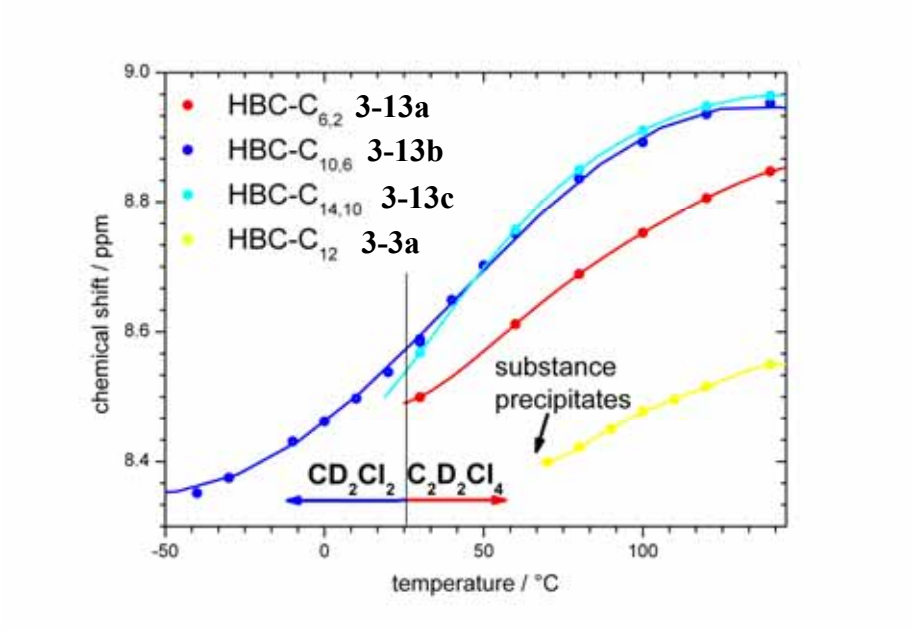

Figure 3-6: *Temperature dependent ^1H NMR of the investigated HBC derivatives in 1,1,2,2-tetrachloroethane-d^2 and dichloromethane-d^2, respectively at a concentration of $4.75x10^{-3}$ M (500 MHz), fitted polynomially (second order).*

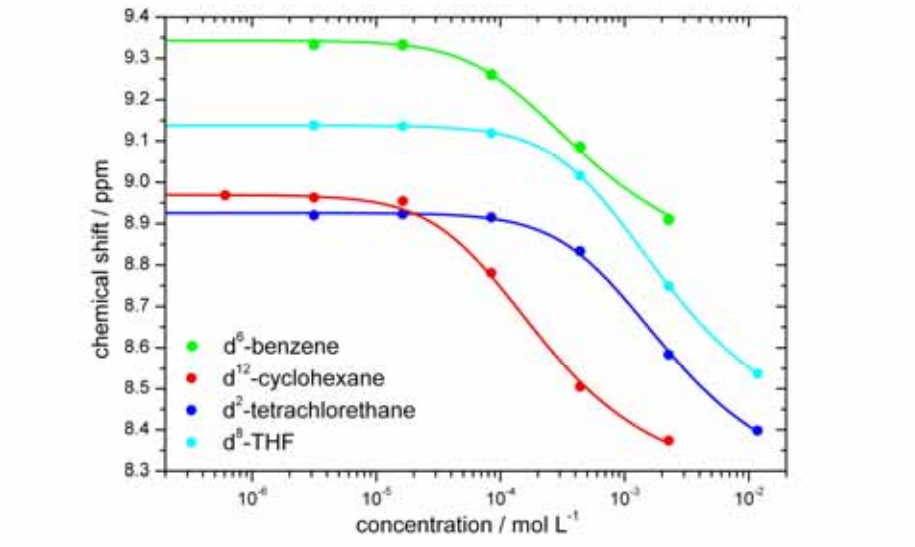

Figure 3-7: *Solvent dependent aggregation behavior of HBC-$C_{14,10}$* **3-13c** *at 30 °C (500MHz), fitted with the indefinite self-association model including next nearest neighbor relations.*

Figure 3-7 shows the concentration dependent ^{1}H NMR fits for HBC-$C_{14,10}$ **3-13c** in different solvents and Table 3-2 summarizes the determined association constants of HBC-C_{12} **3-3a** and HBC-$C_{14,10}$ **3-13c**. The aggregation of these two HBC derivatives in 1,1,2,2-tetrachloroethane-d^2 and THF-d^8 were moderate compared to the values in cyclohexane-d^{12} or benzene-d^6. The self-association in benzene-d^6 was higher than in

other solvents, although, the chemical compatibility to the aromatic HBCs should be better.

Table 3-2: *Association constants of HBC-C_{12}* **3-3a** *and HBC-$C_{14,10}$* **3-13c** *in different solvents at 30 °C.*

NMR solvent	K_a / L mol^{-1} for 3-13c	K_a / L mol^{-1} for 3-3a
cyclohexane-d_{12}	23.4	not soluble
1,1,2,2-tetrachloroethane-d_2	2.9	900
THF-d_8	3.6	5500[a]
benzene-d_6	420	14900

[a] recorded at 40 °C

Since the investigated polyaromatic hydrocarbons were insoluble in polar solvents like acetone-d^6, acetonitrile-d^3, or DMSO-d^6 at NMR concentration level, the NMR experiments were carried out in a mixed solvent system of 1,1,2,2-tetrachloroethane-d^2 and methanol-d^4, with several different compositions. HBC-$C_{14,10}$ **3-13c** at concentration of 4.75x10^{-3} M exhibited an increasing tendency to self-aggregate with an increasing portion of the nonsolvent, methanol-d^4, relative to 1,1,2,2-tetrachloroethane-d^2, (Figure 3-8).

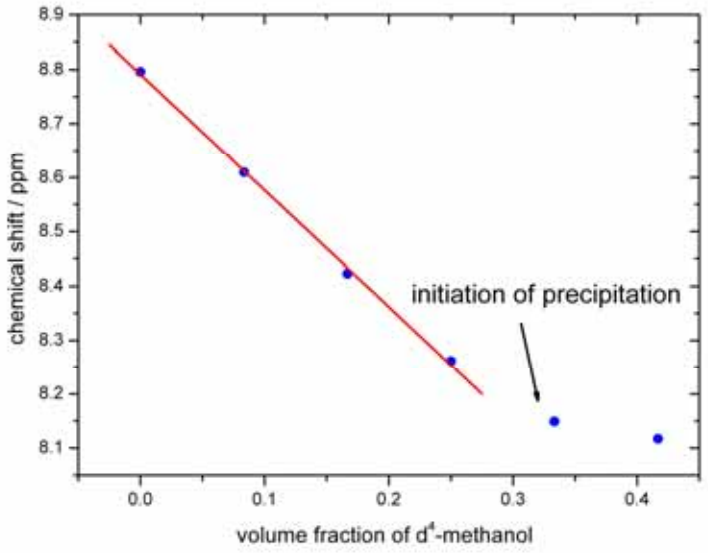

Figure 3-8: *Chemical shift dependence of HBC-$C_{14,10}$* **3-13c** *in a mixture of methanol-d^4 and 1,1,2,2-tetrachloroethane-d^2 with different compositions (concentration: 4.75x10^{-3} M).*

The aromatic resonance of **3-13c** shifted upfield linearly, until the substance precipitated at a methanol-d^4 volume fraction of 30%. As a control experiment, concentration dependent measurements in a constant ratio of methanol-d^4 and 1,1,2,2-tetrachloroethane-d^2 were carried out (not shown here). This led to the same results as the previously described experiment, confirming no influence of the chemical shift upon the solvent polarity in the investigated concentration range.

Thermodynamic parameters of the self-association behavior were obtained from the determination of association constants at different temperatures in THF-d^8 (Figure 3-9). Probably either due to changes of the conformation of the HBC molecules (deviation from planarity) or to changes of the disc mobility in the solvent cage with increasing temperature, the electronic environment of the protons varied and thus the chemical shifts for the monomeric HBCs at low concentrations decreased with increasing temperature.

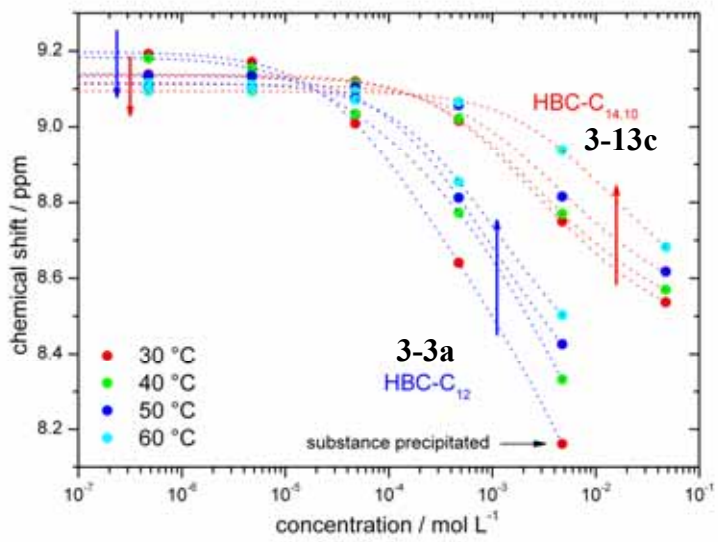

Figure 3-9: *Temperature and concentration dependent ^{1}H NMR data of HBC-$C_{14,10}$* **3-13c** *and HBC-C_{12}* **3-3a** *in THF-d^8 (500 MHz), fitted with the indefinite self-association model including next nearest neighbor relations.*

The VAN'T HOFF plots for the strongly aggregating HBC-C_{12} **3-3a** and the less aggregating HBC-$C_{14,10}$ **3-13c** are shown in Figure 3-10, while the thermodynamic data is presented in Table 3-3. At the lowest temperature and highest concentration, the HBC-C_{12} **3-3a** sample became cloudy during the measurement. Since the solution

NMR measurement detected only aggregates in solution, the determined association constant was too small to fit into the linearized VAN'T HOFF plot.

Table 3-3*: Association constant K_a and thermodynamic parameters for self-aggregation of HBC-$C_{14,10}$* **3-13c** *and HBC-C_{12}* **3-3a** *in THF-d^8 at 30 °C.*

Compound	K_a / L mol^{-1}	ΔH / kJ mol^{-1}	ΔG[a] /kJ mol^{-1}	ΔS /Jmol^{-1}K^{-1}
HBC-$C_{14,10}$ **3-13c**	3.60	-91.7	-5.82	-290
HBC-C_{12} **3-3a**	5500	-283	-36.7	-832

[a] at 296 K

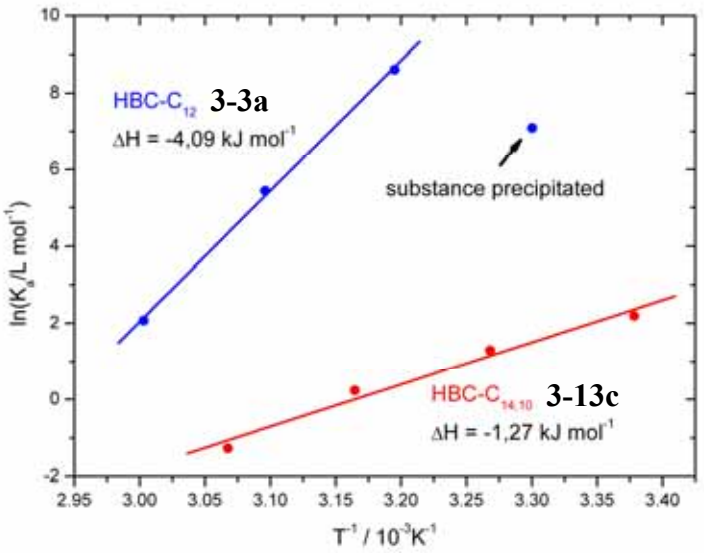

Figure 3-10: *van't Hoff plot of self-association constants K_a for HBC-$C_{14,10}$* **3-13c** *and HBC-C_{12}* **3-3a**.

3.2.2 Electronic Spectroscopy

The electronic spectrum provided a sensitive probe for interactions between molecules within an aggregate.[49] The absorption spectra of HBCs were typical for polycyclic aromatic hydrocarbons (PAHs), showing the characteristic groups of bands of different extinction coefficients according to the CLAR nomenclature: *α*, *p*, *β* (see chapter 5.3). In C_6-symmetric HBCs, the α transition was only weakly allowed and thus difficult to observe, since the transition is symmetrically forbidden.[50] According to KASHAS law[51], the photoluminescence spectra exhibit only transitions from S_1 into vibrational levels of S_0.

To gain deeper insight into the self-association behavior, concentration dependent UV/vis spectra of the feebly self-associating HBC-$C_{14,10}$ **3-13c** and the strongly aggregating HBC-C_{12} **3-3a** were recorded, showing only small differences upon concentration changes in the range from $1x10^{-4}$ to $1x10^{-7}$ M (not shown). In the same concentration range, the photoluminescence (PL) and photoluminescence excitation (PLE) spectra revealed a more pronounced effect (Figure 3-11).

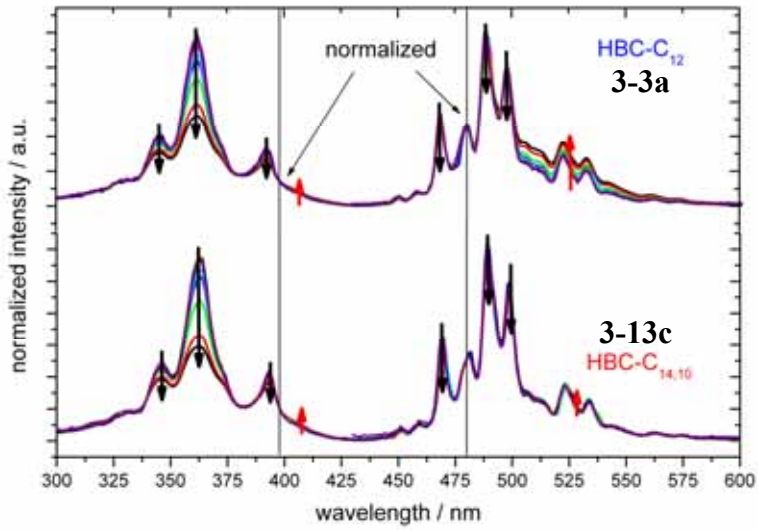

Figure 3-11: *PL and PLE spectra of HBC-$C_{14,10}$* **3-13c** *and HBC-C_{12}* **3-3a** *in $CHCl_3$ at concentrations between $1x10^{-4}$ to $1x10^{-7}$M (black to blue); normalized at 480 nm and 398 nm, respectively. Arrows point into the direction of the highest concentration.*

The PL spectra for both compounds were normalized at 480 nm, since this band was only weakly influenced by concentration. While increasing the concentration, the intensity of the fluorescence bands at 469, 489 and 497 nm decreased for both investigated HBCs. In contrast, the broad band in the region above 500 nm became higher in intensity, indicating the formation of aggregates. The PLE spectra turned out to be a much more sensitive probe for the presence of aggregation. The bands at 345, 360, and 390 nm were strongly dependent on the concentration and lost intensity in concentrated solutions. At high concentrations, a weak, broad band appeared for both investigated HBC derivatives at a wavelength of 407 nm, which could be assigned to an emission from the aggregates. The UV/vis spectra showed, when adding methanol as a non-solvent, an isosbestic point at a wavelength of 398 nm, pointing toward a linear dependence of the two bands at 390 (*p*-Band) and 407 nm,

respectively (Figure 3-12). All PLE spectra in Figure 3-11 were normalized at the isosbestic point.

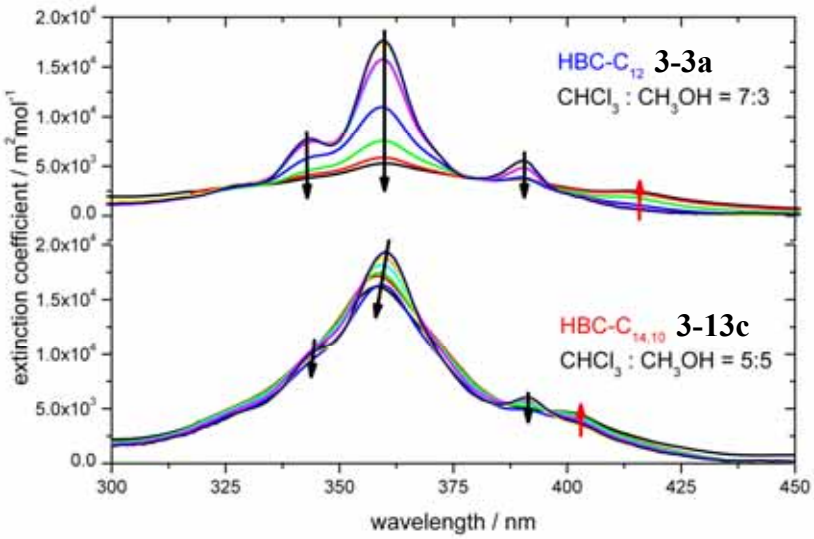

Figure 3-12: *Concentration dependent UV/vis spectra of HBC-C_{12}* **3-3a** *and HBC-$C_{14,10}$* **3-13c** *in $CHCl_3$:CH_3OH = 7:3 and 5:5 respectively (concentration from $6x10^{-5}$ to $4x10^{-7}$ M, black to blue).*

The strength of the self-association appeared to be sensitive to solvent effects, which was supported by the above described ^{1}H NMR results. Due to the aggregation, a non-LAMBERT-BEER law behavior was observed for the investigated derivatives. The extinction coefficient decreased slightly, when the concentration was increased. A more pronounced effect was observed, when the polarity of the solvent was changed.

In the case of HBC-$C_{14,10}$ **3-13c**, the maximum absorption in the UV/vis spectrum (β - band) shifted hypsochromically from 362 to 358 nm as either the content of methanol or the concentration increased, whereas the same band for HBC-C_{12} **3-3a** did not shift at all (Figure 3-13). The photoluminescence spectra of HBC-$C_{14,10}$ **3-13c** and HBC-C_{12} **3-3a**, recorded concentration dependent ($1x10^{-4}$ to $1x10^{-7}$ M) in a mixture of chloroform and methanol with a ratio of 7:3 and 5:5, respectively, exhibited a dramatic change with respect to the polarity of the solvent (Figure 3-14).

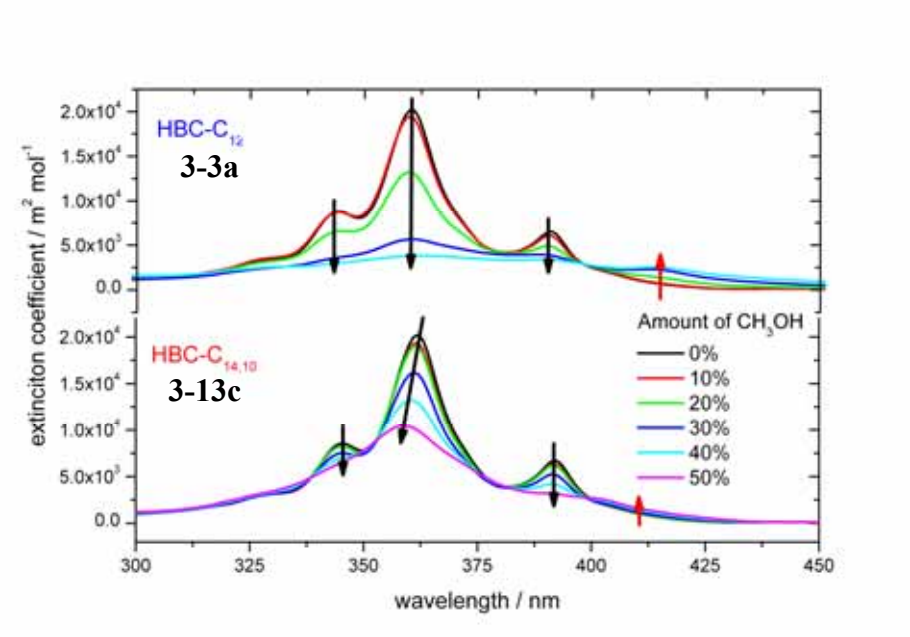

Figure 3-13: *UV/vis spectra of HBC-C_{12}* **3-3a** *and HBC-$C_{14,10}$* **3-13c** *in $CHCl_3/CH_3OH$ of different compositions.*

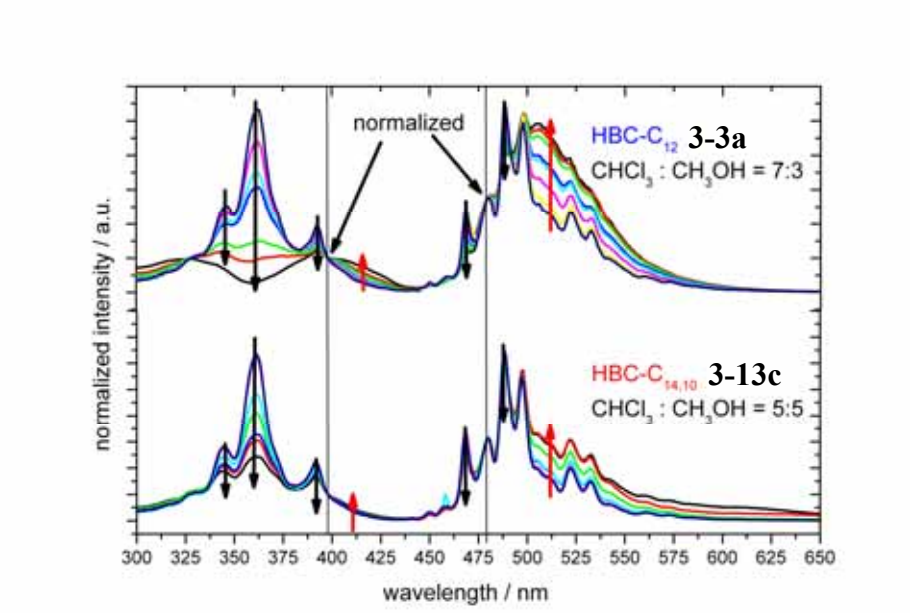

Figure 3-14: *Concentration dependent PL and PLE spectra of HBC-C_{12}* **3-3a** *and HBC-$C_{14,10}$* **3-13c** *in $CHCl_3$:CH_3OH = 7:3 and 5:5, respectively (concentration from $6x10^{-5}$ to $4x10^{-7}$ M, black to blue).*

The main band in the PLE for HBC-C_{12} **3-3a** disappeared completely, whereas, the band at 415 nm intensified. The changes in the PL and PLE spectra for HBC-$C_{14,10}$ **3-13c** were identical to the concentration dependent measurements in chloroform, where the region above 500 nm pointed towards self-association.

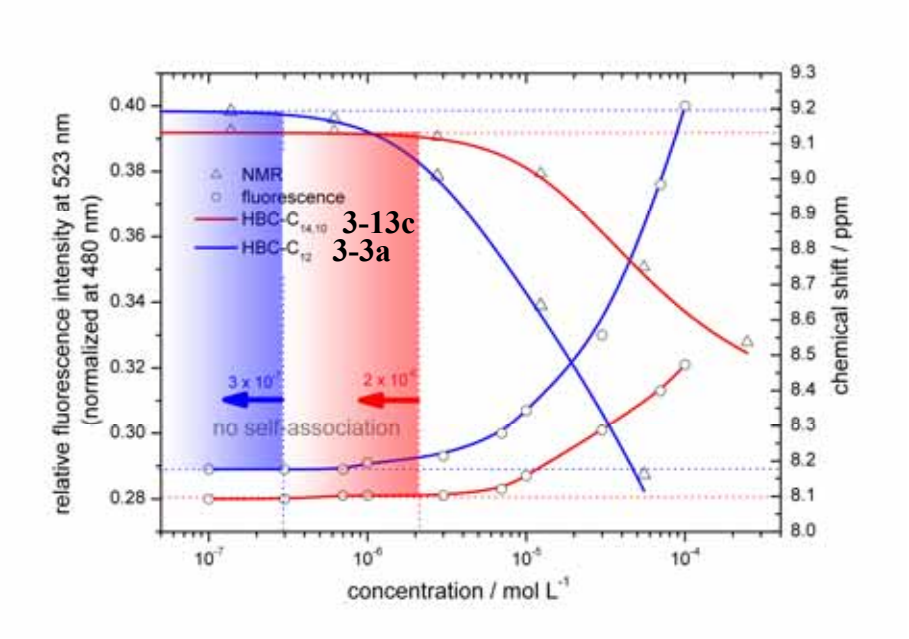

Figure 3-15: *Comparison of PL and ^{1}H NMR (500MHz) results of HBC-C_{12}* **3-3a** *and HBC-$C_{14,10}$* **3-13c***: PL intensity at 523 nm of the at 480 nm normalized spectra, recorded in THF, and the chemical shift from the ^{1}H NMR, recorded in THF-d^8, are plotted against concentration.*

Plotting the change of the relative intensity of the band at e.g. 523 nm from the normalized photoluminescence spectrum versus the concentration gave a curve which was comparable to the concentration dependent ^{1}H NMR plot (Figure 3-15).

At a nominal concentration of $3x10^{-7}$ M for HBC-C_{12} **3-3a** and $2x10^{-4}$ M for HBC-$C_{14,10}$ **3-13c**, the concentration dependent plots from both measurements leveled out, indicating the presence of only the monomeric species in solution. Plotting the values for absorbance at 360 nm determined by UV/vis spectroscopy versus the area under the corresponding PL curve (excitation at 360 nm), yielded two different curves for HBC-C_{12} **3-3a** and HBC-$C_{14,10}$ **3-13c** (Figure 3-16).

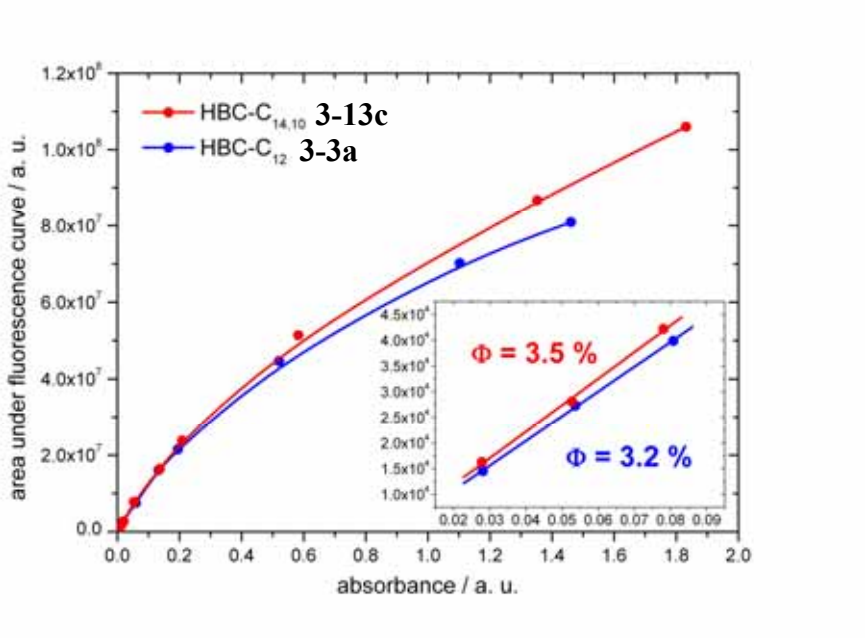

Figure 3-16: *Fluorescence yields of HBC-C_{12}* **3-3a** *and HBC-$C_{14,10}$* **3-13c***, inset: determination of the fluorescence quantum yields of the two materials in the linear regime at low concentrations (no self-association), all measurements (pathway = 1 cm; 25 °C; absorption and excitation wavelength = 360 nm; integration range = 425-600 nm).*

The inner filter effect became dominant at high absorbances making an interpretation difficult. On the other hand, since both derivatives possess almost identical extinction coefficient at low concentrations, the difference between the two plots at large absorbances was remarkable. For HBC-C_{12} **3-3a**, the extinction coefficient was far more dependent on the concentration and furthermore the fluorescence compared to HBC-$C_{14,10}$ **3-13c** was strongly quenched, which could be attributed to the higher self-association of HBC-C_{12} **3-3a**. The inset in Figure 3-16 suggests only a slight difference in the fluorescence quantum yield between HBC-C_{12} **3-3a** (3.2%) and HBC-$C_{14,10}$ **3-13c** (3.5%), proving the similar electronic behavior of the two substances in the absence of self-association. Temperature dependent UV/vis and PL spectroscopy were conducted on samples of different concentration, exhibiting only very small effects with temperature changes.

3.2.3 Conclusion

Since the investigated HBC derivatives did not possess any functional group, which were capable of forming e.g. hydrogen bonds, one assumed a face-to-face π-stacking of the aromatic cores, based on the concentration dependence of the aromatic resonance in the NMR.[32] The influence of the ring current from neighboring

molecules caused the shift of the aromatic protons, decreasing with increasing distance from the core.[38] The α-carbon of the aliphatic side chain exhibited a much smaller concentration dependence; whereas, the chemical shift of the next carbon in the chain was almost independent upon concentration (Figure 3-3).

The observed self-association equilibria for the hexa-alkylated HBCs were fast on the timescale of the NMR experiment, leading to only one broadened, averaged peak for all aggregates. Recently, an oligophenylene dendronized HBC was described, which enhanced the attractive interactions between the molecules.[52] There, the equilibrium kinetics of the dendronized HBC was much slower compared to the timescale of the NMR, as indicated by the observation of distinct aromatic resonances for monomeric and dimeric species.

The self-association behavior of the HBCs with branched alkyl substituents occurred in a different concentration range as compared to the parent HBC-C_{12} **3-3a**. Bulky *t*-butyl-groups in the HBC periphery suppressed aggregation completely and possessed a low solubilizing effect, which has already been confirmed by UV/vis and time-resolved fluorescence measurements.[53] It is presumed that substituents, exhibiting a large steric demand in the close vicinity of the disc, prevent the molecules from closely approaching each other, thereby hindering π-stacking.[48] This observation confirmed the notion that HBCs were cofacially stacked. In our study, HBC-C_{12} **3-3a** showed the strongest aggregation in the concentration range from ~10^{-4} M to ~10^{-7} M accompanied by the lowest solubility. Depending on the temperature and the nature of the solvent, the HBC existed on average as monomer at a concentration at ca. 10^{-7} M, which was at least an order of magnitude lower than that reported for the other π-systems.[43] The solubilizing dodecyl chains possessed only a small steric demand in the periphery of the aromatic disc, which allowed the molecules to approach easily, resulting in a high association constant. The three new HBC derivatives, which carried space-filling alkyl, dove-tailed substituents self-associate only at much higher concentrations, showing substantially smaller association constants compared to HBC-C_{12} **3-3a**. The steric hindrance induced by the side chains prevented the discs from approaching one another.[54] Comparing HBC-$C_{6,2}$ **3-13a** to HBC-$C_{10,6}$ **3-13b**, the length of the side chains increased and led to a diminished self-association. Further extension to HBC-$C_{14,10}$ **3-13c** did not reduce the aggregation in solution at room temperature since now the interactions between the chains became significant. The

attractive interactions, initiated by the long chains, enhanced the self-association slightly, resulting in a higher association for HBC-$C_{14,10}$ **3-13c** compared to the derivative **3-13b**. At higher temperatures, the van der Waals forces decreased and HBC-$C_{14,10}$ **3-13c** exhibited as expected the lowest self-association among the investigated HBCs. Thus, the steric hindrance modulated the strength of the self-association in solution and temperature affected the aggregation size additionally as can be seen from Figure 3-6.

Furthermore, the self-association was strongly dependent on the nature of the solvent.[55] The association constant for HBC-$C_{14,10}$ **3-13c** in cyclohexane-d^{12} as solvent was about ten times higher than those in THF-d_8 and 1,1,2,2-tetrachloroethane-d^2, which could be attributed to the solvophobic effect. It was assumed that aromatic solvents suppress π-stacking between aromatic solutes because such interactions between the solute and solvent would have prevailed over those between solutes. On the contrary, it was observed that HBCs self-associate stronger in benzene-d^6, which was confirmed in previous studies for macrocycles such as PAMs.[38]

Addition of methanol to the solution of HBCs enhanced the solvophobic interactions, leading to stronger aromatic stacking.[56] At the same concentration, the resonance of the aromatic HBC protons shifted with increasing methanol content upfield, indicating a stronger self-association. Additionally, the concentration dependent UV/vis (Figure 3-12) and photoluminescence measurements in a constant mixture of chloroform and the non-solvent methanol revealed the existence of aggregates. The presence of an isosbestic point at a wavelength of 398 nm, proved a linear dependence between the monomer absorption and the absorption of aggregates. In the PL, the broad, less resolved, concentration dependent bands above 500 nm pointed toward the existence of aggregates. The photophysical changes in the case of HBC-$C_{14,10}$ **3-13c** were less pronounced because of the reduced self-association in solution or the hindered electronic coupling between neighboring molecules. The hypsochromic shift in the case of HBC-$C_{14,10}$ **3-13c**, which was not observed for the parent HBC-C_{12} **3-3a**, suggesting a different electronic coupling between the aromatic discs and thus a different geometrical arrangement in the aggregated stacks. This is possibly due to a different geometry in the aggregate caused by the large steric demand of the substituents in the corona.

Quantum mechanical calculations including electron configuration interactions were performed for a better understanding of the spectral changes in the UV/vis of both investigated compounds (Software: Hypercube, Inc., HyperChem 6.0 for Windows). After the optimization of the HBC geometry with an *ab initio* calculation (basis set: 6-31G*), PM3 calculations (20 occupied and 20 unoccupied orbitals for electron configuration) were applied to dimeric HBC stacks with a distance between the cores of 3.6 Å, as was experimentally determined by powder X-ray diffractometry. Translation and lateral rotation of the discs with respect to each other, which is energetically favored,[57] (Figure 3-17) influenced significantly the calculated electronic spectra. Therefore, it is reasonable to assume the existence of different averaged stacking motifs for the two HBCs. On the basis of the performed calculations, it is not possible to identify specific geometrical arrangements of the HBCs in solution.

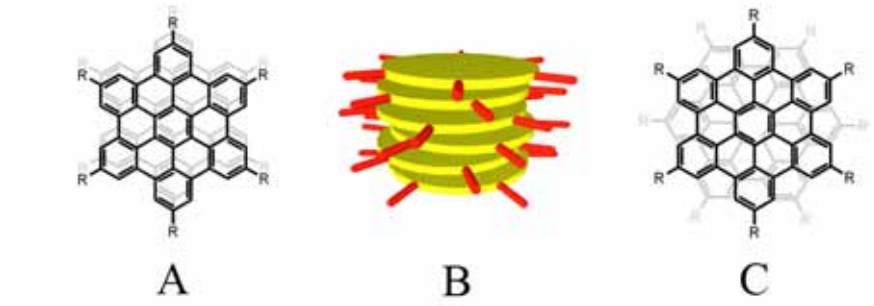

Figure 3-17: *Stacking motif for neighboring HBCs: A: lateral displacement B: schematical structure of an aggregate with rotational and translational offsets in the lateral direction C: rotational offset along the stacking axis.*

For all investigated HBCs, the fluorescence quantum yields were in the same range, but the behavior of HBC-C_{12} **3-3a** and HBC-$C_{14,10}$ **3-13c** differed significantly at high concentrations, indicating either different mechanisms of fluorescence quenching due to different geometries of the molecules with respect to each other or a stronger self-association behavior at high concentration, which was supported by the ^{1}H NMR solution measurements.

NMR and fluorescence spectroscopy allowed the independent determination of the critical concentrations for self-association of HBC-$C_{14,10}$ **3-13c** and HBC-C_{12} **3-3a**.

The thermodynamic parameters derived from the temperature and concentration dependent NMR data suggested that there was an enthalpy gain accompanied with an entropy punishment during the aggregation process, which was also observed for

PAMs. In contrast to the PAMs, which have a much smaller π-area, the association enthalpy for the investigated HBCs were much higher.

3.3 Processing

After having gained an insight into the basic solution self-organization, the material scientist can take the next crucial step towards a successful implementation of the synthesized material in an organic electronic device – the processing into long-range ordered films. The knowledge of the solution association propensity of a specific material helps to narrow the selection of solvents, concentrations and temperatures in the solution based processing.

For solution casting, it is required to deposit pre-aggregated species onto the substrate.[58] It was recently shown that the solution based zone-casting processing is highly dependent on the solubility and thus on the solution self-aggregation of the single building blocks.[59] Thereby, HBC-C_{12} **3-3a**, which is known to possess a limited solubility, was successfully aligned by the above mentioned technique resulting in highly ordered and uniaxially oriented layers. Field-effect transistors (FETs) of **3-3a** were built exploiting zone-cast films and gave charge carrier mobilities up to 10^{-2} cm^2/Vs.[59] On the other hand, the optimal processing parameters of discotic materials with an enhanced solubility are more difficult to determine but leading to highly oriented films as well.[60]

Next to a solubility enhancement, extending the length of the alkyl chain on a HBC disc from 3,7-dimethyl-octyl **3-21** to 3,7,11,15-tetramethyl-hexadecyl **4-28** resulted in a lowering of the isotropization temperature of about 200 °C.[61] If the melting temperature of a material is significantly lower than its decomposition temperature, crystallization from the molten state can be considered as an inexpensive, elegant alternative to the above described solution processing techniques.

In the following chapter, both processing alternatives – from solution and from the melt – will be discussed on the example of the novel HBC derivatives with the branched alkyl chains in the corona.

3.3.1 Solution Processing

To investigate the effect of self-association at the interface between solvent and substrate onto the film morphology[62-64] of the HBC derivatives, the organization from solution was investigated by the AFM technique. Therefore, the samples were first prepared by spin-coating at room temperature on HOPG surfaces.

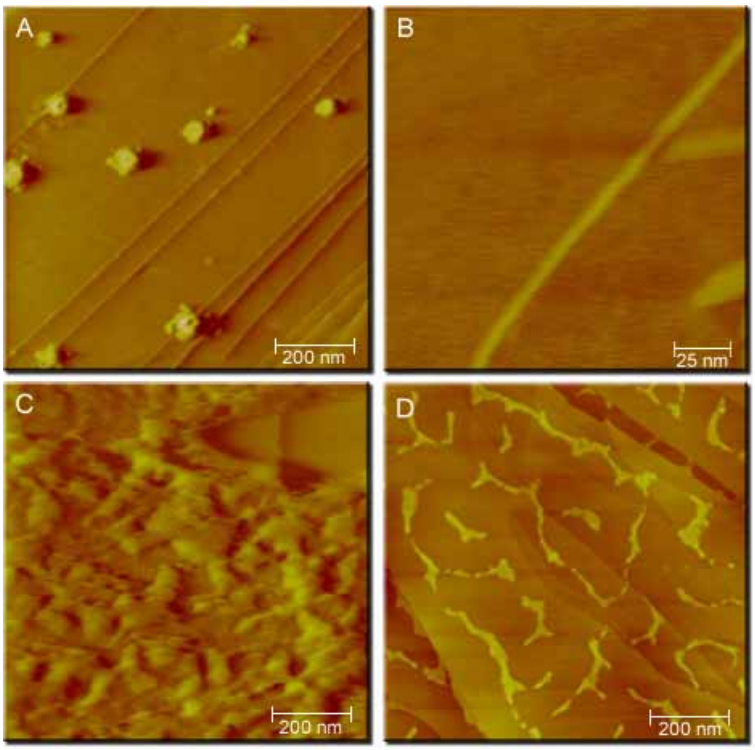

Figure 3-18: *AFM topography images in tapping mode on HOPG surface of spin-coated films HBC-$C_{14,10}$* **3-13c** *from A: a 10^{-7} M THF solution and C: from 10^{-4} M; HBC-C_{12}* **3-3a** *from B: a 10^{-7} M THF solution and D: 10^{-4} M.*

When HBC-$C_{14,10}$ **3-13c** was spin-cast from a 10^{-4} M THF solution, the freshly cleaved graphite surface was covered by an inhomogeneous ~100 nm thick film which showed no nanoscopic order (Figure 3-18C), whereas the film from HBC-C_{12} **3-3a** prepared under the same conditions, exhibited a more pronounced anisotropy in the structure, such as fibrous features (Figure 3-18D). When decreasing the concentration down to 10^{-7} M, in the case of HBC-$C_{14,10}$ **3-13c** single 60 to 80 nm wide blobs with a height of ca. 3 nm, appeared, which were randomly distributed over the surface (Figure 3-18A). From a solvent mixture of methanol and chloroform (1:1) at the same concentration, single flat pancake shaped features with a constant thickness of ca. 2.5 nm were formed (not shown).

Single long nanofibers were found from a 10^{-7} M solution of HBC-C_{12} **3-3a** in THF, which were 1.2 nm high and ca. 20 nm wide, exceeding even several hundreds of nanometers in length (Figure 3-18B). Analyzing the object dimensions, these fibers seemed to consist of a monomolecular layer with several columns lying parallel along the fiber axis, whereby the molecules were arranged edge-on. Very similar nano-fibers have been found for a star-shaped HBC derivative by J. Wu[65,66], when spin-

coated from a THF solution onto HOPG. These fibers consisted of bundles of edge-on organized columnar stacks. The formation of anisotropic nano-objects emphasized the pronounced nucleation and growth propensity of HBC derivatives.

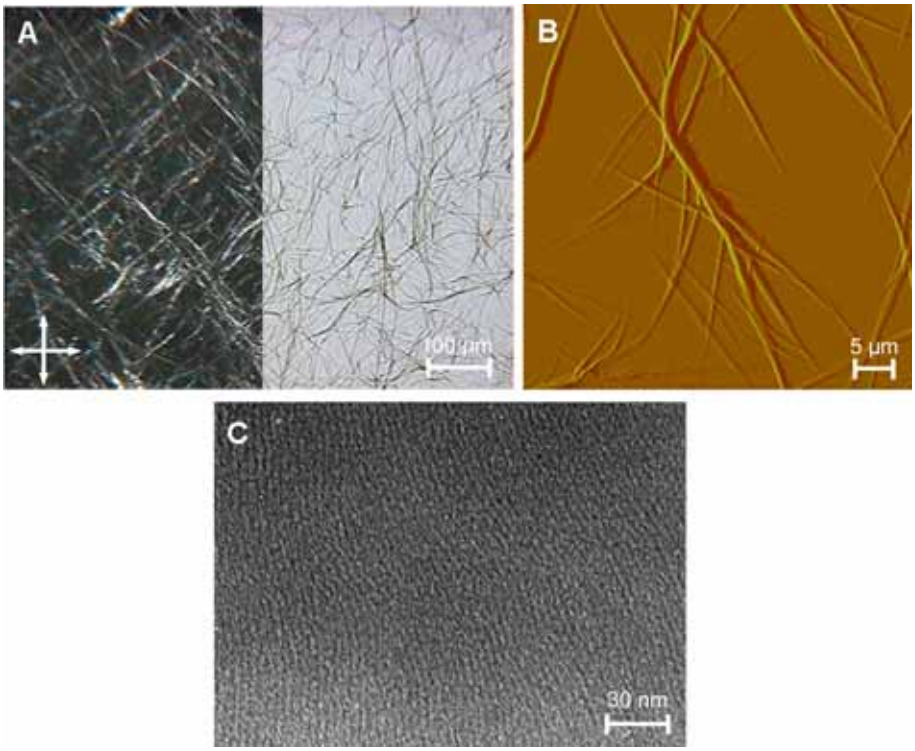

Figure 3-19: *A: POM image of drop-cast HBC-C_{12}* **3-3a** *from a 10^{-4} M toluene solution (right with and left without cross-polarizer), B: AFM topography of the microfiber morphology (tapping mode); C: TEM image of a spin coated HBC-C_{12}* **3-3a** *film (10^{-4} M, toluene).*

The morphology of a drop-cast film (10^{-4} M in toluene) of HBC-C_{12} **3-3a** (Figure 3-19A,B) consisted of several hundred micrometer long, birefringent microfibers. Their dimensions slightly changed with different solvents. By casting from toluene longer, but thinner microfibers were observed in comparison to the films prepared from THF or other solvents with lower evaporation temperatures. In all cases, the morphology was uniform within the drop-cast film, whereby the columnar alignment coincided with the microfiber axis as it was previously proven.[33] Indeed the spin-coated HBC-C_{12} **3-3a** films revealed highly oriented columnar domains as visualized by transmission electron microscopy (TEM) (Figure 3-19C). This tendency to create highly anisotropic structures was even observed within a polymer matrix.[34] The growth of defined fibrous objects is important for device applications, since free charge carriers can migrate along these stacks of molecules.

On the other hand, drop-cast HBC-$C_{14,10}$ **3-13c** and HBC-$C_{10,6}$ **3-13b** films from 10^{-4} M THF solutions were completely amorphous. By using toluene as solvent, the film morphology changed slightly revealing birefringent parts which appeared at the rim of the drop-cast films where most of the material was deposited.

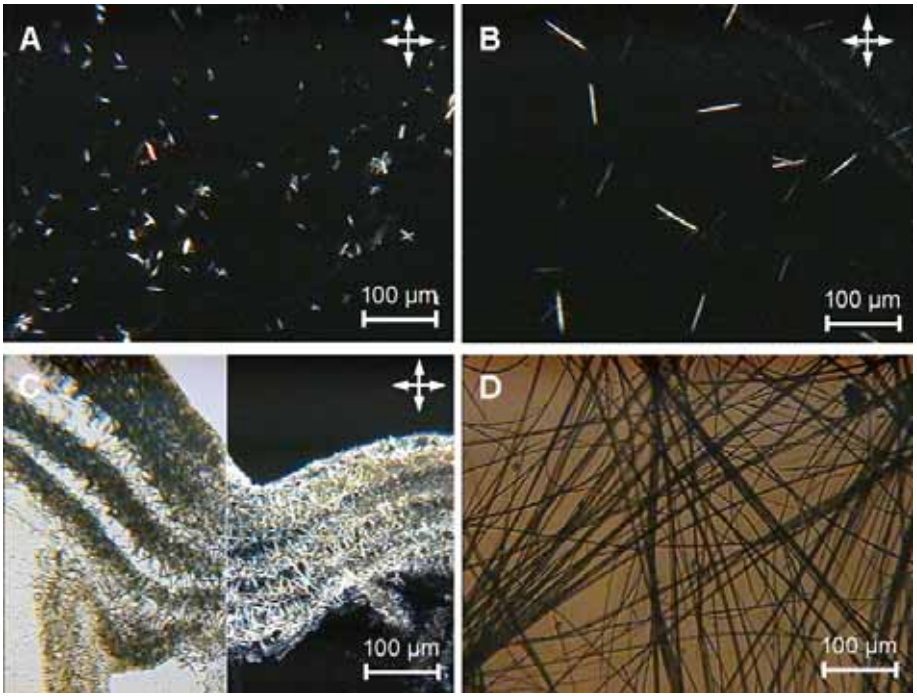

Figure 3-20: *POM of HBC-$C_{6,2}$* **3-13a** *drop-cast from A: toluene and B: xylene both at a concentration of 10^{-4} M, C: optical image of the rim of the drop-cast film prepared in a) (left without and right with cross-polarizer) and D: optical image obtained after evaporation of a HBC-$C_{6,2}$* **3-13a** *solution with a concentration close to the saturation.*

The drop-cast film of HBC-$C_{6,2}$ **3-13a** (Figure 3-20) prepared from a 10^{-4} M THF solution also did not show any birefringence in polarized light, but small particles precipitated randomly from the solution. When the same material was processed from toluene with an identical concentration short crystalline needles appeared at the rim of the film (Figure 3-20C). These structures were highly birefringent and were mainly oriented in the direction of the drop evaporation, whereas the interior of the film revealed the same, but shorter structures (Figure 3-20A). By using a comparable solvent with respect to the association such as xylene, which possesses a significant higher evaporation temperature, the length of these crystalline needles within the film interior increased considerably (Figure 3-20B). Finally, when a saturated toluene solution of HBC-$C_{6,2}$ **3-13a** was slowly evaporated from a small vessel, centimeter long, crystalline fibers were obtained on the bottom of the vessel (Figure 3-20D).

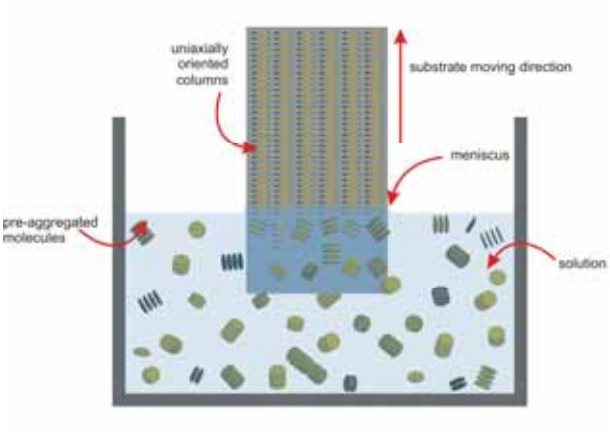

Figure 3-21: *Set-up for the dipping experiment of HBC-$C_{6,2}$* **3-13a***; at the deposition zone a meniscus is formed at which the material crystallized onto the moving support.*

Due to this extraordinary crystallization or nucleation and growth of the material into such large fibers in solution, a dipping experiment was performed by W. PISULA in order to align these structures uniaxially as shown in Figure 3-21. At a concentration of 10^{-1} M in toluene and a low moving velocity of the support, a homogenous film was acquired with indeed oriented microfibers (Figure 3-22). Moreover, these fibers consisted of uniaxially aligned HBC columns as the 2D WAXS pattern indicated (Figure 3-23).

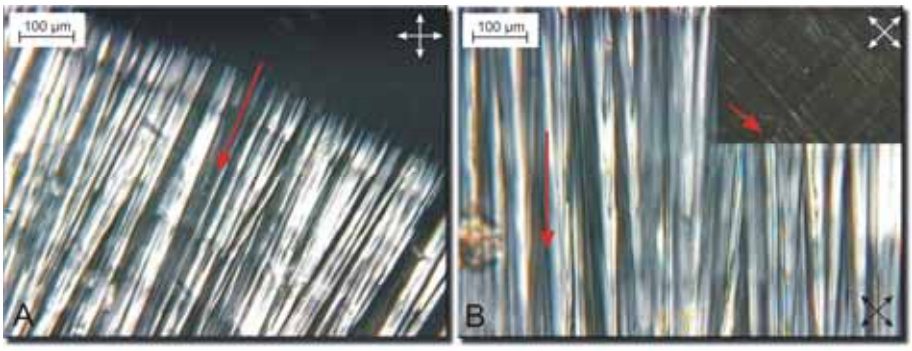

Figure 3-22: *A: POM of the nucleation site, at which the structures begin to grow in the moving direction of the support; B: POM of the interior of the film revealing an uniaxial orientation of the mircofibers.*

The investigation of the film morphology obtained through solution casting revealed additional information about the solution behavior of the HBC derivatives. It has been found that in addition to the thermodynamical aspect (see chapter 3.2) the organization from solution is also dominated by kinetics. This has been impressively demonstrated in the case of HBC-$C_{6,2}$ **3-13a**, which was prepared from different solvents with different evaporation rates.

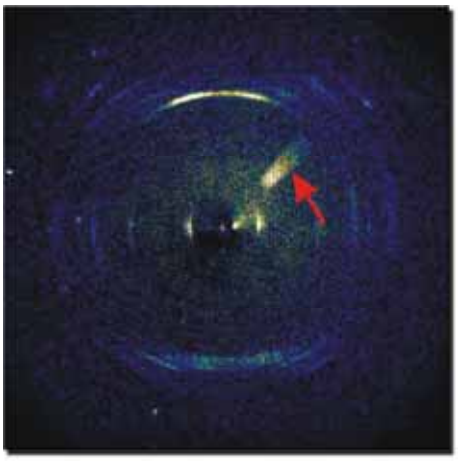

Figure 3-23: *2D WAXS pattern of the oriented HBC-$C_{6,2}$* **3-13a** *film (arrow indicates an artifact).*

Comparing the films of HBC-$C_{6,2}$ **3-13a** which were drop-cast from solvents like toluene and xylene, in which the self-association is known to be very similar, one observed larger micro-objects in the case of the higher boiling xylene. The morphology of a film obtained from THF differed significantly, since only an amorphous structure was obtained. In the latter case, it should be noted that the degree of self-association is smaller.

Nevertheless, the evaporation time of the solvent in the casting process influenced significantly the macroscopic self-organization on the substrate. A slow evaporating solvent like xylene allowed the formation of large anisotropic objects, whereas a solvent with a lower boiling point did not give enough time to exhibit a similar organization. The role of the kinetics in the case of HBC-$C_{6,2}$ **3-13a** is more pronounced compared to HBC-C_{12} **3-3a**. This effect can be explained by the steric requirement induced by the dove-tailed alkyl substituents, which hampered the discs to approach one another. Therefore, the self-assembly of these molecules occurs on a relatively large time scale. This stands in contrast to HBC-C_{12} **3-3a**, which revealed homogeneously distributed micro-ribbons over the drop-cast film independent of the used solvent. These extraordinary structures resulted on one hand from the strong self-association tendency and on the other hand from the low steric demand of the attached alkyl chains.

Consequently, HBC-C_{12} **3-3a** was successfully processed by the zone-casting technique into highly ordered surface layers, supported by the pronounced size of the pre-aggregates, which existed already before the deposition from solution. Contrary, it is difficult to zone-cast HBC-$C_{6,2}$ **3-13a** due to its slow self-aggregation and the

necessity to use high concentrations to reach a sufficient pre-aggregation in solution. On the other hand, adequate processing conditions during a dipping experiment (higher concentrations and low solvent evaporation rates) allowed a uniaxial orientation into surface layers. This solution processing promises a successful implementation of the material in a FET device.

Due to the increase of the peripheral steric demand of the longer dove-tailed side chains, both compounds HBC-$C_{14,10}$ **3-13c** and HBC-$C_{10,6}$ **3-13b** showed a limited tendency to create anisotropic structures from solution. No enhancement in the self-organization onto the surface was observed, even though larger pre-aggregates were observed by the addition of methanol. Both HBC derivatives only formed small domains after the deposition, since the association rate decreased extremely compared to HBC-$C_{6,2}$ **3-13a**. As an alternative, melt processing can be applied to these derivatives, which will be discussed in the following.

3.3.2 Melt Processing

3.3.2.1 Morphology

The crystallization behavior from the isotropic state was investigated by means of thermally controlled POM to gain a better understanding of the supramolecular organization.

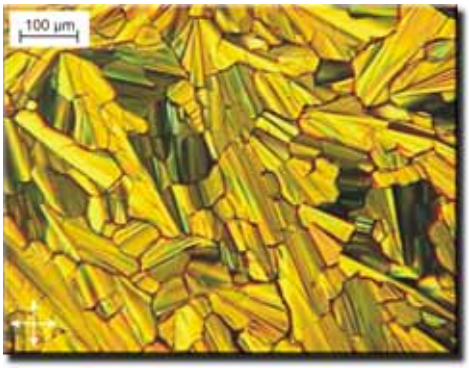

Figure 3-24: *POM image of HBC-$C_{6,2}$* **3-13a** *between two glass slides cooled at 1 °C/min from the isotropic state.*

For this purpose, a sample of HBC-$C_{6,2}$ **3-13a** was sandwiched between two glass slides and heated to the isotropic phase (T_i = 410 °C) under a nitrogen atmosphere. The material was then immediately cooled down at a rate of 1 °C/min, exhibiting a characteristic texture at 380 °C, which appeared typical for a discotic columnar phase

forming pseudo focal conic fan-shapes (Figure 3-24). This arrangement remained stable in the crystalline state. In addition, the size of the domains was strongly dependent on the cooling rate. In contrast to this, HBC-$C_{10,6}$ **3-13b** revealed completely different textures on cooling the sample from the melt (T_i = 96 °C). In this case, the crystallization from the isotropic phase and, thus, the resulting morphology depended strongly on the surface contact. When placing the sample between two glass slides and cooling, HBC-$C_{10,6}$ **3-13b** formed highly birefringent dendritic structures during the initial crystallization process (Figure 3-25, left).

When cooling down to room temperature, the texture of the same sample diversified significantly (Figure 3-25 right). Highly ordered, large, birefringent domains became apparent and indicated a considerable difference in the supramolecular order during the crystallization process when the dendritic shapes began to coincide. This resulted in mosaic textures with large ordered domains which remained stable down to room temperature. The size of these domains was temperature dependent and exceeded even millimeters in size. This change of the morphology can be correlated with the phase transition from the liquid crystalline (LC) phase to a plastic crystalline state of the sandwiched material which forces the molecules to adopt a more favorable organization leading to huge oriented domains at room temperature. The term plastic crystallinity emphasizes a partial crystallinity, where in this case the aromatic HBC moiety occupied defined positions in the crystal lattice. However, the racemic alkyl surrounding only partially crystallized and kept residual flexibility, which was investigated with solid state NMR experiments (3.3.3.3).

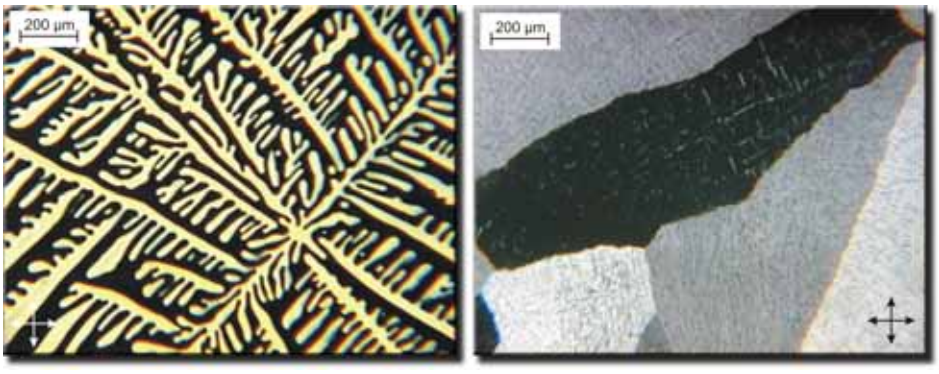

Figure 3-25: *POM images of HBC-$C_{10,6}$* **3-13b** *cooled annealed at 0.1 °C/min from the isotropic state between two glass slides at 95 °C (left) and room temperature (right).*

During crystallization of HBC-$C_{10,6}$ **3-13b** only on one surface, different types of texture were observed. Depending on the cooling rate small, cyclic clusters (Figure

3-26, right) or finger-print, band-structures (0.05 °C /min) appeared which significantly differed from the large domains observed when the sample was sandwiched between glass slides.

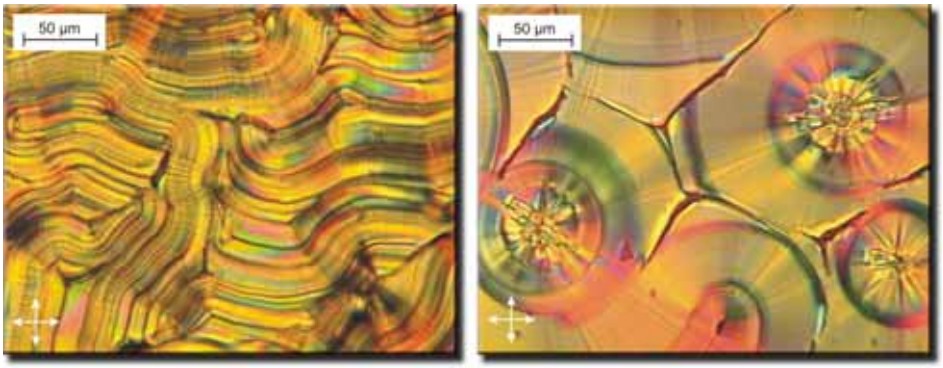

Figure 3-26: *POM images of HBC-$C_{10,6}$* **3-13b** *cooled from the isotropic state on one glass surface with a cooling rate of 0.05°C/min (left) and 0.01°C/ min (right) down to room temperature.*

For the 50-100 µm large cyclic clusters, it is important to note that the nucleus center is surrounded by planar rings, indicating a non-radial growth direction as shown by both the POM image and the topography (Figure 3-27).

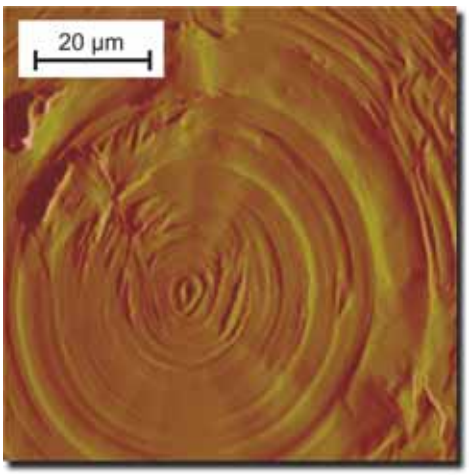

Figure 3-27: *Topography of the cyclic clusters recorded for HBC-$C_{10,6}$* **3-13b**, *when crystallized on one glass surface.*

Interestingly, the surface of the texture, which grew on one surface only, was quite rough what can be seen by the reflected light dark-field optical microscopy image (Figure 3-28).

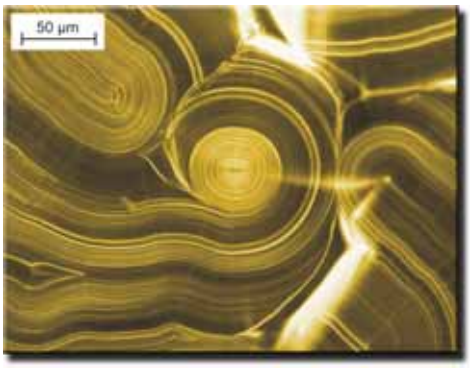

Figure 3-28: *Reflected light dark-field optical microscopy image of HBC-$C_{10,6}$* **3-13b***, crystallized on one surface.*

A very surprising texture was observed for the HBC derivative with the longest side chains, HBC-$C_{14,10}$ **3-13c**. During the cooling from the isotropic state, well-ordered spherulites nucleated randomly over the whole sample (Figure 3-29). This crystallization behavior was atypical for discotic systems, especially for such with large aromatic cores. Spherulite formation of discotics has been reported only for low molecular mass liquid crystals or discotics with substantially smaller cores.[67] The spherulites revealed high anisotropy and therefore coherent long-range order. This gives rise to the well-known MALTESE cross where the isogyres followed the extinction of the analyzer/polarizer direction and indicate a radial alignment of columns from the center. The columns were doubtless oriented in the spherulite growth direction with an edge-on arrangement of the molecules. This supramolecular order was also verified by the determination of the index of refraction. The index was smaller parallel to the radial direction than perpendicular to it as indicated by the red-blue distribution by using a λ-plate (Figure 3-29).

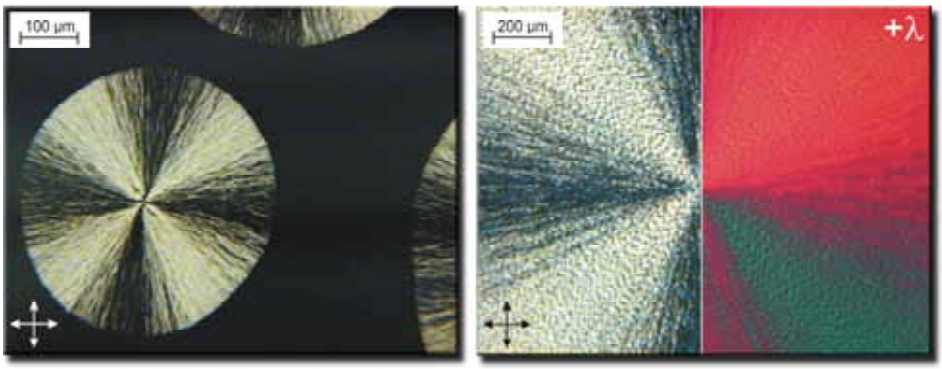

Figure 3-29: *Cross-polarized optical microscopy images of HBC-$C_{14,10}$* **3-13c** *with an isothermal crystallization at 35 °C (during crystallization, left) and at 38 °C (after crystallization, right, with and without lambda plate).*

Therefore, this observation was in strong correlation with the arrangement of the molecules within the spherulitic domains and characterized this phase of the material as optically negative.

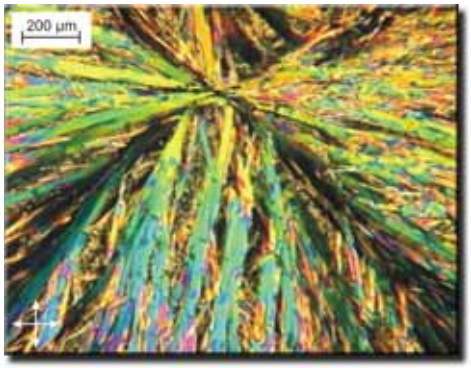

Figure 3-30: *Cross-polarized optical microscopy image of HBC-$C_{14,10}$* **3-13c** *during isothermal crystallization at 45 °C.*

The size of the spherulites varied with the crystallization temperature, whereby in the temperature range from 20 °C to 35 °C the size of the spherulites was not significantly dependent on the temperature and above 35 °C the growth increased exponentially exceeding a spherulite size even of 4 mm. At temperatures higher than 44 °C, the texture changed, exposing a more colorful image (Figure 3-30). Both, the absence of the Maltese cross and the lower contrast of the textures reflected the absence of long-range order.

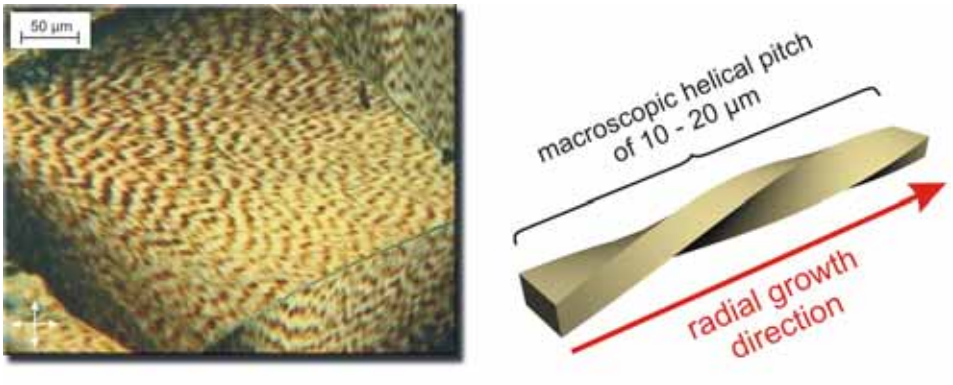

Figure 3-31: *An example of a cross-polarized optical microscopy image illustrating the periodic features along the spherulite radius (left) and a schematic illustration of the helical fibrous structure (right).*

Atomic force microscopy (AFM) was used for closer inspection of the spherulitic domains and revealed a typical lamellar morphology with many of the lamellae performing a twisting which was the origin of a periodic contrast in the POM. This periodic contrast along the radius in the POM was because of birefringent effects and

appears on single fibrous structures suggesting a helical twist of crystallites within the fibers[68] as presented in Figure 3-31. Extinction occurred when the optical axis of crystallites coincided with the polarization plane.

In conclusion, the branched alkyl chains on the HBC molecules exerted a strong influence on the supramolecular self-organization which has been monitored using POM. The obtained textures differed significantly from other HBC derivatives. All three structures impressed with their pronounced tendency to organize from the isotropic state. Interestingly, HBC-$C_{6,2}$ **3-13a** and HBC-$C_{14,10}$ **3-13c** crystallized independent on the surface contact in the same texture, whereas the morphology of HBC-$C_{10,6}$ **3-13b** dramatically differed when cooled down on one or sandwiched between two glass slides.

However, the POM images suggested a deeper investigation of the morphological structures, since the actual molecular orientation is of major importance when the material is aimed to be implemented in an electronic device. Therefore, scanning X-ray scattering experiments have been performed on the obtained films using a micro-focused synchrotron beam, which will be described in the following chapter.

3.3.2.2 Characterization of the molecular orientation

The local order and molecular orientation in the above presented film textures have been investigated at the European Synchrotron Radiation Facility (ESRF) in Grenoble, France. The photographs in Figure 3-32 show the experimental hutch II at the beamline ID13. The beamline utilizes a 46 mm period, tunable undulator with liquid nitrogen cooled Si-111 double monochromator to provide a beam with a wavelength of 0.98 Å. The samples were glued on glass capillaries and mounted and aligned to the exit of the waveguide (Figure 3-32, right).

The C6-symmetrically substituted HBC-$C_{6,2}$ **3-13a** which seemed to crystallize in a typical pseudo focal conic fan-shape texture, did unexpectedly not pack in a hexagonal unit cell, unlike all other known symmetrically substituted HBC derivatives. In fact, the novel HBC derivatives with the branched alkyl chains organized themselves in a monoclinic unit cell, which must be caused by packing effects of the substituents.

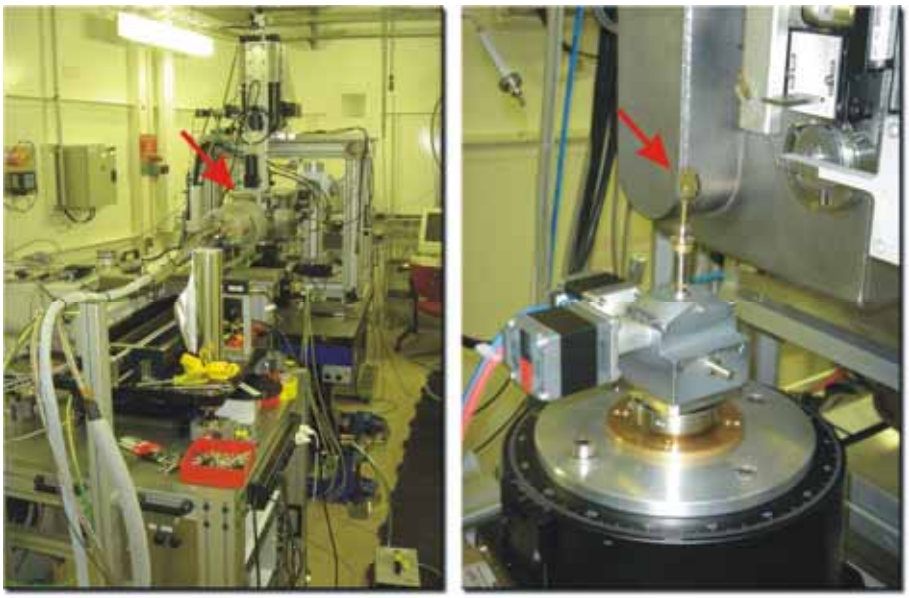

Figure 3-32: *Photographs from the experimental hutch II at the beamline ID13 at the ESRF, Grenoble with the detector in the middle, picture of the mounted sample at the exit of the waveguide (right), red arrows mark the position of the sample.*

Figure 3-33 presents the synchrotron scanning X-ray results on the organized HBC-$C_{6,2}$ **3-13a** sample. The microfocus allowed 2D-WAXS diffractograms to be locally recorded and the molecular orientation to be determined. The birefringence of the POM image is usually a strong indication for an edge-on arranged columnar organization. However, the diffraction pattern indicated a face-on orientation of the molecules. Since the monoclinic unit cell is biaxial, the face-on arrangement led to strong birefringence. Only uniaxial unit cells, such as hexagonal and rhomboedrical reveal the absence of birefringence in the case of face-on organized molecules.[69] The array of 2D-WAXS patterns (Figure 3-33B) was recorded by scanning the focused X-ray beam across the sample which was monitored using optical microscopy. This allowed optical textures to be directly correlated with the molecular superstructure.

It occurred that the orientation of the monoclinic unit cell changed, which is illustrated with the vector array in Figure 3-33C. The determined domain boundaries fit in good agreement the optical textures (Figure 3-33D). This is a very rare example, where the optical textures could be correlated with the local structural orientation.[70]

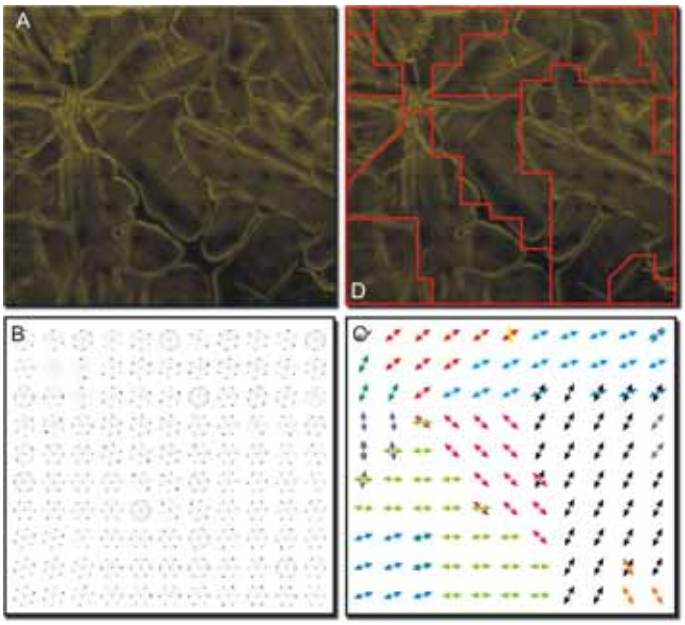

Figure 3-33: *(A) Optical microscopy image of HBC-$C_{6,2}$* 3-13**a**, *sandwiched between glass slides, (B) array of transmission diffraction patterns recorded by scanning across the local texture (200 x 200 µm), (C) array of the orientations of the monoclinic unit cell, (D) domain boundaries detected by X-ray scattering superimposed on the optical microscopy image.*

The same molecular face-on orientation was found in the case of HBC-$C_{10,6}$ **3-13b**, when sandwiched during the crystallization process. The slight distortion of a uniaxial hexagonal to a biaxial monoclinic unit cell caused the appearance of the strong birefringent domains (Figure 3-25). The domains were characterized analogous to the above example by a uniform orientation of the crystal lattice.

In contrast, the molecular orientation for HBC-$C_{10,6}$ **3-13b**, when crystallized only on one surface, appeared to be edge-on. The POM revealed non-radially grown cyclic clusters, which was confirmed by the synchrotron experiment. The orientation of the disc-like molecules can be extracted from the array in Figure 3-34C, which translates the molecular orientation into vectors. This indicates circular grown columns of molecules as displayed in Figure 3-34D. This supramolecular self-organization behavior is unique and has never been observed before.

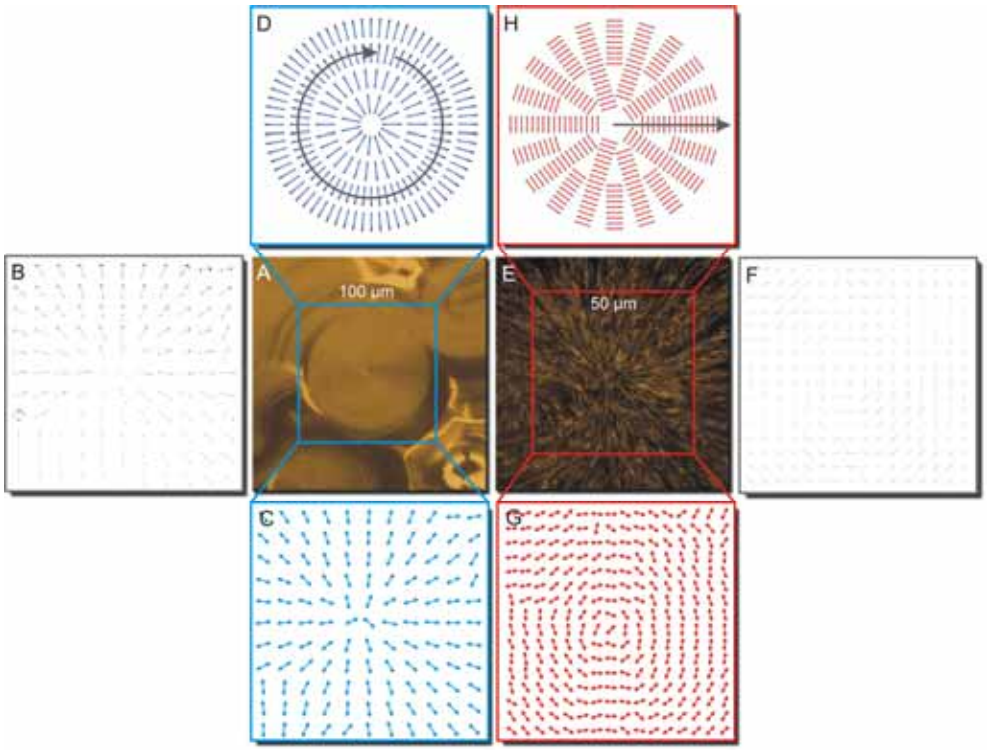

Figure 3-34: *Optical microscopy image of (A) HBC-$C_{10,6}$* **3-13b***, crystallized on one surface and (E) HBC-$C_{14,10}$* **3-13c***; (B) array of transmission 2D-WAXS diffraction patterns recorded by scanning the blue marked area in (A) (100 x 100 µm) and (F) by scanning the red marked area in (E) (50 x 50 µm); vector array displaying the orientation of the monoclinic unit cells for (C) HBC-$C_{10,6}$* **3-13b** *and (G) HBC-$C_{14,10}$* **3-13c***; molecular orientation of (D) HBC-$C_{10,6}$* **3-13b** *and (H) HBC-$C_{14,10}$* **3-13c**.

Extending the alkyl chain from the 2-hexyl-decyl **b** to the 2-decyl-tetradecyl chain **c**, a spherulitic texture was observed (Figure 3-29). The growth of the structure occurs strictly radially from the nucleation center, which was supported by the synchrotron experiments. The center of one spherulite was subjected to the scanning experiment, revealing the typical polycrystalline, edge-on molecular arrangement (Figure 3-34G,H). It is well known, that HBC derivatives adopt a tilted columnar arrangement in their crystalline state. The determination of a possible tilted organization within the described films is currently investigated.

In summary, the extension of the branched alkyl chain has an unforeseen impact on the self-organization beyond the solution. While HBC-$C_{6,2}$ **3-13a** and HBC-$C_{14,10}$ **3-13c** strictly organized independent upon the surface contact face-on and edge-on, respectively, HBC-$C_{10,6}$ **3-13b** allows the molecular orientation to be controlled by changing the surface contact (Figure 3-35).

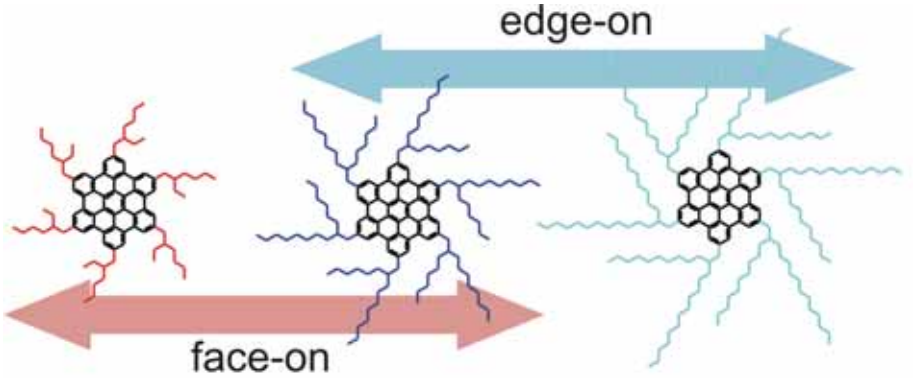

Figure 3-35: *Transition of the face-on to the edge-on orientation when extending the length of the branched substituents on the HBC.*

The formation of a homeotropic phase in the case of HBC-$C_{6,2}$ **3-13a** and HBC-$C_{10,6}$ **3-13b**, which corresponds to a molecular face-on arrangement, has never been observed for all-hydrocarbon discotic materials before. For triphenylenes, it was even claimed that heteroatoms are responsible for the successful formation of a homeotropic phase.[71] The mechanism has not been investigated in the literature.

In conclusion, the processing of non-associated species, like in the isotropic melt, gave also in other cases the face-on oriented molecules.[6] Monomeric molecules seemed to thermodynamically favor a large surface contact and the following molecules grow epitaxially onto the first formed layer of molecules. On the other hand, pre-aggregated molecules, i.e. in solution or in the mesophase, organized in the common edge-on arrangement.

This allows the desired molecular orientation to be controlled by adapting the processing technique.[72] However, most known HBC derivatives possess an isotropization temperature, which was far higher than the clearing point.

The reason why HBC-$C_{14,10}$ **3-13c** adopted exclusively the edge-on orientation is not obvious. The steric demand close to the proximity of the disc did not change when extending the chain in the end. However, the entire chain became more bulky and requested more space when packed. In solution, it was obvious that HBC-$C_{14,10}$ **3-13c** was stronger associated at room temperature, which has been attributed to chain-chain interactions. To gain a deeper insight into this phenomenon, a HBC derivative has been synthesized, where a rigid phenyl-spacer was inserted between the aromatic disc and the flexible, branched alkyl chain. In this case, the steric requirement of the

substituents has been moved away from the aromatic disc, which should allow a better interaction between the molecules.

3.3.2.3 Mechanism of the Homeotropic Phase Formation

FECHTENKÖTTER has described the synthesis of a six-fold 4-*n*-dodecylphenyl substituted HBC derivative[73], which has been successfully implemented in an heterojunction photovoltaic device.[74] Unfortunately, the analogous synthesis with the branched alkyl chain failed, because the necessary Grignard reagent could not be prepared.

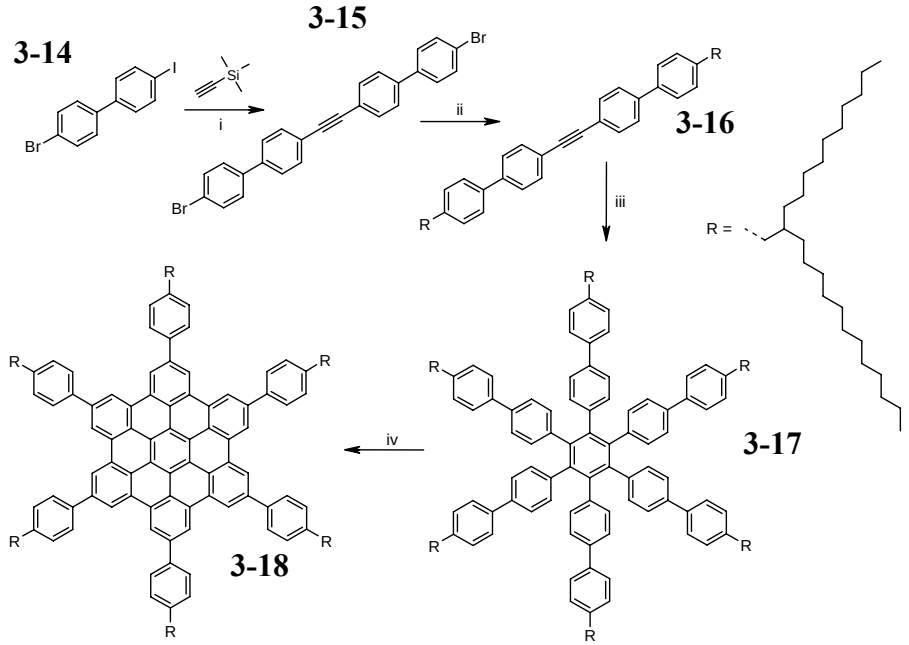

Scheme 3-5: *i) DBU, H_2O, toluene, $(PPh_3)_4Pd$, 89%; ii) BrMgR, THF, $Cl_2Pd(dppf)$, 39% iii) $Co_2(CO)_8$, dioxane, 90% iv) $FeCl_3$, CH_3NO_2, CH_2Cl_2, rt, 120 min, 85%.*

Therefore, the synthetic concept was revised. Commercially available 4-bromobiphenyl was iodinated following the literature procedure to yield 4-bromo-4'-iodobiphenyl **3-14**[75], which was selectively converted to bis(4,4''-dibromo-4-biphenyl)-acetylene **3-15**. Although hardly soluble, the KUMADA conversion with the GRIGNARD reagent of **3-10** yielded the fluorescent alkylated bis(biphenyl)acetylene **3-16**. The yield was low, because the preparative column chromatographical separation turned out to be quite difficult. The cyclotrimerization with cobaltoctacarbonyl proceeded smoothly with satisfying yields. Interestingly, the successful oxidative cyclodehydrogenation reaction required 60 equivalents of iron (III) chloride, which is about 4 times higher than needed for the dodecyl-substituted analogue[73], together with an extended reaction time. Chlorination as an undesired

side-reaction was always a problem for the para-*n*-dodecylphenyl substituted HBC, while HBC-PhC$_{14,10}$ **3-18** did not mass-spectrometrically show any chlorination, despite of the amount of iron(III) chloride and the extended reaction time.The ^{1}H NMR spectrum of HBC-PhC$_{14,10}$ **3-18** at 25 °C exhibited only very broad and unresolved aromatic resonances (Figure 3-36, lower spectrum), which has been observed for the *n*-dodecyl substituted analogue as well.[76] Upon heating, the resonances narrowed and the spectrum got resolved (Figure 3-36, upper spectrum). Despite of the great solubility of this derivative, the solution NMR spectrum indicated a strong association propensity of the compound. Attempts to analyze the temperature dependence of the aromatic resonances with a least-squares curve fitting to assume an indefinite self-assocation process (see chapter 3.2.1) failed which indicates a different mechanism of the association. One can speculate that the additional phenyl substituents slowed down the kinetics of the association-dissociation process significantly. Therefore, the assumption that this process is fast on the timescale of the NMR experiment would not be fulfilled.[46]

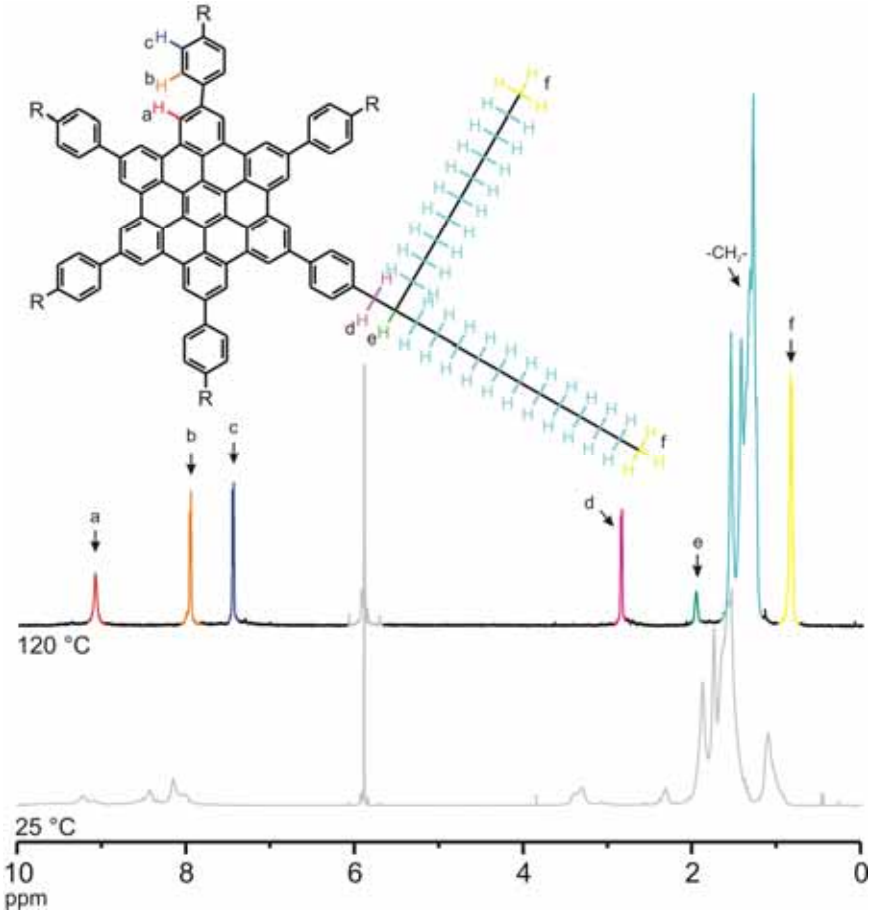

Figure 3-36: *^{1}H NMR spectrum of HBC-PhC$_{14,10}$* **3-18** *in 1,1,2,2-tetrachloroethane-d^{2} at a temperature of 25 °C and 120 °C.*

The UV/vis spectrum (Figure 3-37) resembled the ones of other HBC derivatives, although the lines are broader independent of concentration, which has been seen for other phenyl-substituted PAHs.[77] The β-band was shifted by about 20 nm, which was expected because of the extended π-conjugation. The PL spectrum appeared broader than the one for six-fold alkyl substituted HBCs (Figure 3-11). This can be attributed to the phenyl-substitution and has been observed for other PAHs, i.e. anthracene and 9,10-diphenylanthracene, as well.[50] The additional phenyl rings lead to a conformation-dependent splitting and more transitions are symmetry-allowed.[78]

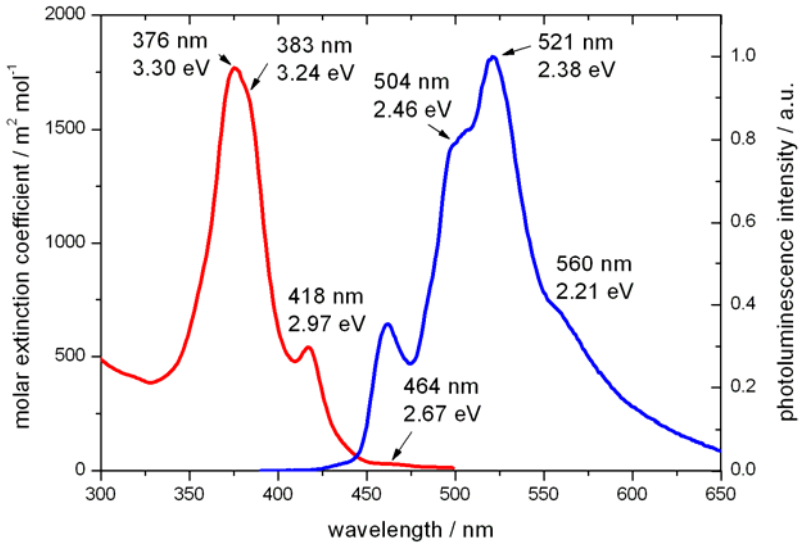

Figure 3-37: *UV/vis (red) and photoluminescence spectrum (λ_{ex} = 376 nm, blue) of HBC-PhC$_{14,10}$* **3-18** *recorded at room temperature in chloroform.*

The melting temperature of HBC-PhC$_{14,10}$ **3-18** was 115 °C, clearly higher than for HBC-C$_{14,10}$ **3-13c**. The intermolecular interactions were greater because of two arguments. Firstly, the phenyl unit developed additional interactions between the aromatic molecules and secondly the steric demand close to the disc was significantly reduced.

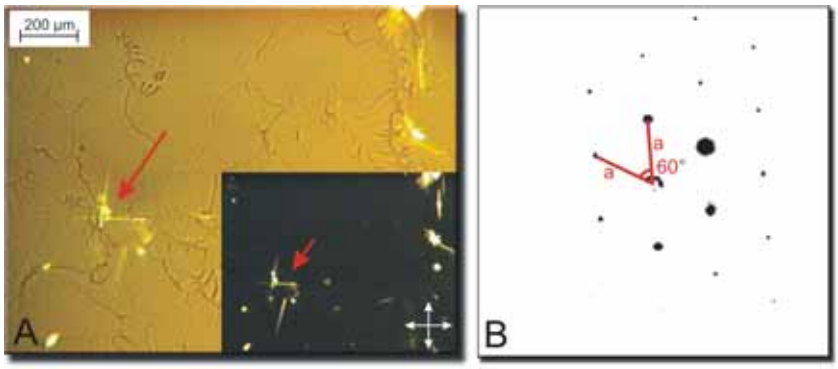

Figure 3-38: *(A) Optical microscopy image of HBC-PhC$_{14,10}$* **3-18** *after crystallization from isotropic state (cooling rate = 0.1 °C/min), inset: cross-polarized optical microscopy image at same position, red arrows mark defects (B) transmission 2D WAXS.*

To investigate the molecular orientation which is spontaneously formed, the sample was sandwiched between glass slides, heated to the isotropization temperature and slowly cooled down to room temperature. As a very striking result, HBC-PhC$_{14,10}$ **3-18** formed typical dendritic structures, which could be observed under the optical microscope (Figure 3-38A).[6] However, when cross-polarizers were applied, the images did not reveal birefringence except of some disordered material, which is marked with red arrows in the Figure 3-38A. The absence of birefringence indicated a face-on orientation of the molecules, which had to pack in a uniaxial unit cell. Indeed, 2D-WAXS allowed a perfect hexagonal unit cell to be determined (Figure 3-38B). Scanning X-ray experiments using the synchrotron microfocussed beam revealed that the material crystallized in very large domains, which exceeded millimeters in size. The "small" dendritic texture can be attributed to dewetting effects from the surface, when the material was crystallized and thus the density shrunk.

It is astonishing, that the introduction of a phenyl unit has a strong impact on the packing and organization behavior of the material. While HBC-C$_{14,10}$ **3-13c** could not establish a face-on orientation, the sterically less hindered derivative HBC-PhC$_{14,10}$ **3-18** formed spontaneously a homeotropic phase, which has been observed for ether-bearing, branched side chains as well.[6]

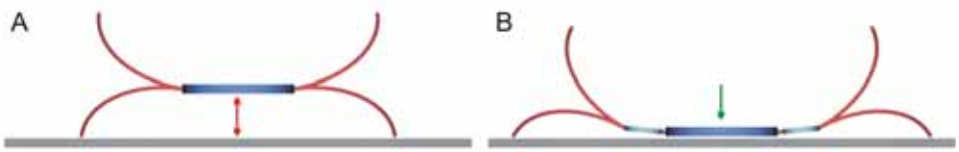

Figure 3-39: *Schematic model of the surface approach of A) HBC-C$_{14,10}$* **3-13c** *and B) HBC-PhC$_{14,10}$* **3-18**.

One can speculate, that the phenyl ring between the bulky alkyl chain and the aromatic disc bestowed the molecule more flexibility. Therefore, the face-on approach onto the surface became thermodynamically more favored, because the chains could be distorted away (Figure 3-39). In contrast, HBC-$C_{14,10}$ **3-13c** nucleated only in the edge-on manner. The edge-on arrangement of the semi-conducting molecules is advantageous for the implementation in FETs, because the charge would have to propagate along the surface. However, one has to direct the growth of the material to span the gap between the source and drain in the FET setup.

A considerable effect of the introduced phenyl spacer onto the formation of the mesophase has been observed. Analogous to FECHTENKÖTTER's HBC, the mesophase was stabilized down to room temperature, since the crystallization of the discotic material was hampered due to the out-of-plane rotated phenyl substituents, leading to a better soluble and processable material.

3.3.2.4 Zone-Crystallization

The extraordinary self-assembly properties of compound HBC-$C_{14,10}$ **3-13c**, consisting in nucleation and directed growth of structures and its ability to create spherulitic textures suggested the application of the zone-crystallization technique to obtain macroscopically controlled order for possible application in electronic devices. It was shown that the processing of materials from their isotropic state by using a temperature gradient is an appropriate method to control the order of supramolecular structures over large areas. W. PISULA built a zone-crystallization device, consisting of two heating blocks which could be independently, thermally controlled. During the alignment process, the sample was moved at a controlled velocity from a heating block with temperature T_1, at which the material was at the isotropic state, to a cooled block with a lower temperature T_2, lower than the crystallization temperature. The set-up is shown schematically in Figure 3-40. The processing conditions depend mainly on the crystallization kinetics of the material. Therefore, the optimal parameters are strongly based on the crystallization kinetics of the material.

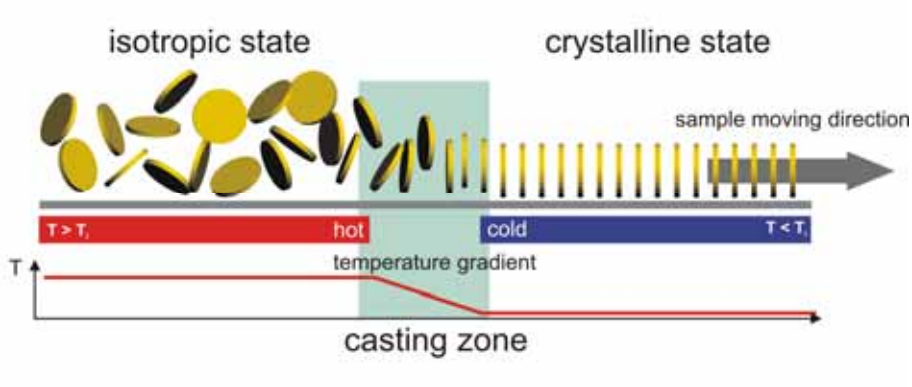

Figure 3-40: *Schematic presentation of zone-crystallization processing.*

After zone-crystallization processing, the aligned HBC-$C_{14,10}$ **3-13c** sample revealed high homogeneous structural order with columns oriented uniaxially along the temperature gradient, as could be seen in Figure 3-41A presenting the 2D-WAXS pattern.

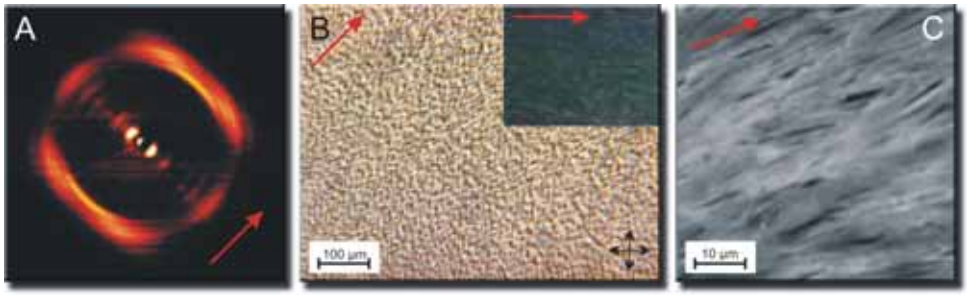

Figure 3-41: *(A) 2D-WAXS of the zone-crystallized HBC-$C_{14,10}$* **3-13c** *sample; (B) POM image with 45° to the polarizer/analyzer axes (inset: same image at 0° to the polarizer/analyzer axes); (C) AFM topography image of zone-crystallized HBC-$C_{14,10}$* **3-13c** *film (tapping mode); the arrows indicate the moving direction of the sample along he temperature gradient.*

The intra- and intercolumnar arrangement within the thermally processed sample was identical as determined for the mechanically extruded filament (see chapter 3.3.3.2). The discotic molecules were "edge-on" arranged with respect to the substrate. The observed high optical anisotropy of the POM images in Figure 3-41B confirmed the long-range order over large areas. The maximum birefringence appeared at an angle of 45° to the polarizer/analyzer axis suggesting that the columnar growth during crystallization takes place along the temperature gradient. The topography of the aligned layers was investigated by means of AFM (Figure 3-41C) which displayed a lamella morphology. These structures were over several hundreds of micrometer long, 2–3 µm wide and aligned in the moving direction of the sample during the processing; the strands were threaded and entangled into each other. From the AFM

image it is obvious that most of the lamellae are face-on arranged and that a twisting of these lamellae occurs. Synchrotron microfocus experiments revealed a high crystallinity in the polycrystalline feature.

This has been an impressive example, how to make use of the natural nucleation and growth of a specific material. HBC-$C_{14,10}$ **3-13c** has been the first extended discotic system, which could be organized over macroscopic dimensions by the zone-crystallization technique. So far, only HBC-C_{12} **3-3a** had been processed with the zone-casting technique (see chapter 1.5), which could even be transferred into a well performing electronic device.[59]

3.3.3 Mechanical Alignment - Structural Investigation

In the previous chapters, the three HBC derivatives with the branched alkyl chain have been investigated in terms of their self-association in solution and self-organization on a surface. The gained results silhouetted the derivatives against the known derivatives, mainly because the typically strong aromatic stacking interactions were modulated because of the steric demand of the used substituents.

To complete the picture, we gained from the described investigation, the thermal behavior and the organization in the respective phases was examined and described in the following.

3.3.3.1 Thermal Behavior

The thermal behavior was verified for all three compounds HBC-$C_{6,2}$ **3-13a**, HBC-$C_{10,6}$ **3-13b** and HBC-$C_{14,10}$ **3-13c** by using differential scanning calorimetry (DSC) in the temperature range from -150 °C to 220°C (10 °C/min). Hereby, the strong influence of the alkyl substituent on the thermal behavior could be observed (Figure 3-42, Table 3-4).

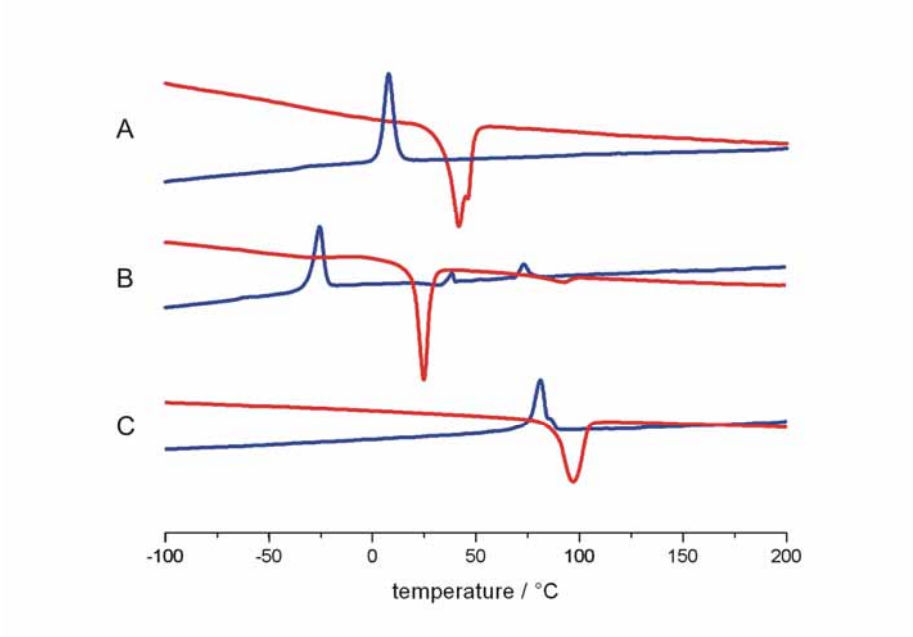

Figure 3-42: *DSC traces of HBC-$C_{6,2}$* **3-13a**, *HBC-$C_{10,6}$* **3-13b** *and HBC-$C_{14,10}$* **3-13c**, *applying heating/cooling rates of 10 °C/min (red = heating, blue = cooling).*

Table 3-4: Thermal characterization for the investigated dove-tailed HBC derivatives.

Sample	Temperature	Enthalpy /J g^{-1}	Phase
HBC-$C_{6,2}$ **3-13a**	97 (81)	21.4 (17.3)	Cr – Col_d
	420 (380)	–	Col_d – I
HBC-$C_{10,6}$ **3-13b**	24 (-26)	26.1 (16.4)	Col_p – Col_d
	93 (73, 45)	2.3 (2.6, 1.0)	Col_d – I
HBC-$C_{14,10}$ **3-13c**	46 (7)	33.4 (32.2)	Col_p – I

Abbreviations: Cr = crystalline phase, Col_p = plastic crystalline, Col_d = columnar disordered mesophase, I = isotropic phase. Brackets indicate values during cooling.

While HBC-$C_{10,6}$ **3-13b** and HBC-$C_{14,10}$ **3-13c** are considered to form a "plastic crystalline" phase because of their plastic deformability at room temperature[79], which stands in contrast to powdery, micro-crystalline materials such as HBC-$C_{6,2}$ **3-13a**.

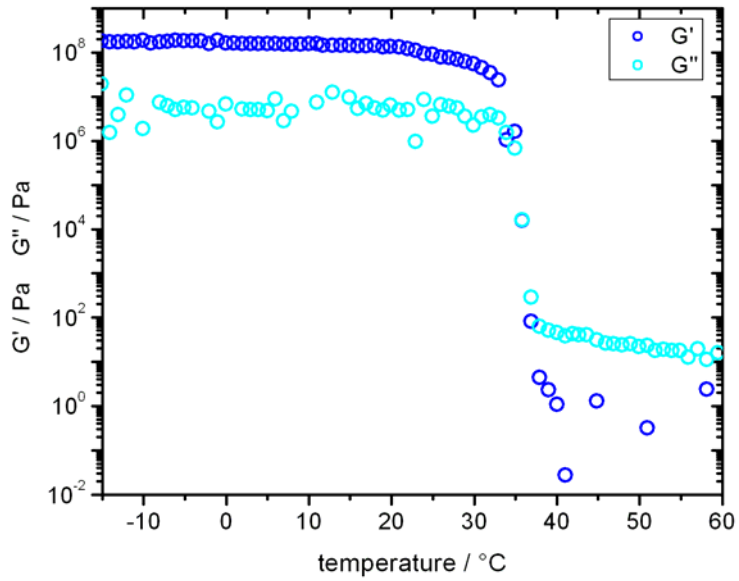

Figure 3-43: *Dynamic mechanical test of HBC-$C_{14,10}$* **3-13c***, the shear storage, G', and loss, G'', modules were recorded temperature dependent at a frequency of 10 rad/sec at a cooling rate of 2 °C/min.*

HBC-$C_{6,2}$ **3-13a** and HBC-$C_{10,6}$ **3-13b** enter the LC state at 97 °C and 24 °C, respectively, whereas HBC-$C_{14,10}$ **3-13c** showed a phase transition directly from the plastic crystalline phase to the isotropic state. The endothermic peak prior the isotropization temperature of **3-13c** might be an indication for a short liquid crystalline range.

Mechanical measurements (Figure 3-43) down to a temperature of -100 °C did not reveal any additional transition. By polarized optical microscopy (POM), HBC-$C_{6,2}$ **3-13a** was found to become an isotropic melt at *ca.* 420 °C. During heating, HBC-$C_{10,6}$ **3-13b** showed only a single transition to the isotropic phase at 93 °C, which was in contrast to the cooling cycle, where two exothermic peaks appeared at 73 °C and 45 °C.

3.3.3.2 Mechanically Aligned Fibers

The relation between molecular structure and the supramolecular organization has been investigated by temperature dependent two-dimensional wide-angle X-ray scattering (2D-WAXS) and powder X-ray diffraction. The samples for 2D-WAXS experiments were prepared by filament extrusion.[80] This mechanical orientation, where the discotic molecules are ordered due to shearing forces, has been developed

and routinely applied in our institute. The described data have been acquired by W. PISULA.

The distinct equatorial reflections in the 2D-WAXS pattern of the compounds **3-13a-c** suggested a well ordered supramolecular structure of the macroscopically oriented filaments with columns aligned along the extrusion direction. The high degree of order for HBC-$C_{6,2}$ **3-13a** and HBC-$C_{10,6}$ **3-13b** was obvious from the large number of higher order reflections in the room temperature patterns (Figure 3-44A,C).

For all three investigated HBCs, the off-meridional reflections indicated an identical tilt of the discotic cores with respect to the columnar axis with an intracolumnar period of 0.48 nm leading to a "herringbone" structure.[81] The large number of higher order off-meridional reflections of HBC-$C_{6,2}$ **3-13a** implied strong intra- as well as intercolumnar correlations between the discs. Contrary to HBC-$C_{10,6}$ **3-13b** and HBC-$C_{14,10}$ **3-13c**, where the corresponding phase was assigned to a plastic-crystalline phase due to plasticity and a slightly lower long-range correlation, HBC-$C_{6,2}$ **3-13a** formed a crystalline phase at room temperature. The distribution of the equatorial reflections in the 2D-WAXS patterns corresponded to the lateral intercolumnar arrangement.

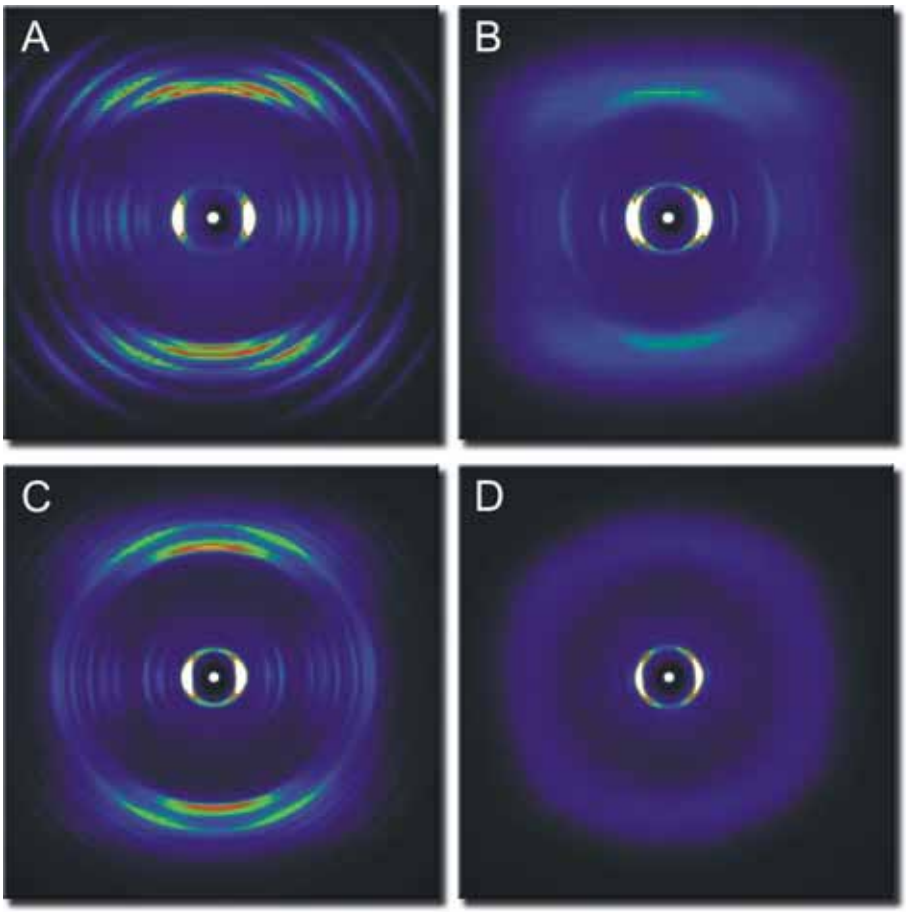

Figure 3-44: *2D-WAXS pattern of filament extruded of HBC-$C_{6,2}$* **3-13a** *(A) in the crystalline and (B) in the liquid crystalline phase, and HBC-$C_{10,6}$* **3-13b** *(C) in the plastic crystalline and (D) in the liquid crystalline phase at 60 °C.*

The intracolumnar order of HBC-$C_{6,2}$ **3-13a** and HBC-$C_{10,6}$ **3-13b** underwent a significant change when heating above the first transition as seen from the 2D-WAXS patterns (Figure 3-44B,D) typical for a LC phase. With increasing temperature, the meridional reflections corresponding to the disc-to-disc distance for HBC-$C_{10,6}$ **3-13b** faded until they completely disappeared at a temperature of 50 °C, indicating a significant decrease of the intracolumnar order in the higher temperature LC phase. For HBC-$C_{6,2}$ **3-13a**, the X-ray pattern showed that the discs maintained a tilted intracolumnar arrangement with a significantly lower degree of order than in the crystalline phase. Therefore, for both compounds the higher temperature was identified as a columnar, disordered phase, Col_d. After cooling back to room temperature and annealing at ambient conditions the initial structure of HBC-$C_{6,2}$ **3-13a** and HBC-$C_{10,6}$ **3-13b** was recovered.

The intercolumnar arrangement of the materials in different phases was investigated using powder X-ray scattering. However, the complex diffractograms and the high crystallinity at room temperature complicated the determination of a two-dimensional lateral unit cell characterizing the intercolumnar organization. A lateral monoclinic model was found to give the best fits for the room temperature diffractograms, whereby the unit cell parameters were dependent on the length of the side chains.

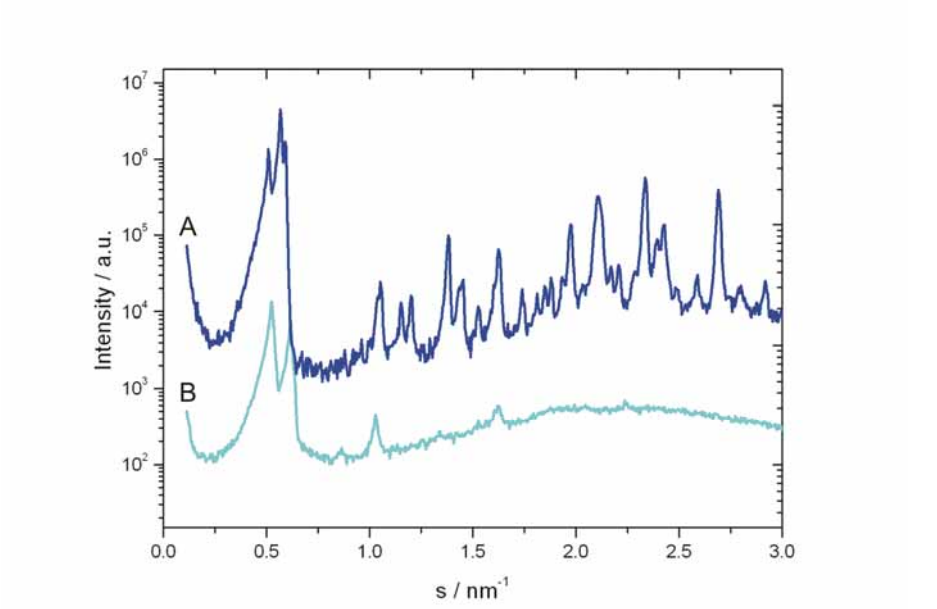

Figure 3-45: *Powder X-ray diffraction of HBC-$C_{6,2}$* **3-13a** *at (A) room temperature in the crystalline phase and (B) at the mesophase.*

The large number and high intensity of sharp reflections observed in the diffractogram of HBC-$C_{6,2}$ **3-13a**, confirmed the high crystallinity and the pronounced long-range order of the material. Especially, the intensive reflections in the wide-angle range (2 – 3 nm^{-1}) emphasized again the high degree of intracolumnar order (Figure 3-45).

A similar degree of order was found for HBC-$C_{10,6}$ **3-13b** (Figure 3-46A) and HBC-$C_{14,10}$ **3-13c** in the plastic crystalline phase, whereby the number of reflections was slightly smaller. Upon heating HBC-$C_{6,2}$ **3-13a** (Figure 3-45B) and HBC-$C_{10,6}$ **3-13b** (Figure 3-46B) to the Col_d phase, a considerable structural change occurred, accompanied by the disappearance of most reflections. Analogous to the synchrotron results, the columnar arrangement in this phase could not be assigned to a hexagonal lattice, which was unusual for six-fold substituted HBCs. Nevertheless, as implied by the high intensity of the split small-angle reflections, a well-ordered intercolumnar

packing was maintained. On the contrary, the reflections corresponding to the molecular stacking disappeared, what supported the 2D-WAXS results.

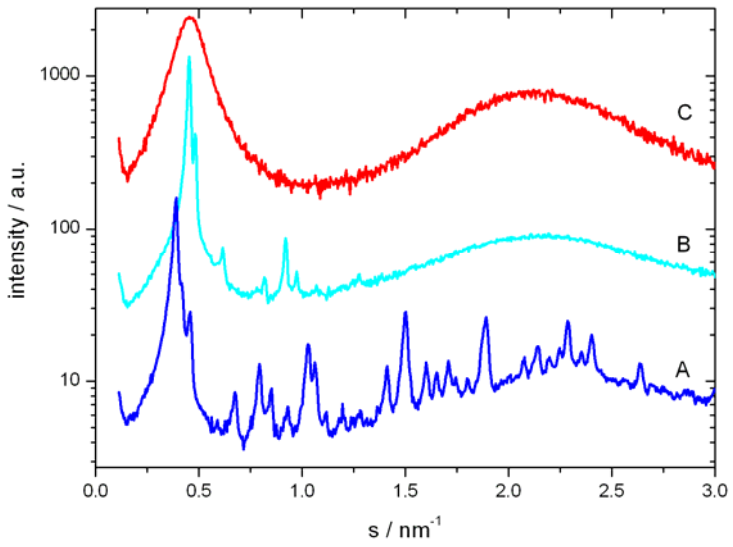

Figure 3-46: *Powder X-ray diffraction of HBC-$C_{10,6}$* **3-13b** *at (A) room temperature in the plastic crystalline phase, (B) in the Col_d liquid crystalline state, (C) in the isotropic phase.*

While heating HBC-$C_{10,6}$ **3-13b** to the optically isotropic state, a broad small-angle reflection appeared, corresponding to a periodicity of 2.2 nm as derived from the X-ray diffraction (Figure 3-46C). This reflection was attributed to a position correlation of molecular aggregates which exhibited a contrast of electron density between the aromatic core stacks and the substituents. From this relation, an average of about four HBC-$C_{10,6}$ **3-13b** molecules was determined with a relatively broad distribution, suggesting that the molecules were not monomeric in the isotropic state, but formed aggregates consisting of several discs. The same stacking number for HBC-$C_{14,10}$ **3-13c** was also calculated from the X-ray scattering pattern recorded for the isotropic state. This dynamic self-aggregation behavior in the optical isotropic, molten state resembled the organization in solution, where a similar correlation between the disc-shaped molecules has been found (chapter 3.2.1).[6]

3.3.3.3 Molecular Dynamics

^{1}H magic angle spinning (MAS) and ^{1}H-^{1}H double-quantum (DQ) MAS NMR experiments were conducted by M. MONDESHKI to probe the type of columnar packing of the HBC derivatives in their crystalline states. The ^{1}H-^{1}H DQ MAS

spectra revealed typical NMR signal patterns[82] arising from a tilted arrangement of the HBC discs, which was also referred to a "herringbone"-type packing. 1D and 2D ^{1}H-^{1}H DQ spectra exhibited three distinct resonances of the aromatic protons situated in the "bays" of the HBC cores, which were known to arise from the packing and different π-electron densities as experienced by the aromatic protons (see Figure 4-16).[83,84] When heating the samples to the respective transition temperatures into the mesophase, the HBC molecules underwent a reorientation from the tilted to a planar arrangement and started a rapid rotation around their columnar axis. In the ^{1}H MAS spectra, this transition manifested itself in the narrowing of the resonance lines. Moreover, the three distinct aromatic peaks observed in the solid state merged into a single aromatic ^{1}H resonance.

The molecular dynamics of the HBC derivatives were investigated by means of sideband patterns observed in ^{1}H-^{13}C REREDOR NMR experiments performed under fast MAS conditions. The experiments yielded local dynamic order parameters, (S), which represented the residual motional anisotropy of a given molecular segment. For alkyl side chains attached to rigid groups or backbones, a mobility gradient was expected, while the α-CH_2 group should be almost as rigid as the core, the ω-CH_3 group should exhibit the highest mobility.

For corresponding molecular segments of HBC-$C_{6,2}$ **3-13a** and HBC-$C_{10,6}$ **3-13b**, similar dynamic order parameters were found in the crystalline and plastic crystalline phase, which confirmed the expectations of a relatively rigid aromatic core and more mobile side chains. In the case of HBC-$C_{6,2}$ **3-13a**, the alkyl chain segment mobility gradually increased from the anchoring point (S ~ 0.7) at the core towards the chain ends (S ~ 0.5), while a more uniform chain mobility was determined for HBC-$C_{10,6}$ **3-13b** with a similar regional order of ~ 0.65 along the chain. For HBC-$C_{14,10}$ **3-13c**, again a pronounced mobility gradient was found, but the overall chain mobility (S ~ 0.5 → 0.15 at 16 °C) was significantly higher than in HBC-$C_{10,6}$ **3-13b** and HBC-$C_{6,2}$ **3-13a**.

When heating to the liquid-crystalline state, the fast disc rotation decreased the ^{1}H-^{13}C dipole-dipole couplings in the aromatic CH groups by a factor of two, as long as the rotation axis paralleled the columnar axis and both were perpendicular to the HBC core plane.[85] Comparing the dynamic order parameter of the cores in the LC phase, HBC-$C_{10,6}$ **3-13b** exhibited the most stable disc rotation with a maximum out-of-

plane excursion of ~ 24°. At the same time, HBC-$C_{6,2}$ **3-13a** showed a less stable rotation, as reflected by ~ 42° out-of-plane excursion, while HBC-$C_{14,10}$ **3-13c** underwent a direct transition from solid phase into melt, such that there was no well-defined liquid-crystalline phase to be studied.

The solid-state NMR experiments revealed that the core and chain mobilities in crystalline or plastic crystalline state were quite similar for HBC-$C_{6,2}$ **3-13a** and HBC-$C_{10,6}$ **3-13b** with a "cone-shaped" mobility gradient of the chain starting from the core towards the ends. On the other hand, HBC-$C_{14,10}$ **3-13c** exhibited even in the plastic crystalline state a high chain mobility due to its length. A slight temperature increase resulted in extremely high dynamics longest branched side chains and finally in the breaking of the columnar structures leading to the isotropic phase. For HBC-$C_{10,6}$ **3-13b**, the isotropization was reached at slightly higher temperatures (T_i = 93 °C). Both examples are in contrast to linear alkyl substituted derivatives, where the isotropization temperature was not reached before 400 °C. Certainly, the branching site close to the aromatic core bears steric demand during the assembly and resulted in a suppression of the mesophase for HBC-$C_{14,10}$ **3-13c** and in a direct melting from the plastic crystalline phase.

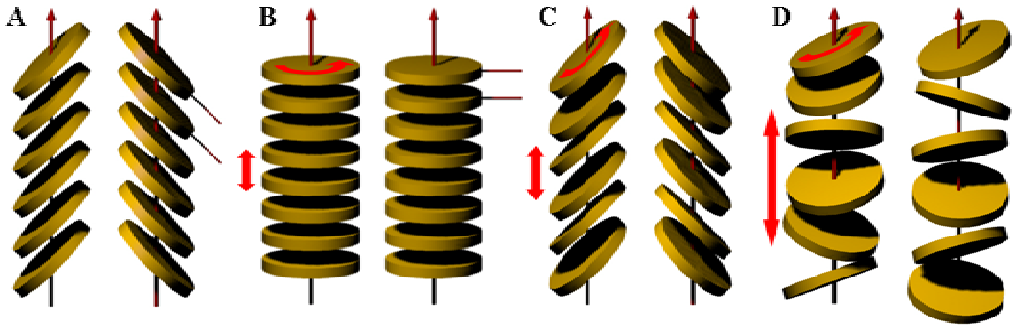

Figure 3-47: *Schematic illustration of the arrangement of the aromatic core in (A) the herringbone order, (B) the planar arrangement which is characteristic mesophase-organization for HBCs substituted by alkyl chains with a low steric demand, (C) the disordered columnar arrangement of the HBC-$C_{6,2}$* **3-13a** *and (D) of the HBC-$C_{10,6}$* **3-13b** *discs in the mesophase. Thereby, the discs possess a rapid rotation around the columnar axes, whereby the longitudinal fluctuations increase with longer side chains.*

The investigation of the thermal behavior indicated that the introduction of a high steric demand can efficiently lower the phase transitions and open the opportunity for the melt processing, what has been exploited in the previous chapters.

Solid-state NMR and X-ray diffraction experiments were conducted to provide an insight into the influence of the side chains on both the macro- and nanoscopic level. At the room temperature phase of HBC-$C_{6,2}$ **3-13a**, HBC-$C_{10,6}$ **3-13b** and HBC-$C_{14,10}$ **3-13c** revealed a high degree of order confirmed by the X-ray scattering results. The herringbone arrangement was verified for all investigated compounds by both solid-state NMR and X-ray experiments (Figure 3-47A). In comparison to other discotics substituted by bulky alkoxy side chains possessing a relatively low isotropization temperature, a high intracolumnar organization at ambient temperatures is quite exceptional as other discotics show an ordered columnar phase far below 0 °C. The reason for the pronounced intracolumnar packing might be the crystallization of the purely hydrocarbon alkyl chains at ambient temperatures due to sufficient rigidity. The introduction of functional groups containing oxygen atoms would increase the chain flexibility, but lower the intracolumnar order.[6] On the other hand, the heating of HBC-$C_{6,2}$ **3-13a** and HBC-$C_{14,10}$ **3-13c** to the mesophase resulted in the increase of the intracolumnar disorder because of the higher dynamics of the resulting bulkiness of the side chains, what was pronounced for HBC-$C_{10,6}$ **3-13b**. Together with the value for the out-of-plane motion, it became clear, that the disc-like molecules were 24° arranged with respect to the columnar axis and bounced on top of each other (Figure 3-47D), which led to a fading of the π-stacking reflection in the X-ray diffractogram. On the other hand, the shorter chains in HBC-$C_{6,2}$ **3-13a** did not prevent the core from approaching, but caused a wobbling of the discs, leading to the appearance of the intracolumnar correlation in the X-ray pattern for the mesophase. The solid-state NMR experiments verified the out-of-plane excursion of ca. 42°, which was identical to the tilting angle in the crystalline phase (Figure 3-47C). Due to this asymmetric shape of the columns, both HBC-$C_{6,2}$ **3-13a**, and HBC-$C_{10,6}$ **3-13b** did not reveal a hexagonal intercolumnar arrangement in the LC phase, which was atypical for symmetrically six-fold substituted HBCs. In contrast to the pronounced order in the room temperature phases, the columnar mesophases at elevated temperatures revealed a significant degree of disorder. This behavior was exceptional, especially when compared to HBC derivatives where linear alkyl substituents were introduced.[80,81]

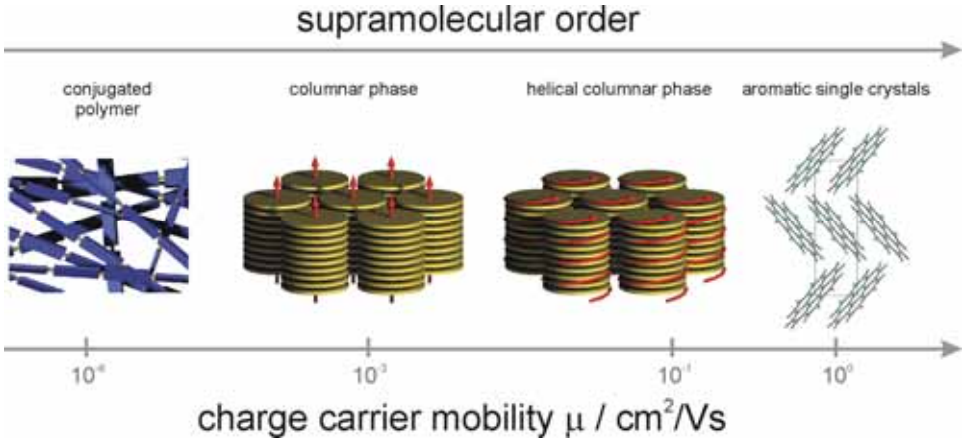

Figure 3-48: *Illustration of the relation between supramolecular order and the charge carrier mobility.*

The three HBC derivatives with the branched alkyl substituents exhibited ordered columnar structures in their crystalline, room temperature state. The discotic molecules were organized in a regular columnar stacking, which packs in a two-dimensional lattice. However, the molecules within the columnar arrangement are not crystallized on a large length scale. Translational or rotational motions could still be excerted by the disc-like molecules, what has been observed in solid state NMR experiments.[81] Such molecular motions are not desired because the charge-carrier mobility depends sensitively upon the perfection of a structure. It is well known that crystalline, discotic columnar arrangements, such as a helical discotic superstructure, where the molecules are crystalline within the three-dimensional lattice, is beneficial for a high mobility of charge carriers along the columnar structure.[86] The following chapter presents a concept, how to modify the intracolumnar stacking behavior of the electron rich HBC molecules by adding an electron poor, discotic system.

3.3.3.4 Manipulation of the Superstructure

A concept to tune properties of materials is the blending of two different compounds. Analogous to the mixing of two linear polymers, various effects can be expected reaching from a phase separation in the blend to the formation of a homogenous one-phase system. For two polymers the blending enthalpy determines whether the mixture will be homogenous or phase separated.[87] The mixing of two macromolecules, which self-assemble into superstructures, is complex, since additional interactions between the different components complicate the description of the system.[88] As illustrated in Figure 3-49, several different supramolecular

organizations can be formed in the mixture. For discotic molecules, which self-assemble in columnar superstructures by π-stacking, ranging from a heterogeneous phase to micro- as well as nanoseparation.

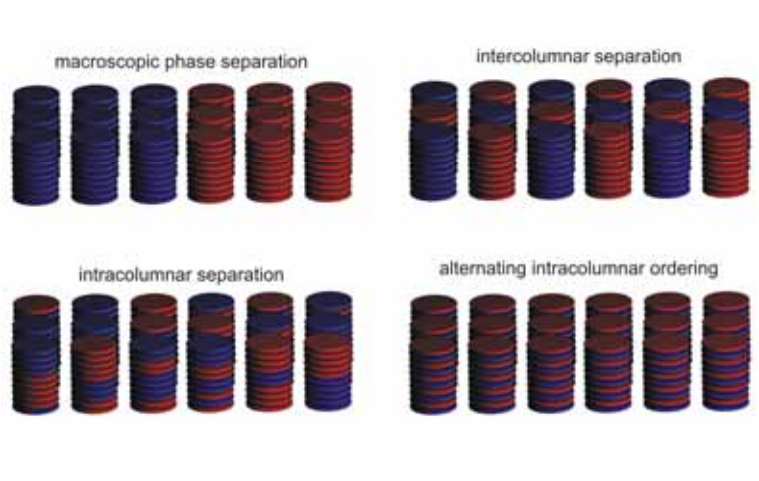

Figure 3-49: *Schematic illustration of different possible supramolecular organizations in a mixture of two discotic compounds with different molecular architectures.*

Intensive investigations of mixtures containing triphenylene as the donor compound have been carried out, whereby trinitrofluorenone,[88,89] azatriphenylenes[90,91] or mellitic triimides[92] were used as acceptor molecules. For equimolar mixtures alternated stacking of the acceptor and donor molecules has been observed leading to an enhanced columnar stability. Time-of-flight experiments verified an enhanced columnar organization by revealing considerably higher charge carrier mobilities for the blends.[93-95]

In this chapter, the effect of blending two discotic materials, which differ significantly in their electronic properties, will be presented. While the already described HBC-$C_{10,6}$ **3-13b** is an electron donating agent, perylene diimide (PDI-$C_{8,7}$) **3-19** or terrylene diimide (TDI-$C_{8,7}$) **3-20** derivatives are acceptors.

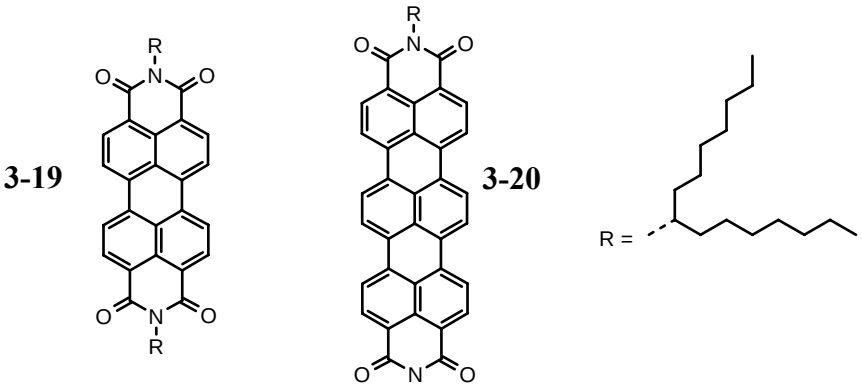

Figure 3-50: *Chemical structure of PMI-$C_{8,7}$* **3-19** *and TDI-$C_{8,7}$* **3-20**

Therefore, the two molecules showed a weak electronic interaction which was indicated by semiempirical calculations (Figure 3-51). One expected a stabilization due to alternating stacking in the columnar structure and thus an induction of ordering in this donor-acceptor mixture. Additionally, the blended molecules were compatible in size, permitting a matched intracolumnar packing, leading to a different self-organization on a surface.

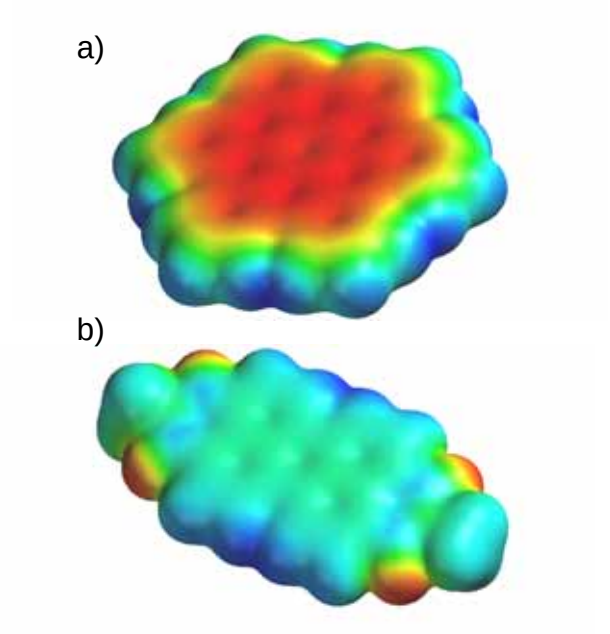

Figure 3-51: *Semiempirical AM1 show the electrostatic potential of a)* **3-13b** *and b)* **3-19** *(red indicates electron-rich areas, blue electron-poor).*

The rylene dyes have been synthesized by F. NOLDE and C. KOHL in our research group. The following investigations were carried out in a collaboration with W. PISULA, who recorded and interpreted *inter alia* the 2D-WAXS diffractograms and supported me with the POM experiments.

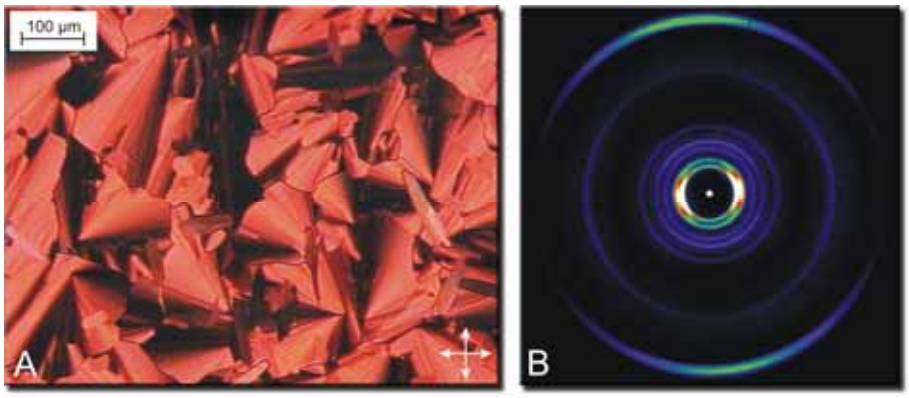

Figure 3-52: *A) POM image after crystallization and B) room temperature 2D-WAXS pattern of PDI-$C_{8,7}$* **3-19**.

The columnar organization of the HBC with the branched alkyl chain has been exhaustively discussed in the previous chapters, showing 2D-WAXS and POM results (see chapter 3.3.2.1 and 3.3.3.2). For PDI-$C_{8,7}$ **3-19**, an optical texture with pseudo focal conical fan-shapes during crystallization (T_i = 130°C) was observed in the POM, indicating the formation of a mesophase, where the molecules were orthogonally arranged with respect to the stacking axis, as was confirmed by the 2D-WAXS (Figure 3-52B). An identical intracolumnar arrangement was determined for **3-20** which formed large ordered domains during cooling from the isotropic phase with edge-on oriented molecules.

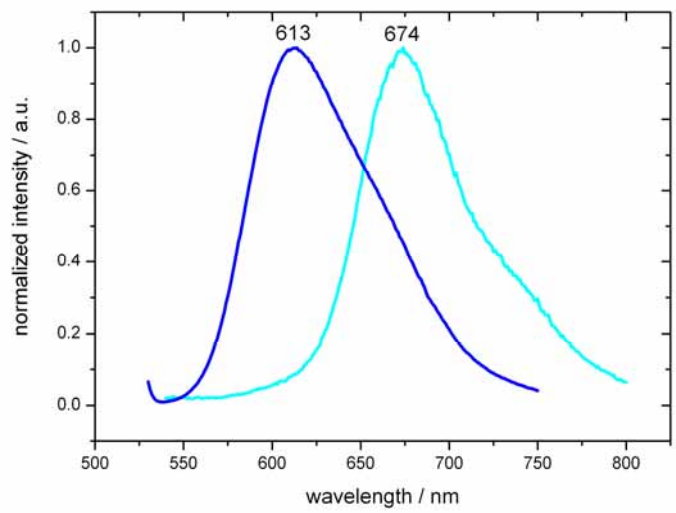

Figure 3-53: *Photoluminescence excitation spectra at an excitation of 360 nm for a equimolar mixture of HBC-$C_{10,6}$* **3-13b** *and PDI-$C_{8,7}$* **3-19** *in solution (blue) and in a drop-cast film (cyan).*

Mixtures of HBC-$C_{10,6}$ **3-13b** with PDI-$C_{8,7}$ **3-19** or TDI-$C_{8,7}$ **3-20** were first prepared at a certain molar ratio in solution and afterwards blended in the isotropic phase to avoid demixing due to different solubilities. The investigation of the thermal behavior

by differential scanning calorimetry (DSC) revealed that all prepared mixtures formed a macroscopic, homogeneous phase.

Photoluminescence excitation spectra for an equimolar mixture of HBC-$C_{10,6}$ **3-13b** and PDI-$C_{8,7}$ **3-19** in solution showed a superposition of the spectra of the pure components. In contrast, drop-cast films of the blend showed a shift of the fluorescence signal of PDI-$C_{8,7}$ **3-19** by 60 nm accompanied by a strong quenching which was expected because of energy transfer processes (Figure 3-53). The significant change of the electronic environment of the chromophore was supported by the differential pulse voltammetry measurements. These displayed an additional peak for the mixture which was shifted by 0.18 eV in comparison to pure PDI-$C_{8,7}$ **3-19** (Figure 3-54).

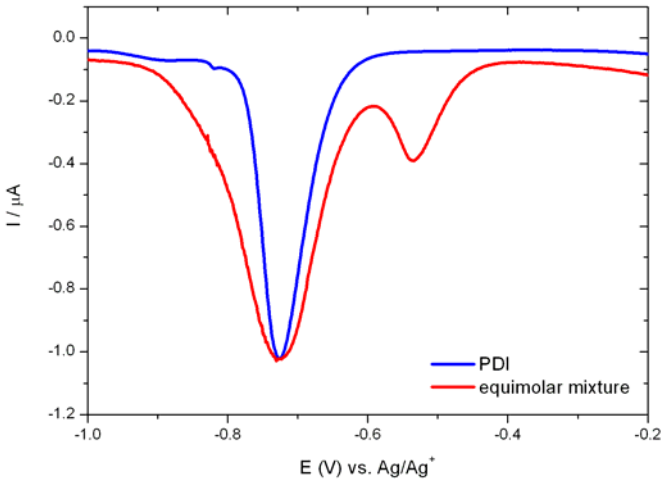

Figure 3-54: *Differential pulse voltammetry for a equimolar mixture (red) of HBC-$C_{10,6}$* **3-13b** *and PDI-$C_{8,7}$* **3-19** *and of pure PDI-$C_{8,7}$* **3-19***, both as a drop-cast film.*

The 2D-WAXS pattern of the equimolar mixture of HBC-$C_{10,6}$ **3-13b** and PDI-$C_{8,7}$ **3-19** exhibited a considerable difference of the supramolecular arrangement in the blend (Figure 3-55). The X-ray pattern changed significantly, when the extruded sample was annealed for 48 hours at ambient conditions, whereby the number of distinct reflections increased dramatically. A set of new higher order reflections appeared, indicating an exceptional long-range order and a complex helical arrangement of the two discotic species within the columnar stacks. The transformation of the first equatorial reflection was thereby particularly impressive which converted from the isotropic shape (Figure 3-55A) to three sharp peaks. This

implied not only a simple intracolumnar reorganization but also a rearrangement of entire columnar segments.

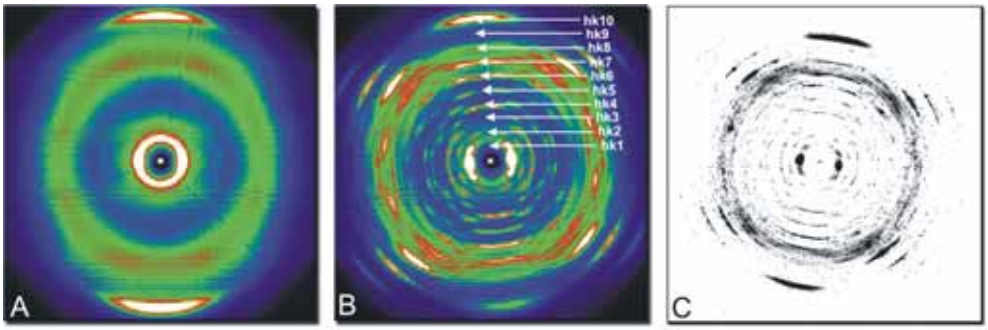

Figure 3-55: *2D-WAXS of an equimolar mixture of HBC-$C_{10,6}$* **3-13b** *and PDI-$C_{8,7}$* **3-19***, A) directly after extrusion and B) after annealing for 48 hours C) local resolution obtained with microfocussed synchrotron beam.*

The layered distribution of the reflections in the meridional direction in the WAXS pattern in Figure 3-55B is identified by the MILLER's indices (hkl) which were assigned to the intracolumnar packing.[96] The nearest intracolumnar repeating distance between single building blocks was 0.34 nm and related to the meridional reflection, which determined the number of 10 molecules per helical pitch, indicating strong correlations over long distances (helical pitch distance 3.4 nm).

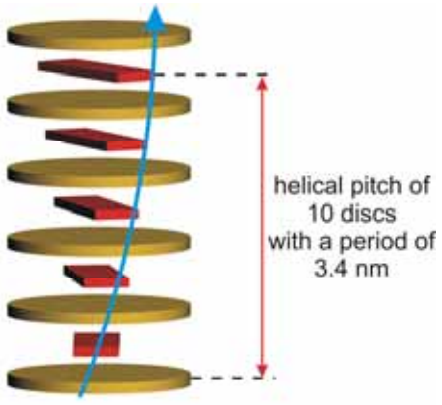

Figure 3-56: *Schematic packing model of an alternating intracolumnar arrangement for the binary mixture. PDI-$C_{8,7}$* **3-19** *are intercalated between HBC-$C_{10,6}$* **3-13b** *which was displaced by 12° with respect to each other leading to the formation of a helical pitch of 3.4 nm.*

The suggested model for the supramolecular arrangement is illustrated in Figure 3-56. It is assumed that an alternating molecular packing gave rise to the helical organization. Thereby, PDI-$C_{8,7}$ **3-19** intercalated between the HBC-discs, which were rotated with respect to each other by 12° providing the necessary contrast for the helical pitch. This molecular rotation was induced by the space demand of the

attached alkyl chains in both derivatives. Recently, helical columnar arrangements have been observed for HBC derivatives substituted by rigid side groups.[97] The electronic donor-acceptor interactions are held responsible for the observed pronounced alternating intracolumnar ordering as reported for a single crystal arrangement consisting of hexafluorobenzene and fullerene which were confirmed by fluorescence and differential pulse voltammetry measurements.[98] 2D WAXS scattering experiments using the microfocussed synchrotron beam revealed locally an even higher crystallinity (Figure 3-55C) in the extruded fiber.

To gain a more detailed insight into the supramolecular arrangement of other mixtures, complementary compositions of 1:2 and 2:1 have been investigated. All extruded samples revealed significantly higher order after annealing. The 2D-WAXS pattern of both blends displayed reflections at identical positions as observed for the 1:1 blend, but with different reflection intensities, which depended on the composition ratio. The additional reflections reached their maximum intensity for the 1:1 molar ratio, possibly due to homo-sequences of excess components in the non-equimolar mixtures.

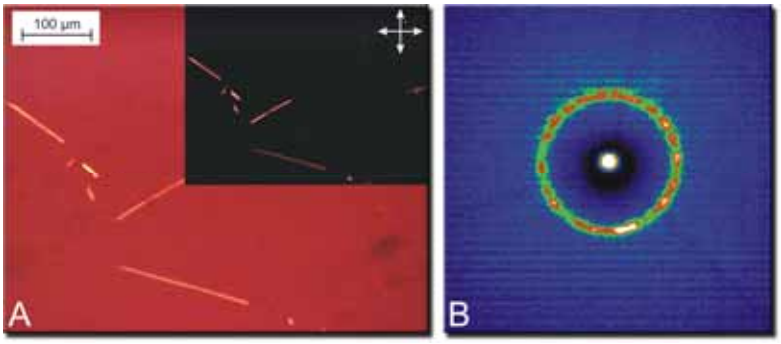

Figure 3-57: *Example for a homeotropically aligned sample based on the mixture of HBC-$C_{10,6}$* **3-13b** *and PDI-$C_{8,7}$* **3-19** *of a molar ratio of 2:1 a) image from the optical microscopy (inset in cross-polarizers) and b) characteristic 2D-WAXS pattern of the film with homeotropic order (identical hexagonal lattice in different small domains led to the multiple appearance of reflections).*

The new supramolecular structure in the blends influenced significantly the thermal behavior and the morphology. When a mixture of HBC-$C_{10,6}$ (**3-13b**): PDI-$C_{8,7}$ (**3-19**) of a ratio 2:1 was cooled from the isotropic phase between two glass slides, a homogenous film was obtained not revealing significant birefringence in polarized light, which is characteristic for a homeotropic phase (Figure 3-57A). The transmission 2D-WAXS pattern of the film confirmed the proposed orientation (Figure 3-57B), whereby the lateral arrangement of the lattice differed considerably

between the domains. This morphology stands in contrast to the one of the homo-components. A similar morphology was also obtained for mixtures of other compositions, however, the number of birefringent defects increased significantly.

Films of mixed samples of HBC-$C_{10,6}$ **3-13b** and TDI-$C_{8,7}$ **3-20** revealed a homeotropic organization analogous to the decribed mixture with PDI-$C_{8,7}$ **3-19**. The morphology of the crystallized mixture, however, exhibited beautiful morphologies (Figure 3-58). The monoclinic unit cell for pure HBC-$C_{10,6}$ **3-13b** (see chapter 3.3.2.2) was changed to a hexagonal packing when the rylene dyes were added, which led to the disappearance of the birefringence in the POM.

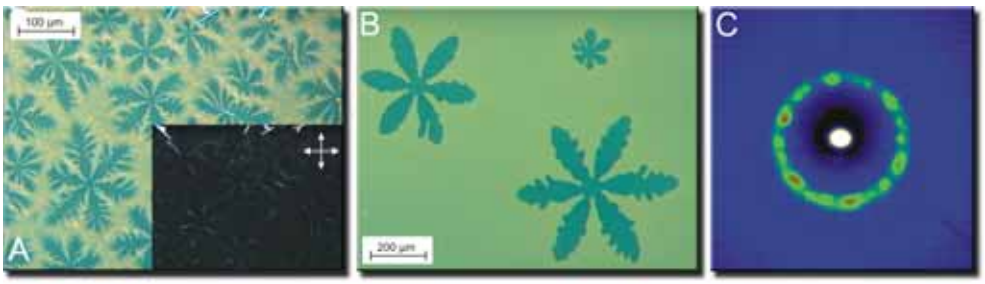

Figure 3-58: *Example for a homeotropically aligned sample based on the mixture of HBC-$C_{10,6}$* **3-13b** *and PDI-$C_{8,7}$* **3-19** *of a molar ratio of 2:1 image from the optical microscopy (inset in cross-polarizers) (A) after crystallization and (B) during crystallization. (C) characteristic 2D-WAXS pattern of the film with homeotropic order.*

In general, HBCs with alkyl substituents possessing a low steric requirement close to the aromatic disc align homeotropically when cooled down from the isotropic phase.[6] When the π-stacking interaction between the aromatic cores is significantly reduced in the isotropic phase, the molecules arrange face-on towards the surface (see chapter 3.3.2.3). This arrangement is assumed to be the most thermodynamically favorable, since the interaction, such as VAN-DER-WAALS, between the molecule and the surface is maximized. On the other hand, high steric demand of the alkyl chains at the vicinity of the aromatic core might hinder an approaching of the disc to the surface as seen for HBC-$C_{14,10}$ **3-13c**[99] (chapter 3.3.2.2).

The electronic interaction between HBC-$C_{10,6}$ **3-13b** and PDI-$C_{8,7}$ **3-19** resulted in the strictly alternating stacking of the donor and acceptor species. The enhancement of the columnar packing due to the addition of an auxilary component is a new approach, which has not been described before. The interactions lead to a helical crystallization of the columns, which is thought to yield a higher charge carrier

mobility along the stacks. However, one can speculate that excitons become trapped between the molecules of different polarity, which is currently under investigation.

The following chapter deals with the investigation of the charge carrier mobility of pure HBC derivatives with different methods. This is an important step to investigate weather the material possess promise for a successful implementation in an electronic device.

3.4 Charge Carrier Mobility

3.4.1 Pulse-Radiolysis Time-Resolved Microwave Conductivity

The charge transport properties of the presented branched HBC derivatives were studied by pulse-radiolysis time-resolved microwave conductivity (PR-TRMC, see introduction) technique. In this method charge carriers are generated in a nondestructive way by means of a very short pulse of high-energy radiation and are concurrently monitored with a time-resolved microwave detection system. The short formation time (nanoseconds) of the charge carriers and the high frequency of the microwave field used, make the PR-TRMC technique capable of monitoring charge carriers within the organized domains of polycrystalline materials. Furthermore, ohmic contacts or tedious sample preparations are redundant. These advantages make this technique highly appropriate for a charge transport study of discotic liquid crystalline materials. The measurements were conducted by J. PIRIS in the group of J. WARMAN in Delft, Netherlands.

Pulse irradiation of compounds **3-13a-c** resulted in very long-lived conductivity transients, relatively to other HBC derivatives studied before. This was evidenced not only by the long-range intracolumnar order but also by the high purity of the materials as a result of their high solubility and, hence, ease of purification.

Table 3-5: *Intracolumnar charge carrier mobilities for the dove-tailed HBC derivatives.*

Sample	Phase	$\Sigma\mu_{1D}$ / $cm^2V^{-1}s^{-1}$
HBC-$C_{6,2}$ **3-13a**	C_r	0.25
	Col_d	0.29
HBC-$C_{10,6}$ **3-13b**	Col_p	0.73
	Col_d	0.08
HBC-$C_{14,10}$ **3-13c**	Col_p	0.47

From the end-of-pulse conductivity the sum of the intracolumnar charge carrier mobilities, $\Sigma\mu_{1D}$, has been determined as a function of temperature. The values obtained for the different phases are summarized in Table 3-5. The temperature behavior of the present compounds differed notably from the previously studied HBC derivatives;[100] in general, the mobility increases slightly with temperature in the

crystalline phase until it experiences a sudden decrease by a factor of *ca*. 2 on entering the mesophase.

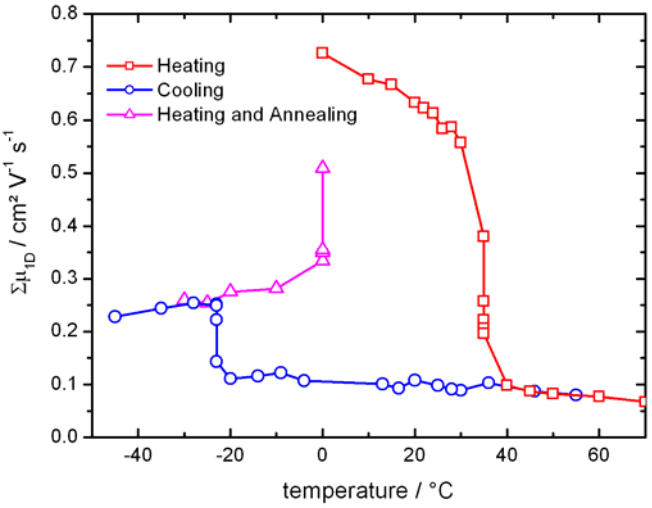

Figure 3-59: *The temperature dependence of the one-dimensional mobility for the first heating (red squares), cooling (blue circles) and final heating back to room temperature (magenta triangles) for the dove-tailed HBC-$C_{10,6}$* **3-13b**.

Most HBC derivatives showed a similar $\Sigma\mu_{1D}$ value of *ca*. 0.3 cm^2/Vs in their columnar hexagonal mesophases. In contrast, the mobility of 0.3 cm^2/Vs for HBC-$C_{6,2}$ **3-13a** did not experience any significant change when going from the crystalline to the liquid crystalline phase. Figure 3-59 represents the temperature behavior of the intracolumnar charge carrier mobility for HBC-$C_{10,6}$ **3-13b**. The room temperature value $\Sigma\mu_{1D}$ = 0.73 cm^2/Vs was the highest measured for a non-crystalline phase and was only overcome by the crystalline tetradecyl substituted derivative (HBC-C_{14}) ($\Sigma\mu_{1D}$ = 1.00 cm^2/Vs).[101] Upon heating the mobility decreased almost linearly with temperature until it experienced a sudden drop of almost an order of magnitude upon conversion to the liquid crystalline phase.

Compound HBC-$C_{14,10}$ **3-13c** was also plastic crystalline at room temperature and accordingly showed a mobility value comparable to the crystalline HBC derivatives. The PR-TRMC measurements provided information about the charge carrier mobility in different phases and were correlated with results described for the columnar packing. The one-dimensional charge carrier transport of HBC-$C_{10,6}$ **3-13b** was strongly dependent on the intracolumnar order and the molecular packing. Disorder resulted in a lowering of the mobility as observed for the liquid crystalline phase of

this compound (see chapter 3.3.3.3). In the highly ordered phases, however, HBC-$C_{10,6}$ **3-13b** and HBC-$C_{14,10}$ **3-13c** yielded exceptionally charge carrier mobilities comparable with highly crystalline HBCs. Identical mobility values for a non-crystalline discotic phase were only observed for lutetium phthalocyanine dimers, but rather due to a small intermolecular distance of 0.33 nm.[102] The two features, long life-time and high mobility of charges, are important requirements for the application of these HBC derivatives in electronic devices and make them very attractive as organic semiconductors.

A very striking result was the extraordinary long life-times of the charge carriers induced in the PR-TRMC measurement, compared to other known HBC derivatives, which have been synthesized in our group. Therefore, it became possible to compare HBC derivatives with different side chains to gain insight into the mechanism of charge carrier recombination, which will be discussed in the following.

3.4.2 Life-Time of Charge Carriers

Pulsed ionization of the peripherally alkyl-chain-substituted HBC derivatives, shown in Figure 3-60, resulted in the temporary formation of mobile charge carriers as evidenced by readily measureable transient changes in conductivity.

The interest in such measurements was mainly focused on the one-dimensional, intracolumnar charge mobilities, $\Sigma\mu_{1D}$, which can be derived from the end-of-pulse value of the conductivity, $\Delta\sigma_{eop}$.[100] The mobilities determined for the crystalline solid phase of all of the HBC derivatives studied are listed in Table 3-6. The values of $\Sigma\mu_{1D}$ are seen to vary by less than a factor of 4 from a high of 1.00 cm^2/Vs for HBC-C_{14} **3-22** to a low of 0.26 cm^2/Vs for HBC-$C_{6,2}$, with no systematic dependence on the structure of the peripheral alkyl chains. These mobility values correspond to intra-columnar charge hopping times of 40 and 160 fs respectively. The relative insensitivity of the mobility to the nature of the alkyl group substituents is as expected if charge transport occurs within the columnarly stacked HBC cores. In contrast to the mobility, which is derived from the end-of-pulse conductivity, the after-pulse decay is found to depend dramatically on the nature of the alkyl chains. This can be qualitatively extracted from Figure 3-61.

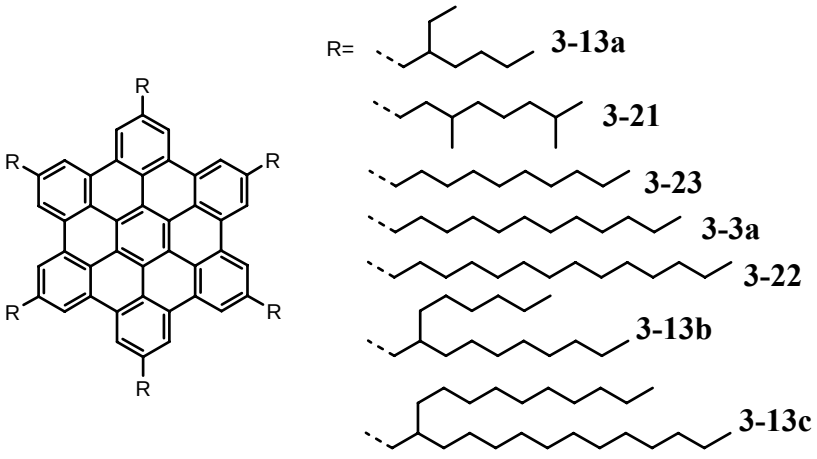

Figure 3-60: *Molecular structures of the investigated HBC derivatives.*

Table 3-6: *The molecular weight, M, disk diameter, d, charge mobility, $\Sigma\mu_{1D}$, kinetic dispersion parameter, α, and exponentional decay time, τ_e, determined for peripherally substituted derivatives of HBC.*

derivative	M / g mol^{-1}	D / Å	$\Sigma\mu_{1D}$ /cm^2 V^{-1} s^{-1}	α	τe / µs
HBC-$C_{6,2}$ **3-13a**	1182	23.4	0.26	0.22	0.24
HBC-$C_{8,2}$ **3-21**	1350	25.4	0.50	0.22	0.49
HBC-C_{10} **3-23**	1350	25.4	0.43	0.28	0.32
HBC-C_{12} **3-3a**	1518	26.8	0.70	0.33	1.55
HBC-C_{14} **3-22**	1686	29.0	1.00	0.46	6.80
HBC-$C_{10,6}$ **3-13b**	1854	30.7	0.72	0.39	24.20
HBC-$C_{14,10}$ **3-13c**	2526	36.6	0.48	0.47	840.00

The results demonstrate the pronounced systematic increase in the timescale of the decay, from a few hundred nanoseconds to almost a millisecond, as the length of the alkyl main chain increases from 6 to 10 to 14 carbon atoms. If one compares data for derivatives with the same main chain length but with and without an additional alkyl side chain, considerably longer decay times for the branched-chain compounds

clearly indicate that the decay is a function of the total number of aliphatic carbon atoms rather than the length of the longest chain. An analogous dramatic increase in the timescale for the decay of the radiation-induced conductivity was previously reported for a series of octa-*n*-alkoxy-subsituted phthalocyanines with chain lengths varying from 6 to 18 carbon atoms.[103,104]

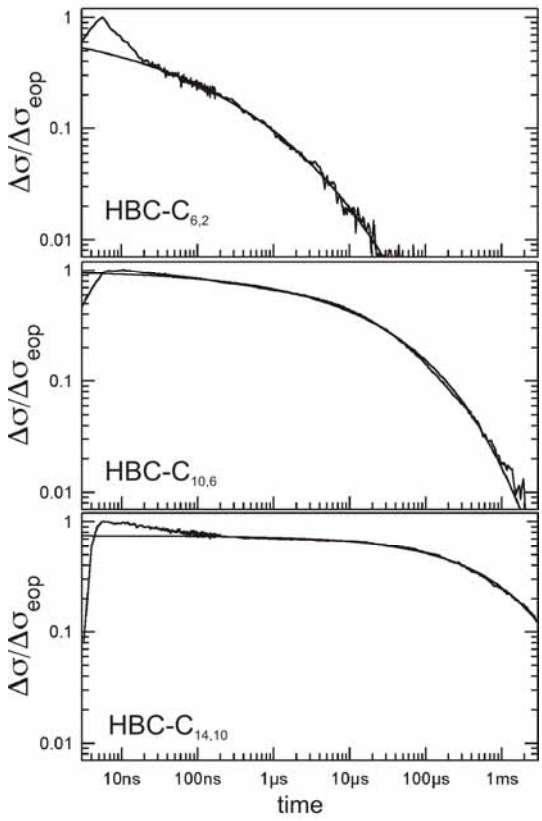

Figure 3-61: *The temporal dependence of the conductivity, normalized to the end-of-pulse value, on 5 ns pulsed ionization of HBC-$C_{6,2}$* **3-13a**, *HBC-$C_{10,6}$* **3-13b**, *and HBC-$C_{14,10}$* **3-13b** *illustrating the dramatic increase in lifetime of the charge carriers with increasing length of the alkyl chains.*

This was explained by a mechanism in which the "long-lived", after-pulse conductivity was attributed to those electron hole pairs for which the electron and the hole become localized on separate columnar stacks. Their recombination is then retarded by the aliphatic hydrocarbon mantle between the stacks and can only occur via intercolumnar electron tunneling. The processes envisaged are illustrated schematically in Figure 3-62. In accordance with this explanation, the decay time was found to obey an exponential dependence on the intercolumnar distance.[103,104] We conclude that the same explanation underlies the systematic increase by 4 orders of magnitude in decay time with increasing size of the peripheral alkyl substituents observed for the present HBC derivatives. An alternative explanation of such a

dramatic systematic effect can be considered, in terms of trapping of the mobile carriers by spurious impurities or domain boundaries, to be extremely unlikely.

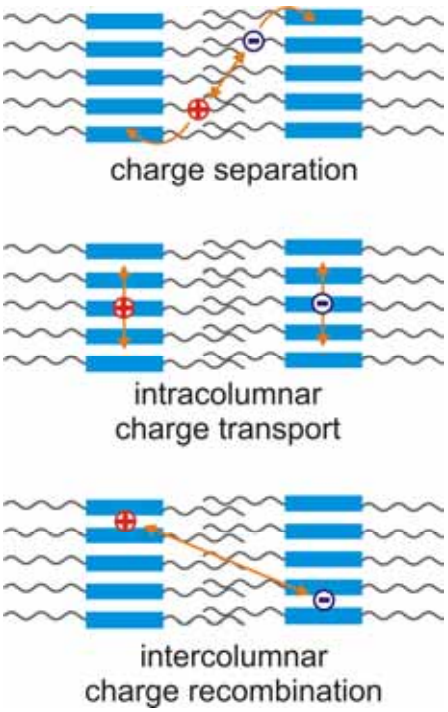

Figure 3-62: *A schematic representation of the processes occurring subsequent to pulsed ionization of the discotic materials studied in the present work.*

The timescale of the after-pulse decay of the conductivity is found to increase dramatically and systematically by orders of magnitude with increasing carbon number of the chains. The 1/e decay time, τ_e, is in fact found to depend exponentially on the effective diameter of the discotic molecules, D, according to[105]

$$D = \sqrt{4\frac{V_c + (M - M_c)}{\rho_m N_A}} \Big/ \pi \cdot d$$

with d as the disk thickness, V_c is the volume of the HBC core, M is the molecular weight, M_c is the molecular weight of the core, ρ_m is the density of the aliphatic mantle, and N_A is Avogadro's constant. The values of d and V_c are taken to be 3.5 Å (the cofacial distance between the stacked aromatic cores) and 410 Å^3 respectively as determined by X-ray diffraction.[106] The value of ρ_m is taken to be 0.95 g/cm^3 as determined for the density of the intervening alkane regions for a series of crystalline octa-*n*-alkoxy-substituted phthalocyanines.[104] The values of D derived are listed in Table 3-6. The decay time τ_e can be calculated with

$$\tau_e = \tau_e(0) \exp(\beta D)$$

which is in very good agreement with the experimental data (Figure 3-63) with $\tau_e(0)$ = 48 fs and $\beta = 0.63$ Å^{-1}.

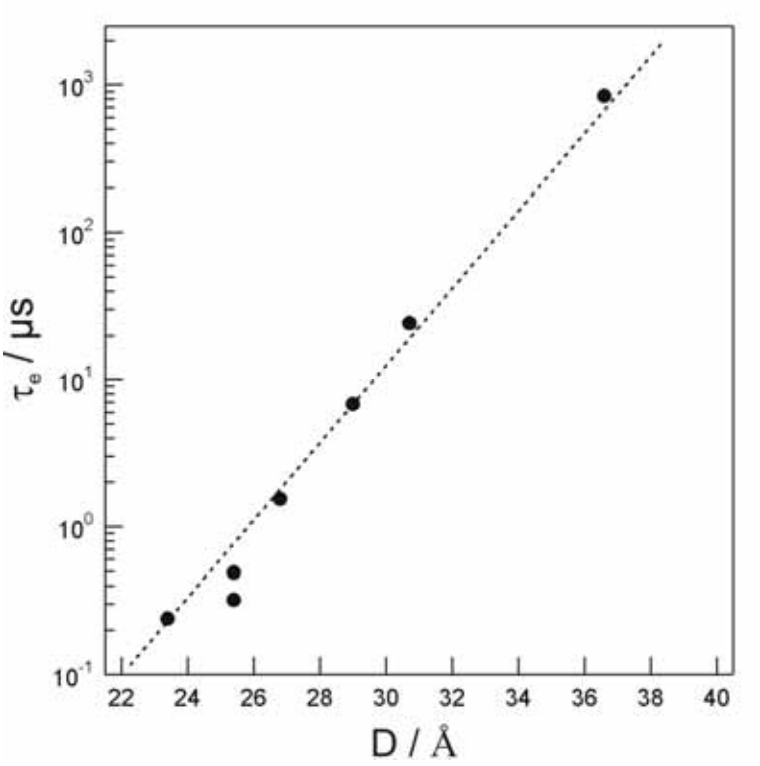

Figure 3-63: *A semilogarithic plot of the exponential conductivity decay time, τ_e, versus the calculated disk diameter, D, for hexa-alkyl derivatives of HBC. The straight line drawn through the points corresponds to an exponential dependence of τ_e on D with $\beta = 0.63$ Å^{-1} and τ_e (0) = 48 fs.*

This exponential dependence is attributed to the occurrence of charge recombination via intercolumnar electron tunnelling through the aliphatic hydrocarbon medium separating the aromatic columnar stacks. Taking into account the tilted stacking configuration of the molecules in the crystalline phase, the β parameter for the distance dependence of intercolumnar electron tunnelling is estimated to be close to 0.8 Å^{-1}. The absolute values of τ_e for a given value of D found for the present HBC derivatives are close to those determined in a previous investigation of octa-*n*-alkoxy-phthalocyanines suggesting the tunnelling kinetics to be independent of the nature of the (hetero)aromatic core.[107] In view of the similarity between the interdigitated alkyl chains within the mantles of the present HBC derivatives and those of the hydrocarbon chains in lipid bilayers, we suggest that the information obtained in the present work may be relevant to electron tunneling through cellular membranes. For a

membrane thickness of 40 Å, a cross-membrane tunneling time of close to one millisecond would be predicted.

3.4.3 Time-of-Flight

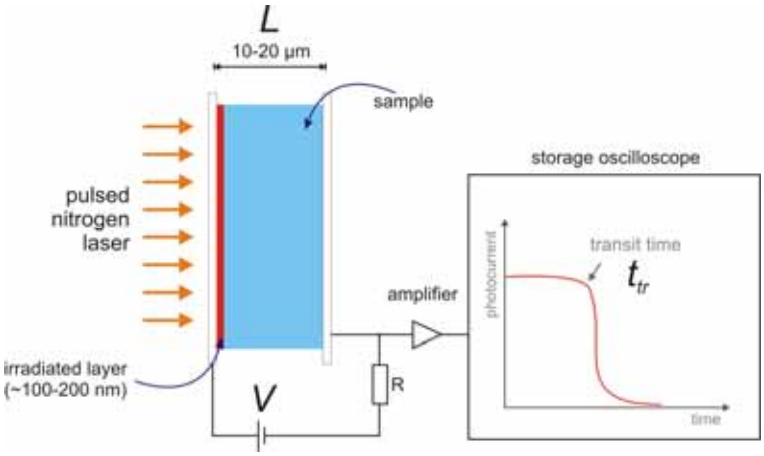

Figure 3-64: *Schematic representation of the TOF set-up.*

In the time-resolved technique[108,109], which is schematically depicted in Figure 3-64, the charge carriers are generated in a constant electric field by illumination with a short laser pulse. Owing to the small penetration depth of the incident laser light, charge carriers are formed only in the thin layer at the transparent, front electrode. The transport of the charge carriers in the applied electric field to the counter electrode induces a displacement current which can be detected with a current amplifier and a storage oscilloscope. Examples of typical photocurrent transients are shown in Figure 3-65.

Such a transient can be approximated by two linear components with different slopes at short and long times. The time-of-flight or transit time, t_{tr}, is defined as the time where these lines intersect. The mobility of the charge carriers, μ, can be calculated from t_{tr} as follows:

$$\mu = \frac{L^2}{V \cdot t_{tr}}$$

where L is the sample thickness and V the applied voltage. The TOF method provides a direct measurement of the charge carrier mobility and requires no knowledge of the concentration of charge carriers. An important advantage of the TOF method is that the contributions of positive and negative carriers can be measured separately, simply by inverting the polarity of the applied electric DC field.

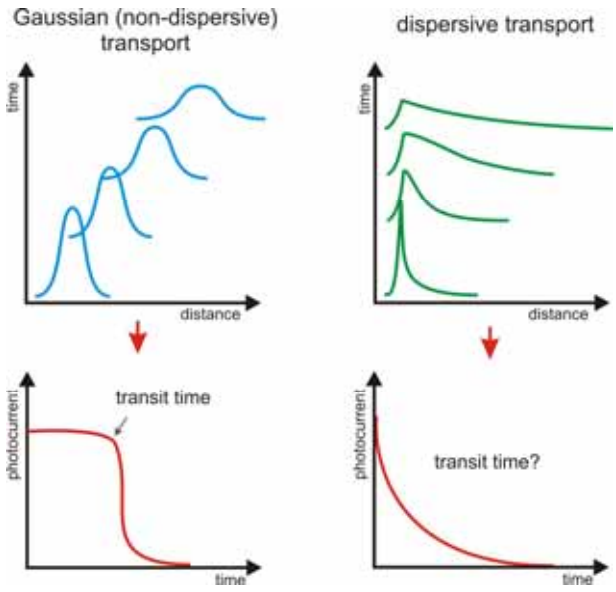

Figure 3-65: *Gaussian or non-dispersive transport with corresponding TOF transients.*

A TOF signal as given in Figure 3-65 with a clear flat region is characteristic for non-dispersive or Gaussian transport, implying that on passing through the organic material in the TOF cell the spatial distribution of charge carriers is Gaussian. From such a non-dispersive TOF transient, the transit time can be readily obtained and thickness-independent charge carrier mobilities can be derived. In contrast, dispersive transport results in a constantly decaying TOF signal without a flat region and without a clear transit time. Both cases are illustrated in Figure 3-65. The two transport regimes, dispersive and Gaussian, have often been studied analytically.[110] Determination of the intrinsic intracolumnar charge carrier mobility in discotic materials demands a high degree of self-organization of the discotic molecules within the inter-electrode gap. Domain boundaries or columnar misalignments can act as barriers or traps to charge migration. Therefore, polycrystalline or other heterogeneous samples will result in dispersive TOF signals from which no mobility value can be determined. This clearly diminishes the possibilities for mobility measurements on solid phases of discotic materials since it is an extremely difficult task to produce single crystals of these compounds. Fortunately, large liquid crystalline domains can be obtained in the TOF cell by slowly cooling the material from the isotropic liquid. For mesomorphic triphenylenes this strategy has been shown to be successful[86,111,112], while for larger columnar systems with significantly high melting points, such as phthalocyanines, porphyrins, and HBCs no reliable TOF mobilities have been published.

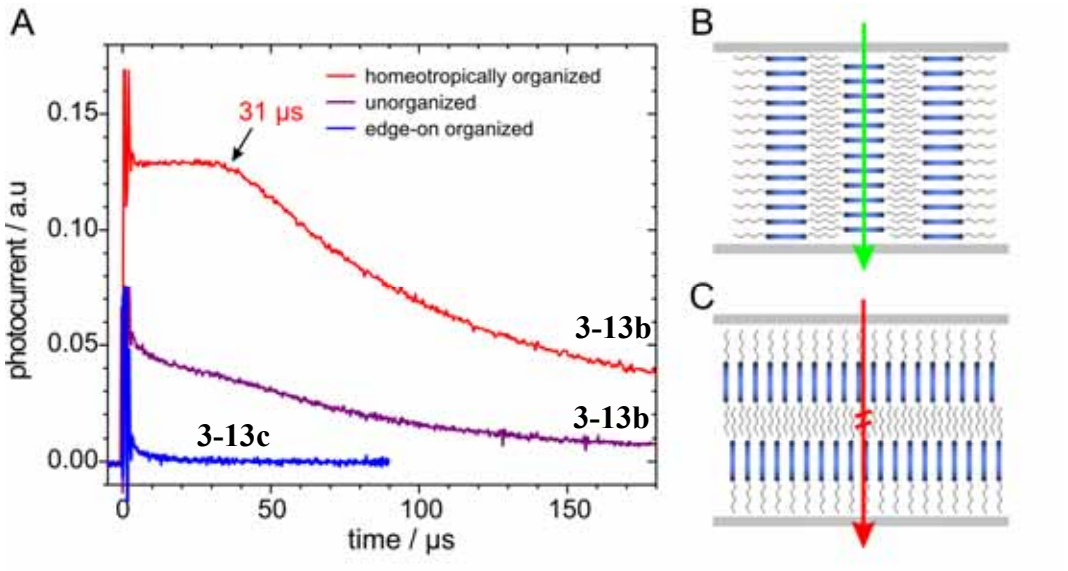

Figure 3-66: *(A) Room temperature hole current transients of face-on organized and unorganized* **3-13b** *and edge-on organized* **3-13c**, *12 µm thick sample in an electric field of 2.9 x 10^4 V/cm; (B) schematic illustration of the theoretical charge percolation pathway for face-on organized molecules; (C) for edge-on arranged molecules in the TOF experiment, tilting of the molecules was for simplicity not shown, arrows indicate direction of the charge carrier migration.*

In contrast to the known HBC derivatives, both HBC-$C_{10,6}$ **3-13b** and HBC-$C_{14,10}$ **3-13c** exhibit very low melting points, which suggested a charge carrier mobility determination with the TOF technique. Furthermore, the different molecular orientation with respect to the substrate for the two compounds opened the possibility to investigate the charge carrier transport, both along and perpendicular to the stacking axis.

For this purpose, the hole transients of sandwiched HBC-$C_{10,6}$ **3-13b** and HBC-$C_{14,10}$ **3-13c** samples were recorded to correlate the degree of order and orientation of the columnar structures with the charge carrier mobility. Furthermore, the transient photocurrent generated by a strongly absorbed short laser pulse in an electrically biased cell with ITO electrodes was recorded. F. LAQUAI and A. KUMAR taught and supported me preparing the cells and performing the experiments, which are presented in the following.

Figure 3-66 depicts the room temperature current transient for the positive charge carriers. HBC-$C_{14,10}$ **3-13c**, which was strictly edge-on oriented in the TOF cell did not allow one to record any meaningful signal of charge carrier transport. The bulky alkyl corona which surrounds the aromatic core may prohibit a charge carrier migration perpendicular to the stacking axis (Figure 3-66C).[105] This result

emphasized the importance to control the organization of the charge carrier percolation pathways, when discotic materials being implemented in organic devices.

When HBC-$C_{10,6}$ **3-13b** was filled into the cell from the molten state and cooled rapidly to room temperature, a dispersive transport of charge carriers was observed. This can be interpreted as a result of charge carriers being retained in traps having different depths, which led to significant different retention periods of charge carriers. This could be evidenced using POM by small domain sizes and increased disorder due to the fast cooling, which inherently leads to the formation of scattering sites for charges. When the sample was annealed slightly above the melting point and subsequently cooled slowly to room temperature (cooling rate of 0.01 °C /min), the hole transient changed its shape as a consequence of the significantly increased order, what has been investigated by POM and 2D-WAXS experiments. The signal of the ordered sample exhibited a clear plateau indicative of a non-dispersive hole transport followed by a pronounced tail. From the transit time and the applied electrical field, the mobility of the positive carriers was determined to be 1.4 x 10^{-3} $cm^2V^{-1}s^{-1}$. This stands in distinct contrast to other discotic systems such as triphenylene[108,113,114] or phthalocyanines[115,116], where no charge carrier mobility could be extracted for the room-temperature phase, implying an apparently low trap concentration in the investigated material. The charge carrier mobility was found to be independent of the applied electric field indicating that charge transport in the oriented HBC does not follow the disorder model.[117] This model is commonly used to describe the temperature and field-dependence of mobility in amorphous organic solids. Figure 3-66B presents schematically the percolation pathway for the charges, when the stacking axis of the discotic material was aligned parallel to the substrate surface. According to POM, the slow cooling process extended the domain sizes, reduced the poly-crystallinity of the sample and led therefore to a non-dispersive charge carrier transport mechanism.

The determined mobility for HBC-$C_{10,6}$ **3-13b** in its crystalline phase was significantly lower, compared to the one obtained by the PR-TRMC technique, where a local, microscopic process is being probed. This suggested an inherently lower long-range intramolecular organization in the plastic crystalline phase, which has been determined by 2D-WAXS experiments before. Temperature dependent TOF measurements on this sample, which A. KUMAR performed, revealed an increase of

the mobility of about one order of magnitude when the sample was heated to the mesophase. This can be interpreted as the material possessed a higher mobility and therefore the charge carrier hopping along the columnar structures was more efficient. However, X-ray scattering results exhibited that the columnar superstructure of that material was disordered, which inherently hampered a good charge carrier transport along the superstructure.

W. PISULA has found that well known HBC-$C_{16,4}$ **4-28** derivative formed a stable, homeotropic phase when slowly cooled from the isotropic state.[6,61] The investigation of the superstructure revealed in this case, that the disc-like molecules in the mesophase were much better organized compared to HBC-$C_{10,6}$ **3-13b**. This suggested to probe the charge carrier mobility of HBC-$C_{16,4}$ **4-28**, which is at room temperature in its mesophase. Very thick samples had to be prepared (44 μm) to allow the TOF transients to be recorded. Figure 3-67 presents the two TOF signals for both compounds, which already indicated a much more efficient hole carrier transport in the better ordered HBC-$C_{16,4}$ **4-28** material. The thermal organization of the columnar structures in these thick samples was not good, which caused the transport mechanism to be dispersive. However, the double-logarithmic plot showed a kink in the transient which could be correlated to a hole carrier mobility of 0.06 $cm^2V^{-1}s^{-1}$ for HBC-$C_{16,4}$ **4-28** and 3.5 x 10^{-3} $cm^2V^{-1}s^{-1}$ for HBC-$C_{10,6}$ **3-13b**, respectively. Although these are only preliminary results and the measurement and the organization have to be optimized to yield better transients, the result is very clear. This proved, that intracolumnarly better organized molecules in the columnar stacking allow the charge carriers to be transferred much more effectively.

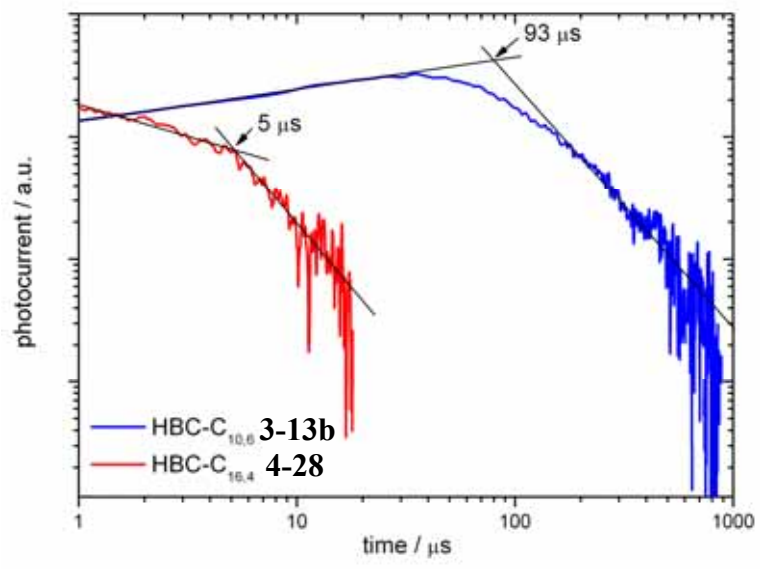

Figure 3-67: *Comparison of the hole current transients for thick samples (44 µm) of HBC-$C_{10,6}$* **3-13b** *and HBC-$C_{16,4}$* **4-28**, *both recorded at 40°C in their mesophase with an electric field of 1.36 x 10^4 V/cm.*

The control of the disc orientation and intracolumnar organization is a vital step to process materials for different electronic devices, which require different orientations of the percolation pathways for the charges with respect to the device setup. The TOF results revealed that the quality of the molecular organization is crucial for the charge carrier mobility. Furthermore, it emphasized again that the described HBC are promising candidates for a successful application in organic electronics. The room-temperature hole mobility which has been obtained by the TOF technique is higher in comparison to other discotic materials. Additionally, the propensity of the materials to organize into large, long-range domains increased the applicability of the material. The anisotropy of the charge carriers was very pronounced since the edge-on arrangement did not reveal any meaningful TOF transient signal of charge carrier transport.

3.5 Implementation in Photovoltaic Devices

The excellent self-organization behavior and the high charge carrier mobility of the introduced HBC derivatives with the bulky, branched alkyl chains make the materials promising for device applications. HBC-PhC_{12} **3-24** was successfully incorporated into a bulk heterojunction photovoltaic element with PDI-$C_{3,2}$ **3-25** as the acceptor component.[74,118] The adequate processing from solution gave self-organized films with vertically segregated donor and acceptor components and a large interfacial surface are. In the diode structure, these films showed photovoltaic response with external quantum efficiencies (EQEs) of 34% at 490 nm, which correspond to a power efficiency of 2%. Inspired by this great result, the novel HBC derivatives have been tested by J. LI in photovoltaic elements together with PDI-$C_{3,2}$ **3-25**.

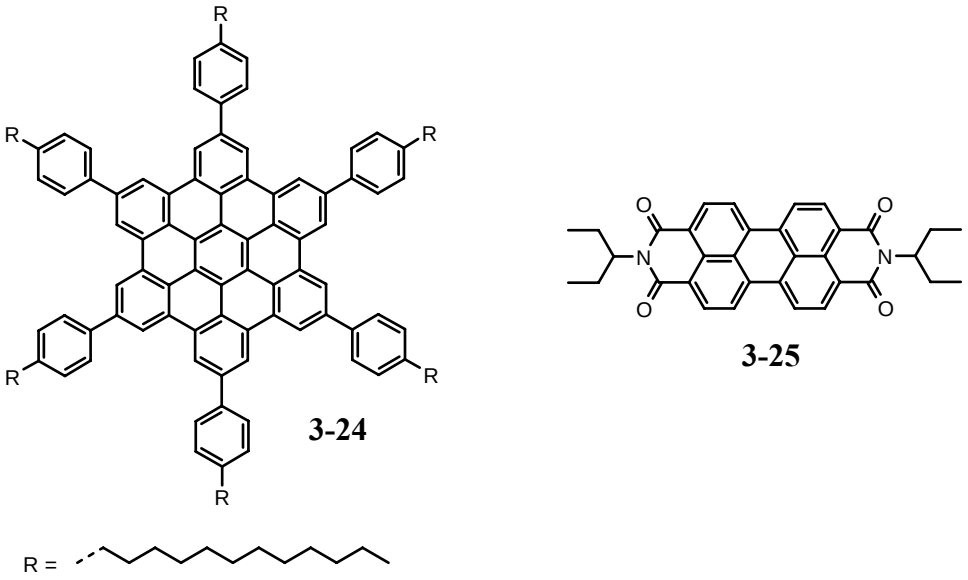

Figure 3-68: *Chemical structure of the donor HBC-PhC_{12}* **3-24** *and the acceptor PDI-$C_{3,2}$* **3-25**.

Expectedly, thin films of the three HBC derivatives **3-13a-c** with the same thickness showed different absorptions due to different chromophore concentrations (Figure 3-69). Assuming the same packing density, the HBC chromophore density in HBC-$C_{6,2}$ **3-13a** is 77 mol%, in HBC-$C_{10,6}$ **3-13b** 38 mol% and in HBC-$C_{14,10}$ **3-13c** 26 mol%, respectively. The extension of the alkyl chains "diluted" the "active" aromatic core, which is directly visible in the absorption spectra. The higher absorption cross-section for HBC-$C_{6,2}$ **3-13a** makes it to the most promising material, since a potential solar cell would collect much more photons.

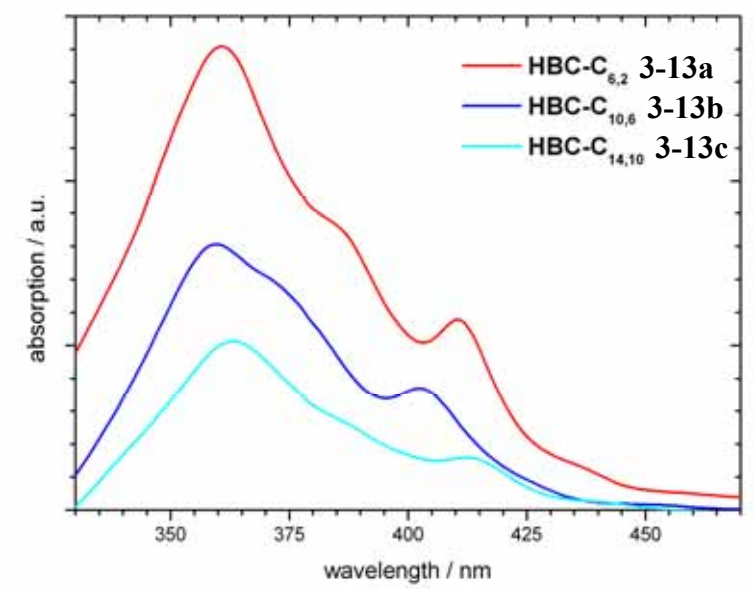

Figure 3-69: *UV/vis absorption spectra of spin coated thin films of HBC-$C_{6,2}$* **3-13a**, *HBC-$C_{10,6}$* **3-13b**, *and HBC-$C_{14,10}$* **3-13c** *(film thickness 100±10 nm).*

HBC-$C_{10,6}$ **3-13b** and HBC-$C_{14,10}$ **3-13c** revealed excellent solubilities in common organic solvents and formed excellent, homogeneous films from the mixture with the acceptor. The RMS roughness was determined by AFM for the spin-coated films to be less than 5 nm. The much more crystalline HBC-$C_{6,2}$ **3-13a** was less well soluble, however the necessary concentrations were obtained by stirring and slight heating. The spin-coated, crystalline films showed rougher surfaces (RMS ~5-10 nm). J. LI has shown that annealing distinctly influenced the appearance of the surface and the film morphology, which could be imaged with scanning electron microscopy (SEM) and AFM (not shown).

The composition of photovoltaic devices requires the knowledge of the electronic levels of both donor and acceptor component. Cyclic voltammetry (CV) was utilized to obtain the electronic levels of the spin-coated HBC derivatives. Reversible oxidation peaks were observed in all the positive scans, while no reduction peaks were detected in the negative scans, because the solvent window did not permit going to high potentials. The oxidation peak positions were used to estimate the HOMO energy levels. For HBC-$C_{6,2}$ **3-13a**, from the onset oxidation potential a HOMO level of -5.2 eV was calculated, while HBC-$C_{10,6}$ **3-13a** and HBC-$C_{14,10}$ **3-13c** showed a level at -5.3 eV. This small difference can be explained by the crystallinity of HBC-$C_{6,2}$ **3-13a** which created from solution large domains of organized molecules and thus lowered the band gap due to an efficient overlap of molecular orbitals. From

solution, both derivatives with the longer chains do not organize that well and the value corresponds to un-aggregated HBC molecules. With the optical band gap of 2.9 eV (onset of the p-band, solid-state UV/vis spectra), the LUMO energies have been calculated to be -2.3 and -2.4 eV, repectively. The determined levels proved that HBC might be a suitable donor material for PDI-$C_{3,2}$ **3-25**, which energies for HOMO and LUMO are -5.3 and -3.3 eV, respectively. The energy difference for the LUMO levels suggested a charge transfer between the two components.[119,120]

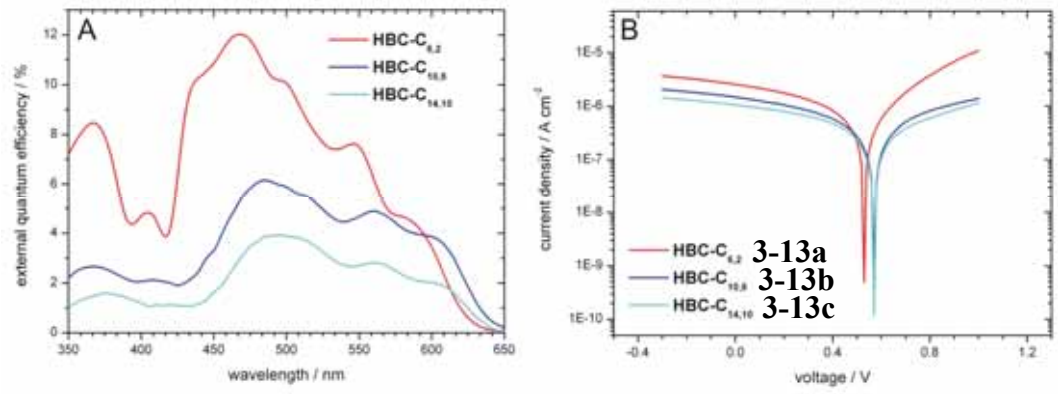

Figure 3-70: *ITO/ HBC:PDI /Al device: optimized EQE spectra at weight ratio of HBC:PDI = 4:6 (film thickness 100 nm, annealed at 120 °C) with corresponding I-V characteristics under monochromatic illumination at 490 nm (incident light intensity 0.3 W/m²) for the three HBC derivatives HBC-$C_{6,2}$* **3-13a**, *HBC-$C_{10,6}$* **3-13b**, *and HBC-$C_{14,10}$* **3-13c**.

Photovoltaic cells of the branched alkyl chain carrying HBCs with PDI-$C_{3,2}$ **3-25** were fabricated with different ratios of HBC:PDI, where an optimal weight ratio of 4:6 was determined independent on the used HBC. The performance of the device was significantly influenced by the attached alkyl side chains and by the annealing procedure. For the solar cell with HBC-$C_{6,2}$ **3-13a**, an EQE of 12 % was found with optimal annealing conditions (120 °C, 1h), which corresponds to a power efficiency of 1.5% (Figure 3-70A). The HBC derivatives with the longer alkyl chains revealed lower performances. Interestingly, the shape of the EQE plot for HBC-$C_{6,2}$ **3-13a** differed significantly from the ones for derivatives with the extended chains. The I-V curves showed the same behavior (Figure 3-70B). Both HBC-$C_{10,6}$ **3-13b** and HBC-$C_{14,10}$ **3-13c** exhibited an open circuit voltage of 0.56 V, whereby the one for HBC-$C_{6,2}$ **3-13a** was with 0.52 V slightly lower. This can be explained by the slightly higher HOMO energy for the derivative with the shortest chain. The short circuit current was the highest for HBC-$C_{6,2}$ **3-13a**, which absorbed more photons than the other two materials. The differences observed for the two materials with the longer

side chains can be interpreted by a different supramolecular structure. While HBC-$C_{6,2}$ **3-13a** formed spontaneous microcrystalline domains, the other two materials only organize in a plastic crystalline phase, where a lower columnar order is being found. The higher self-association propensity of HBC-$C_{6,2}$ **3-13a** might lead to a better vertical segregation, which allows the charge carriers to migrate along these percolation pathways. The presented investigation of mixtures of HBC-$C_{10,6}$ **3-13b** and PDI-$C_{8,7}$ **3-19** promote a different speculation. If some of the material formed an alternating stacking during the processing or annealing procedure, the necessary formation of separated percolation pathways for holes and electrons would fail and the performance of the device would be low. Even after extensive optimization, the performance of the produced solar cells was lower than for other HBC derivatives such as HBC-Ph-C_{12} **3-24** and HBC-C_{12} **3-3a**. The more promising implementation of the HBCs into FET structures is planned and will be conducted by N. TSAO during his PhD work.

3.6 Organization in porous materials – Pyrolysis

Nanostructuring of electronically interesting materials, such as conjugated polymers or discotics is an important process that modifies their electronic and charge carrier transport properties.[121-123] Nanostructuring plays a crucial role in device applications, for example in the fabrication of photovoltaic cells, where the self-assembly of an interpenetrating network of donor and an acceptor component is the critical factor for success.[124,125] Nanostructuring is of interest in photonic band gap materials[126] and fabrication of heterojunction devices in which two different conjugated polymers have to interact intimately to increase their interface.[127]

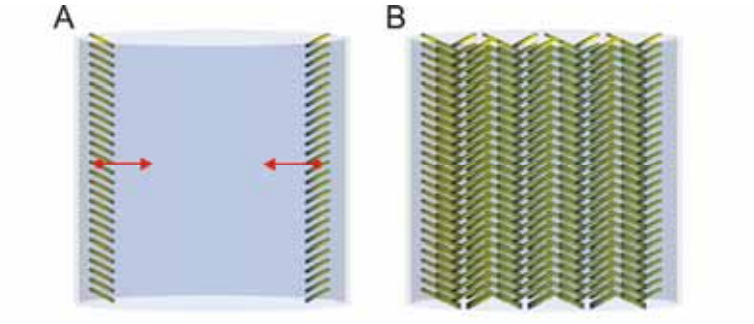

Figure 3-71: *Schematic illustration of (A) the organizing discs, with the red arrows pointing the crystallization direction along the temperature gradient and (B) after controlled cooling to room temperature.*

The striking self-organization behavior of HBC-$C_{14,10}$ **3-13c** in the bulk motivated the use of that material for nanostructuring. When the material was cooled in a macroscopic glass capillary (diameter = 2mm) from its isotropic state down to room temperature, a pronounced tendency to organize was monitored using 2D-WAXS experiments, which have been recorded by W. PISULA.

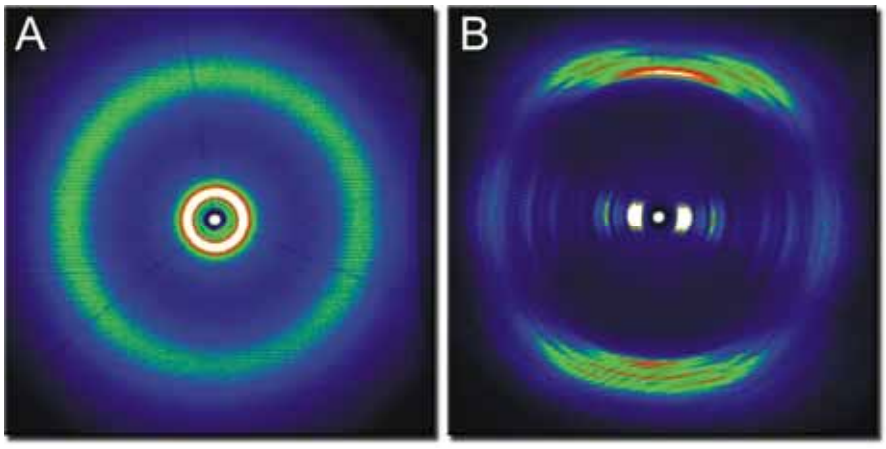

Figure 3-72: *2D-WAXS pattern of (A) the isotropic state and (B) after controlled crystallization.*

Figure 3-71 illustrates the nucleation occurring at the glass walls of the glass capillary and propagation the propagation of the crystallization along the temperature gradient during the cooling. The 2D-WAXS pattern in the molten state exhibits clearly an isotropic distribution of the reflections (Figure 3-72A). After cooling the sample to room temperature, a characteristic pattern was observed (Figure 3-72B), where the supramolecular organization was identical to that determined for extruded filaments of HBC-$C_{14,10}$ **3-13c**. Interestingly, the organization order was even higher as indicated by more and sharper X-ray reflections. The pattern indicated a high, uniaxial orientation of the columnar superstructures along the capillary axis, which was uniform over the whole capillary.

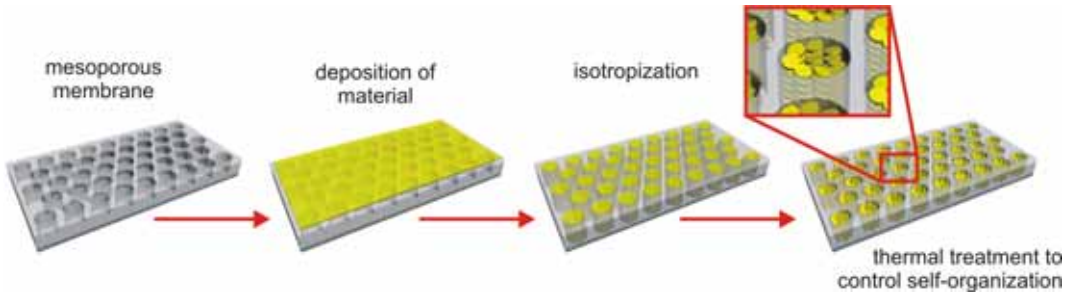

Figure 3-73: *Schematic illustration of the template processing of HBC-$C_{14,10}$* **3-13c** *by controlled thermal treatment.*

The pronounced directional growth and low nucleation propensity of HBC-$C_{14,10}$ **3-13c** promised the desired thermal organization of the material in even smaller volumes. To test the nanostructuring ability, commercially available inorganic aluminum oxide membranes were used as template. The thickness of the membrane was 60 µm and the pore size *ca.* 200 nm. The processing of the material (Figure 3-73) started with the deposition of HBC-$C_{14,10}$ **3-13c** on top of the membrane, which was subsequently heated to melt the HBC. Capillary forces filled the fine pores and the material was organized by controlled cooling to room temperature with a cooling rate of 0.1 °C.

SEM images show the membrane before and after the filling process (Figure 3-74). It is obvious that the pores were completely filled. X-ray diffraction experiments probed the supramolecular organization.

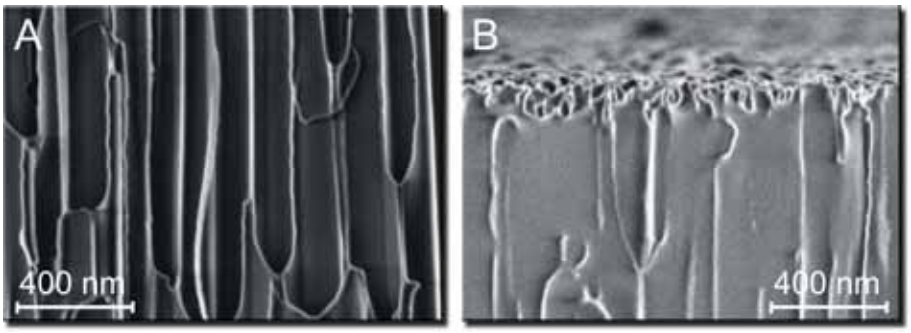

Figure 3-74: *SEM images of the aluminum oxide membrane pores (A) before and (B) after filling with HBC-$C_{14,10}$* **3-13c**. *The membranes were broken and imaged from the side.*

Three different experiments have been conducted (Figure 3-75A). A microfocussed synchrotron beam was carefully aligned perpendicular to the pore channels and 2D-WAXS patterns were recorded (Figure 3-75B). Impressively, the pattern was identical to the one obtained from the macroscopically organized material. Conventional reflection X-ray diffraction experiments revealed a tilting angle, which was identical to the one obtained in the bulk state (Figure 3-75C). As expected, when the X-ray beam penetrated the membrane along the columnar structures, only isotropic rings were recorded indicating different orientation of the columnar unit cell with respect to the pores (Figure 3-75D).

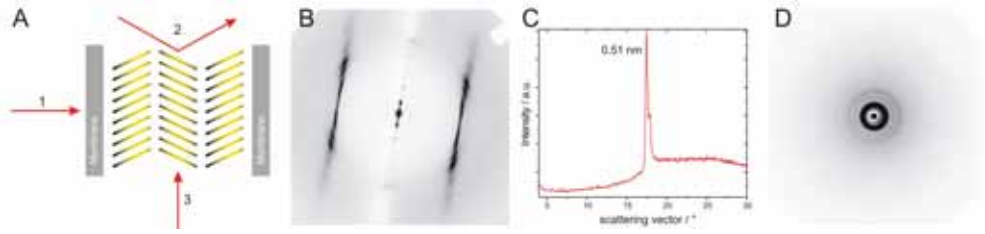

Figure 3-75: *X-ray diffraction analysis of the organized HBC-$C_{14,10}$* **3-13c** *molecules within the mesoporous membrane. (A) Schematic illustration of the three performed scattering experiments, (B) synchrotron microfocus X-ray diffraction with a beam perpendicular to the pores (beam 1 in (A)), (C) X-ray diffraction in reflection showing the intracolumnar periodicity of the tilted discs (beam 2 in (A)), (D) transmission X-ray diffraction along the membrane pore (beam 3 in (A)).*

In conclusion, the material organized both in the macroscopic glass capillary and in the small pores edge-on with respect to the templating walls, as illustrated in Figure 3-75A. In the case of the mesoporous material, this led to a "pseudo-homeotropic" alignment, which could permit TOF studies to probe the charge carrier mobility along the pores.

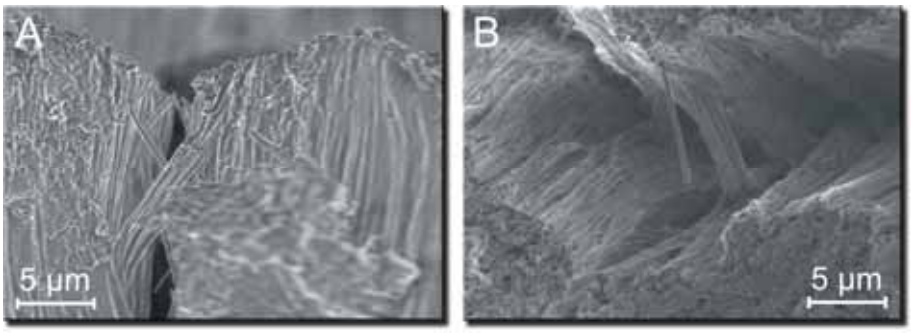

Figure 3-76: *(A) and (B) show SEM images which illustrate organized nanotubes after the removal of the inorganic template.*

Interestingly, it was possible to dissolve the aluminum oxide membrane after the filling with the HBC material with aqueous, dilute, cold sodium hydroxide solution (0.05 M, 4 °C). SEM images depict after the complete removal of the inorganic template, intact, organized nanofibers, although the material was waxy at room temperature (Figure 3-76). However, the mechanical unstable tubes could not be manipulated.

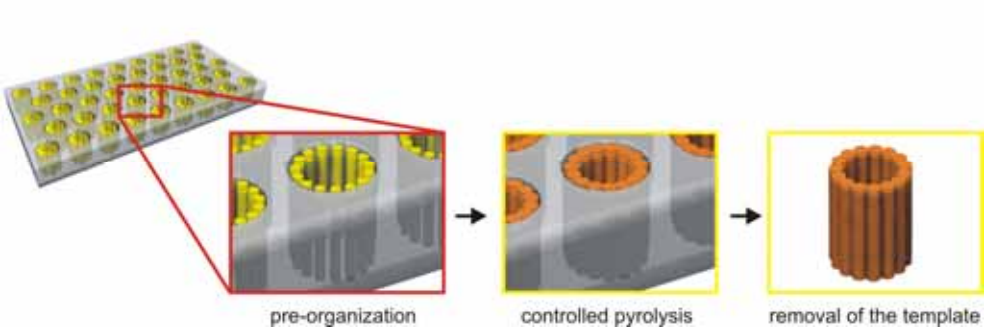

Figure 3-77: *Pyrolysis process of pre-organized HBC molecules.*

L. ZHI performed pyrolytic experiments on the HBC-$C_{14,10}$ **3-13c** -filled templates. For this purpose, less material was introduced into the pores to only wet the surfaces. The loaded membrane was sealed under vacuum and heat-treated at 200 °C for 2h, then 400 °C for 2h, and finally at 600 °C for 5h. The tubes were obtained after removing the template with aqueous sodium hydroxide solution (0.1 M). The whole process is schematically shown in Figure 3-77.

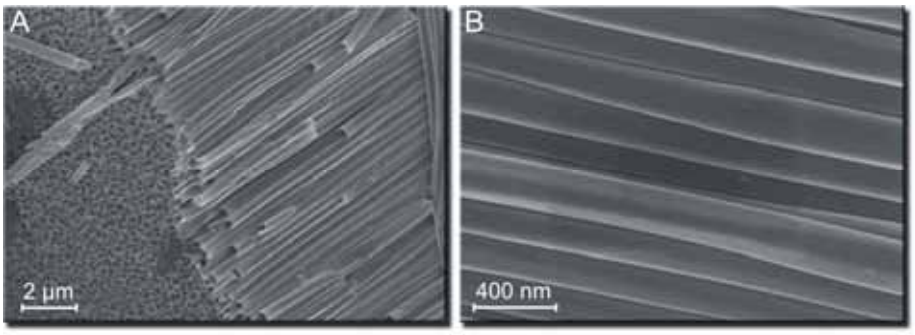

Figure 3-78: *SEM images of nanotubes obtained after pyrolysis and removal of the inorganic template.*

SEM images show highly aligned nanotubes which are very uniform in length and thickness (Figure 3-78). The inside of the nanostructures was hollow which is also indicated in the image in Figure 3-78A. High-resolution transmission electron microscopy (HRTEM) visualized the hollow carbon nanotubes, which consisted of thermally fused PAH molecules (Figure 3-79). Clearly ordered wall structures were found which could further be proved by electron diffraction analysis (Figure 3-79B, inset). This is a new type of carbon nanotubes, which consist of stacked, large aromatic rings along the length of the tube. Theoretically, the tubes should be semiconducting, which is attempted to be tested in a FET setup. Furthermore, conductivity measurements will be performed to implement the material in other applications.

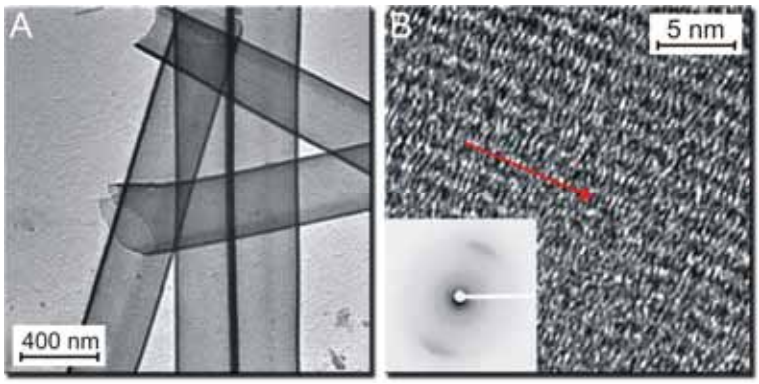

Figure 3-79: *HRTEM images of pyrolytically produced nanotubes (A) uniform, hollow tubes, (B) high magnification visualizing the wall structure, inset: electron diffraction pattern.*

The nanostructuring has been accomplished on different lengths scale. Going from a macroscopic capillary down to 200 nm sized pores, HBC-$C_{14,10}$ **3-13c** proved to be an ideal material with a striking ability to self-organize. It is planned to fill semiconducting, mesoporous titanium dioxide membranes to create a heterojunction

photovoltaic device with a large interface between the donor and the acceptor component.

Recently, L. Zhi presented the fabrication of carbonaceous nanotubes utilizing the template method. Differently substituted HBCs and Ni-naphthocyanine were used as building blocks and thermally cross-linked to obtain nano-objects.[128-130] The striking ability of the novel HBC derivatives to self-assemble into long-range organized domains allowed nanotubes of much higher quality (dispersity, wall structure) to be obtained.

3.7 Summary

The simple chemical introduction of branched alkyl chains into the periphery of the aromatic HBC core exerted a dramatic influence onto the self-organization of the material and the processing. Solution based investigations of the self-aggregation propensity revealed that the steric demand, induced by the branching close to the aromatic entity, reduced the intermolecular attractive forces.[131] The space demand of such a flexible alkyl chain is illustrated in Figure 3-80.

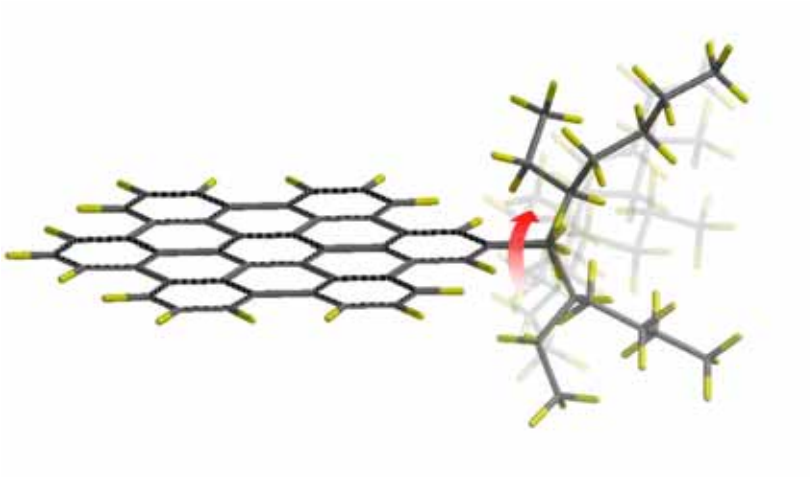

Figure 3-80: *Simulation of the space demand of a single, rotating branched alkyl chain attached to the HBC core.*

This modulation of the π-stacking lowered the isotropization temperature, which opened the possibility to process from the molten state. The length of the attached side chains controlled thereby the orientation of the discotic molecules with respect to the substrate surface. Both edge-on and face-on arrangements can be achieved by changing the length of the alkyl chain, which is required for the processing of the material in thin films for electronic devices. The PR-TRMC technique revealed very long life-times for the induced charge carriers compared to other HBC derivatives, because dense alkyl surrounding hampered the direct recombination of the free charge carriers.[105] Distinct differences of the charge carrier mobilities between the crystalline and the liquid crystalline phase were observed, supporting the X-ray results, which indicated a disordered columnar superstructure in the mobile mesophase. In TOF experiments, the comparison with other HBC derivatives, exhibiting ordered mesophases, emphasized the importance to molecularly order the active component for an unperturbed charge carrier transport process. However, the better ordered crystalline phases permitted the charge carriers to migrate very

effectively and perfect non-dispersive signals could be recorded. Expectedly, strictly edge-on organized molecules did not allow a meaningful TOF signal to be recorded.

The excellent propensity to self-organize the derivatives with the bulky branched alkyl chains were exploited to nanostructure these materials in inorganic templates. Thereby, the high organizations could be fixed in a controlled pyrolysis process and after the template was removed, the networked discotic materials gave monodisperse nanotubes. These objects were the walls were composed of stacked aromatic molecules can be considered a new allotrope of carbon.

3.8 References

(1) van de Craats, A. M.; Warman, J. M. *Advanced Materials* **2001**, *13*, 130-133.

(2) Lemaur, V.; Da Silva Filho, D. A.; Coropceanu, V.; Lehmann, M.; Geerts, Y.; Piris, J.; Debije, M. G.; Van de Craats, A. M.; Senthilkumar, K.; Siebbeles, L. D. A.; Warman, J. M.; Bredas, J. L.; Cornil, J. *J. Am. Chem. Soc.* **2004**, *126*, 3271-3279.

(3) Adam, D.; Schuhmacher, P.; Simmerer, J.; Haussling, L.; Siemensmeyer, K.; Etzbach, K. H.; Ringsdorf, H.; Haarer, D. *Nature* **1994**, *371*, 141-143.

(4) Boden, N.; Bushby, R. J.; Clements, J.; Movaghar, B.; Donovan, K. J.; Kreouzis, T. *Physical Review B* **1995**, *52*, 13274-13280.

(5) Tracz, A.; Jeszka, J. K.; Watson, M. D.; Pisula, W.; Müllen, K.; Pakula, T. *Journal of the American Chemical Society* **2003**, *125*, 1682-1683.

(6) Pisula, W.; Tomovic, Z.; El Hamaoui, B.; Watson, M. D.; Pakula, T.; Müllen, K. *Advanced Functional Materials* **2005**, *15*, 893-905.

(7) Karthaus, O.; Ringsdorf, H.; Tsukruk, V. V.; Wendorff, J. H. *Langmuir* **1992**, *8*, 2279-2283.

(8) Mindyuk, O. Y.; Heiney, P. A. *Adv. Mater.* **1999**, *11*, 341-344.

(9) Piris, J.; Pisula, W.; Tracz, A.; Pakula, T.; Müllen, K.; Warman, J. M. *Liq. Cryst.* **2004**, *31*, 993-996.

(10) van de Craats, A. M.; Stutzmann, N.; Bunk, O.; Nielsen, M. M.; Watson, M.; Mullen, K.; Chanzy, H. D.; Sirringhaus, H.; Friend, R. H. *Advanced Materials* **2003**, *15*, 495-499.

(11) Bunk, O.; Nielsen, M. M.; Solling, T. I.; van de Craats, A. M.; Stutzmann, N. *J. Am. Chem. Soc.* **2003**, *125*, 2252-2258.

(12) Zimmermann, S.; Wendorff, J. H.; Weder, C. *Chem. Mater.* **2002**, *14*, 2218-2223.

(13) Fechtenkötter, A.; Tchebotareva, N.; Watson, M.; Müllen, K. *Tetrahedron* **2001**, *57*, 3769-3783.

(14) Herwig, P.; Kayser, C. W.; Müllen, K.; Spiess, H. W. *Adv. Mater.* **1996**, *8*, 510-513.

(15) Barber, H. J.; Slack, R. *J. Chem. Soc.* **1944**, 612-615.

(16) Mio, M. J.; Kopel, L. C.; Braun, J. B.; Gadzikwa, T. L.; Hull, K. L.; Brisbois, R. G.; Markworth, C. J.; Grieco, P. A. *Org. Lett.* **2002**, *4*, 3199-3202.

(17) Hurd, R. N.; Delamater, G.; McElheny, G. C.; Wallingford, V. H.; Turner, R. J. *J. Org. Chem.* **1961**, *26*, 3980-3987.

(18) Watson, J. D.; Crick, F. H. C. *Nature* **1953**, *171*, 737-738.

(19) Bong, D. T.; Clark, T. D.; Granja, J. R.; Ghadiri, M. R. *Angew. Chem. Int. Ed.* **2001**, *40*, 988-1011.

(20) Percec, V.; Ahn, C. H.; Ungar, G.; Yeardley, D. J. P.; Moller, M.; Sheiko, S. S. *Nature* **1998**, *391*, 161-164.

(21) Brunsveld, L.; Folmer, B. J. B.; Meijer, E. W.; Sijbesma, R. P. *Chem. Rev.* **2001**, *101*, 4071-4097.

(22) Ciferri, A. *Macromol. Rapid Commun.* **2002**, *23*, 511-529.

(23) Prins, L. J.; Reinhoudt, D. N.; Timmerman, P. *Angew. Chem. Int. Ed.* **2001**, *40*, 2383-2426.

(24) Sherrington, D. C.; Taskinen, K. A. *Chem. Soc. Rev.* **2001**, *30*, 83-93.

(25) Hirschberg, J.; Brunsveld, L.; Ramzi, A.; Vekemans, J.; Sijbesma, R. P.; Meijer, E. W. *Nature* **2000**, *407*, 167-170.

(26) Hunter, C. A.; Lawson, K. R.; Perkins, J.; Urch, C. J. *J. Chem. Soc. - Perk. Trans. 2* **2001**, 651-669.

(27) Gallivan, J. P.; Schuster, G. B. *J. Org. Chem.* **1995**, *60*, 2423-2429.

(28) van Gorp, J. J.; Vekemans, J.; Meijer, E. W. *J. Am. Chem. Soc.* **2002**, *124*, 14759-14769.

(29) Gearba, R. I.; Lehmann, M.; Levin, J.; Ivanov, D. A.; Koch, M. H. J.; Barbera, J.; Debije, M. G.; Piris, J.; Geerts, Y. H. *Adv. Mater.* **2003**, *15*, 1614-1618.

(30) Nguyen, T. Q.; Martel, R.; Avouris, P.; Bushey, M. L.; Brus, L.; Nuckolls, C. *J. Am. Chem. Soc.* **2004**, *126*, 5234-5242.

(31) Würthner, F.; Thalacker, C.; Sautter, A. *Adv. Mater.* **1999**, *11*, 754-758.

(32) Hoeben, F. J. M.; Jonkheijm, P.; Meijer, E. W.; Schenning, A. *Chem. Rev.* **2005**, *105*, 1491-1546.

(33) Hunter, C. A.; Sanders, J. K. M. *J. Am. Chem. Soc.* **1990**, *112*, 5525-5534.

(34) Zhao, D. H.; Moore, J. S. *Chem. Comm.* **2003**, 807-818.

(35) Lin, C. H.; Tour, J. *J. Org. Chem.* **2002**, *67*, 7761-7768.

(36) Höger, S.; Bonrad, K.; Rosselli, S.; Ramminger, A. D.; Wagner, T.; Silier, B.; Wiegand, S.; Haussler, W.; Lieser, G.; Scheumann, V. *Macromol. Symp.* **2002**, *177*, 185-191.

(37) Zhao, D. H.; Moore, J. S. *J. Org. Chem.* **2002**, *67*, 3548-3554.

(38) Tobe, Y.; Utsumi, N.; Kawabata, K.; Nagano, A.; Adachi, K.; Araki, S.; Sonoda, M.; Hirose, K.; Naemura, K. *J. Am. Chem. Soc.* **2002**, *124*, 5350-5364.

(39) Phillips, K. E. S.; Katz, T. J.; Jockusch, S.; Lovinger, A. J.; Turro, N. J. *J. Am. Chem. Soc.* **2001**, *123*, 11899-11907.

(40) Nakamura, K.; Okubo, H.; Yamaguchi, M. *Org. Lett.* **2001**, *3*, 1097-1099.

(41) Kano, K.; Fukuda, K.; Wakami, H.; Nishiyabu, R.; Pasternack, R. F. *J. Am. Chem. Soc.* **2000**, *122*, 7494-7502.

(42) Farina, R. D.; Swinehar.Jh; Halko, D. J. *J. Phys. Chem.* **1972**, *76*, 2343-2348.

(43) Terekhov, D. S.; Nolan, K. J. M.; McArthur, C. R.; Leznoff, C. C. *J. Org. Chem.* **1996**, *61*, 3034-3040.

(44) Schutte, W. J.; Sluytersrehbach, M.; Sluyters, J. H. *J. Phys. Chem.* **1993**, *97*, 6069-6073.

(45) Law, W. F.; Lui, K. M.; Ng, D. K. P. *J. Mater. Chem.* **1997**, *7*, 2063-2067.

(46) Martin, R. B. *Chem. Rev.* **1996**, *96*, 3043-3064.

(47) Wu, J. S.; Fechtenkötter, A.; Gauss, J.; Watson, M. D.; Kastler, M.; Fechtenkötter, C.; Wagner, M.; Müllen, K. *J. Am. Chem. Soc.* **2004**, *126*, 11311-11321.

(48) Shetty, A. S.; Zhang, J. S.; Moore, J. S. *J. Am. Chem. Soc.* **1996**, *118*, 1019-1027.

(49) Prince, R. B.; Saven, J. G.; Wolynes, P. G.; Moore, J. S. *J. Am. Chem. Soc.* **1999**, *121*, 3114-3121.

(50) Clar, E. *Polycyclic Hydrocarbons*; Academic: New York, 1964; Vol. 1+2.

(51) Kasha, M. *Faraday Discuss.* **1950**, 14-19.

(52) Wu, J. S.; Fechtenkötter, A.; Gauss, J.; Watson, M. D.; Kastler, M.; Fechtenkötter, C.; Wagner, M.; Müllen, K. *Journal of the American Chemical Society* **2004**, *126*, 11311-11321.

(53) Biasutti, M. A.; Rommens, J.; Vaes, A.; De Feyter, S.; De Schryver, F. D.; Herwig, P.; Müllen, K. *Bull. Soc. Chim. Belg.* **1997**, *106*, 659-664.

(54) Luz, Z.; Poupko, R.; Wachtel, E. J.; Zimmermann, H.; Bader, V. *Mol. Cryst. Liq. Cryst.* **2003**, *397*, 367-377.

(55) Höger, S.; Bonrad, K.; Mourran, A.; Beginn, U.; Möller, M. *J. Am. Chem. Soc.* **2001**, *123*, 5651-5659.

(56) Lahiri, S.; Thompson, J. L.; Moore, J. S. *J. Am. Chem. Soc.* **2000**, *122*, 11315-11319.

(57) Gauss, J.; Ochsenfeld, C. - *manuskript in preparation* **2005**.

(58) Pisula, W., Johannes Gutenberg Universität 2005.

(59) Pisula, W.; Menon, A.; Stepputat, M.; Lieberwirth, I.; Kolb, U.; Tracz, A.; Sirringhaus, H.; Pakula, T.; Müllen, K. *Advanced Materials* **2005**, *17*, 684-689.

(60) Pisula, W.; Tomovic, Z.; Stepputat, M.; Kolb, U.; Pakula, T.; Müllen, K. *manuscript in preparation* **2005**.

(61) Liu, C. Y.; Fechtenkötter, A.; Watson, M. D.; Müllen, K.; Bard, A. J. *Chemistry of Materials* **2003**, *15*, 124-130.

(62) Nguyen, T. Q.; Bushey, M. L.; Brus, L. E.; Nuckolls, C. *J. Am. Chem. Soc.* **2002**, *124*, 15051-15054.

(63) Klok, H. A.; Jolliffe, K. A.; Schauer, C. L.; Prins, L. J.; Spatz, J. P.; Moller, M.; Timmerman, P.; Reinhoudt, D. N. *J. Am. Chem. Soc.* **1999**, *121*, 7154-7155.

(64) Jonkheijm, P.; Hoeben, F. J. M.; Kleppinger, R.; van Herrikhuyzen, J.; Schenning, A.; Meijer, E. W. *J. Am. Chem. Soc.* **2003**, *125*, 15941-15949.

(65) Wu, J., Johannes Gutenberg Universität, 2004.

(66) Wu, J. S.; Watson, M. D.; Zhang, L.; Wang, Z. H.; Müllen, K. *J. Am. Chem. Soc.* **2004**, *126*, 177-186.

(67) Bushey, M. L.; Hwang, A.; Stephens, P. W.; Nuckolls, C. *J. Am. Chem. Soc.* **2001**, *123*, 8157-8158.

(68) Imai, H.; Oaki, Y. *Angew. Chem. Int. Ed.* **2004**, *43*, 1363-1368.

(69) Patzelt, W. J. *Polarisationsmikroskopie*; Ernst Leitz Wetzlar GmbH: Wetzlar, 1985.

(70) Gazzano, M.; Focarete, M. L.; Riekel, C.; Scandola, M. *Biomacromolecules* **2004**, *5*, 553-558.

(71) Hatsusaka, K.; Ohta, K.; Yamamoto, I.; Shirai, H. *J. Mater. Chem.* **2001**, *11*, 423-433.

(72) Kopitzke, J.; Wendorff, J. H. *Chem. unserer Zeit* **2000**, *34*, 4-16.

(73) Fechtenkötter, A.; Saalwächter, K.; Harbison, M. A.; Müllen, K.; Spiess, H. W. *Angewandte Chemie-International Edition* **1999**

38, 3039-3042.

(74) Schmidt-Mende, L.; Fechtenkötter, A.; Müllen, K.; Moons, E.; Friend, R. H.; MacKenzie, J. D. *Science* **2001**, *293*, 1119-1122.

(75) Wirth, H. O.; Königstein, O.; Kern, W. *Justus Liebig's Annalen der Chemie* **1960**, *634*, 84-104.

(76) Fechtenkötter, A., Johannes Gutenberg University Mainz, 2001.

(77) Harvey, R. G. *Polycyclic Aromatic Hydrocarbons*; Wiley-VCH: New York, Chichester, Weinheim, Brisbane, Singapore, Toronto, 1997.

(78) Becker, R. *Theory and Interpretation of Fluorescence and Phosphorescence*; Wiley Interscience: New York, 1969.

(79) Glusen, B.; Heitz, W.; Kettner, A.; Wendorff, J. H. *Liquid Crystals* **1996**, *20*, 627-633.

(80) Pisula, W.; Tomovic, Z.; Simpson, C.; Kastler, M.; Pakula, T.; Müllen, K. *Chemistry of Materials* **2005**, *17*, 4296-4303.

(81) Fischbach, I.; Pakula, T.; Minkin, P.; Fechtenkötter, A.; Müllen, K.; Spiess, H. W.; Saalwächter, K. *J. Phys. Chem. B* **2002**, *106*, 6408-6418.

(82) Wasserfallen, D.; Fischbach, I.; Chebotareva, N.; Kastler, M.; Pisula, W.; Jäckel, F.; Watson, M. D.; Schnell, I.; Rabe, J. P.; Spiess, H. W.; Müllen, K. *Adv. Funct. Mater.* **2005**, *in press*.

(83) Brown, S. P.; Schnell, I.; Brand, J. D.; Müllen, K.; Spiess, H. W. *J. Am. Chem. Soc.* **1999**, *121*, 6712-6718.

(84) Brown, S. P.; Schnell, I.; Brand, J. D.; Müllen, K.; Spiess, H. W. *J. Mol. Struct.* **2000**, *521*, 179-195.

(85) Schnell, I. *Prog. Nucl. Magn. Reson. Spectrosc.* **2004**, *45*, 145-207.

(86) Adam, D.; Closs, F.; Frey, T.; Funhoff, D.; Haarer, D.; Ringsdorf, H.; Schuhmacher, P.; Siemensmeyer, K. *Phys. Rev. Lett.* **1993**, *70*, 457-460.

(87) Scott, R. L. *J. Chem. Phys.* **1949**, *17*, 279-284.

(88) Kranig, W.; Boeffel, C.; Spiess, H. W.; Karthaus, O.; Ringsdorf, H.; Wustefeld, R. *Liq. Cryst.* **1990**, *8*, 375-388.

(89) Tsukruk, V. V.; Wendorff, J. H.; Karthaus, O.; Ringsdorf, H. *Langmuir* **1993**, *9*, 614-618.

(90) Boden, N.; Bushby, R. J.; Lu, Z. B.; Lozman, O. R. *Liquid Crystals* **2001**, *28*, 657-661.

(91) Arikainen, E. O.; Boden, N.; Bushby, R. J.; Lozman, O. R.; Vinter, J. G.; Wood, A. *Angew. Chem. Int. Ed.* **2000**, *39*, 2333-2336.

(92) Park, L. Y.; Hamilton, D. G.; McGehee, E. A.; McMenimen, K. A. *J. Am. Chem. Soc.* **2003**, *125*, 10586-10590.

(93) Wegewijs, B. R.; Siebbeles, L. D. A.; Boden, N.; Bushby, R. J.; Movaghar, B.; Lozman, O. R.; Liu, Q.; Pecchia, A.; Mason, L. A. *Phys. Rev. B* **2002**, *65*.

(94) Pecchia, A.; Lozman, O. R.; Movaghar, B.; Boden, N.; Bushby, R. J.; Donovan, K. J.; Kreouzis, T. *Phys. Rev. B* **2002**, *65*.

(95) Kreouzis, T.; Scott, K.; Donovan, K. J.; Boden, N.; Bushby, R. J.; Lozman, O. R.; Liu, Q. *Chem. Phys.* **2000**, *262*, 489-497.

(96) Holst, H. C.; Pakula, T.; Meier, H. *Tetrahedron* **2004**, *60*, 6765-6775.

(97) Wu, J. H.; Watson, M. D.; Müllen, K. *Angew. Chem. Int. Ed.* **2003**, *42*, 5329-5333.

(98) Wang, Z. H.; Dötz, F.; Enkelmann, V.; Müllen, K. *Angew. Chem. Int. Ed.* **2005**, *44*, 1247-1250.

(99) Pisula, W.; Kastler, M.; Wasserfallen, D.; Pakula, T.; Müllen, K. *Journal of the American Chemical Society* **2004**, *126*, 8074-8075.

(100) Warman, J. M.; Van de Craats, A. M. *Molecular Crystals and Liquid Crystals* **2003**, *396*, 41-72.

(101) van de Craats, A. M.; Warman, J. M.; Fechtenkötter, A.; Brand, J. D.; Harbison, M. A.; Müllen, K. *Advanced Materials* **1999**, *11*, 1469-1472.

(102) Ban, K.; Nishizawa, K.; Ohta, K.; de Craats, A. M. V.; Warman, J. M.; Yamamoto, I.; Shirai, H. *J. Mater. Chem.* **2001**, *11*, 321-331.

(103) Warman, J. M.; Schouten, P. G. *Applied Organometallic Chemistry* **1996**, *10*, 637-647.

(104) Schouten, P. G.; Warman, J. M.; Gelinck, G. H.; Copyn, M. J. *J. Phys. Chem.* **1995**, *99*, 11780-11793.

(105) Warman, J. M.; Piris, J.; Pisula, W.; Kastler, M.; Wasserfallen, D.; Müllen, K. *Journal of the American Chemical Society* **2005**, *in press*.

(106) Ito, S.; Wehmeier, M.; Brand, J. D.; Kübel, C.; Epsch, R.; Rabe, J. P.; Müllen, K. *Chem. Eur. J.* **2000**, *6*, 4327-4342.

(107) van de Craats, A. M.; Warman, J. M. *Synthetic Metals* **2001**, *121*, 1287-1288.

(108) Müller-Horsche, E.; Haarer, D.; Scher, H. *Phys. Rev. B* **1987**, *35*, 1273-1280.

(109) Kepler, R. G. *Phys. Rev.* **1960**, *119*, 1226-1229.

(110) Bassler, H. *Physica Status Solidi B-Basic Research* **1993**, *175*, 15-56.

(111) Ochse, A.; Kettner, A.; Kopitzke, J.; Wendorff, J. H.; Bassler, H. *PCCP* **1999**, *1*, 1757-1760.

(112) Arikainen, E. O.; Boden, N.; Bushby, R. J.; Clements, J.; Movaghar, B.; Wood, A. *J. Mater. Chem.* **1995**, *5*, 2161-2165.

(113) Boden, N.; Bushby, R. J.; Lozman, O. R.; Lu, Z. B.; McNeill, A.; Movaghar, B. *Molecular Crystals and Liquid Crystals* **2004**, *410*, 541-549.

(114) Ohta, K.; Hatsusaka, K.; Sugibayashi, M.; Ariyoshi, M.; Ban, K.; Maeda, F.; Naito, R.; Nishizawa, K.; van de Craats, A. M.; Warman, J. M. *PCCP* **2003**, *397*, 325-345.

(115) Iino, H.; Hanna, J.; Bushby, R. J.; Movaghar, B.; Whitaker, B. J.; Cook, M. J. *Appl. Phys. Lett.* **2005**, *87*.

(116) Fujikake, H.; Murashige, T.; Sugibayashi, M.; Ohta, K. *Appl. Phys. Lett.* **2004**, *85*, 3474-3476.

(117) Borsenberger, P. M.; Pautmeier, L.; Bässler, H. *Journal of Chemical Physics* **1991**, *94*, 5447-5454.

(118) Schmidt-Mende, L.; Fechtenkötter, A.; Müllen, K.; Friend, R. H.; MacKenzie, J. D. *Physica E-Low-Dimensional Systems & Nanostructures* **2002**, *14*, 263-267.

(119) Brabec, C. J.; Cravino, A.; Meissner, D.; Sariciftci, N. S.; Rispens, M. T.; Sanchez, L.; Hummelen, J. C.; Fromherz, T. *Thin Solid Films* **2002**, *403*, 368-372.

(120) Brabec, C. J.; Sariciftci, N. S.; Hummelen, J. C. *Adv. Funct. Mater.* **2001**, *11*, 15-26.

(121) Kietzke, T.; Neher, D.; Landfester, K.; Montenegro, R.; Guntner, R.; Scherf, U. *Nature Mater.* **2003**, *2*, 408-U7.

(122) Kulbaba, K.; Cheng, A.; Bartole, A.; Greenberg, S.; Resendes, R.; Coombs, N.; Safa-Sefat, A.; Greedan, J. E.; Stover, H. D. H.; Ozin, G. A.; Manners, I. *J. Am. Chem. Soc.* **2002**, *124*, 12522-12534.

(123) Grimsdale, A. C.; Bauer, R.; Weil, T.; Tchebotareva, N.; Wu, J. S.; Watson, M.; Müllen, K. *Synthesis* **2002**, 1229-1238.

(124) Wudl, F. *J. Mater. Chem.* **2002**, *12*, 1959-1963.

(125) Yu, G.; Gao, J.; Hummelen, J. C.; Wudl, F.; Heeger, A. J. *Science* **1995**, *270*, 1789-1791.

(126) Müller, M.; Zentel, R.; Maka, T.; Romanov, S. G.; Torres, C. M. S. *Adv. Mater.* **2000**, *12*, 1499-1503.

(127) Granstrom, M.; Petritsch, K.; Arias, A. C.; Lux, A.; Andersson, M. R.; Friend, R. H. *Nature* **1998**, *395*, 257-260.

(128) Zhi, L. J.; Gorelik, T.; Friedlein, R.; Wu, J. S.; Kolb, U.; Salaneck, W. R.; Müllen, K. *Small* **2005**, *1*, 798-801.

(129) Zhi, L. J.; Gorelik, T.; Wu, J. S.; Kolb, U.; Müllen, K. *J. Am. Chem. Soc.* **2005**, *127*, 12792-12793.

(130) Zhi, L. J.; Wu, J. S.; Li, J. X.; Kolb, U.; Müllen, K. *Angew. Chem. Int. Ed.* **2005**, *44*, 2120-2123.

(131) Kastler, M.; Pisula, W.; Wasserfallen, D.; Pakula, T.; Müllen, K. *J. Am. Chem. Soc.* **2005**, *127*, 4286-4296.

4 Functionalization of Hexa-*peri*-hexabenzocoronenes

Particularly in recent years, having been spurred on by the increasing technological promise of the π-stacks as conducting pathways in organic-based electronics, the synthetically driven ultimate aim of this work is to design and prepare new functional materials for use in electronic or other devices.[1] Control of their optical and electronic properties by synthetic design and the evaluation of their potential for electronic applications are thus key features of our work.[2] A vital aspect of this is the control of the supramolecular order of the materials in the solid state, by regulation of their intermolecular interactions.[3]

Derivatives of hexa-*peri*-hexabenzocoronene (HBC), as presented in the previous chapters, offer a great balance between straight forward synthetic approach and excellent properties, which make this group of materials very promising for applications in different organic devices.[4] However, the fine-tuning of the supramolecular organization and a decoration of the aromatic cores with different functionalities remains an interesting field to design novel materials. Hydrogen bonding groups have been introduced into the corona, which improved the intermolecular organization.[5] However, the additional interactions rendered the material insoluble and hampered therefore a reasonable processing into films, required for the implementation into devices. A particular aim is to obtain materials that can be readily processed for use in electronic and optoelectronic devices.

4.1 Attachment of a Chromophore

D. BRAND investigated the *a posteriori* functionalization of bromo-substituted, soluble HBC derivatives with palladium catalyzed cross-coupling reactions (Scheme 4-1).[6]

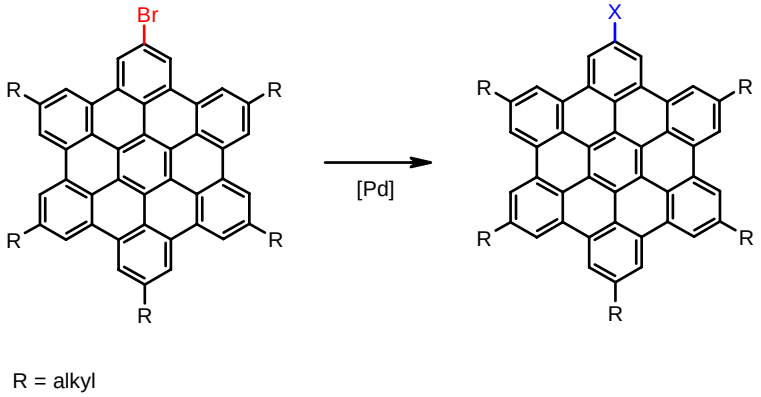

Scheme 4-1: *Functionalization of bromo-functionalized HBC derivatives using palladium catalyzed cross-coupling reactions.*

This functionalization open N. TCHEBOTAREVA the possibility to design a whole variety of functionalized HBC derivatives and to investigate the influence of distinct substitutions onto the supramolecular organization of these materials.[7] HBC derivatives emerged from her work, which were carrying different acceptor components connected via alkyl tethers of different lengths. These dyads phase segregated on the nanoscale and formed stable mono-layers on HOPG, which were imaged with scanning tunneling microscopy (STM).[8,9]

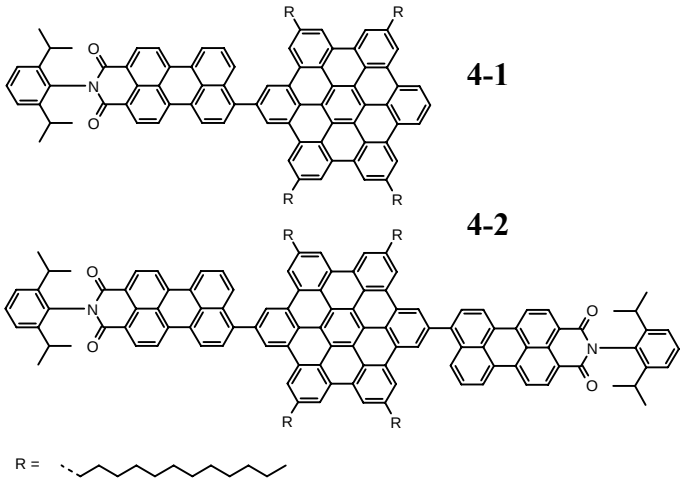

Figure 4-1: *Donor and acceptor dyads synthesized by A. FECHTENKÖTTER and E. REUTHER.*

In my diploma thesis, I worked on the BUCHWALD derivatization of HBC derivatives to influence the energy gap. However, it turned out, that single amino-groups caused

only a small change of the electronic levels of the large, aromatic disc.[10] In the literature, there has been an impressive example, where six perylenedicarboximonoimid (PMI) moieties were attached into the shell of an dendronized HBC derivative, which allowed studying the intramolecular energy transfer processes.[11] E. REUTHER and A. FECHTENKÖTTER worked together on the synthesis of PMI functionalized HBC derivatives **4-1** and **4-2** (Figure 4-1), where the rylene dye moiety was directly attached to the aromatic HBC core.[12] These covalently linked donor-acceptor systems revealed an ultrafast excitation energy transfer, which could not be resolved with the picosecond time correlated single photon counting technique. However in the bulk state, the materials did not organize forming long-range order. Furthermore, the synthesis of these dyads required SUZUKI coupling and the synthesis of adequate starting materials, which resulted in low yields of the desired materials.

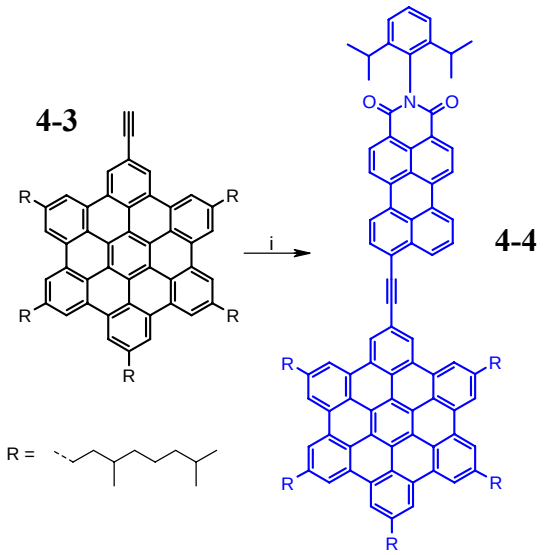

Scheme 4-2: *i) 9-Bromo-N-(2,6-di-iso-propylphenyl)-perylene-3,4-dicarboxiimide, PPh_3, CuI, $Pd(PPh_3)_4$, 72%.*

In the following, the synthesis of a donor-acceptor dyad will be presented, where the accepting and the donating entity are separated by a conjugating carbon-carbon triple bond. In contrast to the known derivatives **4-1** and **4-2**, the tedious purification after the palladium catalyzed cross-coupling reaction should be prevented by using a HAGIHARA-SONOGASHIRA protocol, which can be conducted in higher yields and produces usually less side-products. The introduction of a carbon-carbon-triple bond onto a phenyl unit causes less steric problems than the formation of an aryl-aryl bond. Besides these synthetic advantages, the triple bond between the two chromophores

would allow the dyad to be planar and therefore in better conjugation. The material suggested the implementation as auxiliary component in heterojunction photovoltaic devices to tune the phase-segregation and therefore the interface between donor and acceptor component.

The first starting materials consisted of the ethynyl substituted HBC derivative **4-3**, which has been previously prepared over 11 steps with an overall yield of around 4%.[7,10] This compound was coupled in a straight forward HAGIHARA-SONOGASHIRA cross-coupling reaction with 9-bromo-N-(2,6-di-iso-propylphenyl)-perylene-3,4-dicarboxiimide, which was obtained from BASF.

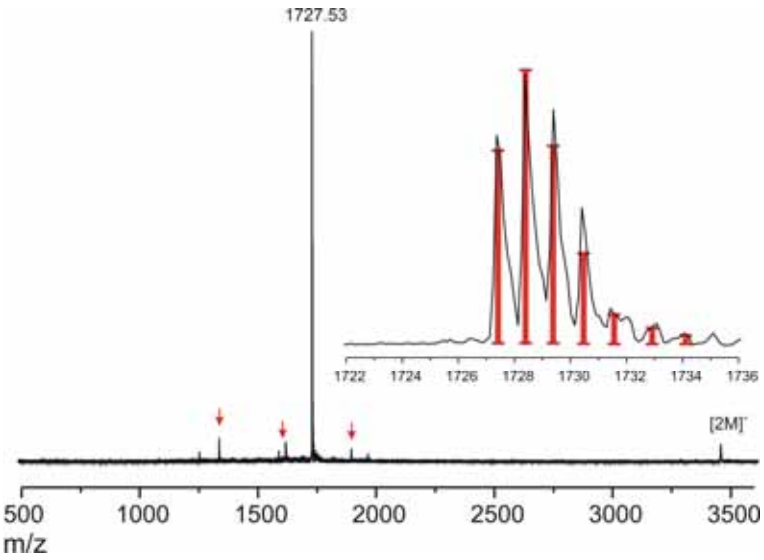

Figure 4-2: *MALDI-TOF spectrum of HBC-PMI* **4-4***, solid-state preparation using TCNQ as the matrix substance.*

After the column chromatographical purification, the HBC-PMI **4-4** was obtained in good yield and pure, as indicated by the MALDI-TOF spectrum (Figure 4-2). The determined isotope distribution was in good agreement with the simulation. However, the spectrum showed traces of impurities which could not be assigned. Furthermore, NMR spectra could be recorded of the very well soluble, purple HBC-PMI **4-4**. All proton resonances could be assigned to their corresponding nuclei (Figure 4-3) using two dimensional NMR experiments (HH COSY and NOESY). The ^{1}H NMR spectrum did not reveal any impurity.

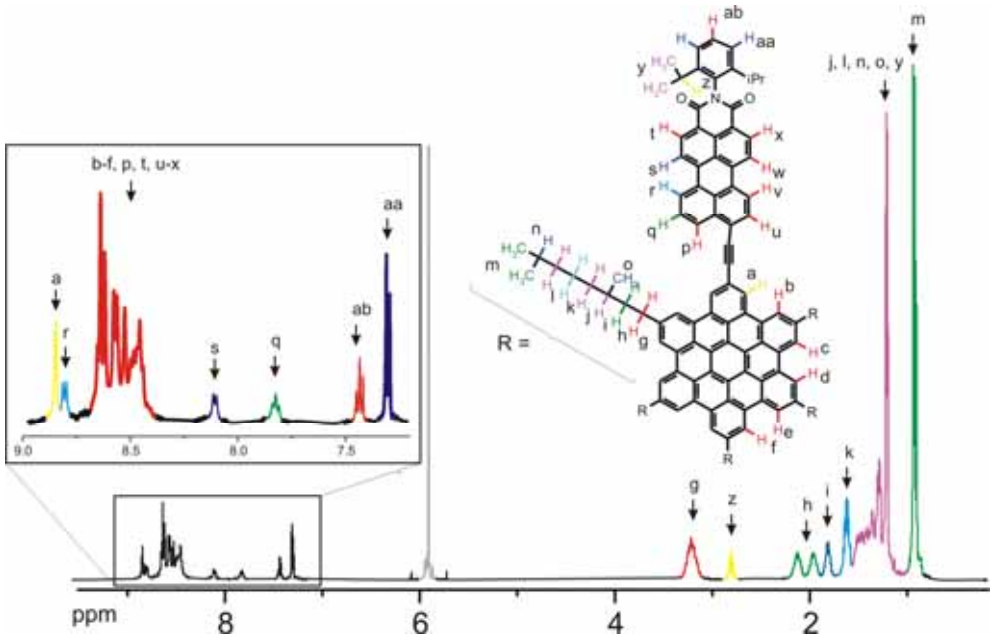

Figure 4-3: *^{1}H NMR spectrum of HBC-PMI* **4-4**, *recorded in 1,1,2,2-tetrachloroethane-d^{2} at 127 °C, solvent peak was colorized in grey.*

The UV/vis spectrum of HBC-PMI **4-4** consisted of two distinct maxima: the structured ultraviolet absorption with the maximum at around 380 nm and the other at the blue edge of the spectrum with a maximum of 540 nm. It is clear, that the ultraviolet absorption originated from the donor and the blue absorption from the accepting PMI moiety. This suggests a weak coupling in the dyad, which has been observed for similar compounds as well.[12] Excitation of the acceptor at 540 nm led to a strong, broad yellow photoluminescence which was shifted bathochromically by 50 nm compared to **4-1** and **4-2**. This indicated a better coupling of the donor and the acceptor component due to an unperturbed rotation of both components around the triple bond. The investigation of the energy transfer between donor and acceptor revealed a process with an efficiency of more than 98%.

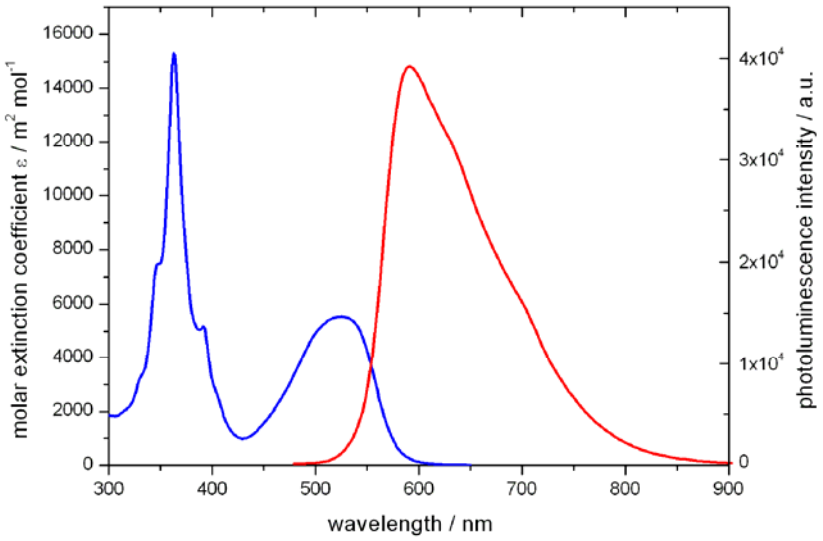

Figure 4-4: *UV/vis and PL (excitation at 370 nm) spectrum of HBC-PMI* **4-4** *recorded in chloroform.*

Expectedly, the photoluminescence quantum efficiency (Φ_f) was with 54% much higher than for unsubstituted HBC derivatives, which originated from the rylene chromophore.

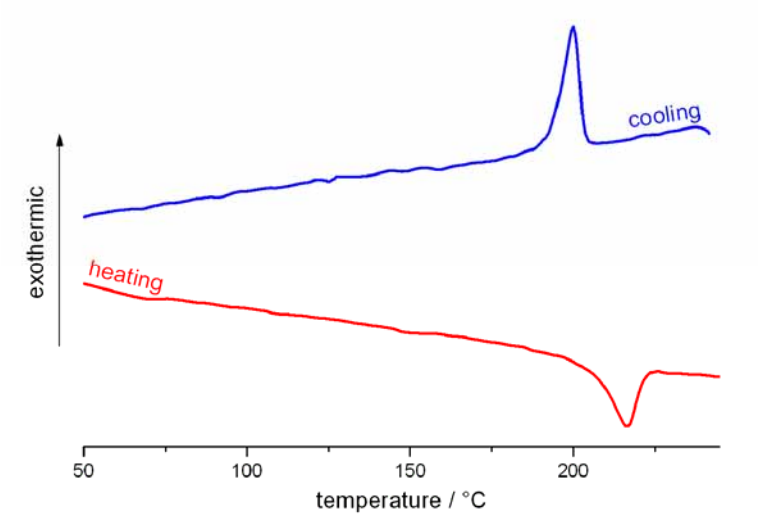

Figure 4-5: *DSC trace of HBC-PMI* **4-4**, *exhibiting a phase transition at 217 °C during heating (200 °C during cooling), recorded with a heating rate of 10 °C / min.*

The thermal behavior was investigated by differential scanning calorimetry (DSC). In the temperature range from -150 – 300 °C, one clear, endothermic peak at 217 °C was found, which was assigned to the crystalline-mesophase transition by means of two-dimensional wide-angle X-ray scattering (2D-WAXS). Compared to the parent HBC, which carries six identical alkyl chains HBC-$C_{8,2}$ **3-21** (C_r-Col_{ho} @ 81 °C), the

mesophase for HBC-PMI **4-4** was reached at far higher temperatures, which was due to the extended π-area and therefore a better packing in the crystalline phase.

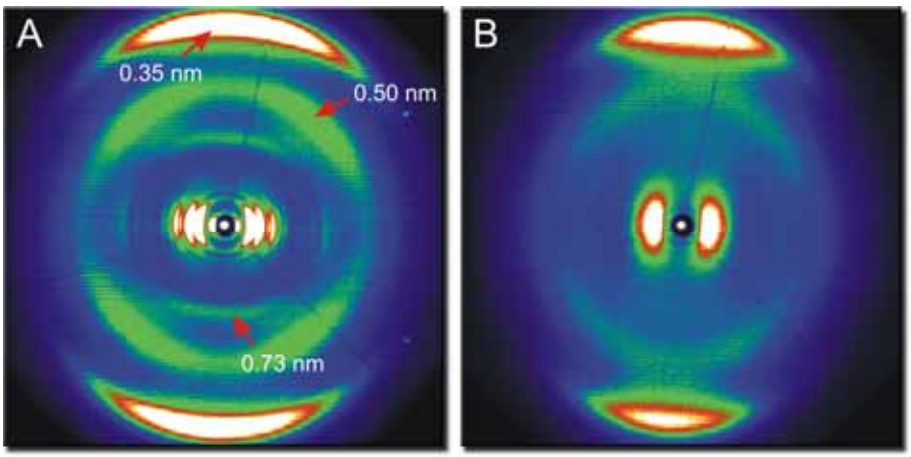

Figure 4-6: *2D-WAXS patterns of HBC-PMI* **4-4***, recorded (A) at room temperature phase (cubic unit cell with a = 5.31 nm) and (B) at 225 °C in the mesophase (hexagonal unit cell with a = 3.0 nm).*

The 2D-WAXS pattern of a mechanically extruded HBC-PMI **4-4** filament at room temperature (Figure 4-6A) showed a well organized, crystalline material. The equatorial reflex distribution allowed an untypically, large cubic unit cell to be determined, which is presented in Figure 4-7.

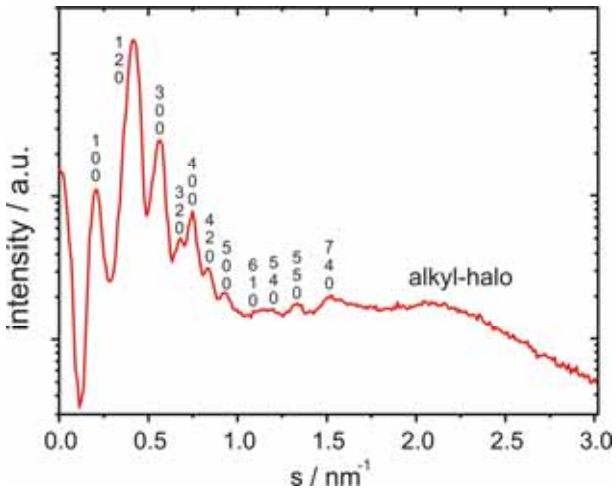

Figure 4-7: *Equatorial scattering intensity distribution as a function of the scattering vector s, the reflection positions are assigned by the* MILLER*'s indices according to the determined cubic unit cell.*

A series of meridional reflexes were found, which correspond to different stacking distances within the discotic material and suggested a high lateral order of the columns. The 2D-WAXS pattern at a temperature of 225 °C revealed to be typical for a columnar, ordered, hexagonal mesophase with a packing parameter of the size of the molecule.[13] Most of the higher order reflections disappeared indicating that also

the degree of structural order decreased significantly. The 2D-WAXS pattern is dominated by reflections indicating the short-range correlations.

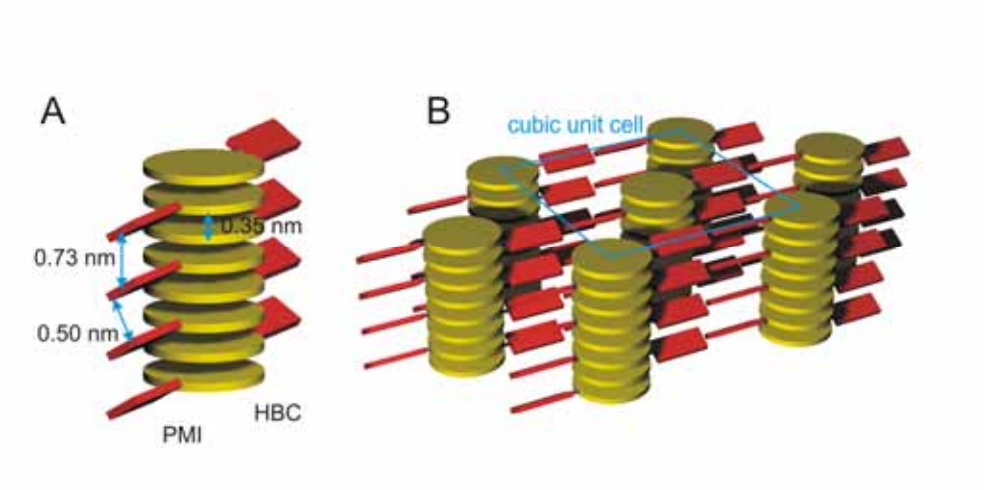

Figure 4-8: *Schematical representation of the supramolecular structure of HBC-PMI* **4-4** *in its room temperature phase. HBC and PMI core are colorized in yellow and red, respectively. The molecular dimensions fit the meridional reflections of the 2D-WAXS.*

Combining all information, the supramolecular organization of the HBC-PMI **4-4** molecules could be simulated (Figure 4-8). It is known that bulky units induce large steric requirements in the core periphery and induce a rotation of the molecules, which fits also in this case. Since the aromatic perylene unit is rotated out-of-plane with respect to the HBC core, as indicated by the off-meridional reflexes, two adjacent discs are not able to stack on top of each other with the same configuration, resulting in the lateral rotation of the molecules. The rotation of the donor and the acceptor against each other was confirmed by density functional calculations (DFT, 3-21G), which is not shown here. The meridional reflection peak, corresponding to a real space distance of 0.73 nm (correlation of very second disc) indicated that the molecules adopt only two different conformations in the stacked arrangement. This means that every second molecule within the stack was oriented the same way. The off-meridional reflections can be explained by the calculated tilting of the perylene moieties with an angle of nearly 45° which is also the azimuthal angle of the reflections. The correlation of 0.5 nm is in very good accordance with every second tilted perylene unit attached to the aromatic core. The large aromatic HBC moieties dominate the stacking and form a non-tilted columnar superstructure.

Interestingly, both the donating and the accepting entities within the dyad form a nano-separated columnar superstructure. The charge carrier mobilities for both parts

are very high, whereby HBC possibly transports holes and the PMI the electrons. This spontaneous formed “coaxial cable” suggests a testing in organic devices, such as solar cells. The interface between the donor and the acceptor component is very high. However, the risk for a fast recombination of charge carriers might limit the performance. Furthermore, the material could be added in small amounts as an auxiliary material to the heterojunction photovoltaic element of an HBC and a perylene derivative. Since the material is theoretical compatible to both components of the solar cell, the de-mixing in the fabrication process could be tuned. The high photoluminescence quantum yield in solution qualifies the material for testing as active component in organic light emitting diodes (oLED). Unfortunately, the material was not tested up to now in a device structure which is planned for the future.

The use of the higher-yielding HAGIHARA-SONOGASHIRA protocol to prepare a conjugated dyad between HBC and PMI allowed the material to be obtained on a multi-gram scale. This offered the opportunity to investigate the packing by means of 2D-WAXS experiments. The previously prepared materials **4-1** and **4-2** have been obtained only in very small quantities due to a very difficult separation from side-products. Therefore, the packing organization could not be investigated in the past.

4.2 a posteriori Functionalizations

In the previous chapter, the functionalization of the discotic HBC was described. However, the synthesis route comprised many synthetic steps and a relatively low overall yield.[4] The synthesis of many different derivatives based on that method becomes very tedious. Since the scope of the SCHOLL cyclodehydrogenation reaction does not permit a whole variety of different functions, the derivatizations have to be carried out on the already fused aromatic molecule.[14] This causes on the other hand difficulties to purify the usually strongly aggregating species, which hampered in many cases the isolation of the desired product. Therefore different concepts have been introduced using adequately functionalized HBC derivatives for a posteriori functionalizations.

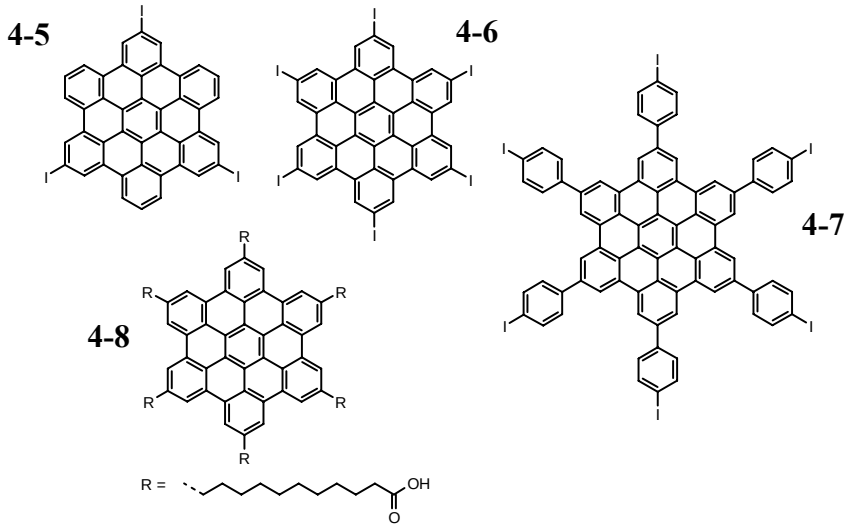

Figure 4-9: *Chemical structures of a posteriori functionizable HBC derivatives.*

J. WU introduced different iodo-functionalized HBC derivatives **4-5**, **4-6**, and **4-7**, which underwent successfully palladium HAGIHARA-SONOGASHIRA cross-coupling reactions.[15] Although hardly soluble, these building blocks were functionalized in many cases in a straight forward fashion.[16] However, some attempted conversions failed unexpectedly and in other cases the purification of the desired product could not be accomplished. The synthesis of large amounts of these precursors was complicated because of a long, multi-step synthesis.[17] D. BRAND presented a hexa-carboxy acid functionalized HBC **4-8**, which could be esterified with different alcohols.[6] Due to hydrogen bonds and thereby associated aggregation, this building block was not suitable for a whole variety of functionalizations. The overall yield of the nine step containing synthesis of **4-8**was smaller than 10%.

Gram-quantities of materials have to be obtained by a preferably simple synthesis, to allow the potential of a material to be tested in electronic applications.

4.2.1 Synthesis

In the following, the straight forward, high yielding synthesis of a HBC building block will be presented. Hydroxyl functions were used, which can be converted using many different methods. Very reactive carboxylic acid chlorides or anhydrides react quantitatively with the alcohol groups without producing side-products, which makes difficult purification steps needless.

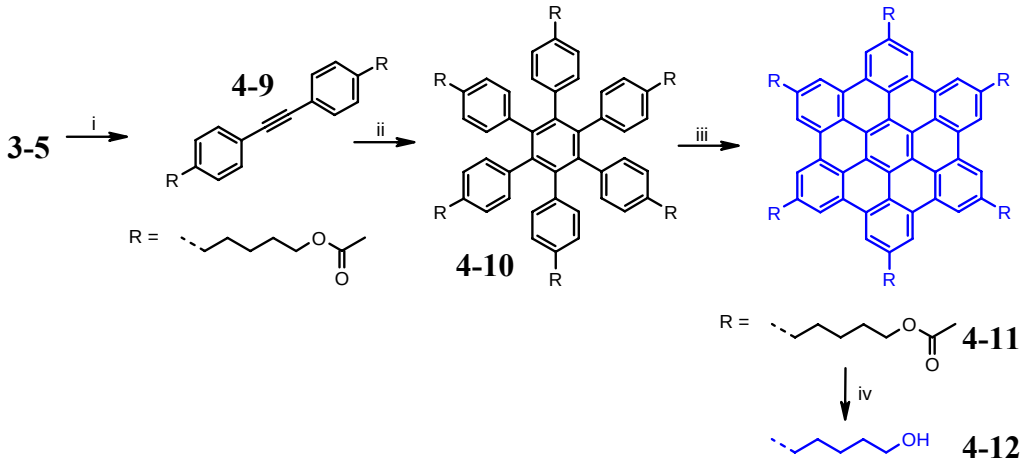

Scheme 4-3: *Synthesis of HBC-C_5OH* **4-12**, *i) 5-acetoxypen-1-ene, 9-BBN, NaOH, $Cl_2Pd[dppf]$, 81%; ii) $Co_2(CO)_8$, 91%; iii) $FeCl_3$, 95%; iv) KOH, MeOH, H_2O, 99%.*

The synthesis started with dibromotolane **3-5**, which was obtained in one step from commercially available 1-bromo-4-iodobenzene (**3-4**).[18] The conversion of the bromo functions in a palladium catalyzed SUZUKI coupling with the hydroboration adduct of 5-acetoxypent-1-ene yielded the desired tolane **4-9** in good yield. After the successful cobalt promoted cyclotrimerization, the hexaphenylbenzene derivative **4-10** was subjected to a SCHOLL reaction. Interestingly, large amounts of iron(III) chloride were necessary to planarize the molecule, because the acetyl esters coordinated iron, which could not take part in the reaction. HBC-C_5-OAc **4-11** was obtained as a yellow waxy, well soluble material, which permitted a column chromatographic purification to remove residual iron salts.After the purification, the acetyl protection groups were cleaved quantitatively with base to afford the crystalline HBC-C_5OH **4-12**. This building block was synthesized in five, straight forward steps starting from commercially available compounds in an overall yield of 64%. The scale-up of the

synthesis worked without any problem and multi-gram amounts of the HBC-C_5OH **4-12** were made. In most organic solvents, the material was even at elevated temperatures hardly soluble. However, in pyridine and DMF the HBC derivative showed a good solubility even at room temperature.

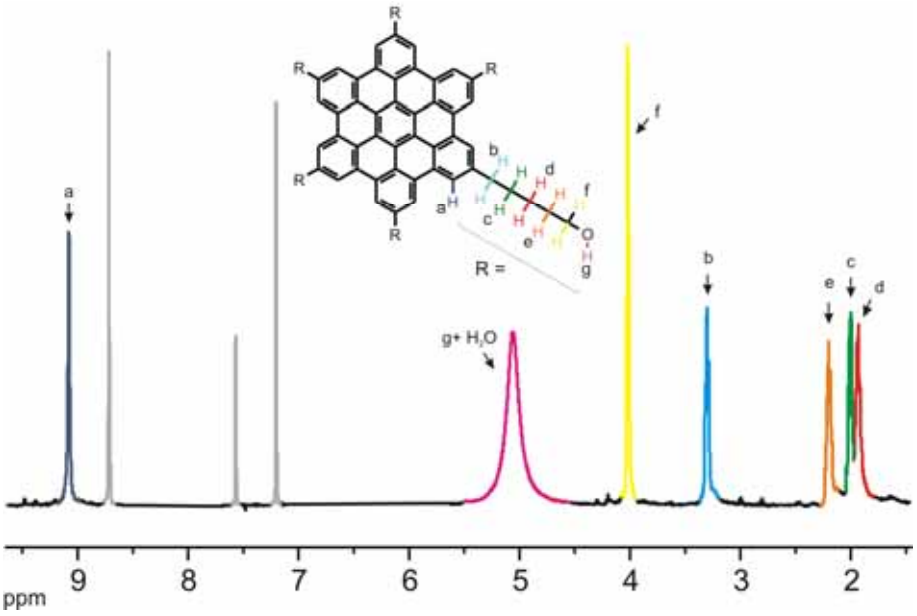

Figure 4-10: *^{1}H NMR spectrum of HBC-C_5OH* **4-12***, recorded in pyridine-d^5 (500 MHz), solvent signals are colorized in grey.*

Both ^{1}H NMR (Figure 4-10) and MALDI-TOF (Figure 4-11) analytics revealed the successful preparation of the desired material. All proton resonances could be assigned to their corresponding nuclei and the determined isotope pattern was in good agreement with the simulation.

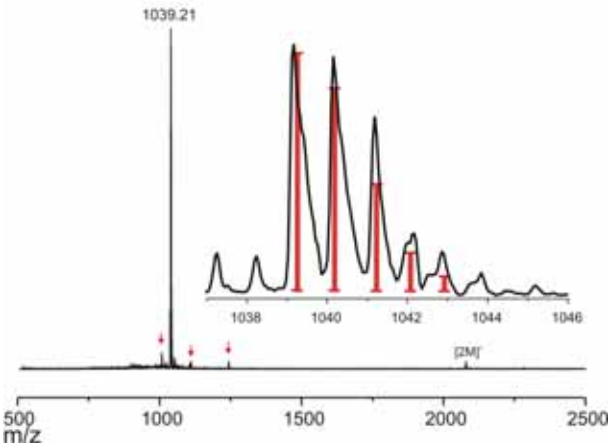

Figure 4-11: *MALDI-TOF spectrum of HBC-C_5OH* **4-12***, using the solid state preparation with TCNQ as the matrix substance; red arrows indicate traces of impurities, which could not be assigned.*

The success of the described synthesis towards HBC-C_5OH **4-12** motivated the synthesis of an analogous derivative carrying a longer alkyl tether. This allows the effect of proximity of the introduced function to be studied, when two derivatives with different tether lengths can be compared.

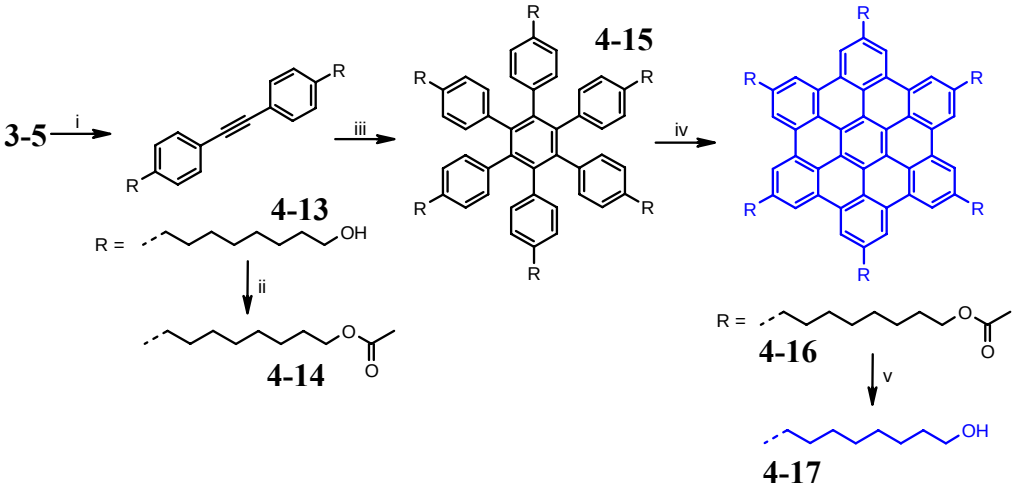

Scheme 4-4: *i) oct-7-en-1-ol, 9-BBN, NaOH, $Pd(PPh_3)_4$, 96%; ii) pyridine, Ac_2O, 96%; iii) $Co_2(CO)_8$, 89%; iv) $FeCl_3$, 74%; v) KOH, MeOH, H_2O, 99%.*

An HBC derivative with an alkyl tether length of eight carbon atoms has been synthesized analogously to HBC-C_5OH **4-12**. The conversion of the bromo functions of **3-5** was carried out with hydroborated oct-7-en-1-ol, which gave the alcohol functionalized tolane. The free hydroxyl groups were protected with acetyl, before the cyclotrimerization. After the SCHOLL reaction, the protection groups were cleaved to afford HBC-C_8OH **4-17** in an overall yield of 60%.

Figure 4-12 presents the recorded MALDI-TOF spectrum, which clearly indicated the successful reaction of the material. Similar to analogous acid functionalized HBCs[7], the longer tether imposed the molecule a better solubility, because the strong hydrogen bonding between the more flexible chains become weaker.[5]

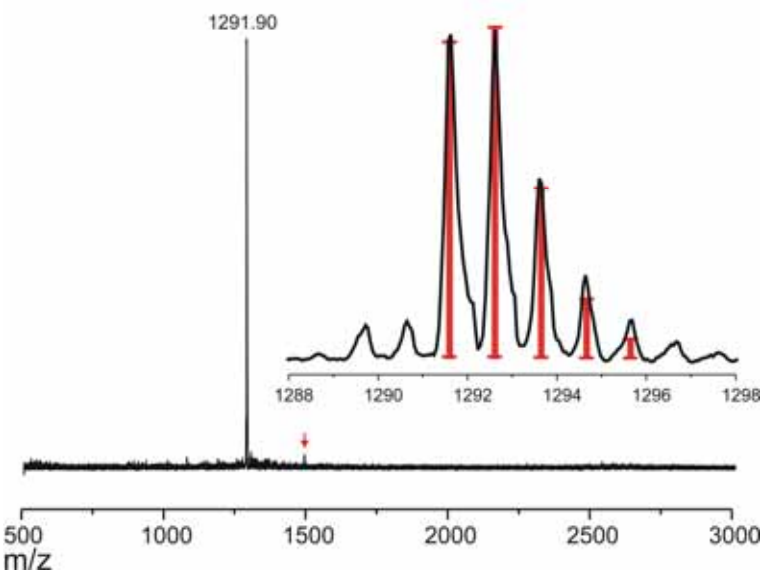

Figure 4-12: *MALDI-TOF spectrum of HBC-C_8OH* **4-17***, using the solid state preparation technique with TCNQ as the matrix substance, red arrow indicates a small amount of an unassigned impurity.*

Large amounts of both HBC-C_5OH **4-12** and HBC-C_8OH **4-17** were easily accessible and therefore the synthesis of tailored materials became possible. Hydroxy-functions were introduced at the ω-position of alkyl tethers onto the aromatic core of the HBC, which allow many different, high-yielding functionalizations.

Interestingly, the small extension of the alkyl tether by only three carbon atoms visually changed the bulk properties. While HBC-C_5OH **4-12** was a crystalline powder, the longer tether rendered the molecule waxier. In the following the supramolecular organization in the solid state will described.

4.2.2 Supramolecular Organization

The investigations of HBC derivatives bearing carboxylic acid functions in the periphery revealed a pronounced influence onto the columnar π-stacking.[5] The functionalization improved the order in the bulk and influenced the surface patterning.[19,20] In contrast to these acid group bearing derivatives, the alcohol substituted HBCs possessed a reasonable solubility in solvents like DMF or pyridine, because the established hydrogen bonds were not dimeric and therefore easier to break. This already suggested a different propensity to organize, since the introduction of only one acid function reduced the solubility in common organic solvents dramatically.

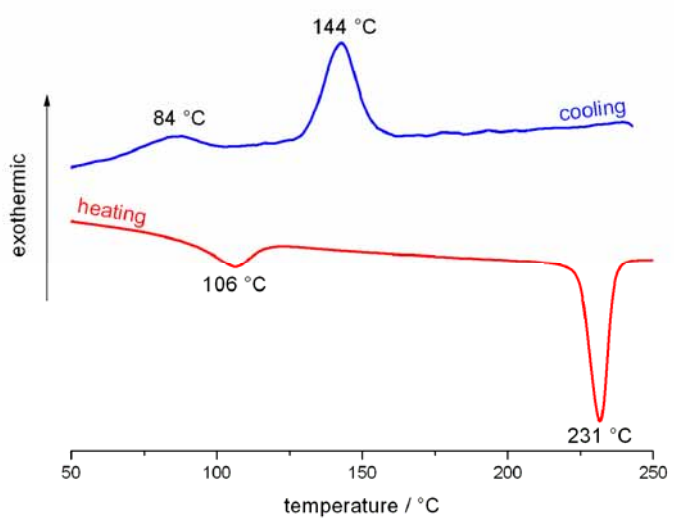

Figure 4-13: *DSC trace of HBC-C_5OH* **4-12***, recorded with a heating rate of 10 °C / min.*

The supramolecular organization of both HBC-C_5OH **4-12** and HBC-C_8OH **4-17** has been elucidated by means of 2D-WAXS and solid-state NMR experiments. The thermal behavior has been investigated with DSC. HBC-C_5OH **4-12** revealed two distinct phase transitions, as can be seen in Figure 4-13. Together with the following X-ray experiments, the room temperature phase was assigned to a crystalline phase (Cr_1). At 106 °C, the compound changed its crystalline packing and entered a second crystalline phase (Cr_2). Above 230 °C, the mesophase was reached.

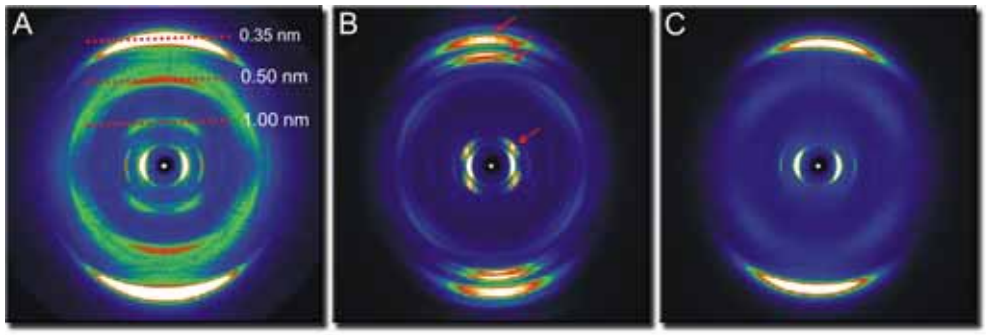

Figure 4-14: *2D-WAXS pattern of an extruded filament (extrusion temperature 250 °C) of HBC-C_5OH* **4-12***, (A) at room temperature, hexagonal (a = 2.18 nm) (B) at 150 °C, hexagonal (a = 2.14 nm) and (C) at 250 °C in the mesophase (hexagonal a = 2.21 nm).*

Filaments of HBC-C_5OH **4-12** were extruded from the mesophase to obtain mechanically well aligned samples.[13] The following experiments have been carried out by W. PISULA.

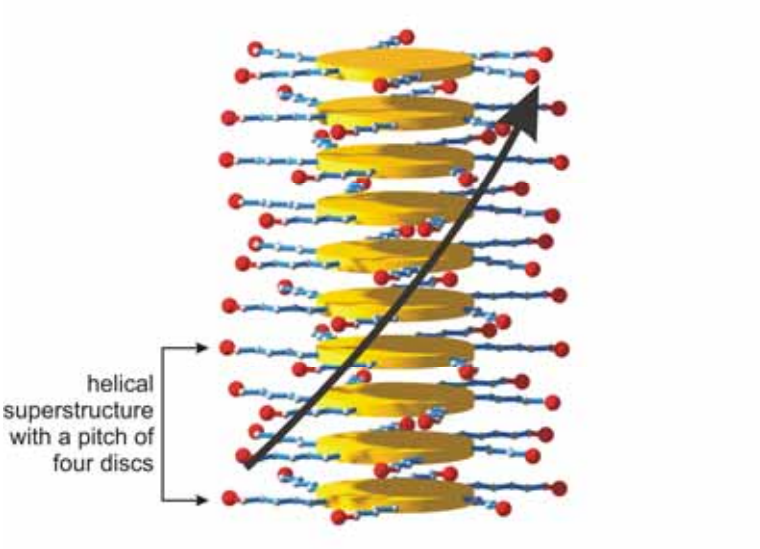

Figure 4-15: *Helical superstructure in the room temperature crystalline phase Cr_1 with a pitch of four HBC-C_5OH* **4-12** *molecules. Oxygen atoms are drawn as red balls, aromatic part was drawn as yellow disc.*

The 2D-WAXS pattern from the hexagonal Cr_1-phase showed a high order due to many sharp reflections (Figure 4-14A). The detailed interpretation allowed a helical arrangement to be elucidated, where the molecules are rotated by 20°, which means that every fourth disc is oriented in the same direction. The solid-state NMR investigations allowed a non-tilted planar stacking to be determined, whereby both substituents and the aromatic system are packed tightly and rigid. Entering the Cr_2 phase, the mobility of the side-chains increased which suggested a breaking of the hydrogen bonds.

As Figure 4-16 illustrates, the ^{1}H-^{1}H double quantum BaBa spectrum revealed the characteristic three aromatic resonances for a herringbone stacking.[21,22] The breaking of the hydrogen bonds allowed the aromatic discs to adopt the more favorable tilted stacking which is typical for crystalline HBC derivatives.[13] The analysis of the NMR sideband patterns (not shown) proved much higher chain mobilities for the substituents in the Cr_2 than in the room temperature Cr_1 phase.

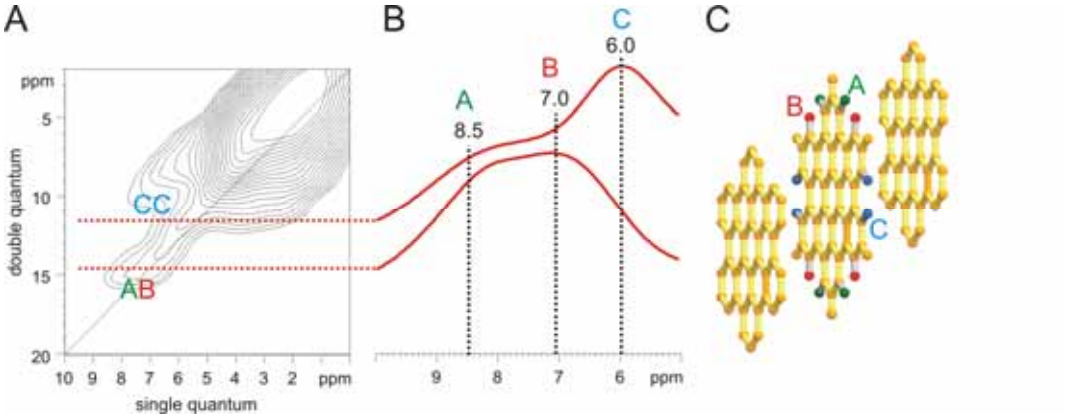

Figure 4-16: *(A) ^{1}H-^{1}H DQ BaBa spectrum of HBC-C_5OH* **4-12** *in its Cr_2 phase, recorded at 425 K with magic angle spinning of 30 kHz, (B) slices through (A) and (C) geometrical alignment of the discs in a tilted, columnar structure (herringbone type). The magnetically different hydrogens are labeled and colorized in the simulation and in (A) and (B).*

The 2D-WAXS pattern indicated a complex supramolecular, hexagonal organization with a high intracolumnar order as the multiple meridional reflections suggested (Figure 4-14B). A definite interpretation of the intracolumnar reflections was not possible up to now, however a helical arrangement is possible to be superimposed onto the columnar stacking. In contrast to that, the supramolecular structure of the mesophase was typical for HBC derivatives, where the columns are packed in a non-tilted, hexagonal lattice with molecules rotating on top of each other.[13] Figure 4-17 illustrates schematically the organization of HBC-C_5OH **4-12** in the three phases. Analogous to observations made for other hydrogen bonded HBCs, the hydrogen bonds are pulling the disc-like molecules into the atypical non-tilted stacking, forming a highly crystalline, helical columnar packing. Increasing the temperature, the hydrogen-bond equilibrium was shifted to the "open" form, which allowed at some point to establish the common tilted organization.[23]

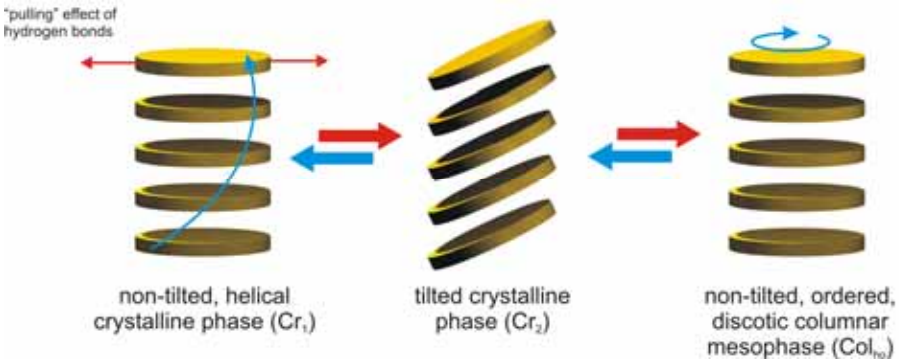

Figure 4-17: *Illustration of the intracolumnar organization of HBC-C_5OH* **4-12** *in its three observed phases.*

The substituents possessed flexibility and were not tightly packed anymore. Increasing the temperature further, the HBC derivative entered a typical ordered mesophase, observed for many similar materials before. In this phase both the aromatic disc and the substituents gained mobility. HBC-C_5OH **4-12** revealed an interesting supramolecular packing, which has not been observed for discotic materials before.

Surprisingly, the extension of the alkyl tether, as in the case of HBC-C_8OH **4-17**, allowed weakly ordered superstructures to be formed. As for carboxylic acid derivatives observed, longer alkyl spacers led to a higher flexibility in space and the hydrogen bonds are therefore much weaker and do not support the columnar stability. HBC-C_8OH **4-17** did not show an interesting superstructure.[5]

4.3 "Tailoring" Supramolecular Properties

The motivation for the synthesis of the alcohol decorated derivatives HBC-C_5OH **4-12** and HBC-C_8OH **4-17** was the potentially simple functionalization. Alcohols are known to react readily with "activated" carboxylic acids such as carboxylic acid chlorides and anhydrides. Alternative methods are known from the peptide synthesis.[24,25] Carbodiimides are well known agents for the formation of peptide bonds and are widely used for esterifications.[26] The decoration of the HBC core with different alkyl substituents has been shown to influence the phase behavior, the solubility and the supramolecular organization, as been described in chapter 1. However, the change of the alkyl chain required a novel multi-step synthesis with many purification steps.[27,28] The one-step functionalization of the hydroxyl group carrying HBCs as building blocks with alkyl carboxylic acids should give easily a large amount of different derivatives which can be tested in electronic devices.

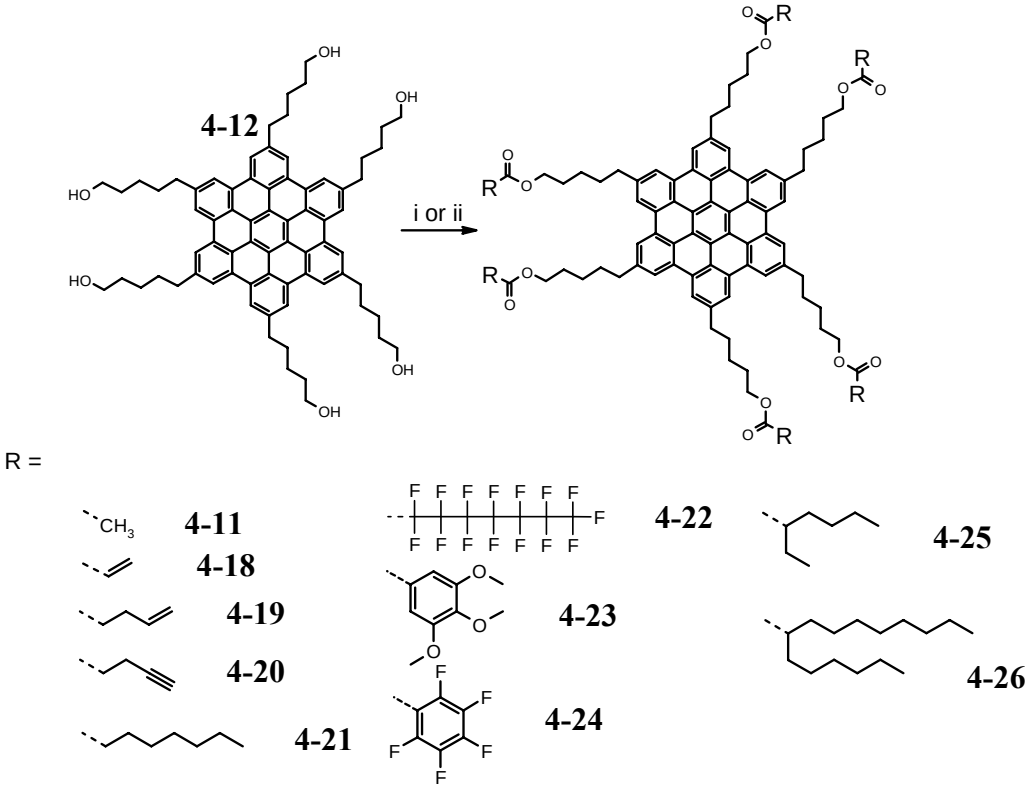

Figure 4-18: *Esterification of HBC-C_5OH* **4-12***; i) R-COCl or (R-CO)$_2$O, NEt$_3$, 59-89%; ii) R-COOH, DCC, DMAP, 75-89%.*

The first tested conversion on HBC-C_5OH **4-12** was the straight forward reaction of acetic anhydride in pyridine to re-protect the free hydroxyl groups, which was achieved quantitatively after one hour of reaction time. The reaction of commercially available acryloyl chloride with the HBC building block gave, in the presence of a

radial scavenger, HBC-C_5-acrylate **4-18** in a yield of 75% after several reprecipitation steps.[29]

The reaction with pent-4-enoyl chloride gave HBC-C_5-penten **4-19**, which carried six double bonds. These olefins can be converted into derivatives with other functionalities. Hydrosilylation of the double bonds has been performed.[30] However, the isolation of the product was difficult, because the reactive silyl groups underwent a condensation to form oligomers. Intended coating of glass substrates with this material failed because the condensation of the reactive groups proceeded in an intramolecular fashion and did not react with free hydroxy groups on the surface. Pent-4-ynoic acid was coupled in the presence of DCC and DMAP six times onto HBC-C_5OH **4-12**, which proved the high reactivity of the building block also in the reaction with free carboxylic acids. The six terminal triple bonds in HBC-C_5-pentyne **4-20** are potential reaction sites for "click"-chemistry or additions. Further functionalizations have not been tested so far. The decoration of the hydroxy groups with octanoic acid proceeded very smoothly and the well soluble HBC-C_5-C_8 **4-21** was isolated in a yield of 89%. The analogous reaction with the pentadecafluoro-octanoyl chloride gave the desired HBC-C_5-C_8F_{15} **4-22**, which was hardly soluble in the used solvent. In this case, although both the starting material and the product were not well soluble in the reaction solvent, the esterification worked with a yield of 79% after purification. Furthermore, donating and accepting benzoic acid chlorides were successfully subjected to the esterification. Both the HBC-C_5-$Ph(OMe)_3$ **4-23** and HBC-C_5-PhF_5 **4-24** are possible candidates for single-molecular field-effect transistors.[31] In these experiments, the derivatives are deposited onto HOPG and the aromatic core permits electrons to tunnel from the tip into the conducting support. The peripheral donor or acceptor moieties act as the gate, which can be biased by introducing charge-transfer complex partners. The tunneling current through the HBC core modulates by the nanometer-sized charge transfer complex in the periphery, which has been shown for an anthrachinone carrying HBC derivative, synthesized by Z. WANG.[32] The novel donor and acceptor materials were sent to the STM group of Prof. RABE, Berlin, where the molecules are currently tested. In the future, different donor and acceptor components have to be introduced onto the HBC core with varying tether lengths to gain a deeper understanding into the function of these chemically switchable, single-molecular FETs. The functionalization of

corresponding hydroxyl group carrying HBCs might offer access towards these materials. Analogous to the described examples, HBC-C_5-$C_{6,2}$ **4-25** and HBC-C_5-$C_{10,6}$ **4-26** have been synthesized and isolated purely.

Table 4-1: *Phase behavior of the functionalized HBC derivatives.*

Derivative	Temperature / °C	Enthalpy /Jg^{-1} (heating)	Phase-transition
HBC-C_5-OAc **4-11**	128 (98)	32.4	C_r – Col_{ho}
	~450*		Col_{ho} – I
HBC-C_5-acrylate **4-18**	112 (92)	26.5	C_r – Col_{ho}
	>150		polymerization
HBC-C_5-penten **4-19**	-1 (36)	27.9	C_r – Col_{ho}
	360*		Col_{ho} – I
HBC-C_5-pentyne **4-20**	85 (73)	8.86	C_r – Col_{ho}
	350*		Col_{ho} – I
HBC-C_5-C_8 **4-21**	53 (32)	43.3	C_r – Col_{ho}
	350*		Col_{ho} – I
HBC-C_5-C_8F_{15} **4-22**	-	-	
	>500*		melting
HBC-C_5-$Ph(OMe)_3$ **4-23**	34 (-22)	8.38	C_r – Col_{ho}
	>500*		Col_{ho} – I
HBC-C_5-PhF_5 **4-24**	53 (-18)	13.4	C_r – Col_{ho}
	>500*		Col_{ho} – I
HBC-C_5-$C_{6,2}$ **4-25**	15 (-3)	10.7	C_r – Col_{hd}
	205	7.47	Col_{hd} – I
HBC-C_5-$C_{10,6}$ **4-26**	-1 (-36)	8.25	C_r – Col_{hd}
	122	4.86	Col_{hd} – I

List of abbreviations: Cr – crystalline phase, Colho – mesophase (hexagonal ordered columnar phase), Colhd – mesophase (disordered hexagonal columnar phase) I – isotropic phase, phase transitions upon cooling are given in brackets, * - assigned by polarized optical microscopy.

Table 3-1 summarizes the thermal data obtained by DSC for the novel materials based on the functionalization of HBC-C_5OH **4-12**. It becomes quite obvious that the functionalization has a strong impact onto the position and broadness of the mesophase. Furthermore, the crystallinity, which is derived from the enthalpy of the crystal-mesophase transition, and the melting temperature could be tailored over a wider range. The functionalization of HBC-C_8OH **4-17** could be conducted by applying the same reaction conditions.

In conclusion, the hydroxy group carrying building blocks opened an elegant approach towards a large number of different HBC based derivatives. Going from the highly crystalline HBC-C_5-C_8 **4-21**, over its fluorinated analogue, which did not exhibit a stable mesophase anymore, to in its mesophase disordered HBC-C_5-$C_{6,2}$ **4-25**, many different derivatives with different properties have been obtained in a one-step synthesis. The peripheral decoration with perfluorinated chains, well-known for their low VAN-DER-WAALS forces[33], is known to reduce the intracolumnar interactions.[34]

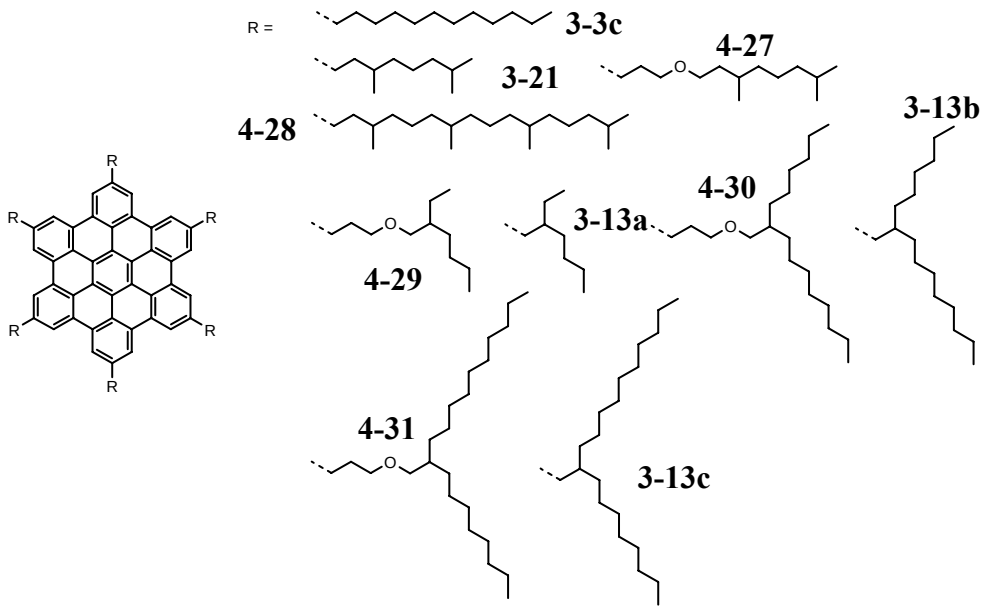

Figure 4-19: *Different alkyl chain carrying HBC derivatives.*

M. WATSON introduced a new type of alkyl chain onto the HBC core, which contained an ether function. The four derivatives HBC-$C_3OC_{8,2}$ **4-27**, HBC-$C_3OC_{6,2}$ **4-29**, HBC-$C_3OC_{10,6}$ **4-30**, and HBC-$C_3OC_{14,10}$ **4-31** have been prepared, which show homeotropical alignment when cooled from their isotropic state.[35]

However, the final SCHOLL reaction caused problems, since already a small excess of iron(III) chloride cleaved some of the ether chains, which made the isolation of the desired HBC derivative impossible. A tedious optimization of the right cyclodehydrogenation conditions was required. Only small amounts of these interesting materials could therefore be obtained. Interestingly, the 2D-WAXS patterns (Figure 4-20) recorded for filaments of the branched alkyl chain containing novel "HBC-ester" derivatives resembled the one of these "ether-HBCs". Both HBC-C_5-$C_{6,2}$ **4-25** and HBC-C_5-$C_{10,6}$ **4-26** revealed a weakly ordered, hexagonal mesophase at room temperature.

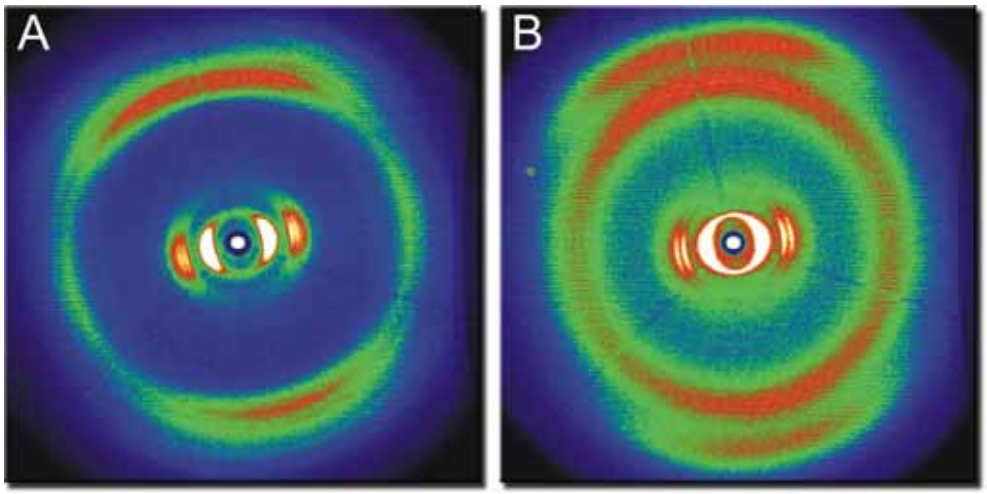

Figure 4-20: *2D-WAXS pattern of a filament of HBC-C_5-$C_{10,6}$* **4-26***, (A) at -70°C in its "plastic" columnar phase and (B) at room temperature in its disordered mesophase.*

Both derivatives showed, when crystallized from the isotropic state, a homeotropic alignment analogous to the previously synthesized ether containing derivatives.

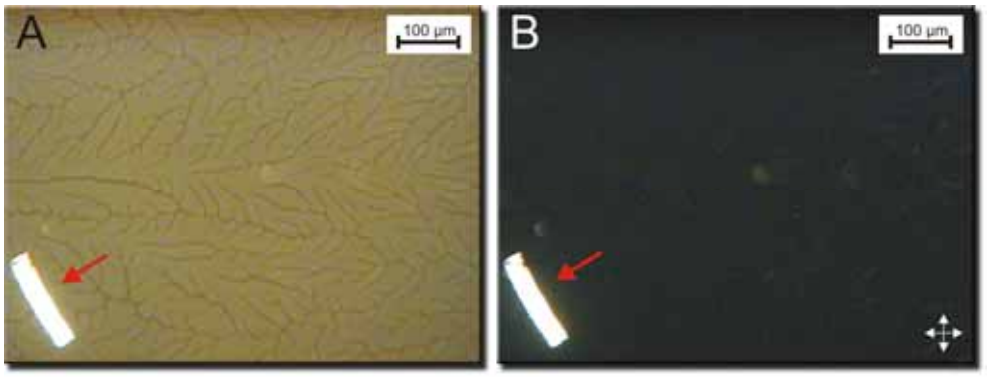

Figure 4-21: *HBC-C_5-$C_{10,6}$* **4-26***, cooled slowly from the isotropic state to room temperature (A) optical microscopy image and (B) with crossed polarizers, red arrows indicate a dust particle as reference point.*

As has presented in Figure 4-21, the optical microscopy image exhibits typical dendritic textures, which are not birefringent as seen with crossed polarizers. Large defect-free domains could be obtained when thin films of the sample were crystallized between glass slides (not shown).

The simpler synthetic access compared to the ether-chain decorated HBCs qualifies both HBC-C_5-$C_{6,2}$ **4-25** and HBC-C_5-$C_{10,6}$ **4-26** for the implementation into solar cells, since the “face-on” orientation is theoretically beneficial for a high performance. Preliminary TOF results revealed high mobilities for positive charge carriers. A detailed investigation will be performed in the near future.

4.4 Structure-Property Relation

In the last years, a whole variety of HBC derivatives has been synthesized, which carried different solubilizing alkyl substituents in the periphery.[36,37] Interestingly, the nature of these substituents heavily influenced the supramolecular organization of the discotic materials. Long-range ordering, self-healing ability, thermal position and broadness of the mesophase are only some properties, which can be controlled by tuning the flexible surrounding around the disc-like molecules.[2] Linear *n*-alkyl chains impose the material a high crystallinity, which causes a pronounced aggregation propensity and therefore a low solubility together with high isotropization temperatures.[38] A modulation of the strong π-stacking was achieved by introducing racemic, branched chains, which reduce the intermolecular, attractive forces. This led to a lowering of the crystallinity and the isotropization temperature.[4]

Simple volume calculations for the substituents around the HBC molecules have been performed, assuming a cylindrical space demand for linear chains and a conical for the branched analogues (Figure 4-22).

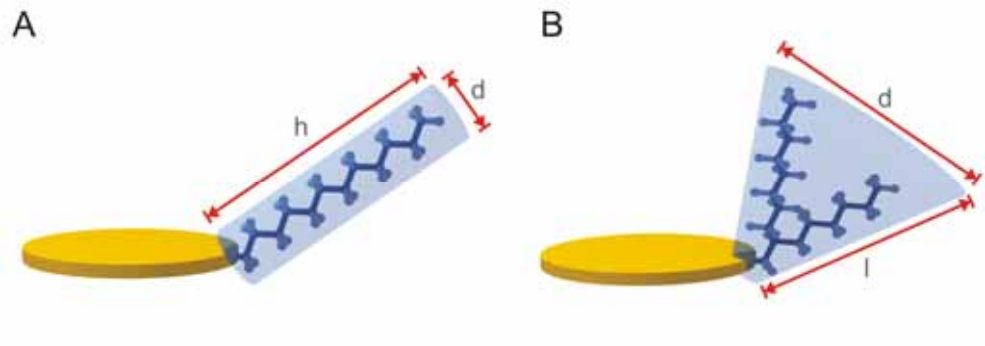

Figure 4-22: *Schematical illustration of (A) cylindrical space requirement of a linear chain (-C_{12}) and (B) conical space requirement of a branched alkyl chain (-$C_{10,6}$) on the aromatic HBC core.*

Plotting the calculated space demand for the substituents on different HBC derivatives on a logarithmic scale versus the isotropization temperature, one obtains a linear dependence (Figure 4-23). Intuitively, bulkier substituents caused a lowering of the isotropization temperature, compared to less demanding chains in the corona of the disc-like molecules, because these substituents sterically reduced the intermolecular interactions.[39]

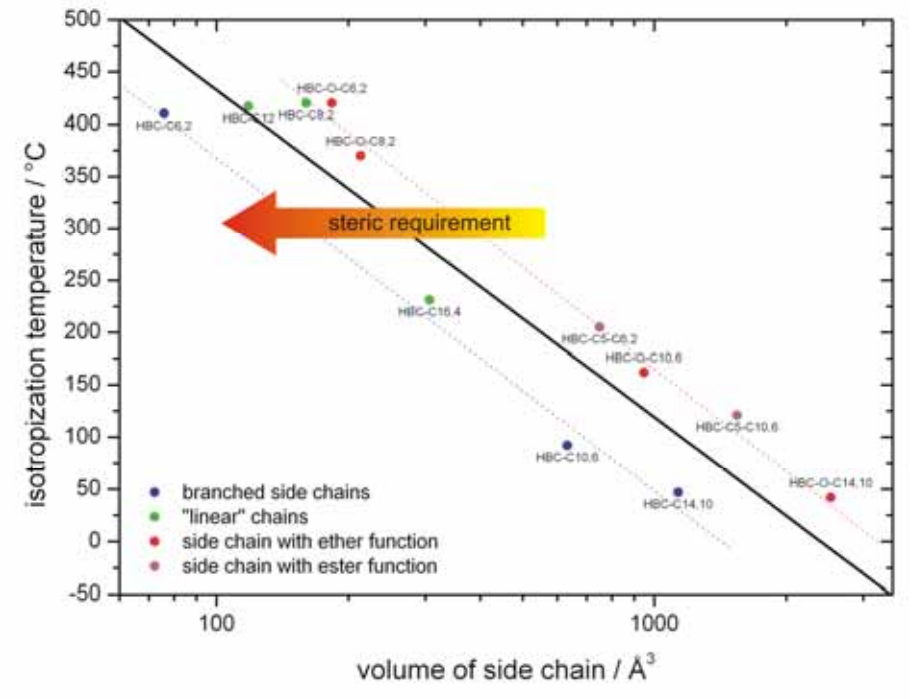

Figure 4-23: *Relation between the side-chain volume and the isotropization temperature of several different HBC derivatives.*

Comparing the derivatives with the branched alkyl chains, one observed that the isotropization temperature was lower for derivatives, where the branching site was in close proximity to the aromatic core. The derivatives, which have been introduced in the previous chapter, where the branching site is at the β-position, exhibited the lowest melting temperatures per volume side chain. Moving the branching site further away from the aromatic core, the ratio between melting temperature and side chain volume became smaller. Expectedly, the steric demand of the attached substituents allowed the intermolecular interaction to be controlled over a wide range.

This example impressively shows how the molecular properties such as the isotropization temperature can be tuned. This is a prerequisite for the successful implementation of such materials in devices.

4.5 Chemical Cross-Linking of Hexa-peri-hexabenzocoronene

Time-of-flight (TOF) experiments revealed that the macroscopic charge carrier mobility for most of the discotic materials can not be determined in their crystalline state due to a high trap concentration originating from grain boundaries.[40,41] In the mesophase, these inherent traps heal and high charge carrier mobilities can be determined, often with a non-dispersive transport mechanism.[42] This suggests operating electronic devices based on such semiconductors in their mesophase, which is usually at elevated temperatures and therefore difficult to realize.

4.5.1 Fixation of supramolecular organizations

In the following, the previously described HBC-C_5-acrylate **4-18** will be used to "freeze in" the supramolecular organization by an induced cross-linking of the acrylic ester functions. D. BRAND has synthesized two similar derivatives, where an acrylate or methacrylate moiety was attached in the ω-position of undecyl tethers (Figure 4-24).[29] In this case, the mesophase could not be reached without inducing a parallel cross-linking of the discotic molecules, what hampered the organization of the material and a successful processing into well ordered films.

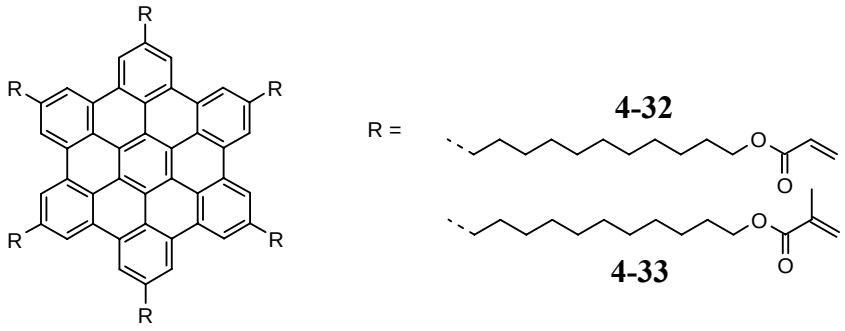

Figure 4-24: *"Polymerizable" HBC derivatives by D. BRAND, HBC-C_{11}-acrylate* **4-32** *and HBC-C_{11}-Methacrylate* **4-33**.

Figure 4-25 presents two separate heating-cooling DSC cycles. For HBC-C_5-Acrylat **4-18**, it was possible to reach the mesophase without initiating the cross-linking of the flexible surrounding. This is an important qualification to mechanically induce a macroscopic order by filament extrusion. During the first heating, the mesophase transition showed two endothermic peaks which was observed for HBC-C_{11}-acrylate **4-32** as well.[29] However, 2D-WAXS experiments could not elucidate the nature for this "double transition".

When the HBC-C_5-acrylate **4-18** was heated higher than 150 °C, the polymerization of the reactive acrylate moieties occurred without the addition of a photoinitiator, as can be seen be the strong exothermic peak in the DSC (Figure 4-25).

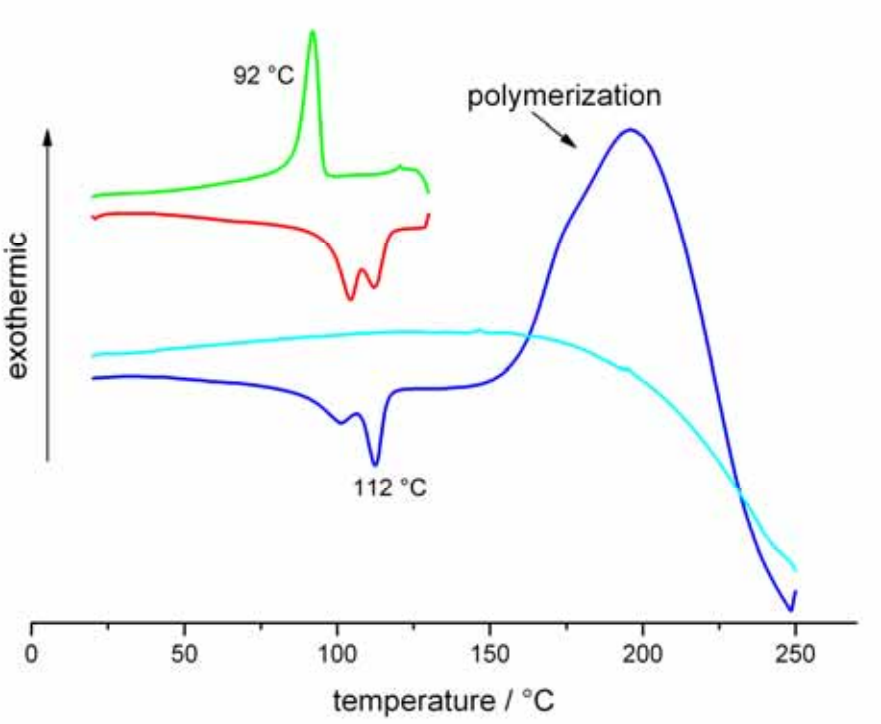

Figure 4-25: *DSC traces of HBC-C_5-acrylate* **4-18***, upper cycle shows the reversible transition into the mesophase and back to the crystalline room temperature phase, lower cycle indicates the polymerization during heating starting at 150 °C.*

The conversion of the acrylates to the corresponding polymer was calculated from the heat of polymerization (obtained by integration of the DSC trace) using the literature known value for acrylates (78 kJ mol^{-1}). The achieved polymerization degree was found to be 58% of double bonds, corresponding to 3-4 polymerized groups per molecule, which has been identical for the previously synthesized derivatives **4-32** and **4-33**.[29] Such a high degree of polymerization prevents any further phase transitions after the formation of the network, as evidenced that no glass transition was observed even down to temperatures as low as -150 °C. In addition, the brittle 3D network obtained did not show any solubility in common organic solvents even at high temperatures, prohibiting further characterization of the product by GPC or MALDI-TOF mass spectrometry.

In the case of the HBC-C_{11}-acrylate **4-32**, which D. BRAND synthesized, the photopolymerization failed, because the decomposition of the material during the

process was significant. Interestingly, the light-induced cross-linking of the reactive acrylate moiety in HBC-C_5-acrylate **4-18** proceeded much more effectively. The UV/vis spectrum of a freshly spin-coated and the subsequently polymerized (low pressure mercury lamp, 255 nm) and hydrazine treated films were identical (Figure 4-26). This indicated the absence of decomposed side-products, which was not observed for HBC-C_{11}-acrylate **4-18**. The shortening of the alkyl tethers led to an enhancement of the light-induced polymerization, because the reactive entities were less flexible in space and could form a network more easily.

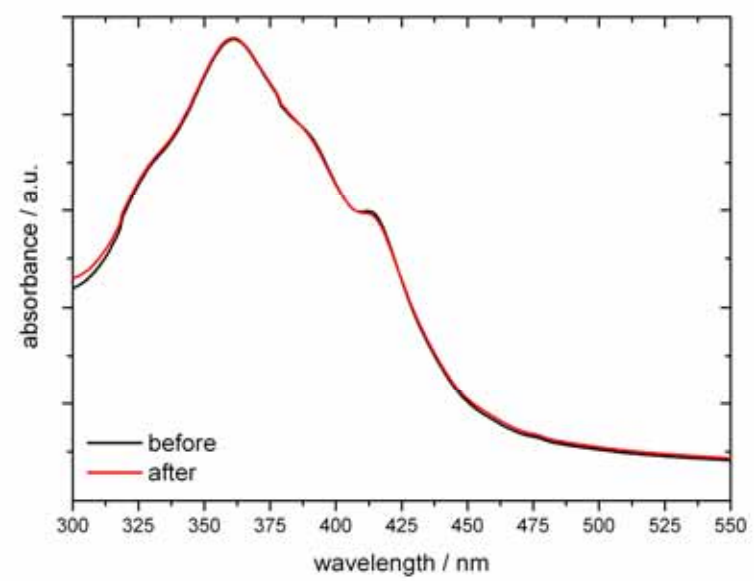

Figure 4-26: *Solid-state UV/vis spectrum of HBC-C_5-acrylate* **4-18** *before and after photo-polymerization (after polymerization, treatment with hydrazine gas).*

The irradiation of a concentrated THF solution of HBC-C_5-acrylate **4-18** did not yield polymerized high-molecular weight HBC-stacks. The MALDI-TOF spectrum showed even after long reaction times a significant amount of monomer (Figure 4-27). However, the spectrum, recorded in linear mode, revealed the presence of oligomers.

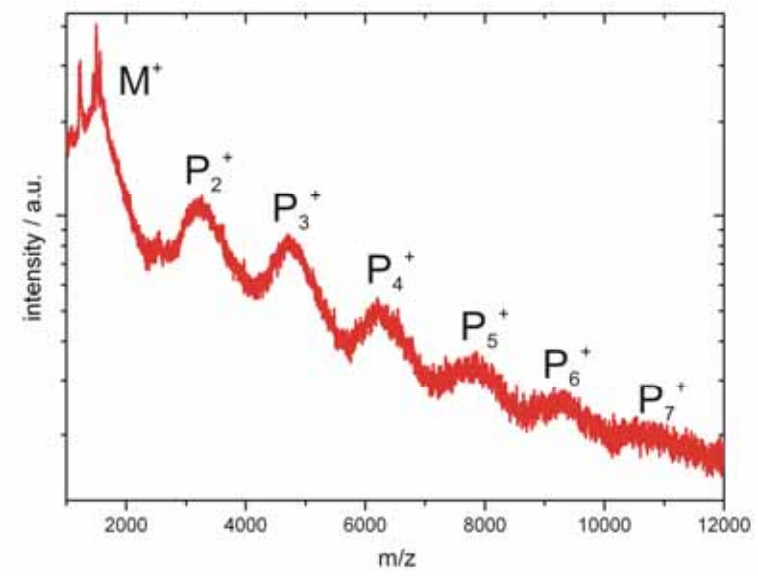

Figure 4-27: *MALDI-TOF spectrum (linear mode) of the attempted photopolymerization of HBC-C_5-acrylate* **4-18** *after an irradiation time of 48 hours. Spectrum shows monomer (M^+) and oligomers (P_n^+).*

The thermal polymerization of HBC-C_5-acrylate **4-18** proceeded also very smooth. A freshly spin-coated film of that material from a concentrated THF solution and subsequent cross-linking at a temperature of 160 °C for 15 minutes in an argon atmosphere rendered the material completely insoluble. The film was rinsed with dichloromethane, THF and even CS_2 for long times, but even after concentration of these solutions the photoluminescence did not exhibit characteristic spectra for HBC chromophores.

As already been observed in the DSC traces, the mesophase of HBC-C_5-acrylate was reached without initiating a parallel cross-linking of the peripheral chains. This opened the possibility to align the material mechanically by filament extrusion from the mesophase, which has been performed by W. PISULA.[13] The supramolecular organization of the extruded filaments was investigated by means of 2D-WAXS experiments. The room-temperature pattern (Figure 4-28A) revealed a typical hexagonal, highly ordered crystalline packing with very sharp and distinct reflections. The short substituents in the corona of that HBC derivative pack well and allow a highly organized lattice to be formed. When the filament was heated to 130 °C, the X-ray pattern indicated a typical organization of a discotic mesophase with more diffuse reflections (Figure 4-28B). When the sample was not heated higher that 140 °C, the crystalline organization was maintained after cooling back to room

temperature, what has been already indicated by the DSC experiment. However, when the material was brought above 150 °C, the cross-linking of the acrylate functions set in. The organization did not change during this process, as observed by the 2D-WAXS pattern, which resembled the one observed in the un-polymerized mesophase. After the cross-linking, the room temperature organization was identical to the one in the mesophase, what indicated a successful fixing of the supramolecular organization of the mesophase.

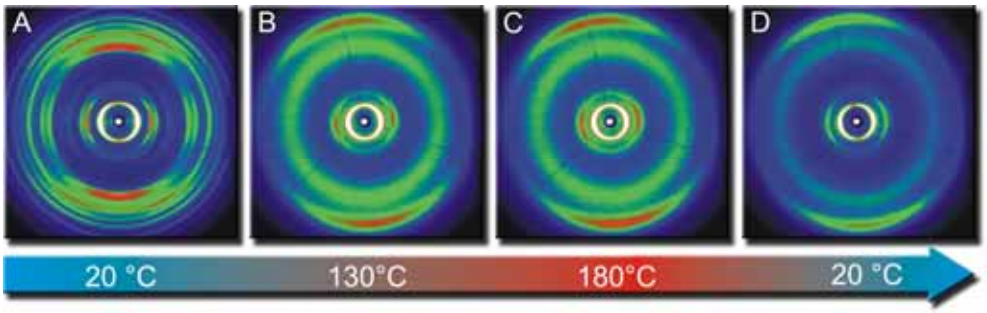

Figure 4-28: *2D-WAXS patterns of HBC-C_5-acrylate* **4-18**, *(A) room temperature, (monoclinic a = 2.16 nm, 2.06 nm, γ = 60°, 30° tilting of the discs with respect to the columnar axis, 0.35 nm distance between the discs) (B) in mesophase at 130 °C (hexagonal a = 2.41 nm, 0.36 nm distance between the discs), (C) during polymerization at 180 °C and (D) after polymerization at room temperature.*

Both tested external stimuli induce a cross-linking of the acrylate moieties in the periphery of HBC-C_5-acrylate **4-18**, which freezes the organization of the discs in.[43] For applications, it might be interesting to operate the device with a specific organization independent upon temperature to obtain the optimal performance.[44,45] The light-induced polymerization allowed the crystalline organization to be fixed, while thermal energy permitted to freeze in the supramolecular structure of the mesophase.

4.5.2 Nanostructuring

Most crucial for the performance of electronic devices is the formation of adequate morphologies which offer unperturbed percolation pathways to allow charge carriers to migrate between the working electrodes.[46] Especially for heterojunction photovoltaic devices, the self-assembly of the active components into interpenetrating networks is a critical factor for success.[47,48] The nanostructuring of donor or acceptor component into adequate assemblies promises success.

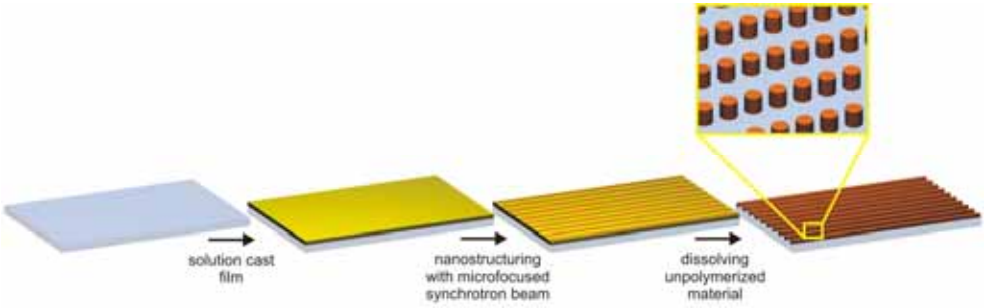

Figure 4-29: *Schematical illustration of the nanostructuring process with the focused synchrotron beam.*

The light induced polymerization using the light of an unfocussed mercury lamp has already been tested. Focused photon sources such as lasers or the synchrotron beam offer an elegant way to locally polymerize solution cast films of i.e. HBC-C_5-acrylate **4-18** into nanostructured assemblies. [49] A drop-cast film of the material from a concentrated chloroform solution was subjected to the microfocused synchrotron radiation with a beam diameter of *ca.* 800 nm. The cast film was moved in the synchrotron beam with a piezo stage and line scans were performed with a step width of 10 µm to locally cross-link the acrylate entities with the high-energy beam. After the exposure, the films were rinsed with THF and put over night into CS_2 to dissolve un-polymerized material. The complete process is illustrated in Figure 4-29.

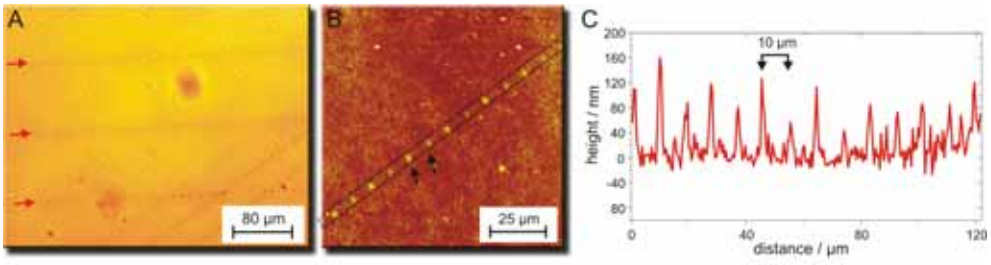

Figure 4-30: *Analysis of the nanostructured HBC-C_5-acrylate* **4-18** *(A) optical microscopy image, red arrows mark the written point-lines (B) AFM topology image, dotted box indicates the written "columns", black arrows point onto two "columns" and (C) height profile of the dotted box in (B), written "columns" are separated by ~10 µm.*

Already the optical microscopy allowed visualizing the polymerized, microscopic columnar structures (Figure 4-30). The images clearly exhibit lines composed of discrete points. The AFM topography image (Figure 4-30B) showed the same discrete columns which were separated by ~10 µm. The height of these columns varied between 120-160 nm (Figure 4-30C), which corresponded to the thickness of the cast films.

This experiment impressively showed the potential of the light-induced cross-linking of the HBC derivative into well organized nanostructured films. After having removed the un-polymerized material, one could fill the space between the structures with an adequate donor and test the performance in a heterojunction photovoltaic device. However, the cross-linked films were not macroscopically organized which would be required for electronic applications.

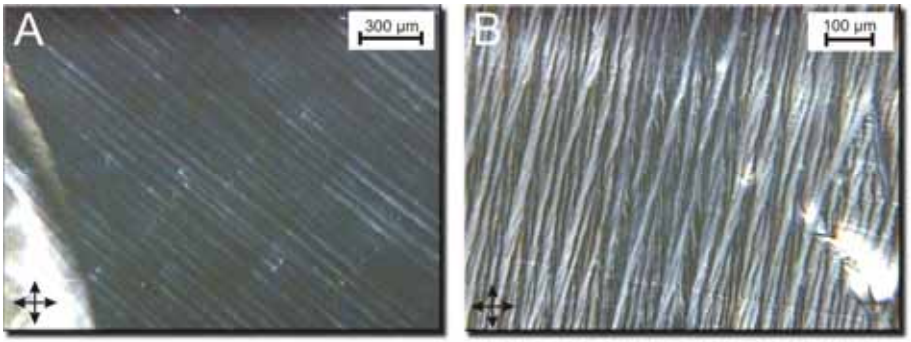

Figure 4-31: *POM images of zone-cast HBC-C_5-acrylate* **4-18** *films, different magnifications.*

Motivated by this idea, N. TSAO optimized the zone-casting (see chapter **1.1**) conditions for HBC-C_5-acrylate **4-18**. A detailed description of the casting parameters will be presented in his dissertation. Recently, he managed to obtain macroscopically, highly oriented thin films (Figure 4-31) of the polymerizable material, which could now be subjected to nanostructuring. Unfortunately, the solution casting only gives edge-on arranged molecules, due to the pronounced pre-aggregation of the utilized solution. This arrangement of the columnar structures is not favorable for fabrication of photovoltaic elements, where the charge carriers are supposed to travel vertically to the support. In contrast, FETs require the obtained organization of the columnar structures. With a focused photon source, single column bundles could be cross-linked and isolated to record the field-effect in such nanostructures. Experiments, where these structures are obtained either by a focused photon source or a heated AFM tip, are planed and will be conducted by N. TSAO in the future.

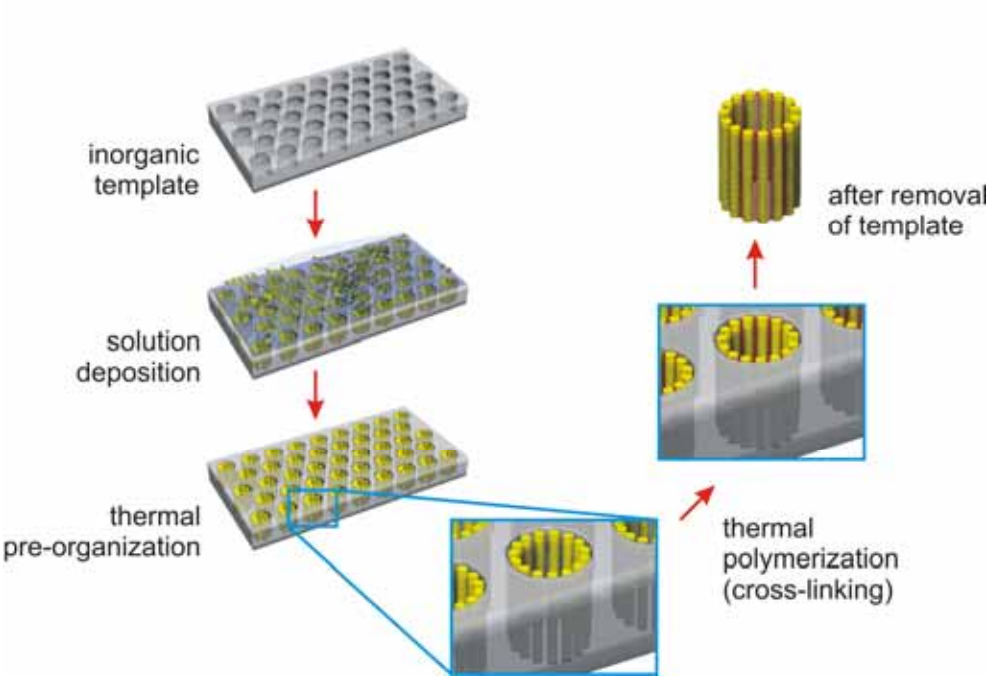

Figure 4-32: *Schematical illustration of templated polymerization process of HBC-C_5-acrylate* **4-18**.

A different method to nanostructure materials requires the use of adequate templates. Firstly introduced by M. WATSON, commercially available inorganic, mesoporous membranes permit the organization of columnar superstructures to be obtained in the pores.[50] As demonstrated in the previous chapter, the HBC derivatives bearing branched alkyl substituents were perfectly organized in the mesoporous material and subsequently cross-linked by a controlled pyrolysis as performed by L. ZHI.[51,52] The use of HBC-C_5-acrylate **4-18** would allow the pyrolysis process to be exchanged by a technologically cheaper, milder thermal cross-linking at a temperature below 200 °C.

Commercially available mesoporous aluminum oxide membranes have been filled by capillary forces with a solution of HBC-C_5-acrylate **4-18**. Thereby, the concentration and the solvent played an essential role to pre-organize the material within the pores. A 0.5 M solution of the compound in dichloromethane appeared to be ideal yielding pre-organized structures within the pores. As solution processing of pre-aggregated HBC molecules gave always edge-on arranged discs, the illustrated organization is expected (Figure 4-32). The filled membranes were heated in a heating stage at a rate of 0.1 °C per minute to 170 °C, where the sample was kept for one hour. After having cooled the sample again to room temperature, the inorganic membrane was dissolved with concentrated sodium hydroxide. The residue was carefully washed with water, before optical microscopy was utilized to visualize the obtained structures. The whole

process is illustrated in Figure 4-32. As expected, thin rod-like objects were found, which revealed birefringence with crossed polarizers (Figure 4-33A,B), indicating a high organization. SEM images emphasized the formation of nanotubes, which are organized in bundles (Figure 4-33C,D

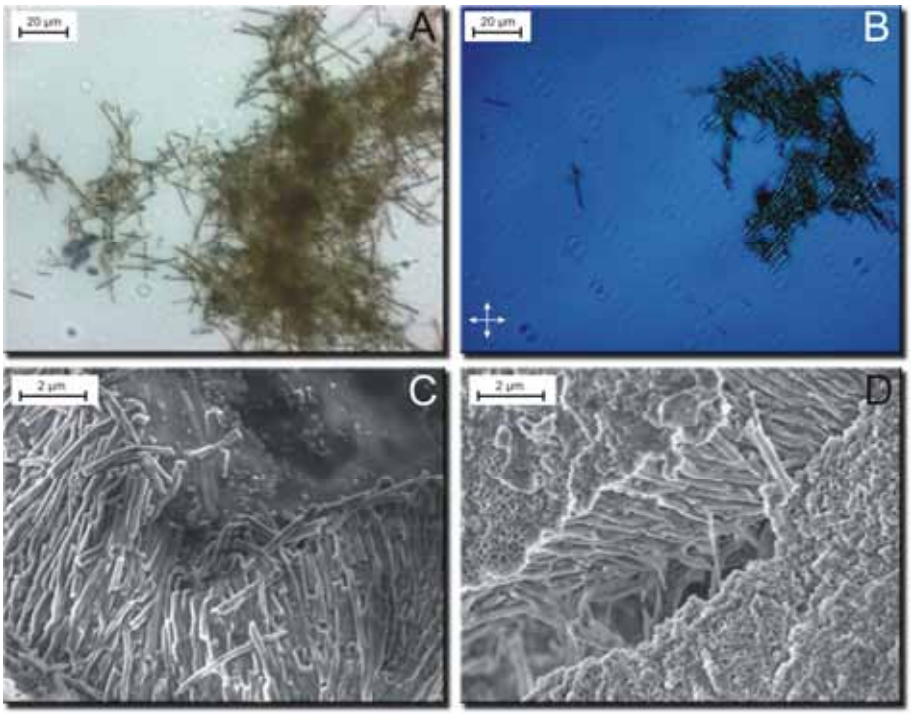

Figure 4-33: *Polymerized HBC-C_5-acrylate* **4-18** *after removal of the template, (A) optical microscopy image of the nanotubes, (B) POM image and (C) and (D) SEM images of the organized nanotubes.*

High resolution transmission electron microscopy (HRTEM) showed nanotubes with a well defined wall-structure (Figure 4-34B). As expected before, the molecules were aligned in the edge-on fashion before the polymerization. Some defects nanotubes were found (Figure 4-34A), which emphasized the necessity to optimize the process. Apparently, not enough material was available to wet the inner surface completely. Polymerization experiments in the membrane with higher concentrated solutions have been performed, but the TEM results are not available yet.

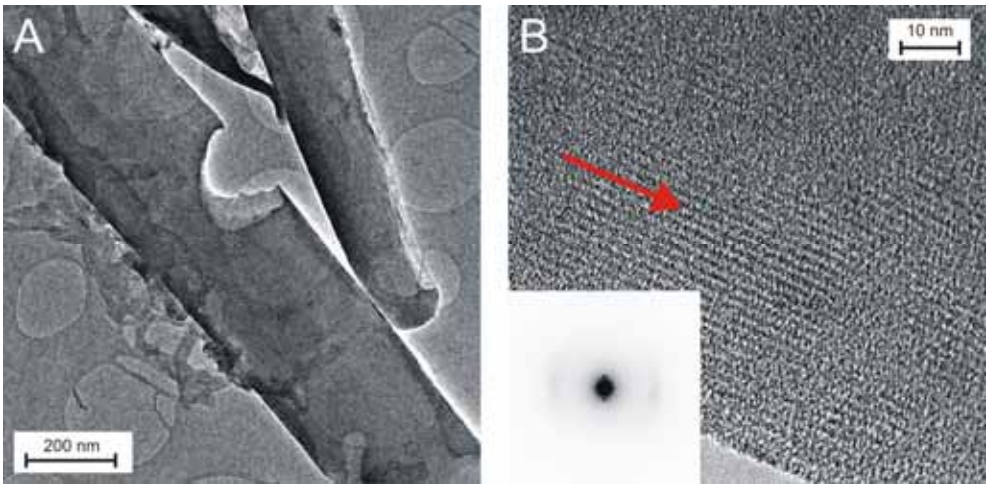

Figure 4-34: *(A) HRTEM image of the polymerized HBC-C_5-acrylate* **4-18** *nanotubes, (B) high magnification of the wall structure, inset: electron diffraction analysis; red arrow points into the direction of the columnar structures along the length of the tube.*

4.6 Summary

The chemical functionalization of discotic materials opened the possibility to tune the desired properties, such as electronic or self-assembly behavior. The conjugation of a PMI rylene dye to HBC's aromatic system severely influenced the stacking organization and expectedly the electronic properties. The control of HOMO and LUMO allows novel materials for applications in heterojunction photovoltaic devices to be designed, where the positions of the electronic level are important to guarantee the polarization of the excitons and thus a successful charge transfer process. However, the lengthy synthesis hampered to synthesize large quantities and to obtain differently substituted derivatives. The testing of materials in electronic devices requires a simple synthetic approach to react to the needs of the device fabrication. Therefore, a reactive HBC building block was synthesized which permitted very simple *a posteriori* functionalizations. A whole variety of differently substituted HBC ester derivatives has been made, which are currently investigated. In this case, the synthesis of the material was not the bottle-neck in the process to implement materials into electronic devices.

One very interesting material was obtained which carried cross-linkable entities attached at the end of a short flexible alkyl tether. Both thermal energy and photons can be used as external stimuli to polymerize the material and to freeze in an established organization. This is an important requirement for electronic applications, where a distinct morphology of the active component between the electrodes has to be maintained. Preliminary experiments with a focused, high energy photon source proved that the material could be patterned microscopically. In the future, this could allow semi-conducting wires to be produced by a lithographic process. The successful, macroscopic alignment of edge-on arranged molecules has already been accomplished by the zone-casting technique, which offers an elegant testing of the material in an FET setup. Finally, inorganic templates were utilized to nanostructure this polymerizable HBC derivative into nanotubes after the template was removed. Optimization of this process and subsequent electronic studies on these potentially semiconducting nanotubes are planned.

4.7 References

(1) Adam, D.; Schuhmacher, P.; Simmerer, J.; Haussling, L.; Siemensmeyer, K.; Etzbach, K. H.; Ringsdorf, H.; Haarer, D. *Nature* **1994**, *371*, 141-143.

(2) Wu, J. S.; Grimsdale, A. C.; Müllen, K. *J. Mater. Chem.* **2005**, *15*, 41-52.

(3) Pisula, W., Johannes Gutenberg Universität 2005.

(4) Fechtenkötter, A.; Tchebotareva, N.; Watson, M.; Müllen, K. *Tetrahedron* **2001**, *57*, 3769-3783.

(5) Wasserfallen, D.; Fischbach, I.; Chebotareva, N.; Kastler, M.; Pisula, W.; Jäckel, F.; Watson, M. D.; Schnell, I.; Rabe, J. R.; Spiess, H. W.; Müllen, K. *Adv. Funct. Mater.* **2005**, *15*, 1585-1594.

(6) Brand, D., Johannes Gutenberg Universität, 1999.

(7) Tchebotareva, N., Johannes Gutenberg Universität, 2003.

(8) Jäckel, F.; Yin, X.; Samori, P.; Tchebotareva, N.; Watson, M. D.; Venturini, A.; Müllen, K.; Rabe, J. P. *Synth. Met.* **2004**, *147*, 5-9.

(9) Samori, P.; Yin, X. M.; Tchebotareva, N.; Wang, Z. H.; Pakula, T.; Jackel, F.; Watson, M. D.; Venturini, A.; Müllen, K.; Rabe, J. P. *J. Am. Chem. Soc.* **2004**, *126*, 3567-3575.

(10) Kastler, M., Johannes Gutenberg Universität, 2002.

(11) Wu, J. S.; Qu, J. Q.; Tchebotareva, N.; Müllen, K. *Tetrahedron Lett.* **2005**, *46*, 1565-1568.

(12) Fechtenkötter, A., Johannes Gutenberg Universität, 2001.

(13) Pisula, W.; Tomovic, Z.; Simpson, C.; Kastler, M.; Pakula, T.; Müllen, K. *Chem. Mater.* **2005**, *17*, 4296-4303.

(14) Wasserfallen, D.; Kastler, M.; Müllen, K. *in preparation*.

(15) Wu, J. H.; Watson, M. D.; Müllen, K. *Angew. Chem. Int. Ed.* **2003**, *42*, 5329-5333.

(16) Wu, J., Johannes Gutenberg Universität, 2004.

(17) Wu, J. S.; Watson, M. D.; Zhang, L.; Wang, Z. H.; Müllen, K. *J. Am. Chem. Soc.* **2004**, *126*, 177-186.

(18) Mio, M. J.; Kopel, L. C.; Braun, J. B.; Gadzikwa, T. L.; Hull, K. L.; Brisbois, R. G.; Markworth, C. J.; Grieco, P. A. *Org. Lett.* **2002**, *4*, 3199-3202.

(19) Samori, P.; Yin, X. M.; Tchebotareva, N.; Wang, Z. H.; Pakula, T.; Jäckel, F.; Watson, M. D.; Venturini, A.; Müllen, K.; Rabe, J. P. *J. Am. Chem. Soc.* **2004**, *126*, 3567-3575.

(20) Jäckel, F.; Watson, M. D.; Müllen, K.; Rabe, J. P. *Phys. Rev. Lett.* **2004**, *92*.

(21) Brown, S. P.; Schnell, I.; Brand, J. D.; Müllen, K.; Spiess, H. W. *J. Am. Chem. Soc.* **1999**, *121*, 6712-6718.

(22) Brown, S. P.; Schnell, I.; Brand, J. D.; Müllen, K.; Spiess, H. W. *J. Mol. Struct.* **2000**, *521*, 179-195.

(23) Brown, S. P.; Schnell, I.; Brand, J. D.; Müllen, K.; Spiess, H. W. *Phys. Chem. Chem. Phys.* **2000**, *2*, 1735-1745.

(24) Bodanszky, M. *Int. J. Pept. Protein Res.* **1985**, *25*, 449-474.

(25) Hughes, D. L. *Org. Prep. Proced. Int.* **1996**, *28*, 127-164.

(26) Shelkov, R.; Nahmany, M.; Melman, A. *Org. Biomol. Chem.* **2004**, *2*, 397-401.

(27) Herwig, P. T.; Enkelmann, V.; Schmelz, O.; Müllen, K. *Chem. Eur. J.* **2000**, *6*, 1834-1839.

(28) Ito, S.; Wehmeier, M.; Brand, J. D.; Kübel, C.; Epsch, R.; Rabe, J. P.; Müllen, K. *Chem. Eur. J.* **2000**, *6*, 4327-4342.

(29) Brand, J. D.; Kübel, C.; Ito, S.; Müllen, K. *Chem. Mater.* **2000**, *12*, 1638-1647.

(30) Fensterbank, L.; Malacria, M.; Sieburth, S. M. *Synthesis* **1997**, 813-854.

(31) Jäckel, F.; Wang, Z.; Watson, M. D.; Müllen, K.; Rabe, J. P. *Synth. Met.* **2004**, *146*, 269-272.

(32) Jäckel, F.; Wang, Z.; Watson, M. D.; Müllen, K.; Rabe, J. P. *Chem. Phys. Lett.* **2004**, *387*, 372-376.

(33) Visjager, J.; Tervoort, T. A.; Smith, P. *Polymer* **1999**, *40*, 4533-4542.

(34) Alameddine, B.; Aebischer, O. F.; Amrein, W.; Donnio, B.; Deschenaux, R.; Guillon, D.; Savary, C.; Scanu, D.; Scheidegger, O.; Jenny, T. A. *Chem. Mater.* **2005**, *17*, 4798-4807.

(35) Pisula, W.; Tomovic, Z.; El Hamaoui, B.; Watson, M. D.; Pakula, T.; Müllen, K. *Adv. Funct. Mater.* **2005**, *15*, 893-904.

(36) Hill, J. P.; Jin, W. S.; Kosaka, A.; Fukushima, T.; Ichihara, H.; Shimomura, T.; Ito, K.; Hashizume, T.; Ishii, N.; Aida, T. *Science* **2004**, *304*, 1481-1483.

(37) Zhang, Q.; Prins, P.; Jones, S. C.; Barlow, S.; Kondo, T.; An, Z. S.; Siebbeles, L. D. A.; Marder, S. R. *Org. Lett.* **2005**, *7*, 5019-5022.

(38) Liu, C. Y.; Fechtenkötter, A.; Watson, M. D.; Müllen, K.; Bard, A. J. *Chem. Mater.* **2003**, *15*, 124-130.

(39) Wu, J. S.; Fechtenkötter, A.; Gauss, J.; Watson, M. D.; Kastler, M.; Fechtenkötter, C.; Wagner, M.; Müllen, K. *J. Am. Chem. Soc.* **2004**, *126*, 11311-11321.

(40) Pecchia, A.; Lozman, O. R.; Movaghar, B.; Boden, N.; Bushby, R. J.; Donovan, K. J.; Kreouzis, T. *Phys. Rev. B* **2002**, *65*.

(41) Iino, H.; Hanna, J.; Jager, C.; Haarer, D. *Mol. Cryst. Liq. Cryst.* **2005**, *436*, 1171-1178.

(42) Müllerhorsche, E.; Haarer, D.; Scher, H. *Phys. Rev. B* **1987**, *35*, 1273-1280.

(43) Contoret, A. E. A.; Farrar, S. R.; O'Neill, M.; Nicholls, J. E. *Chem. Mater.* **2002**, *14*, 1477-1487.

(44) Melzer, C.; Brinkmann, M.; Krasnikov, V. V.; Hadziioannou, G. *Chem. Phys. Chem* **2005**, *6*, 2376-2382.

(45) Reichmanis, E.; Katz, H.; Kloc, C.; Maliakal, A. *Bell Labs Technical Journal* **2005**, *10*, 87-105.

(46) Witte, G.; Woll, C. *J. Mater. Res.* **2004**, *19*, 1889-1916.

(47) Hoppe, H.; Sariciftci, N. S.; Egbe, D. A. M.; Muhlbacher, D.; Koppe, M. *Molecular Crystals and Liquid Crystals* **2005**, *426*, 255-263.

(48) Brabec, C. J.; Sariciftci, N. S.; Hummelen, J. C. *Adv. Funct. Mater.* **2001**, *11*, 15-26.

(49) Korte, F.; Serbin, J.; Koch, J.; Egbert, A.; Fallnich, C.; Ostendorf, A.; Chichkov, B. N. *Appl. Phys. A* **2003**, *77*, 229-235.

(50) Watson, M. D. 2004.

(51) Zhi, L. J.; Gorelik, T.; Wu, J. S.; Kolb, U.; Müllen, K. *J. Am. Chem. Soc.* **2005**, *127*, 12792-12793.

(52) Zhi, L. J.; Wu, J. S.; Li, J. X.; Kolb, U.; Müllen, K. *Angew. Chem. Int. Ed.* **2005**, *44*, 2120-2123.

5 Polycyclic Aromatic Hydrocarbons with Different Peripheries

Polycyclic aromatic hydrocarbons (PAHs) or polyarenes constitute an extraordinarily large and diverse class of organic molecules.[1] The correct nomenclature for these aromatic systems are given by the IUPAC[2]. However, the enormous diversity of that class and the existence of old, obsolete nomenclatures complicate the naming of structures. In this chapter, I will give a very short summary of the most important rules of the IUPAC nomenclature.

5.1 Nomenclature

In the IUPAC system, the names of several basic ring systems with a long history of use, such as naphthalene and chrysene, are retained. A small selection of these rings systems are listed in Figure 5-1. All of the compounds are in the oxidation state where they contain the maximum number of conjugated double bonds, and this is denoted by the ending "-ene". More complex ring systems are named by using the names of the prescribed hydrocarbon as base components and prefixing the names of additional component rings. The base component should contain as many rings as possible. The attached components should be as simple as possible. The prefixes of the attached components are formed by changing the ending "-ene" to "-eno". Isomers are distinguished by lettering the peripheral sides of the base component, beginning with "a" for the side "1-2", "b" for the side "2-3", etc., lettering every side around the periphery. The side where the ring fusion occurs is then designated by assigning a letter as early in the alphabet as possible. To this letter is prefixed, if necessary, the numbers of the positions of fusion of the attached components; these numbers are chosen to be as low as possible, and their numbering conforms to the direction of the lettering of the base component. The letters and numbers are enclosed in square brackets and are placed immediately after the designation of the attached component.

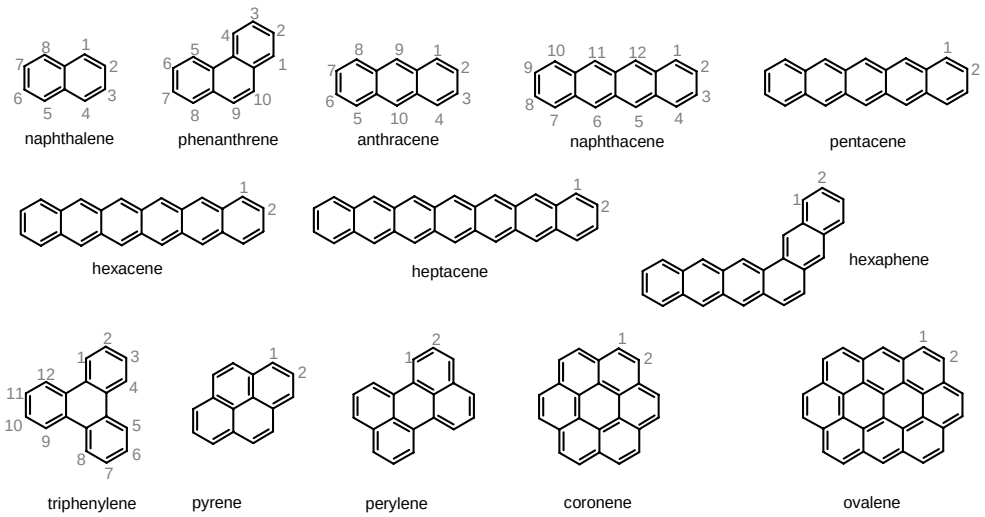

Figure 5-1: *Names and numbering of a selection of basic PAH ring systems*

For the purpose of numbering the ring positions, the polycyclic ring system is oriented so that (a) the maximum number of rings lies in a horizontal row and (b) as many rings as possible are above and to the right of the horizontal row (upper right quadrant).(Figure 5-2)

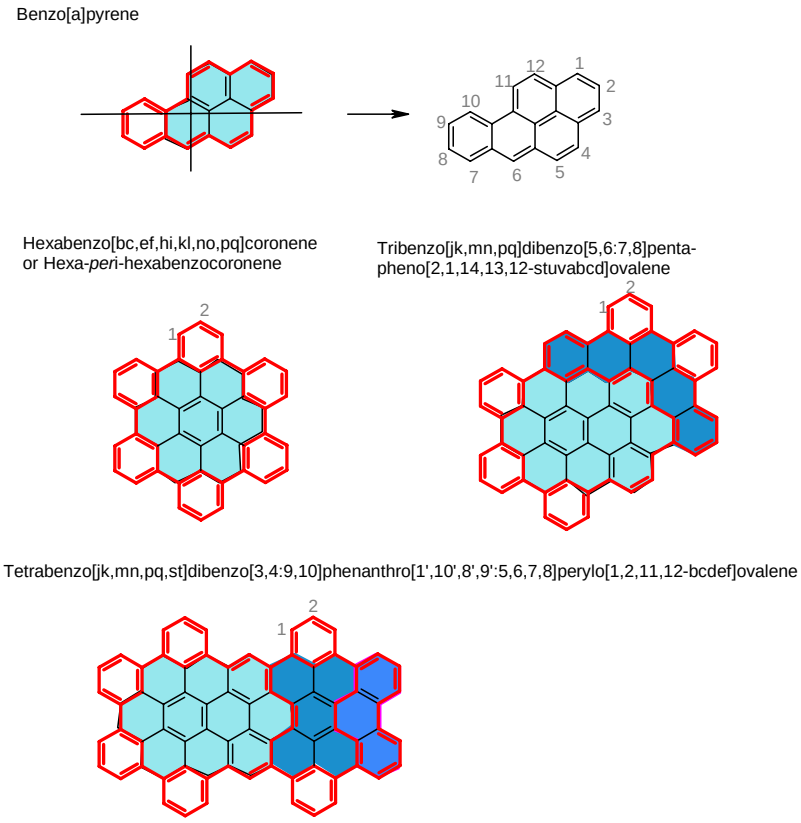

Figure 5-2: *Orientation, numbering and naming of PAH systems.*

If two or more orientations meet these requirements, the one having as few rings as possible in the lower left quadrant is chosen. Numbering commences with the carbon

atom in the most counterclockwise position in the uppermost ring farthest to the right, and proceeds in a clockwise direction, omitting atoms common to two or more rings.

From Figure 5-2 it becomes obvious that the nomenclature works well for small PAHs, however, for the extended PAH systems, synthesized in the MÜLLEN group, the naming becomes very difficult and does not clarify the structure anymore. For example, the 222 carbon containing hydrocarbon, which has been synthesized[3], the IUPAC nomenclature suggests bis(benzonaphthacenoheptacenodecacenononaceno-[2,1,22,21,20,19,8,7,6,5,4-*a1b1c1d1e1f1g1h1i1j1k1l1m1n1o1p1*:2',1',22',21',20',-19',18',17',16',15',14'-*y'z'a'1b'1c'1d'1e'1f'1g'1h'1i'1j'1k'1l'1m'1n'1o'1p'1*])nonaceno-[2,1,22,1,20,19,8, 7,6,15,14-*defghijklmnopqrstu*:3,4,5,6,7,8,9,10,11,12,13-*d'e'f'g'h'-i'j'k'l'm'n'o'p'q' r's't'u'*]didecacene. It is clear that such a name is too long and to complicated to be of any practical use. Therefore it makes more sense to introduce a different naming, which relates a chemical structure with a short meaningful name, like i.e. HBC-$C_{10,6}$ **3-13b** as used in the previous chapters.

5.2 Clar-Rule and Peripheries

The energies of PAHs are dependent upon both the number of fused aromatic rings and their topology, i.e., their arrangement in space. CLAR[4,5] proposed that the chemical reactivities and other properties of polyarenes could be best understood in terms of localization of the aromatic sextets presents in the molecule. He empirically found that the chemical reactivity and other properties of PAHs could be predicted by his model. He assigned π-electron sextets to discrete benzene rings and the remaining π-electrons to double bonds. Such sextet rings are usually indicated by solid circles in the rings concerned.

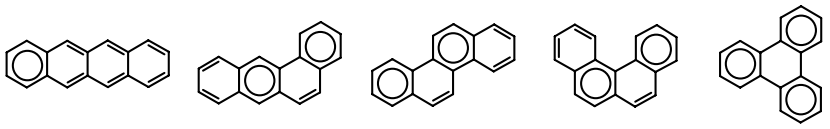

ionization potential	6.97 eV	7.41 eV	7.59 eV	7.61 eV	7.87 eV
HOMO-LUMO gap	2.71 eV	3.53 eV	3.87 eV	3.84 eV	4.36 eV

Figure 5-3: *Structure, ionization potential, and HOMO-LUMO gap of PAH isomers with four benzene units.*

Fully benzoid PAHs can formally be drawn only with ROBINSON rings without isolated "double" bonds and are known to be kinetically very stable, unreactive substances. Triphenylene, one of the five isomeric PAHs with four benzene rings (Figure 5-3) differs distinctly concerning its properties from the other isomers. It has the highest resonance energy[6], the highest ionization potential[7], the largest HOMO-LUMO gap[7], and is the thermally most stable and chemically least reactive of the compounds (Figure 5-3).

It becomes quite obvious that the energy gap between HOMO and LUMO depends mostly on the number of fused rings, the topology and therefore the nature of the periphery. DIAS[8,9] showed that there are four types of CH perimeter units on the outer boundary of PAHs (Figure 5-4), which have different reactivities towards chemical reactions.[10] The "acene"- or "zigzag edge" corresponds to higher reactive PAHs, while the "phenanthrene" or "arm-chair edge" leads to very stable aromatic systems, such as triphenylene.

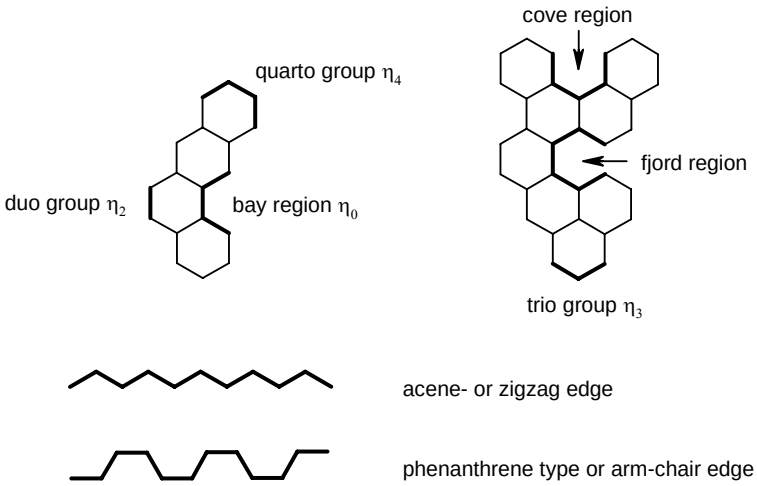

Figure 5-4: *Schematic representation of the structural parameters in PAHs and the different type of edges in the structures.*

5.3 Electronic Spectroscopy of PAHs

One of the most striking properties of the PAHs that set them apart from other classes of organic compounds is the nature of their UV/Vis absorbance spectra. When the absorbance spectrum of a solution of any PAH is examined, several observations are made[4,11]. Various transitions in the UV absorption spectrum of PAHs can be observed, which can be classified by different terminologies.[4,12,13] E. CLAR identified three main types of transitions with different intensities and designated them the α, β and p bands, which originated from empirically determined correlations between the so-called "ortho" and "para" reactivity and the absorption spectra. Corresponding nomenclatures have been developed by J. R. PLATT[12] and originate from group theory[13].

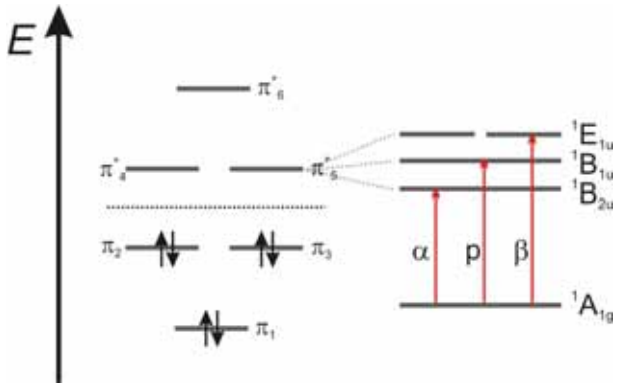

Figure 5-5: *Energy scheme of the π-orbitals and electronic transitions for the case of benzene.*

The electronic situation for benzene, as the formal monomer for the class of PAHs, is well understood. The HOMO and the LUMO form both a pair of degenerate molecular orbitals. The four possible transitions from the $\pi_{2/3}$ into $\pi^*_{4/5}$ lead, what can be derived theoretically, to transitions from the $^1A_{1g}$ ground state into the excited singlet states $^1B_{2u}$, $^1B_{1u}$ and the degenerate $^1E_{1u}$. The electron correlation abolishes the excited state, therefore, three electronic transitions (α, β and p) with different energies are observed (Figure 5-5).

The time-dependent perturbation theory for an undisturbed system like an atom or molecule gives for the transition rate (transition probability per time unit) Γ_{if} of a system from the initial state i to the final state f under the influence of a time-dependent perturbation V the so-called Fermis golden rule:

$$\Gamma_{if} = \tfrac{2\pi}{\hbar}\delta(E_f - E_i)\left|\langle f|V|i\rangle\right|^2$$

with E_i and E_f as the energies for the initial and the final state. For a periodic perturbation exp(±iωt) (electromagnetic field), one receives in dipole approximation

$$\Gamma_{if} \propto \delta(E_f - E_i \pm \hbar\omega)\left|\langle f|er|i\rangle\right|^2$$

where *er* is the dipole operator with the elemental charge *e* and the distance vector *r*. The first term corresponds to the energy conservation and the second term is called transition matrix element M_{if}:

$$M_{if} = \langle f|er|i\rangle = \int \Psi_f er \Psi_i d\tau$$

This term is responsible, that additional to the common dipole selection rules (angular momentum quantum number $\Delta\Lambda = \pm 1$, total spin $\Delta\Sigma = 0$, rotational quantum number $\Delta J = 0$ or ± 1, change of parity) a symmetry selection rule exists for molecules with a high symmetry (at least D_{3h}). For highly symmetric molecules, the transition matrix element can show an anomaly.[14] For distinct symmetries of the states *i* and *f*, the integral in the transition matrix element can vanish independent of the other selection rules. Such a transition is called symmetry forbidden.

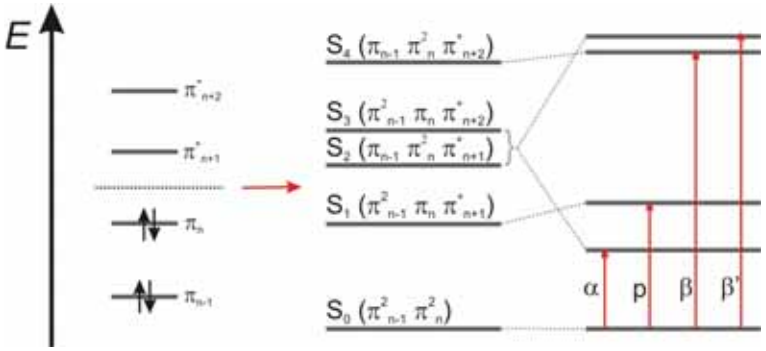

Figure 5-6: *Orbitals, configurations and electronic transitions considering configuration interactions in PAHs.*

In the corresponding UV/vis spectrum of benzene, the structure rich α and the p-band correspond to symmetry-forbidden transitions. The p-band "borrows" intensity from the neighboring β-band. Substituents on the benzene ring lower the symmetry and therefore these two transitions gain intensity.

In the spectra of extended, condensed PAHs, one notices interesting similarities. In contrast to benzene, the HOMOs π_{n-1} and π_n and the LUMOs π^*_{n+1} and π^*_{n+2} are not necessarily degenerate anymore. There are theoretically four transitions between these orbitals possible (Figure 5-6).

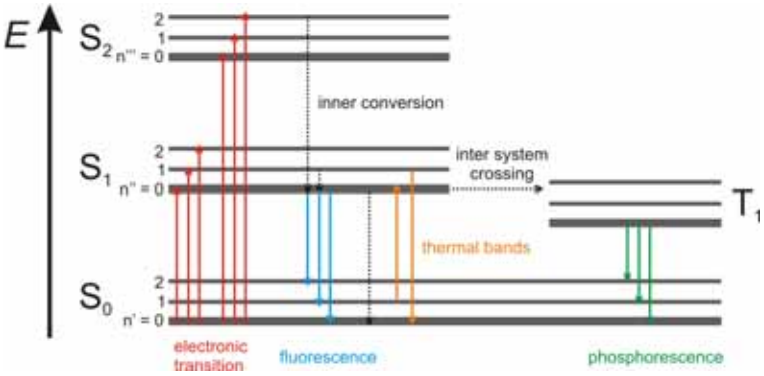

Figure 5-7: *Jablonski diagram.*

Configuration interactions between electrons cause a splitting of degenerate configuration states. Therefore, the shape and the topology of the PAH determines the position of the α-band with respect to the p-transition. Annelation of benzene units shifts the band to longer wavelengths. In the case of the polyacenes, the p-band passes the α-band, when going from benzene to anthracene. In all case, the transition from the HOMO into the LUMO corresponds to the p-band, which is often confused.[15,16]

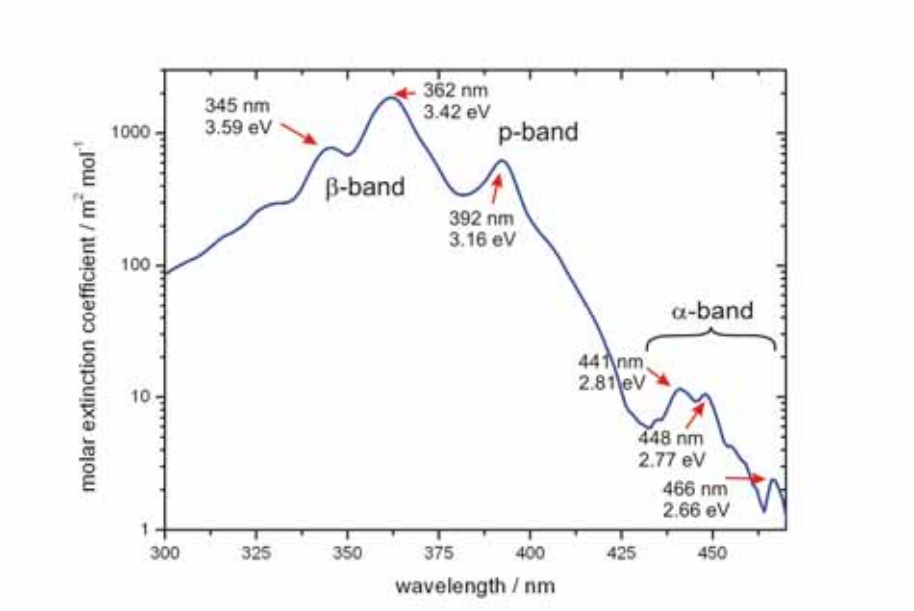

Figure 5-8: *Logarithmically plotted UV/vis absorption spectrum of HBC-C_{12}* **3-3a** *(oDCB).*

In the case of the D_{6h} symmetric HBC, one observes a typical UV/vis response with the three distinct bands α, β and p (Figure 5-8).[17,18] The α-bands appear at longest wavelength and are very weak in intensity. Analogous to benzene, the α-band is symmetry forbidden and therefore has only small molar extinction coefficients and corresponds to a transition from the second highest occupied molecular orbital

(HOMO-1) to the lowest unoccupied molecular orbital (LUMO). The p-band, which relates to the transition between the HOMO and the LUMO, is located at 392 nm. The onset of that band is at 425 nm, which corresponds to an optical band gap of 2.92 eV. The most intense band is the β-band at 362 nm with a molar extinction coefficient of around 2000 m^2 mol^{-1}, which corresponds to a transition from the highest occupied molecular orbital (HOMO) to the second lowest unoccupied orbital (LUMO+1). The band shows typical vibronical bands in the range of 1300 to 1350 cm^{-1}.[19]

The photoluminescence emission (PL) spectrum of HBC-C_{12} **3-3a** exhibits a typical vibrational fine structure, which is typical for symmetry forbidden transitions.[20] The spectrum is analogous to most PAHs independent on the excitation wavelength.

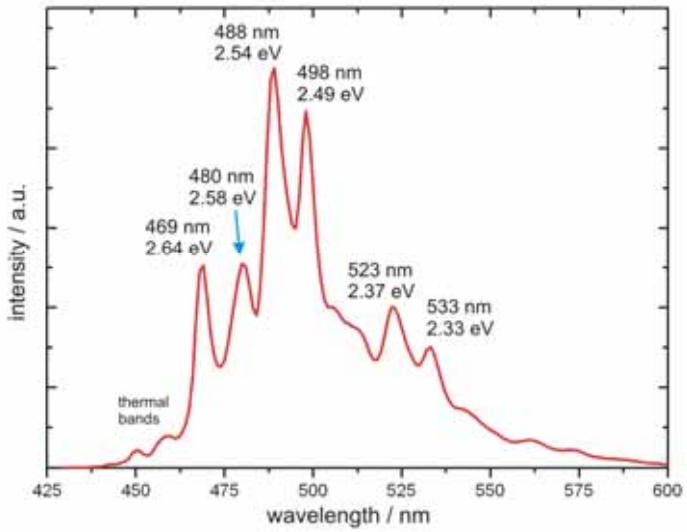

Figure 5-9: *PL spectrum of HBC-C_{12}* **3-3a** *(λ_{ex} = 362 nm, in oDCB).*

The 0-0 transition has been identified as the band at 469 nm.[21] The relatively small Stokes shift of 3 nm, which is almost independent on the solvent, indicates no polarity difference of ground and excited state. According to KASHAS rule[22] (Figure 5-7), the fluorescence occurs only from the first excited state S_1, which corresponds in this case to the weak α transitions in the UV/vis spectrum. At lower wavelength, one can observe two thermal bands in the PL spectrum, which vanish at low temperatures.

The UV/vis and the photoemission spectra have been used to study association phenomena in solution (see chapter 3.2.2).[23] The transitions and the oscillator

strengths of electronic transitions are influenced by neighboring molecules, due to a partial overlap of π-orbitals.[24]

5.4 Introduction of "zigzag" Sites

In the previous chapters, the synthesis, characterization and the investigation of suitable processing techniques for differently substituted HBCs has been described in detail. As a striking feature, the supramolecular organization was very dependent upon the functionalization in the periphery. A simple manipulation of the alkyl chain which decorates the corona of the disc leads to different orientations and organizations on substrates and in the bulk phase. However, all described derivatives are electronically identical. The position of HOMO and LUMO are mainly determined by the HBC core and only very weakly influenced by substitution and self-association.[23] In my diploma thesis[25], electron rich mono-amino substituted HBC derivatives have been synthesized, which only caused a small change of the energy gap of the substance of about 0.04 eV compared to the parent hexa-alkylated cases. This pointed out, that the difficult chemical derivatization of the HBCs does not lead to dramatic electronic changes.

A possible implementation of compounds as active components in electronic devices requires next to a "good" morphology and purity suitable electronic properties to minimize i.e. contact problems on the electrodes.[26-28] The charge transport in semi-conducting discotic materials can be explained using the band model[26,29], which applies also for inorganic semi-conductors. It has been stressed out, that the energy of overlapping orbitals is a crucial parameter that guarantees unhindered charge carrier propagation through the material. Furthermore, the charge carrier injection barrier between the semiconductor and the electrode depends distinctly from the oxidation and redox potentials. Therefore, it is a synthetic task to tune the HOMO and LUMO levels and to understand how to influence *inter alia* the electronic properties.

In the past, a parameter to manipulate the electronic properties has been the size of the synthesized PAH.[30-33] A series of different PAHs of different shapes and sizes up to 222 carbon atoms in the aromatic system have been made and characterized.[34,35] However, the simple extension of the PAHs caused various problems, starting with the reproducibility of the cyclodehydrogenation reaction, in which up to 108 hydrogen atoms have to quantitatively be removed from the precursor, solubility and purification of the PAH.[36,37] However, most of the synthesized, extended PAHs with more than 40 aromatic carbon atoms were fully-benzoid and possessed exclusively an

"arm-chair" periphery.[9] PAHs with different types of peripheries are valuable model systems to understand the properties of graphite.[38]

As a different approach, the variation of the periphery is suggested to be a sensitive parameter to influence the electronic properties. This has been shown for small aromatic molecules[11] and theoretically predicted for larger aromatic systems.[39] In the following chapters, the synthesis of a homologous series of extended, not fully-benzoid PAHs with a partial "zigzag" edges will be described. These introduced "phenanthrene-like" peripheries with formally localized, nucleophilic double-bonds should theoretically be susceptible to further functionalizations like oxidations unlike the "arm-chair" analogues. The influence of the periphery on the electronic spectra and on the packing organization was investigated and the results will be presented.

5.4.1 Tetrabenzo[*bc,ef,hi,uv*]ovalene

The formal annelation of one benzene unit to the 42 carbon containing HBC gives the 44 carbon containing tetrabenzo[*bc,ef,hi,uv*]ovalene, which will be called in following TBO. When looking at the chemical structure in Figure 5-10, one notices that only one benzene subunit cannot obtain a ROBINSON ring; TBO is a not fully-benzoid PAH, with a potentially reactive formal double bond according to the CLAR description.

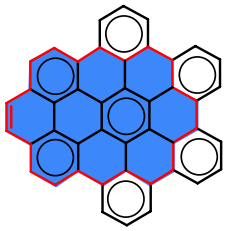

Tetrabenzo[bc,ef,hi,uv]ovalene

Figure 5-10: *Chemical structure of TBO, the name defining ovalene subunit is colorized in blue.*

In our research group, the synthesis of appropriate oligophenylenes, which are planarized in a SCHOLL reaction, has been used to access extended PAHs.[40] Retro-synthetically, the desired precursor could be obtained via a DIELS-ALDER cycloaddition reaction, where the additional phenyl ring can be introduced on one of the two starting materials. As a first attempt, which has been performed by Z. WANG, the phenyl ring was formally "attached" onto the cyclopentadienone derivative (Scheme 5-1). Starting from the synthesis of the literature known pyrene-4,5-dione[41]

(**5-1**) (three steps, over all yield = 76%), the two-fold potassium hydroxide promoted KNOEVENAGEL condensation with 1,3-diphenylpropan-2-one gave the thermally instable derivative **5-2** in moderate yields. In solution, NMR spectra of **5-2** showed already after minutes unidentified decomposition products, which have been observed in similar cases as well.[42] The use of ethanol as solvent turned out to be crucial for the success of the reaction, because the product **5-2** precipitated from the reaction, which circumvented the complete decomposition.

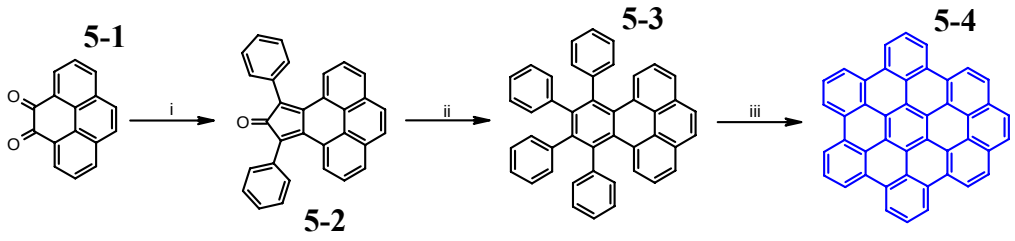

Scheme 5-1: *i) 1,3-diphenylpropan-2-one, KOH, 41%; ii) diphenylacetylene, microwave radiation, 20%; iii) $FeCl_3$, 82%.*

However, the DIELS-ALDER reaction of **5-2** with commercially accessable diphenylacetylene yielded in a microwave furnace the PAH precursor **5-3**. The microwave radiation enhanced the reaction speed (reaction time 45 min, conventional: over night) dramatically, which allowed the isolation of **5-3** in 20% yield.[43] Conventional heating did not reveal any product, because most of the starting material decomposed before the conversion. The final SCHOLL reaction with iron(III) chloride proceeded smoothly to the desired, unsubstituted TBO **5-4** in good yields, what is indicated in the MALDI-TOF spectrum (Figure 5-11), using the solid state preparation method.[44] However, some traces of bis-chlorinated side product could be identified, which has been observed in the synthesis of other unsubstituted, extended PAHs as well.[45] The insufficient solubility prevented a further characterization from solution. However, scanning tunneling microscopy (STM) results will be presented in a later chapter 5.6.3.

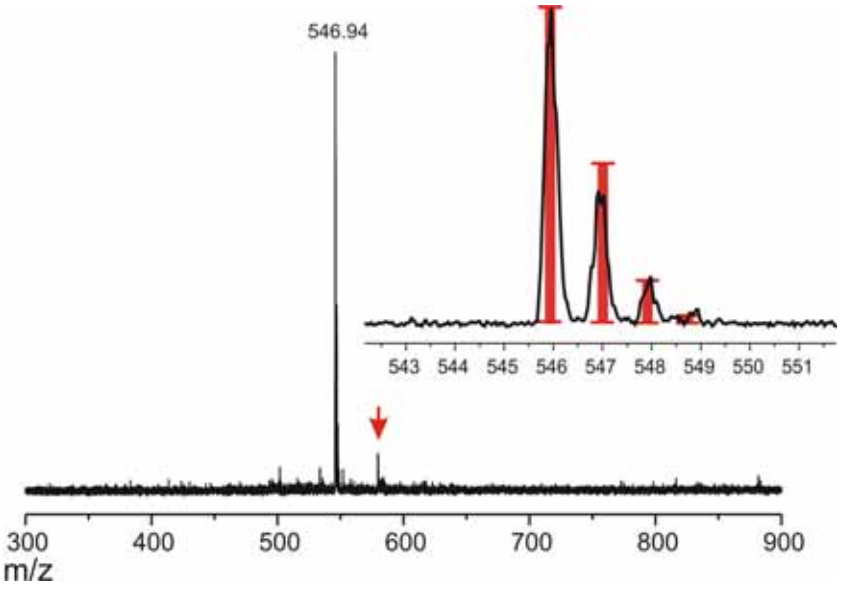

Figure 5-11: *MALDI-TOF spectrum of TBO* **5-4***, using solid state preparation with TCNQ as matrix substance; the red arrow indicates traces of bis-chlorinated species.*

The overall yield toward the unsubstituted TBO with the described synthetic route was about 5%, what renders a multi-gram synthesis difficult.

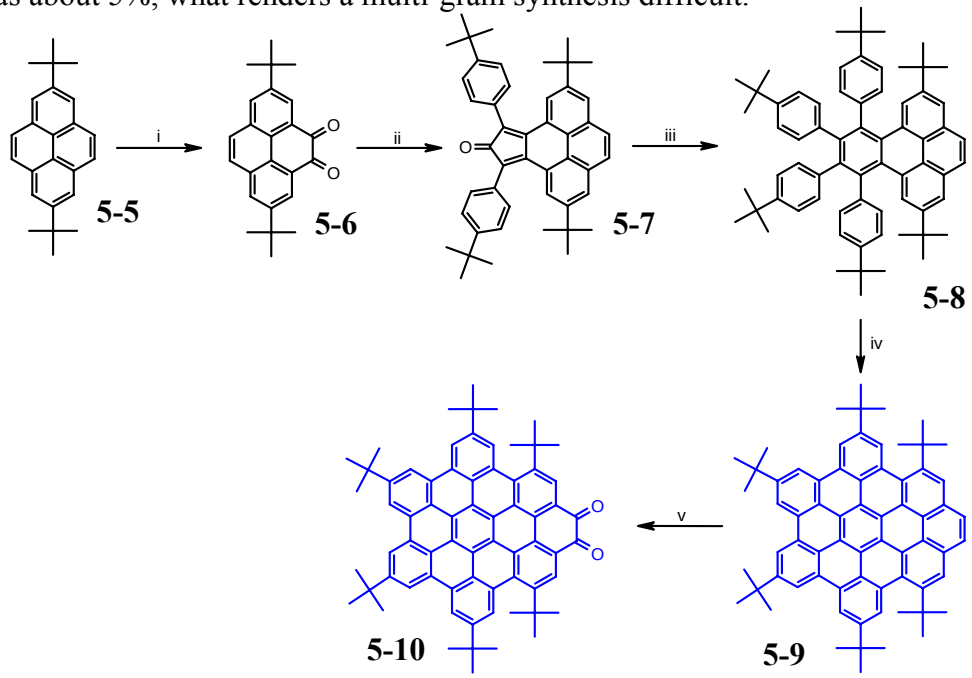

Scheme 5-2: *i) RuO_2, $NaIO_4$, 10%; ii) 2,7-di-tert-butylpyrene-4,5-dione, KOH, 87%, iii) 4,4'-di-tert-diphenylacetylene, 80%, iv) $FeCl_3$, 95%, v) RuO_2, $NaIO_4$, 11%.*

However, Z. WANG synthesized a six-fold *tert*-butylated TBO(^{t}Bu)$_6$ **5-9** following the same synthetic concept.[46] It turned out that the *tert*-butyl groups stabilized the cyclopentadienone derivative **5-7**, which allowed the DIELS-ALDER reaction to be conducted in good yields. The *tert*-butyl groups in position 1 and 6 distorted the PAH what can be seen from the crystal structure (Figure 5-12).

The reasonable solubility of **5-9** opened the possibility to oxidize the formal double bond (Scheme 5-2) under mild conditions to the respective dione **5-10**.[46] Stronger oxidants increased the yield of the oxidation, but the de-*tert*-butylation became more prominent. The separation of the side-products from the desired compound was impossible. However, the reaction proved the CLAR rule, that the "zigzag" edge is more electron rich and therefore more susceptible for an oxidation.[4]

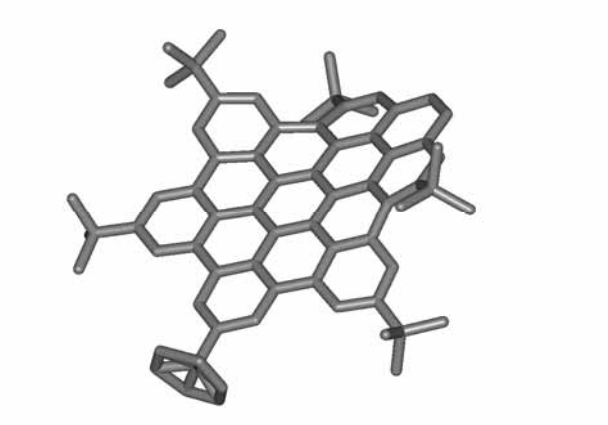

Figure 5-12: *Crystal structure of the distorted TBO(^{t}Bu)$_6$* **5-9***, hydrogen atoms are omitted for clarity.*

In order to receive better soluble and eventually phase-forming TBO derivatives, it has been attempted to introduce *n*-dodecyl chains into the cyclopentadienone-derivative, which would allow a four-fold *n*-alkylated TBO to be synthesized.

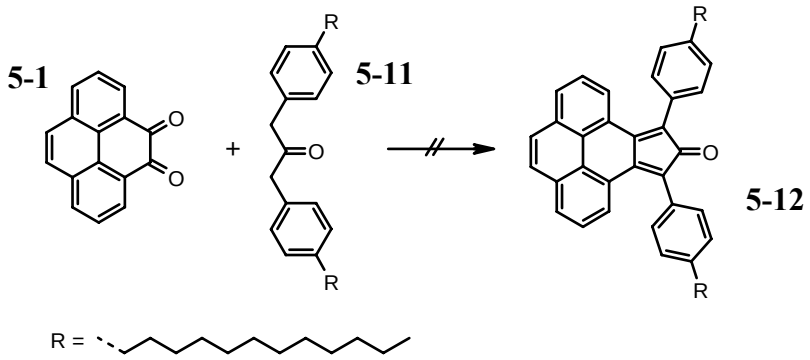

Scheme 5-3: *Attempted synthesis of an alkylated cyclopentadienone-derivative* **5-12**.

Unfortunately, the KNOEVENAGEL reaction of pyrene-4,5-dione (**5-1**) with 1,3-bis-(4-*n*-dodecyl-phenyl)propan-2-one (**5-11**)[47] did not give the desired product, since it decomposes because of the good solubility in the reaction solvent. Therefore, the scope of the presented synthetic concept does not allow a broad variety of different functionalities to be introduced. It seemed to be significant that the cyclopentadienone derivative is either sterically shielded or that it precipitates during the course of the KNOEVENAGEL condensation to avoid its decomposition.

A novel synthetic concept was developed based on the experience, which D. WASSERFALLEN gained with the selective mono-DIELS-ALDER reaction of tetraalkylated tetraphenylcyclopentadienone with 2,2'-diethynyl-biphenyl (**5-14**).[48] The terminal triple bond was rearranged with platinum(II) chloride in a FÜRSTNER protocol[49,50] to a phenanthrenyl moiety. Although the reaction yield was high, the separation from small amounts of side products occurred to be of difficulty and time consuming.

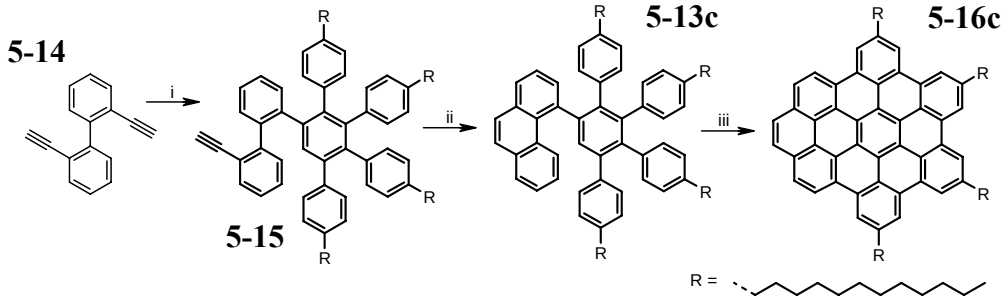

Scheme 5-4: *i) 2,3,4,5-Tetrakis(4-n-dodecyl-phenyl)-cyclopentadienone, 62% ii) $PtCl_2$, 93%; iii) $FeCl_3$, 79%.*

Interestingly, the ^{1}H NMR spectrum (Figure 5-13) exhibited distinct aromatic resonances for all protons in the asymmetric precursor molecule **5-13c**, which could

all be assigned with the use of H,H COSY and NOESY experiments. The large downfield shift of the proton a (H-4 position of the phenanthrenyl unit, Figure 5-13) has been observed for all phenanthrene units substituted in the 4 position.

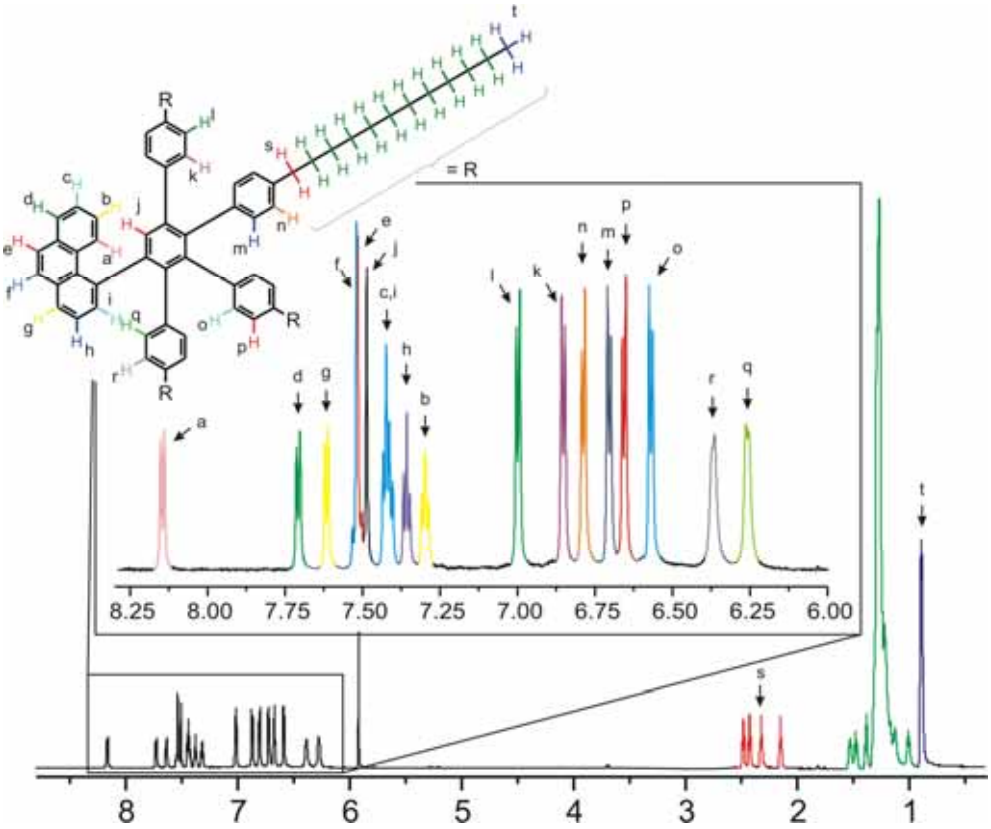

Figure 5-13: *^{1}H NMR spectrum of* **5-13c**, *recorded in 1,1,2,2-tetrachloroethane-d^{2} at 80 °C (700 MHz).*

Quantum-chemical calculations revealed that this shift is caused by the distorted geometry and misshapen orbitals induced by the bulky substituent in the bay area of the phenanthrene and therefore not due to an anisotropic ring current.[51] Nevertheless, the resonance of the proton on the small PAH subunit in **5-13c** was downfield shifted compared to the resonances from the phenyl rings because of the stronger anisotropic, diamagnetic ring current.[52] The protons r and q (Figure 5-13) on the phenyl moiety which is located next to the phenanthrenyl unit, were very broad at room temperature and narrowed with increasing temperature. This suggests a hindered rotation on the timescale of the NMR experiment at room temperature, which has been seen for other DIELS-ALDER adducts as well.[53,54] Astonishingly, the proton resonance and the carbon resonances (not shown) of the four α-CH_2 groups exhibited a distinct chemical shift difference, which is for protons around 0.4 ppm. The peaks revealed only a weak concentration dependence which excludes an intramolecular contribution. It seems

that the inductive effect of the phenanthrene unit changed the electron density in the attached phenyl rings, which was additionally indicated by different aromatic resonances for all phenyl units.

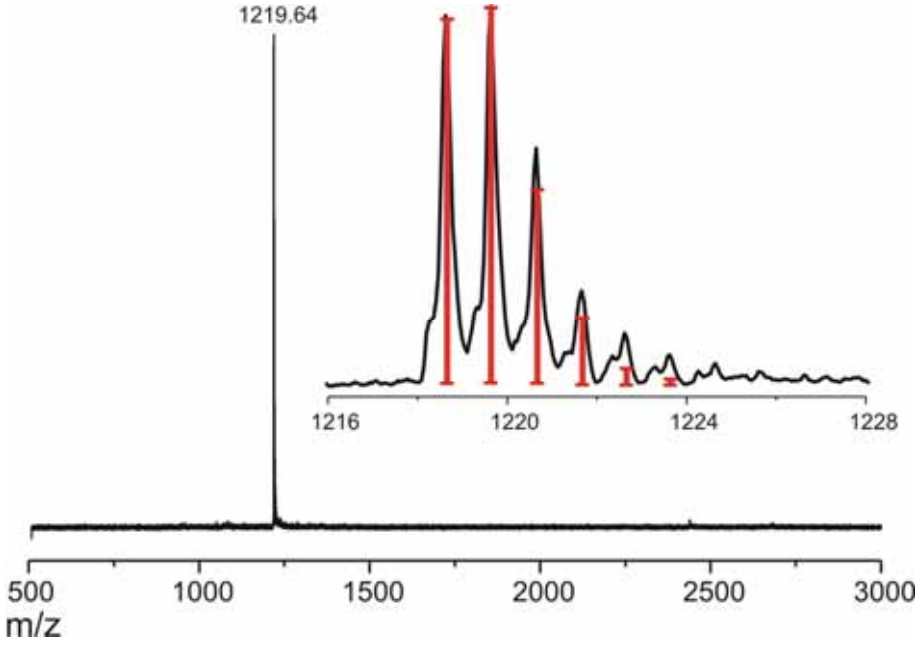

Figure 5-14: *MALDI-TOF spectrum of TBO(C_{12})$_4$* **5-16c***, solid-state prepared sample using TCNQ as the matrix substance.*

The final SCHOLL reaction allowed TBO(C_{12})$_4$ **5-16c** to be obtained in good yields from the precursor **5-13c**. Thereby, 2.7 equivalents of iron(III) chloride were necessary to fully planarize **5-13c**, which is about twice as much as for the analogous reaction with hexa-phenyl benzenes. The cyclodehydrogenation reaction with less equivalents in the case of the TBO(C_{12})$_4$ **5-16c** gave partially closed by-products where the phenanthrene unit was not fused to the rest of the molecule. This goes along with observations of D. WASSERFALLEN for rotationally flexible subunits that fuse on a slower timescale and need therefore more iron(III) chloride to fuse.[48] The MALDI-TOF spectrum (Figure 5-14) indicates the pure, desired product without any evidence of chlorination despite of the amount of oxidant used. The experimental isotope distribution is in good agreement with the calculated spectrum and proves the existence of only the fully closed specie. TBO(C_{12})$_4$ **5-16c** could be recrystallized from toluene to afford a microcrystalline powder whose color was slightly darker orange than the one of HBC-C_{12} **3-3a**. The ^{1}H NMR spectrum of the weakly soluble compound could be obtained (not shown) and will be discussed on a different TBO derivative (see below).

The oxidation reaction of TBO$(C_{12})_4$ **5-16c** to the corresponding dione analogously to the described example Z. WANG presented[46] failed since the oxidative decomposition of the alkyl substituents was prominent even when using very mild oxidation conditions.

The problems with the preparative work-up after the isomerization reaction towards **5-13c** narrowed the versatility of the presented synthetic concept. Attempts to synthesize a *tert*-butylated TBO following that method were unsuccessful. Because of this reason, another approach was designed which should avoid the problems of the first two reaction routes.

Retro-synthetically, the necessary precursor can be obtained via a DIELS-ALDER cycloaddtion reaction of tetraphenylcyclopentadienone and 4-ethynylphenanthrene (Scheme 5-5). The latter compound is literature known and synthesized in 10 steps starting from diphenic acid in an overall yield of less than 1%.[51,55]

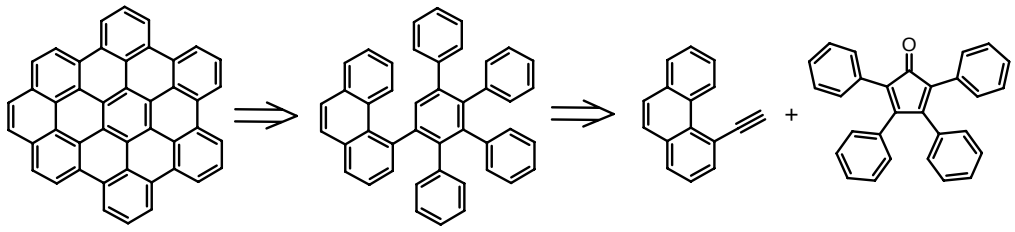

Scheme 5-5: *Retro-synthesis of TBO.*

In order to have a chance to potentially utilize TBO derivatives in electronic applications in the future, such a lengthy synthesis would hamper the ability to gain enough material. Consequently, a novel synthesis towards the suitable substituted phenanthrene derivative had to be developed, which allows a multi-gram scale-up and a high over-all yield.

The first idea started with a palladium catalyzed SUZUKI cross-coupling, which had to be conducted selectively. In HAGIHARA-SONOGASHIRA reactions, the different reactivity of iodo versus bromo substituents is commonly used as a preparative concept. However, in the case of a SUZUKI reaction only very few examples are published where this was utilized.[56,57] The reason is that the temperature windows for both halogen substituents are smaller and strongly dependent upon the used substrates.

After optimization, the desired, selective SUZUKI reaction of (2-iodo-phenyl)-acetonitrile **5-17** with 2-bromophenylbrononic acid **5-18** afforded the biphenyl derivative **5-19** in high yields. The reduction of the nitrile group to the corresponding aldehyde **5-20** with DIBAL failed since the basicity of the reaction promoted an Aldol condensation and addition reaction of the desired product to compounds with higher molecular weights. Even in a STEPHENS reaction, the Aldol reactions could not be suppressed which did not allow a clean product to be isolated.

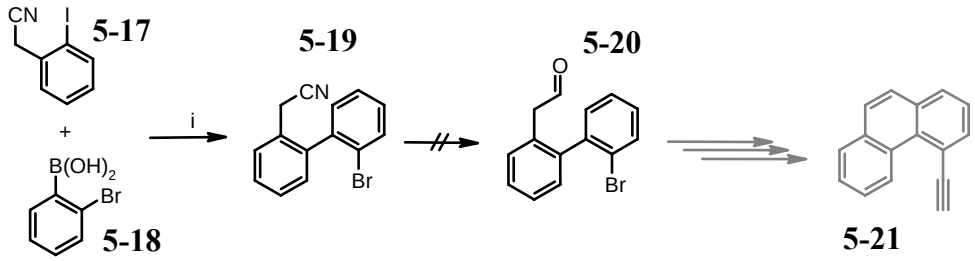

Scheme 5-6: *i) $Pd(PPh_3)_4$, 93%.*

Attempts to conduct the FRIEDEL-CRAFTS reaction on impure **5-20** towards 4-bromophenanthrene were unsuccessful.

Another synthetic route towards the desired phenanthrene derivative **5-21**, starting with a statistically conducted HAGIHARA-SONOGASHIRA reaction towards the substituted tolane **5-24** was suggested.

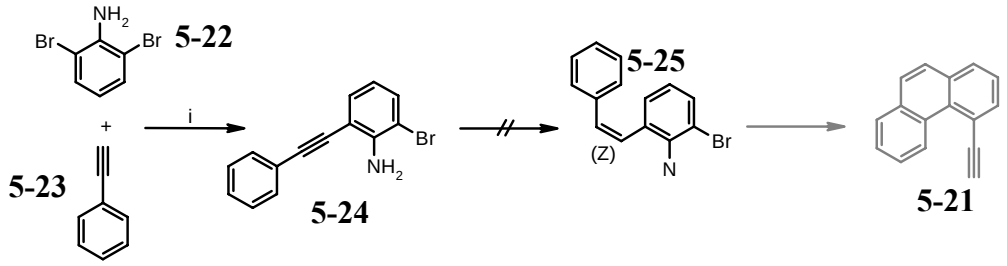

Scheme 5-7: *i) $Cl_2Pd(PPh_3)_2$, 42%.*

However, the hydrogenation of the triple bond using the LINDLAR catalyst to the corresponding (Z)-stilbene **5-25**, which was thought to be fused in a PSCHORR reaction to the desired phenanthrene, failed. Also other partial hydrogenation attempts with DIBAL or silanes did not lead to the desired formation of the double bond.

A more successful synthetic concept is presented in Scheme 5-8, which allowed 4-ethynylphenanthrene (**5-21**) to be synthesized in seven steps in an overall yield of 31%. The straight forward palladium catalyzed SUZUKI cross coupling reaction of 2-formylphenylbronic acid (**5-27**) and 2-bromoanisol (**5-26**) gave the corresponding

biphenyl derivative **5-28** in satisfying yields. The formyl-functionality was converted into the corresponding alkyne **5-29** with lithio trimethylsilyl diazomethane[58] and subsequently isomerized according the already used FÜRSTNER method[49,50] to yield 4-methoxyphenanthrene (**5-30**) in good yields.

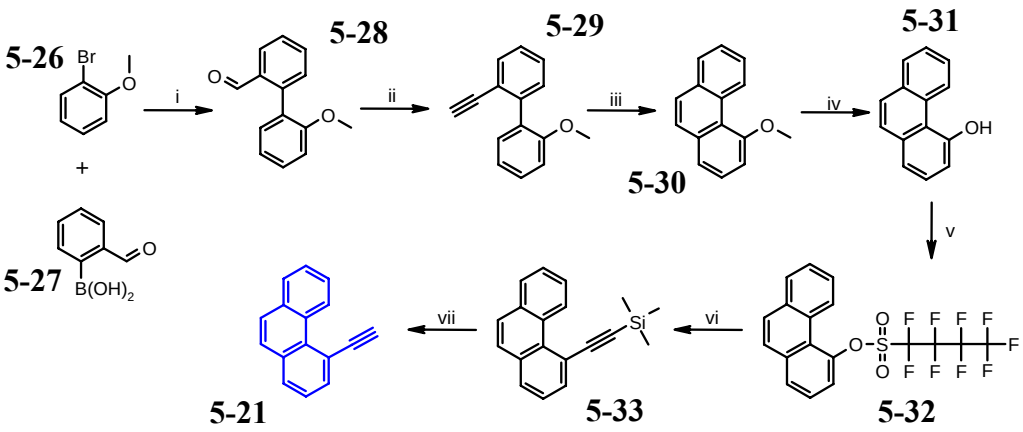

Scheme 5-8: *i) $Pd(PPh_3)_4$, 73%; ii) trimethylsilyldiazomethane, LDA, 84%; iii) $PtCl_2$, toluene, 76%; iv) BBr_3, 86%; v) NfF, 93%; vi) trimethylacetylene, CuI, 87%; vii) K_2CO_3, 95%.*

After a standard demethylation reaction with borontribromide, the hydroxyl function was converted to the nonaflate derivative **5-32**, which proved to be more suitable than triflate or tosylate in the following reaction step, because of a better kinetical stability. The HAGIHARA-SONOGASHIRA cross-coupling reaction yielded with the nonaflate derivative **5-32** the desired silylacetylene carrying phenanthrene **5-33** in 87% yield, while the analogous triflate and tosylate gave unsubstituted phenanthrene as the main product. The final removal of the silyl protection group proceeded smoothly with potassium carbonate as base in methanol to afford the desired phenanthrene derivative **5-21**. All reaction steps scaled well and it was possible to obtain this compound on a multi-gram scale.

This building block was converted with differently substituted tetraphenylcyclpentadienones **5-34a-c** to the corresponding precursors which were subsequently planarized to the corresponding TBO derivatives **5-16** (Scheme 5-9). Following this route, unsubstituted TBO **5-16a**, TBO(^{t}Bu)$_4$ **5-16b** and again TBO(C_{12})$_4$ **5-16c** were obtained in higher yields than with the before mentioned synthetic concepts. The difficult work with the thermal unstable compounds and the difficult purification were successfully circumvented and the PAHs could be obtained on a multi-gram scale.

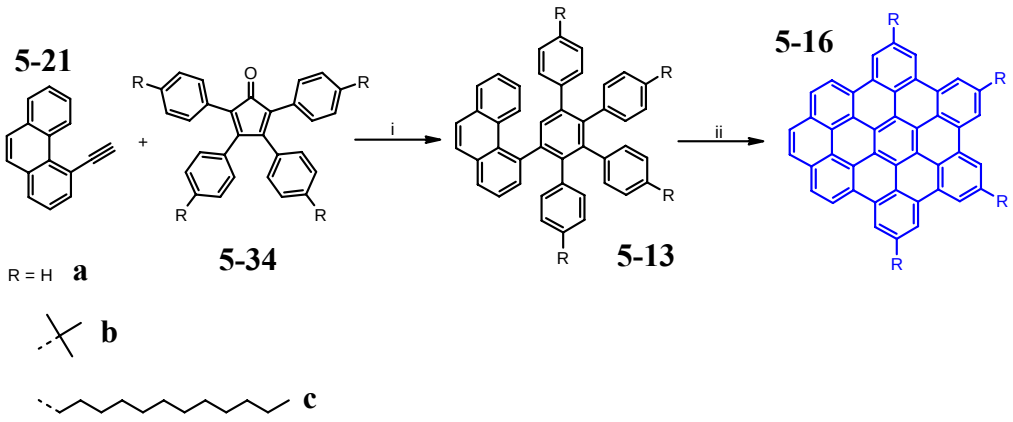

Scheme 5-9: *Synthetic concept towards TBO derivatives using 4-ethynylphenanthrene as building block. i) 84-95%; ii) $FeCl_3$, 79-83%.*

The *tert*-butylated precursor **5-13b** revealed a similar ^{1}H NMR spectrum (Figure 5-15) than the previously decribed *n*-dodecyl substituted analogue **5-13c** (Figure 5-13). Again the sterically overcrowded phenyl ring gave at room temperature broad resonances for protons suggesting a hindered rotation.

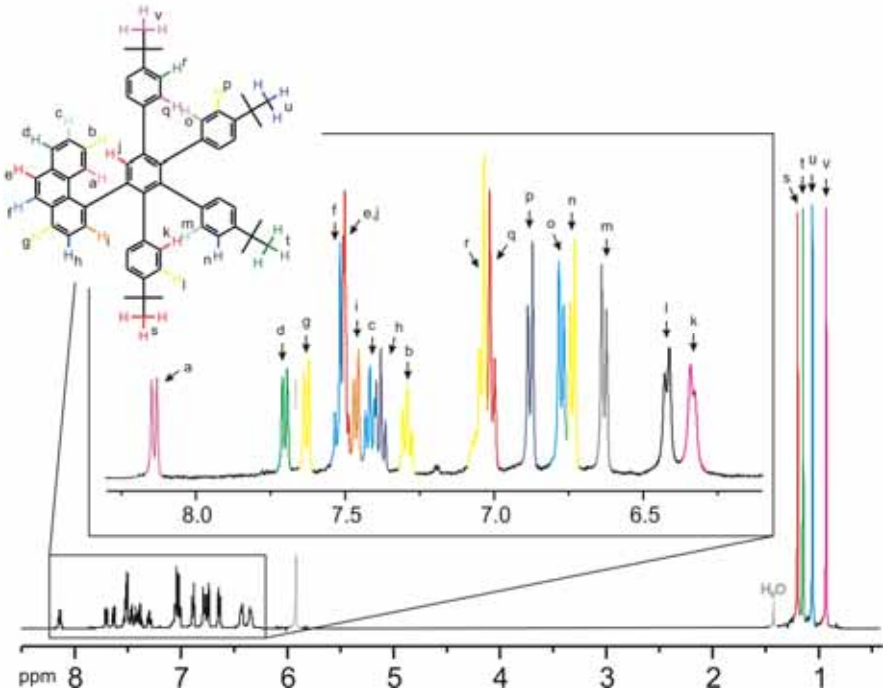

Figure 5-15: *^{1}H NMR spectrum of* **5-13b**, *recorded in 1,1,2,2-tetrachloroethane-d^2 at 80 °C (500 MHz).*

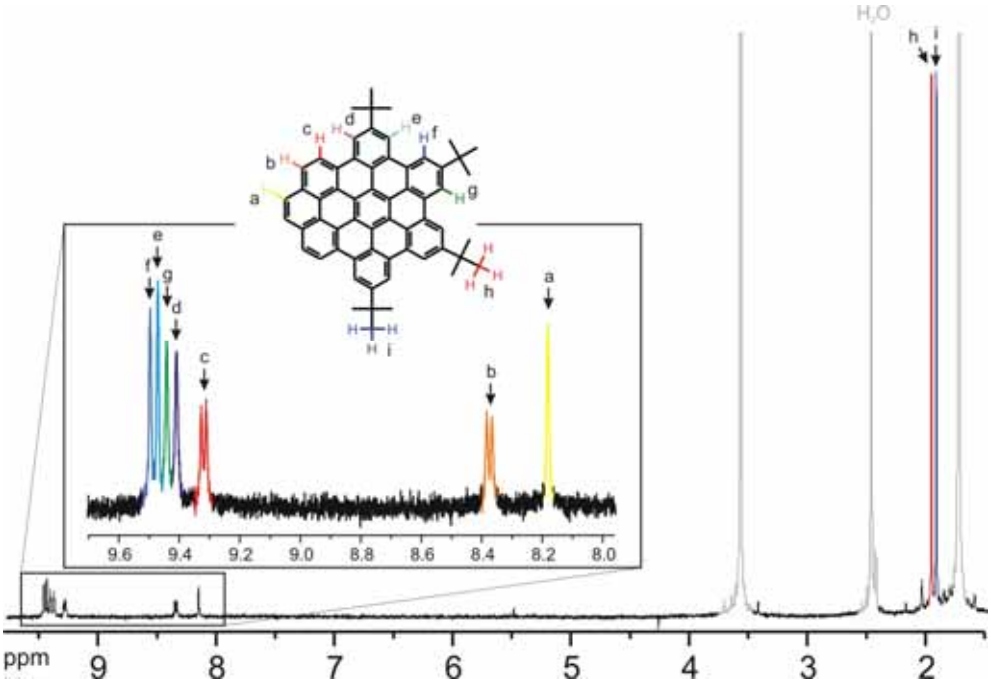

Figure 5-16: *^{1}H NMR spectrum TBO(^{t}Bu)$_4$* **5-16b**, *recorded in THF-d^{8} at 60 °C (500 MHz).*

The spectrum became better resolved when heating over 70 °C. All proton resonances could be assigned using 2D NMR spectroscopy experiments. Interestingly, the resonances of the protons on the *t*-butyl groups appeared isolated with a difference of the chemical shift of about 0.5 ppm, which has analogously been observed for the *n*-dodecyl substituted analogue **5-13c**. After the SCHOLL planarization, it was possible to obtain a resolved ^{1}H NMR spectrum of the hardly soluble TBO(^{t}Bu)$_4$ **5-16b** (Figure 5-16). Together with H,H COSY experiments and the exemplary shown NOESY spectrum (Figure 5-17), the resonances could be undoubtedly assigned to their corresponding protons.

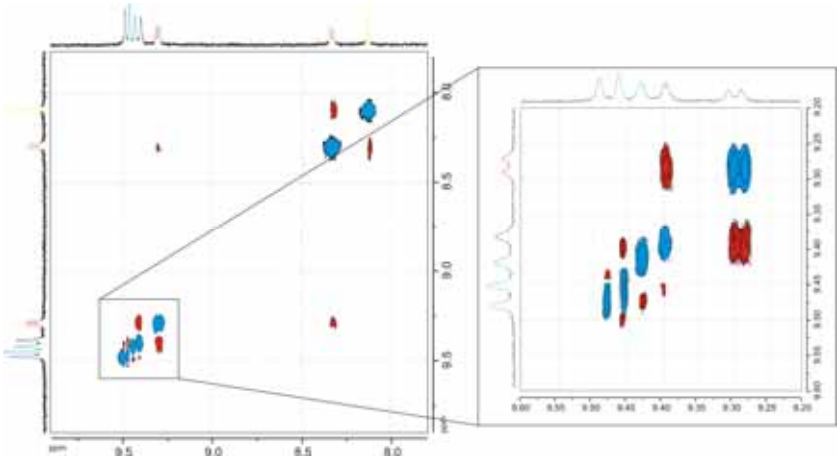

Figure 5-17: *NOESY spectrum of TBO(^{t}Bu)$_4$* **5-16b**, *recorded in THF-d^{8} at 60 °C (500 MHz), diagonal peaks are colorized in blue, cross-peaks in red.*

Most upfield shifted appeared the protons which are located on the "zigzag" edge, since there are more shielded due to an increased electron density at that site according to CLAR's rule. With increasing distance to that site, the resonances shifted downfield (Figure 5-16). The effect, which has to be taken into account, is that the ring current shields and deshields nuclei depending on their position. This secondary effect might be responsible for the shift difference of the aromatic protons.

X-ray crystal structures of HBC(^{t}Bu)$_6$ **3-3c**, its radical cation salt and several metal complexes have been obtained, which gave an insight into the packing behavior of extended PAHs.[59] All attempts to obtain crystals of pure TBO(^{t}Bu)$_4$ **5-16b** that have the dimensions and the quality for single crystal diffractometry, failed. The compound crystallized in very small needles (Figure 5-18), which were too small for the analysis. This propensity to form small crystallites when slowely evaporating the solvent, suggests a processing of saturated solutions with the zone-casting technique to obtain macroscopically organized films which is currently tested by N. TSAO.

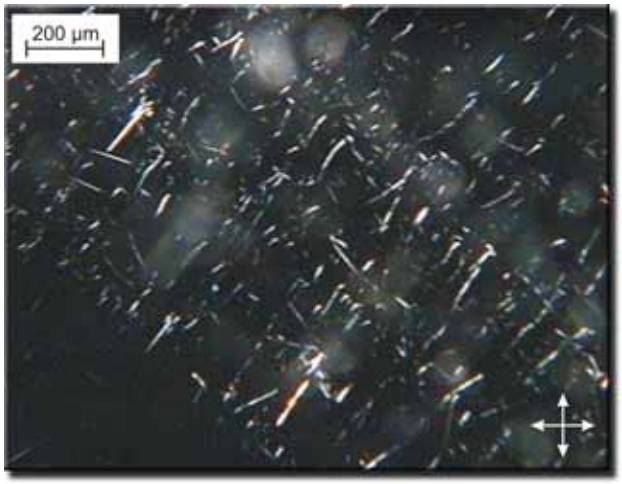

Figure 5-18: *Polarization optical microscopy (POM) of a drop-cast film of TBO(^{t}Bu)$_4$* **5-16b** *from toluene.*

Z. WANG managed to co-crystallize the PAH together with the strongly electron accepting TCNQ from THF. Figure 5-19A presents the molecular structure of the co-crystal. One notices that the PAH is expectedly almost perfectly planar with one *tert*-butyl group disordered in the crystal lattice. The acceptor is located close to the "zigzag" site, which is as discussed more electron rich and therefore the ideal position.

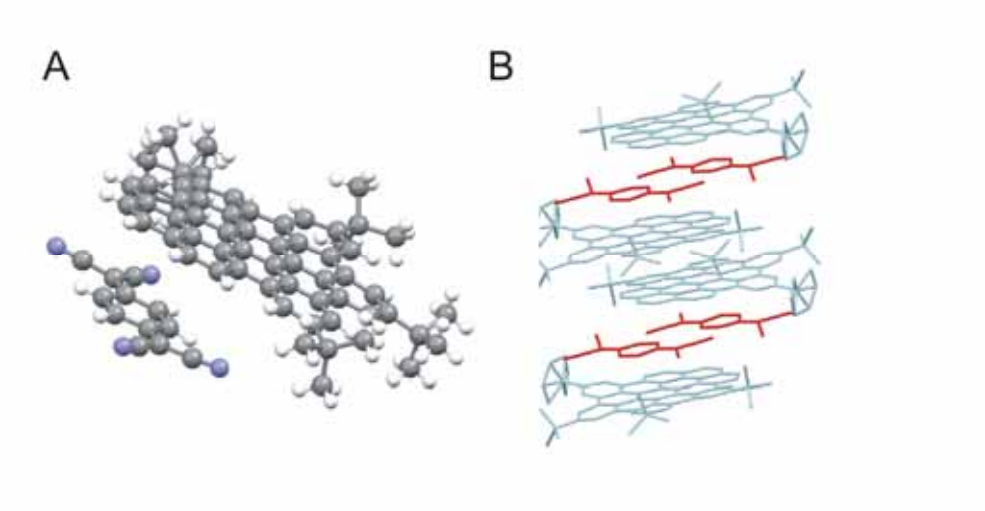

Figure 5-19: *(A) Co-crystal structure represented as balls and sticks of TBO(^{t}Bu)$_4$* **5-16b** *with TCNQ (THF as solvate, not shown); (B) crystal packing represented as wire model, with TBO(^{t}Bu)$_4$* **5-16b** *(light blue) and TCNQ (red).*

The packing of the molecules revealed to be interesting. Every other two PAH disc, two TCNQ molecules intercalated the aromatic stacking and increased the stacking distance from 3.6 to 3.8 Å. Within the stacks of molecules, the "zigzag" edge is packed alternating; every second TBO(^{t}Bu)$_4$ **5-16b** exhibited the same molecular orientation.

5.4.2 Dibenzo[*hi,uv*]phenanthro-[3,4,5,6-*bcdef*]-ovalene

In the previous chapter, the formal introduction of one "zigzag" site into the periphery of HBC has been described. The addition of another "zigzag" site on the opposite site of the aromatic core, leads to a PAH with 44 carbon atoms, which is named after the IUPAC nomenclature dibenzo[*hi,uv*]phenanthro-[3,4,5,6-*bcdef*]-ovalene (pDBPO, Figure 5-20). The structure belongs to the class of not-fully-benzoid PAHs and is predicted by computational chemists to be more reactive than its benzoid analogues.[60,61]

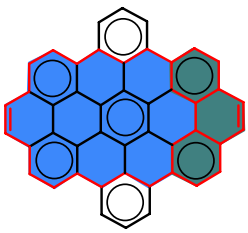

Dibenzo[hi,uv]phenanthro-(3,4,5,6-bcdef)-ovalene

Figure 5-20: *Chemical structure of pDBPO, the name defining ovalene subunit is colorized in blue.*

Synthetically, all building blocks for the reaction towards an adequate precursor have been made and described in the previous chapter. The [4+2] cycloaddition reaction of 4-ethynylphenanthrene **5-21** and the cyclopentadienone derivative **5-2** yielded the PAH **5-35**. Contrary to the reaction towards the precursor **5-3**, the DIELS-ALDER reaction proceeded smoothly and gave a high yield, since the reaction with terminal alkyne requires less thermal activation. Therefore, the decomposition of the starting material **5-2** was much slower.

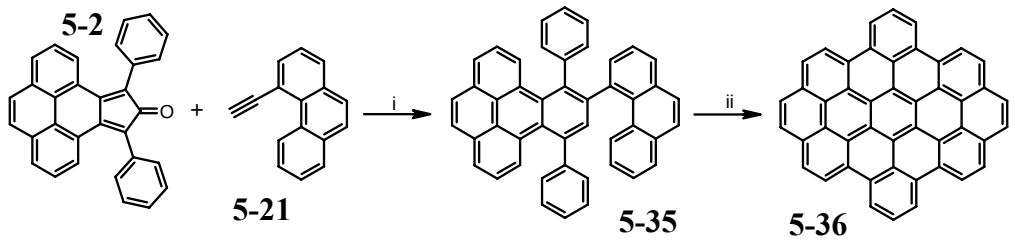

Scheme 5-10: *i) 72%; ii) $FeCl_3$, 88%.*

With two-dimensional NMR experiments, all proton resonances of the precursor molecule **5-35** could be assigned. Most upfield shifted appeared again the protons on the PAHs, which are located at the “zigzag” site. Interestingly, the rotation of the phenyl group, which carries the protons n, o and p (Figure 5-21) appeared to be strongly hindered. The resonances for the protons n and p were doubled which suggested a different chemical environment due to the hindered rotation of the phenyl-phenyl single bond. Temperatures of 180 °C were not sufficient to coalesce the corresponding aromatic resonances, which indicated a very high barrier for the rotation. Unfortunately, one could not determine the activation energy for that process, since the temperature windows for the tested solvents did not allow the intramolecular rotation to became fast.

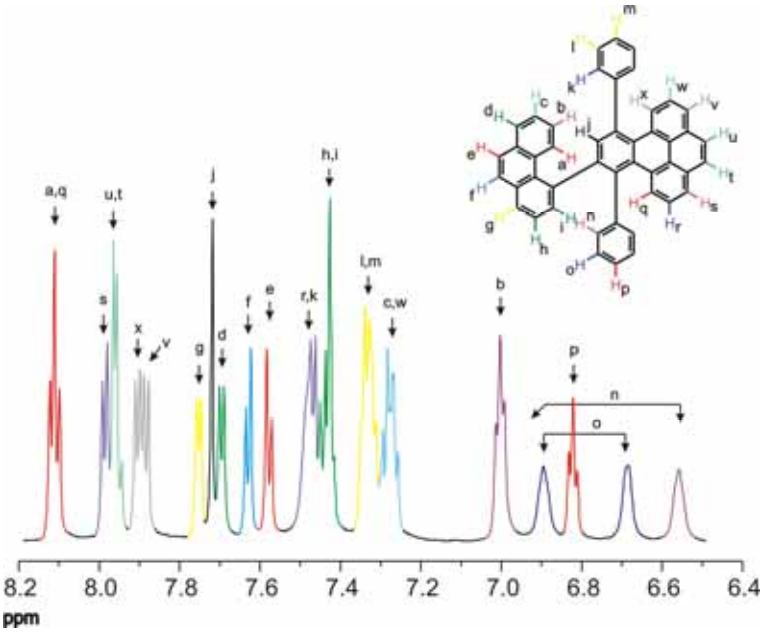

Figure 5-21: *^{1}H NMR of* **5-35***, recorded in THF-d^{8} at 70 °C (700 MHz).*

The final SCHOLL cyclodehydrogenation reaction of the precursor **5-35** yielded the hardly soluble, unsubstituted pDBPO **5-36** in good yields. The MALDI-TOF spectrum indicated the peak for the molecular ion with an isotope distribution which perfectly fits the simulation (Figure 5-22). However, the insufficient solubility of the PAH did not allow any further characterization from solution. In chapter 5.6.3, results from STM of the pDBPO **5-36** will be discussed.

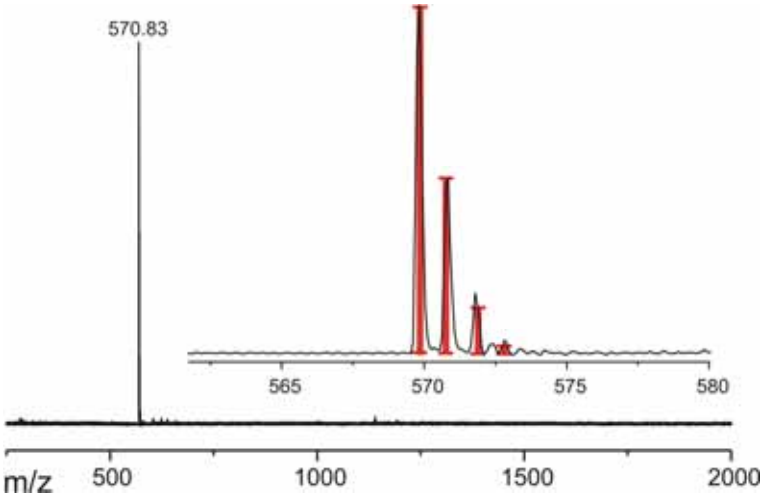

Figure 5-22: *MALDI-TOF spectrum of pDBPO* **5-36***, using solid state preparation with TCNQ as matrix substance.*

To improve the solubility and to obtain NMR spectra of pDBPO, multiple *tert*-butyl groups were introduced into the perimeter of the disc. Scheme 5-11 presents the synthetic concept, starting again with a DIELS-ALDER cycloaddition with the already

prepared compounds **5-7** and **5-21**. The thermal stability of the *tert*-butyl group carrying cyclopentadienone derivative **5-7** increased the yield of the reaction to be almost quantitative after the work-up procedure.

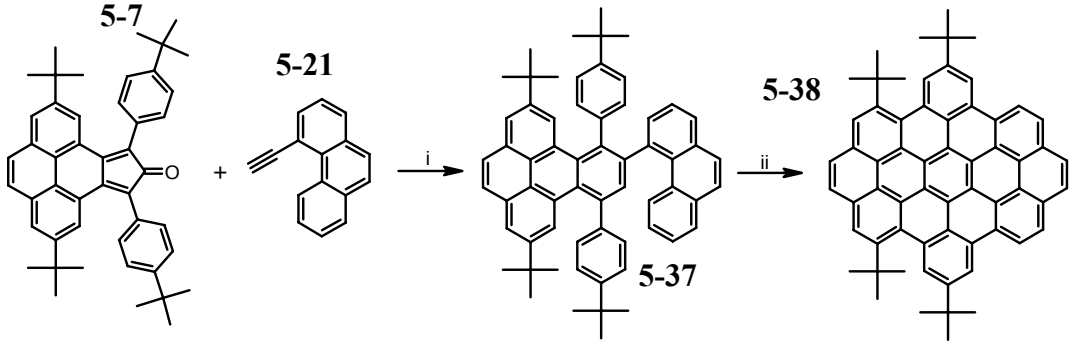

Scheme 5-11: *i) 98%; ii) $FeCl_3$, 85%.*

The ^{1}H NMR spectrum of the new precursor **5-37** emphasized again the hindered rotation of the phenyl ring, which carries the protons k and l (Figure 5-23). Most upfield shifted appeared the signals of the protons located at the PAHs due to a distortion of the local molecular orbitals and the anisotropic ring current effect, which caused a deshielding of the corresponding nuclei.

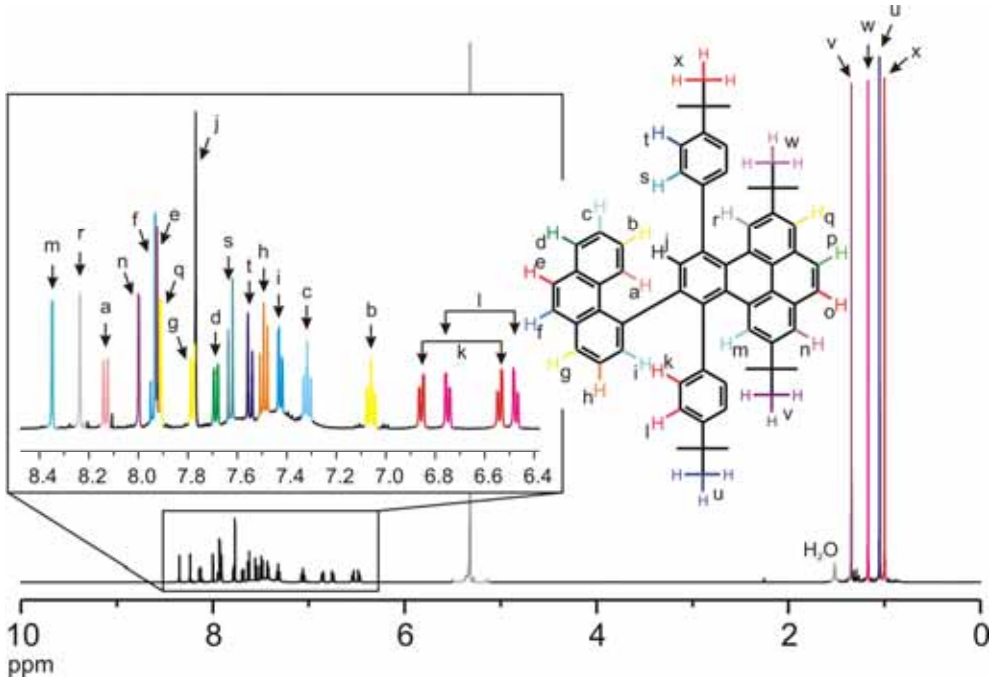

Figure 5-23: *^{1}H NMR of* **5-37***, recorded in dichloromethane-d^2 at 25 °C (500 MHz).*

Figure 5-24 presents a typical H,H COSY spectrum of the aromatic region of the asymmetric precursor **5-37**, recorded at room temperature in dichloromethane-d^2. Most upfield shifted appeared the two spin systems for the protons k and l. The rotation of this moiety around the phenyl-phenyl bond is sterically hindered and

therefore slow on the timescale of the experiment. Furthermore, the spin systems for the PAH moieties could be identified and the corresponding protons could be assigned and labeled as seen in Figure 5-23.

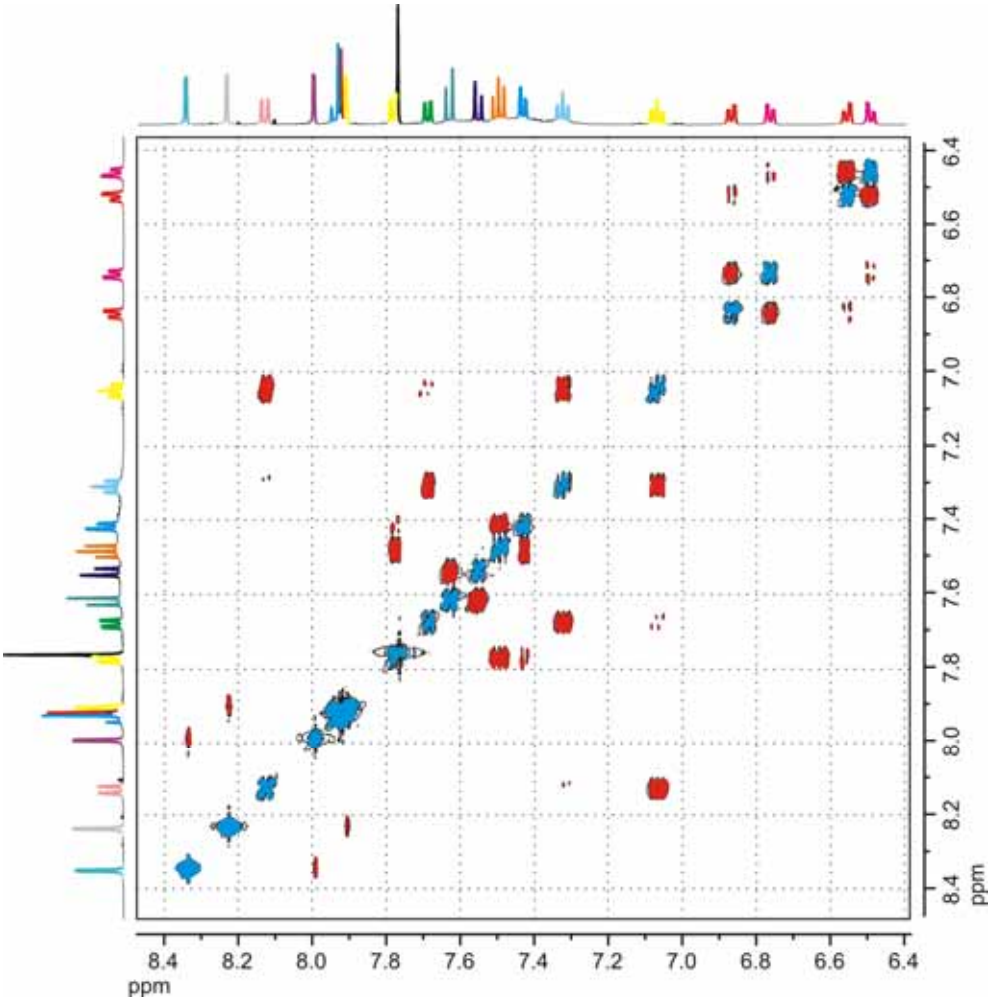

Figure 5-24: *H,H COSY of* **5-37***, recorded in dichloromethane-d*^{2} *at 25 °C (500 MHz), peaks are colorized for better visualization*

After the final Scholl reaction of the precursor molecule **5-37**, one obtained the pDBPO(^{t}Bu)$_4$ **5-37** with a distorted geometry. The *tert*-butyl groups, which are located in an "arm-chair" site of the PAH cause a twisting of the aromatic plane due to steric repulsion. This has been already proved by the single crystal analysis of TBO(^{t}Bu)$_6$ **5-9**.[46] D. WASSERFALLEN even exploited this twisting to enhance solubility for a much larger PAH with 72 carbon atoms in the aromatic core **1-44**, since the π-stacking was disturbed by the distortion.[37] Besides the solubility enhancement due to the non-planarity, the *tert*-butyl groups imposed the molecule a much better solubility in common organic solvents, which allowed NMR spectra to be recorded from solution. Figure 5-25 presents the ^{1}H NMR spectrum of

pDBPO(^{t}Bu)$_4$ **5-37** at slightly elevated temperature in THF. The aromatic region revealed the expected seven proton resonances, which could be assigned using H,H-COSY (Figure 5-26) experiments.

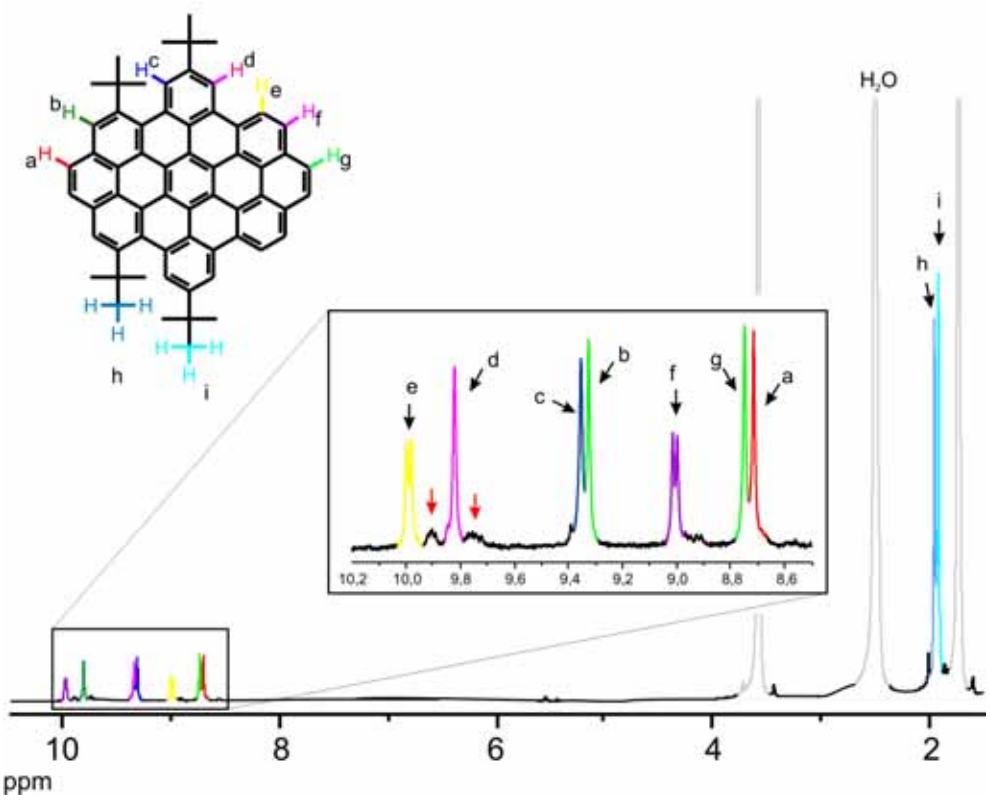

Figure 5-25: *^{1}H NMR of pDBPO(^{t}Bu)$_4$* **5-37***, recorded in THF-d^8 at 57 °C (700 MHz)*

The aromatic resonances of the proton nuclei which are located at the "zigzag" site appeared at higher field, due to a shielding induced by the higher electron density or the different local ring current effects. This again supported the empirically determined CLAR theory of the aromatic sextet (see chapter 5.2). However, a closer inspection of the aromatic region revealed the existence of small amounts of impurities which are marked with the red arrows in Figure 5-25.

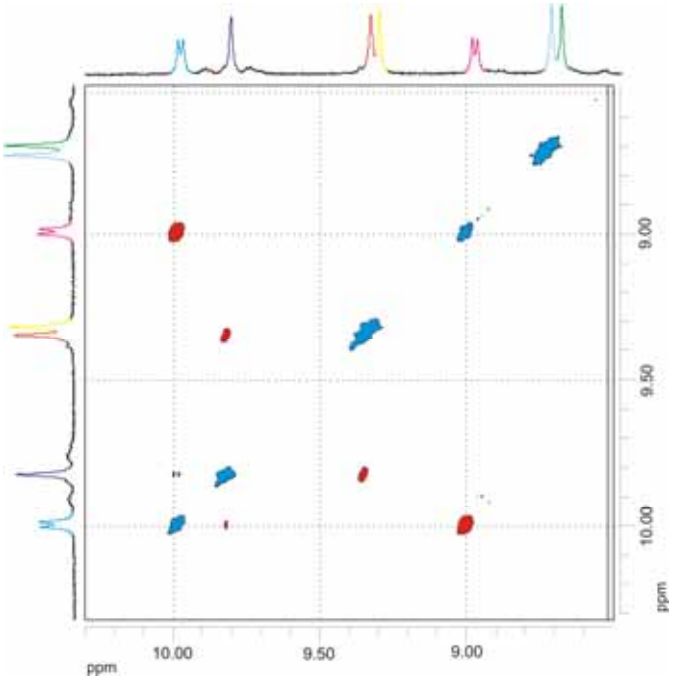

Figure 5-26: *H,H COSY of pDBPO(^{t}Bu)$_4$* **5-37***, recorded in THF-d^8 at 57 °C (700 MHz).*

The MALDI-TOF spectrum, using the solid state preparation method[44] did not indicate the presence of side-products (Figure 5-27). The isotope distribution was in good agreement with the simulation, although the signal-to-noise ratio of the recorded spectrum was not ideal.

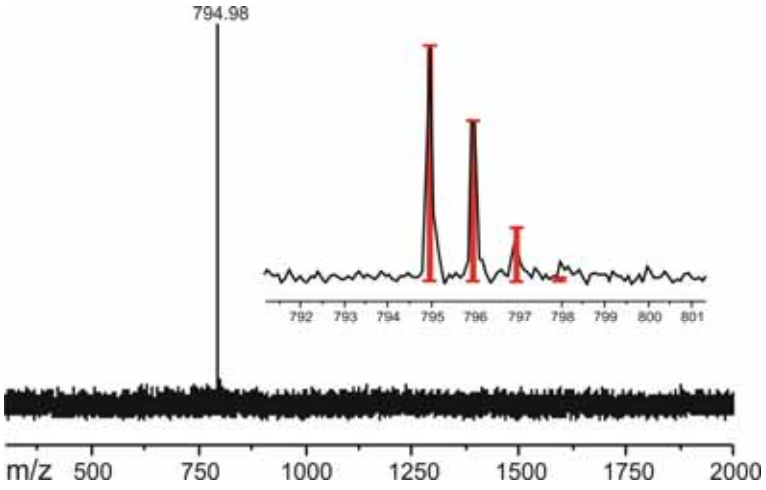

Figure 5-27: *MALDI-TOF spectrum of pDBPO(^{t}Bu)$_4$* **5-37***, solid-state prepared sample using TCNQ as matrix substance.*

Attempts to either "mono-oxidize" or "double-oxidize" pDBPO(^{t}Bu)$_4$ **5-37** according to the previously discussed example (Scheme 5-2) failed. Even when using drastic conditions, mass spectrometrically no desired product could be identified. In contrast to TBO, the electron density is not as strongly polarized towards the rim. Therefore,

the electron density at both zigzag sites is much lower than in the case of TBO, which inhibited the oxidation. This has been supported by DFT calculations (not shown) and will be discussed later.

All undertaken attempts to obtain single crystals of pDBPO(^{t}Bu)$_4$ **5-37** that are suitable for single X-ray diffractometry were unsuccessful so far. The compound crystallizes in tiny needles, which dimensions are not sufficient for the analysis. Furthermore, no co-crystal with accepting molecules like TCNQ, or hexafluorobenzene could be obtained up to now.

In order to obtain a phase forming derivative of pDBPO, one would have to attach flexible alkyl chains to the rigid aromatic backbone. However, as previously described, the *n*-dodecyl substituted cyclopentadienone **5-12** could not be synthesized. Therefore, a different synthetic concept was utilized which allowed the alkyl chains to be introduced on a later stage (Scheme 5-12).

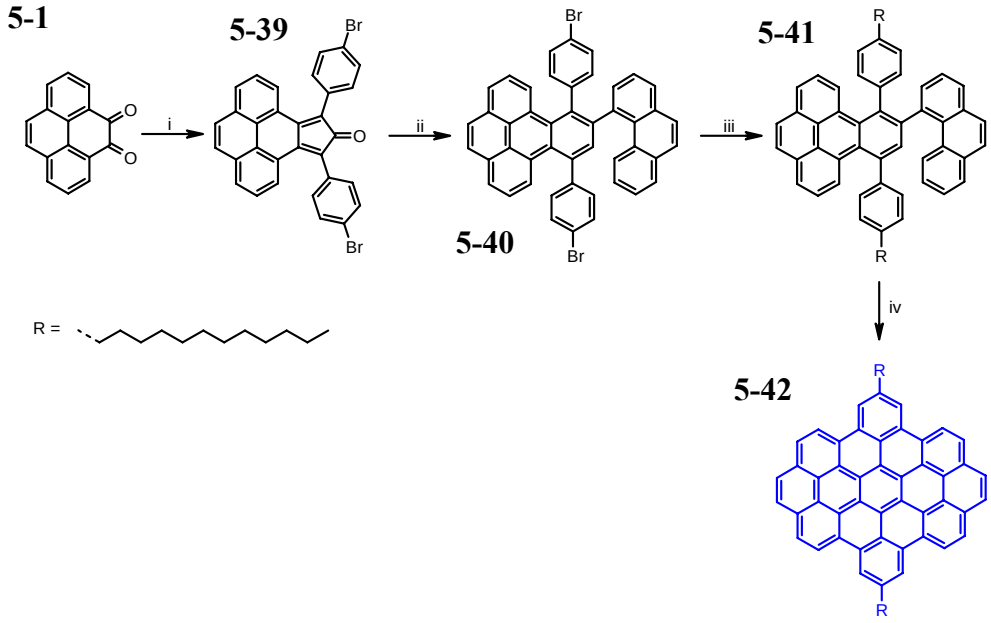

Scheme 5-12: *i) 1,3-bis-(4-bromo-phenyl)-propan-2-one, KOH, 47%; ii) 4-ethynylphenanthrene, 75%; iii) RMgBr, Pd(dppf)Cl$_2$, 91%; iv) FeCl$_3$, 90%*

Starting the literature known synthesis of pyrenedione **5-1**[41], the double KNOEVENAGEL condensation with 1,3-bis-(4-bromo-phenyl)-propan-2-one[62] was conducted. Contrary to the derivative with the *n*-dodecyl chains, the solubility of the double bromine carrying cyclopentadienone **5-39** was low enough to precipitate during the course of the reaction and to be isolated in a moderate yield of 47%. The

low solubility in the reaction solvent circumvented in fact the direct thermal decomposition of the unstable derivative. The subsequent DIELS-ALDER cycloaddition proceeded analogous to the previously described examples with satisfying yields of **5-40**. The two bromo-functionalities of compound **5-40** were convertible into alkyl-substituents using palladium catalyzed cross-coupling reactions, such as NIGISHI, KUMADA or SUZUKI methods. The highest yields were obtained by reacting the hydroboration adduct of *n*-dodec-1-ene and 9-BBN in a SUZUKI protocol with the halogen functions to give the two-fold *n*-dodecyl substituted analogue **5-41**.

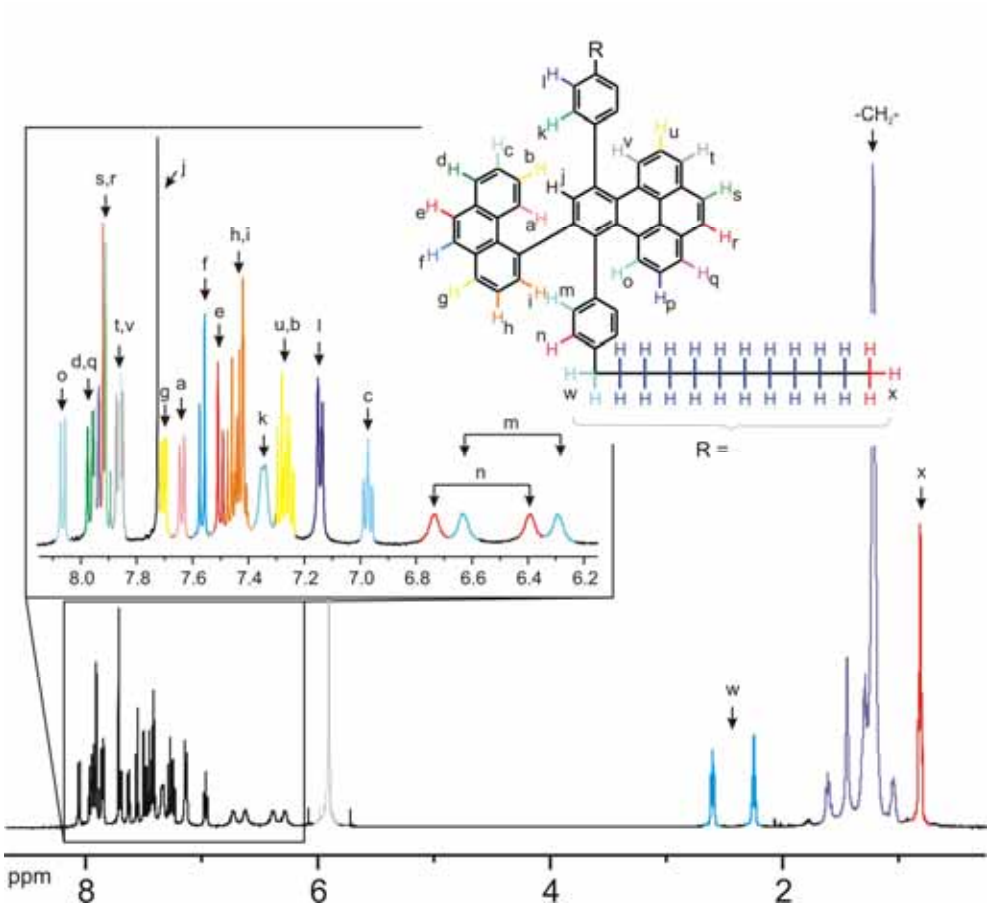

Figure 5-28: *^{1}H NMR of* **5-41**, *recorded in 1,1,2,2-tetrachloroethane-d^2 at 100 °C (500 MHz).*

Following the previous precursors, the ^{1}H NMR spectrum of **5-41** emphasized again the steric hindrance for the rotation of the restricted phenyl (Figure 5-28). Even a temperature of 100 °C did not promote the rotation at the timescale of the NMR experiment. The phenyl group can be considered as locked at room temperature. All aromatic resonances could be assigned to their corresponding nuclei by means of two-dimensional NMR spectroscopy (not shown).

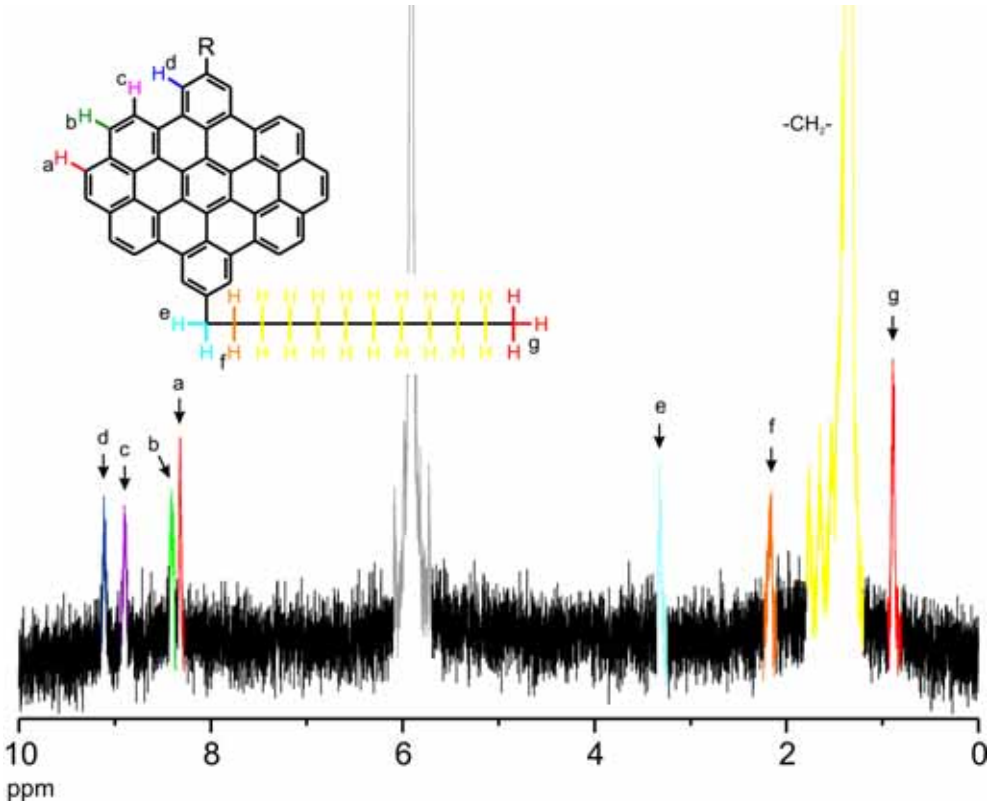

Figure 5-29: *^{1}H NMR of pDBPO(C_{12})$_2$* **5-42***, recorded in 1,1,2,2-tetrachloroethane-d^2 at 137 °C.*

The cyclodehydrogenation reaction with iron(III) chloride proceeded analogous to the previous examples smoothly and pDBPO(C_{12})$_2$ **5-42** was obtained in a yield of 90% after the work-up procedure. Although only two alkyl chains solubilized the extended aromatic molecule, high-field NMR instrumentation allowed resolved ^{1}H NMR spectra to be recorded at elevated temperatures. Figure 5-29 presents the ^{1}H NMR spectrum of pDBPO(C_{12})$_2$ **5-42**, taken in 1,1,2,2-tetrachloroethane-d^2 at 137 °C. Although the signal-to-noise ratio was due to the limited solubility not ideal, the aromatic region clearly showed the four expected aromatic resonances, which could be assigned to their corresponding protons. At highest field, the protons located at the "zigzag" site were found, emphasizing the polarization of the electron density within the PAH molecule. However, the chemical shift difference between the "zigzag" and the "arm-chair" protons is smaller in comparison with TBO(^{t}Bu)$_4$ **5-16b** (Figure 5-16), indicating different local ring current effects and polarizations of the electron density within the aromatic part of the molecule.

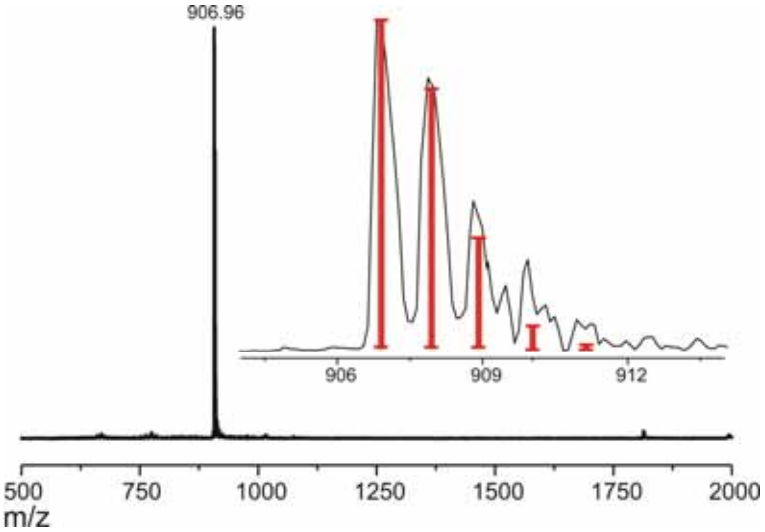

Figure 5-30: *MALDI-TOF of pDBPO(C_{12})$_2$* **5-42***, solid state prepared sample with TCNQ as the matrix substance.*

The MALDI-TOF mass spectrum reveals the successful planarization reaction. The isotope pattern was in good agreement with the simulated spectrum (Figure 5-30).

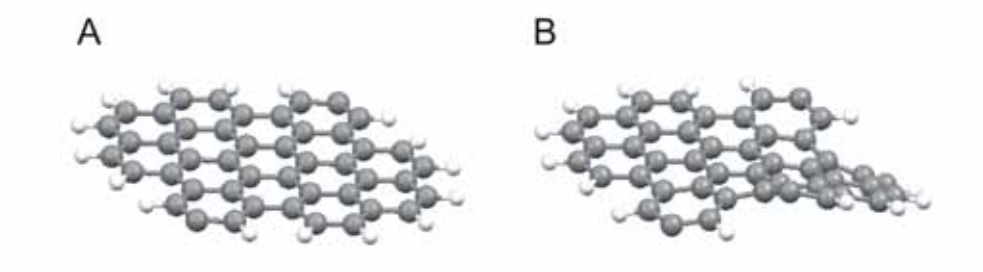

Figure 5-31: *Calculated optimized geometry (semi-empirical, AM1) for (A) pDBPO(C_{12})$_2$* **5-42** *and (B) pDBPO(^{t}Bu)$_4$* **5-38***, substituents are not shown for clarity.*

Figure 5-31 presents the geometry of the planar and the distorted aromatic core of the derivative **5-38** and **5-42**, respectively, which has been calculated using the semi-empirical AM1 method. The Figure emphasizes the steric congestion exerted by the *tert*-butyl groups.

The thermal behavior and the phase formation of the *n*-dodecyl substituted derivative pDBPO(C_{12})$_2$ **5-42** will be described in chapter 5.6. In the following chapter, a synthetic approach towards a PAH with a "tri-zigzag" edge structure will be described.

5.4.3 Diphenanthro[3,4,5,6-*uvabc*;3',4',5',6'-*efghi*]ovalene

To extend our homologous series of "zigzag" site containing PAHs, the next logical step was to introduce formally a third "zigzag" edge into the periphery of the 42

carbon atom containing HBC. One possible isomer is the diphenanthro[3,4,5,6-*uvabc*;3',4',5',6'-*efghi*]ovalene (DPO), which structure is shown in Figure 5-32. According to CLAR's rule of the aromatic sextet, this PAH is again not-fully-benzoid since three "isolated" double bonds are existent next to benzene rings which contain ROBINSON rings.

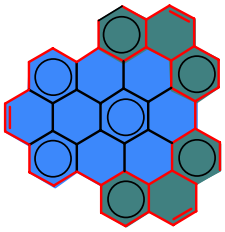

Diphenanthro[3,4,5,6-uvabc;3',4',5',6'-efghi]ovalene

Figure 5-32: *Chemical structure of DPO written according the CLAR nomenclature.*

Retro-synthetically, a simple cobalt promoted cyclotrimerization according to the VOLLHARD protocol[63] of the already prepared 4-ethynylphenanthrene (**5-21**) should lead to a suitable PAH precursor which one could oxidatively planarize in a SCHOLL reaction (Scheme 5-13).

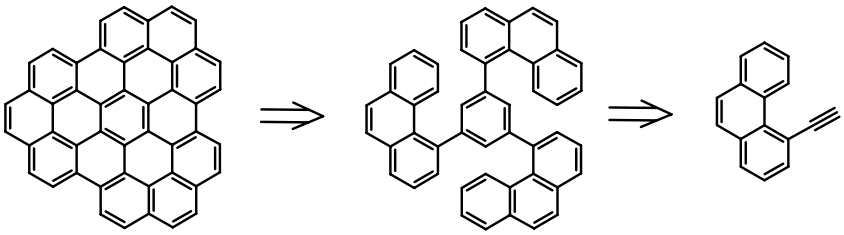

Scheme 5-13: *Retro-synthesis of DPO.*

Unfortunately, the suggested cyclotrimerization reaction was unsuccessful since access to the alkyne is sterically hindered, which has been observed for other cases as well.[64] Because of that reason, the initial cobalt adduct does not react to the necessary metallacycle and the reaction stops at the stage of the adduct.

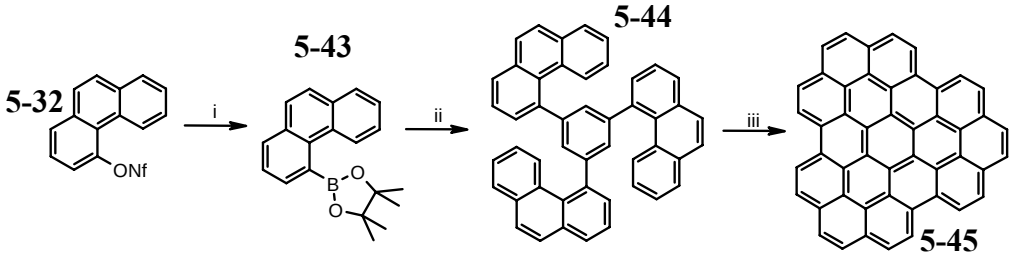

Scheme 5-14: *i) Bispinacolatodiboron, $Pd(PPh_3)_4$, AcOK, 83 %; ii) 1,3,5-tribromobenzene, $Pd(PPh_3)_4$, $Ba(OH)_2$, 15%; iii) $FeCl_3$, 65%.*

Therefore, a novel synthetic concept had to be found. Starting from the already prepared nonaflate **5-32**, the boronic ester **5-43** was obtained using a modified SUZUKI-MIYAURA coupling. The standard reaction conditions with a palladium(II) catalyst in THF or toluene did not allow any product to be obtained. Reaction temperatures of 90 °C and the use of tetrakis(triphenylphosphino)palladium(0) in DMF were optimal for the conversion and the desired product could be obtained in satisfying yields of 83%. The crystal structure elucidated, why the standard conditions did not allow the desired product to be obtained in satisfying yields (Figure 5-33). The substitution with the sterically demanding boron ester function leads to a distortion of bond angle and the aromatic system.

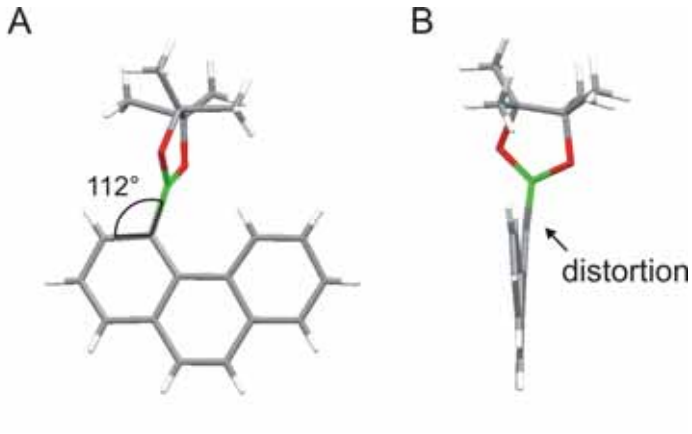

Figure 5-33: *X-ray crystal structure of* **5-43***, (A) top view, decreased angle and (B) side view which illustrates the distortion of the phenanthrene unit.*

As a little draw-back, the reaction yield of the subsequent, optimized SUZUKI coupling of the boronic ester **5-43** with 1,3,5-tribromobenzene was quite low.

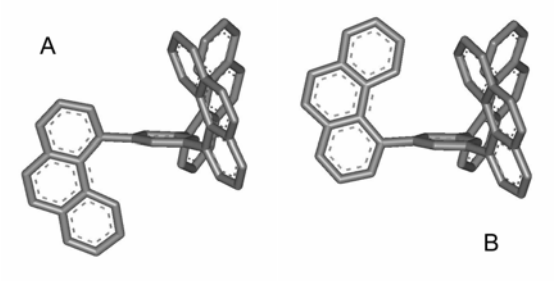

Figure 5-34: *Simulated atropisomers of* **5-44A** *and* **5-44B** *(molecular mechanic force field, MMF).*

This stands in contrast to the analogues reaction of 1,3,5-tribromobenzene with a 2-biphenylbronic ester derivative, where J. WU obtained reaction yields of 91%.[65] The reaction with 1,3,5-tribromobenzene requires strong bases to obtain the sterically crowded precursor molecule **5-44**. The conversion with bases of moderate basicity

was much lower compared to the reaction when using barium hydroxide, which has been observed for other SUZUKI on sterically demanding substrates.[66] At room temperature, the molecule existed as two stable atropisomers **5-44A** and **5-44B** (Figure 5-34) in solution and temperatures of about 180°C are needed to promote the free rotation of the phenanthrenyl-units around the central benzene ring, which has been observed with temperature dependent ^{1}H NMR spectroscopy (Figure 5-35). The room temperature spectrum shows three doublets for the downfield shifted proton resonances of the 5-position of the phenanthrenyl-units, with the intensities of 0.8, 2 and 1. This is related to a ratio between **5-44A** and **5-44B** of around 9:1, showing that the formation of B is sterically hindered during the reaction. When heating the sample in 1,2-dichlorobenzene-d^4, the observed doublets started to coalesce. However, the temperature window of the NMR solvent did not permit to completely coalesce the resonance; the peak remained broad. Therefore, it was not possible to calculate the activation energy for the isomerization process.

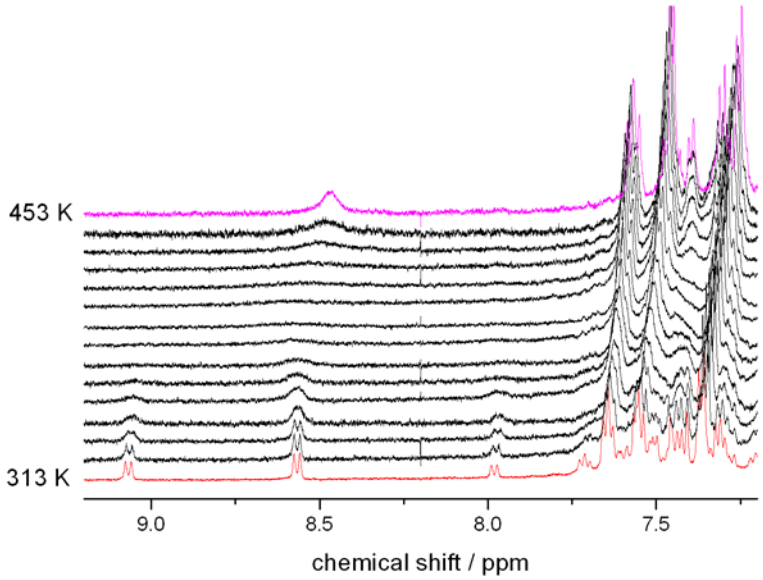

Figure 5-35: *Stacked plot of temperature dependent ^{1}H NMR spectra of* **5-44** *(aromatic region), recorded in oDCB-d^4.*

The final SCHOLL reaction gave the unsubstituted, hardly soluble PAH, DPO **5-45**, which did not allow any solution based analytics. However, the MALDI-TOF mass spectrum indicated the successful conversion of the precursor into the PAH (Figure 5-36).

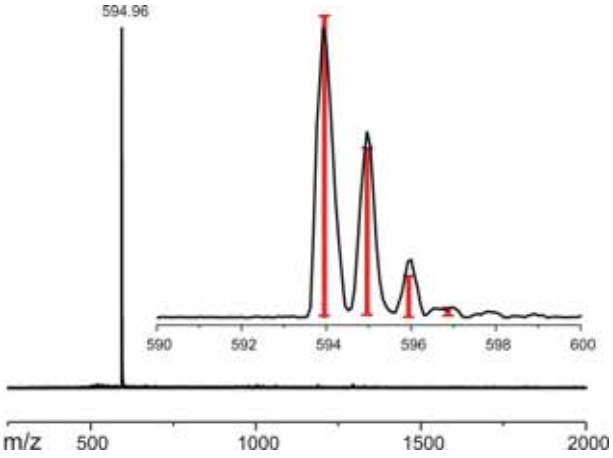

Figure 5-36: *MALDI-TOF spectrum of DPO* **5-45***, using the solid state preparation technique with TCNQ as the matrix substance.*

In order to get a better characterizable, soluble and even phase-forming DPO derivative, long, flexible alkyl chains should be introduced in the corona of the aromatic molecule.

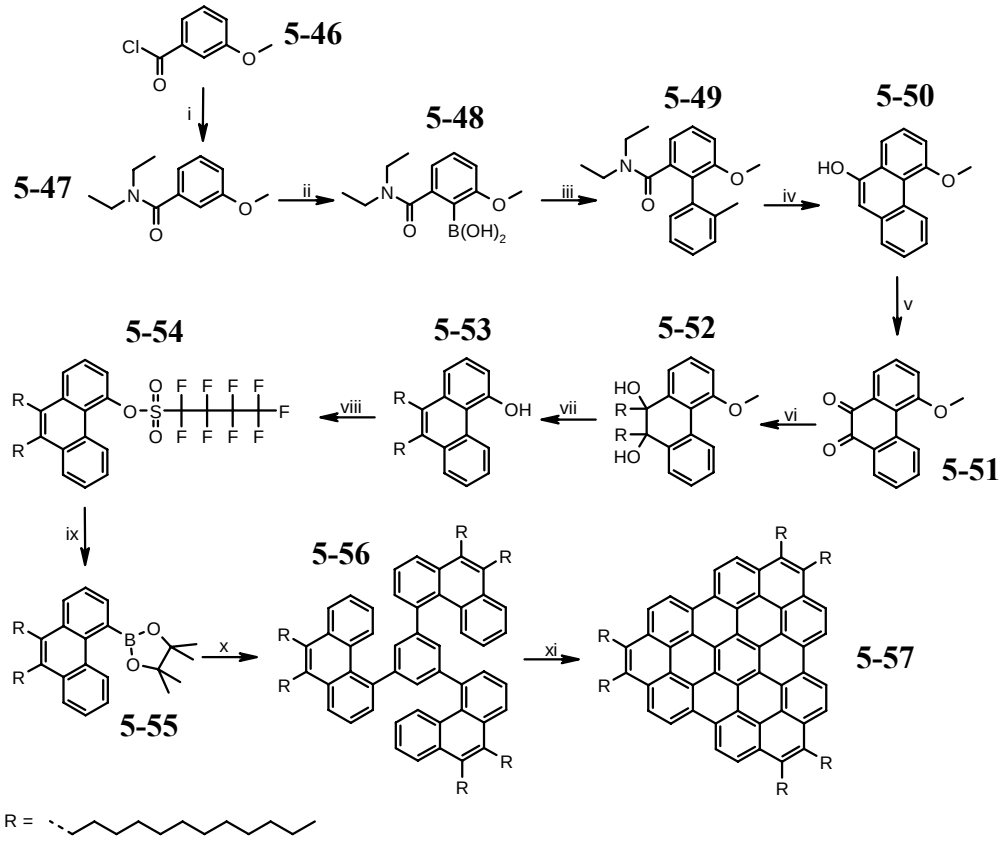

Scheme 5-15: *i) NEt_2, 99%; ii) ^tBuLi, $B(OMe)_3$, 62%; iii) $Pd(PPh_3)_4$, 2-iodotoluene, Na_2CO_3, 81%; iv) LDA, 94%; v) O_2, salcomine, 99%; vi) RMgBr; vii) HIO_3, AcOH; viii) NfF, 90% (three steps); ix) $Pd(PPh_3)_4$, bispinacolatodiborane, KOAc, 72%; x) 1,3,5-tribromobenzene, $Pd(PPh_3)_4$, $Ba(OH)_2$, 8%; xi) $FeCl_3$, 83%.*

The synthetic concept (Scheme 5-15) was based on the phenanthrene synthesis following the SNIEKUS method.[67] Commercially available 3-methoxy benzoyl chloride (**5-46**) was converted to the N,N-diethyl-3-methoxy-benzamide (**5-47**). A directed-ortho-metallation reaction was conducted using *tert*-butyl lithium and subsequently quenched to yield the boronic acid analogue **5-48**. This component was coupled with 2-iodotoluene in a standard SUZUKI cross-coupling reaction to obtain the biphenyl derivative **5-49**. With strong, sterically demanding bases such as LDA, the phenanthrene derivative **5-50** was obtained after an intramolecular cyclization, which was very sensitive to oxidation. The oxidation could be conducted quantitatively using oxygen and salcomine, a catalyst which binds molecular oxygen in solution. After this oxidation, the quinone **5-51** was reacted with the GRIGNARD reagent of 1-bromo-dodecane. The corresponding diol **5-52** was directly reduced with iodic acid to the 9,10 –dialkylated phenanthrene **5-53**. The applied reaction conditions allowed the methoxy function to be demethylated in situ. The separation of the desired phenanthrenol from side products turned out to be difficult, so that the crude compound was converted with nonafluoro-butane-1-sulfonyl fluoride to the nonaflate **5-54**, which could be easily purified. The above described, optimized reaction conditions allowed also in this case **5-54** to be converted to the pinacol boronic ester **5-55** in good yields. The SUZUKI cross-coupling reaction with 1,3,5-tribromobenzene required strong bases to afford the sterically crowded precursor molecule **5-56**. Analogous to the unsubstituted case, the reaction yield was very low and the propeller molecule **5-56** formed two stable atropisomers in solution at room temperatures. ^{1}H NMR spectroscopy (not shown) revealed that temperatures of more than 180 °C would be necessary to activate the rotation completely.

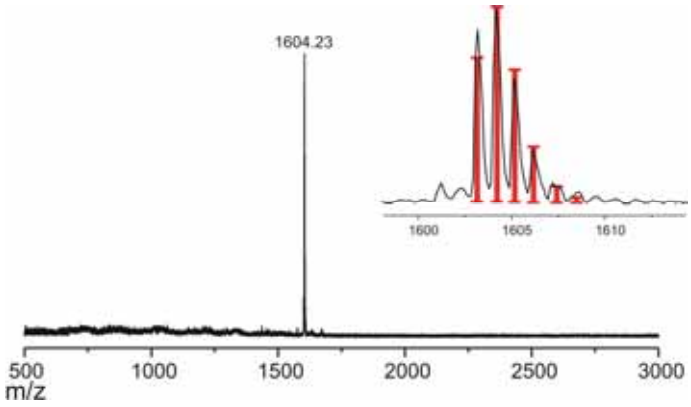

Figure 5-37: *MALDI-TOF spectrum of DPO(C_{12})$_6$* **5-57***, using solid-state preparation with TCNQ as the matrix substance.*

Again, the final cyclodehydrogenation reaction gave the desired DPO(C_{12})$_6$ **5-57**, which is clearly proven by the MALDI-TOF mass spectrum (Figure 5-37). Interestingly, the solubility of the compound was quite low at room temperature, although six long alkyl arms were attached in the periphery of the molecule. ^{1}H NMR spectra could only be resolved when CS_2 as a good solvent for the aromatic part was added to the NMR tube (Figure 5-38). The aromatic region of the molecule remained broad and not very well resolved, which can be explained by pronounced self-association processes in solution. Two aromatic signals could be resolved, which were assigned to the corresponding nuclei by simulation. With the knowledge of the previously described PAHs with "zigzag" sites, the more downfield shifted resonance was assigned to the proton which is located closer to the "zigzag" site.

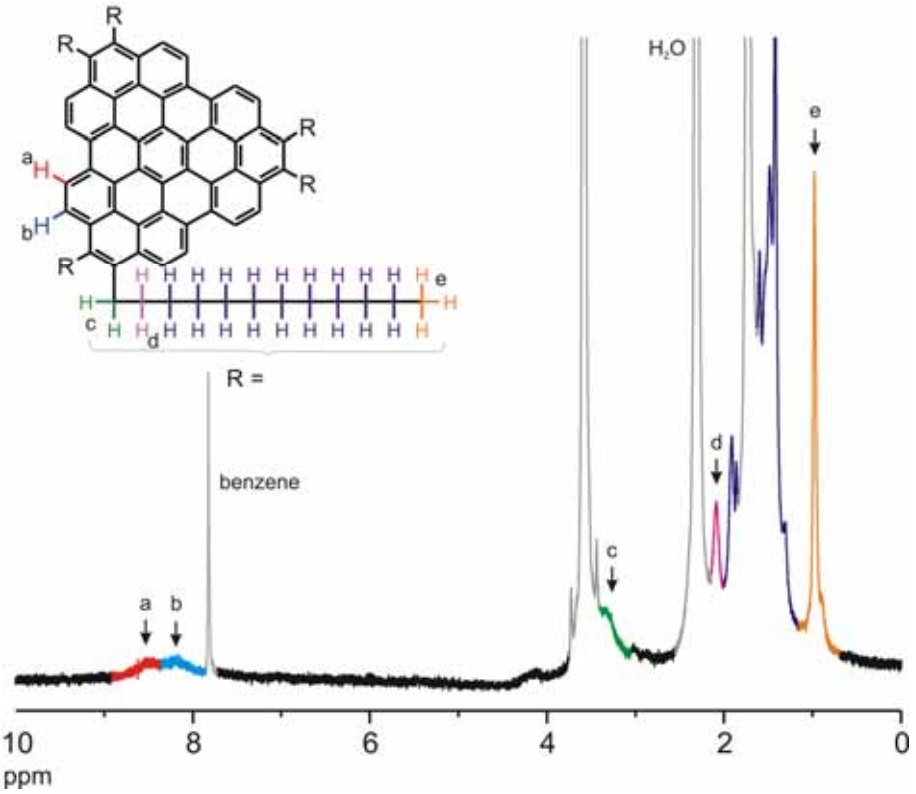

Figure 5-38: *^{1}H NMR of DPO(C_{12})$_6$* **5-57***, recorded in a mixture of THF-d^8 and CS_2 at room temperature (500 MHz).*

The DPO(C_{12})$_6$ **5-57** was phase forming, which will be described in chapter 5.6.

An alternative synthetic concept was recently developed by X. FENG. He utilized a cyclocondensation reaction of acetyl substituted with $SiCl_4$ to obtain a triphenylbenzene derivative **5-58**, which was converted over two steps into a suitable DPO precursor (Scheme 5-16). The reaction pathway was much shorter, higher

yielding and opened the possibility to introduce different alkyl chains to study the phase formation behavior and the surface organization dependent as a function of the alkyl substitution.

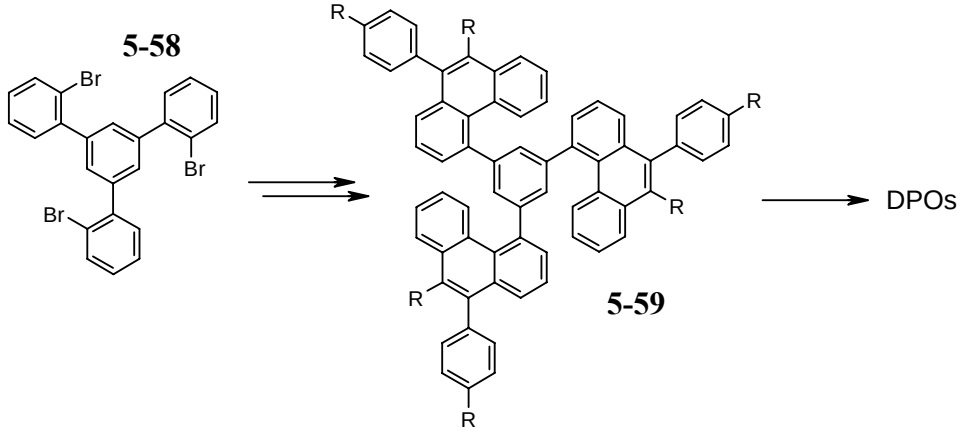

Scheme 5-16: *Novel synthetic concept towards DPO derivatives developed by X. FENG.*

5.4.4 Dibenzo[*ef,hi*]phenanthro[3,4,5,6-*u,v,a,b,c*]ovalene

In the previous chapters, the synthesis of extended PAHs with one, two and three "zigzag" sites was described. In the case of the pDBPO, two "zigzag" edges have been introduced which stand "para" to each other. Figure 5-39 presents an analogous PAH dibenzo[*ef,hi*]phenanthro[3,4,5,6-*u,v,a,b,c*]ovalene (mDBPO), where two such sites are "meta" to each other.

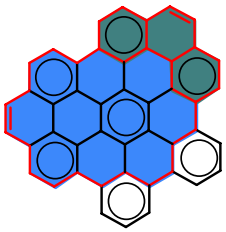

Dibenzo[ef,hi]phenanthro[3,4,5,6-u,v,a,b,c]ovalene

Figure 5-39: *Chemical structure of mDBPO written according the CLAR nomenclature.*

The analysis of the product mixture of the SUZUKI reaction with the phenanthrene boronic ester **5-55** and 1,3,5-tribromobenzene, which has been described in chapter 5.4.3, revealed that the two-fold reacted, sterically less crowded species was present as the main product and could be isolated in 71% yield. In the case of the unsubstituted boronic ester **5-43** with 1,3,5-tribromobenzene, it was even possible to crystallize the main product **5-60** (Figure 5-40). The crystal structure elucidated the

steric crowding at the halogen position, which hindered the "third" SUZUKI conversion.

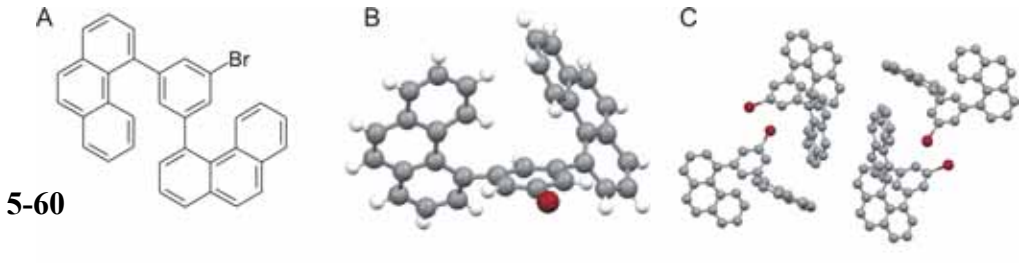

Figure 5-40: *(A) chemical structure of the main product in the SUZUKI reaction of* **5-43** *with 1,3,5-tribromobenzene, (B) X-ray crystal structure and (C) packing in the crystal.*

Nevertheless, **5-60** gave the chance to obtain a suitable precursor after the successful SUZUKI reaction with commercially available 2-biphenyl boronic acid. Interestingly, the biphenyl unit did not hinder the rotation of the two neighboring phenanthrene units and hence the precursor **5-61** did not show the formation of atropisomers at room temperature, which has clearly been seen from the ^{1}H NMR spectrum (not shown).

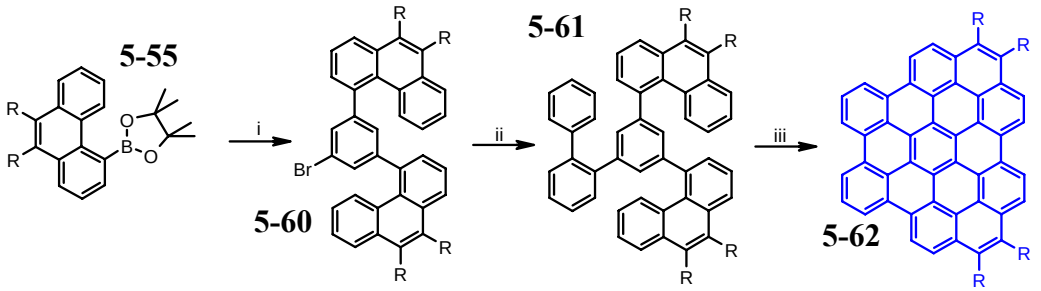

Scheme 5-17: *i) $Pd(PPh_3)_4$, $Ba(OH)_2$, 74%; ii) 2-biphenylboronic acid, $Ba(OH)_2$, 71%; iii) $FeCl_3$, 91%.*

The MALDI-TOF spectrum (Figure 5-41) indicated the successful planarization of the precursor with iron(III) chloride to the desired PAH, mDBPO$(C_{12})_4$ **5-62**.

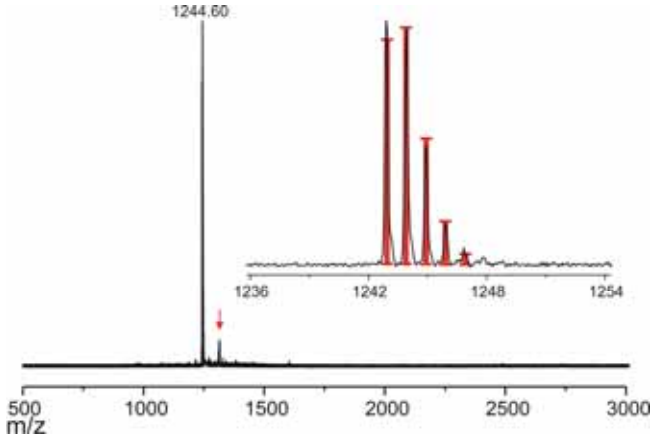

Figure 5-41: *MALDI-TOF of mDBPO(C_{12})$_4$* **5-62***, using solid-state preparation with TCNQ as matrix substance, red arrow indicates peak for an unassigned impurity.*

The red arrow in the mass spectrum marks an impurity which could not be assigned. High-field NMR instrumentation allowed the expected seven aromatic resonances to be resolved when heating the NMR tube to 140 °C in 1,1,2,2-tetrachloroethane-d^2 (Figure 5-42).

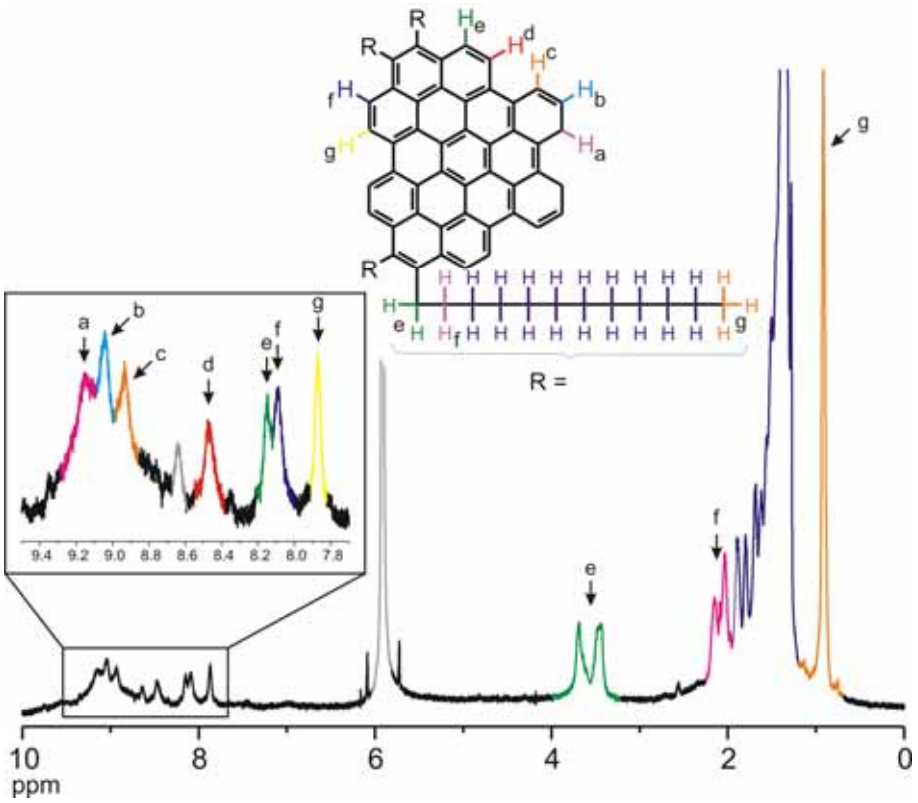

Figure 5-42: *^{1}H NMR of mDBPO(C_{12})$_4$* **5-62***, recorded in 1,1,2,2-tetrachloroethane-d^2 at 140 °C (500 MHz)*

Strong self-association caused again a broadening of the proton resonances, which are at room temperature not resolved. The *n*-dodecyl chains imposed the molecule a phase forming behavior which will be discussed separately in chapter 5.6.

5.4.5 Circumcoronene

In the last chapters, the successful implementation of "zigzag" sites into the perimeter of extended PAH was described. As a logic consequence, the homologous series of mono-, bis- and tris-"zigzag" carrying compounds was intended to be extended. A very interesting compound, which has been many times in focus for computational chemists, is the six "zigzag" sites containing circumcoronene.[68,69] This PAH has synthetically not been described so far and was approached *via* a dodecabenzyl hexaphenylbenzene derivative **5-70**.

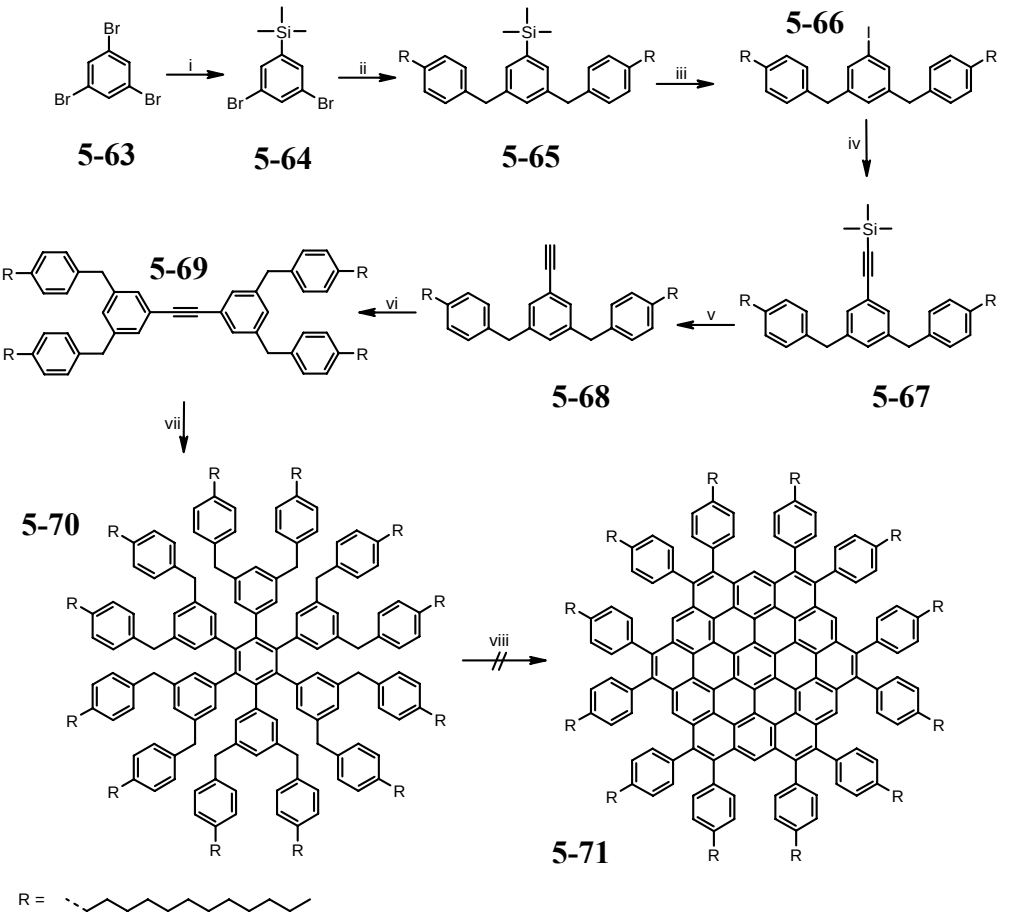

Scheme 5-18: *i) n-BuLi, TMS-Cl, 79%; ii) 4-n-dodecylbenzylmagnesium bromide, $Cl_2Ni(dppp)_2$, 29%; iii) ICl, 87%; iv) PPh_3, CuI, trimethylsilylacetylene, $Cl_2Pd(PPh_3)_2$, 92%; v) TBAF, 96%; vi)* **5-66**, *PPh_3, CuI, $Cl_2Pd(PPh_3)_2$, 84%; vii) $Co_2(CO)_8$, 86%; viii) $FeCl_3$*

The reaction concepts started with the selective mono-lithiation of 1,3,5-tribromobenzene **5-63** and subsequent reaction with trimethylsilyl chloride to afford 3,5-dibromo-1-(trimethylsilyl)benzene (**5-64**) in good yields.[70] The KUMADA cross-coupling reaction with the GRIGNARD reagent of 4-*n*-dodecylbenzyl bromide[71] provided in low conversions the desired bis-benzyl derivative **5-65**, because the majority of the benzyl GRIGNARD coupled in the presence of the catalyst oxidatively. The analogous reaction with a palladium catalyst did not yield the desired product. In this case, only dibenzyl could be mass spectrometrically detected. The conversion of the TMS group with iodomonochloride and the subsequent HAGIHARA-SONOGASHIRA cross-coupling reaction proceeded smoothly and gave the ethynyl substituted derivative **5-68**. The following cross-coupling reaction required a careful degassing to avoid the bisacetylene formation. With multiple freeze-pump-thaw cycles, the undesired side-product formation could be completely suppressed and the tolane derivative **5-69** could be isolated in good yields. The cyclotrimerization with dicobaltoctacarbonyl afforded the hexa-(3,5-bis-(4-*n*-dodecylbenzyl))phenylbenzene **5-70**.

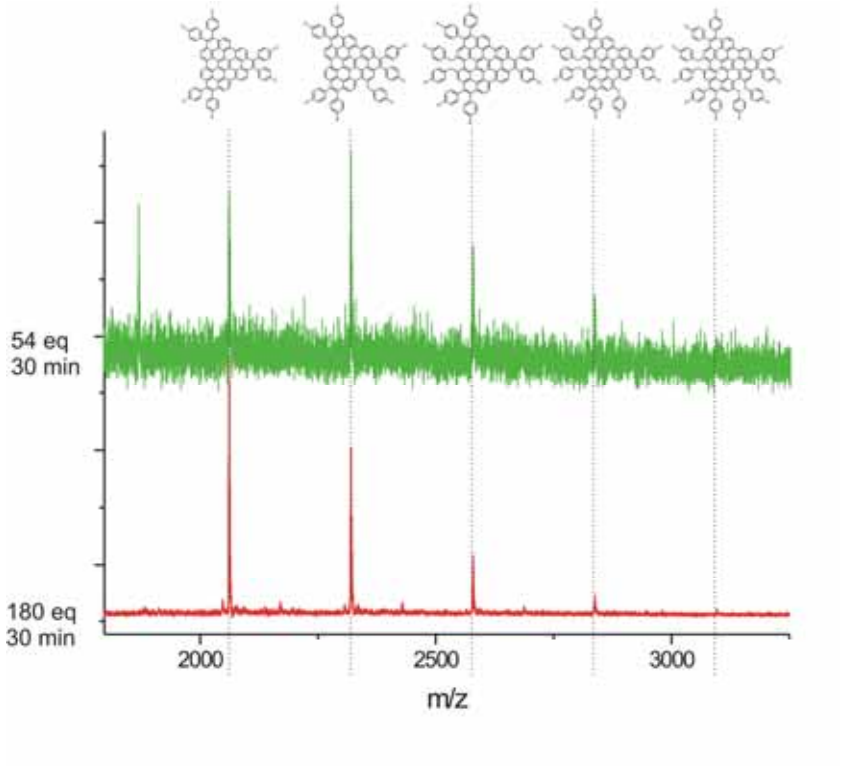

Figure 5-43: *MALDI-TOF spectrum indicating fragmentation during the cyclodehydrogenation reaction independent on the reaction conditions.*

Unfortunately, the final SCHOLL planarization reaction with iron(III) chloride did not give the desired PAH. The MALDI-TOF spectrum of the obtained product undoubtedly indicated a fragmentation during the reaction. All spectra, independent upon the applied laser power, revealed clearly debenzylated species.

Figure 5-43 presents two MALDI spectra of reaction which have been conducted with different amounts of oxidant. It becomes clear that the amount of iron(III)chloride influenced the fragmentation process. However, when using only very small amounts, the fragmentation was suppressed but partially fused by-products were detected. This is one example, where the optimal reaction conditions for the SCHOLL reaction could not be found. All attempts changing concentration, temperature and amount of oxidant did not reveal a successful reaction, which was additionally supported by broad and unresolved UV/vis spectra. Another clear indication for the incomplete SCHOLL reaction was the incongruence of absorption and photoluminescence excitation (PLE) spectra.[48] Furthermore, the reductive cyclodehydrogenation with potassium metal gave the same experimental results.

However, the analysis of a series of MALDI spectra of reactions applying different conditions revealed doubtlessly that the oxidative cyclodehydrogenation fused sp^3 centers together. This is the first example of a SCHOLL reaction, where bonds between non-aromatic carbon atoms are established. Although in the presented case not successful, because of the partial fragmentation, this result motivates the synthesis of benzyl unit containing precursors with different topologies. A successful planarization of such precursors suggests a simple access towards not fully benzoid, extended PAHs.

As an alternative reaction concept to obtain circumcoronene derivatives, one could introduce benzophenone moieties instead of the benzyl units, which could be fused with i.e. a MCMURRAY reaction.

5.5 Electronic Spectroscopy of the “zigzag” PAHs

The successful manipulation of the perimeter starting from the all-“armchair” HBC to the tree “zigzag” site containing DPO gave a homologous series of PAHs with varying size, periphery and topology (Figure 5-44).

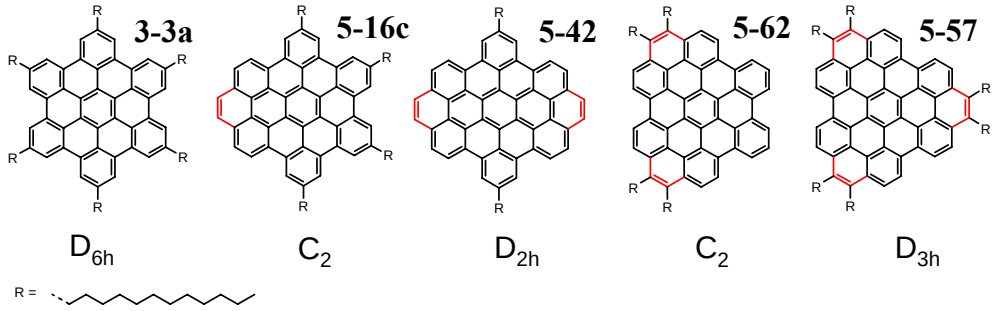

Figure 5-44: *Homologous series of PAHs with different size, periphery and topology.*

One of the most striking properties of PAHs, which sets them apart from other classes of organic molecules, is the nature of their UV/vis absorption spectra. The spectral response is very high, because the incident photons are interacting strongly with the PAH’s π-electrons. The number and the oscillator strength of the transitions in the usually structure-rich absorption spectra are mainly dependent upon the symmetry and the topology of the molecule.[4] The novel PAHs (Figure 5-44) revealed very characteristic concentration dependent absorption spectra and PL spectra, which will be compared in the following with the parent compound HBC-C_{12} **3-3a** (see also chapter 5.3).

5.5.1 Aromatic Core Symmetry

For the D_{6h} symmetric HBC-C_{12} **3-3a**, only the β-bands at 362 and 345 nm exhibited a high intensity, while the p-band borrows intensity from the latter band and appeared at a wavelength of 392 nm. At longest wavelength, a set of very weak bands were observed, which correspond to α- transitions. The PL gave a spectrum with a lot of sharp transitions, which is typical for a symmetry forbidden transition from the S_1 to the ground state S_0. Therefore, different vibronic levels of the ground state were reached from the excited state, leading to a set of distinct peaks.

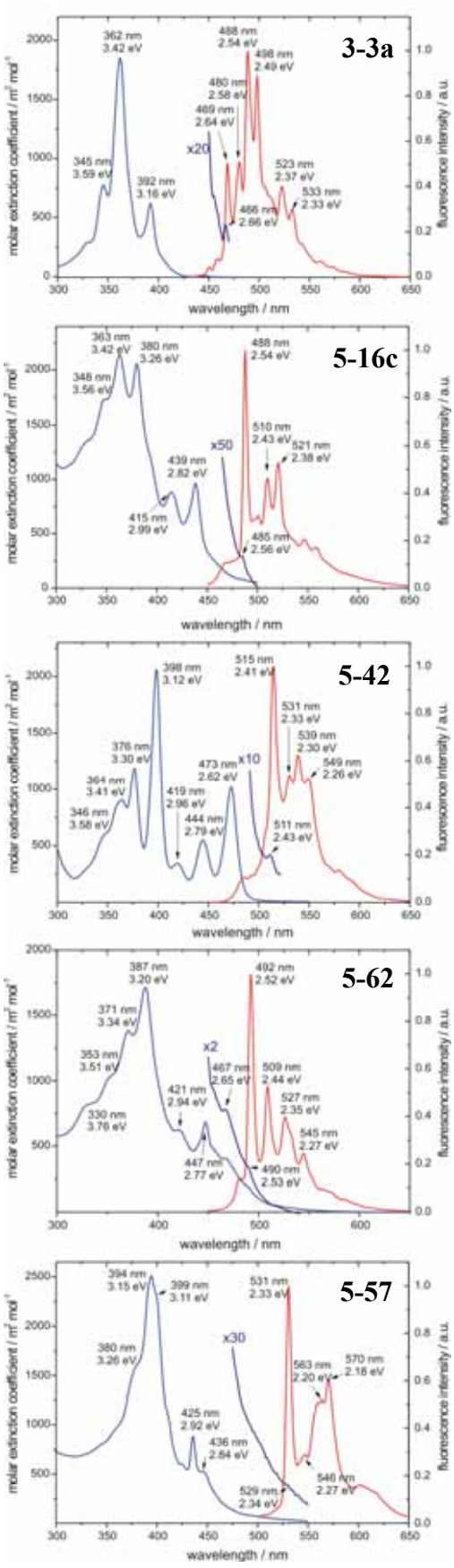

Figure 5-45: *UV/vis and PL spectra of the "zigzag" PAHs.*

It has been shown that HBC(C_{12})$_4$ **5-74**, whose synthesis will be described later (chapter 5.6.1), revealed identical spectra. This indicated that the substitution pattern had no impact on the electronic spectra of these PAH, which were only influenced by the nature of the aromatic core. This allowed the synthesized "zigzag" PAHs to be compared, although decorated with different numbers of *n*-dodecyl chains in different substitution patterns.

The formal annelation of an additional phenyl ring into an "arm-chair" site of HBC(C_{12})$_4$ **5-74** gives the TBO(C_{12})$_4$ **5-16c**. The symmetry reduction led to more allowed transitions, and therefore to a much broader UV/vis response. Even the α-bands were broader and stronger in intensity. In the fluorescence, the 0-0 transition is the strongest band, since the corresponding transition is not symmetry forbidden anymore. The same arguments hold for the mDBPO(C_{12})$_4$ **5-62**, which gave also a broad structure-poor spectrum compared to the one of HBC-C_{12} **3-3a**. Increasing the symmetry group to D_{2h} in the case for pDBPO(C_{12})$_2$ **5-42**, the peaks in the UV/vis spectrum became again sharper and fewer. When going to the D_{3h} symmetric DPO(C_{12})$_6$ **5-57**, the amount of transitions was again reduced and the UV/vis spectrum resembled the one of the parent compound HBC-C_{12} **3-3a**. Furthermore, the energy space between the intense absorption bands and the PL bands increased again compared to

the PAHs with the lower symmetry, TBO(C_{12})$_4$ **5-16c**, pDBPO(C_{12})$_2$ **5-42** and mDBPO(C_{12})$_4$ **5-62**.

Comparing the spectra of all investigated PAHs, one notices that the molar extinction coefficients of the most intense bands were in the same range. Furthermore, the Stokes shift was in all cases very small (< 5 nm) and independent of the used solvent, which indicated no polarity difference of the ground and the excited state as been observed for other PAHs as well.[33]

To gain a deeper insight into the origin of the distinct absorption bands, quantum chemical calculations were carried out to compute energies and intensities of the excitations, using a Density Functional Theory (DFT) approach. Therefore, the structures of “zigzag” PAHs have first been optimized on the B3LYP/3-21G level and subsequently a TDDFT (Time-dependent DFT) calculation (B3LYP/6-31G*) was conducted. The results of the calculation are summarized in Table 5-1.

Plotting the absorption maximum of the α- and the β-band respectively versus the number of carbon atoms in the aromatic system, one finds both for the experimental and the calculated data a linear dependence (Figure 5-46). The calculations were in good agreement with the experimentally determined peak positions and exhibited only a small systematical deviation, due to the relatively small basis set used in the TDDFT calculation. For all investigated PAHs, the ratio between the peak wavelength of the α- and the β-band were constant, which has been empirically reported already by CLAR for substantially smaller compounds.

Table 5-1: *Calculated and experimentally determined energies of the CLAR bands (oscillator strength* f *is also given).*

compound	transition	E(eV) exp.	E(eV) calc.	f (calc)
HBC-C_{12} 3-3**a**	α	2.66	2.90	0.00
	p	3.16	3.03[a]	0.00
	β	3.42	3.48	0.72
		3.59	3.48	0.72
TBO(C_{12})$_4$ 5-16**c**	α	2.56	2.75	0.0001
	p	2.62	2.79[b]	0.15
			3.16	0.18
			3.26	0.31
	β	3.26	3.39	0.36
			3.53	0.11
			3.61	0.23
pDBPO(C_{12})$_2$ 5-42	α	2.43	2.72	0.0003
	p	2.62	2.62[c]	0.26
	β	3.12	3.21	0.71
			3.23	0.00
			3.24	0.00
			3.30	0.00
			3.65	0.0039
mDBPO(C_{12})$_4$ 5-62	α	2.53	2.66	0.0003
	p	2.77	2.64[d]	0.18
	β	3.20	3.26	0.02
			3.28	0.74
			3.35	0.41
			3.53	0.00
			3.60	0.0039
DPO(C_{12})$_6$ 5-57	α	2.33	2.55	0.00
	p	2.92	2.67[d]	0.00
			3.20	0.91
	β	3.11	3.20	0.91
			3.45	0.01
			3.45	0.01
			3.60	0.00

[a]wavefunction composition: -0.49 (H-1→L+1), 0.49 (H→L)
[b]wavefunction composition: 0.27 (H-1→L+1), 0.11 (H-1→L+2), 0.62 (H→L)
[c]wavefunction composition: -0.23 (H-1→L+1), 0.63 (H→L)
[d]wavefunction composition: -0.23 (H-1→L+1), 0.64 (H→L)
[e]wavefunction composition: 0.50 (H-1→L+1), 0.50 (H→L)

Surprisingly, the p-band, which corresponds to the transition between the HOMO and the LUMO, does not reveal a linear dependence upon the size of the aromatic system. For the 48 carbon containing molecule DPO$(C_{12})_6$ **5-57**, the p-band was in the same range as for the smaller, 44 carbon containing TBO$(C_{12})_4$ **5-16c**. The p-band in the case of pDBPO$(C_{12})_2$ **5-42** was shifted most bathochromically within the investigated homologous series of PAHs. This proves that the p-band depended upon the topology and less upon the total size of the π-system. The extension of the aromatic system does not necessarily decrease the energy gap.

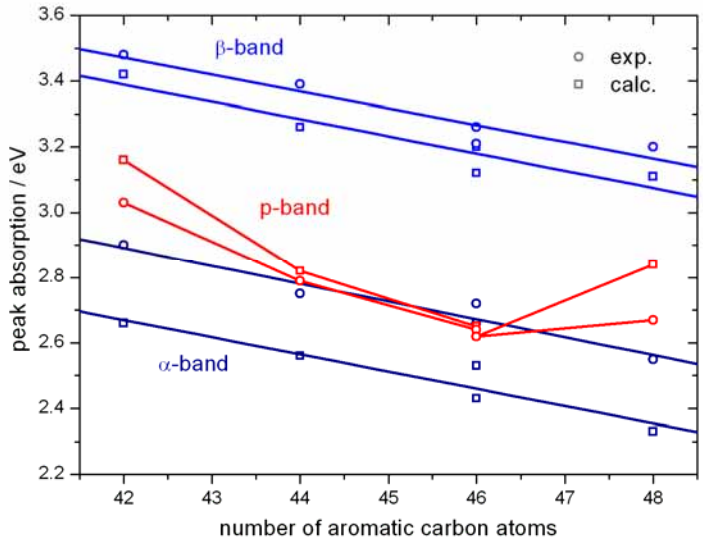

Figure 5-46: *Dependence of the absorption bands from the size of the aromatic core for the "zigzag" PAHs.*

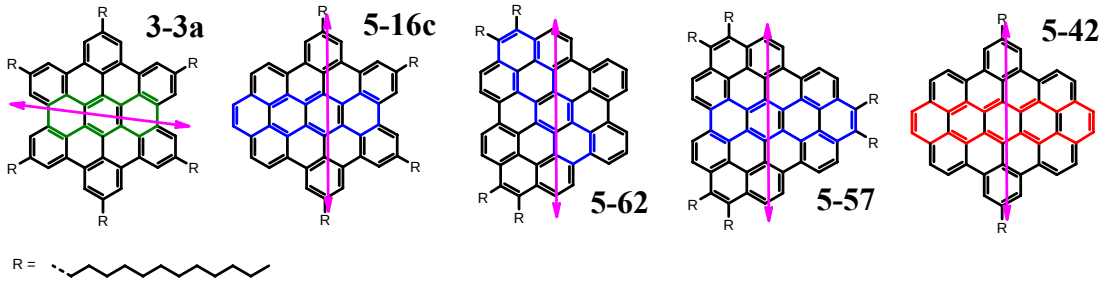

Figure 5-47: *Investigated PAHs where the "enclosed" acene is colorized, the magenta arrow indicates the calculated polarization direction of the transition dipole moment of the p-band.*

While compound pDBPO$(C_{12})_2$ **5-42** formally contained a pentacene subunit, the TBO$(C_{12})_4$ **5-16c**, mDBPO$(C_{12})_4$ **5-62** and DPO$(C_{12})_6$ **5-57**, where the position of the p-band is similar, enclosed only a tetracene moiety (Figure 5-47). The polarization of

the transition dipole moments for the p-bands in all cases were calculated, which did not support the above speculation. The transitions of the p-bands were not polarized in the direction of the central acene subunit (Figure 5-47).

Cyclovoltametry of the strongly aggregating "zigzag" PAHs revealed a distinct dependence of the oxidation potential upon the degree of association. Measurements in solution gave scattering values with a deviation of about 0.2 eV depending upon parameters such as temperature, concentration and nature of the used solvent. Cyclovoltametry on films revealed a pronounced dependence upon cast conditions and annealing. Unfortunately, not enough material was available to study these dependencies in greater detail. Therefore, absolute values for the HOMOs could not be gained experimentally and were determined in quantum mechanical calculation, which are in good agreement with the experimental levels of HBC.[72] These results allow a qualitative speculation and emphasize the influence of size, topology and nature of the periphery onto the molecular properties (Figure 5-48). The HOMO levels ranged in these calculations from -5.24 eV for HBC to -4.82 eV for pDBPO **5-36**. Since the applied quantum mechanical algorithms did not allow the energy of unoccupied orbitals to be determined accurately, the optical bandgap (onset of p-band) was used to determine the position of the LUMO levels (Figure 5-48).

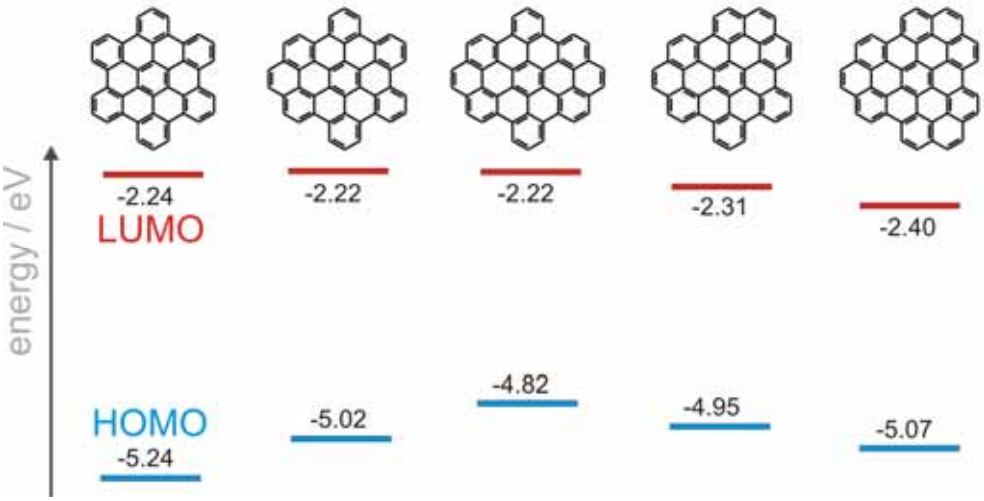

Figure 5-48: *„zigzag" PAHs with calculated HOMO and LUMO levels (density functional theory, B3LYP/3-21G).*

Evidently, the size, topology and symmetry of the aromatic core component sensitively influenced the position of the HOMO and LUMO, although experimental data is missing.

The introduction of bulky substituents such as *tert*-butyl groups into the bay position of PAHs caused due to steric reasons a distortion of the aromatic core (Figure 5-31). This twisting of the PAH enhanced the solubility and reduced the aggregation propensity. Furthermore, since the symmetry of the aromatic part was reduced due to the distortion the UV/vis response clearly differed. TBO(^{t}Bu)$_6$ **5-9** exhibited a less featured absorption spectrum compared to the undistorted analogue TBO(^{t}Bu)$_4$ **5-16b** (Figure 5-49). Again, one observed that the number of substituents and the substitution pattern had only a weak influence on the electronic spectra. For both derivatives **5-9** and **5-16b**, the characteristic bands revealed the same energy.

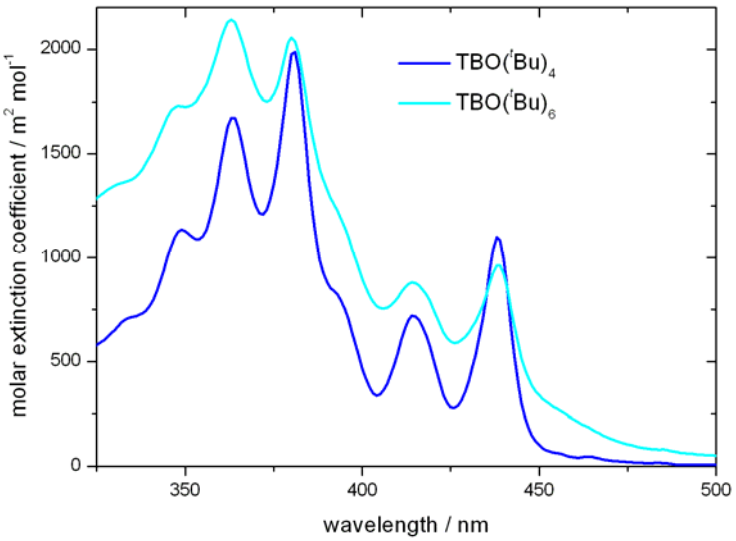

Figure 5-49: *UV/vis spectra of TBO(^{t}Bu)$_4$* **5-16b** *and TBO(^{t}Bu)$_6$* **5-9**, *recorded in chloroform.*

The same results were found when comparing the absorption spectra of pDBPO(^{t}Bu)$_4$ **5-38** and pDBPO(C_{12})$_2$ **5-42**. The non-planar derivative **5-38** gave again a broader absorption spectrum compared to the undisturbed and therefore planar PAH **5-42** (not shown). Since the nature of the alkyl substituents in the two pDBPO was different, the energy of the transitions slightly differed.

The change of the symmetry, which goes along with the partial change of the periphery type, had a distinct influence upon the electronic spectra. Both the experimental and computational UV/vis spectra were in very good agreement and reveal that the spectra of highly symmetric molecules were transition-poor compared to the PAHs with lower symmetries. The PAH typical bands α- and β depended linearly upon the overall size of the aromatic system, while the position of the p-band

which corresponds to the HOMO-LUMO transition, was mainly controlled by the topology of the PAH. More detailed quantum-mechanical calculations are currently performed to gain a deeper understanding into the dependence of the p-band from molecular parameters such as the topology. The number and the substitution pattern of the *n*-alkyl chains did expectedly not have any influence upon these molecular properties.

5.5.2 Self-Association in Solution

The self-association behavior of differently substituted HBCs has already been described in detail in chapter 3.2. Both NMR and electronic spectroscopy helped to elucidate the association propensities of the different derivatives in solution.

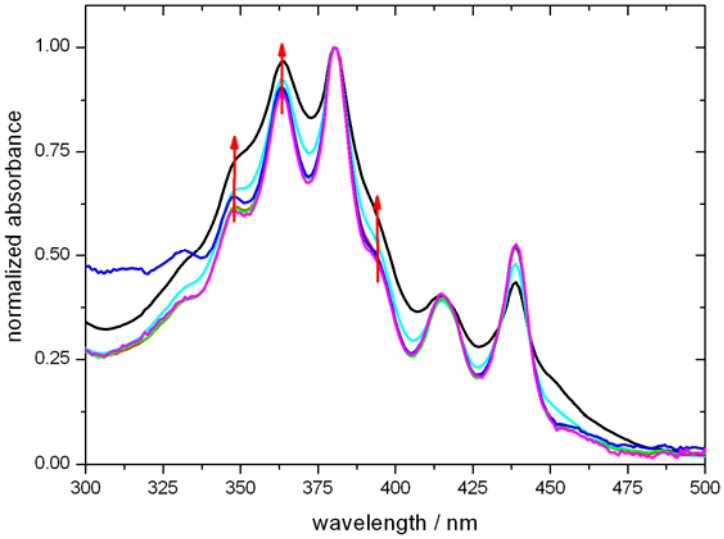

Figure 5-50: *Concentration dependent UV/vis spectra of TBO(C_{12})$_4$* **5-16c***, recorded in chloroform (concentration from 4x10^{-5} to 4x10^{-7} M, black to magenta).*

In the case of the "zigzag" site containing PAHs, ^{1}H NMR experiments turned out to be difficult, since much longer experimental times would have been necessary to resolve the multiple aromatic resonances of the sparingly soluble PAHs. However, solution UV/vis and PL spectroscopy was utilized to investigate potential aggregation phenomena. Expectedly, all investigated "zigzag" PAHs exhibited a very pronounced tendency to form aggregates in solution. In the following, selected results of the "zigzag" containing PAHs will be presented. Figure 5-50 depicts the concentration dependent UV/vis spectra of TBO(C_{12})$_4$ **5-16c**, which emphasizes the pronounced

self-association propensity of extended PAHs. With increasing concentration, the structure-rich spectrum became broader and less resolved. The same behavior has been found for HBC-C_{12} **3-3a** (chapter 3.2.2) and is found for the other investigated examples, as well.[23] These PAHs all showed similar solubilities in common organic solvents, qualitatively indicating a similar self-association propensity.

The PL spectroscopy was a much more sensitive method to probe the self-association in solution.[73] The PLE spectra revealed once again strong concentration dependence, which is a clear indication for association phenomena (Figure 5-51). The PL spectra were normalized.

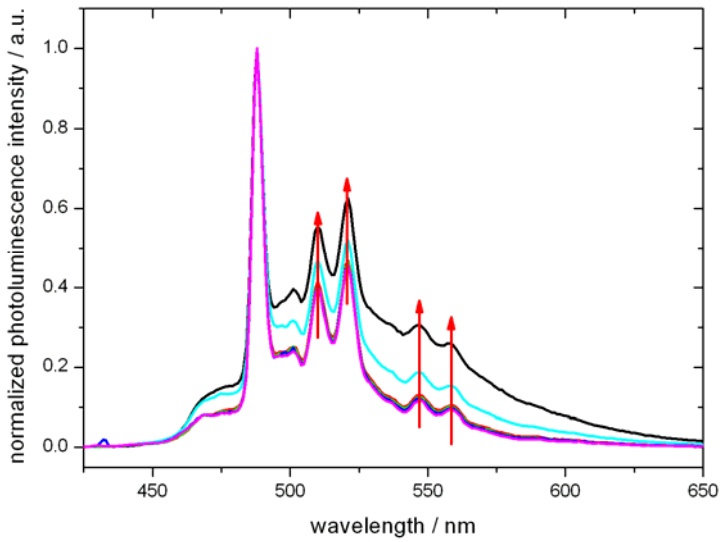

Figure 5-51: *Concentration dependent photoluminescence emission of TBO(C_{12})$_4$* **5-16c**, *recorded in chloroform (concentration from 4x10^{-5} to 4x10^{-7} M, black to magenta).*

The self-association propensity of the “zigzag” site containing PAHs were similar to the one of HBC-C_{12} **3-3a**, where a high association constant in different solvents was determined.

5.6 Supramolecular Organization

The substitution of the aromatic systems with flexible alkyl chains enhanced on one hand the solubility to obtain a material which could be characterized by solution analytics. On the other hand, the flexible substituents impose the rigid aromatic cores in many cases a discotic phase behavior.[74] In the past, discotic materials have gained great importance as promising, active components in organic devices.[75-78] In these applications, are long-range and defect-free organization of the planar, aromatic molecules is required to yield high performance values in the electronic device.[79]

In the following, the supramolecular organization of the novel PAHs (Figure 5-44) will be described to gain a further understanding how size, symmetry, substitution pattern and topology of the PAH influence the quality of the packing in the bulk. Only materials, which show a strong tendency to self-assemble into adequate supramolecular arrangements, promise a high performance when implemented in electronic devices.

The results which will be presented in the following chapter originate from a fruitful cooperation with W. PISULA, who recorded and analyzed the 2D-WAXS patterns obtained from experiments on extruded filaments.

5.6.1 Introduction of a Novel Substitution Pattern

The novel *n*-dodecyl substituted PAHs, which are presented in Figure 5-44, differed not only in their shape, symmetry and topology of the aromatic core. Different substitution patterns and numbers of the attached alkyl chains may have a vital influence upon the organization in the bulk. Therefore, an *n*-dodecyl HBC derivative with a modified substitution pattern was synthesized to study the effect on the self-ordering. The synthesis will be presented in the following.

The straight forward synthesis started with the DIELS-ALDER cycloaddition of the known *n*-dodecyl substituted cyclopentadienone **5-34c**[62] with commercially available diphenylacetylene **5-72**. The subsequent cyclodehydrogenation reaction yielded the HBC(C_{12})$_4$ **5-74** in good yields.

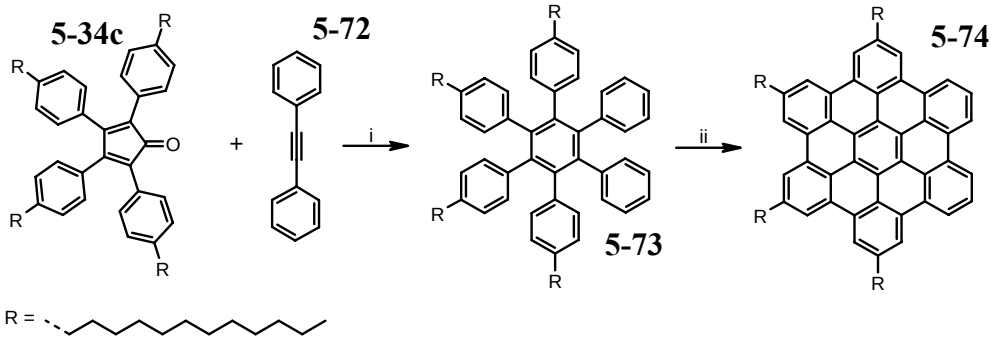

Scheme 5-19: *i) 93%; ii) $FeCl_3$, 93%.*

The solubility of **5-74** was compared to the two chains more carrying HBC-C_{12} **3-3a** clearly higher. This already indicated an influence upon the association in solution. The ^{1}H NMR spectrum recorded at elevated temperatures in THF-d^8 revealed the expected resonance which could be assigned to the corresponding nuclei. Furthermore, the MALDI-TOF spectrum supported the NMR spectroscopy and revealed the successful planarization of the precursor.

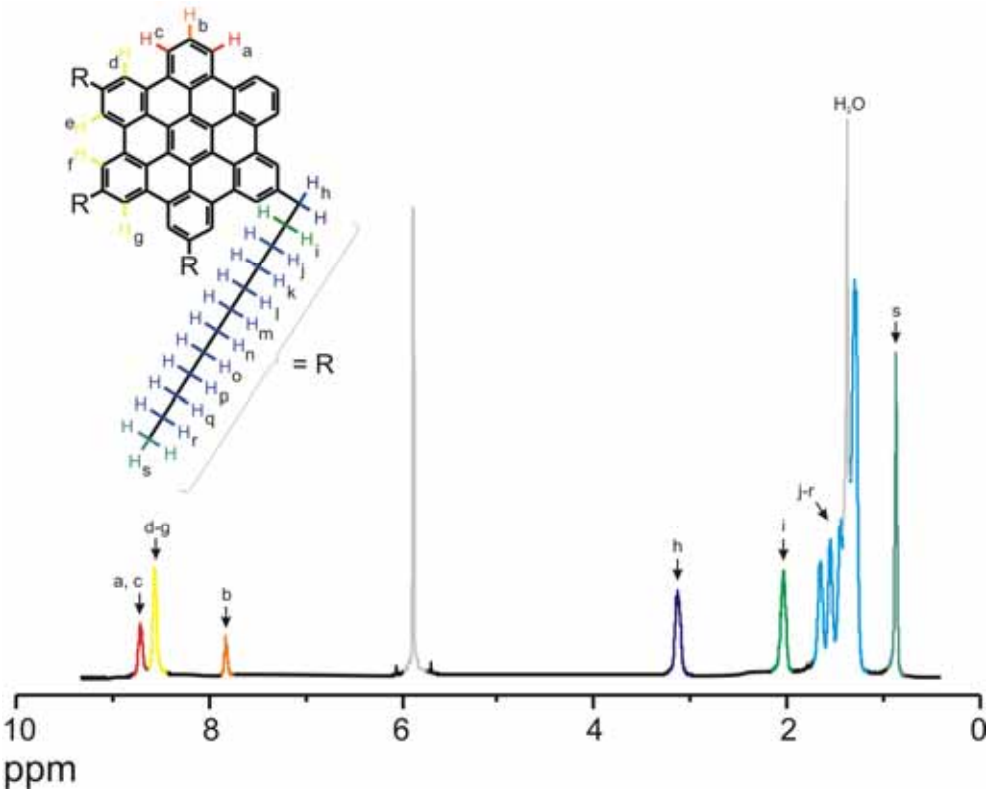

Figure 5-52: *^{1}H NMR of HBC(C_{12})$_4$* **5-74**, *recorded in THF-d^8 at 57 °C.*

HBC(C_{12})$_4$ **5-74** and HBC-C_{12} **3-3a** will be used in the following as model systems to compare the results of the PAHs with partial "zigzag" character.

5.6.2 Self-Assembly in the Bulk Phase

The thermal behavior, which is summarized in Table 5-2, was determined by differential scanning calorimetry (DSC) and polarized optical microscopy (POM). The phase evaluation was performed on the basis of X-ray scattering results discussed in the next section. All investigated derivatives were crystalline-like at room temperature. The comparison of the thermal data showed a stronger dependence on the number and the substitution pattern of the *n*-dodecyl side chains at the corona than on the shape and symmetry of the aromatic core. Thus, with increasing number of alkyl chains the phase transition temperature from the crystalline phase to the mesophase decreased. Therefore, independent upon the aromatic core symmetry, derivatives HBC(C_{12})$_4$ **5-74**, TBO(C_{12})$_4$ **5-16c** and mDBPO(C_{12})$_4$ **5-62** entered the mesophase at significantly higher temperatures than HBC-C_{12} **3-3a** and DPO(C_{12})$_6$ **5-57** with more alkyl side chains. Moreover, the density of substitution and consequently the steric hindrance played an additional effect, as it was obvious for the symmetric compound DPO(C_{12})$_6$ **5-57** which revealed the lowest first transition temperature among the investigated samples. On the other hand, the thermal results suggested that the core symmetry influenced the columnar stability and thus affected the isotropization temperature, which is much higher for the symmetric HBC-C_{12} **3-3a**, pDBPO(C_{12})$_2$ **5-42** and DPO(C_{12})$_6$ **5-57** in comparison to the derivatives consisting of an asymmetric core like mDBPO(C_{12})$_4$ **5-62**, melting already at 210°C. The enthalpy of the phase transition (Table 5-2) is an indication for the change of the organization between two phases. Therefore, by assuming an identical order in the mesophase for all derivatives, which is reasonable, the enthalpy of the first phase transition increases with increasing crystallinity of the material and thus with higher supramolecular order in the C_r phase. This relation was in good agreement with the structural results described in the next section.

Table 5-2: *Phase behavior of "zigzag" PAHs, comparison to HBCs.*

Derivative	Temperature / °C	Enthalpy / Jg^{-1} 1st transition (heating)	Phase-transition
HBC-C_{12} 3-3**a**	107 (82)	45.8	C_r – Col_{ho}
	420*		Col_{ho} – I
HBC$(C_{12})_4$ **5-74**	147 (123)	15.7	C_r – Col_{ho}
	400*		Col_{ho} – I
TBO$(C_{12})_4$ **5-16c**	148 (98)	13.8	C_r – Col_{ho}
	400*		Col_{ho} – I
pDBPO$(C_{12})_2$ **5-42**	226 (216)	28.3	C_r – ?
	> 500*		Col_{ho} – I
mDBPO$(C_{12})_4$ **5-62**	173 (144)	11.5	C_r – Col_{co}
	210		Col_{co} – I
DPO$(C_{12})_6$ **5-57**	48 (22)	18.4	C_r – Col_{ho}
	> 500*		Col_{ho} – I

List of abbreviations: C_r – crystalline phase, Col_{ho} – mesophase (hexagonal ordered columnar phase), Col_{co} – mesophase (cubic ordered columnar phase) I – isotropic phase, phase transitions upon cooling are given in brackets, * - assigned by polarized optical microscopy.

The samples for the structure evaluation by 2D-WAXS were prepared by filament extrusion as described previously.[80] All derivatives were extruded in their deformable, plastic state to ensure an adequate alignment of the columnar structures along the shear direction. For a reasonable comparison of the supramolecular organization of all derivatives, the patterns were recorded at room temperature before annealing which could influence strongly the molecular packing as observed for HBC$(C_{12})_4$ **5-74**.[80]

Temperature dependent measurements gave an additional insight into the order prevailing in the higher temperature phases. Except compound mDBPO$(C_{12})_4$ **5-62**, all derivatives revealed a characteristic hexagonal mesophase with a non-tilted

intracolumnar organization above the first transition. In contrast, the pronounced asymmetry of mDBPO(C_{12})$_4$ **5-62** resulted in a tilted packing of the discs towards the columnar axis and a cubic intercolumnar arrangement in the mesophase. The organization of pDBPO(C_{12})$_2$ **5-42** in its higher temperature phase could experimentally not be determined.

The room temperature 2D-WAXS results were used to correlate the supramolecular organization to the molecular architecture. All derivatives, except pDBPO(C_{12})$_2$ **5-42**, arranged in a "herringbone" manner with tilted molecules within the columns, whereby the tilting angle varied only slightly as it was derived from the azimuthal angle of the off-meridional reflections. The variation of the positions of the equatorial reflections implied differences of the lateral 2D unit cells which were dependent on the size of the aromatic core and the number of *n*-dodecyl side chains. In general, the strength and sharpness of the reflections were a strong indication for the degree of supramolecular order. The reflections in the 2D-WAXS patterns suggested a close relation between the core symmetry and the number of alkyl substituents and the self-organization. A higher symmetry of the core component led to sharper reflections proving a better correlation of the molecules and long-range organization.

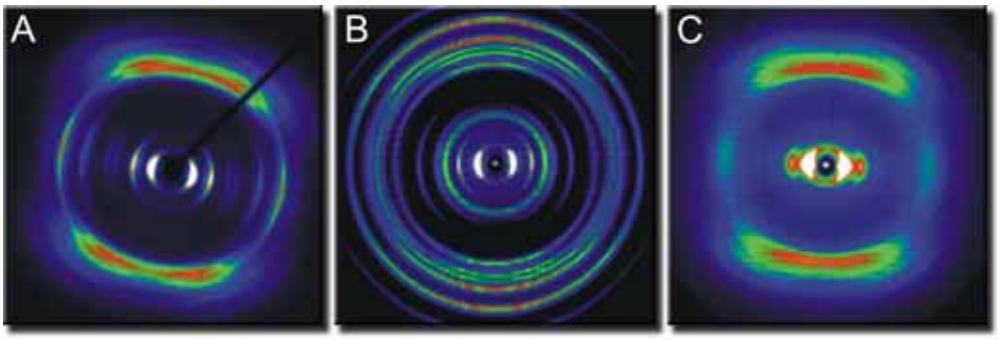

Figure 5-53: *Temperature 2D-WAXS patterns of derivatives with a symmetrical architecture as (A) HBC-C_{12}* 3-3**a**, *(B) pDBPO(C_{12})$_2$* **5-42** *and (C) DPO(C_{12})$_6$* **5-57**.

Figure 5-53 shows the patterns for the higher symmetric compounds HBC-C_{12} **3-3a**, pDBPO(C_{12})$_2$ **5-42** and DPO(C_{12})$_6$ **5-57**, whereby in Figure 5-54 the X-ray results for the "asymmetric" derivatives are presented. It is obvious that the degree of molecular symmetry enhanced the supramolecular order. The reflections, indicating both inter- and intracolumnar arrangement for the compounds, possessing a higher symmetric design were sharper and more distinct in comparison to the ones for the less symmetric PAHs.

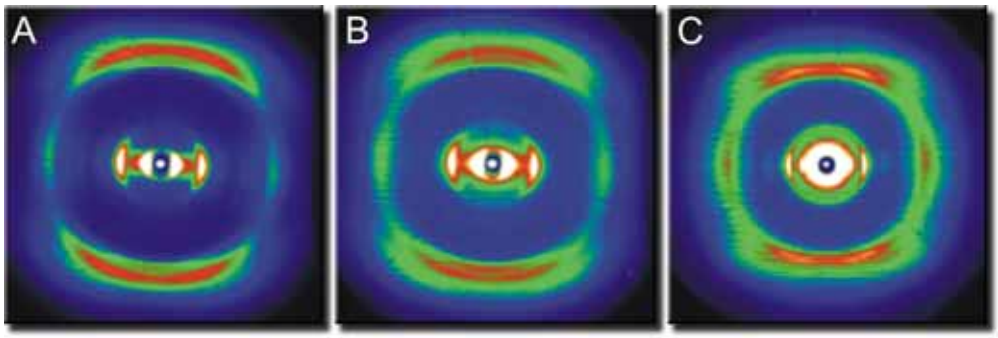

Figure 5-54: *Room temperature 2D-WAXS pattern of derivatives with an asymmetrical architecture as (A) HBC(C_{12})$_4$* **5-74***, (B) TBO(C_{12})$_4$* **5-16c** *and (C) mDBPO(C_{12})$_4$* **5-62**.

The highest degree of crystallinity was observed for pDBPO(C_{12})$_2$ **5-42** due to the small number of only two *n*-dodecyl side chains and the relatively high D_{2h} core symmetry. The resulting structure gave rise to multiple meridional reflections with a non-tilted intracolumnar arrangement implying an extraordinarily high intracolumnar order. Both symmetric HBC-C_{12} **3-3a** and DPO(C_{12})$_6$ **5-57** differed in the core size and the position of substitution of the six *n*-dodecyl chains. Since the pattern of HBC-C_{12} **3-3a** revealed more distinct higher order reflections, one can assume that in this case the slight core increase did not play any role on the organization of the molecules. However, the distribution of the alkyl side around the core influenced the packing in a greater extent.

In the case of DPO(C_{12})$_6$ **5-57**, the alkyl substituents are paired on two neighboring carbon atoms in the periphery of the PAH, which leads due to steric reasons to a worse packing than compared to the HBC-C_{12} **3-3a**, where the substitution point of the *n*-dodecyl chains are well distributed in the corona.

The lower symmetry decreased additionally the supramolecular order as in the case of HBC(C_{12})$_4$ **5-74**, TBO(C_{12})$_4$ **5-16c**, and mDBPO(C_{12})$_4$ **5-62**. In all three 2D-WAXS patterns both equatorial and meridional reflections became more diffuse and weak. Especially compound mDBPO(C_{12})$_4$ **5-62**, consisting of a core with a low symmetry and a high number of directly "neighboring" substituents, revealed the highest degree of disorder. The equatorial first order reflections, characteristic for the intercolumnar arrangement, were almost isotropic suggesting a poor alignment of the columnar structures in the extruded samples. However, sharper off-meridional reflections might imply a more uniform tilting of the discs than in the other investigated cases. According to the thermal behavior of compounds HBC(C_{12})$_4$ **5-74** and TBO(C_{12})$_4$

5-16c, the additional two carbon atoms within the core also did not affect the molecular packing to a great extent.

In conclusion, the type of the corona of the PAH imposed its character onto the supramolecular organization of the synthesized mesogenes. All investigated compounds exhibited a columnar mesophase, whereby the symmetry of the aromatic part influenced only the stability of the arrangement probed by the thermal transitions in the DSC. However, the number and the position of the flexible alkyl chains dramatically influenced both the thermal behavior and the quality of the supramolecular organization, which was derived from the analysis of the X-ray patterns. Fewer chains with a symmetric arrangement around the aromatic disc cause a stabilization of the columnar organization due to an unperturbed aromatic π-stacking. More chains, which are asymmetrically distributed in the periphery of the PAH, are more difficult to pack and hence the columnar arrangement exhibited more defects and a smaller long-range correlation. This is the first study on discotics, where the influence on the supramolecular organization was investigated with respect to shape, symmetry or topology.

The tuning of both the electronic properties and the propensity to organize defect-free into long-range organized molecular stacks is a challenge for material science to quest for novel, semi-conduction materials with specific properties. The UV/vis absorption behavior together with the position of the molecular orbitals were two important parameters which influence the performance of organic heterojunction photovoltaic devices.[81] The high supramolecular order enhances the charge carrier transport along the one-dimensional structures. Therefore, the development of organic semiconductors which self-assemble into highly organized arrays is one major goal. This study elucidated the importance of the molecular design on the molecular properties and the self-organization and gave important insights for the future development of semi-conducting materials based on extended PAHs.

5.6.3 Self-Assembly on Surfaces

In the quest for the fabrication of molecular electronic devices based on π-conjugated molecules, an important goal is the visualization and possibly manipulation of single molecules or small aggregates. To this end, the molecules need to be first localized on a substrate surface, preferably in monolayers. These can be prepared by LANGMUIR-

BLODGETT technique[82,83], sublimation[84,85] or by self-assembled monolayers (SAM) from solution.[86-88] The LANGMUIR-BLODGETT technique requires soluble and amphiphilic molecules, prerequisites which can only be met by specially functionalized PAHs.[83] Sublimation takes place under high vacuum and high temperatures, conditions where alkyl substituents and functional groups are thermally decomposed, therefore it is only applicable for unsubstituted PAHs up to a certain size.[89] Self-assembled monolayers are gratuitously formed spontaneously by absorption of long chain substituted organic molecules on the surface of suitable substrates.[90-92] In order to explore organic surfaces on different length scales in various environments, scanning probe microscopes have played a paramount role.[93,94] Applications have already gone far beyond the pure imaging of a surface. Some examples are the manipulation of single molecules at room temperature,[95] stimulating photochemical reactions with light and following the reaction in real time at interfaces[96,97] and the probing of the electronic properties of single molecules by means of scanning tunneling spectroscopy (STS).[98]

The following scanning tunneling microscopy (STM) results emerged from a strong collaboration with P. RUFFIEUX and O. GRÖNING (EMPA, Thun, Switzerland, Group of P. GRÖNING). The ultra-high vacuum (UHV) deposition of unsubstituted HBC (~300 °C, 10^{-10} mbar) onto a Cu(111) surface was visualized with STM. With a negative sample bias voltage, the electrons tunneled through occupied orbitals with an energy around the HOMO orbital (Figure 5-55A). A simple integration and weighting of molecular orbitals with a similar energy, which were obtained with an extended HÜCKEL calculation, gave simulated STM images (inset Figure 5-55A). Figure 5-55B depicts the same monolayer of HBC molecules with a positive sample bias. The observed structuring fitted again the simulation (inset).

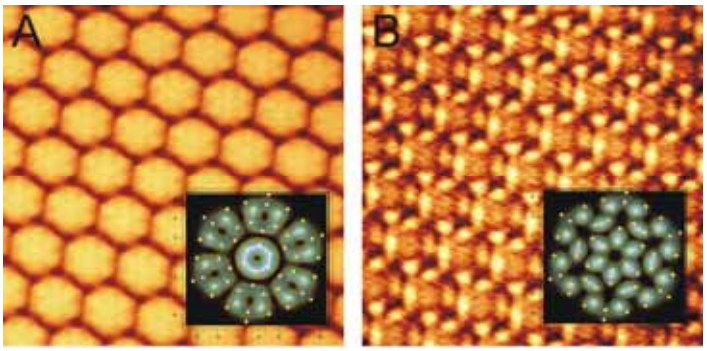

Figure 5-55: *STM picture, 10 x 10 nm^2; (A) sample bias: -2 V (occupied states), inset: simulation (extended Hückel); (B) sample bias: +2 V (unoccupied states, inset: simulation (extended Hückel).*

STM images of a monolayer of HBC on Cu(111) reveal a hexagonal arrangement of the molecules with a nearest-neighbor distance of 14.2(1) Å (Figure 5-56). This is in excellent agreement with the nearest-neighbor (NN) distance of 14.2 Å determined from low energy electron diffraction (LEED) where the pattern can be directly related to a superstructure with respect to the surface unit cell of Cu(111). Furthermore, the hexagonal molecular shape resolved by STM allows the determination of the molecular orientation. Comparison of the molecular orientation and the NN direction reveals that the molecular orientation in the monolayer structure deviates from the orientation expected for a close-packed structure of hexagonal molecules in the way that the molecular axis m of the molecule is rotated by ~9° with respect to the NN direction.

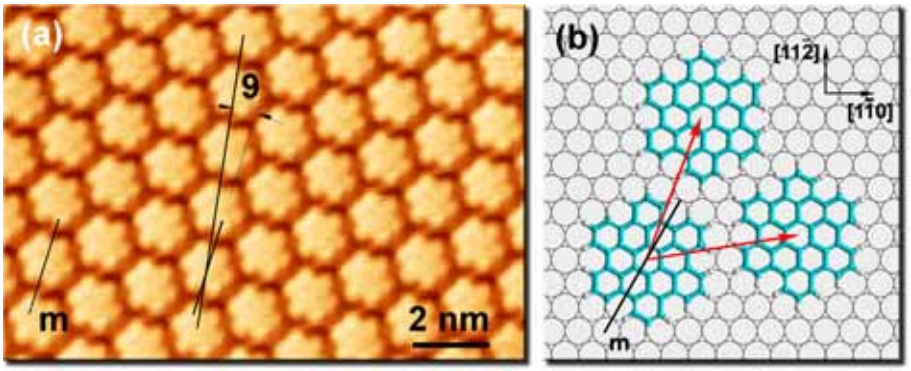

Figure 5-56: *Monolayer structure of HBC on Cu(111). (a) STM image (U = 5 mV, I = 0.03 nA). The molecular axis m is indicated. (b) Proposed molecule orientation and superstructure.*

Comparison with the structure of the Cu surface atoms shows that the molecular axis m is parallel to the direction of Cu atom rows, which is in agreement with results from an X-ray photoelectron diffraction study.[85] This molecular orientation is apparently stabilized by the alignment of the Cu atom rows and the carbon rings of the molecule due to the nearly identical separations between Cu atoms (d_{Cu} = 2.55 Å) and the benzene rings (2.5 Å). The same orientation is found for isolated single molecules adsorbed on the Cu(111) surface[99], where the lock into registry of the molecule with the Cu lattice is observed during lateral manipulation of the molecule with the STM tip. These observations evidence a molecule-substrate interaction which is strongly modulated with the periodicity of the Cu atom lattice and explain the growth of adequate superstructures for the HBC monolayer on the Cu(111) surface. Accordingly, the observed monolayer structure with the molecules rotated by ~9° with respect to the NN direction results in the densest possible commensurate

packing of the molecules with the carbon rings oriented in the direction of the Cu atom rows.

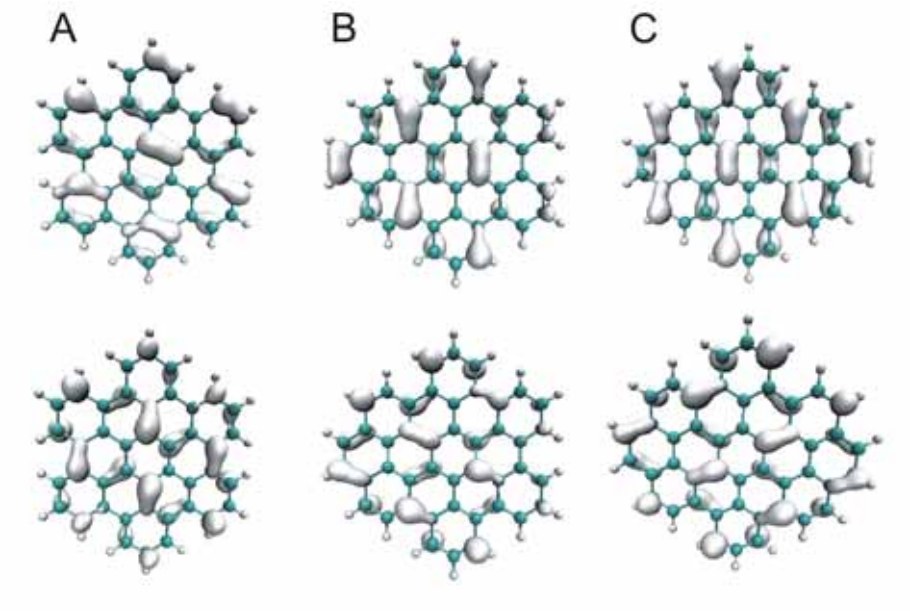

Figure 5-57: *Computed images of HOMO (upper image) and LUMO (lower image) with DFT (B3LYP/3-21G) of (A) HBC; (B) TBO* **5-16a** *and (C) DBPO* **5-36**.

In the previous chapters, the successful synthesis of three novel PAHs with a partial "zigzag" edge structure was described. The CLAR rule predicted for the "zigzag" sites a higher electron density, which was intended to be visualized with STM. A pronounced polarization of the electron cloud on these aromatic molecules would have a strong influence on the contrast of the STM images. For both, TBO **5-16a** and pDBPO **5-36** the HOMO orbital revealed a high orbital coefficient at the "zigzag" site. For HBC, the orbital lobes are in the periphery well distributed.

However, the tunneling occurs not strictly through one single energy state, since large molecules possess a large number of orbitals which are almost degenerate. A much better simulation for the STM experiment would require a summation over all orbitals, which are energetically close to the HOMO or the LUMO.

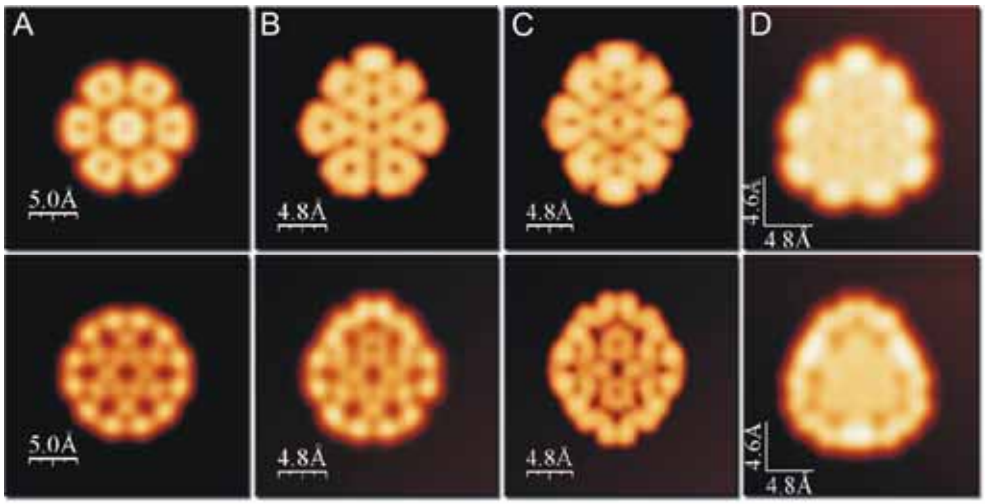

Figure 5-58: *Simulation of STM images of (A) HBC 3-3***d***; (B) TBO* **5-16a***; (C) pDBPO* **5-36***; (D) DPO* **5-45***; upper picture: HOMO (U = -1.5 V), lower picture: LUMO (+1.5 V).*

Figure 5-58 presents this simulation of the potential STM images of HBC **3-3d**, TBO **5-16a**, pDBPO **5-36**, and DPO **5-45** (negative and positive sample bias voltage). As already discussed, HBC revealed a symmetric intensity distribution within the PAH. For both, TBO **5-16a** and pDBPO **5-36**, the simulated STM image for the occupied states exhibited a slightly stronger contrast at the "zigzag" sites. Unfortunately, the resolution of the experimental images is far lower, so that one can not expect to resolve the small intramolecular contrast differences. For the D_{3h} symmetric DPO **5-45**, the simulated STM image did not indicate a contrast difference at the "zigzag" sites. The calculation predicted a similar contrast of the STM picture in the perimeter of the extended PAH. Conclusively, the eligible detection of the nature of the modified periphery within the novel series of PAHs will be not accomplished by STM.

Compared to the HBC, pDBPO **5-36** has a lower rotational symmetry (C_2) due to the 4 additional carbon atoms in the aromatic core. This leads formally to two additional benzene rings along the long axis of the molecule.

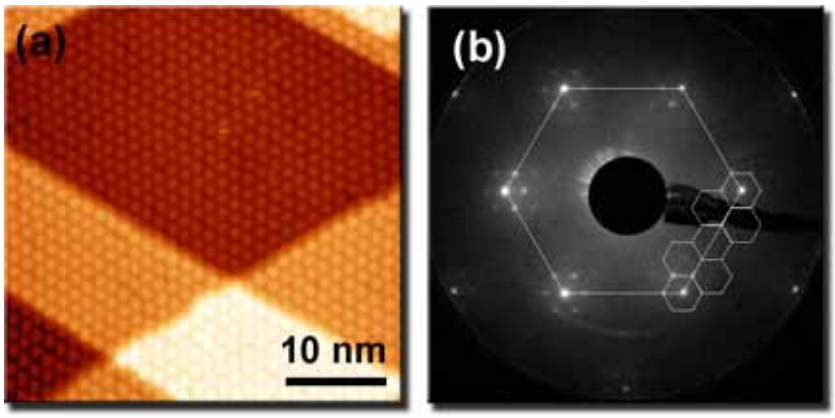

Figure 5-59: *pDBPO* **5-36** *monolayer structure on Cu(111). (a) STM image (U = 0.1 V, I = 0.05 nA). (b) LEED: 186 eV at 150 K.*

In Figure 5-50, an STM overview image and a LEED pattern of the monolayer structure of pDBPO **5-36** on Cu(111) is shown. The LEED pattern reveals a commensurate (6 x 6) structure with respect to the Cu(111) lattice. The according NN molecule separation is 15.3 Å. From STM images we determine an average NN molecule separation of 15.4 Å, in good agreement with the diffraction experiment.

High-resolution STM images of the monolayer structure reveal further details about the orientation of the pDBPO molecules **5-36**, as shown in Figure 5-60.

Three possible orientations of the molecule with respect to the Cu lattice are found. The arrangement of the differently orientated molecules results in a molecular superstructure including 8 molecules in the unit cell. According to the symmetry of the Cu(111) surface, three orientations of the superstructure unit cell are possible and for each of them two equivalent domains with a mirror axis along the close-packed rows of the Cu atoms are possible. The superstructure is also resolved in the Fast Fourier Transform (FFT) of the STM image (Figure 5-60b). The wave vectors related to this superstructure are indicated with arrows.

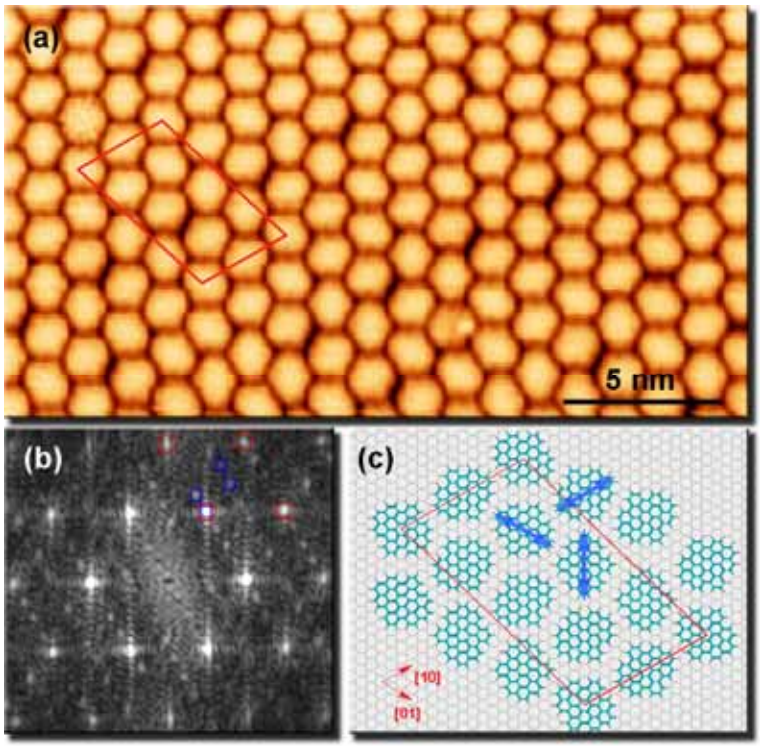

Figure 5-60: *Local structure of pDBPO* **5-36** *on Cu(111). (a) High resolution STM image (U = -1.5 V, I = 0.05 nA). (b) Calculated FFT image of (a) Red circles highlight the spots originating from quasi-hexagonal arrangement of the molecules. Blue squares highlight spots related to the orientational superstructure.*

Despite the small structural difference of the pDBPO **5-36** with respect to HBC the self-ordering at the surface is fundamentally different. The slightly larger size inhibits the arrangement in the same commensurate superstructure as HBC due to repulsive intermolecular forces along the axis with the additional atoms. Accordingly, the average NN molecule separation is increased. Compared to HBC, an increase of ~8 % was determined by LEED and STM measurements. According to the lower symmetry, different non-equivalent orientations of the molecule exist at the surface. However, we observe only orientations where neighboring carbon rings are aligned with the Cu atom rows, i.e. only three orientations are identified. The simulation revealed that a theoretical closed packed mono-orientation domain (Figure 5-61A) would be about 2.9% closer packed than the experimentally found hexagonal multi-orientation domain (Figure 5-61B).

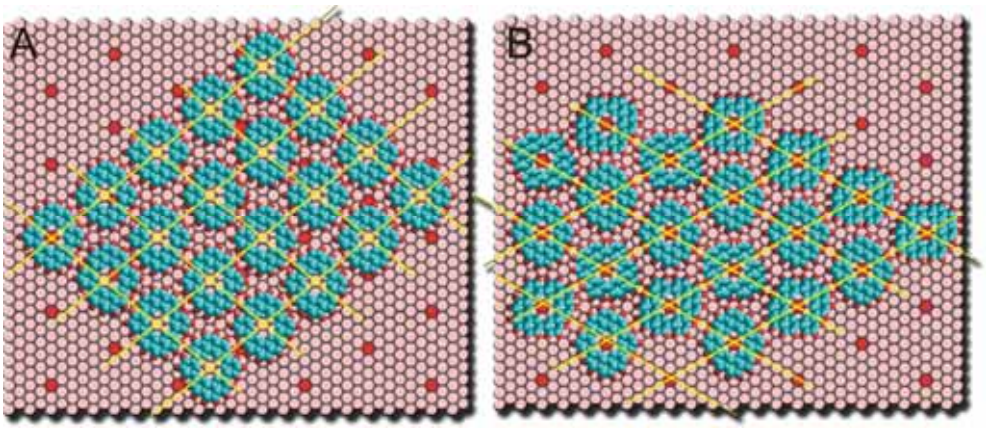

Figure 5-61: *(A) theoretically calculated closed packed mono-orientation domain; (B) experimentally found hexagonal multi-orientation domain.*

This indicates that in the case of pDBPO **5-36** the molecule-substrate interaction plays a key role in the self-ordering of the monolayer film. The molecular superstructure observed in STM images reveals a unit cell containing all three non-equivalent orientations of the molecule. However, for a given domain the monolayer structure does not show a uniform occupation of the three possible molecule orientations. Four of the molecules in the superstructure unit cell are oriented with the molecular axis m aligned with the short lattice vector of the superstructure unit cell. The remaining molecules have orientations in the other two allowed directions with two molecules for each direction. According to these observations we propose a molecular arrangement, as shown in Figure 5-60c. The model accounts for the molecular orientations observed with STM and the average NN separation of 6 d_{Cu} on Cu(111). Despite the large size of the unit cell structure (containing 288 Cu atoms), only few defects in molecular ordering are observed.

The lower symmetric TBO **5-16a** exhibited an interesting behavior, which is not fully understood. Figure 5-62A presents a STM image of *ca.* 1.3 monolayers of this PAH. The first monolayer organized probably in a hexagonal fashion. The second monolayer is present in two domains with a twist of ± 4-6°. However, the ordering of the second monolayer seems to be higher than the first one. The weaker molecule-substrate interaction may allow a better, unperturbed packing which is not disturbed by the aromatic locking with the Cu(111) surface.

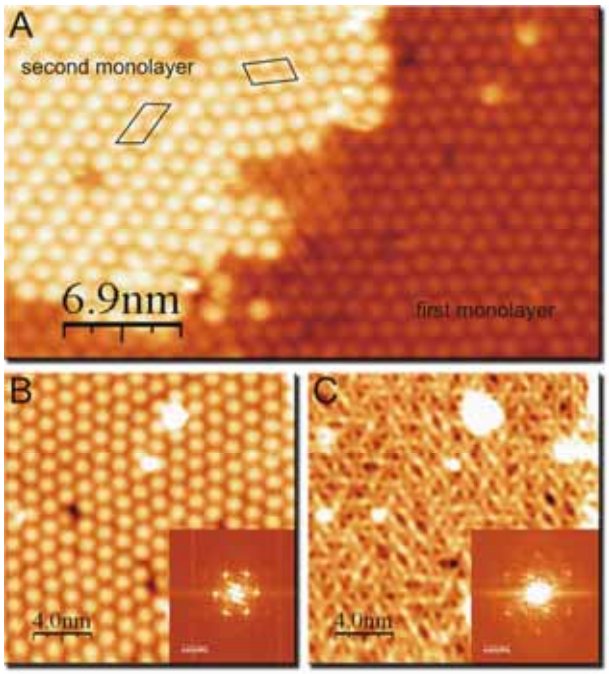

Figure 5-62: *(A) 1.3 monolayer of TBO* **5-16a** *on Cu(111), substrate held at room temperature during evaporation no post deposition annealing, second monolayer orders better than first and is present in two domains (unit cell); (B) occupied states of the first monolayer (-1.75 V) inset: FFT; (C) unoccupied states of the first monolayer (+1.75 V) inset: FFT.*

Figure 5-62B,C presents the image of a complete monolayer with negative and positive sample bias voltage. Surprisingly, the STM image of the unoccupied states revealed linear structures, which are longer than the actual size of the PAH. This phenomenon is not understood and under current investigation.

The self-ordering of all molecules presented here is largely influenced by a prominent substrate-molecule interaction. This leads to a restriction on possible molecule orientations in the way that molecules are only adsorbed with carbon rings aligned with the Cu atom rows. Furthermore, the molecule-substrate interaction determines the nearest-neighbor separation of the molecules allowing only distances that are translationally equivalent with respect to the substrate lattice. However, it should be noted that this checkerboard behavior is not generally observed for monolayer structures of PAHs but rather depends on the molecular size and the geometrical shape of the molecular periphery as shown for monolayer structures of HBC and the rhombus-shaped $C_{54}H_{22}$ on GeS.[84,100] Accordingly, the monolayer structures depend on the interplay of molecule-substrate and molecule-molecule interactions. The monolayer structures of PAHs on Cu(111) presented here are largely dominated by the molecule-substrate interaction and no structural units are observed which could be

related to a specific attractive molecule-molecule interaction. More specifically, the monolayer structures observed here are the densest possible commensurate arrangements of molecules that are allowed by steric repulsion between neighboring molecules.

Another, experimentally easier technique is the STM on SAMs at the solid-liquid interface. For this purpose, alkyl substituted PAHs have been used to guarantee a minimum solubility which is required. The following experiments were conducted by M. PENG in the group of J. P. RABE. A semi-concentrated solution of tetra-*n*-dodecyl derivative TBO(C_{12})$_4$ **5-16c** has been prepared in 1,2,4-trichlorobenzene, put on a freshly cleaved highly oriented pyrolytic graphite (HOPG) surface and the spontaneous physisorbed SAM has been investigated with a STM tip. The mono-"zigzag" site containing PAH revealed a dimer-structure with the unit cell parameters of a = (2.60 ± 0.10) nm, b = (3.01 ± 0.10) nm and α = (72 ± 2) ° (Figure 5-63A). The light areas correspond to the aromatic and the dark areas to the aliphatic part of the molecule. Individual alkyl chains are not resolved since their mobility is too high. The detailed analysis of the organization together with STS is still in focus of ongoing investigations. However, the morphology on HOPG of the alkylated derivative differed distinctly from the results of the UHV on Cu(111) deposited unsubstituted TBO **5-16a** analogue. This indicated that the alkyl substituents improve the adsorption on surfaces.

The PAH pDBPO(C_{12})$_2$ **5-42** organized itself from a 1,2,4-trichlorbenzene solution on HOPG in a rectangular lattice (Figure 5-63B). In this case, only a mono-orientation domain was found, where the elongated direction was identical for all molecules within the SAM. STS was performed and the results are currently analyzed in the group of J. P. RABE. The imaged SAM resembles the organization of the rhombus shaped PAH[35] on a molybdenum sulfide substrate, since both molecules belong to the D_{2h} symmetry group. Investigation on the other "zigzag" site containing PAHs are still ongoing.

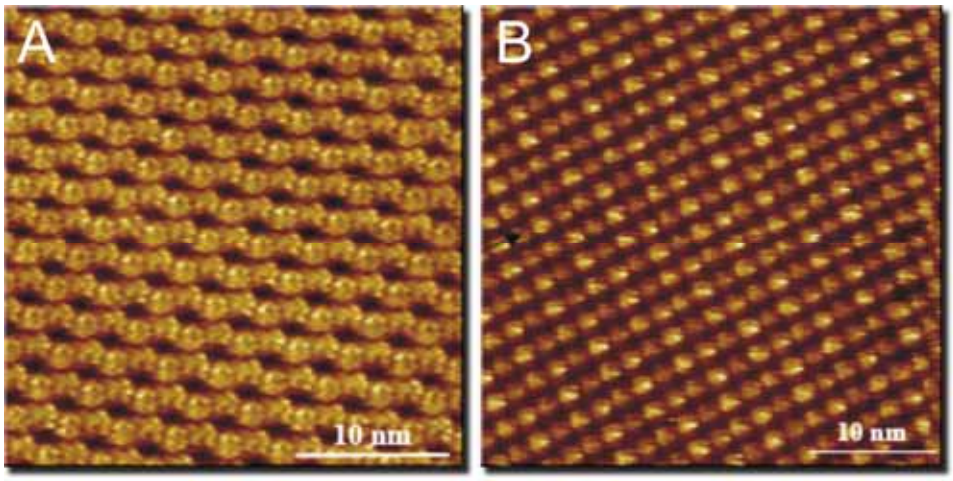

Figure 5-63: *STM images of SAMs, obtained at the solution-HOPG interface (A) TBO(C_{12})$_4$* **5-16c***, exhibiting a dimer structure with a = (2.60 ± 0.10) nm, b = (3.01 ± 0.10) nm, α = (72 ± 2) °, sample bias: -1.2 V, 200 pA; (B) pDBPO(C_{12})$_2$* **5-42** *arranged in arrays with a = (2.17 ± 0.10) nm, b = (1.81 ± 0.10) nm, α = (81 ± 1) °, sample bias: -1.0 V, 100 pA.*

In conjunction with the high spatial resolution of the STM, the probing of defined areas of the single molecules in their SAMs was made possible. All investigated compounds revealed a pronounced tendency to epitaxially form two-dimensional crystalline structures both on Cu(111) and on HOPG. Thereby, the molecule-substrate interactions dominated and forced the molecules into a geometric arrangement. The slight change of the PAH perimeter exerted a fundamental effect onto the self-organization on substrates. This emphasizes the analogy to the bulk organization, where the symmetry of the molecular architecture determined the three-dimensional self-assembly of the discotic molecules. The design of well-defined molecular building blocks with specific symmetries and defined intermolecular interactions allows the tailoring of two- and three-dimensional architectures, which is of major interest in the fields of microporous materials[101], molecular electronics[102-105], and molecular machines.[106] Experiments with the DPO derivatives **5-45** and **5-57**, both with UHV technique and at the solid-liquid interface, are currently performed.

5.7 Functionalization of PAHs in the Periphery

The synthesis and the characterization of electronic and supramolecular properties of a homologous series of PAHs which contain "zigzag" sites have been described in the previous chapter. One motivation to modify the nature of the PAH perimeter was to change its chemical reactivity. The empirical CLAR rule of the aromatic sextet would predict a localization of electron density at the "zigzag" positions, which leads in the case of smaller PAHs to a pronounced regiospecific reactivity towards oxidations or aromatic substitution reactions, such as FRIEDEL-CRAFTS-type reactions.[107] Optimized oxidation conditions allowed the mono-"zigzag" TBO(^{t}Bu)$_6$ **5-9** to be converted into the corresponding diketone.[46] However, all attempts to conduct this reaction on differently substituted TBO derivatives such as *n*-dodecyl analogues failed, because the alkyl substituents decomposed during the reaction. PAHs with more "zigzag" sites were not susceptible for oxidations. Even with harsh conditions, one could not observe traces of the desired oxidation products.

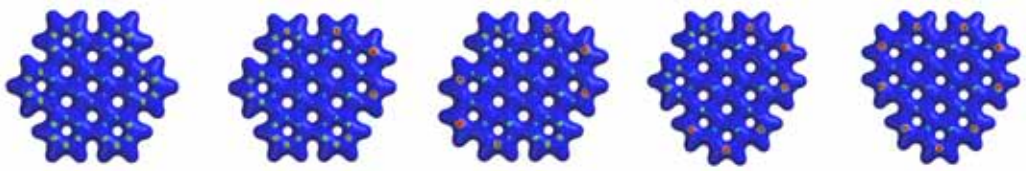

Figure 5-64: *Quantum-mechanical calculation of the potential density in the "zigzag"-PAHs and HBC, red color indicates the highest electron density (Hartree-Fock, 3-21G(*)).*

The potential density distribution over the "zigzag" PAHs has been quantum-mechanically calculated and is depicted in Figure 5-64. In the case of HBC, the electron density in the aromatic perimeter is expectedly uniformly distributed. Introducing "zigzag" sites, one clearly notices a slight localization of electron density at these positions, what has been supported by ^{1}H NMR spectroscopy as well. The calculations clearly proved, that the polarization of the potential curve within the aromatic core was pronounced for the TBO **5-16a** derivative. The electron density in PAHs with multiple "zigzag" sites is less localized in the periphery, leading to a reduced tendency to become oxidized.

Functionalizations of extended PAHs have mostly been achieved by converting bromo- or iodo functions with palladium-catalyzed cross-coupling reactions.[108] These conversions need to be high yielding to avoid an often tedious and complicated purification in the lab. The introduction of different functions before the PAH

forming SCHOLL reaction has proved to be unsuccessful in many examples.[36] Heteroatoms like oxygen, nitrogen or sulfur suppress in most cases the planarization reaction of the precursor molecules completely. Therefore, the chemical *a posteriori* functionalization of the PAH's periphery would be also in this case an eligible alternative to tailor the molecular and supramolecular properties of the PAH after the problematic SCHOLL reaction. In the following chapter, we present the synthesis and the characterization of a PAH which contains an odd number of carbon atoms in the aromatic core.

5.7.1 3H-Cyclopenta[*cde*]hexa-*peri*-hexabenzocoronene

Introducing a five-membered ring into the "armchair" periphery of HBC, one obtains 3H-cyclopenta[*cde*]hexa-peri-hexabenzocoronene (CPHBC), which belongs to the large group of nonalternant PAHs.[107] An important feature of the chemistry of these molecules is the formation of cation, anion and radical intermediates at the bridge position.

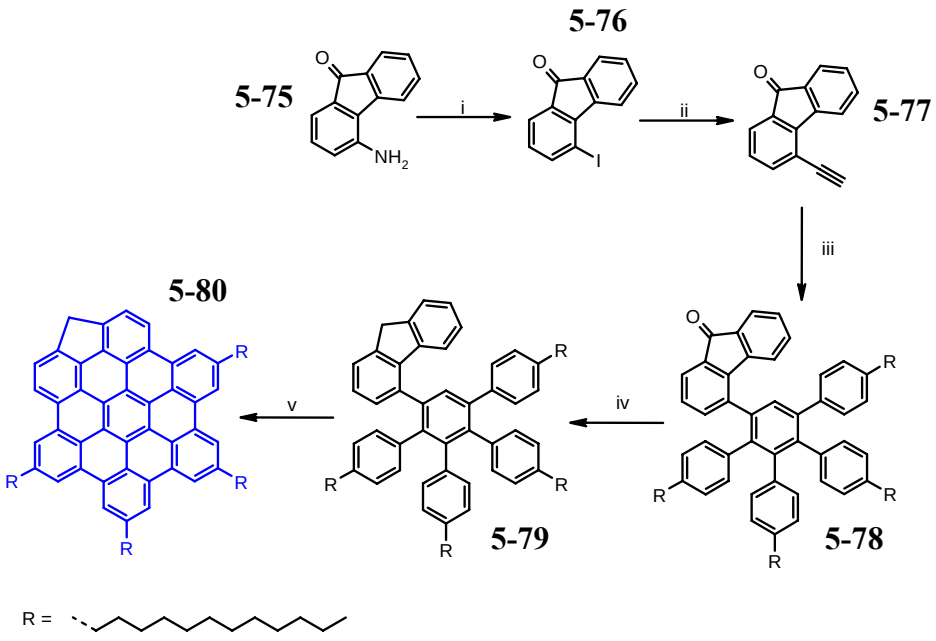

Scheme 5-20: *i) $NaNO_2$, KI, 65%; ii) trimethylsilylacetylene, $Cl_2Pd(PPh_3)_2$, 71%; K_2CO_3, 92%; iii)* **5-34c**, *93%; iv) Pd/C, H_2, 95%; v) $FeCl_3$, 87%.*

These intermediates are inherently nonalternant. The alternative isomer structures in which the extra hydrogen atom resides at other positions in the molecule are also obviously nonalternant. The bridge-sites in such molecules are very reactive and thus open an opportunity to modify the perimeter of a PAH.

The synthesis route towards CPHBC(C_{12})$_4$ **5-80** started with the literature present SANDMEYER conversion of the commercially available 4-aminofluoren-9-one (**5-75**) into the iodo analogue **5-76**.[109] After the HAGIHARA-SONOGASHIRA cross-coupling reaction with trimethylsilylacetylene, the TMS group was chipped off with potassium carbonate to afford 4-ethynyl-fluoren-9-one (**5-77**) in a good yield. The ethynyl group was reacted as dienophile in a DIELS-ALDER reaction with 2,3,4,5-tetrakis-(4-*n*-dodecyl-phenyl)-cyclopenta-2,4-dienone **5-34c**[62] to the "dendronized" fluorenone **5-78**. Attempts to planarize this molecule using iron(III)chloride failed. However, after the successful reduction of the ketone to the fluorene analogue **5-79** using hydrogen gas and palladium on char coal as catalyst, the SCHOLL reaction yielded the desired CPHBC($_{12}$)$_4$ **5-80** in good yields.

The MALDI-TOF spectrum using the solid state preparation with TCNQ as the matrix substance revealed a successful planarization reaction (Figure 5-65). The experimental isotope distribution was in good agreement with the simulation.

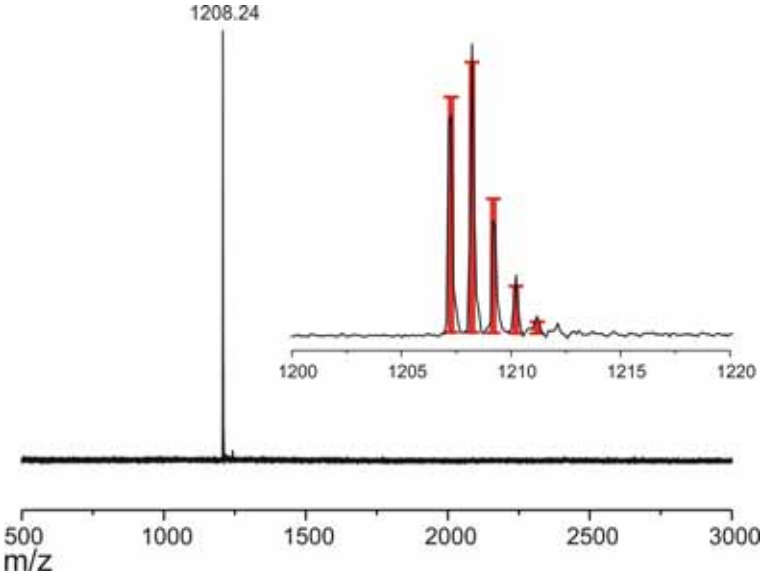

Figure 5-65: *MALDI-TOF spectrum of CPHBC(C_{12})$_4$* **5-80***, using solid-state preparation with TCNQ as the matrix substance.*

The PAH was recrystallized from toluene to yield a yellow, microcrystalline powder. The ^{1}H NMR spectrum in THF-d^8 showed at elevated temperatures sharp resonance peaks of all protons, which could be assigned to the corresponding nuclei (Figure 5-66). The resonances of the aromatic protons closest to the methylene bridge are more shielded. The spectrum indicates the presence of small amounts of impurities, which are marked with red arrows.

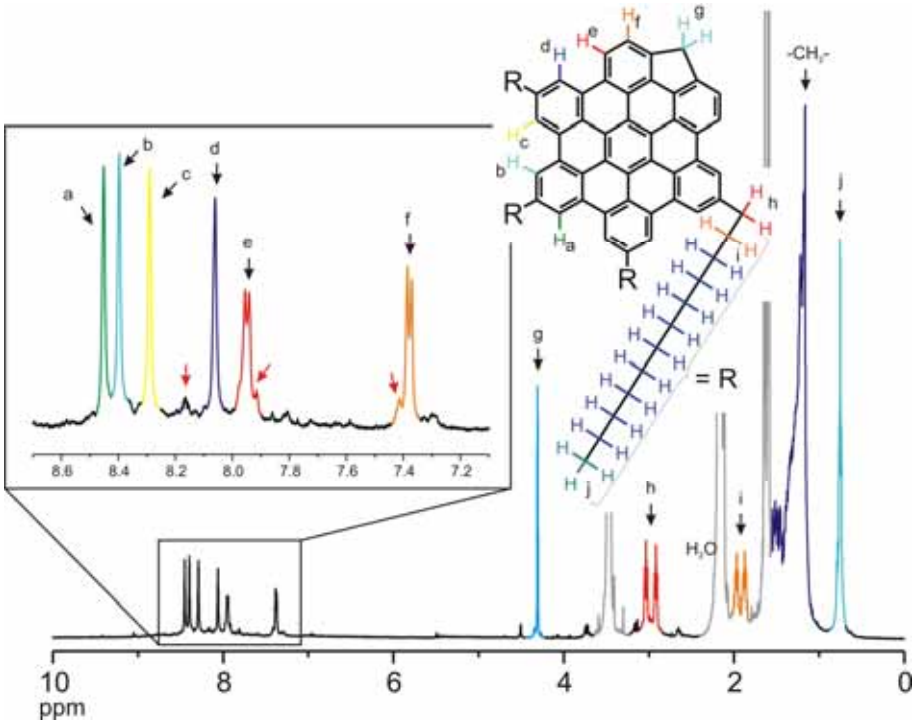

Figure 5-66: *^{1}H NMR of CPHBC(C_{12})$_4$* **5-80**, *recorded in THF-d^8 at 55 °C, red arrows mark impurties, solvent peaks are colorized in grey.*

The desired *a posteriori* functionalization of the bridge-site in CPHBC(C_{12})$_4$ **5-80** was attempted on the example of an oxidation. Already weak bases such as LHDMS allowed the deprotonation of one proton at the methylene bridge. The anion turned out to be very reactive, analogous to the fluorene as the parent compound.[110] Already molecular oxygen was sufficient to convert the anion into the ketone **5-81**.

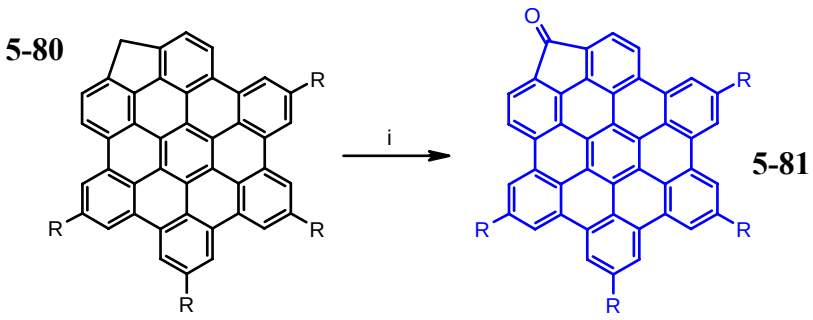

Scheme 5-21: *i) LHDMS, O_2, 82%.*

Cyclopenta[*cde*]hexa-*peri*-hexabenzocoronene-3-one (CPHBCCO(C_{12})$_4$) **5-81** was isolated in high yields. The MALDI-TOF spectrum revealed the quantitative oxidation reaction (Figure 5-67). The simulation fitted the experimentally determined isotope distribution quite well. However, the isotope pattern indicates the loss of an

additional proton which was attributed to an artifact of the solid-state prepared MALDI sample (different heights of the solid analyte on the target).[48]

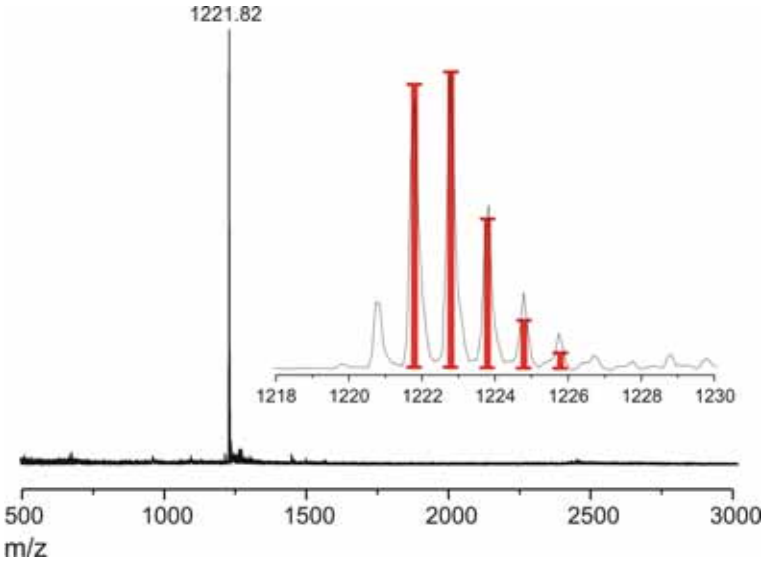

Figure 5-67: *MALDI-TOF spectrum of CPHBCCO(C_{12})$_4$* **5-81**, *using solid-state preparation with TCNQ as the matrix substance.*

The CPHBCCO(C_{12})$_4$ **5-81** turned out to be clearly less soluble than its precursor. However, it was possible using high-field NMR spectrometer to resolve a ^{1}H NMR at elevated temperatures. The resonances were assigned using simulated spectra.

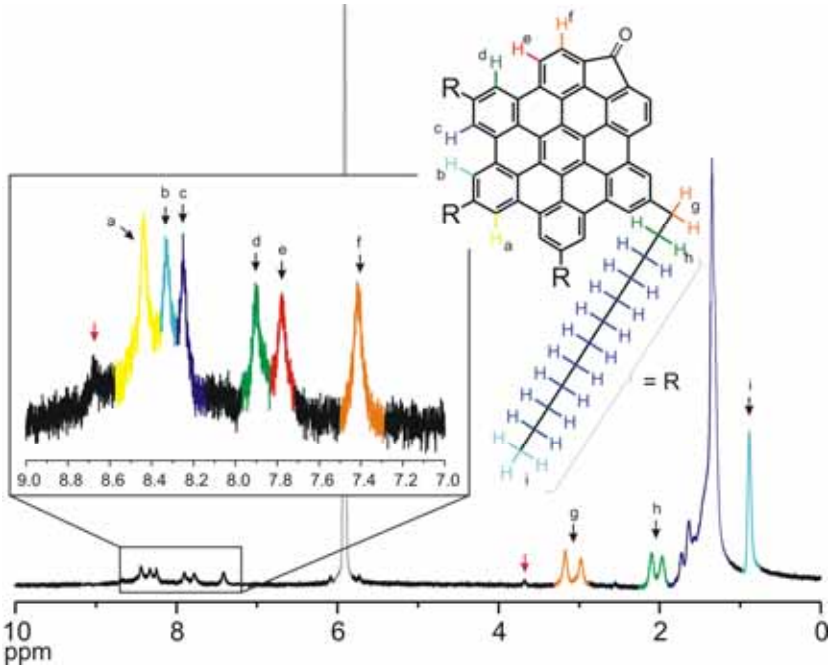

Figure 5-68: *^{1}H NMR of CPHBCCO(C_{12})$_4$* **5-81**, *recorded in THF-d^8 at 55 °C, red arrows mark impurties, solvent peak was colorized in grey.*

While the electronic spectroscopy on CPHBC(C_{12})$_4$ **5-80** did not reveal any difference to the parent case, HBC-C_{12} **3-3c** or HBC(C_{12})$_4$ **5-74**, CPHBCCO(C_{12})$_4$ **5-81** differed. The symmetry reduction due to the introduction of the electron rich heteroatom rendered the normally weak α-transitions "more allowed".

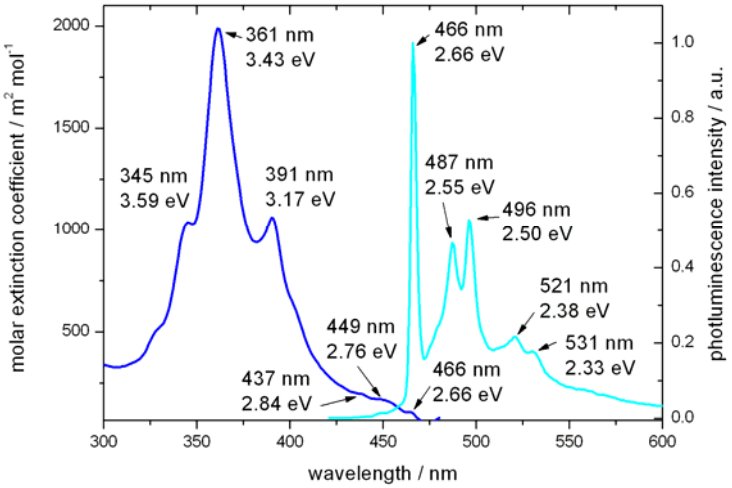

Figure 5-69: *UV/vis and photoluminescence spectra of CPHBCCO(C_{12})$_4$* **5-81**, *recorded in chloroform.*

Surprisingly, the electronegative oxygen did not significantly change the position of the bands. However, the PL spectrum clearly emphasized the symmetry reduction, since the 0-0 transition at 466 nm was the strongest, which stands in contrast to HBC-C_{12} **3-3c**. The spectrum showed far less transitions.

5.7.2 Investigation of the Supramolecular Self-Organization

In the next section, the supramolecular organization of the two novel PAHs will be elucidated. The question is whether the methylene-bridge in CPHBC(C_{12})$_4$ **5-80** or the dipole inducing keto-group in CPHBCCO(C_{12})$_4$ **5-81** impose any effect onto the self-assembly in the bulk phase. Since the molecular architecture is very similar to HBC(C_{12})$_4$ **5-74**, which has been described before, the compound will be used as model system to compare the thermal behavior and the bulk organization. The presented X-ray diffraction experiments have been performed together with W. PISULA, who gave me also valuable help during the analysis.

Already the data obtained from the DSC indicated a pronounced influence of the small chemical modification onto the position of the thermal transitions (Table 5-3).

While both HBC(C_{12})$_4$ **5-74** and CPHBC(C_{12})$_4$ **5-80** entered the mesophase at roughly the same temperature, the introduction of the keto-function lowered the transition from the crystalline phase to the mesophase in the case of CPHBCCO(C_{12})$_4$ **5-81** significantly to 73 °C. Furthermore, the enthalpy of the first transition for **5-80** was more than two times higher than for the other two investigated derivatives, which clearly indicated a pronounced change of the organization at that transition.

Table 5-3: *Phase behavior of the PAHs* **5-74**, **5-80** *and* **5-81**.

Derivative	Temperature / °C	Enthalpy / Jg^{-1}	Phase-transition
$HBC(C_{12})_4$ **5-74**	147 (123)	15.7	C_r – Col_{ho}
	400*		Col_{ho} – I
$CPHBC(C_{12})_4$ **5-80**	139 (101)	41.3	C_r – Col_{ho}
	420*		Col_{ho} – I
$CPHBCCO(C_{12})_4$ **5-81**	73 (22)	17.6	C_r – Col_{ho}
	410*		Col_{ho} – I

List of abbreviations: Cr – crystalline phase, Colho – mesophase (hexagonal ordered columnar phase), Colco – mesophase (cubic ordered columnar phase) I – isotropic phase, phase transitions upon cooling are given in brackets, * - assigned by polarized optical microscopy.

For the system $HBC(C_{12})_4$ **5-74**, the typical orthogonal disc orientation with respect to the column axes was detected for the mesophase (Figure 5-70A). In its room-temperature crystalline state, the disc revealed the characteristic tilted intracolumnar arrangement (Figure 5-70B). Thereby, the degree of the supramolecular order was strongly dependent on the thermal treatment of the extruded sample. After repetitive annealing procedure in the mesophase, the X-ray pattern for the crystalline phase exposed more distinct reflections (Figure 5-70C).

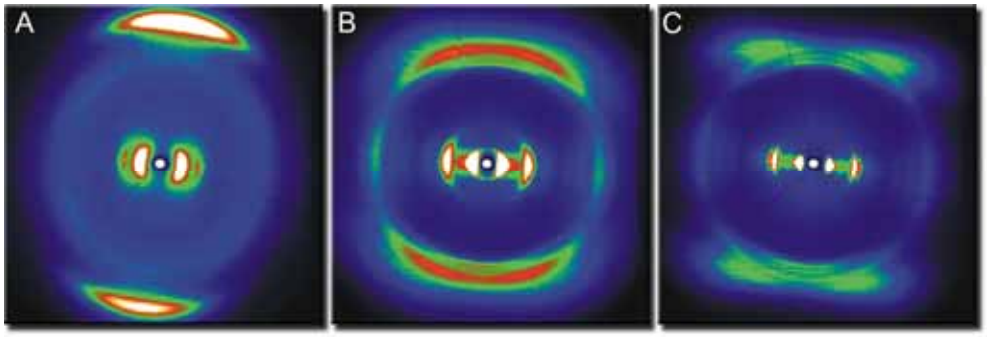

Figure 5-70: *2D-WAXS patterns for an extruded* $HBC(C_{12})_4$ **5-74** *filament (A) in the mesophase, (B) in the crystalline room temperature phase before annealing, and (C) in the crystalline room temperature phase after repetitive annealing in the mesophase; all patterns are recorded applying the same conditions and displayed with the same contrast.*

Finally, the off-meridional reflections corresponding to the disc tilting were separated. Unusually, the intercolumnar arrangement was improved as well being reflected by more pronounced equatorial reflections. The unit cell for the crystalline phase was fitted to two different arrangements; a hexagonal lattice with a unit cell of a = 3.60 nm, and an orthorhombic lattice with a = 1.81 nm and b = 3.13 nm. Because of the asymmetrical substitution of the aromatic core, a lamellar arrangement of alternating single rows of aromatic cores and alkyl side chains was established (Figure 5-71).[111]

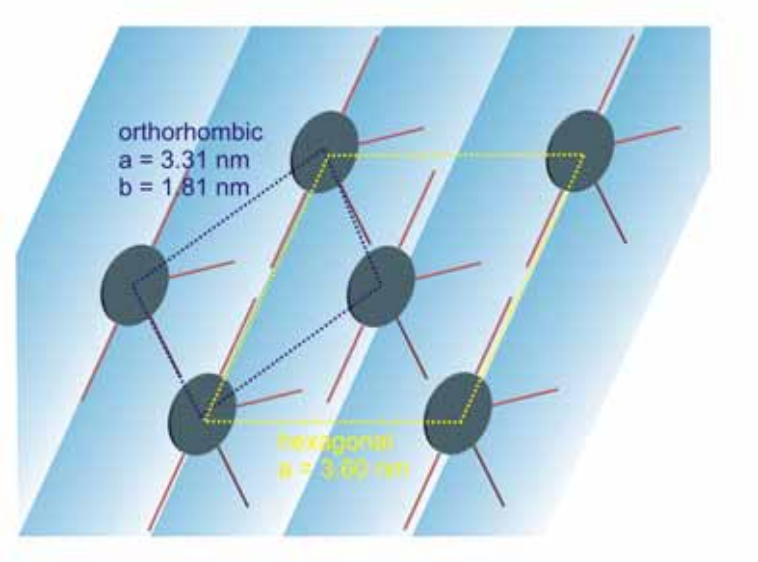

Figure 5-71: *Illustration of the supramolecular arrangement with alternating aromatic core and alkyl chain rows (the side chains are indicated as straight lines due to simplicity).*

Already the first look at the 2D-WAXS pattern recorded on a mechanically aligned filament of CPHBC(C_{12})$_4$ **5-80** allowed a remarkable difference to be noticed to the chemically similar previously described derivative without the methylene bridge (Figure 5-72). As indicated by the enthalpy of the first transition in the DSC, the organization in the crystalline phase revealed a very high degree of long-range order. The room temperature pattern (Figure 5-72B) exhibited clearly sharper reflexes in the equatorial plane, which correlated to a hexagonal columnar organization. The determined unit cell with a = 4.1 nm is large, suggesting a complex supramolecular packing with a correlation of every second discotic column. Atypical for a crystalline phase, the molecules aligned orthogonal to the stacking direction, which stands once again in contrast to HBC(C_{12})$_4$ **5-74**, which adopted a "normal" tilted columnar organization. One can speculate, that the methylene protons do not allow the

necessary offset shifting of the disc, which thus hampered sterically the molecular tilting.

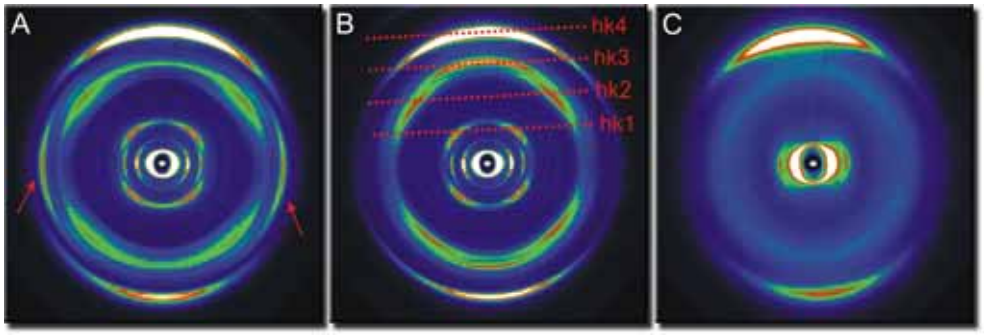

Figure 5-72: *2D-WAXS patterns for an extruded CPHBC(C_{12})$_4$* **5-80** *filament (A) of the crystalline phase at -100 °C, red arrows indicate the reflections from crystallized alkyl chains, (B) of helical arrangement in the room-temperature crystalline phase with a pitch of 1.4 nm (every 5th molecule correlates by rotation of each disc by 15°, hexagonal columnar packing with a = 4.1 nm), the MILLER's indices describe the periodicity along the columnar structures and (C) of the hexagonal columnar mesophase at 150 °C (a = 2.53 nm, stacking distance 0.35 nm).*

The intramolecular organization exhibited a helical arrangement of the CPHBC(C_{12})$_4$ **5-80** molecules, in which every 5th molecule is oriented in the same way. Since we are not dealing with a single-crystalline material, we assume that every disc is rotated by 15° (Figure 5-73). In this case the electron-rich and therefore strongly scattering aromatic part of every 5th molecule is oriented in the same way (rotation of 60°). This postulates that both the alkyl substituents and the methylene-bridge are not influencing the D_{6h}-symmetry of the aromatic part in the scattering experiment. However, it would be also possible that every disc is rotated by 72°, which we believe makes physically no sense, because this angle does not reflect the PAH symmetry.

At lower temperatures (-100 °C), additional equatorial reflexes appeared in the 2D-WAXS pattern (Figure 5-72A, red arrows), which could be correlated to a crystallization of the linear *n*-dodecyl chains. The 2D-WAXS pattern recorded at 150 °C in the mesophase of CPHBC(C_{12})$_4$ **5-80** appeared to be a hexagonal arrangement typical for discotic molecules of that size with a unit cell parameter of a = 2.53 nm.

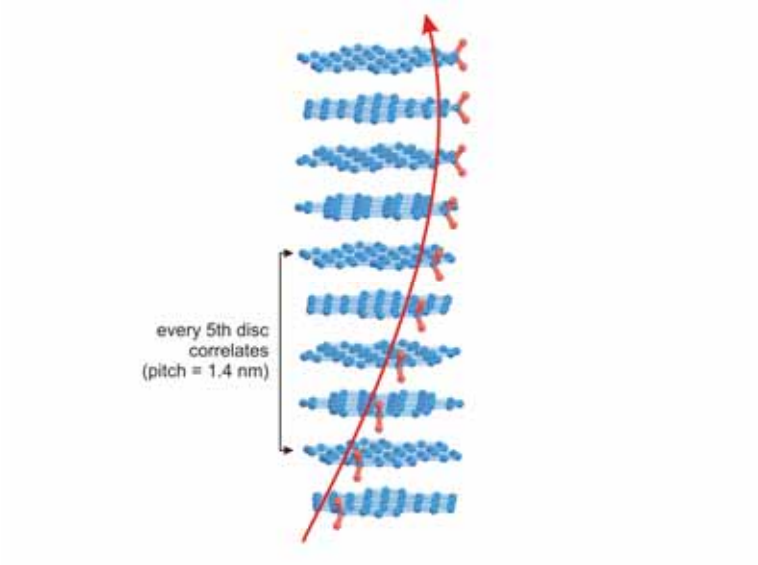

Figure 5-73: *Suggested helical superstructure in the crystalline phase of CPHBC(C_{12})$_4$* **5-80** *with a helical pitch of 1.4 nm (5 discs); alkyl chains are omitted for clarity.*

One can state, that the supramolecular organization of CPHBC(C_{12})$_4$ **5-80** differed significantly from other similar derivatives. Astonishingly, the small steric demand which was excerted from the methylene group caused a helical, non-tilted intracolumnar arrangement, which has been rarely observed in discotic PAHs.[112,113] This enhanced order within the columns promises a better charge carrier mobility along the stacking directions. It is planed to test this material as active component in an FET setup.

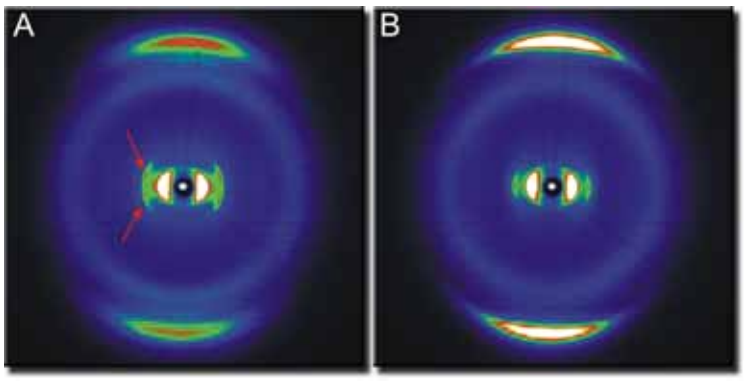

Figure 5-74: *2D-WAXS patterns for an extruded CPHBCCO(C_{12})$_4$* **5-81** *filament (A) of the room temperature, crystalline phase after annealing in the mesophase (complicated superstructure) and (B) of the hexagonal, columnar mesophase at 100 °C with a = 2.78 nm and a typical stacking distance of 0.35 nm.*

After the oxidation, the room-temperature 2D-WAXS pattern still revealed a columnar, hexagonal of CPHBCCO(C_{12})$_4$ **5-81**, but the intracolumnar organization

appeared to be less ordered (Figure 5-74). Two distinct off-equatorial reflexes were found, which indicated a complex supramolecular organization, which could not be elucidated so far. The mesophase of the molecules was very similar to the one of CPHBC(C_{12})$_4$ **5-80** with a good intercolumnar, less dense, non-tilted hexagonal columnar arrangement (a = 2.78 nm). The effect of the dipole-moment induced by the keto-group was expected to have a stonger influence onto the packing. Further experiments, to align the molecules in a magnetic field are planed.

The organization of CPHBCCO(C_{12})$_4$ **5-81** differed also from the one of HBC(C_{12})$_4$ **5-74**. It is very surprising, that the apparently small chemical modifications had a pronounced impact upon the supramolecular organization. As previously discussed (chapter 5.6.2), the symmetry reduction excerted by the substitution pattern going from HBC-C_{12} **3-3c** to HBC(C_{12})$_4$ **5-74** lowered the degree of crystallinity in the self-organized stacks significantly. The bridging of the "arm-chair" site with either a methylene- or a keto-group changed the symmetry of the molecule, but enhanced the supramolecular order to a great extent.

5.7.3 Functionalization

The main motivation for the synthesis of CPHBC(C_{12})$_4$ **5-80** was the promising possibility to easily modify the PAHs perimeter. In the last chapter, the high-yielding oxidation to CPHBCCO(C_{12})$_4$ **5-81** has been described as one example for a successful derivatization. Several different reactions have been tested to functionalize the fluorene-analogous periphery, which are summarized in Scheme 5-22. As a very reactive intermediate, the corresponding anion was obtained after the deprotonation with sterically hindered bases such as LHDMS. This anion reacted readily with methyl vinyl ketone in a MICHAEL-Addition or underwent a S_{N2} reaction with primary *n*-alkyl bromides. The reactions were monitored with mass spectrometry. However, the purification of these compounds was very tedious, since the solubility of the derivatives was limited and therefore a column chromatographic separation could not be successfully conducted. The four *n*-dodecyl chains do not impose this PAH enough solubility. A change to a more solubilizing alkyl chain such as branched alkyl chains suggests which would allow an isolation of the pure synthesized derivatives.[114] Conclusively, I observed that the fluorene-moiety in the PAH underwent the typical reactions, however only the oxidation product was isolated cleanly. The lack of

experimental time disallowed a better soluble analogue of the discussed PAH to be synthesized.

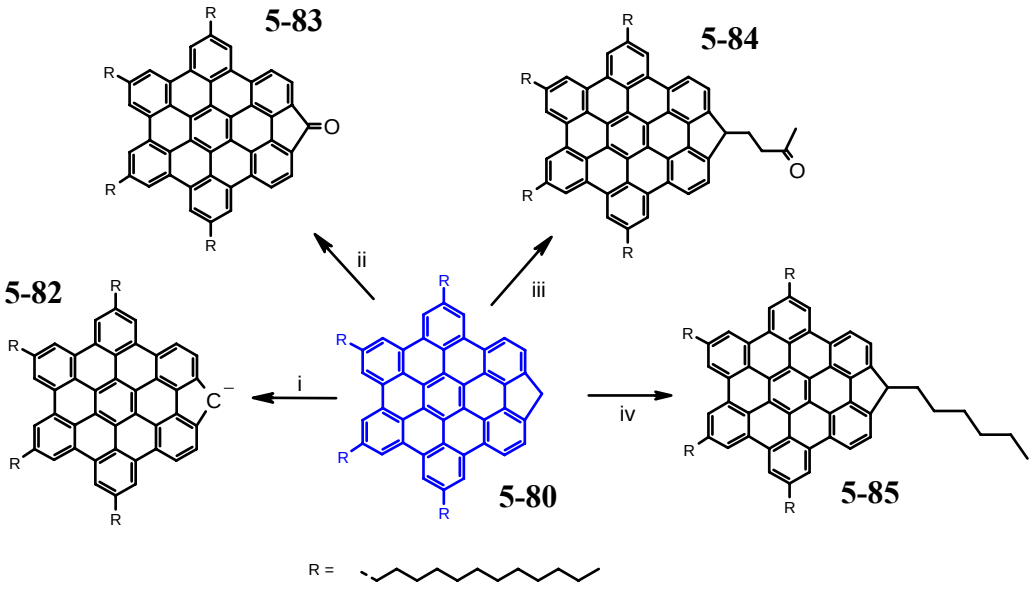

Scheme 5-22: *Tested reactions for the functionalization of CPHBC(C_{12})$_4$* **5-80***: i) Deprotonation with LHDMS; ii) Oxidation (see above); iii) MICHAEL-Addition with methyl vinyl ketone; iv) alkylation with 1-bromohexane.*

Since CPHBCCO(C_{12})$_4$ **5-81** was obtained and isolated purely, the carbonyl center offered an even simpler chance to functionalize the periphery of that PAH. S. BERNHARDT recently showed that carbonyl centers incorporated into a dendrimer scaffold are accessible for a vide variety of *a posteriori* derivatizations.[115] Again several reaction-types have been tested to evaluate the reactivity of the "fluorenone"-moiety in the PAH.

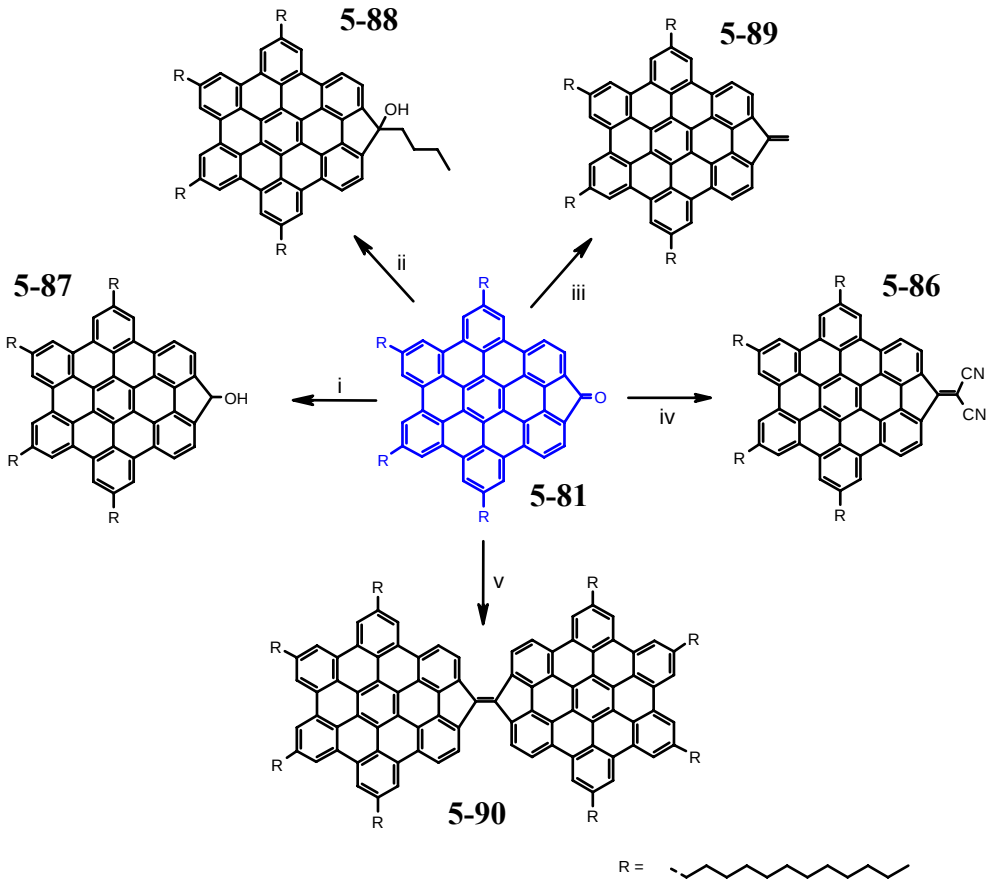

Scheme 5-23: *Tested reactions for the functionalization of CPHBCCO(C_{12})$_4$* **5-81***: i) Reduction with LiAlH$_4$; ii) reaction with n-BuLi; iii) WITTIG reaction; iv) KNOEVENAGEL with malononitrile; v) MCMURRAY reaction.*

Straight forward reduction with lithium aluminum hydride afforded the corresponding secondary alcohol. The carbonyl function readily reacted with *n*-butyl lithium to the tertiary alcohol. An exocyclic double bond could be obtained in a standard WITTIG conversion, which would certainly allow further functionalizations. As a typical carbonyl reaction, the KNOEVENAGEL conversion with malonitrile permitted an acceptor substituted PAH to be obtained. The mass spectrum of the crude MCMURRAY reaction of two CPHBCCO(C_{12})$_4$ **5-81** molecules indicated a successful conversion to the large fully conjugated, extended PAH. All these reaction have been tested on small scale and the difficult purification has not been performed. Similar to the previous reactions, the conversion of CPHBCCO(C_{12})$_4$ **5-81** yielded in all cases the product, which could not be isolated easily due to solubility reasons. Also in this case, the change of the alkyl substituents would be an attempt to solve that problem. Conclusively, one can state, that for both CPHBC(C_{12})$_4$ **5-80** and CPHBCCO(C_{12})$_4$ **5-81** could be functionalized at their periphery following different methodologies.

5.7.4 Other "Reactive" Peripheries

Another type of "chemical" reactive peripheries are "arm-chair" sites in not-fully benzoid PAHs. S. MÜLLER has recently shown that the bay position of perylenetetracarboxdiimide derivatives (PDI) were susceptible for DIELS-ALDER cycloaddition reactions (Scheme 5-24).[116]

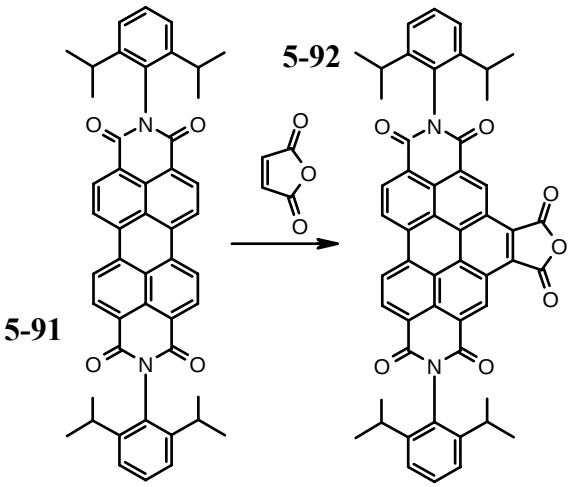

Scheme 5-24: *Diels-Alder cycloaddition in the bay position of PDI.*

Analogous to this concept, a synthetic route towards a large extended PAH was developed, which included six potentially reactive "perylene" bay areas. Starting with the partial hydrogenation of pyrene (**5-93**) [117], which gave the chromatographically purified pure tetrahydropyrene isomer **5-94**, 2,7-dibromopyrene (**5-95**) was obtained after two further steps in an overall yield of 69%.[118] The following KUMADA coupling was conducted under kinetic control to selectively obtain the mono-alkylated pyrene **5-97**. The HAGIHARA-SONOGASHIRA cross-coupling reaction following GRIECO's procedure[119] yielded the strongly fluorescent dipyrenylacetylene derivative **5-98** in very high yield.

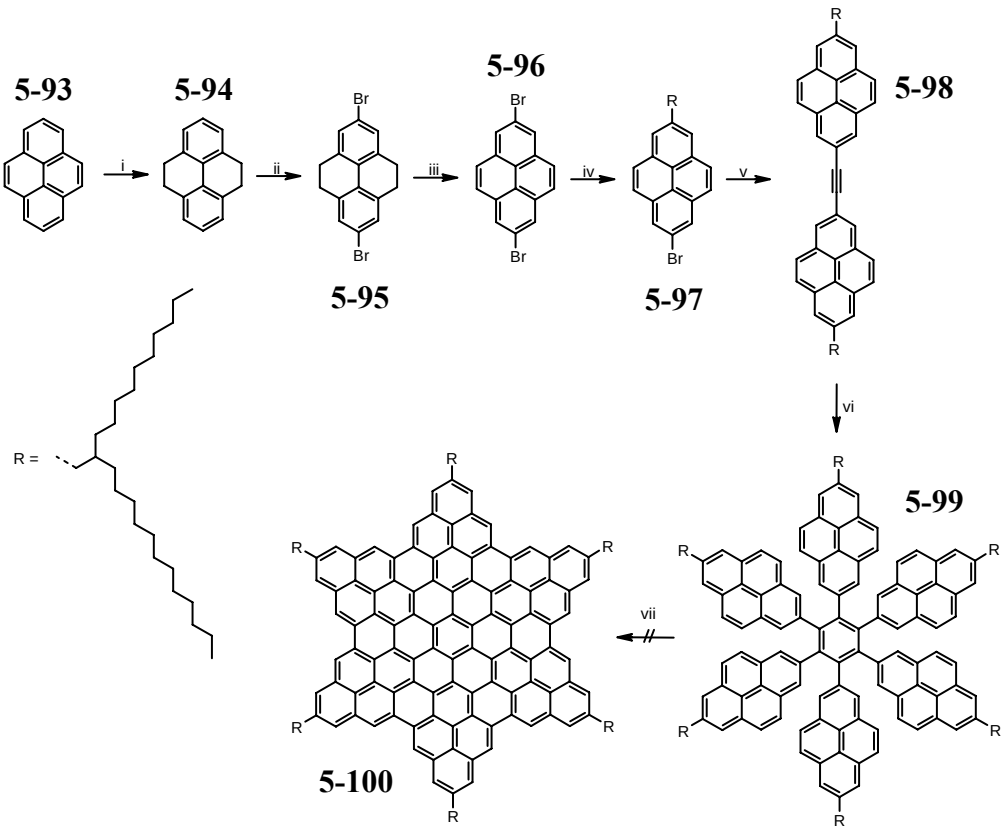

Scheme 5-25: *i) H_2, Pd/C, 72%; ii) Br_2, $FeCl_3$, 99%; iii) Br_2, CS_2, 99%; iv) RMgBr, $Cl_2Pd(dppf)$, 77%; v) CuI, $Pd(PPh_3)_2$, trimethylsilylacetylene, DBU, H_2O, 96%; vi) $Co_2(CO)_8$, 83%; vii) $FeCl_3$.*

After the successful cyclotrimerization with dicobaltoctacarbonyl, the precursor molecule **5-99** with an average molecular mass of 3299 dalton could be isolated purely after column chromatography. Very surprising, the SCHOLL cyclodehydrogenation did not yield the aimed PAH **5-100**. Independent of the amount of used oxidant (< 60 eq), the reaction stopped after six aryl-aryl bonds had been fused, which was clearly indicated by the MALDI-TOF spectra. When using a large excess of iron(III) chloride (> 60 eq.) in that reaction, the MALDI-TOF spectrum showed a very broad peak which suggested strong fragmentation during the reaction. The isolated, highly soluble material had a pink color, but showed on the thin-layer chromatography different bands, suggesting a complex mixture of different PAHs. The attempted separation failed since the compounds are streaking on the stationary phase of the preparative column, which made an isolation of distinct bands impossible.

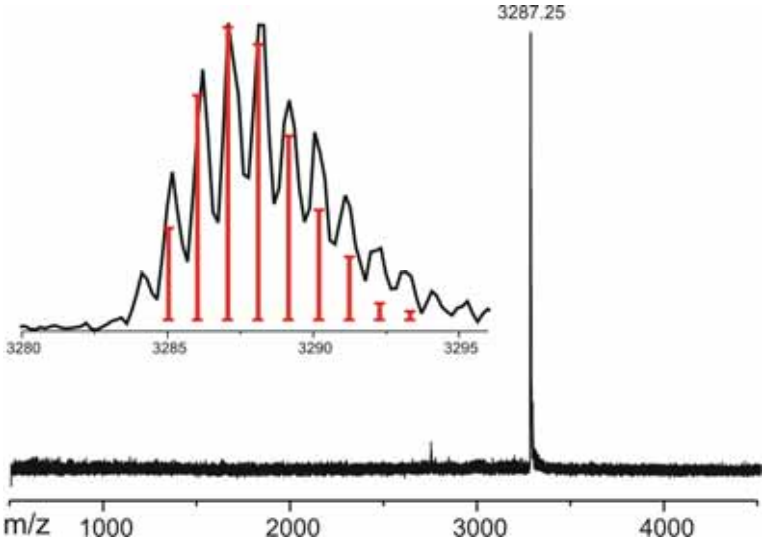

Figure 5-75: *MALDI-TOF spectrum of the crude product after the cyclodehydrogenation of* **5-99***, using the solid state preparation technique with TCNQ as the matrix substance.*

A very interesting question still remained unanswered. The reason why the SCHOLL reaction stopped after the formation of 6 aryl-aryl bonds is not apparent. Furthermore, the chemical structure of the main product was ambiguous.

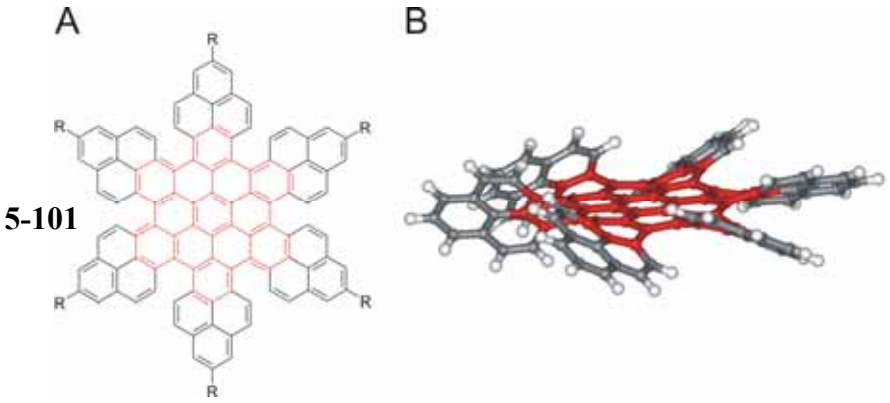

Figure 5-76: *(A) postulated chemical structure and (B) optimized geometry (alkyl chains are omitted for clarity) of the PAH, which is found as the major product.*

The analysis of ^{1}H NMR, MALDI-TOF and UV/Vis spectra of the product mixture obtained in many cyclodehydrogenations attempts revealed to be very complicated. However, the sum of all indications allowed the structure of the main product to be postulated. The MALDI-TOF spectra suggested, analogous to the planarization of hexaphenylbenzene towards HBC, the successful removal of 12 hydrogen atoms during the reaction. Together with the UV/vis spectra, which resembled the one of HBC (not shown), the distorted PAH structure **5-101** (Figure 5-76) was postulated. In pyrene, the carbon atoms at the positons 1, 3, 6, and 8 are very reactive and undergo regioselective aromatic substitutions. One can speculate that this caused the

planarization reaction to end after having fused six aromatic bonds. However, the ^{1}H NMR spectra (not shown) exhibited a large number of different partially closed bye-products which could not be assigned to a specific structure. The alternative reductive cyclodehydrogenation reaction of the precursor **5-99** with potassium has been tried. The MALDI-TOF indicated in this case mostly starting material and some partially closed species. The described results emphasized the difficulty to predict the cyclodehydrogenation reaction.

5.8 Graphite with “Defects”

In the previous section, the synthesis and the characterization of PAHs with different types of peripheries have been introduced. Small PAHs can be considered as the monomeric, well-defined analogues to graphite. Theoreticians appreciate such model systems to improve their understanding of graphite.[9] Surface and bulk (structural) defects in graphite play an essential role in many processes involving this material. They influence physical (electronic and thermal conductivity, electronic structure) and chemical (reactivity, activation of adsorbed molecules) properties of graphite.[120,121] It is well known that structural defects are beneficial for the reaction of molecular oxygen with graphite.[122] Next to model substances with different peripheral structures, the synthesis of specific graphitic segments with defects is of importance to study the excerted influence onto the properties.[123]

5.8.1 Synthesis of an Extended PAH with “Hole”

Pentagon-heptagon pairs[124], mono-vacancies[125,126] and multi-vacancies[127,128] and adatoms[129] are typical stable graphene defects that have been predicted. These FRENKEL and SCHOTTKY defects are atomic-scale defects which alter the physical and chemical properties of carbon nanostructures.[130,131] A very impressive example was published by HASHIMOTO ET. AL., who managed visualizing knock-on atom displacements[129] on single-walled carbon nanotubes, induced by high-energetic particles such as electrons and ions, with high resolution transmission electron microscopy (TEM).[132]

A SCHOTTKY defect is the formal removal of a central benzene unit, which leads to a “hole” in the graphene sheet. Recently, the group of Prof. MÜLLEN presented the synthesis of a 222 carbon atom containing planar graphite segment, following the concept of cyclodehydrogenating a suitable oligophenylene precursor.[3] This PAH will be used in the next section as the parent compound for a novel “hole”-containing analogue.

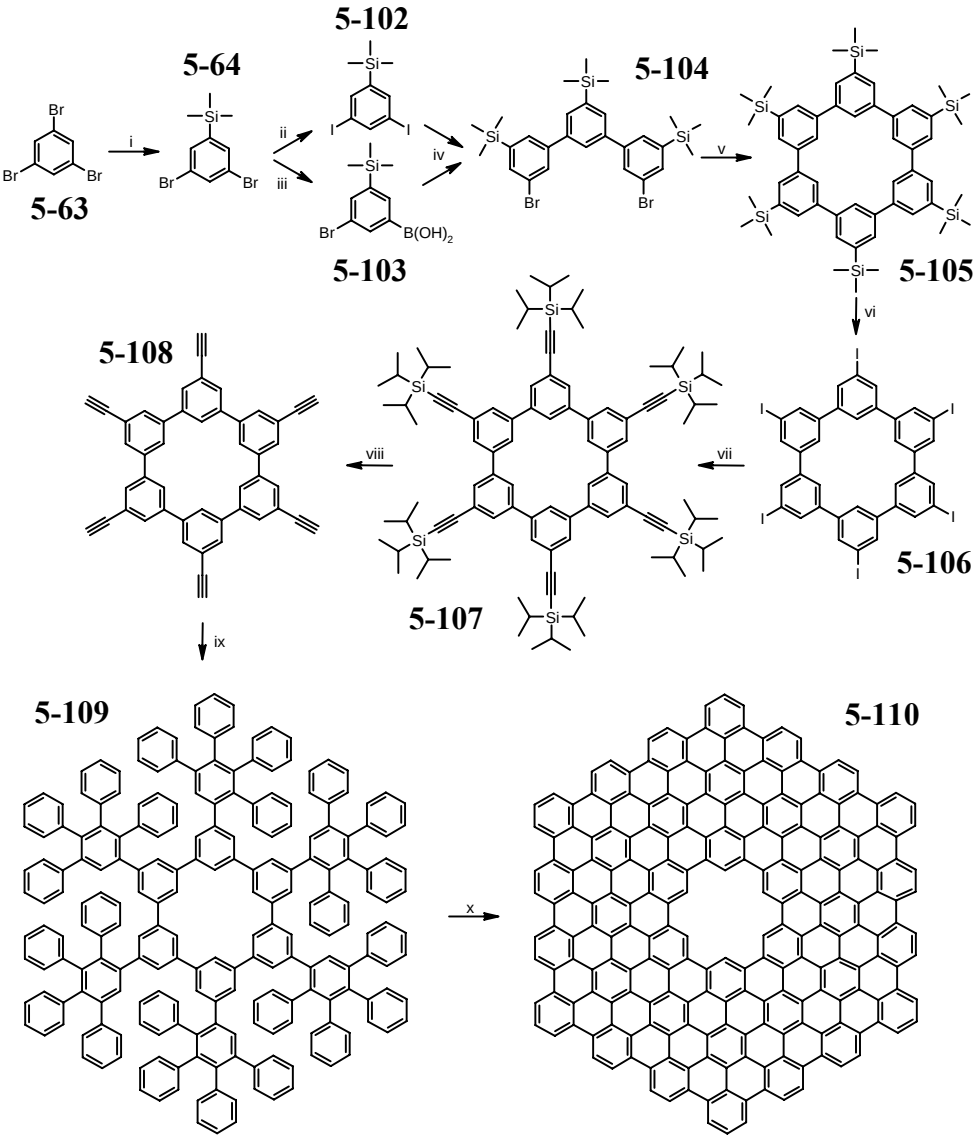

Scheme 5-26: *i) n-BuLi, TMS-Cl, 79%; ii) t-BuLi, I_2, 82%; iii) n-BuLi, $B(O^iPr)_3$, 97%; iv) K_2CO_3, $Pd(PPh_3)_4$, 81%; v) COT, bipy, $Ni(COT)_2$, 58%; vi) ICl, 84%; vii) CuI, PPh_3, $Pd(PPh_3)_4$, TIPS-acetylene, 55%; viii) TBAF, 76%; ix) 2,3,4,5-tetraphenyl-cyclopenta-2,4-dienone, 85%; x) $FeCl_3$.*

The synthetic concept targeted at first the hexa-*m*-phenylene ring **5-105**, which has been synthesized unsubstituted in the literature in very low yield (~1%) by the oxidative coupling of the bis-GRIGNARD reagent of 1,3-dibromobenzene.[133] Such an unsatisfying yield would not allow synthesizing the desired PAH in a reasonable quantity. Therefore, the macrocycle synthesis was performed in a step-wise fashion using regioselective SUZUKI reactions (Scheme 5-26). Commercially available 1,3,5-tribromobenzene (**5-63**) was converted to the mono-TMS substituted dibromo-derviative **5-64**, as described before.[70] This compound was double lithiated with *t*-butyl lithium and subsequently quenched to the bis-iodo analogue **5-102** as the first

building block. 1,3-dibromo-5-trimethylsilylbenzene (**5-64**) was on the other hand reacted to the boronic acid **5-103**, after mono-lithiation and quenching tri-*iso*-propyl borate. The subsequent SUZUKI cross-coupling reaction of **5-102** with **5-103** could be conducted selectively at room temperature yielding the *m*-terphenyl derivative **5-104**. This high selectivity for cross-coupling reactions is well known for HAGIHARA-SONOGASHIRA, where one used the different temperature-reactivity windows for different halogen functions.[66]

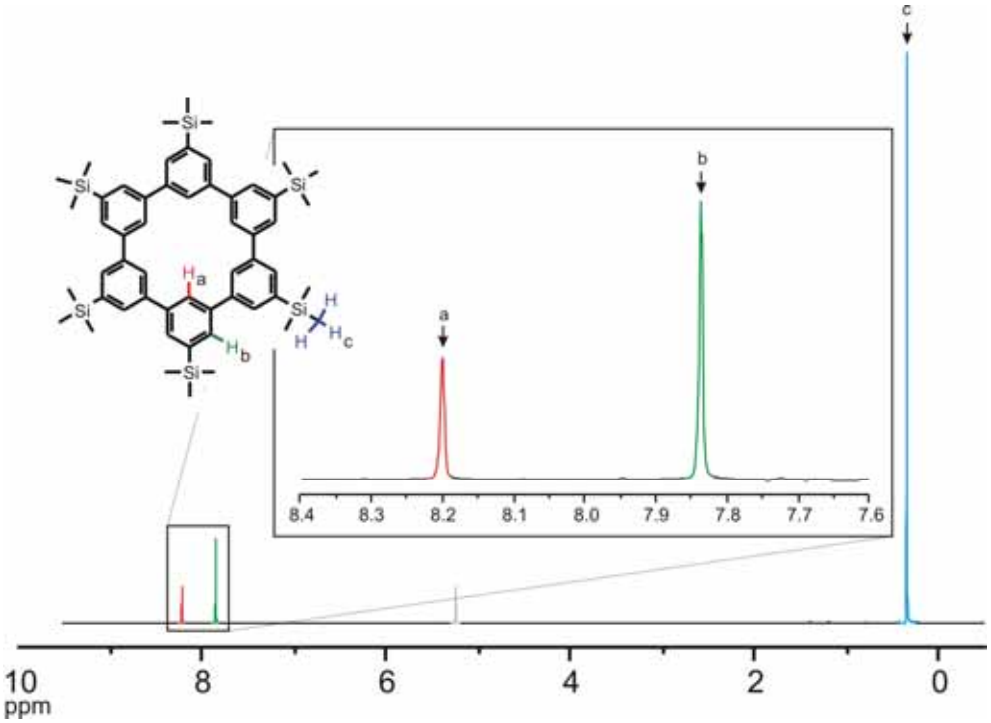

Figure 5-77: *^{1}H NMR spectrum of* 5-105 *recorded at room temperature in dichloromethane-d^2, solvent peak was colorized in grey.*

The most critical step concerned the dimerization of the *m*-terphenyl **5-104** unit following YAMAMOTO's protocol. Expectedly, the concentration influenced the yield to a great extent and different reaction conditions had to be tested to allow the substituted hexa-*m*-phenylene **5-105** to be obtained in a satisfying yield of 58%. Mass-spectometrically, it was not possible to prove undoubtedly the successful fusion to the ring-molecule, since the open form differed only by two dalton. However, the ^{1}H-NMR spectrum revealed a highly symmetric molecule. The resonances could clearly be assigned to the corresponding nuclei in the ring molecule **5-105** (Figure 5-77). As a very elegant structure proof, it was further possible to grow a single-crystal of the compound, which structure could be resolved using X-ray diffraction. The analysis clearly confirmed the successful reaction (Figure 5-78A). The side view

of the molecule indicated that the *m*-jointed ring possessed enough flexibility to establish a chair conformation, analogous to cyclohexane (Figure 5-78B,C). The cyclo-*m*-phenylene **5-105**, which carried masked halogen and therefore reactive groups for further functionalizations, was obtained in an overall yield of 32% in five steps, which is far higher than for the reported synthesis of the unsubstituted analogue.[133]

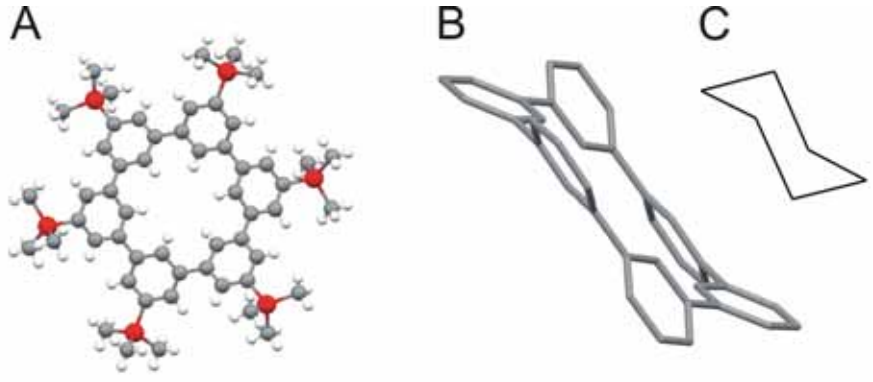

Figure 5-78: *crystal structure of* **5-105** *(A) top view, (silicon atoms are colorized in red, carbon in grey and hydrogen in white, solvent molecules are not show) (B) side view (TMS groups and hydrogen atoms omitted for clarity) and (C) chair conformation of cyclohexane.*

In the next synthesis step, the TMS-groups were converted to iodo-functions using iodomonochloride to afford compound **5-106**. Although hardly soluble, the six-fold HAGIHARA-SONOGASHIRA reaction of **5-106** with tri-*iso*-propylsilylacetylene could be performed to afford the well-soluble macrocycle **5-107**. The multiple HAGIHARA-SONOGASHIRA cross-coupling reaction on an almost insoluble starting material has been published by J. WU. He converted six iodo functions around an HBC in high yields into different acetylene derivatives and studied the self-assembly in the bulk state.[134,135]

It was again possible to obtain single crystals with sufficient quality to be analyzed by single-crystal X-ray diffraction. The ring adopted again a chair conformation in the crystal lattice (Figure 5-79). Interestingly, the analogous reaction of **5-106** with trimethylsilylacetylene yielded the corresponding compound only in very low yields. The cleavage of the TIPS groups from the acetylenes was performed with TBAF, analogous to many dendrimer synthesis performed in the MÜLLEN group.[136] Compound **5-108** was reacted with commercially available 2,3,4,5-tetraphenyl-cyclopenta-2,4-dienone (**5-34a**) in a six-fold [4+2] cycloaddition yielding in the

dendronized macrocycle **5-109**, which can be considered as a suitable precursor for the SCHOLL planarization reaction.

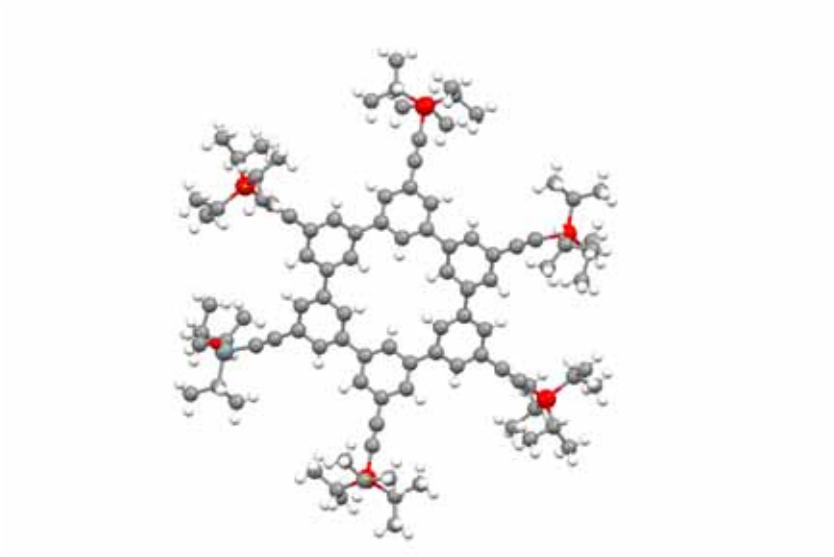

Figure 5-79: *Crystal structure of* **5-107***, solvating molecules are removed for clarity (silicon atoms are colorized in red, carbon in grey and hydrogen in white, solvent molecules are not shown).*

Although, the central macrocycle was not planar, the treatment of **5-109** with iron(III) chloride yielded mass-spectrometrically the expected PAH. However, the standard conditions did not avoid the chlorination as a prominent side-product in this reaction (not shown). The same problem occurred in the synthesis of C222, the analogous PAH without the hole. For extended PAHs, the suppression of the chlorination could not be achieved and was thus a serious problem.[137] Optimization attempts showed that the use of a stream of argon saturated with dichloromethane, which was bubbled through the reaction mixture, reduced the amount of chlorination almost completely.

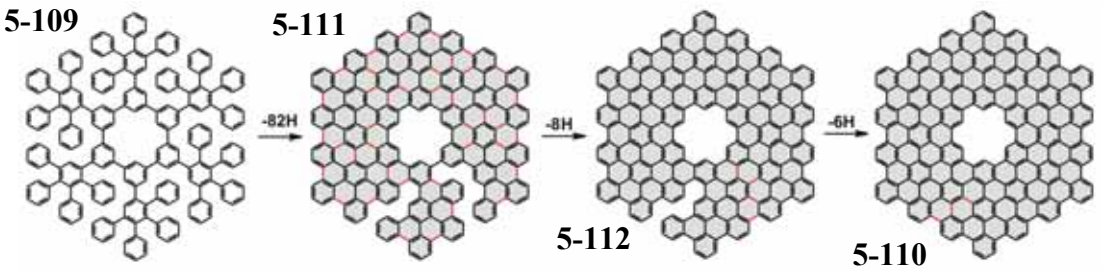

Scheme 5-27: *Suggested intermediates* **5-111** *and* **5-112** *during the cyclodehydration of* **5-109***, indicated by a series of MALDI-TOF spectra.*

This change of the reaction conditions allowed using much harsher reaction conditions with iron(III) chloride amounts up to 480 equivalents without a significant

amount of chlorination. Experiments proved that the planarization of **5-109** required long reaction times, as was seen in the recorded MALDI-TOF spectra (Figure 5-80Figure 5-71).

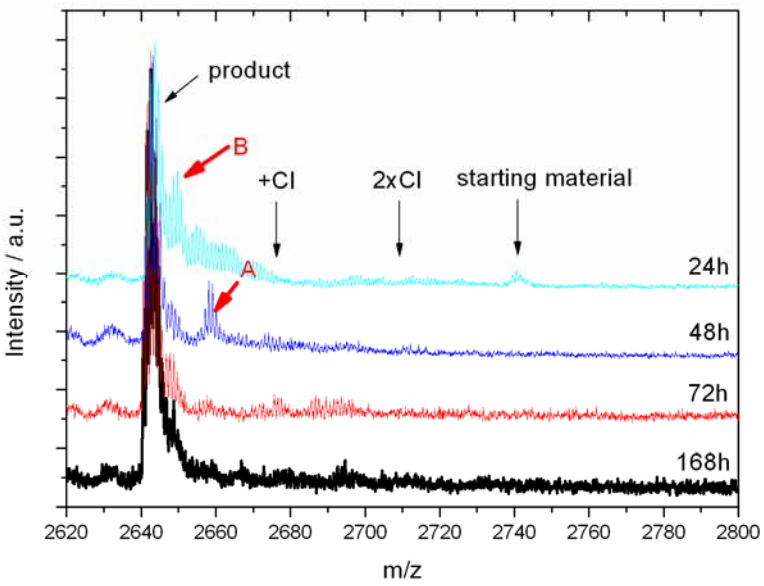

Figure 5-80: *MALDI-TOF spectra taken during the cyclodehydrogenation of* **5-109** *(after 24, 48, 72, and 168 hours) recorded using the solid-state preparation with TCNQ as matrix substance. Side-products A and B are indicated.*

The analysis of a large number of recorded MALDI-TOF spectra revealed two "trapped" partially fused intermediates **5-111** and **5-112**, which are presented in Scheme 5-27. Together with D. WASSERFALLEN, we investigated the SCHOLL reaction on different, extended PAHs and recorded mass and NMR spectra during the course of the reaction.[48] The results from that study and semi-empirical quantum mechanical calculations allowed the mechanism of the planarization reaction for extended PAHs to be speculated. "Dendritic" 2,3,4,5-tetraphenylbenzene-subunits fused during the course of the reaction in elemental steps with different kinetics. In the first step, the planarization produced a singly bonded tribenzo[*b,n,pqr*]perylene moiety (Figure 5-81). The next extension of the polycyclic aromatic system created a more strained, distorted system and proceeded therefore kinetically much slower than the first three aryl-aryl bond formations. Incorporation of the next phenyl unit in the "growing" PAH created a very strained intermediate, which lay energetically higher than the previous intermediate. The final planarization step gained a lot of stabilization

towards the fully fused PAH. This reaction pathway was found to fit for all investigated examples and the speculated intermediates were mass-spectrometrically identified.[48]

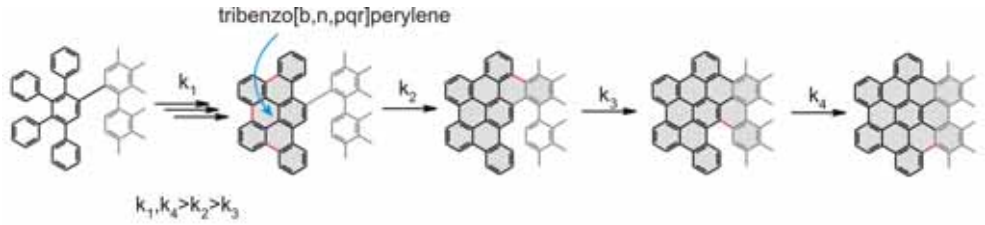

Figure 5-81: *Suggested reaction mechanism; elemental steps with different kinetics.*

Furthermore, MALDI-TOF spectra using the solid-state preparation method, concealed the true state of the sample purity, since desorption- and ionization propensity for the completely fused PAH differed significantly from partially fused by-products. This was emphasized for the 216 carbon containing PAH with hole **5-110**, where a reasonable MALDI-TOF spectrum was obtained. However, further characterizations with solid state UV/vis and NMR exhibited the imperfect synthesis (not shown). The absorption profile differed significantly from batch to batch and the solid-state NMR spectra clearly indicated a large number of different by-products, which could not be identified. Quantification of the amount of impurities in these insoluble mixtures proved to be difficult since the relaxation behavior of the different components in the mixture might differ. As a very rough estimation, the interpretation of the solid state NMR spectra, assuming a relaxation of the proton nuclei on the same timescale, allowed a maximum amount of impurities to be determined as high as 70%.

Purification attempts to extract partially fused side-products, due to a potentially better solubility, failed. Furthermore, STM experiments to visualize the central hole of deposited **5-110** on a HOPG surface at the solid-liquid interface were unsuccessful, which might be due to the discussed impurities or a bad organization on the surface.

The synthesis of extended PAHs remains a very challenging field, since the lack of analytical techniques for insoluble materials hamper the determination of the purity state. Next to the pronounced self-association propensity of the huge π-areas within these compounds, a large number of impurities impeded resolving the aromatic region in ^{1}H NMR spectra of soluble PAHs.[3,33] Recently, D. WASSERFALLEN managed to synthesize a pure PAH with a size of 72 aromatic carbon atoms, which is

so far the largest, clearly characterized PAH **1-44**.[138] The complicated synthetic approach required the step-wise planarization of a suitable precursor to allow the final SCHOLL reaction to be performed without problems with chlorination and partially fused species. It turned out that the introduction of distortion rendered the PAH reasonable soluble, because the aggregation was dramatically reduced.[48] As a very elegant method, soft-landing promises to purify and to process the unsublimable, insoluble material (see chapter 5.8.5).

5.8.2 Engineering of microporous organic crystals

Construction of porous organic solids relies mainly on arrangements of organic molecules into extensive networks via such intermolecular interactions as hydrogen bonding and metal coordination to generate cavities for guest inclusion.[139] Many efforts along this line have afforded various crystals or amorphous solids[140] which have guest-binding and/or catalytic[140] properties. “Low-temperature building block” approaches to design and synthesize porous 3D crystals have been exploited employing a variety of building blocks mostly in the form of organic or organometallic molecules that can bind to metal ions[141] or form hydrogen bonds to other molecules.[142] Large-pore metal-organic frameworks have been used as materials for gas adsorption.[143] As graphene units have been shown to intercalate lithium atoms[144] and to bind hydrogen molecules[145,146], such materials would have potential applications in lithium batteries or in hydrogen storage.[147] The controlled pyrolysis of graphitic precursors can be used to obtain carbonaceous materials with controlled geometries.[148]

Crystals of precursor **5-109**, which has been described in the last chapter, would fulfill theoretically the necessary prerequisites for the storage of guest molecules. Intrinsically, the material can not form a closed packing, which is hampered by the molecular architecture. However, attempts to grow crystals of that material from different solvents failed. The compound precipitates from all tested solvents as a colorless, micro-crystalline powder. It is well known, that “low symmetric” dendritic molecules do not pack into macroscopical crystals.[136]

Therefore, the 2,3,4,5-tetraphenyl-dendrons were replaced by the better packing 2,3,4,5,6-pentaphenyl analogues, according to Scheme 5-28. The ring molecule **5-106** was reacted in a six-fold HAGIHARA-SONOGASHIRA cross-coupling with

phenylacetylene into compound **5-113**. The yield of that reaction was quite astonishingly, since both starting material and product were only sparingly soluble in the used solvent. An analogous reaction has been performed by J. WU et al. who reacted hardly soluble HBC derivatives using that methodology.[134,135] Finally, a six-fold DIELS-ALDER cycloaddition reaction with **5-113** and 2,3,4,5-tetraphenyl-cyclopenta-2,4-dienone **5-34a** was conducted, yielding the dendronized ring molecule **5-114** in good yields. Microwave radiation was utilized to accelerate the reaction speed and to increase the yield, which took under conventional conditions several days.

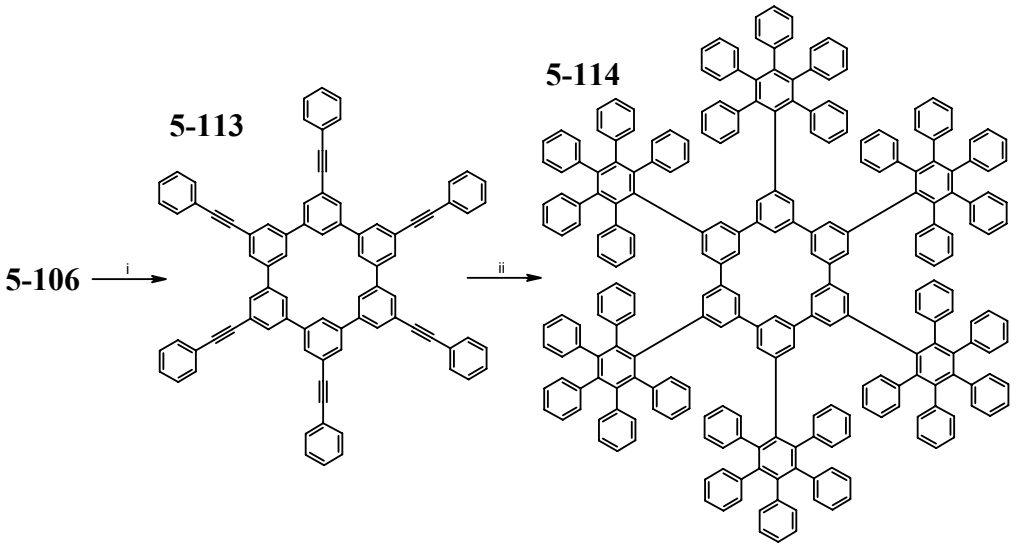

Scheme 5-28: *i) PPh_3, phenyl acetylene, CuI, $Pd(PPh_3)_4$, 90%; ii) 2,3,4,5-tetraphenyl-cyclopenta-2,4-dienone, microwave radiation, 88%.*

Interestingly, **5-114** crystallized in contrast to **5-109** from different solvents into large needle-like crystals, which were suitable for single-crystal X-ray diffractometry. The analysis validated again the chair-conformation of the central ring, which resembled the one of cyclohexane (Figure 5-82A,B). As expected, the three-dimensional packing of the molecules created a channel-like superstructure (Figure 5-82C,D), which was filled with molecules of the crystallization solvent.

Two kinds of channels were observed, one formed by the inner ring and the other by the packing of the dendrons of the molecule. Unfortunately, the crystals were not stable under atmospheric conditions, since the solvated molecules were too volatile. Experiments to gain crystals from higher boiling solvent are still in progress. The measurement of the hydrogen gas uptake is planned and promising, since the

graphitic material possesses a lot of hollow cavities within its crystal structure, which can be theoretically filled with guest molecules.

Supramolecular chemistry provides ways and means to design and generate organized equilibrium architectures of nanoscopic dimensions with novel structural and functional properties.[149] Peptides are short molecules yielding to numerous examples of molecular self-organized systems.[150] Urea, which is one of the smallest molecules containing the peptide linkage, forms seval polymorphs of extended linear[151], orthogonal[152], or helicoidal[153] networks of hydrogen bonds. The organization of suitable, large, organic building blocks utilizing aromatic π-stacking is a fairly new concept to obtain nanostructured crystals and has not been reported in the literature.

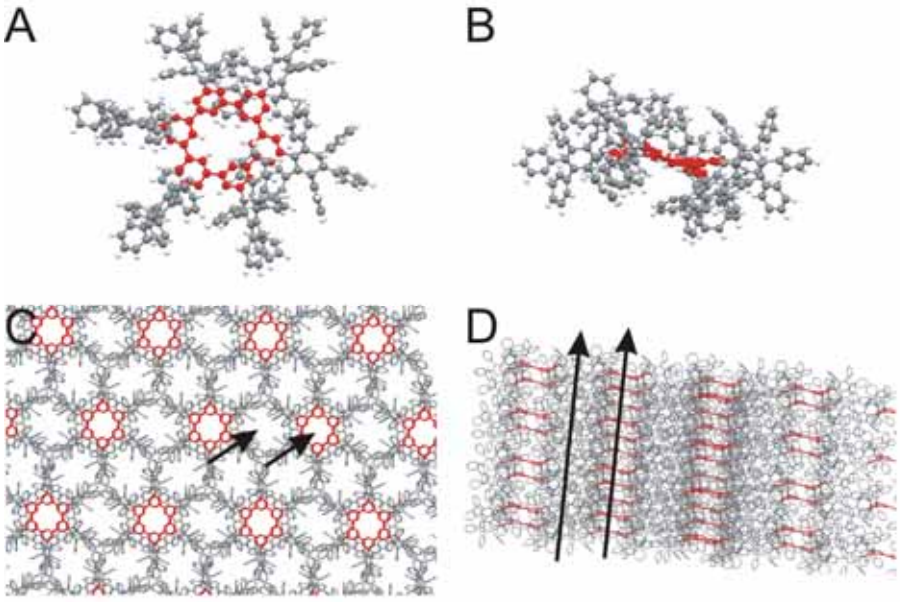

Figure 5-82: *Crystal structure of* **5-114***, inner ring was colorized in red, solvent molecules removed for clarity; (A) top view; (B) side view indicating the chair conformation of the inner ring, (C) packing motif from top, and (D): side view of the packing motif; arrows indicate the two channels in (C) and (D).*

5.8.3 Phase Forming Ring

The high reactivity of **5-106** in HAGIHARA-SONOGASHIRA couplings opened the elegant possibility to decorate the ring structure with flexible, long alkyl arms, which theoretically should impose discotic properties onto the molecule. S. HÖGER et al. and J. MOORE et al. published a series of much larger, phase forming, self-associating phenylacetylene-based macrocycles (PAM), which have been investigated in great detail.[154-158]

The cross-coupling reaction with tetradec-1-yne was performed analogous to the previously described examples and gave the desired compound **5-115** in reasonable yield.

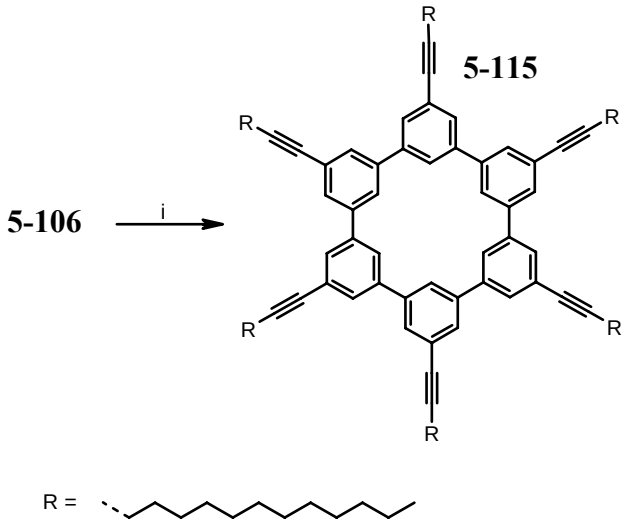

Scheme 5-29: *i) tetradec-1-yne, PPh_3, CuI, $Pd(PPh_3)_4$, 51%.*

A detailed ^{1}H NMR analysis revealed a weak self-association behavior in concentrated solutions, since the aromatic resonances depended both from concentration and temperature (Figure 5-83).

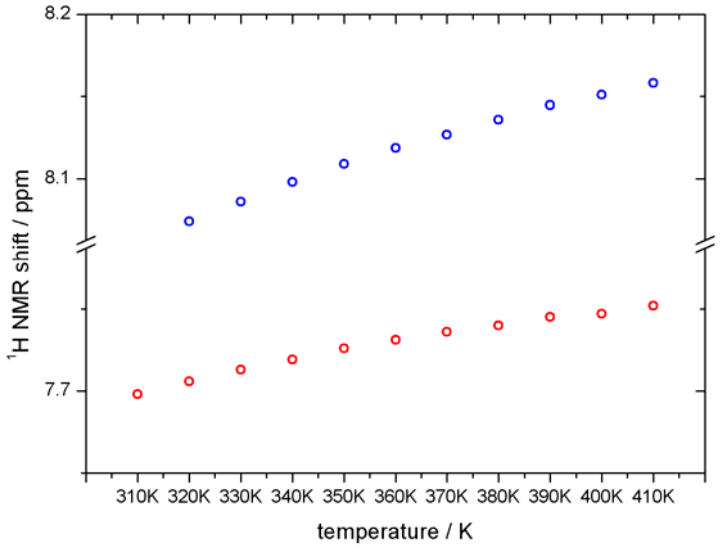

Figure 5-83: *Temperature dependent ^{1}H NMR shifts of the aromatic ring protons of* **5-115***, recorded in tetrachloroethane-d^2.*

The maximal shift difference for both aromatic ring protons was in the range of 0.1 ppm, which suggests a formation of only dimeric structures.[159] Using solvophobic interactions, the self-association behavior of the molecule was amplified, which has

been observed for other PAMs, as well.[160,161] The residual flexibility and the non-planarity of the central ring weakened the intermolecular interactions compared to the form persistent HBC analogue, which carried the same alkyl substituents and revealed a much more pronounced self-association behavior in solution.

In the DSC, the compound exhibited one endothermic transition at 45 °C, which corresponded to a melting point. The analysis of the room temperature phase by X-ray diffraction revealed a badly organized crystalline phase. The 2D-WAXS pattern of a mechanically oriented sample revealed a weak reflection for the π-stacking (Figure 5-84). However, the material differed distinctly from HBC analogues, which were much higher oriented and better organized. Figure 5-84B illustrates the simulated stacking of the flexible ring-molecules.

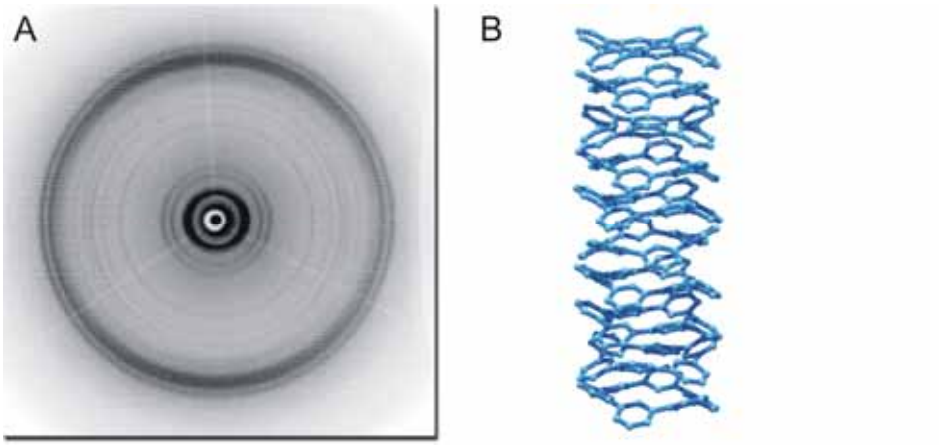

Figure 5-84: *(A) 2D-WAXS diffraction pattern of an extruded sample of* **5-115** *at room temperature (monoclinic unit cell, with a = b = 4.66 nm and γ = 97°) and (B) simulated stacking of the flexible* **5-115** *molecules.*

In conclusion, the flexible “HBC with hole” revealed only a very weak tendency to self-organize into columnar superstructures, which makes compounds based on that concept less interesting for applications. The stiff, extended PAH core of HBC derivatives imposed almost all derivatives a pronounced propensity to self-organize and to form very stable mesophases, with a temperature broadness up to 250 °C.[162] The necessary nanophase separation to obtain a discotic mesogens between the flexible surrounding and the rigid core component is not perfectly fulfilled in this case. Numerous examples of stiffer and therefore more shape-persistent disc-like macrocycles exhibit a more pronounced self-aggregation behavior, which form more stable and broader discotic mesophases.[158,160,163-167]

5.8.4 Non-planar PAHs with hole

Nonplanar aromatic hydrocarbons, in which the inside and outside carbon surfaces exhibit different chemical and physical properties, have always attracted considerable attention.[168,169] The discovery of fullerenes[170] sparked a renewed interest in curved surface polycyclic aromatic hydrocarbons (PAHs) and stimulated the developments of new synthetic methods for their preparation.

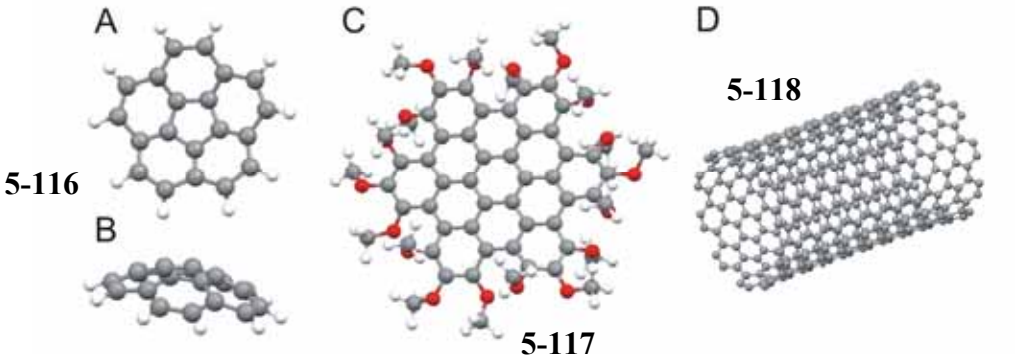

Figure 5-85: *Structure of corannulene* **5-116** *(A) top view and (B) side view; (C) non-planar structure of HBC(OMe)$_{18}$* **5-117***; (D) armchair nanotube* **5-118** *(10,10)*

In the past, attempts to induce chemically a distortion on the molecular level were thought to be not successful, since PAHs were considered as the prototype for planar compounds. The synthesis of very aesthetic molecules such as the bowl-shaped corannulene (**5-116**)[171,172] (Figure 5-85A,B) or helicenes[173] drew the attention to non-planar PAHs, which have been inaccessible due to their inherent strain. In the case of the octadeca-methoxy substituted HBC(OMe)$_{18}$ **5-117**, the non-planarity was induced by sterical congestion excerted by the methoxy groups located in the "bay"-regions of the PAH.[174] The introduction of two *tert*-butyl groups into a PAH with 72 carbon atoms **1-44** twisted the molecule significantly leading to better processability due to an hampered aggregation propensity.[48,138] The distorted examples of PAH represent the connection between two- and three-dimensional graphitic segment, and are called "missing links".[175]

All these non-planar examples of PAHs (Figure 5-85) are higher in energy as their planar counterparts.[107] For the synthesis of such derivatives, it becomes clear, that the price for the distortion has to be paid at one level.

One approach which has been tested was the attempted cyclodehydrogenation of 1,2,3,4,5-pentaphenylcyclopentadiene (**5-119**) applying the SCHOLL method (Scheme 5-30). However, the analysis of the product mixture emphasized that the desired

strain could not be introduced in this reaction step. A wild product mixture was detected by mass spectrometry with different partially fused species. Traces of the planar PAH, where three aryl-aryl bonds were fused could be detected. Also, other cyclodehydrogenation conditions were applied giving similar results.

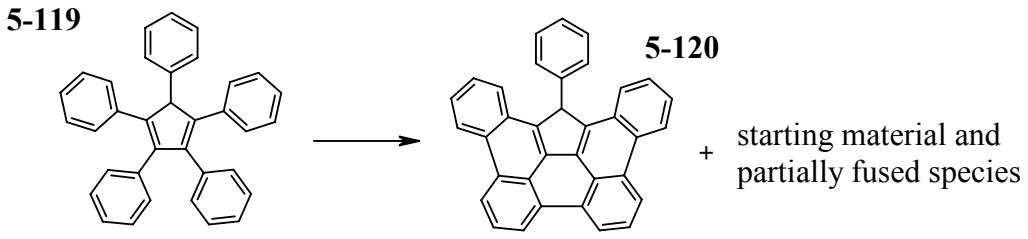

Scheme 5-30: *i) $FeCl_3$ or K.*

As a consequence, a synthetic concept was developed which planned to introduce the distortion prior to the planarization reaction. The desired intermediate in this reaction route was the known cyclopenta-*m*-phenylene, which was isolated in the literature in small traces from the oxidative coupling of the bis-GRIGNARD reagent of 1,3-dibromobenzene. In our case, the strained cycle would have to be substituted with TMS groups to allow a further “dendronization” analogous to the previously described extended PAH with hole (Scheme 5-31). The reaction path started with a double lithiation of the already synthesized molecule **5-104** and a subsequent quenching with elemental iodine. The iodinated *m*-terphenyl **5-121** was converted in a selective Suzuki reaction to the corresponding *m*-pentaphenyl **5-122**. Different attempts to cyclize this derivative using oxidative couplings of various prepared metal-organic intermediates (i.e. YAMAMOTO coupling) failed. Therefore, the mono-boronic ester derivative **5-123** was prepared which promised a Suzuki reaction to form the cyclopenta-*m*-phenylene **5-124**. As a major drawback, also with this material, it was not possible to fuse the desired ring structure. Not even traces of that compound were found in the complex product mixture. The TMS groups did not allow the temperature to be increased dramatically, since temperatures above 120 °C led to a cleavage of TMS groups.

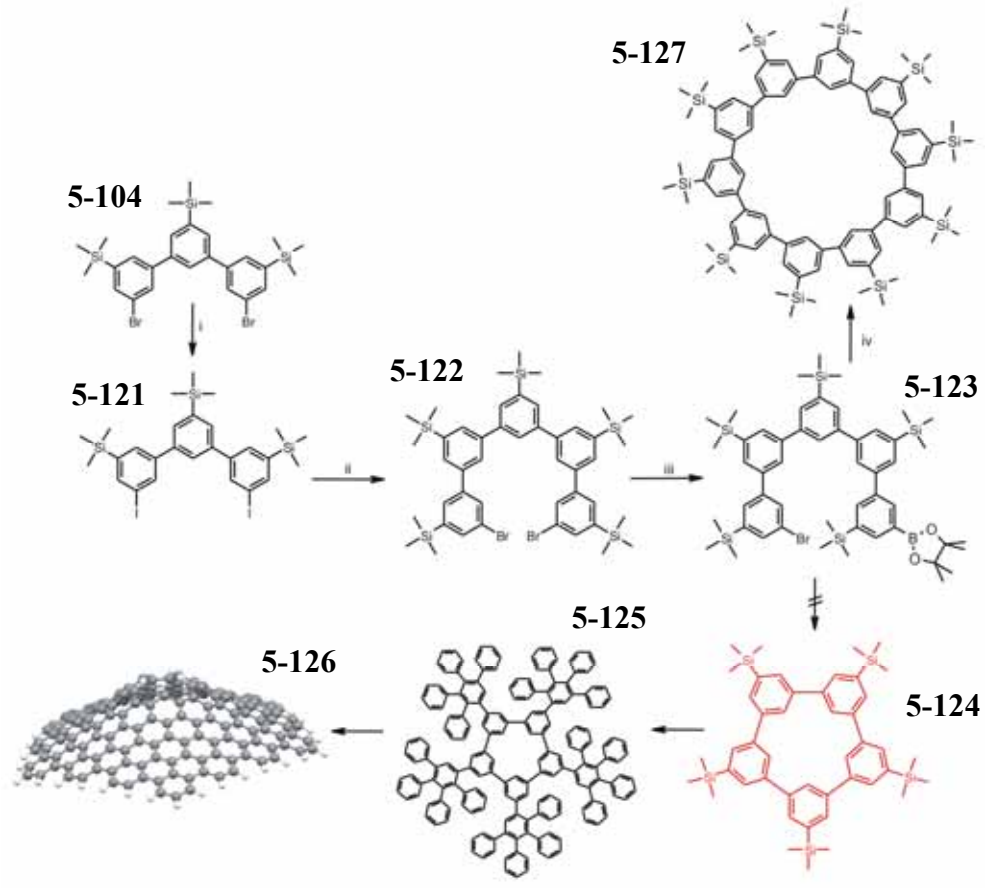

Scheme 5-31: *i) n-BuLi, I_2, 86%; ii)* **5-103***, K_2CO_3, $Pd(PPh_3)_4$, 85%; iii) bis(pinacolato)diboron, KOAc, $Cl_2Pd(dppf)$, 44%; iv) K_2CO_3, $Pd(PPh_3)_4$, 44%.*

Interestingly, the "undesired" cyclodeca-*m*-phenylene **5-127** was formed in surprisingly high yields in almost all cyclization attempts (up to 44%). After column chromatographical isolation from the complex product mixtures, the material was crystallized and the structure analyzed by single-crystal X-ray diffractometry. Although the structure could not be fully resolved yet, the large macrocycle organized analogous to cyclodecane in the same "chair" conformation as depicted in Figure 5-86.[176,177] The analogous unsubstituted macrocycle was obtained in low yields by H. STAAB et. al already in 1967.[178]

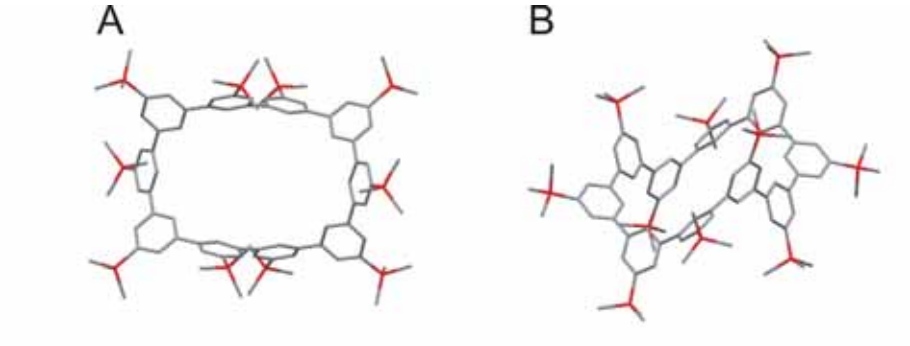

Figure 5-86: *Crystal structure of* **5-127** *(A) top view and (B) side view; silicon atoms are in red, carbon in grey, hydrogen atoms omitted for clarity.*

The described example emphasized the challenge to synthesize non-planar extended PAHs. Unfortunately, I was not able to obtain the desired intermediate to test the cyclodehydrogenation after the dendronization.

5.8.5 Softlanding

The development of novel methods for depositing organic macromolecules or biomolecules such as proteins, nucleotides, antibodies etc. on specific surfaces with high purity and preservation of the structure is of increasing importance for future applications.[179] G.R. COOKS proposed already 1977 the soft-landing concept which focused mainly on studies of modified surfaces by mass selected inorganic cluster.[180,181]

The mass spectrometry subgroup of J. RÄDER acquired valuable know-how to perform softlanding experiments of extended PAH molecules using MALDI as a pulsed technique and the soldi-state preparation method. As already mentioned the synthesis towards large, extended and insoluble PAHs lacks of purification methods. Sublimation of PAHs with more than 60 carbon atoms has not been successful since the existing vacuum systems do not reach low enough pressures. Besides a surface modification, the softlanding technique provides a valuable purification of materials, since the molecules can be deposited with a single isotope consistency. The deposition of electronically suitable molecules opens a unique possibility to fabricate electronic devices such as FETs.

5-128

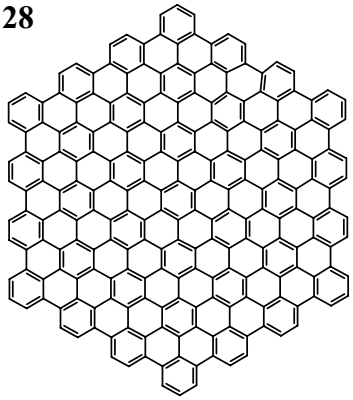

Figure 5-87: *Chemical structure of C222.*

For this purpose, the published synthesis of the 222 carbon containing PAH **5-128** (Figure 5-87) was repeated and improved. Analogous to the hole-containing PAH **5-110** with 216 aromatic carbon atoms, the SCHOLL reaction was performed with dichloromethane saturated argon gas bubbling through the reaction solution. This change allowed the chlorination side reaction to be almost completely suppressed. The MALDI-TOF spectrum using the solid-state preparation revealed the successful planarization (not shown). Analogously to the previous described PAH **5-110**, solid-state NMR experiments indicated the presence of partially fused side-products, which were not detected by MALDI-TOF. Quantification of the amount of impurities was also in this case very difficult due to different relaxation behaviors of partially and completely fused species. Nevertheless, softlanding opened a unique possibility to purify and to process the insoluble material into films with organized molecules.

The material was subjected to MALDI based softlanding experiments which have been performed by A. ROUHANIPOUR. The ionized molecules were decelerated and landed on HOPG and the resulting morphology was investigated with AFM.

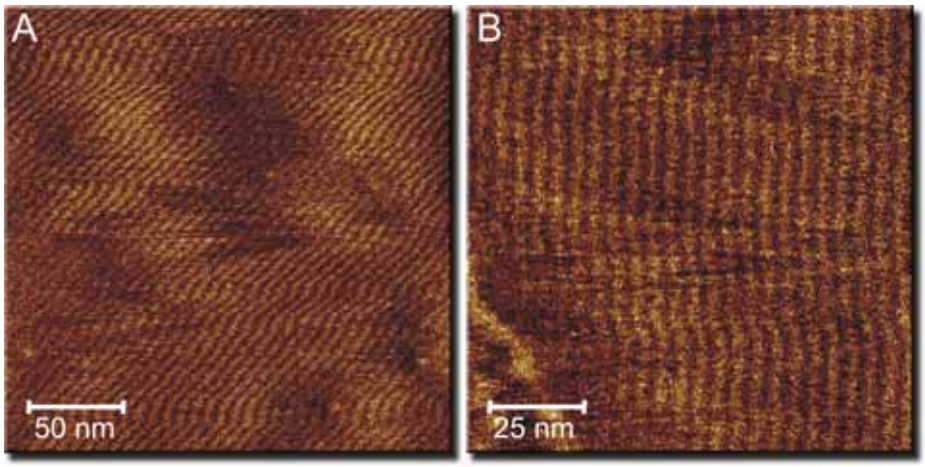

Figure 5-88: *Topographical AFM images of soft-landed C222* **5-128** *onto HOPG.*

Very astonishingly, the large PAH molecules organized into large columnar superstructures with an edge-on orientation (Figure 5-88). This behavior is not fully understood, since PAHs usually deposited face-on onto HOPG (i.e. in sublimation).

Currently, the fabrication of a top-down built FET using the deposited and purified material is conducted to gain an impression into the device performance of the usually unprocessable, extended PAHs. In parallel, the deposition of C216 **5-110** is optimized to possibly compare device properties and the influence of the hole within the aromatic structure.

5.9 Summary

Theoretically, two main approaches are possible to influence the HOMO and LUMO levels of PAHs. In the past, the extension of the aromatic π-area led to different all-hydrocarbon chromophores which showed a substantially bathochromically shifted UV/vis response compared to their smaller counterparts. However, the increasing size of the PAHs caused difficulties to process the material due to the even more pronounced tendency to self-associate, which rendered most of these materials insoluble in common organic solvents. The second approach, which has only theoretically been discussed, is the change of the nature of the periphery. The introduction of "zigzag" sites was theoretically predicted to lower the energy gap and to lead to a higher chemical reactivity, which would allow to functionalize the PAH *a posteriori*. To synthetically achieve the change of the periphery, different precursors for the SCHOLL planarization reaction have been made, which incorporated for the first time PAH units. Interestingly, the attempted cyclodehydrogenation reaction were successful, leading to different, extended PAHs, which contained a partial "zigzag" sites in their perimeters. All these compounds could be decorated with solubilizing linear alkyl chains, which allowed the complete chemical characterization in solution to be performed. The electronic spectroscopy emphasized the influence of the introduced "zigzag" sites and thus the symmetry of the aromatic system. Quantum chemical calculation supported the analysis of the experimental spectra. Expectedly, all alkyl substituted derivatives exhibited a discotic behavior and a pronounced self-association behavior in solution whereby the substitution pattern of the alkyl chains influenced the stability, crystallinity and self-organization to a great extent. STM images of some of these novel PAHs have been obtained by either UHV deposition or by self-assembly at the solid-liquid interface on HOPG. Unlike the smaller PAHs, the extended derivatives did not allow the "zigzag" sites to be imaged, because of a weaker electron polarization towards the "zigzag" edges.

Unfortunately, the predicted *a posteriori* functionalization of the "zigzag" sites was only successful for TBO, where the oxidation to the diketone structure could be accomplished in poor yields. As a new concept, a five membered ring was formally introduced into one "arm-chair" site of HBC, which allowed the chemical modification to be conducted in good yields. However, the poor solubility of the *n*-dodecyl derivatives was in many cases not sufficient to purify the PAHs.

Finally, the nature of the aromatic core was changed by creating an artificial defect structure, which can be considered as a model for SCHOTTKY defects in graphite. Using a macrocyclic precursor for the SCHOLL cyclodehydrogenation, a 216 carbon atom containing PAH was obtained, which carried a hole in the centre. However, the problems, which D. WASSERFALLEN experienced during the cyclodehydrogenation towards larger PAHs caused also in this case problems. Although the analytical techniques are limited to prove the purity of such insoluble materials, partially closed intermediates were still present and could not be separated. A potential purification and processing promised the in the MÜLLEN group established softlanding technique, which allowed large PAHs to be isolated in their pure state. A 222 carbon containing, giant PAH was purified and deposited onto HOPG using this technique. The deposition led to extended domains of edge-on arranged PAH molecules, which will be used as the semiconductor for thin-film FETs.

5.10 References

(1) Fetzer, J. C. *Org. Prep. Proced. Int.* **1989**, *21*, 47-65.

(2) Loening, K.; Merritt, J.; Later, D.; Wright, W. *Polynuclear Aromatic Hydrocarbons: Nomenclature Guide*; Batelle: Columbus, 1990.

(3) Simpson, C. D.; Brand, J. D.; Berresheim, A. J.; Przybilla, L.; Rader, H. J.; Müllen, K. *Chem. - Eur. J.* **2002**, *8*, 1424-1429.

(4) Clar, E. *The Aromatic Sextet*; Wiley: New York, 1972.

(5) Zander, M. *Handbook of Polycyclic Aromatic Hydrocarbons*; Marcel Dekker: New York, 1983.

(6) Hess, B. A.; Schaad, L. J. *J. Am. Chem. Soc.* **1971**, *93*, 305-&.

(7) Biermann, D.; Schmidt, W. *J. Am. Chem. Soc.* **1980**, *102*, 3173-3181.

(8) Dias, J. R. *Polycycl. Aromat. Comp.* **2005**, *25*, 113-127.

(9) Dias, J. R. *J. Chem. Inf. Model* **2005**, *45*, 562-571.

(10) Ruiz-Morales, Y. *J. Phys. Rev. A* **2002**, *106*, 11283-11308.

(11) Clar, E. *Polycyclic Hydrocarbons*; John Wiley and Sons: New York, 1964; Vol. 1+2.

(12) Klevens, H. B.; Platt, J. R. *J. Chem. Phys.* **1949**, *17*, 470-481.

(13) Par, R. G. *The Quantum Theory of Molecular Electronic Structure* New York, Amsterdam, 1963.

(14) Becker, R. *Theory and Interpretation of Fluorescence and Phosphorescence*; Wiley Interscience: New York, 1969.

(15) Clar, E. *Angew. Chem. Int. Ed.* **1956**, *68*, 528-528.

(16) Clar, E.; Kuhn, O. *Liebigs Ann.* **1956**, *601*, 181-192.

(17) Clar, E.; Ironside, C. T.; Zander, M. *J. Chem. Soc.* **1959**, 142-147.

(18) Clar, E.; Ironside, C. T. *Proc. R. Soc. London, Ser. A* **1958**, 150-150.

(19) Herzberg, G. *Molecular Spectra and Molecular Structure, III. Electronic Spectra and Electronic Structure of Polyatomic Molecules*; VNR: New York, 1966.

(20) Wu, J. S.; Qu, J. Q.; Tchebotareva, N.; Müllen, K. *Tetrahedron Lett.* **2005**, *46*, 1565-1568.

(21) Beier, J., Universität Bayreuth, 2001.

(22) Kasha, M. *Discussions of the Faraday Society* **1950**, 14-19.

(23) Kastler, M.; Pisula, W.; Wasserfallen, D.; Pakula, T.; Müllen, K. *J. Am. Chem. Soc.* **2005**, *127*, 4286-4296.

(24) Segade, A.; Castella, M.; Lopez-Calahorra, F.; Velasco, D. *Chem. Mater.* **2005**, *17*, 5366-5374.

(25) Kastler, M., Johannes Gutenberg Universität, 2002.

(26) Lemaur, V.; Da Silva Filho, D. A.; Coropceanu, V.; Lehmann, M.; Geerts, Y.; Piris, J.; Debije, M. G.; Van de Craats, A. M.; Senthilkumar, K.; Siebbeles, L. D. A.; Warman, J. M.; Bredas, J. L.; Cornil, J. *J. Am. Chem. Soc.* **2004**, *126*, 3271-3279.

(27) Adam, D.; Schuhmacher, P.; Simmerer, J.; Haussling, L.; Siemensmeyer, K.; Etzbach, K. H.; Ringsdorf, H.; Haarer, D. *Nature* **1994**, *371*, 141-143.

(28) Boden, N.; Bushby, R. J.; Clements, J.; Movaghar, B.; Donovan, K. J.; Kreouzis, T. *Phys. Lett. B* **1995**, *52*, 13274-13280.

(29) Lever, L. J.; Kelsall, R. W.; Bushby, R. J. *Phys. Rev. B* **2005**, *72*.

(30) Dötz, F.; Brand, J. D.; Ito, S.; Gherghel, L.; Müllen, K. *J. Am. Chem. Soc.* **2000**, *122*, 7707-7717.

(31) Watson, M. D.; Fechtenkötter, A.; Müllen, K. *Chem. Rev.* **2001**, *101*, 1267-1300.

(32) Debije, M. G.; Piris, J.; de Haas, M. P.; Warman, J. M.; Tomovic, Z.; Simpson, C. D.; Watson, M. D.; Müllen, K. *J. Am. Chem. Soc.* **2004**, *126*, 4641-4645.

(33) Tomovic, Z.; Watson, M. D.; Müllen, K. *Angew. Chem. Int. Ed.* **2004**, *43*, 755-758.

(34) Simpson, C. D.; Brand, J. D.; Berresheim, A. J.; Przybilla, L.; Rader, H. J.; Mullen, K. *Chemistry-a European Journal* **2002**, *8*, 1424-1429.

(35) Müller, M.; Kubel, C.; Müllen, K. *Chem. - Eur. J.* **1998**, *4*, 2099-2109.

(36) Wasserfallen, D.; Kastler, M.; Müllen, K. 2006.

(37) Wasserfallen, D.; Kastler, M.; Pisula, W.; Fogel, Y.; Wang, Z.; Müllen, K. 2005.

(38) Kobayashi, Y.; Fukui, K.; Enoki, T.; Kusakabe, K.; Kaburagi, Y. *Phys. Rev. B* **2005**, *71*.

(39) Stein, S. E.; Brown, R. L. *J. Am. Chem. Soc.* **1987**, *109*, 3721-3729.

(40) Müller, M.; Kübel, C.; Morgenroth, F.; Iyer, V. S.; Müllen, K. *Carbon* **1998**, *36*, 827-831.

(41) Young, E. R. R.; Funk, R. L. *J. Org. Chem.* **1998**, *63*, 9995-9996.

(42) Marchand, A. P.; Srinivas, G.; Watson, W. H. *Arkivoc* **2003**, 8-15.

(43) Abramovitch, R. A. *Org. Prep. Proced. Int.* **1991**, *23*, 685-711.

(44) Przybilla, L.; Brand, J. D.; Yoshimura, K.; Räder, H. J.; Müllen, K. *Anal. Chem.* **2000**, *72*, 4591-4597.

(45) Yoshimura, K.; Przybilla, L.; Ito, S. J.; Brand, J. D.; Wehmeir, M.; Räder, H. J.; Müllen, K. *Macromol. Chem. Physic.* **2001**, *202*, 215-222.

(46) Wang, Z. H.; Tomovic, E.; Kastler, M.; Pretsch, R.; Negri, F.; Enkelmann, V.; Müllen, K. *J. Am. Chem. Soc.* **2004**, *126*, 7794-7795.

(47) Schlicke, B.; Frahn, J.; Schluter, A. D. *Synth. Met.* **1996**, *83*, 173-176.

(48) Wasserfallen, D., Johannes Gutenberg Universität, 2006.

(49) Fürstner, A.; Mamane, V. *J. Org. Chem.* **2002**, *67*, 6264-6267.

(50) Mamane, V.; Hannen, P.; Furstner, A. *Chem. - Eur. J.* **2004**, *10*, 4556-4575.

(51) Kleinpeter, E.; Klod, S. *J. Am. Chem. Soc.* **2004**, *126*, 2231-2236.

(52) Mallory, F. B.; Baker, M. B. *J. Org. Chem.* **1984**, *49*, 1323-1326.

(53) Marshall, K.; Rothchild, R. *Spectrosc. Lett.* **2004**, *37*, 469-492.

(54) Ramirez, O.; Tokhunts, R.; Rothchild, R. *Spectrosc. Lett.* **2004**, *37*, 421-436.

(55) Newman, M. S.; Patrick, T. B.; Darlak, R. S.; Zuech, E. A. *J. Org. Chem.* **1969**, *34*, 1904-&.

(56) Merschaert, A.; Gorissen, H. J. *Heterocycles* **2003**, *60*, 29-45.

(57) Hensel, V.; Schluter, A. D. *Eur. J. Org. Chem.* **1999**, 451-458.

(58) Miwa, K.; Aoyama, T.; Shioiri, T. *Synlett* **1994**, 107-108.

(59) Herwig, P. T.; Enkelmann, V.; Schmelz, O.; Müllen, K. *Chem. - Eur. J.* **2000**, *6*, 1834-1839.

(60) Morikawa, T.; Narita, S.; Klein, D. J. *J. Chem. Inf. Model* **2004**, *44*, 1891-1896.

(61) Morikawa, T.; Narita, S.; Klein, D. J. *Polycycl. Aromat. Comp.* **2004**, *24*, 195-206.

(62) Ito, S.; Wehmeier, M.; Brand, J. D.; Kübel, C.; Epsch, R.; Rabe, J. P.; Müllen, K. *Chem. - Eur. J.* **2000**, *6*, 4327-4342.

(63) Vollhardt, K. P. C. *Acc. Chem. Res.* **1977**, *10*, 1-8.

(64) Schore, N. E. *Chem. Rev.* **1988**, *88*, 1081-1119.

(65) Wu, J., Johannes Gutenberg Universität, 2004.

(66) Diederich, F.; Stang, J. P. *Metal-catalyzed Cross-coupling Reactions*; Wiley-VCH: Weinheim, Berlin, New York, Chichester, Brisbane, Singapore, Toronto, 1998.

(67) Fu, J. M.; Snieckus, V. *Can. J. Chem.* **2000**, *78*, 905-919.

(68) Gutman, I.; Cyvin, S. J.; Ivanov-Petrovic, V. *Z. Naturforsch. A* **1998**, *53*, 699-703.

(69) Disch, R. L.; Schulman, J. M.; Peck, R. C. *J. Phys. Chem.* **1992**, *96*, 3998-4002.

(70) Gong, L. Z.; Hu, Q. S.; Pu, L. *J. Org. Chem.* **2001**, *66*, 2358-2367.

(71) Wehmeier, M.; Wagner, M.; Müllen, K. *Chem. - Eur. J.* **2001**, *7*, 2197-2205.

(72) Schmidt-Mende, L.; Fechtenkötter, A.; Müllen, K.; Moons, E.; Friend, R. H.; MacKenzie, J. D. *Science* **2001**, *293*, 1119-1122.

(73) Hoeben, F. J. M.; Jonkheijm, P.; Meijer, E. W.; Schenning, A. *Chem. Rev.* **2005**, *105*, 1491-1546.

(74) Jin, W.; Fukushima, T.; Kosaka, A.; Niki, M.; Ishii, N.; Aida, T. *J. Am. Chem. Soc.* **2005**, *127*, 8284-8285.

(75) Xiao, S. X.; Myers, M.; Miao, Q.; Sanaur, S.; Pang, K. L.; Steigerwald, M. L.; Nuckolls, C. *Angew. Chem. Int. Ed.* **2005**, *44*, 7390-7394.

(76) Shklyarevskiy, I. O.; Jonkheijm, P.; Stutzmann, N.; Wasserberg, D.; Wondergem, H. J.; Christianen, P. C. M.; Schenning, A.; de Leeuw, D. M.; Tomovic, Z.; Wu, J. S.; Müllen, K.; Maan, J. C. *J. Am. Chem. Soc.* **2005**, *127*, 16233-16237.

(77) Levitsky, I. A.; Euler, W. B.; Tokranova, N.; Xu, B.; Castracane, J. *Appl. Phys. Lett.* **2004**, *85*, 6245-6247.

(78) Schmidt-Mende, L.; Watson, M.; Müllen, K.; Friend, R. H. *Mol. Cryst. Liq. Cryst.* **2003**, *396*, 73-90.

(79) Piris, J.; Debije, M. G.; Stutzmann, N.; van de Craats, A. M.; Watson, M. D.; Müllen, K.; Warman, J. M. *Adv. Mater.* **2003**, *15*, 1736-+.

(80) Pisula, W.; Tomovic, Z.; Simpson, C.; Kastler, M.; Pakula, T.; Müllen, K. *Chem. Mater.* **2005**, *17*, 4296-4303.

(81) Brabec, C. J.; Sariciftci, N. S.; Hummelen, J. C. *Adv. Funct. Mater.* **2001**, *11*, 15-26.

(82) Kubowicz, S.; Pietsch, U.; Watson, M. D.; Tchebotareva, N.; Müllen, K.; Thunemann, A. F. *Langmuir* **2003**, *19*, 5036-5041.

(83) Reitzel, N.; Hassenkam, T.; Balashev, K.; Jensen, T. R.; Howes, P. B.; Kjaer, K.; Fechtenkötter, A.; Tchebotareva, N.; Ito, S.; Müllen, K.; Bjornholm, T. *Chem. - Eur. J.* **2001**, *7*, 4894-4901.

(84) Günther, C.; Karl, N.; Pflaum, J.; Strohmaier, R.; Gompf, B.; Eisenmenger, W.; Müller, M.; Müllen, K. *Langmuir* **2005**, *21*, 656-665.

(85) Ruffieux, P.; Gröning, O.; Bielmann, M.; Simpson, C.; Müllen, K.; Schlapbach, L.; Gröning, P. *Phys. Rev. B* **2002**, *66*.

(86) Piot, L.; Marchenko, A.; Wu, J. S.; Müllen, K.; Fichou, D. *J. Am. Chem. Soc.* **2005**, *127*, 16245-16250.

(87) Jäckel, F.; Ai, M.; Wu, J. S.; Müllen, K.; Rabe, J. P. *J. Am. Chem. Soc.* **2005**, *127*, 14580-14581.

(88) Watson, M. D.; Jäckel, F.; Severin, N.; Rabe, J. P.; Müllen, K. *J. Am. Chem. Soc.* **2004**, *126*, 1402-1407.

(89) Sellam, F.; Schmitz-Hubsch, T.; Toerker, M.; Mannsfeld, S.; Proehl, H.; Fritz, T.; Leo, K.; Simpson, C.; Müllen, K. *Surf. Sci.* **2001**, *478*, 113-121.

(90) Delamarche, E.; Michel, B.; Biebuyck, H. A.; Gerber, C. *Adv. Mater.* **1996**, *8*, 719-&.

(91) Delamarche, E.; Michel, B. *Thin Solid Films* **1996**, *273*, 54-60.

(92) Rabe, J. P.; Buchholz, S. *Science* **1991**, *253*, 424-427.

(93) Yazdani, A.; Lieber, C. M. *Nature* **1999**, *401*, 227-230.

(94) Gimzewski, J. K.; Joachim, C. *Science* **1999**, *283*, 1683-1688.

(95) Jung, T. A.; Schlittler, R. R.; Gimzewski, J. K.; Tang, H.; Joachim, C. *Science* **1996**, *271*, 181-184.

(96) Abdel-Mottaleb, M. M. S.; De Feyter, S.; Gesquiere, A.; Sieffert, M.; Klapper, M.; Müllen, K.; De Schryver, F. C. *Nano Lett.* **2001**, *1*, 353-359.

(97) Heinz, R.; Stabel, A.; Rabe, J. P.; Wegner, G.; Deschryver, F. C.; Corens, D.; Dehaen, W.; Suling, C. *Angew. Chem. Int. Ed.* **1994**, *33*, 2080-2083.

(98) Uji-i, H.; Miura, A.; Schenning, A.; Meijer, E. W.; Chen, Z. J.; Wurthner, F.; De Schryver, F. C.; Van der Auweraer, M.; De Feyter, S. *Chemphyschem* **2005**, *6*, 2389-2395.

(99) Gross, L.; Moresco, F.; Ruffieux, P.; Gourdon, A.; Joachim, C.; Rieder, K. H. *Phys. Rev. B* **2005**, *71*.

(100) Karl, N.; Günther, C. *Cryst. Res. Technol.* **1999**, *34*, 243-254.

(101) Kitagawa, S.; Kitaura, R.; Noro, S. *Angew. Chem. Int. Ed.* **2004**, *43*, 2334-2375.

(102) Joachim, C.; Gimzewski, J. K.; Aviram, A. *Nature* **2000**, *408*, 541-548.

(103) Maruccio, G.; Cingolani, R.; Rinaldi, R. *J. Mater. Chem.* **2004**, *14*, 542-554.

(104) Nitzan, A.; Ratner, M. A. *Science* **2003**, *300*, 1384-1389.

(105) Carroll, R. L.; Gorman, C. B. *Angew. Chem. Int. Ed.* **2002**, *41*, 4379-4400.

(106) Desiraju, G. R. *Angew. Chem. Int. Ed.* **1995**, *34*, 2311-2327.

(107) Harvey, R. G. *Polycyclic Aromatic Hydrocarbons*; Wiley-VCH: New York, Chichester, Weinheim, Brisbane, Singapore, Toronto, 1997.

(108) Fechtenkötter, A.; Tchebotareva, N.; Watson, M.; Müllen, K. *Tetrahedron* **2001**, *57*, 3769-3783.

(109) Newman, M. S.; Blum, J. *Israel J. Chem.* **1964**, *2*, 301-&.

(110) Rodriguez, D.; Martinez-Esperon, M. F.; Navarro-Vazquez, A.; Castedo, L.; Dominguez, D.; Saa, C. *J. Org. Chem.* **2004**, *69*, 3842-3848.

(111) Pisula, W., Johannes Gutenberg Universität 2005.

(112) Bushby, R. J.; Boden, N.; Kilner, C. A.; Lozman, O. R.; Lu, Z. B.; Liu, Q. Y.; Thornton-Pett, M. A. *J. Mater. Chem.* **2003**, *13*, 470-474.

(113) Praefcke, K.; Eckert, A.; Blunk, D. *Liq. Cryst.* **1997**, *22*, 757-757.

(114) Pisula, W.; Kastler, M.; Wasserfallen, D.; Pakula, T.; Müllen, K. *J. Am. Chem. Soc.* **2004**, *126*, 8074-8075.

(115) Bernhardt, S.; Baumgarten, M.; Wagner, M.; Müllen, K. *J. Am. Chem. Soc.* **2005**, *127*, 12392-12399.

(116) Müller, S., Johannes Gutenberg Universität, 2006.

(117) Fu, P. P.; Lee, H. M.; Harvey, R. G. *J. Org. Chem.* **1980**, *45*, 2797-2803.

(118) Lee, H.; Harvey, R. G. *J. Org. Chem.* **1986**, *51*, 2847-2848.

(119) Mio, M. J.; Kopel, L. C.; Braun, J. B.; Gadzikwa, T. L.; Hull, K. L.; Brisbois, R. G.; Markworth, C. J.; Grieco, P. A. *Org. Lett.* **2002**, *4*, 3199-3202.

(120) Atamny, F.; Baiker, A.; Schlogl, R. *Fresen. J. Anal. Chem.* **1997**, *358*, 344-348.

(121) Osing, J.; Shvets, I. V. *Surf. Sci.* **1998**, *417*, 145-150.

(122) Henschke, B.; Schubert, H.; Blocker, J.; Atamny, F.; Schlogl, R. *Thermochim. Acta* **1994**, *234*, 53-83.

(123) Baranovsky, R. E.; Eltsov, K. N.; Elesin, V. F.; Suvorov, A. L.; Shevlyuga, V. M.; Yurov, V. Y. *Phys. Low -Dimens. Str.* **1999**, *5-6*, 161-168.

(124) Stone, A. J.; Wales, D. J. *Chem. Phys. Lett.* **1986**, *128*, 501-503.

(125) Krasheninnikov, A. V.; Nordlund, K.; Sirvio, M.; Salonen, E.; Keinonen, J. *Phys. Rev. B* **2001**, *6324*.

(126) Krasheninnikov, A. V.; Nordlund, K.; Lehtinen, P. O.; Foster, A. S.; Ayuela, A.; Nieminen, R. M. *Phys. Rev. B* **2004**, *69*.

(127) Telling, R. H.; Ewels, C. P.; El-Barbary, A. A.; Heggie, M. I. *Nature Materials* **2003**, *2*, 333-337.

(128) Ewels, C. P.; Telling, R. H.; El-Barbary, A. A.; Heggie, M. I.; Briddon, P. R. *Phys. Rev. Lett.* **2003**, *91*.

(129) Nordlund, K.; Keinonen, J.; Mattila, T. *Phys. Rev. Lett.* **1996**, *77*, 699-702.

(130) Ewels, C. P.; Heggie, M. I.; Briddon, P. R. *Chem. Phys. Lett.* **2002**, *351*, 178-182.

(131) Hansson, A.; Paulsson, M.; Stafstrom, S. *Phys. Rev. B* **2000**, *62*, 7639-7644.

(132) Hashimoto, A.; Suenaga, K.; Gloter, A.; Urita, K.; Iijima, S. *Nature* **2004**, *430*, 870-873.

(133) Staab, H. A.; Binnig, F. *Tetrahedron Lett.* **1964**, 319-321.

(134) Wu, J. H.; Watson, M. D.; Müllen, K. *Angew. Chem. Int. Ed.* **2003**, *42*, 5329-5333.

(135) Wu, J. S.; Watson, M. D.; Zhang, L.; Wang, Z. H.; Müllen, K. *J. Am. Chem. Soc.* **2004**, *126*, 177-186.

(136) Bernhardt, S., Johannes Gutenberg Universität, 2006.

(137) Simpson, C. D., Johannes Gutenberg Universität, 2003.

(138) Wasserfallen, D.; Kastler, M.; Pisula, W.; Fogel, Y.; Wang, Z.; Müllen, K. *J. Am. Chem. Soc.* **2006**, *in press*.

(139) Eddaoudi, M.; Kim, J.; Rosi, N.; Vodak, D.; Wachter, J.; O'Keefe, M.; Yaghi, O. M. *Science* **2002**, *295*, 469-472.

(140) Endo, K.; Sawaki, T.; Koyanagi, M.; Kobayashi, K.; Masuda, H.; Aoyama, Y. *J. Am. Chem. Soc.* **1995**, *117*, 8341-8352.

(141) Reineke, T. M.; Eddaoudi, M.; Fehr, M.; Kelley, D.; Yaghi, O. M. *J. Am. Chem. Soc.* **1999**, *121*, 1651-1657.

(142) Aakeroy, C. B.; Beatty, A. M.; Leinen, D. S. *Angew. Chem. Int. Ed.* **1999**, *38*, 1815-1819.

(143) Rosi, N. L.; Eckert, J.; Eddaoudi, M.; Vodak, D. T.; Kim, J.; O'Keeffe, M.; Yaghi, O. M. *Science* **2003**, *300*, 1127-1129.

(144) Sato, K.; Noguchi, M.; Demachi, A.; Oki, N.; Endo, M. *Science* **1994**, *264*, 556-558.

(145) Schlapbach, L.; Zuttel, A. *Nature* **2001**, *414*, 353-358.

(146) Baughman, R. H.; Zakhidov, A. A.; de Heer, W. A. *Science* **2002**, *297*, 787-792.

(147) Grimsdale, A. C.; Wu, J. S.; Müllen, K. *Chem. Comm.* **2005**, 2197-2204.

(148) Renouard, T.; Gherghel, L.; Wachtler, M.; Bonino, F.; Scrosati, B.; Nuffer, R.; Mathis, C.; Müllen, K. *J. Power. Sources* **2005**, *139*, 242-249.

(149) Lehn, J.-M. *Supramolecular Chemistry - Concepts and Perspectives*; Wiley-VCH: Weinheim, 1995.

(150) Zhang, S. G. *Biotechnol. Adv.* **2002**, *20*, 321-339.

(151) Ranganathan, D.; Lakshmi, C.; Karle, I. L. *J. Am. Chem. Soc.* **1999**, *121*, 6103-6107.

(152) Johnson, M. R.; Parlinski, K.; Natkaniec, I.; Hudson, B. S. *Chem. Phys.* **2003**, *291*, 53-60.

(153) Hollingsworth, M. D.; Harris, K. D. M. *Comprehensive Supramolecular Chemistry, Solid State Supramolecular Chemistry: Crystal Engeneering Vol. 6*; Pergamon: New York, 1996.

(154) Höger, S.; Bonrad, K.; Mourran, A.; Beginn, U.; Möller, M. *J. Am. Chem. Soc.* **2001**, *123*, 5651-5659.

(155) Höger, S.; Bonrad, K.; Rosselli, S.; Ramminger, A. D.; Wagner, T.; Silier, B.; Wiegand, S.; Haussler, W.; Lieser, G.; Scheumann, V. *Macromol. Symp.* **2002**, *177*, 185-191.

(156) Tobe, Y.; Utsumi, N.; Kawabata, K.; Nagano, A.; Adachi, K.; Araki, S.; Sonoda, M.; Hirose, K.; Naemura, K. *J. Am. Chem. Soc.* **2002**, *124*, 5350-5364.

(157) Zhao, D. H.; Moore, J. S. *J. Org. Chem.* **2002**, *67*, 3548-3554.

(158) Zhao, D. H.; Moore, J. S. *Chem. Comm.* **2003**, 807-818.

(159) Martin, R. B. *Chem. Rev.* **1996**, *96*, 3043-3064.

(160) Lahiri, S.; Thompson, J. L.; Moore, J. S. *J. Am. Chem. Soc.* **2000**, *122*, 11315-11319.

(161) Nelson, J. C.; Saven, J. G.; Moore, J. S.; Wolynes, P. G. *Science* **1997**, *277*, 1793-1796.

(162) van de Craats, A. M.; Warman, J. M.; Fechtenkötter, A.; Brand, J. D.; Harbison, M. A.; Müllen, K. *Adv. Mater.* **1999**, *11*, 1469-1472.

(163) Höger, S.; Cheng, X. H.; Ramminger, A. D.; Enkelmann, V.; Rapp, A.; Mondeshki, M.; Schnell, I. *Angew. Chem. Int. Ed.* **2005**, *44*, 2801-2805.

(164) Höger, S. *Chem. - Eur. J.* **2004**, *10*, 1320-1329.

(165) Moore, J. S. *Acc. Chem. Res.* **1997**, *30*, 402-413.

(166) Meier, H. *Synthesis* **2002**, 1213-1228.

(167) Meier, H.; Schnorpfeil, C.; Fetten, M.; Hinneschiedt, S. *Eur. J. Org. Chem.* **2002**, 537-542.

(168) Wiberg, K. B. *Angew. Chem. Int. Ed.* **1986**, *25*, 312-322.

(169) Poater, J.; Fradera, X.; Duran, M.; Sola, M. *Chem. - Eur. J.* **2003**, *9*, 1113-1122.

(170) Kroto, H. W.; Heath, J. R.; Obrien, S. C.; Curl, R. F.; Smalley, R. E. *Nature* **1985**, *318*, 162-163.

(171) Janata, J.; Gendell, J.; Ling, C. Y.; Barth, W.; Backes, L.; Mark, H. B.; Lawton, R. G. *J. Am. Chem. Soc.* **1967**, *89*, 3056-&.

(172) Scott, L. T.; Cheng, P. C.; Hashemi, M. M.; Bratcher, M. S.; Meyer, D. T.; Warren, H. B. *J. Am. Chem. Soc.* **1997**, *119*, 10963-10968.

(173) Lovinger, A. J.; Nuckolls, C.; Katz, T. J. *J. Am. Chem. Soc.* **1998**, *120*, 1944-1944.

(174) Wang, Z. H.; Dotz, F.; Enkelmann, V.; Müllen, K. *Angew. Chem. Int. Ed.* **2005**, *44*, 1247-1250.

(175) Hagen, S.; Bratcher, M. S.; Erickson, M. S.; Zimmermann, G.; Scott, L. T. *Angew. Chem. Int. Ed.* **1997**, *36*, 406-408.

(176) Shenhav, H.; Schaeffer, R. *Cryst. Struct. Commun.* **1981**, *10*, 1181-1182.

(177) Wiberg, K. B. *J. Org. Chem.* **2003**, *68*, 9322-9329.

(178) Staab, H. A.; Binnig, F. *Chem. Ber. Recl.* **1967**, *100*, 889-&.

(179) Yang, X.; Räder, H. J.; Rouhanipour, A.; Müllen, K. *Eur. J. Org. Chem.* **2005**, *11*, 287-293.

(180) Heiz, U.; Sanchez, A.; Abbet, S.; Schneider, W. D. *J. Am. Chem. Soc.* **1999**, *121*, 3214-3217.

(181) Tsekouras, A. A.; Iedema, M. J.; Cowin, J. P. *J. Chem. Phys.* **1999**, *111*, 2222-2234.

6 Conclusion and Outlook

The modulation of the pronounced aggregation propensity of alkyl substituted hexa-*peri*-hexabenzocoronenes has been achieved by a reduction of the intermolecular attractive forces. Sterically demanding branched, racemic alkyl chains, with the branching site in close proximity to the aromatic core, have been introduced in a synthetically straight forward fashion. Figure 6-1 illustrates the space-fillingness of the flexible peripheral substituents on these novel HBC derivatives.

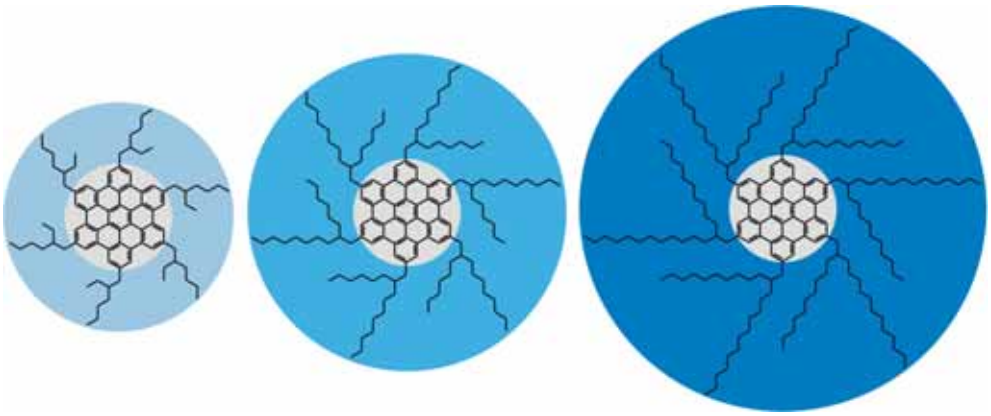

Figure 6-1: *Novel branched alkyl substituted HBCs, shielding of the aromatic core due to the flexible insulating alkyl periphery.*

The reduction of the aromatic π-stacking interactions, which has been elucidated by solution NMR and electronic spectroscopy, dramatically improved the solubility, which is qualitatively around a factor of 1000 times better for the derivative with the longest branched chain **3-13c** than for the *n*-dodecyl substituted derivative **3-3a**. This allowed a better purification by means of preparative column chromatography to obtain better purities for the application in organic electronics. Another striking feature is the ability to melt the HBC derivatives with the bulkiest side chains at temperatures, which are below the thermal decomposition threshold. This opened the possibility to apply cheap melt-processing, such as zone-crystallization to obtain uniaxially organized molecules over macroscopical areas. The melt-processing is believed to further refine the material to even yield higher purities. HBC-$C_{6,2}$ **3-13a** gave well organized film with edge-on orientation applying a solution-dipping method.

Depending on the steric demand excerted by the side-chain, different molecular orientations with respect to the support have been achieved, which is very important

for the successful implementation in electronic devices, which require different orientations of the charge carrier pathways. In general, the discotic materials organize edge-on when processed from solution and face-on from the molten state. Supported by different model systems, if the steric demand of the side-chain is very high, a face-on approaching onto the surface is prohibited – the materials always organized face-on as observed for HBC-$C_{14,10}$ **3-13c**. These are the first important insights, how the formation of face-on alignment and therefore homeotropic phases occurs, which is fundamental to organize discotic materials on surfaces.

Another important requirement for the implementation of materials into organic electronic devices is a high charge carrier mobility to allow an unperturbed migration in a device structure. Time-resolved pulse-radiolysis microwave conductivity (TR-PRMC) measurements revealed good charge carrier mobilities for the novel materials together with very long charge carrier life-times. This was explained by the insulation of the "conducting" columns by the space-filling alkyl surrounding, suppressing the charge carrier recombination. Preliminary results from the time-of-flight (TOF) experiments, to determine the macroscopical charge carrier mobility for HBC-$C_{10,6}$ **3-13b**, which adopted a highly ordered "pseudo"-homeotropic organization from the isotropic state, emphasized the potential of the material.

Implemented in organic heterojunction photovoltaics together with a perylenedi-carboxiimid derivative as acceptor, good performing devices were obtained. However, the large amount of alkyl component "reduced" the chromophore concentration and fewer photons were absorbed. Furthermore, at the interface between the donor and acceptor the polarization of generated excitons might be hampered, due to the large amount of insulating alkyl chains.

Motivated by the result that the flexible alkyl surrounding around the HBC allows molecular and supramolecular properties to be controlled, the synthetic approach had to be optimized and shortened to obtain quicker differently substituted derivatives.

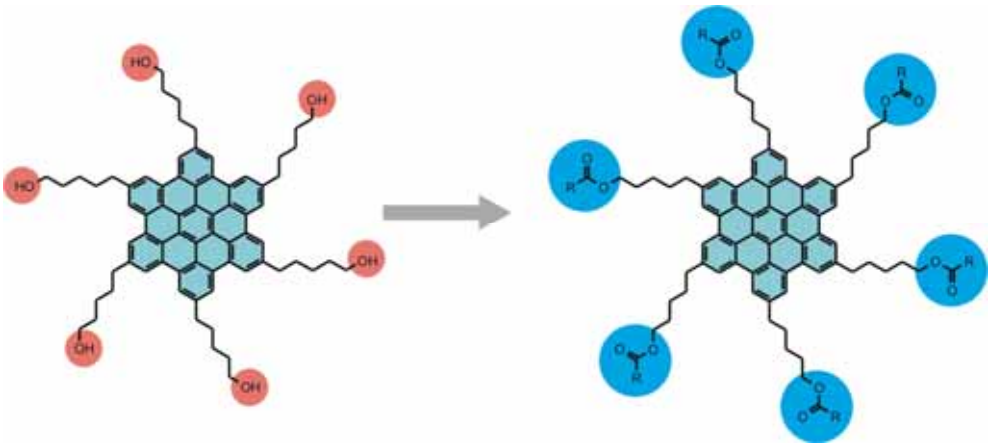

Figure 6-2: *Simple 1-step peripheral functionalization of universal building block HBC-C_5OH* **4-12** *to different ester functionalized HBCs.*

The hexa-hydroxy substituted HBC-C_5OH **4-12** and HBC-C_8OH **4-17** have been therefore synthesized on multi-gram scale which permit a quantitative one-step functionalization of all six reactive groups (Figure 6-2). For example, different branched alkyl chains were introduced by different esterification methodologies. Analogous to HBC derivatives with a much more tedious synthesis, both HBC-C_5-$C_{6,2}$ **4-25** and HBC-C_5-$C_{10,6}$ **4-26** established a well organized homeotropic phase, when cooled from the isotropic melt, which is ideal to test the material as charge injection layers in organic light emitting diodes (LED) or as active component in photovoltaics. Preliminary TOF and impedance spectroscopy experiments revealed very high charge carrier mobilities, which thus can barely be detected with our system.

Other functions, such as donor, acceptor or cross-linkable moieties have been introduced in a straight forward fashion. Peripheral acrylate groups allow a fixation of an established organization either by photons or heat as external stimuli. Uniaxially organization and nanostructuring of this electronically interesting material have been performed, opening novel possibilities for applications.

Functionalization of the peripheral side chains in the terminal position has been accomplished by the esterification of hydroxy groups. However, the introduction of functionalities which are in direct conjugation or directly attached to the aromatic core required new concepts. The fluorene-containing CPHBC$(C_{12})_4$ **5-80** and the fluorenone-containing CPHBCCO$(C_{12})_4$ **5-81** offer the derivatization of the HBC part (Figure 6-3). However, the attached *n*-dodecyl alkyl chains did not guarantee enough solubility to purify the desired products after the conversions. This can easily be

solved in the future by introducing alkyl chains which reduce the intermolecular aggregation.

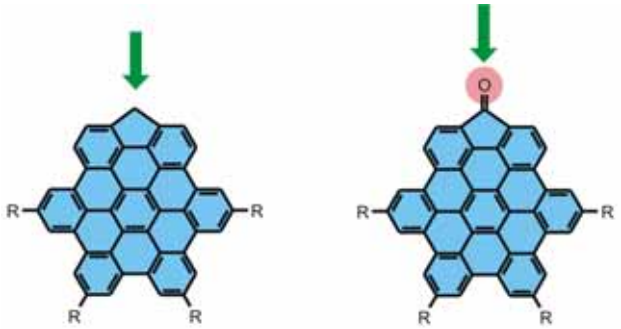

Figure 6-3: *Direct functionalization of the aromatic core in CPHBC(C_{12})$_4$* **5-80** *and CPHBCCO(C_{12})$_4$* **5-81**.

The variation of the polycyclic aromatic hydrocarbon (PAH) perimeter has been theoretically predicted to influence strongly the electronic properties. Going from the "all-arm chair" HBC to PAHs with one, two and three "zigzag" sites (Figure 6-4), the electronic spectroscopy revealed pronounced differences between the derivatives. However, the symmetry and the size of the aromatic core component in these derivatives excerted a strong influence onto molecular properties, such as the number of transitions in the UV/vis spectrum. The tuning of the electronic levels of materials is a fundamental task in material science to optimize the injection of charge carriers from electrodes with a specific work function.

Figure 6-4: *„zigzag" PAHs.*

Finally, the supramolecular order revealed a dependence upon the substitution pattern of the alkyl chains attached in the corona of the PAHs. Higher symmetry substitution patterns with fewer chains stabilized the intracolumnar organization, due to a better crystallization.

In summary, next to the synthesis of new materials holding promise for organic electronics, novel concepts have been developed which allow a simpler functionalization of the PAH based discotic materials both in the periphery and at the

aromatic core. However, the synthesis of CPHBC derivatives with better solubilizing chains is recommended to facilitate the work-up of these materials in the laboratory.

On the presented, interdisciplinary path from the synthesis, over a successful processing to the implementation in devices (Figure 6-5), promising results emerged from the first two fields.

Figure 6-5: "*The interdisciplinary path" from synthesis to the successful implementation in a device structure.*

Uniaxially organized, macroscopic films of HBC-$C_{6,2}$ **3-13a** and HBC-$C_{14,10}$ **3-13c**, obtained by dipping and zone-crystallization, fulfill the requirements – adequate organization and good charge carrier mobility – for the implementation into FET structures. These experiments are planned for the future and will be conducted by N. TSAO during his thesis, who focuses on the processing and implementation of the novel structures in organic, electronic devices.

The experiments with HBC-C_5-acrylate **4-18** opened novel concepts to pattern surfaces to obtain higher interfacial surface contacts in solar cells. Furthermore, the investigation of FET performances dependent upon the local, molecular organization, which can be "frozen" in, would give a deeper insight into the charge carrier mobility – morphology relationship.

7 Experimental Part

7.1 General methods

7.1.1 Chemicals and solvents

All used chemicals and solvents were obtained from the companies ABCR, Acros, Aldrich, Fluka, Lancaster, Merck and Strem. Unless otherwise mentioned, they were used as obtained.

7.1.2 Chromatography

Preparative column chromatography was performed on silica gel from Merck with a grain size of 0.063 – 0.200 mm (silica gel) or 0.04-0.063 mm (flash silica gel, Geduran Si 60). For analytical thin layer chromatography (TLC), silica gel coated substrates "60 F_{254}" from Merck were used. Compounds were detected by fluorescence quenching at 254 nm, self-fluorescence at 366 nm or staining in an iodine vapor chamber. For eluents, analytically pure solvents (p.a. or technical grade) were distilled prior to the use. The compositions of the eluents are given together with the retension value R_f.

7.1.3 Microwave Assisted Reactions

Some reactions were performed in a microwave oven (CEM GmbH, Kamp-Lintfort, Germany, model: Discover) using the maximum power to heat the system. The temperature was adjusted by changing the flow rate for a jet of air around the glass reaction vessel. The reaction vessels were sealed and could hold a pressure of 10 bars.

7.1.4 Inert atmosphere

Oxygen or moisture sensitive reactions were carried out in an argon atmosphere (Linde). If not mentioned specifically, reactions were degassed by bubbling a stream of argon though the reaction mixture.

7.2 Analytical techniques

7.2.1 Mass spectrometry

FD mass spectra were obtained on a VG Instruments ZAB 2-SE-FPD spectrometer. MALDI-TOF spectrometry was conducted on a Bruker Reflex II-TOF spectrometer, utilizing a 337 nm nitrogen laser. If not specifically mentioned, tetracyanoquinodimethane (TCNQ) was used as the matrix substance for solid state prepared samples. Varying thicknesses of the prepared sample on the MALDI target reduced the resolution; therefore only integers of the molecular peaks are given. Isotope patterns are given and compared to the calculation, which are usually in agreement. In some cases, fullerite was used as an internal standard.

7.2.2 NMR spectroscopy

^{1}H NMR, ^{13}C NMR, H,H COSY, C,H COSY and NOESY experiments were recorded in the listed deuterated solvents on a Bruker DPX 250, Bruker AMX 300, Bruker DRX 500 or a Bruker DRX 700 spectrometer. The deuterated solvent was used as an internal standard. In complicated cases, spectra were simulated using ACDLabs NMR prediction software to compare the results.

7.2.3 Elemental Analysis

Elemental analysis of solid samples was carried out on a Foss Heraeus Vario EL as a service of the Institute for Organic Chemistry, Johannes-Gutenberg-Universität of Mainz. Liquid compounds or oils were not analyzed because of the difficulties to remove residual solvents and atmospheric gases like CO_2. The high carbon content of the synthesized large polycyclic aromatic hydrocarbons complicated the detection of the elements. Although all combustions were complete (no soot formation), the analysis in most of the case lacked reproducibility. Repetitive measurements on the same sample gave strongly varying contents of the analyzed elements. This problem could not be solved so far, therefore the given results are associated with some uncertainty.

7.2.4 UV/vis spectroscopy

Solution UV/vis spectra were recorded at room temperature on a Perkin-Elmer Lambda 100 spectrophotometer. The molar extinctions are given in the unit $m^2 \cdot mol^{-1}$,

which is consistent with the SI standard. In order to eliminate aggregation phenomena in solution, spectra of samples of different concentrations were compared to give the properties for the monomeric species in solution, which is usually at a concentration of 10^{-6} – 10^{-7} M. If not specifically mentioned, chloroform (spectroscopic grade) was used as solvent and the measurement was performed at room temperature.

7.2.5 Photoluminescence spectroscopy

Solution photoluminescence spectra were recorded on a SPEX-Fluorolog II (212) spectrometer. Spectra of samples of different concentrations were compared to extracted aggregation behaviors. Quantum yields of selected compounds were calculated by comparing a known standard (three different concentrations). If not specifically mentioned, chloroform (spectroscopic grade) was used as solvent and the measurement was performed at room temperature.

7.2.6 Differential scanning calorimetry (DSC) and thermogravimetric analysis (TGA)

For TGA, a Mettler TG 50 thermogravimetric analyzer was used to determine the decomposition temperature. DSC was measured on a Mettler DSC 30 with heating and cooling rates of 10 °C/min in the range from -150 °C until thermal decomposition. If not specifically mentioned, the transitions were endothermic and the peak values of the second heating and cooling cycle (value in brackets) were given to exclude influences from the thermal history.

7.2.7 Polarization microscopy

A Zeiss Axiophot with a nitrogen flushed Linkam THM 600 hot stage was used to perform polarization microscopy.

7.2.8 X-Ray Diffractometry

Powder X-ray diffraction experiments were performed using a Siemens D 500 Kristalloflex diffractometer with a graphite-monochromatized CuK_α X-ray beam, emitted from a rotating Rigaku RU-300 anode. 2D WAXS measurements of oriented filaments were conducted using a rotating anode (Rigaku 18 kW) X-ray beam (CuK_α, pinhole collimation, double graphite monochromator) and CCD camera. The patterns

were recorded with vertical orientation of the filament axis and with the beam perpendicular to the filament.

Phases of mesogenes are characterized with: C_r = crystalline phase, Col_p = plastic crystalline, Col_d = columnar disordered mesophase, I = isotropic phase.

7.2.9 Single crystal analysis

The single crystal analysis was performed on a Nonius-KCCD diffractometer with a Mo-K_α (λ = 0.71923 Å, graphite monochromatized) at a temperature of 150 K. The structures were solved by direct methods (Shelxs) and refined on F with anisotropic temperature factors for all non-hydrogen atoms. The H atoms were refined with fixed isotropic temperature factors in the riding mode.

7.2.10 Synchrotron experiments

The experiments have been performed at the European Synchrotron Radiation Facility (ESRF) in Grenoble, France. The Microfocus Beamline (ID 13) was used with an one-dimensional waveguide optic. The sample was prepared on glass slides and glued at one end onto a glass capillary using cyanoacrylate adhesive. After curing, the capillary was mounted onto the beamline positioning stage and aligned to the exit of the waveguide. The X-ray waveguide provides a beam of approximately 0.1 µm in the vertical plane at its exit. The horizontal dimension of the beam is defined by the beam profile entering the waveguide and was approximately 3 µm in this instance. The experiments were performed using the TE0 mode, which has a divergence of approximately 1 mrad. Thus, the vertical beam size on the sample at the exit of the waveguide cannot be larger than 0.2 µm intervals. A radiation of wavelength 0.98 Å was used, with each diffraction pattern being generated with a 1 s exposure time. The diffraction patterns were collected on a MARCCD detector with an average size resolution of 64.45 x 64.45 μm^2. The diffraction data were analyzed using the Fit2D software application.

7.2.11 Pulse-radiolysis time-resolved microwave conductivity investigation

For pulse-radiolysis time-resolved microwave conductivity measurements (conducted by J. PIRIS and J. WARMAN, Delft, Netherlands), the polycrystalline materials were

contained in a Ka-band (26.5-42 GHz) microwave cavity. For most of the compounds the measurements were carried out at room temperature. For the longer, branched alkyl-chain derivatives (HBC-$C_{10,6}$ **3-13b** and HBC-$C_{14,10}$ **3-13c**), the measurements were made at 0°C since the transition to the liquid crystalline or isotropic liquid phases occurs close to or only slightly above room temperature. The samples were homogeneously ionized with a single 5 ns pulse of 3 MeV electrons from a Van de Graaff accelerator. The energy deposited in the sample per pulse was ca 20 kJ/m3 which resulted in an initial concentration of charge carriers of ca $1x10^{22}$ m^{-3} (*ca.* $2x10^{-5}$ moles per liter). The transient change in the conductivity of the sample was monitored as the temporary decrease in the microwave power reflected by the sample. By using a transient digitizer with a quasi-logarithmic timebase, transients could be digitally recorded for times from nanoseconds to milliseconds using a single pulse from the accelerator. Noise reduction could be achieved if required by averaging several single-shot transients.

7.2.12 Time-of-flight experiments

Charge carriers were generated by optical excitation of the sample through the semitransparent ITO-electrode using 10 ns light pulses from a frequency-tripled (355 nm) Nd:YAG laser. The transient photocurrent across the cell was amplified using a Stanford low noise current preamplifier (model SR570) and monitored using a Tektronix TDS380 digital storage oscilloscope. The transit time t_T was obtained from the intersection of the tangent to the plateau and the tangent to the tail determined in the linear plot. The hole mobility was calculated using $\mu = d^2/ (t_T V)$ where d is the film thickness, t_T the transit time and V the external bias applied. All TOF measurements were performed under a dynamic vacuum of 10^{-5} mbar. The excitation intensity of the laser pulse was controlled by a set of calibrated neutral density filters. Less than 10% of the sample capacitor charge was generated in the bulk in order to avoid space charge effects that would result in a non-uniform field across the sample. The thickness of the cells was determined with an accuracy of about 4% by recording the interference patterns in an UV/vis spectrometer.

7.2.13 Electrochemical Characterization

Electrochemical measurements were performed on a Voltametric Analyzer (AutoLab PGSTAT-30, Potentiostat/Galvanostat) in a three-electrode cell with an Au working

electrode (3 mm diameter), a silver quasi-reference electrode (AgQRE, calibrated with the Fc/Fc^+ redox couple E° = 4.8 eV) and a Pt counter electrode. Films were drop cast from a solution of toluene. Tetrabutylammonium perchlorate (TBAClO4, 0.1M), and acetonitrile were used as electrolyte and solvent, respectively. Differential pulse voltammetry was measured with 15 mV, 50 ms pulses at 100 ms intervals. Experiments were conducted by J. W. F. ROBERTSON and J. LI.

7.2.14 Preparation of Photovoltaic Devices

The photovoltaic device was fabricated by spin coating HBC:PDI solutions (20 mg / ml, ratios of 2:8, 4:6, 5:5, and 6:4) onto ITO substrates pre-treated with acetone and *iso*-propanol in an ultrasonic bath followed by cleaning for 10 min with oxygen plasma. Thin film was then annealed at 120 °C for 1 h in nitrogen atmosphere. About 100 nm thick Al was subsequently evaporated through a mask on the surface to form the cathode. The effective area of the device is about 6 mm^2 defined by overlap of etched ITO and the top electrode. An accurate value of the area is measured through microscope for subsequent calculation. Incident light is focused on the effective area of each device through a lens. Current-λ curves are recorded with a Keithley 236 Source-Measure Unit. A tungsten-halogen lamp was employed as light source, supplying monochromatic light from 300 nm to 800 nm through a TRIAX 180 monochromator. Incident light intensity was determined by a calibrated silicon diode. The maximum intensity was 1 W/m^2 at *ca.* 600 nm. Solar light was obtained from a solar simulator, (Lichttechnik, Germany) using a 575 W metal halide lamp, in combination with an ODF-Filter, to produce a spectral distribution close to the global radiation AM1.5G. The light intensity can be adjusted and here is set to around 100 W/m^2. Devices are protected by nitrogen during the test.

7.3 Synthesis

7.3.1 4,4'-Bis(2-ethyl-hexyl)diphenylacetylene (3-11a)

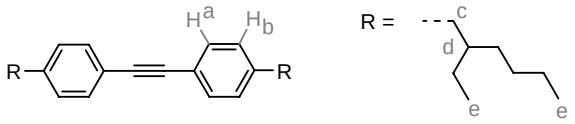

In a dry, two-neck flask, 2.21 g magnesium (90.0 mmol) was initially treated with few iodine crystals. 20 mL of dry THF and 17.4 g 2-ethylhexyl bromide (**3-10a**, 90.0 mmol) were carefully added and the resulting mixture was refluxed for 3 hours. The Grignard agent was transferred *via cannula* to a solution of 5 g 4,4'-dibromodiphenylacetylene (**3-5**, 15 mmol) and 0.35 g dichloro[1,1'-bis(diphenyl-phosphino)ferrocene]palladium(II) (0.48 mmol) in 100 mL of anhydrous THF and was stirred for 4 days at 45 °C. After quenching with methanol, the solvent was removed *in vacuo* and the crude product was purified using column chromatography to obtain 3.30 g of the desired product as a colorless oil (28%, 8.20 mmol).

MS (FS, 8kV): m/z (%) = 402.7 (100%, M^+) (calc. for $C_{30}H_{42}$ = 402.67 g mol^{-1})

^{1}H-NMR (250 MHz, CD_2Cl_2): δ = 7.45 (d, 4H, ^3J(H,H) = 8.07 Hz, H_a), 7.17 (d, 4H, ^3J(H,H) = 8.0 Hz, H_b), 2.58 (d, 4H, ^3J(H,H) = 7,25 Hz, H_c), 1.66 (m, 2H, H_d), 1.5-1.2 (m, 16H, -CH_2-), 0.92 (t, 12H, ^3J(H,H) = 6.20 Hz, H_e)

^{13}C-NMR (63 MHz, CD_2Cl_2): δ = 142.94 (4-Ar-*C*, 4'-Ar-*C*), 131.64 (2-Ar-*C*, 2'-Ar-*C*, 6-Ar-*C*, 6'-Ar-*C*), 129.72 (3-Ar-*C*, 3'-Ar-*C*, 5-Ar-*C*, 5'-Ar-*C*), 120.95 (1-Ar-*C*, 1'-Ar-*C*), 89.32 (*C*≡C), 41.53 (α-*C*H_2), 40.46 (β-*C*H-), 32.76 (3-*C*H_2-hexyl), 29.26 (1-*C*H_3-ethyl), 25.91 (4-*C*H_2-hexyl), 23.48 (5-*C*H_2-hexyl), 14.35 (6-*C*H_3-hexyl), 11.02 (2-*C*H_3-ethyl)

7.3.2 Hexa-(4-(2-ethyl-hexyl-))phenylbenzene (3-12a)

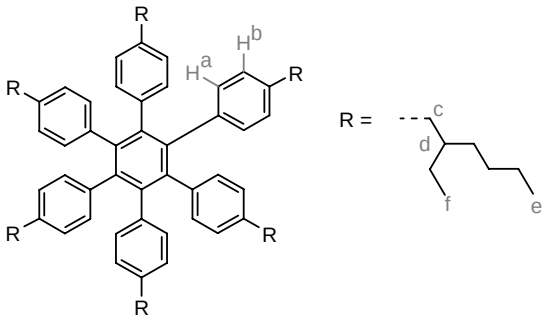

2.00 g 4,4'-Bis(2-ethyl-hexyl)diphenylacetylene (**3-11a**, 4.97 mmol) were dissolved in 400 mL of anhydrous 1,4-dioxane and degassed. 170 mg Dicobaltoctacarbonyl (0.49 mmol, 10 mol%) was added and the resulting mixture was stirred overnight at reflux. The solvent was removed *in vacuo* and the crude product was purified using column chromatography (silica gel, eluent: low boiling petroleum ether, dichloromethane = 9:1, R_f = 0.29) to yield 1.5 g of the desired products as a colorless oil (75%, 1.24 mmol).

MS (FS, 8kV): m/z (%) = 1208.1 (100%, M^+), 2416 (4%, $M^{½+}$) (calc. for $C_{90}H_{126}$= 1208.01 g mol^{-1})

^{1}H-NMR (250 MHz, CD_2Cl_2): δ = 6.71 (d, 12H, ^3J(H,H) = 8.15 Hz, H_b), 6.65 (d, 12H, ^3J(H,H) = 8.22 Hz, H_a), 2.31 (dd, 12H, ^3J(H,H) = 6.71 Hz, ^4J(H,H) = 2.52 Hz, H_c), 1.6-1.0 (m, 54H, -CH_2-), 0.91 (t, 18H, ^3J(H,H) = 6.51 Hz, H_e), 0.81 (t, 18H, ^3J(H,H) = 7.57 Hz, H_f)

^{13}C-NMR (125 MHz, CD_2Cl_2): δ = 144.03, 142.01 (both Ar-*C*), 135.01, 130.91 (both Ar-*C*H), 44.67 (2-*C*H-hexyl), 43.29 (1-*C*H_2-hexyl), 35.91 (3-*C*H_2-hexyl), 32.42 (1-*C*H_2-ethyl), 28.95 (4-*C*H_2-hexyl), 26.74 (5-*C*H_2-hexyl), 17.63 (6-*C*H_3-hexyl), 14.31 (2-*C*H_3-ethyl)

7.3.3 2,5,8,11,14,17-Hexa(4-(2-ethyl-hexyl-)-hexa-*peri*-hexabenzocoronene (3-13a)

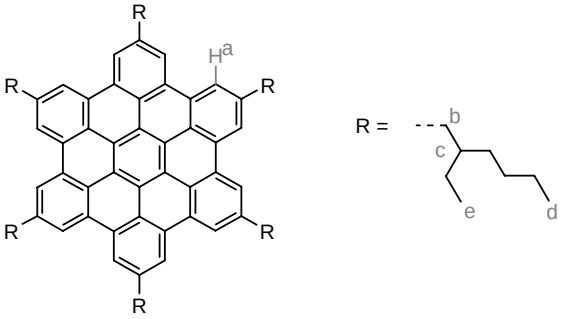

900 mg Hexa-(4-(2-ethyl-hexyl-))phenylbenzene (**3-12a**, 750 mmol) were dissolved in 400 mL dichloromethane. A stream of argon saturated with dichloromethane was bubbled into the solution through a Teflon tube. A solution of 2.00 g iron(III) chloride (12.5 mmol) in 12 mL nitromethane was quickly added. After a reaction time of 45 minutes, the reaction was stopped with methanol. After having evaporated the solvent, the residue was filtered through a short silica pad with hot toluene to yield 840 mg of the desired product as a yellow, crystalline solid (94%, 720 mmol).

MS (MALDI-TOF): m/z (%) = 1195 (36%), 1196 (35%), 1197 (18%), 1198 (7%) , 1199 (4%) (calc. for $C_{90}H_{114}$ = 1195.91 g mol^{-1}, Isotope pattern: 1195 (37%), 1196 (37%), 1197 (19%), 1198 (6%), 1199 (2%))

UV/vis: λ / nm (ε / m^2·mol^{-1}) = 342 (858), 361 (2029), 392 (672), 441 (25), 448(24), 466 (16)

^{1}H-NMR (250 MHz, $C_2D_2Cl_4$): δ = 8.41 (s, 12H, H_a), 2.96 (bs, 12H, H_b), 1.89 (m, 6H, H_c), 1.7-1.0 (m, 46H, -CH_2-), 1.01 (t, 18H, ^3J(H,H) = 7.32 Hz, H_d), 0.91 (t, 18H, ^3J(H,H) = 6.96 Hz, H_e)

^{13}C-NMR (63 MHz, $C_2D_2Cl_4$): δ = 139.58, 130.23, 123.81, 122.47, 120.10 (all HBC-*C*), 41.79 (α-*C*H_2), 41.63 (β-*C*H-), 33.26, 29.44, 26.49, 23.32 (all -*C*H_2-), 14.24 (-*C*H_3), 11.32 (-*C*H_3)

DSC (°C): 97 (81)

Elemental Analysis: 90.35% C, 9.64% H (berechnet: 90,39% C, 9,64% H)

7.3.4 4,4'-Bis(2-hexyl-decyl)diphenylacetylene (3-11b)

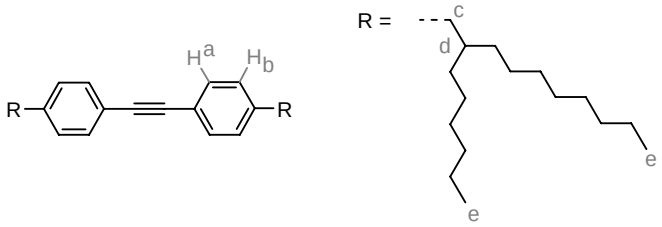

In a dry, two-neck flask, 2.21 g magnesium (90.0 mmol) was initially treated with few iodine crystals. 20 mL of dry THF and 27.5 g 2-hexyldecyl bromide (**3-10b**, 90.0 mmol) were carefully added and the resulting mixture was refluxed over night. The Grignard agent was transferred *via cannula* to a solution of 5 g 4,4'-dibromodiphenylacetylene (**3-5**, 15 mmol) and 0.75 g dichloro[1,1'-bis(diphenyl-phosphino)ferrocene]palladium(II) (1.00 mmol) in 100 mL of anhydrous THF and was stirred for 4 days at 45 °C. After quenching with methanol, the solvent was removed *in vacuo* and the crude product was purified using column chromatography (silica gel, eluent: hexane, R_f = 0.74) to obtain 8.03 g of the desired product as a colorless oil (86%, 12.8 mmol).

MS (FS, 8kV): m/z (%) = 627.4 (100%, M^+) (calc. for $C_{46}H_{74}$ = 627.10 g mol^{-1})

^{1}H-NMR (300 MHz, CD_2Cl_2): δ = 7.47 (d, 4H, ^3J(H,H) = 7.92 Hz, H_a), 7.17 (d, 4H, ^3J(H,H) = 7.92 Hz, H_b), 2.58 (d, 4H, ^3J(H,H) = 7.14 Hz, H_c), 1.66 (m, 2H, H_d), 1.5-1.2 (m, 48H, -CH_2-), 0.92 (t, 12H, ^3J(H,H) = 6.21 Hz, H_e)

^{13}C-NMR (75 MHz, CD_2Cl_2): δ = 142.95 (4-Ar-*C*, 4'-Ar-*C*), 131.66 (2-Ar-*C*, 2'-Ar-*C*, 6-Ar-*C*, 6'-Ar-*C*), 129.74 (3-Ar-*C*, 3'-Ar-*C*, 5-Ar-*C*, 5'-Ar-*C*), 120.97 (1-Ar-*C*, 1'-Ar-*C*), 89.35 (*C*≡ C), 40.95 (α-*C*H_2), 40.14 (β-*C*H-), 33.65, 33.62, 32.45, 32.41, 30.50, 30.18, 30.13, 29.86, 27.01, 23.21 (all -*C*H_2-), 14.41 (-*C*H_3)

7.3.5 Hexa-(4-(2-hexyl-decyl-))phenylbenzene (3-12b)

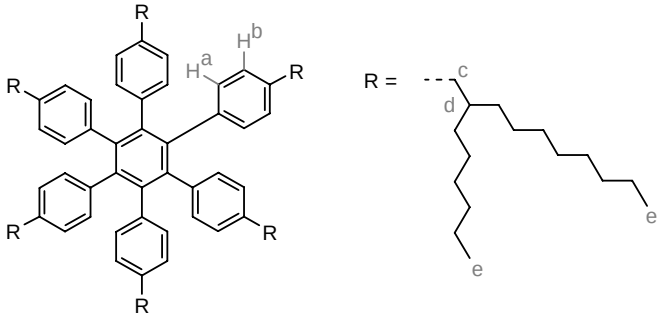

1.00 g 4,4'-Bis(2-hexyl-decycl)diphenylacetylene (**3-11b**, 1.60 mmol) were dissolved in 250 mL of anhydrous 1,4-dioxane and degassed. 27 mg dicobaltoctacarbonyl (70.0 µmol, 5 mol%) was added and the resulting mixture was stirred overnight at reflux. The solvent was removed *in vacuo* and the crude product was purified using column chromatography (silica gel, eluent: low boiling petroleum ether, R_f = 0.62) to yield 930 mg of the desired products as a colorless oil (93%, 0.49 mmol).

MS (FS, 8kV): m/z (%) = 1880.5 (100%, M^+) (calc. for $C_{138}H_{222}$ = 1881.31 g mol^{-1})

^{1}H-NMR (250 MHz, CD_2Cl_2): δ = 6.68 (d, 12H, ^{3}J(H,H) = 8.20 Hz, H_b), 6.62 (d, 12H, ^{3}J(H,H) = 8.20 Hz, H_a), 2.30 (d, 12H, ^{3}J(H,H) = 6.95 Hz, H_c), 1.6-1.0 (m, 150H, -CH_2-), 0.91 (t, 36H, ^{3}J(H,H) = 6.30 Hz, H_e)

^{13}C-NMR (65 MHz, CD_2Cl_2): δ = 140.80, 138.76, 131.80, 127.71 (all Ar-*C*), 40.47 (α-*C*H_2), 39.96 (β-*C*H-), 33.30, 32.47, 30.60, 30.26, 30.21, 29.91, 26.84, 26.81, 23.21 (all -*C*H_2-), 14.40 (-*C*H_3)

7.3.6 2,5,8,11,14,17-Hexa(2-hexyl-decyl)-hexa-*peri*-hexabenzocoronene (3-13b)

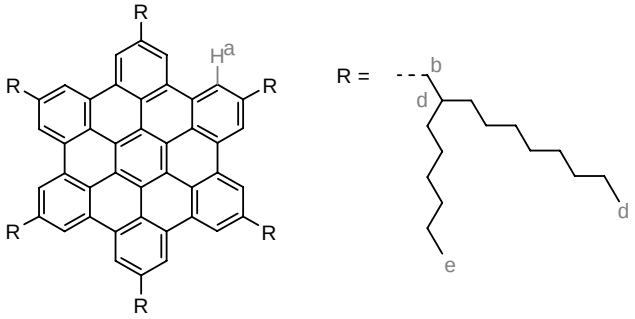

900 mg Hexa-(4-(2-hexyl-decyl-))phenylbenzene (**3-12b**, 470 mmol) were dissolved in 400 mL dichloromethane. A stream of argon saturated with dichloromethane was bubbled into the solution through a Teflon tube. A solution of 1.30 g iron(III) chloride (8.04 mmol) in 9 mL nitromethane was quickly added. After a reaction time of 45 minutes, the reaction was stopped with methanol. After having evaporated the solvent, the residue was purified using preparative column chromatography (silica gel, eluent: hexane, R_f = 0.8) to yield 719 mg of the desired product as a yellow, waxy solid (82%, 719 mmol).

MS (MALDI-TOF): m/z (%) = 1868 (20%), 1869 (27%), 1870 (22%), 1871 (17%), 1872 (7%) (calc. for $C_{138}H_{210}$ = 1869,21 g mol^{-1}, Isotope pattern: 1868 (21%), 1869 (33%), 1870 (26%), 1871 (13%), 1872 (5%))

UV/vis: λ / nm (ε / m^2·mol^{-1}) = 345 (784), 362 (1920), 392 (627), 440 (65)

^{1}H-NMR (250 MHz, CD_2Cl_2): δ = 8.40 (s, 12H, H_a), 3.02 (d, 12H, ^{3}J(H,H) = 6.63 Hz, H_b), 2.03 (m, 6H, H_c), 1.7-1.0 (m, 150H, -CH_2-), 0.92 (t, 18H, ^{3}J(H,H) = 6.63 Hz, H_d), 0.83 (t, 18H, ^{3}J(H,H) = 6.33 Hz, H_e)

^{13}C-NMR (75 MHz, CD_2Cl_2): δ = 139.46, 129.88, 123.42, 122.35, 119.72 (all HBC-*C*), 42.13 (α-*C*H_2), 40.52 (β-*C*H-), 33.86, 32.51, 32.40, 30.73, 30.38, 30.27, 29.90, 27.20, 23.19, 23.10 (all -*C*H_2-), 14.34 (-*C*H_3), 14.25 (-*C*H_3)

DSC (°C): 24 (-26), 93 (73, 45)

Elemental Analysis: 88.77% C, 11.19% H (calc.: 88.68% C, 11.32% H)

7.3.7 2-Decyl-tetradecylbromide (3-10c)

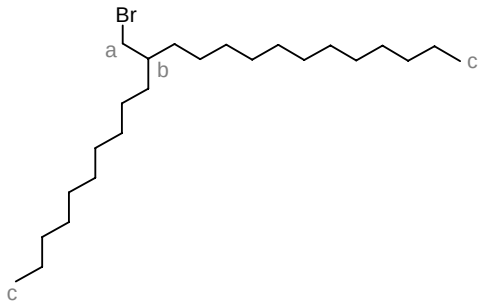

84.2 g 2-Decyl-tetradecanol (**3-9c**, 0.24 mol, 100 mL) and 100 g triphenylphosphine (0.38 mmol) were dissolved in 160 mL dichloromethane and cooled to 0 °C. 65 g N-bromosuccinimide (0.37 mol) was carefully added in small portions, and the reaction mixture was stirred at room temperature for 12 h. Dichloromethane was removed *in vacuo*, the residue dissolved in hexane and filtered over a silica pad. The product was distilled using a Kugelrohr apparatus under reduced pressure to yield 81 g of the desired compound as a colorless oil (80%, 0.19 mol).

MS (FD, 8kV): m/z (%) = 416.6 (100%, M^+), 836.4 (35%, $M^{½+}$) (calc. for $C_{24}H_{49}Br$= 417.56 g mol^{-1})

^{1}H NMR (300 MHz, CD_2Cl2): δ = 3.47 (d, 2H, ^3J(H,H) = 5.7 Hz, H_a), 1.62 (m, 1H, H_b), 1.5-1.1 (m, 40H, -CH_2-), 0.90 (t, 6H, ^3J(H,H) = 7.59 Hz, H_c); ^{13}C-NMR (75 MHz, CD_2Cl_2): δ = 40.15 (α-CH$_2$), 40.05 (β-CH-), 33.09, 32.49, 30.34, 30.19, 30.15, 29.91, 27.07, 23.23 (all -CH$_2$-), 14.42 (-CH$_3$).

7.3.8 4,4'-Bis(2-decyl-tetradecyl)diphenylacetylene (3-11c)

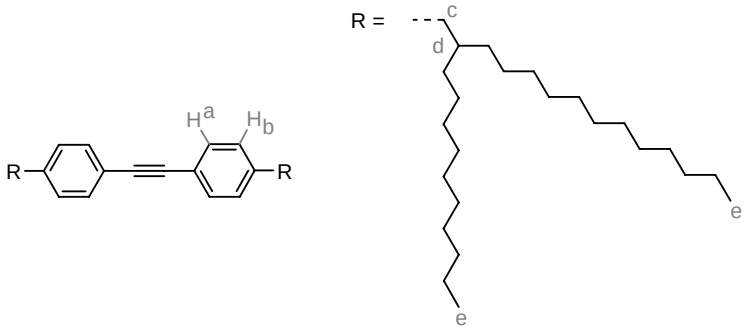

In a dry, two-neck flask, 4.41 g magnesium (0.18 mol) was initially treated with few iodine crystals. 40 mL of dry THF and 75 g 2-decyltetradecyl bromide (**3-10c**, 0.18 mmol) were carefully added and the resulting mixture was refluxed over night. The warm Grignard agent was transferred *via cannula* to a solution of 10 g 4,4'-dibromodiphenylacetylene (**3-11**, 30 mmol) and 1.50 g dichloro[1,1'-bis(diphenyl-phosphino)ferrocene]palladium(II) (2.00 mmol) in 200 mL of anhydrous THF and was stirred for 4 days at 45 °C. After quenching with methanol, the solvent was removed *in vacuo* and the crude product was purified using column chromatography (silica gel, eluent: hexane, R_f = 0.55) to obtain 14.2 g of the desired product as a colorless oil (56%, 16.7 mmol).

MS (FS, 8kV): m/z (%) = 851.3 (100%, M^+) (calc. for $C_{62}H_{106}$= 851.54 g mol^{-1})

^{1}H-NMR (250 MHz, CD_2Cl_2): δ = 7.42 (d, 4H, ^{3}J(H,H) = 8.00 Hz, H_a), 7.15 (d, 4H, ^{3}J(H,H) = 8.25 Hz, H_b), 2.55 (d, 4H, ^{3}J(H,H) = 7.00 Hz, H_c), 1.66 (m, 2H, H_d), 1.5-1.1 (m, 80H, -CH_2-), 0.89 (t, 12H, ^{3}J(H,H) = 6,50 Hz, H_e)

^{13}C-NMR (65 MHz, CD_2Cl_2): δ = 142.95 (4-Ar-*C*, 4'-Ar-*C*), 131.69 (2-Ar-*C*, 2'-Ar-*C*, 6-Ar-*C*, 6'-Ar-*C*), 129.76 (3-Ar-*C*, 3'-Ar-*C*, 5-Ar-*C*, 5'-Ar-*C*), 121.05 (1-Ar-*C*, 1'-Ar-*C*), 89.40 (*C*≡ C), 41.01 (α-*C*H_2), 40.16 (β-*C*H-), 33.69, 32.50, 30.52, 30.24, 30.21, 23.25, 29.93, 27.06 (all -*C*H_2-), 14.41 (-*C*H_3)

7.3.9 Hexa-(4-(2-decyl-tetradecyl-))phenylbenzol (3-12c)

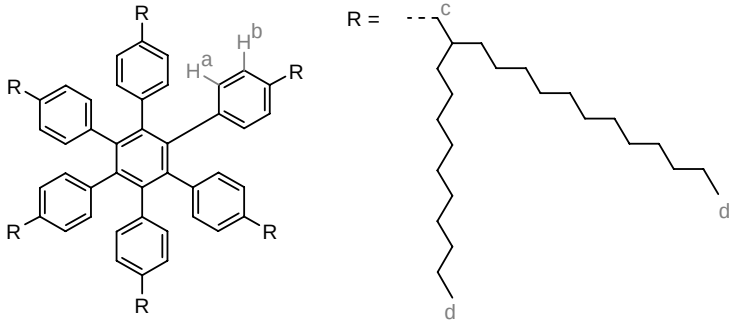

2.00 g 4,4'-Bis(2-decyl-tetradecycl)diphenylacetylene (**3-11c**, 2.35 mmol) were dissolved in 500 mL of anhydrous 1,4-dioxane and degassed. 82.0 mg dicobaltoctacarbonyl (0.24 mmol, 10 mol%) was added and the resulting mixture was stirred overnight at reflux. The solvent was removed *in vacuo* and the crude product was purified using column chromatography (silica gel, eluent: low boiling petroleum ether, dichloromethane = 9:1, R_f = 0.90) to yield 1.59 g of the desired products as a colorless oil (79%, 0.62 mmol).

MS (FS, 8kV): m/z (%) = 2553.0 (calc. for $C_{186}H_{318}$= 2554.61 g mol^{-1})

^{1}H-NMR (250 MHz, CD_2Cl_2): δ = 6.65 (d, 12H, ^{3}J(H,H) = 8.21 Hz, H_b), 6.62 (d, 12H, ^{3}J(H,H) = 8.23 Hz, H_a), 2.28 (d, 12H, ^{3}J(H,H) = 6.95 Hz, H_c), 1.6-1.0 (m, 246H, -CH-, -CH_2-), 0.89 (t, 36H, ^{3}J(H,H) = 6.36 Hz, H_d)

^{13}C-NMR (65 MHz, CD_2Cl_2): δ = 140.71, 138.71, 131.75, 127.65 (all Ar-*C*), 40.41 (α-*C*H_2), 39.90 (β-*C*H-), 33.24, 32.39, 32.38, 30.54, 30.20, 30.14, 29.85, 29.83, 26.80, 23.14 (all -*C*H_2-), 14.31 (-*C*H_3)

7.3.10 2,5,8,11,14,17-Hexa(2-decyl-tetradecyl)-hexa-*peri*-hexabenzocoronene (3-13c)

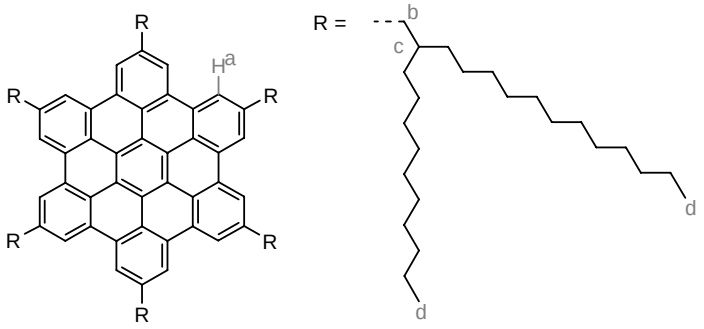

1.00 g Hexa-(4-(2-decyl-tetradecyl-))phenylbenzene (**3-12c**, 390 mmol) were dissolved in 370 mL dichloromethane. A stream of argon saturated with

dichloromethane was bubbled into the solution through a Teflon tube. A solution of 1.10 g iron(III) chloride (6.78 mmol) in 8 mL nitromethane was quickly added. After a reaction time of 45 minutes, the reaction was stopped with methanol. After having evaporated the solvent, the residue was purified using preparative column chromatography (silica gel, eluent: hexane, R_f = 0.7) to yield 744 mg of the desired product as a yellow, waxy solid (75%, 290 mmol).

MS (MALDI-TOF): m/z (%) = 2542 (12%), 2543 (26%), 2544 (25%), 2545 (19%), 2546 (10%), 2547 (6%) (calc. for $C_{186}H_{306}$ = 2542.51 g mol^{-1}, Isotope pattern: 2542 (12%), 2543 (26%), 2544 (27%), 2545 (19%), 2546 (10%), 2547 (4%))

UV/vis: λ / nm (ε / m^2·mol^{-1}) = 345 (773), 362 (1840), 392 (630), 441 (6)

^{1}H-NMR (250 MHz, CD_2Cl_2): δ = 8.40 (s, 12H, H_a), 3.00 (d, 12H, ^3J(H,H) = 6.25 Hz, H_b), 2.00 (m, 6H, H_c), 1.7-1.0 (m, 240H, -CH_2-), 0.81 (t, 36H, ^3J(H,H) = 5.50 Hz, H_d)

^{13}C-NMR (75 MHz, CD_2Cl_2): δ = 139.36, 129.93, 123.50, 122.31, 119.81 (all HBC-*C*), 42.13 (α-*C*H$_2$), 40.48 (β-*C*H-), 33.88, 33.83, 32.36, 32.31, 30.74, 30.36, 30.29, 30.20, 30.11, 29.85, 29.77, 27.25, 23.07 (all -*C*H$_2$-), 14.24 (-*C*H$_3$)

DSC (°C): 46 (7)

Elemental Analysis: 87.20% C, 12.35% H (calc.: 87.87% C, 12.13% H)

7.3.11 Bis(4,4''-dibromo-4-biphenyl)-acetylene (3-15)

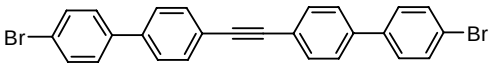

1.19 g 4'-Bromo-4-iodo-biphenyl (**3-14**, 3.31 mmol), 60.8 mg copper(I) iodide (0.32 mmol) and 67 mg bis(triphenylphosphino)palladium(II) chloride (0.10 mmol) were dried in high vacuum in a Schlenk flask. Afterwards, 16 mL anhydrous, freshly distilled toluene, 2.87 mL DBU (19.2 mmol), 228 µL trimethylsilyl acetylene (1.60 mmol) and 23 µL water were added step-wise and the resulting mixture was stirred at room temperature over night. The mixture was poured into methanol and the precipitate was collected and extensively washed with methanol and dichloromethane to afford 719 mg of the desired compound as an colorless, crystalline material (89%, 1.47 µmol). The hardly soluble compound was used without further purification.

MS (FD, 8kV): m/z (%) = 488.4 (100%, M$^+$) (calc. for $C_{26}H_{16}Br_2$= 488.23 g mol^{-1})

7.3.12 Bis(4,4''-di-(2-decyl-tetradecyl)-4-biphenyl)-acetylene (3-16)

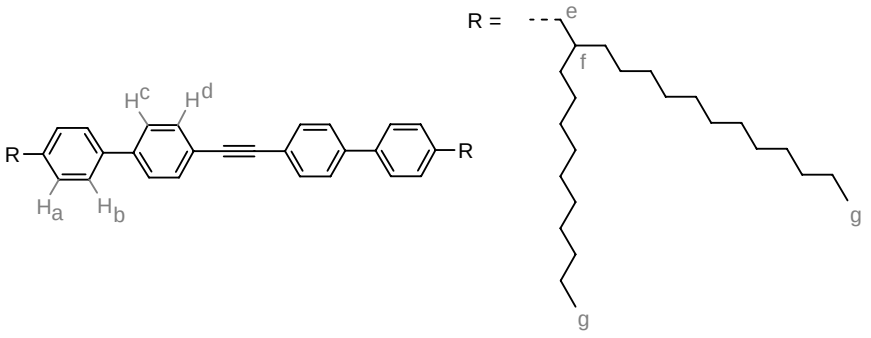

5.26 g Bis(4,4''-dibromo-4-biphenyl)-acetylene (**3-15**, 10.8 mmol) and 540 mg dichloro[1,1'-bis(diphenyl-phosphino)ferrocene]palladium(II) (738 µmol) were

suspended in 540 mg anhydrous THF. A freshly prepared Grignard solution, made from 1.58 g magnesium (65.0 mmol) and 27.2 2-decyl-tetradecyl bromide (**3-10c**, 65.0 mmol) in 40 mL anhydrous THF, were transferred *via cannula* into the suspension. The mixture was stirred at 45 °C for four days. After having removed the solvent *in vacuo*, the residue was purified using preparative column chromatography (flash silica gel, eluent: gradient from low boiling petroleum ether to low boiling petroleum ether, dichloromethane = 9:1) to afford 4.2 g of the desired compound as a colorless oil (39%, 4.18 mmol).

MS (FD, 8kV): m/z (%) = 1003.0 (100%, M^+) (calc. for $C_{74}H_{114}$ = 1003.73 g mol^{-1})

UV/vis: λ / nm (ε / $m^2 \cdot mol^{-1}$) = 322 (3350)

^{1}H NMR (300 MHz, CD_2Cl_2, 353 K): δ = 7.62 (s, 8H, H_a, H_b), 7.55 (d, 4H, ^3J(H,H) = 8.20 Hz, H_c), 7.24 (d, 4H, ^3J(H,H) = 8.20 Hz, H_d), 2.58 (d, 4H, ^3J(H,H) = 6.84 Hz, H_e), 1.67 (m, 2H, H_f), 1.4-1.2 (m, 80H, -CH_2-), 0.91 (t, 12H, ^3J(H,H) = 6.88 Hz, H_g)

^{13}C NMR (75 MHz, CD_2Cl_2, 353 K): δ = 142.21, 141.30, 137.70, 132.33, 130.17, 127.13, 126.90, 122.21, 90.25, 40.54, 40.08, 33.55, 32.35, 30.40, 30.08, 29.78, 26.92, 23.11, 14.30.

7.3.13 Hexa-(4-(2-decyl-tetradecyl)phenyl)phenylbenzene (3-17)

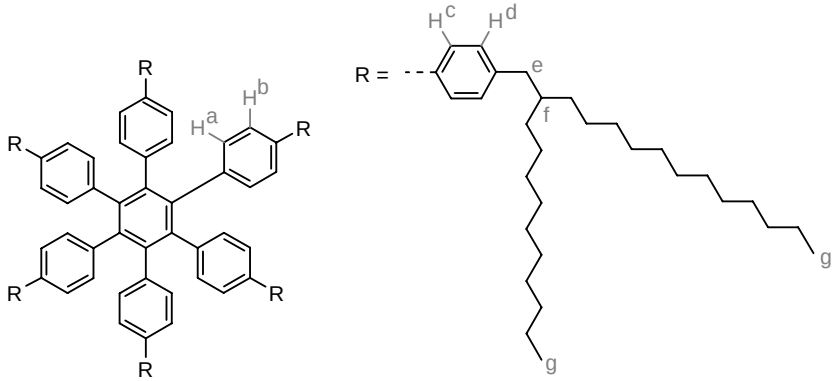

860 mg Bis(4,4''-di-(2-decyl-tetradecyl)-4-biphenyl)-acetylene (**3-16**, 857 µmol) were dissolved in 300 mL of anhydrous 1,4-dioxane and degassed. 25.0 mg dicobaltoctacarbonyl (73 µmol) was added and the resulting mixture was stirred overnight at reflux. The solvent was removed *in vacuo* and the crude product was purified using column chromatography (flash silica gel, eluent: low boiling petroleum ether, dichloromethane = 9:1, R_f = 0.55) to yield 770 mg of the desired products as a colorless oil (90%, 256 µmol).

MS (FD, 8kV): m/z (%) = 3010.1 (100%, M^+) (calc. for $C_{222}H_{342}$ = 3011.20 g mol^{-1})

^{1}H NMR (250 MHz, CD_2Cl_2): δ = 7.35 (d, 12H, ^3J(H,H) = 8.04 Hz, H_d), 7.22 (d, 12H, ^3J(H,H) = 8.19 Hz, H_b), 7.10 (d, 12H, ^3J(H,H) = 8.22 Hz, H_c), 7.05 (d, 12H, ^3J(H,H) = 8.20 Hz, H_a), 2.52 (d, 12H, ^3J(H,H) = 6.46 Hz, H_e), 1.61 (m, 6H, H_f), 1.5-1.1 (m, 240H, -CH_2-), 0.91 (t, 36H, ^3J(H,H) = 6.77 Hz, H_g).

^{13}C NMR (65 MHz, CD_2Cl_2): δ = 141.28, 140.85, 140.08, 138.02, 132.46, 129.89, 126.65, 125.35, 138.05 40.47, 40.13, 33.55, 32.44, 30.50, 30.17, 29.88, 26.97, 23.20, 14.40.

7.3.14 2,5,8,11,14,17-Hexa-(4-(2-decyl-tetradecyl)phenyl)-hexa-*peri*-hexabenzocoronene (3-18)

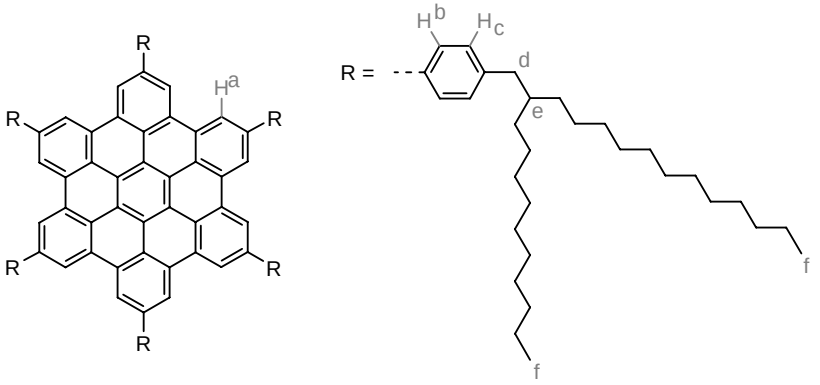

48.6 mg Hexa-(4-(2-decyl-tetradecyl)phenyl)phenylbenzene (**3-17**, 16.1 µmol) were dissolved in 65 mL dichloromethane. A stream of argon saturated with dichloromethane was bubbled into the solution through a Teflon tube. A solution of 157 mg iron(III) chloride (968 µmol) in 1.60 mL nitromethane was quickly added. After a reaction time of 120 minutes, the reaction was stopped with methanol. The precipitate was filtered off and reprecipitated into a methanol/ aqueous hydrazine solution (1000:1). The crude product was purified using preparative column chromatography (silica gel, eluent: toluene, R_f = 0.67). Finally, the material was reprecipitated again into methanol to afford 41 mg of the desired compound as a bright yellow, waxy solid (85%, 13.7 µmol).

MS (MALDI-TOF): m/z (%) = 2997 (11%), 2998 (21%), 2999 (26%), 3000 (20%), 3001 (12%), 3002 (7%), 3003 (2%) (calc. for $C_{222}H_{330}$ = 2999.11 g mol^{-1}, Isotope pattern: 2997 (8%), 2998 (21%), 2999 (26%), 3000 (21%), 3001 (13%), 3002 (7%), 3003 (3%))

UV/vis: λ / nm (ε / m^2·mol^{-1}) = 354 (746), 377 (1760), 417 (542), 467 (29), 506 (11)

^{1}H NMR (500 MHz, $C_2D_2Cl_4$, 393 K): δ = 9.10 (s, 12H, H_a), 7.97 (d, 12H, ^3J(H,H) = 7.85 Hz, H_b), 7.47 (d, 12H, ^3J(H,H) = 7.85 Hz, H_c), 2.86 (d, 12H, ^3J(H,H) = 6.71 Hz, H_d), 1.98 (m, 6H, H_e), 1.6-1.2 (m, 240H, -CH_2-), 0.86 (2xt, 36H, ^3J(H,H) = 7.13 Hz, H_f).

^{13}C NMR (125 MHz, $C_2D_2Cl_4$, 373 K): δ = 141.70, 139.00, 130.81, 130.42, 129.28, 128.46, 127.94, 127.86, 120.54, 41.00, 40.23, 34.14, 32.08, 32.04, 30.52, 30.07, 29.99, 29.96, 29.90, 29.82, 29.51, 29.45, 27.24, 22.77, 22.74, 14.12, 14.10.

DSC (°C): -39 (-44), 114 (63)

Elemental Analysis: 89.04% C, 11.07% H (calc.: 88.91% C, 11.09% H)

7.3.15 9-[5,8,11,14,17-penta(3,7-dimethyloctyl)-hexa-*peri*-hexabenzocoronen-2-yl]-N-(2,6-di-*iso*-propylphenyl)-perylene-3,4-dicarboxiimide (4-4)

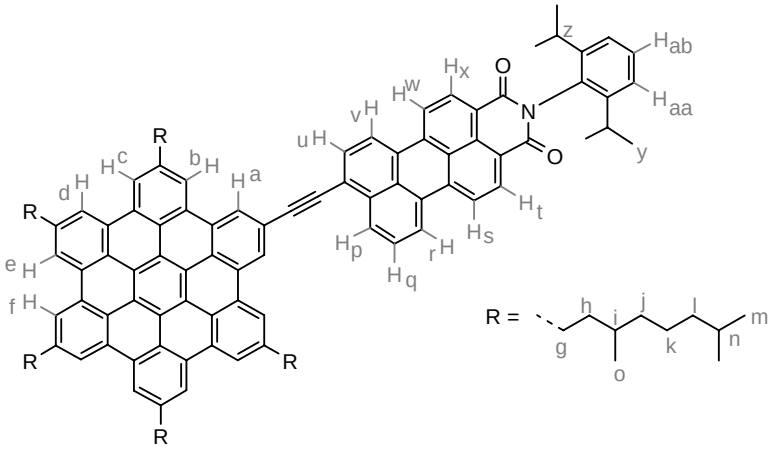

90 mg 9-Bromo-N-(2,6-di-*iso*-propylphenyl)-perylene-3,4-dicarboxiimide (160.3 µmol), 200 mg 2-acetyl-5,8,11,14,17-penta(3,7-dimethyloctyl)-hexa-*peri*-hexabenzocoronene (**4-3**, 160 µmol), 1.1 mg triphenylphosphine (4.2 µmol) and 11 mg copper(I) iodide (5.8 µmol) were dissolved in 10 mL piperidin and degassed with three freeze-vacuum-thaw cycles. Afterwards, 66 mg tetrakis-(triphenylphosphino)-palladium(0) (5.8 µmol) were added and the mixture was stirred at 80 °C for 24 hours. After having removed the solvent *in vacuo*, the residue was purified *via* repetitive column chromatography (silica gel, a) dichloromethane, R_f = 0.3-0.6; b) gradient acetone to acetone, toluene = 1:40, R_f = 0.3-0.4; c) toluene: ethyl acetate = 40:1, R_f = 0.2-0.4). The product was finally reprecipitated into methanol to afford 198 mg of the title compound as a red-violet solid (72%, 115 µmol).

MS (MALDI-TOF): m/z (%) = 1727 (24%), 1728 (30%), 1729 (26%), 1730 (15%), 1731 (4%) (calc. for $C_{128}H_{143}NO_2$ = 1727.57 g mol^{-1}, isotope pattern: 1726 (24%), 1727 (34%), 1728 (25%), 1729 (12%), 1730 (4%))

UV/vis ($CHCl_3$): λ / nm (ε / m^2·mol^{-1}) = 348 (751), 363 (1531), 392 (516), 526 (553)

^{1}H NMR (500 MHz, $C_2D_2Cl_4$, 400 K): δ = 8.87 (s, 2H, H_a), 8.81 (d, 1H, ^3J(H,H) = 8.92 Hz, H_r), 8.66 (s, 2H, H_b), 8.63 (s, 2H, H_c), 8.62 (s, 2H, H_d), 8.59 (s, 2H, H_e), 8.58 (s, 2H, H_f), 8.54 (s, 2H, H_p), 8.5-8.4 (m, 5H, H_t, H_u, H_v, H_w, H_x), 8.11 (d, 1H, ^3J(H,H) = 6.76 Hz, H_s), 7.83 (t, 1H, ^3J(H,H) = 8.44 Hz, H_q), 7.44 (dt, 1H, ^3J(H,H) = 7.36 Hz, ^4J(H,H) = 1.18 Hz, H_{ab}), 7.30 (d, 2H, ^3J(H,H) = 7.70 Hz, H_{aa}), 3.22 (m, 10H, H_g), 2.80 (sept., 2H, ^3J(H,H) = 6.91 Hz, H_z), 2.12 (m, 5H, H_{h*}(chiral)), 1.96 (m, 5H, H_{h*}(chiral)), 1.81 (m, 5H, H_i), 1.60 (m, 10H, H_k), 1.56-1.20 (m, 52H, H_j, H_l, H_n, H_o, H_y), 0.92 (m, 30H, H_m)

^{13}C NMR (125 MHz, $C_2D_2Cl_4$, 400 K): δ = 162.90, 145.28, 144.36, 140.28, 140.13, 140.09, 136.41, 136.10, 133.89, 130.96, 130.89, 130.81, 131.26, 131.15, 130.21, 130.16, 129.80, 129.42, 129.24, 129.15, 129.07, 128.32, 127.48, 127.01, 126.28, 124.38, 123.62, 123.41, 123.31, 123.06, 122.51, 122.45, 122.28, 121.25, 121.09, 121.00, 120.88, 120.82, 120.78, 120.08, 119.91, 119.60, 119.26, 118.92, 98.97, 87.38, 38.79, 38.69, 36.74, 34.02, 33.99, 32.48, 28.50, 27.19, 24.09, 23.14, 21.84, 21.78, 19.12.

DSC (°C): 217 (200)

Elemental Analysis: 89.02% C, 8.39% H, 0.91% N (calc.: 88.99% C, 8.34% H, 0.81% N, 1.85% O)

7.3.16 4,4'-Bis(5-acetoxypentyl)diphenylacetylene (4-9)

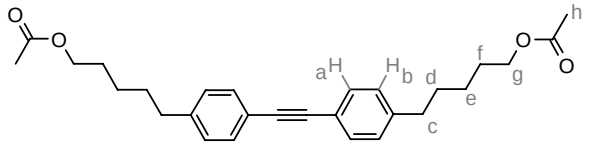

14.0 g 5-Acetoxypent-1-ene (15.4 mL, 109.4 mmol) were transferred into 250 mL of a 0.5 M solution of 9-borabicyclononane in THF and stirred at room temperature for 24 hours. In the next step, 55 mL of a 2M aqueous potassium hydroxide solution were added and the mixture was stirred for an additional 20 minutes. Finally, 9.20 g 4,4'-dibromodiphenylacetylene (**3-5**, 27.4 mmol) and 1.10 g dichloro[1,1'-bis(diphenylphosphino)ferrocene]palladium(II) (1.50 mmol) were put into the reaction solution. After five hours, the solvent was removed *in vacuo* and the residue was purified using preparative column chromatography (silica gel, eluent: hexane, ethyl acetate = 8:2) to yield 9.67 g of the desired compound as a colorless oil (81%, 22.3 mmol).

MS (FD, 8kV): m/z (%) = 434.3 (100%, M^+) (calc. for $C_{28}H_{34}O_4$ = 434.58 g mol^{-1})

^{1}H NMR (250 MHz, CD_2Cl_2): δ = 7.46 (d, 4H, ^3J(H,H) = 8.09 Hz, H_a), 7.16 (d, 4H, ^3J(H,H) = 8.15 Hz, H_b), 4.04 (t, 4H, ^3J(H,H) = 6.68 Hz, H_g), 2.61 (t, 4H, ^3J(H,H) = 7.65 Hz, H_c), 2.01 (s, 6H, H_h), 1.9-1.3 (m, 12H, H_d, H_e, H_f)

^{13}C NMR (65 MHz, CD_2Cl_2): δ = 170.80 (C=O), 143.19, 131.79, 128.79, 121.08 (all Ar-*C*), 89.36 (C≡C), 64.49 (-*C*H_2OAc)), 35.96 (α-*C*H_2-), 31.15, 28.81, 25.89 (all -*C*H_2-), 20.92 (-CO-*C*H_3)

7.3.17 Hexa-4-(5-acetoxypentyl)phenylbenzene (4-10)

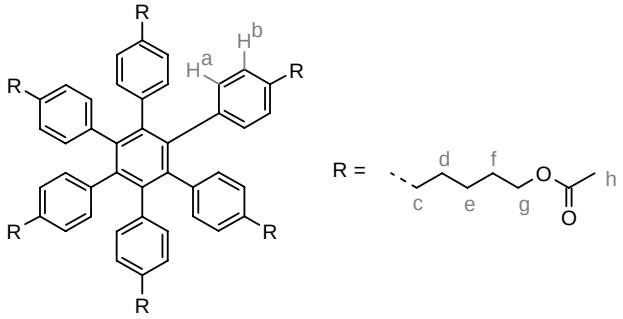

5.00 g 4,4'-Bis(5-acetoxypentyl)diphenylacetylene (**4-9**, 11.51 mmol) were dissolved in 500 mL anhydrous 1,4-dioxane and degassed. 400 mg Dicobaltoctacarbonyl (1.17 mmol) were added and the resulting mixture was refluxed over night. The solvent was removed in vacuo and the residue was purified using preparative column chromatography (silica gel, eluent: hexane, ethyl acetate = 6:4, R_f =0.66) to obtain 4.57 g of the title compound as a colorless oil (91%, 3.51 mmol).

MS (FS, 8kV): m/z (%) = 1303.8 (100%, M^+) (calc. for $C_{84}H_{102}O_{12}$= 1303.74 g mol^{-1})

^{1}H NMR (300 MHz, CD_2Cl_2): δ = 6.70 (d, 12H, ^3J(H,H) = 8.20 Hz, H_b), 6.65 (d, 12H, ^3J(H,H) = 8.14 Hz, H_a), 3.98 (t, 12H, ^3J(H,H) = 6.79 Hz, H_g), 2.37 (t, 12H, ^3J(H,H) =

7.59 Hz, H_c), 2.00 (s, 18H, H_h), 1.60-1.50 (m, 12H, H_f), 1.50-1.35 (m, 12H, H_d), 1.30-1.10 (m, 12H, H_e)

^{13}C NMR (75 MHz, CD_2Cl_2): δ = 171.17 (C=O)), 140.67, 139.41, 138.79, 131.72, 126.79 (all Ar-C), 64.70 (-*C*H_2-OAc), 35.40 (α-*C*H_2), 31.21, 28.74, 25.47 (all -*C*H_2-), 21.10 (-CO-*C*H_3)

7.3.18 2,5,8,11,14,17-Hexa-(5-acetoxypentyl)-hexa-*peri*-hexabenzocoronene (4-11)

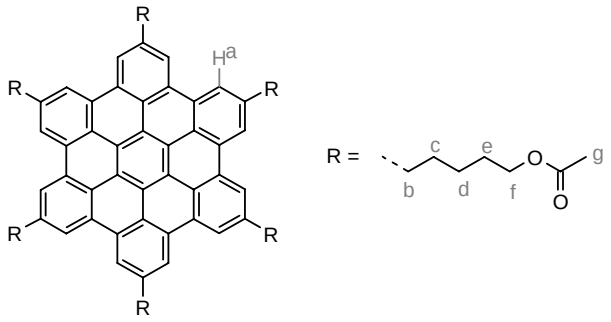

200 mg Hexa-4-(5-acetoxyoctyl)phenylbenzene (**4-10**, 143 µmol) were dissolved in 100 mL dichloromethane. A stream of argon saturated with dichloromethane was bubbled into the solution through a Teflon tube. A solution of 1.50 g iron(III) chloride (9.20 mmol) in 10 mL nitromethane was quickly added. After a reaction time of 120 minutes, the reaction was stopped with water, the organic phase separated, washed, dried with magnesium sulfate and concentrated. The residue was filtered through a short silica pad with hot toluene to remove inorganic impurities. Finally, the crude product was purified using preparative column chromatography (neutral aluminum oxide, gradient from hexane, ethyl acetate = 2:1 to pure ethyl acetate) to yield 175 mg of the desired polycyclic aromatic hydrocarbon as a yellow, waxy solid (95%, 135 µmol).

MS (MALDI-TOF): m/z (%) = 1291 (37%), 1292 (33%), 1293 (16%), 1294 (7%), 1295 (4%) (calc. for $C_{84}H_{90}O_{12}$ = 1291.65 g mol^{-1}, Isotope pattern: 1291 (38%), 1292 (36%), 1293 (18%), 1294 (6%), 1295 (2%))

UV/vis: λ / nm (ε / m^2·mol^{-1}) = 342 (877), 361 (2028), 392 (657), 441 (22), 448(26), 466 (12)

^{1}H NMR (300 MHz, CD_2Cl_2): δ = 7.92 (s, 12H, H_a), 4.20 (t, 12H, ^3J(H,H) = 6.43 Hz, H_f), 2.75 (t, 12H, ^3J(H,H) = 7.31 Hz, H_b), 2.08 (s, 18H, H_g), 2.0-1.5 (m, 36H, H_c, H_d, H_e)

^{13}C NMR (75 MHz, CD_2Cl_2): δ = 171.17 (C=O), 140.67, 139.41, 138.79, 131.72, 126.79 (all HBC-*C*), 64.70 (-*C*H_2-OAc), 35.40 (α-*C*H_2), 31.21, 28.74, 25.47 (all -*C*H_2-), 21.10 (-CO-*C*H_3)

DSC (°C): 128 (98)

Elemental Analysis: 78.19% C, 6.94% H (calc.: 78.11% C, 7.02% H, 14.86% O)

7.3.19 2,5,8,11,14,17-Hexa-(5-hydroxypentyl)-hexa-*peri*-hexabenzocoronene (4-12)

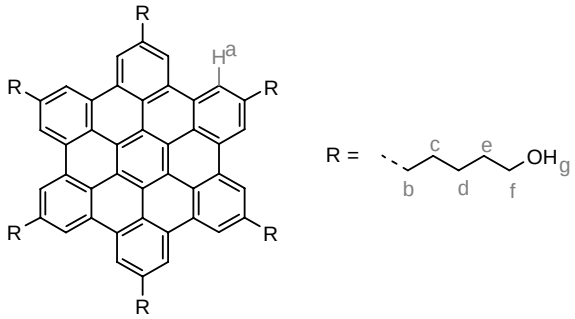

1.00 g 2,5,8,11,14,17-Hexa-(5-acetoxypentyl)-hexa-*peri*-hexabenzocoronene (**4-11**, 0.77 mmol) and 6.00 g potassium hydroxide (0.11 mol) were dissolved in a mixture of 100 mL THF, 2 mL methanol and 2 mL water. The mixture was refluxed for 15 hours and cooled down to room temperature. The basic solution was neutralized with 2M aqueous hydrochloride acid. The precipitate was collected, extensively washed with water, methanol and THF, and dried *in vacuo*. The crude product was dissolved in a minimum amount of DMF and reprecipitated into water to afford 800 mg of the pure title compound as a yellow, crystalline solid (99%, 0.77 mmol).

MS (MALDI-TOF): m/z (%) = 1039 (34%), 1040 (33%), 1041 (25%), 1042 (8%) (calc. for $C_{72}H_{78}O_6$= 1039.42 g mol^{-1}, Isotope pattern: 1039 (44%), 1040 (36%), 1041 (15%), 1042 (4%))

^{1}H NMR: 9.11 (s, 12 H, H_a), 5.06 (bs, 6H, H_g), 4.02 (t, 12H, ^3J(H,H) = 6.35 Hz, H_f), 3.30 (t, 12H, ^3J(H,H) = 7.84 Hz, H_b), 2.19 (pent., 12H, ^3J(H,H) = 7.34 Hz, H_e), 2.00 (pent., 12H, ^3J(H,H) = 7.49 Hz, H_c), 1.92 (pent., 12H, ^3J(H,H) = 7.72 Hz, H_d)

^{13}C NMR: low solubility does not allow recording resolved spectra

DSC (°C): 106 (84), 231 (144)

Elemental Analysis: 83.25% C, 7.51% H (calc.: 83.20% C, 7.56% H, 9.24% O)

7.3.20 4,4'-Bis(8-hydroxyoctyl)diphenylacetylene (4-13)

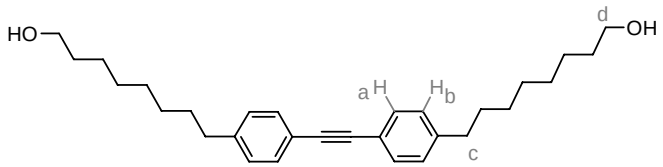

16.5 mL Oct-7-en-1-ol (14.0 g, 109 mmol) were transferred under argon to 250 mL of a 0.5 M 9-borabicyclononane solution in THF. After having stirred the mixture for 15 hours, 55.0 mL of a 3 M aqueous sodium hydroxide solution were added and the reaction was stirred for an additional 10 minutes. 9.20 g 4,4'-Dibromdiphenylacetylene (**3-5**, 27.4 mmol) and 1.1 g dichloro[1,1'-bis(diphenylphosphino)ferrocene] palladium(II) were added and the mixture was stirred over night. The solvent was evaporated and the residue was purified utilizing preparative column chromatography (silica gel, eluent: hexane, ethyl acetate = 1:1, R_f = 0.36) to afford 11.2 g of the title compound as a colorless solid (96%, 25.8 µmol).

MS (FD, 8kV): m/z (%) = 434.5 (100%, M^+) (calc. for $C_{30}H_{42}O_2$ = 434.67 g mol^{-1})

^{1}H NMR (300 MHz, CD_2Cl_2): δ = 7.42 (d, 4H, ^3J(H,H) = 8.20 Hz, H_a), 7.17 (d, 4H, ^3J(H,H) = 8.13 Hz, H_b), 3.58 (t, 4H, ^3J(H,H) = 6.62 Hz, H_d), 2.62 (t, 4H, ^3J(H,H) = 7.45 Hz, H_c), 1.8-1.2 (m, 24H, -CH_2-)

^{13}C NMR (125 MHz, CD_2Cl_2): δ = 143.90 (4-Ar-*C*, 4'-Ar-*C*), 131.71 (2-Ar-*C*, 2'-Ar-*C*, 6-Ar-*C*, 6'-Ar-*C*), 128.89 (3-Ar-*C*, 3'-Ar-*C*, 5-Ar-*C*, 5'-Ar-*C*), 120.88 (1-Ar-*C*, 1'-Ar-*C*), 89.17 (*C*≡C), 63.19 (-*C*H_2-OH), 36.19 (α-*C*H_2), 33.26, 31.63, 29.81, 29.74, 29.57, 26.12 (all -*C*H_2-)

Elemental Analysis: 81.95% C, 10.06% H (calc.: 82.90% C, 9.74% H, 7.36% O)

7.3.21 4,4'-Bis(8-acetoxyoctyl)diphenylacetylene (4-14)

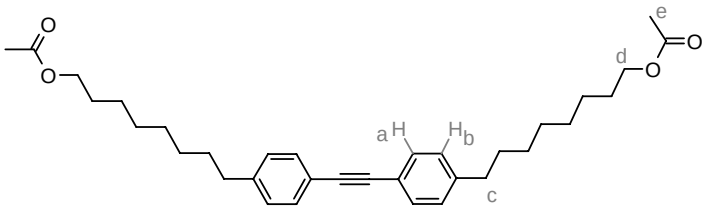

2.36 g 4,4'-Bis(8-hydroxyoctyl)diphenylacetylene (**4-13**, 5.43 mmol) were heated for four hours at 150 °C in a mixture of 4.3 g pyridine (54.3 mmol) and 50 mL acetic anhydride. The reaction was allowed to cool to room temperature and quenched with water. The aqueous phase was extracted with ethyl acetate and the organic phase was dried with magnesium sulfate and concentrated *in vacuo*. The residue was purified using preparative column chromatography (silica gel, eluent: hexane: ethyl acetate = 1:1, R_f = 0.86) to obtain 2.72 g of the desired product as a colorless solid (96%, 5.24 µmol).

MS (FD, 8kV): m/z (%) = 518.7 (100%, M^+) (calc. for $C_{34}H_{46}O_4$ = 518.74 g mol^{-1})

^{1}H NMR (300 MHz, CD_2Cl_2): δ = 7.42 (d, 4H, ^3J(H,H) = 8.14 Hz, H_a), 7.17 (d, 4H, ^3J(H,H) = 8.15 Hz, H_b), 3.58 (t, 4H, ^3J(H,H) = 6.75 Hz, H_d), 2.62 (t, 4H, ^3J(H,H) = 7.44 Hz, H_c), 2.00 (s, 6H, H_e), 1.7-1.2 (m, 24H, -CH_2-)

^{13}C NMR (125 MHz, CD_2Cl_2): δ = 171.25 (*C*=O), 143.86 (4-Ar-*C*, 4'-Ar-*C*), 131.71 (2-Ar-*C*, 2'-Ar-*C*, 6-Ar-*C*, 6'-Ar-*C*), 128.89 (3-Ar-*C*, 3'-Ar-*C*, 5-Ar-*C*, 5'-Ar-*C*), 120.89 (1-Ar-*C*, 1'-Ar-*C*), 89.16 (*C*≡C), 64.82 (-*C*H_2-OAc), 36.18 (α-*C*H_2), 31.62, 29.71, 29.55, 29.52, 29.00, 26.26 (all -*C*H_2-), 21.12 (-CO-*C*H_3)

Elemental Analysis: 77.86% C, 8.76% H (calc.: 78.72% C, 8.94% H, 12.34% O)

7.3.22 Hexa-(8-acetoxyoctyl)phenylbenzene (4-15)

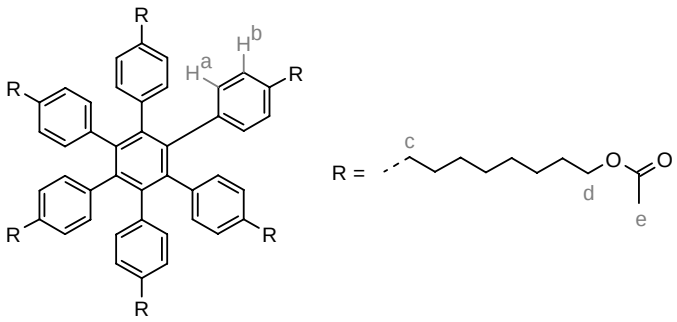

1.00 g 4,4'-Bis(8-acetoxyoctyl)diphenylacetylene (**4-14**, 1.93 mmol) were dissolved in 250 mL anhydrous 1,4-dioxane and degassed. Afterwards, 65 mg dicobaltoctacarbonyl (0.19 mmol, 10 mol%) were added and the resulting mixture was refluxed for 14 hours. The solvent was evaporated and the residue was purified using preparative column chromatography (silica gel, eluent: hexane, ethyl acetate = 2:1, R_f = 0.39) to afford 898 mg of the desired product as a colorless oil (89%, 0.58 mmol).

MS (FS, 8kV): m/z (%) = 1556.9 (100%, M^+) (calc. for $C_{102}H_{138}O_{12}$= 1556.23 g mol^{-1})

^{1}H NMR (250 MHz, CD_2Cl_2): δ = 6.72 (d, 12H, ^3J(H,H) = 8.21 Hz, H_b), 6.65 (d, 12H, ^3J(H,H) = 8.23 Hz, H_a), 4.02 (t, 12H, ^3J(H,H) = 6.71 Hz, H_d), 2.36 (t, 12H, ^3J(H,H) = 7.35 Hz, H_c), 2.00 (s, 18H, H_e), 1.7-1.0 (m, 72H, -CH_2-)

^{13}C NMR (63 MHz, CD_2Cl_2): δ = 171.26 (*C*=O), 140.70, 139.70, 138.72 (all Ar-*C*), 131.68, 126.80 (both Ar-*C*H), 64.82 (-*C*H_2-OAc), 35.62 (α-*C*H_2), 31.61, 29.71, 29.63, 29.17, 29.03, 26.34 (all -*C*H_2-), 2111 (-CO-*C*H_3)

7.3.23 2,5,8,11,14,17-Hexa-(8-acetoxyoctyl)-hexa-*peri*-hexabenzocoronene (4-16)

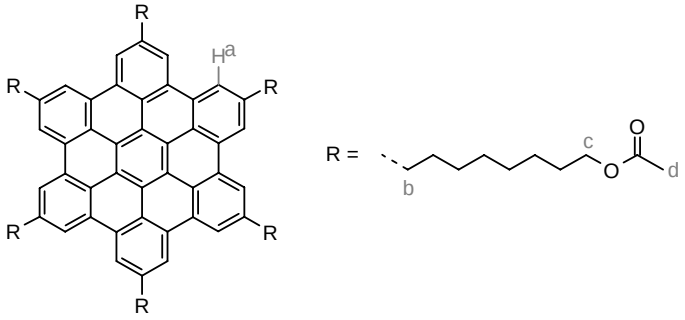

150 mg Hexa-(8-acetoxyoctyl)phenylbenzene (**4-15**, 96.0 µmol) were dissolved in 160 mL dichloromethane. A stream of argon saturated with dichloromethane was bubbled into the solution through a Teflon tube. A solution of 502 mg iron(III) chloride (3.10 mmol) in 6 mL nitromethane was quickly added. After a reaction time of 120 minutes, the reaction was stopped with water, the organic phase separated, washed, dried with magnesium sulfate and concentrated. The residue was filtered through a short silica pad with hot toluene to remove inorganic impurities. Finally, the crude product was purified using preparative column chromatography (neutral aluminum oxide, gradient from hexane, ethyl acetate = 2:1 to pure ethyl acetate) to yield 110 mg of the desired polycyclic aromatic hydrocarbon as a yellow, waxy solid (74%, 71 µmol).

MS (MALDI-TOF): m/z (%) = 1543 (30%), 1544 (33%), 1545 (22%), 1546 (9%), 1547 (4%) (calc. for $C_{102}H_{126}O_{12}$ = 1544.13 g mol^{-1}, Isotope pattern: 1543 (31%), 1544 (36%), 1545 (21%), 1546 (9%), 1547 (3%))

UV/vis: λ / nm (ε / m^2·mol^{-1}) = 342 (817), 361 (2001), 392 (688), 441 (22), 448(19), 466 (23)

^{1}H NMR (300 MHz, CD_2Cl_2): δ = 8.11 (s, 12H, H_a), 4.09 (t, 12H, ^3J(H,H) = 6.76 Hz, H_c), 2.89 (t, 12H, ^3J(H,H) = 7.61 Hz, H_b), 2.03 (s, 18H, H_d), 2.0-1.2 (m, 72H, -CH_2-)

^{13}C NMR (75 MHz, CD_2Cl_2): δ = 171.22 (*C*=O), 139.88, 129.48, 122.89, 121. 04, 119.14 (all HBC-*C*), 64.84 (-*C*H_2-OAc), 37.58 (α-*C*H_2), 32.89, 30.50, 30.25, 29.97, 29.14, 26.51 (all -*C*H_2-), 21.12 (-CO-*C*H_3)

UV/vis: λ / nm (ε / $m^2 \cdot mol^{-1}$) = 342 (826), 362 (2002), 392 (476), 466 (6)

DSC (°C): 50 (36)

Elemental Analysis: 78.36% C, 8.53% H (calc.: 79.34% C, 8.22% H, 12.43% O)

7.3.24 2,5,8,11,14,17-Hexa-(8-hydroxyoctyl)-hexa-*peri*-hexabenzocoronene (4-17)

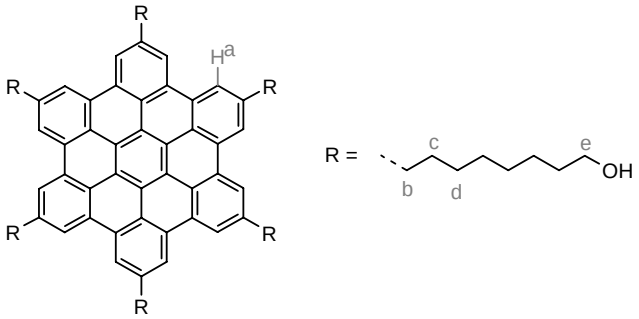

135 mg 2,5,8,11,14,17-Hexa-(8-acetoxyoctyl)-hexa-*peri*-hexabenzocoronene (**4-16**, 87.4 µmol) and 421 mg potassium hydroxide (7.50 mmol) were dissolved in a mixture of 25 mL THF, 1 mL methanol and 1 mL water. The mixture was refluxed for 15 hours and cooled down to room temperature. The basic solution was carefully neutralized with 2M aqueous hydrochloride acid. The precipitate was collected, extensively washed with water, methanol and THF, and dried *in vacuo*. The crude product was dissolved in a minimum amount of DMF and reprecipitated into water to afford 112 mg of the pure title compound as a yellow, crystalline solid (99%, 86.7 µmol).

MS (MALDI-TOF): m/z (%) = 1291 (35%), 1292 (36%), 1293 (20%), 1294 (9%) (calc. for $C_{90}H_{114}O_6$= 1291.90 g mol^{-1}, Isotope pattern: 1291 (36%), 1292 (37%), 1293 (19%), 1294 (7%))

^{1}H NMR (700 MHz, THF, 323 K): δ = 8.41 (s, 12H, H_a), 3.54 (t, 12H, ^3J(H,H) = 6.03 Hz, H_e), 3.02 (t, 12H, ^3J(H,H) = 6.55 Hz, H_b), 2.33 (m, 12H, H_c), 1.99 (m, 12H, H_d), 1.8-1.4 (m, 48H, -CH_2-)

^{13}C NMR (175 MHz, THF, 323 K): δ = 143.83, 133.61, 126.98, 124.96, 123.22, 65.67, 41.09, 37.13, 36.40, 34.01, 33.86, 33.74

DSC: no transition between -150 and 300°C

Elemental Analysis: 83.43% C, 8.05% H (calc.: 83.67% C, 8.89% H, 7.43% O)

7.3.25 2,5,8,11,14,17-Hexa-(5-acryloxypentyl)-hexa-*peri*-hexabenzocoronene (4-18)

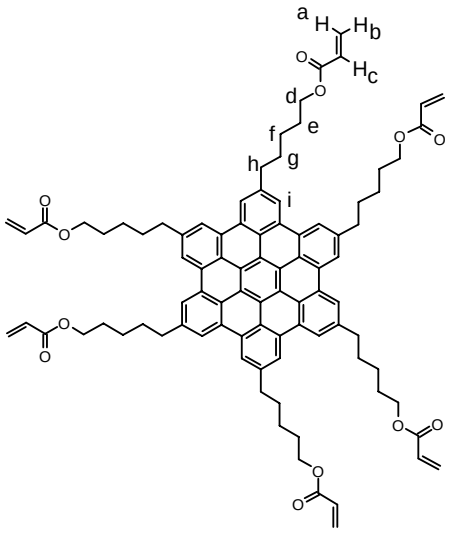

100 mg 2,5,8,11,14,17-Hexa-(5-hydroxypentyl)-hexa-*peri*-hexabenzocoronene (**4-12**, 96 µmol), 4.24 g N,N-dimethylanilin (35.0 mmol) und 77.0 mg 2,6-di-*tert*-butyl-4-methyl-phenole (350 µmol) were dissolved in 200 mL anhydrous 1,4-dioxan. 173 mg acryloyl chloride (2.33 mmol) were added to the solution and the mixture was stirred at 55 °C under light protection over night. The solvent was removed *in vacuo* and the crude material was repetitively reprecipitated into methanol to afford 98 mg of the desired compound as a yellow, waxy solid (75%, 72 µmol).

MS (MALDI-TOF): m/z (%) = 1363 (36%), 1364 (33%), 1365 (18%), 1366 (8%), 1367 (5%) (calc. for $C_{90}H_{90}O_{12}$ = 1363.71 g mol^{-1}, Isotope pattern: 1363 (35%), 1364 (36%), 1365 (20%), 1366 (7%), 1367 (2%))

^{1}H-NMR (500 MHz, CD_2Cl_2, 306 K): δ = 8.33 (s, 12H, H_i), 6.38 (dd, 6H, ^{3}J(H,H) = 17.30 Hz, ^{2}J(H,H) = 1.43 Hz, H_a), 6.15 (dd, 6H, ^{3}J(H,H) = 10.39 Hz, ^{3}J(H,H) = 17.32 Hz,, H_c), 5.79 dd, 6H, ^{3}J(H,H) = -10.36 Hz, ^{2}J(H,H) = 1.40 Hz, H_b), 4.28 (t, 12H, ^{3}J(H,H) = 6.64, H_d), 3.01 (t, 12H, ^{3}J(H,H) = 7.79, H_h), 1.98 (m, 12H, H_e), 1.90 (m, 12H, H_g), 1.70 (m, 12H, H_f)

^{13}C-NMR (125 MHz, CD_2Cl_2, 306 K): δ = 165.46, 139.07, 129.55, 128.82, 128.05, 122.25, 120.39, 118.54, 63.96, 36.38, 31.37, 28.18, 25.63.

UV/vis: λ / nm (ε / m^2·mol^{-1}) = 342 (866), 361 (2096), 392 (688), 466 (7)

DSC (°C): 112 (92) (polymerization starts at 150°C)

Elemental Analysis: 80.38% C, 6.19% H (calc.: 79.27% C, 6.65% H, 14.08% O)

7.3.26 2,5,8,11,14,17-Hexa-(5-pent-5'-ene-oxypentyl)-hexa-*peri*-hexabenzocoronene (4-19)

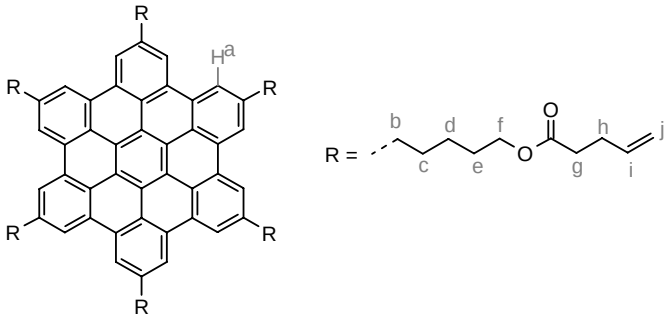

15 mg 2,5,8,11,14,17-Hexa-(5-hydroxypentyl)-hexa-*peri*-hexabenzocoronene (**4-12**, 24.1 µmol) were suspended in a mixture of 10 mL anhydrous toluene and 1 mL freshly distilled triethyl amine. Afterwards, 171 mg pent-4-enoyl chloride (1.46 mmol) was syringed into the reaction and the resulting mixture was stirred over night. The reaction was stopped by the addition of methanol. The precipitate was collected and reprecipitated into methanol to afford 31 mg of the title compound as a yellow solid (84%, 20.2 µmol).

MS (MALDI-TOF): m/z (%) = 1231 (31%), 1232 (33%), 1233 (24%), 1234 (9%), 1235 (2%) (calc. for $C_{102}H_{114}O_{12}$ = 1532.04 g mol^{-1}, Isotope pattern: 1231 (31%), 1232 (36%), 1233 (21%), 1234 (9%), 1235 (3%))

^{1}H NMR (250 MHz, CD_2Cl_2): δ = 8.49 (s, 12H, H_a), 5.8-5.6 (m, 6H, H_i), 5.0-4.8 (m, 12H, H_j), 4.10 (t, 12H, ^3J(H,H) = 6.50 Hz, H_f), 3.04 (t, 12H, ^3J(H,H) = 8.71 Hz, H_b), 2.4-2.2 (m, 12H, H_h), 2.05-1.85 (m, 12H, H_g), 1.85-1.70 (m, 12H, H_e), 1.70-1.55 (m, 12H, H_c), 1.55-1.40 (m, 12H, H_d)

^{13}C NMR (75 MHz, CD_2Cl_2): δ = 173.24 (C=O), 140.36, 137.33, 130.01, 121.62, 119.76 (all Ar-*C*), 115.41, 101.22 (both -CH=CH_3), 64.76, 43.77, 33.89, 29.27, 37.45, 32.40, 26.60 (all alkyl-*C*).

UV/vis: λ / nm (ε / m^2·mol^{-1}) = 342 (823), 361 (1999), 392 (587), 466 (12)

DSC (°C): -1 (-36)

Elemental Analysis: 79.86% C, 7.59% H (calc.: 79.97% C, 7.50% H, 12.53% O)

7.3.27 2,5,8,11,14,17-Hexa-(5-pent-5'-yne-oxypentyl)-hexa-*peri*-hexabenzocoronene (4-20)

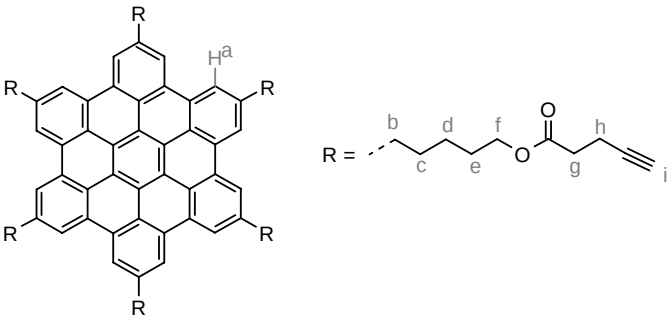

100 mg 2,5,8,11,14,17-Hexa-(5-hydroxypentyl)-hexa-*peri*-hexabenzocoronene (**4-12**, 96.2 µmol), 113 mg pent-4-ynoic acid (1.15 mmol), 237 mg dicyclohexyl-

carbodiimide (1.15 mmol), and 23 mg DMAP (192 µmol) were dissolved in 100 mL anhydrous dichloromethane. The solution was stirred at room temperature over night. After having removed the solvent *in vacuo*, the residue was precipitated into methanol. The solid was filtered off and dried in high vacuum. Residual urea was sublimed out to afford 107 mg of the title compound as a waxy yellow solid (73%, 70.4 µmol).

MS (MALDI-TOF): m/z (%) = 1519 (28%), 1520 (36%), 1521 (20%), 1522 (11%), 1523 (5%) (calc. for $C_{102}H_{102}O_{12}$ = 1519.94 g mol^{-1}, Isotope pattern: 1519 (31%), 1520 (36%), 1521 (21%), 1522 (9%), 1523 (3%))

^{1}H-NMR (300 MHz, CD_2Cl_2, 306 K): δ = 8.43 (s, 12H, H_a), 4.22 (t, 12H, ^3J(H,H) = 6.67 Hz, H_f), 3.06 (t, 12H, ^3J(H,H) = 7.90, H_b), 2.6-2.4 (m, 24H, H_g, H_h), 2.05-1.95 (m, 12H, H_e), 1.98 (t, 6H, ^4J(H,H) = 2.55 Hz, H_i), 1.95-1.80 (m, 12H, H_c), 1.75-1.60 (m, 12H, H_d)

2.4-2.2 (m, 6H, H_d), 2.1-1.2 (m, 84H, -CH_2-), 0.92 (t, 18H, ^3J(H,H) = 7.41 Hz, H_e), 0.91(t, 18H, ^3J(H,H) = 6.48 Hz, H_f)

^{13}C-NMR (75 MHz, CD_2Cl_2, 306 K): δ = 172.07 (*C*=O), 140.01, 129.78, 123.22, 121.33, 119.50 (all Ar-*C*), 83.10, 69.09, 65.14, 37.42, 33.76, 32.40, 29.21, 26.62, 14.70

UV/vis: λ / nm (ε / m^2·mol^{-1}) = 345 (766), 362 (1932), 392 (629), 441 (8)

DSC (°C): 85 (73)

Elemental Analysis: 78.81 % C, 6.53 % H (calc.: 80.60 % C, 6.76 % H, 12.63 % O)

7.3.28 2,5,8,11,14,17-Hexa-(5-octanoyl-oxypentyl)-hexa-*peri*-hexabenzocoronene (4-21)

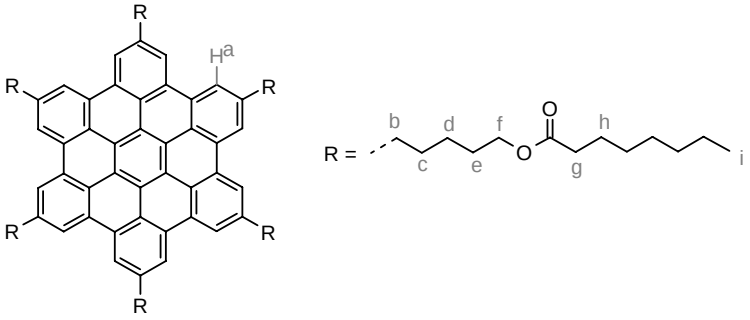

100 mg 2,5,8,11,14,17-Hexa-(5-hydroxypentyl)-hexa-*peri*-hexabenzocoronene (**4-12**, 96.2 µmol) and 939 mg octanoyl chloride (5.77 mmol) were suspended in a mixture of 1 mL triethyl amine and 50 mL THF and stirred at room temperature over night. The solvent was removed *in vacuo* and the crude material was repetitively reprecipitated into methanol to afford 154 mg of the desired compound as a yellow, waxy solid (89%, 85.7 µmol).

MS (MALDI-TOF): m/z (%) = 1795 (26%), 1796 (35%), 1797 (23%), 1798 (11%), 1799 (5%) (calc. for $C_{120}H_{162}O_{12}$ = 1796.62 g mol^{-1}, Isotope pattern: 1795 (25%), 1796 (34%), 1797 (24%), 1798 (11%), 1799 (4%))

^{1}H-NMR (300 MHz, CD_2Cl_2, 306 K): δ = 8.40 (s, 12H, H_a), 4.18 (t, 12H, ^3J(H,H) = 6.63, H_f), 3.06 (t, 12H, ^3J(H,H) = 7.99, H_b), 2.27 (t, 12H, ^3J(H,H) = 7.69 Hz, H_g),

2.10-1.95 (m, 12H, H_e), 1.95-1.80 (m, 12H, H_c), 1.75-1.65 (m, 12H, H_h), 1.65-1.50 (m, 12H, H_d), 1.35-1.10 (m, 48H, -CH_2-), 0.81 (t, 18H, ^3J(H,H) = 6.85 Hz, H_i)

^{13}C-NMR (75 MHz, CD_2Cl_2, 306 K): δ = 174.01 (*C*=O), 140.18, 129.96, 123.39, 121.51, 119.68, 64.59, 37.46, 34.68, 32.39, 32.06, 29.50, 29.41, 29.31, 26.65, 25.42, 22.96, 14.18.

UV/vis: λ / nm (ε / $m^2 \cdot mol^{-1}$) = 342 (844), 361 (2058), 392 (604), 466 (8)

DSC (°C): 53 (32)

Elemental Analysis: 80.34% C, 8.92% H (calc.: 80.22% C, 9.09% H, 10.69% O)

7.3.29 2,5,8,11,14,17-Hexa-(5-(2,2,3,3,4,4,5,5,6,6,7,7,8,8,8-pentadecafluoro-octanoyloxy)-oxypentyl)-hexa-*peri*-hexabenzocoronene (4-22)

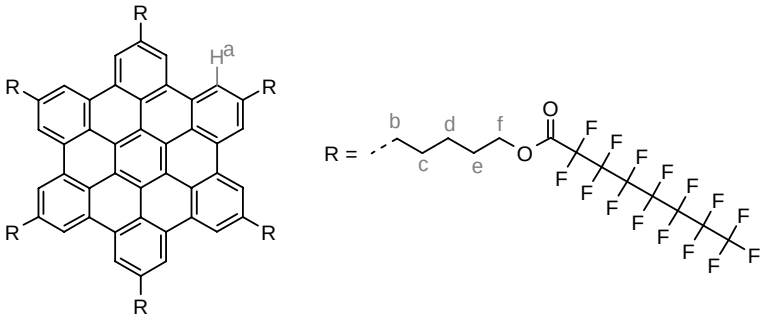

20 mg 2,5,8,11,14,17-Hexa-(5-hydroxypentyl)-hexa-*peri*-hexabenzocoronene (**4-12**, 19.2 µmol) and 499 mg 2,2,3,3,4,4,5,5,6,6,7,7,8,8,8-pentadecafluoro-octanoyl chloride (1.15 mmol) were suspended in a mixture of 1 mL triethyl amine and 50 mL THF and stirred at 45 °C over night. The solvent was removed *in vacuo* and the crude material was repetitively reprecipitated into methanol to afford 52 mg of the desired compound as a yellow, waxy solid (79%, 15.2 µmol).

MS (MALDI-TOF): m/z (%) = 3414 (25%), 3415 (34%), 3416 (22%), 3417 (12%), 3418 (6%) (calc. for $C_{120}H_{72}F_{90}O_{12}$ = 3415.76 g mol^{-1}, Isotope pattern: 3414 (25%), 3415 (34%), 3416 (24%), 3417 (11%), 3418 (4%))

^{1}H-NMR (500 MHz, THF, 354 K): δ = 8.86 (s, 12H, H_a), 4.52 (t, 12H, ^3J(H,H) = 6.46, H_f), 3.20 (tb, 12H, H_b), 2.2-1.9 (m, 24H, H_e, H_c), 1.8-1.6 (m, 12H, H_d)

^{13}C-NMR: no resolved spectrum could be recorded because of the vanishing solubility

^{19}F-NMR (471 MHz, THF, 323 K): δ = -77.83 (3F), -114.99 (2F), -117.97 (2F), -118.34 (2F), -119.02 (4F), -122.62 (2F)

UV/vis: λ / nm (ε / $m^2 \cdot mol^{-1}$) = 342 (816), 361 (1987), 392 (544)

DSC (°C): no transition

Elemental Analysis: 42.17% C, 2.07% H (calc.: 42.20% C, 2.12% H, 50.06% F, 5.62% O)

7.3.30 2,5,8,11,14,17-Hexa-[5-(3,4,5-Trimethoxy-benzoyloxy)-pentyl]-hexa-*peri*-hexabenzocoronene (4-23)

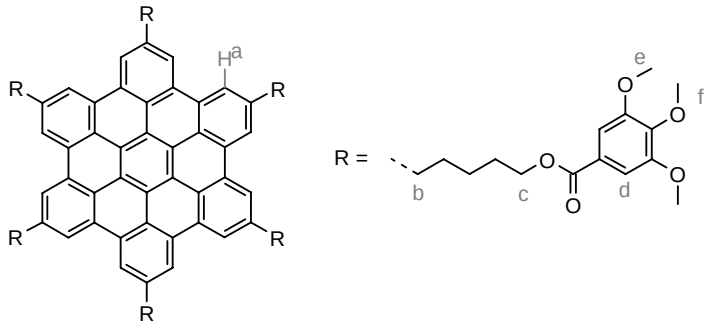

20 mg 2,5,8,11,14,17-Hexa-(5-hydroxypentyl)-hexa-*peri*-hexabenzocoronene (**4-12**, 19.2 µmol) and 266 mg 3,4,5-trimethoxy-benzoyl chloride (1.15 mmol) were dissolved in 25 mL pyridine. The solvent was removed *in vacuo* and the residue was repetitively precipitated into methanol to yield 25 mg of the title compound as a yellow solid (59%, 11.3 µmol).

MS (MALDI-TOF): m/z (%) = 2203 (21%), 2204 (29%), 2205 (23%), 2206 (14%), 2207 (8%), 2208 (5%) (calc. for $C_{132}H_{138}O_{30}$ = 2204.55 g mol^{-1}, Isotope pattern: 2203 (21%), 2204 (32%), 2205 (25%), 2206 (14%), 2207 (6%), 2208 (2%))

^{1}H-NMR (250 MHz, CD_2Cl_2, 306 K): δ = 8.49 (s, 12H, H_a), 7.24 (s, 12H, H_d), 4.38 (t, 12H, ^{3}J(H,H) = 6.42 Hz, H_c), 3.73 (s, 36H, H_e), 3.71 (s, 18H, H_f), 3.08 (t, 12H, ^{3}J(H,H) = 6.44 Hz, H_b), 2.3-1.5 (m, 36H, -CH_2-).

^{13}C-NMR (65 MHz, CD_2Cl_2, 306 K): δ = 166.40, 153.34, 142.52, 140.39, 130.01, 125.81, 121.64, 123.42, 119.77, 107.01, 65.52, 60.74, 56.35, 37.44, 32.40, 29.29, 26.65.

UV/vis: λ / nm (ε / m^2·mol^{-1}) = 342 (800), 362 (1998), 392 (466), 467 (5)

DSC (°C): 34 (-22)

Elemental Analysis: 71.87% C, 6.13% H (calc.: 71.92% C, 6.31% H, 21.77% O)

7.3.31 2,5,8,11,14,17-Hexa-(5-pentafluorobenzoyloxy-pentyl)-hexa-*peri*-hexabenzocoronene (4-24)

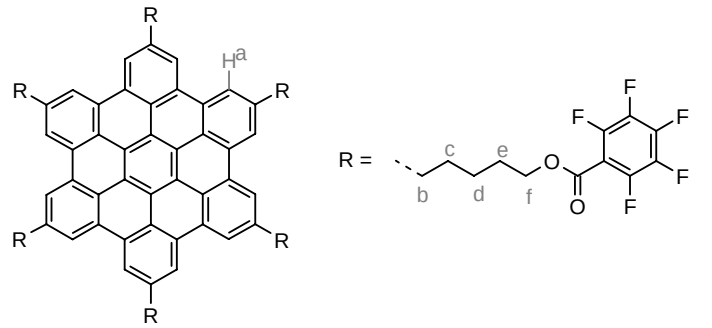

25.1 mg 2,5,8,11,14,17-Hexa-(5-hydroxypentyl)-hexa-*peri*-hexabenzocoronene (**4-12**, 24.2 µmol) and 450 mg 2,3,4,5,6-pentafluoro-benzoyl chloride (1.95 mmol) were suspended in a mixture of 1 mL triethyl amine and 20 mL toluene. After having

removed the solvents in vacuo, the residue was repetitively precipitated into methanol to afford 39 mg of the desired product as a yellow solid (73%, 17.7 µmol). 21715

MS (MALDI-TOF): m/z (%) = 2202 (28%), 2203 (33%), 2204 (23%), 2205 (11%), 2206 (5%) (calc. for $C_{114}H_{72}F_{30}O_{12}$ = 2203.79 g mol^{-1}, Isotope pattern: 2202 (27%), 2203 (35%), 2204 (23%), 2205 (10%), 2206 (3%))

^{1}H-NMR (500 MHz, CD_2Cl_2, 306 K): δ = 8.54 (s, 12H, H_a), 4.48 (t, 12H, ^3J(H,H) = 6.48, H_f), 3.13 (t, 12H, ^3J(H,H) = 7.86, H_b), 2.06 (m, 12H, H_e), 1.97 (m, 12H, H_c), 1.72 (m, 12H, H_d)

^{13}C-NMR (125 MHz, CD_2Cl_2, 306 K): δ = 159.33, 145.76 (^1J(F,C) = 257 Hz), 143.30 (^1J(F,C) = 259 Hz), 140.41, 137.95 (^1J(F,C) = 257 Hz), 130.08, 123.50, 121.81, 119.87, 67.13, 37.21, 31.92, 28.82, 26.06.

UV/vis: λ / nm (ε / m^2·mol^{-1}) = 343 (804), 361 (1958), 392 (477), 466 (5)

DSC (°C): 53 (-18)

Elemental Analysis: 61.97% C, 3.27% H (calc.: 62.13% C, 3.29% H, 8.71% O, 25.86% F)

7.3.32 2,5,8,11,14,17-Hexa-[5-(2-ethyl-hexanoyloxy)-pentyl]-hexa-*peri*-hexabenzocoronene (4-25)

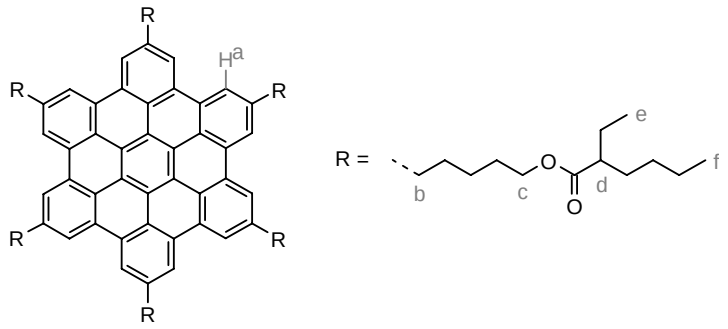

100 mg 2,5,8,11,14,17-Hexa-(5-hydroxypentyl)-hexa-*peri*-hexabenzocoronene (**4-12**, 96.2 µmol) and 939 mg 2-ethyl-hexanoyl chloride (5.77 mmol) were suspended in a mixture of 1 mL triethyl amine and 25 mL dichloromethane and stirred at room temperature over night. The solvent was removed *in vacuo* and the crude material was repetitively reprecipitated into methanol to afford 127 mg of the desired compound as a yellow, waxy solid (73%, 70.7 µmol).

MS (MALDI-TOF): m/z (%) = 1795 (28%), 1796 (36%), 1797 (21%), 1798 (11%), 1799 (4%) (calc. for $C_{120}H_{162}O_{12}$ = 1796.62 g mol^{-1}, Isotope pattern: 1795 (25%), 1796 (34%), 1797 (24%), 1798 (11%), 1799 (4%))

^{1}H-NMR (300 MHz, CD_2Cl_2, 306 K): δ = 8.27 (s, 12H, H_a), 4.23 (t, 12H, ^3J(H,H) = 6.53, H_c), 2.99 (t, 12H, ^3J(H,H) = 7.66, H_b), 2.4-2.2 (m, 6H, H_d), 2.1-1.2 (m, 84H, -CH_2-), 0.92 (t, 18H, ^3J(H,H) = 7.41 Hz, H_e), 0.91(t, 18H, ^3J(H,H) = 6.48 Hz, H_f)

^{13}C-NMR (125 MHz, CD_2Cl_2, 306 K): δ = 176.52 (*C*=O), 139.94, 129.77, 123.22, 121.27, 119.48 (all Ar-*C*), 64.41, 47.75, 37.53, 32.52, 32.21, 30.06, 29.38, 26.77, 25.92, 23.07, 14.20, 12.09.

UV/vis: λ / nm (ε / m^2·mol^{-1}) = 342 (822), 361 (2017), 392 (587), 466 (4)

DSC (°C): 15 (-3)

Elemental Analysis: 80.34% C, 8.92% H (calc.: 80.22% C, 9.09% H, 10.69% O)

7.3.33 2,5,8,11,14,17-Hexa-[5-(2-hexyl-decanoyloxy)-pentyl]-hexa-*peri*-hexabenzocoronene (4-26)

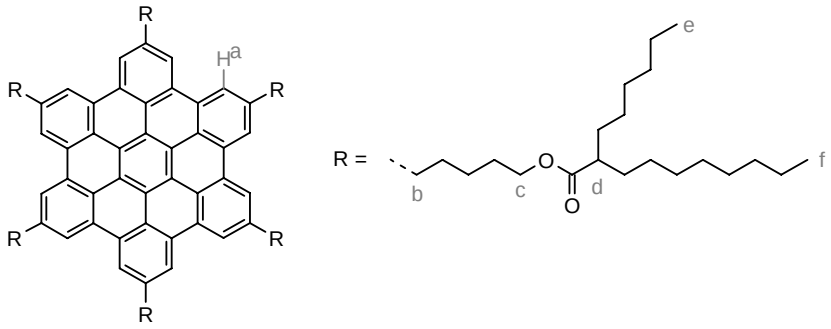

100 mg 2,5,8,11,14,17-Hexa-(5-hydroxypentyl)-hexa-*peri*-hexabenzocoronene (**4-12**, 96.2 µmol), 296 mg 2-hexyl-decanoic acid (1.15 mmol), 198 mg dicyclohexyl-carbodiimide (0.96 mmol), and 19 mg DMAP (154 µmol) were dissolved in 100 mL anhydrous dichloromethane. The solution was stirred at room temperature over night. After having removed the solvent *in vacuo*, the residue was precipitated twice into methanol. Residual urea was sublimed out to afford 211 mg of the title compound as a waxy yellow solid (89%, 85.4 µmol).

MS (MALDI-TOF): m/z (%) = 2468 (17%), 2469 (28%), 2470 (28%), 2471 (15%), 2472 (9%), 2473 (4%) (calc. for $C_{168}H_{258}O_{12}$ = 2469.92 g mol^{-1}, Isotope pattern: 2468 (15%), 2469 (28%), 2470 (27%), 2471 (17%), 2472 (8%), 2473 (3%))

^{1}H-NMR (500 MHz, CD_2Cl_2, 306 K): δ = 8.52 (s, 12H, H_a), 4.18 (t, 12H, ^{3}J(H,H) = 6.47, H_c), 3.12 (t, 12H, ^{3}J(H,H) = 7.64, H_b), 2.4-2.2 (m, 6H, H_d), 2.2-1.0 (m, 180H, -CH_2-), 0.84 (t, 18H, ^{3}J(H,H) = 6.27 Hz, H_e), 0.81(t, 18H, ^{3}J(H,H) = 6.85 Hz, H_f).

^{13}C-NMR (125 MHz, CD_2Cl_2, 306 K): δ = 176.67 (*C*=O), 140.39, 130.13, 123.56, 121.67, 119.88, 64.37, 46.11, 37.53, 32.84, 32.46, 32.24, 32.11, 29.93, 29.83, 29.64, 29.61, 29.34, 27.80, 27.78, 26.68, 23.03, 22.99, 14.25.

UV/vis: λ / nm (ε / m^2·mol^{-1}) = 342 (877), 361 (2056), 392 (577), 466 (14)

DSC (°C): -1 (-36)

Elemental Analysis: 81.69% C, 10.57% H (calc.: 81.70% C, 10.53% H, 7.77% O)

7.3.34 9,11-Diphenyl-cyclopenta[*e*]pyren-10-one (5-2)

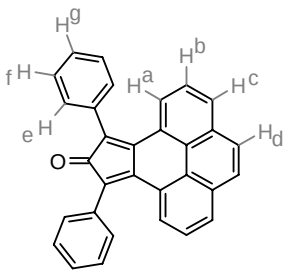

1.00 g Pyren-4,5-dione (**5-1**, 4.30 mmol) and 905 mg 1,3-diphenylpropan-2-one (4.30 mmol) were suspended in 40 mL ethanol. A solution of 133 mg potassium hydroxide

in 1 mL water was added slowly while heating the reaction to 80 °C. After 10 minutes at that temperature, 40 mL water was added in order to stop the reaction. The reaction was quickly extracted with dichloromethane. The organic phase was dried with magnesium sulfate and evaporated *in vacuo*. The residue was purified using preparative column chromatography (silica gel, eluent: low boiling petroleum ether, dichloromethane = 1:1, R_f = 0.78) to afford 720 mg of the thermally unstable product as a dark brown solid (41%, 1.78 mmol). The compound was directly converted, because it is only stable at -20 °C for a couple of days.

MS (FS, 8 kV): m/z (%): 406.5 (100%, M^+) (calc. for $C_{31}H_{18}O$ = 406.49 g mol^{-1})

^{1}H NMR (700 MHz, CD_2Cl_2): δ = 7.90 (dd, ^3J(H,H) = 6.82 Hz, ^4J(H,H) = 1.42 Hz, 2H, H_c), 7.82 (d, ^3J(H,H) = 7.61 Hz, 2H, H_a), 7.76 (t, ^3J(H,H) = 7.81 Hz, 2H, H_b), 7.68 (s, 2H, H_d), 7.50 (m, 4H, H_e), 7.44 (m, 6H, H_f, H_g) (spectrum shows decomposed side products, because of the instability in solution)

^{13}C NMR (125 MHz, CD_2Cl_2): compound not stable in solution for longer measurement durations

7.3.35 9,10,11,12-Tetraphenylbenzo[*e*]pyrene (5-3)

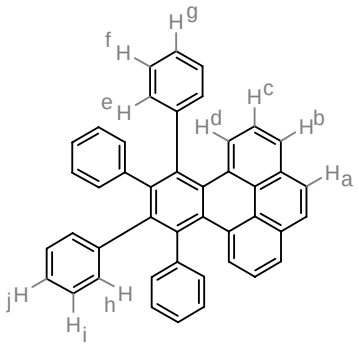

250 mg 9,11-Diphenyl-cyclopenta[*e*]pyren-10-one (**5-2**, 0.62 mmol) and 109 mg (0.62 mmol) diphenyl acetylene were dissolved in 1 mL diphenyl ether and heating in a microwave furnace for 45 min at 280°C (250W, no ramp time). The diphenyl ether was evaporated *in vacuo* and the residue was purified using preparative column chromatography (flash silica gel, eluent: petroleum ether, dichloromethane = 9:1, R_f = 0.12-0.33). The substance was reprecipitated from dichloromethane into methanol to yield 69 mg of the desired product as a colorless solid (20%, 0.12 mmol).

MS (FS, 8 kV): m/z (%): 556.4 (100%, M^+) (calc. for $C_{44}H_{28}$ = 556.71 g mol^{-1})

^{1}H NMR (300 MHz, CD_2Cl_2): δ = 7.97 (s, 2H, H_a), 7.95 (d, ^3J(H,H) = 7.62 Hz, ^4J(H,H) = 1.09 Hz, 2H, H_b), 7.88 (t, ^3J(H,H) = 8.22 Hz, ^4J(H,H) = 0.97 Hz, 2H, H_c), 7.39 (d, ^3J(H,H) = 8.09 Hz, 2H, H_d), 7.15-7.1 (m, 10H, H_e, H_f, H_g), 6.94-6.92 (m, 6H, H_i, H_j), 6.82-6.80 (m, 4H, H_h)

^{13}C NMR: the solubility is too low to record resolved spectra

Elemental Analyis: 94.67% C, 5.02% H (calc. 94.93% C, 5.07% H).

7.3.36 2,7-Di-*tert*-butylpyrene-4,5-dione (5-6)

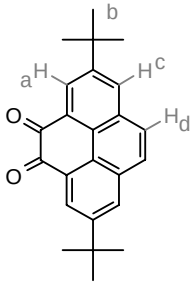

A solution of 10.0 g 2,7-di-*tert*-butylpyrene (**5-5**, 31.8 mmol) in a mixture of 150 mL DMF and 40 mL 6 M aqueous acetic acid was treated with 0.32 g ruthenium dioxide (2.40 mmol) and 6.43 g sodium periodate (30.0 mmol). The mixture was stirred at room temperature for 24 hours, and an additional 4 g of sodium periodate (18.6 mmol) were added. The stirring was continued for 24 hours. The suspension was filtered and the filtrate was poured into cold water and extracted with dichloromethane. The organic layer was washed three times with water, dried over magnesium sulfate, concentrated and the residue was purified by column chromatography (silica gel, eluent: low boiling petroleum ether, dichloromethane = 1:1, R_f = 0.56) to afford 1.09 g of the title compound as a orange solid (10%, 3.16 mmol).

MS (FS, 8kV): m/z (%) = 344.0 (100%, M^+) (calc. for $C_{24}H_{24}O_2$ = 344.46 g mol^{-1})

^{1}H NMR (250 MHz, CD_2Cl_2): δ = 8.51 (d, 2H, ^4J(H,H) = 2.07 Hz, H_c), 8.17 (d, 2H, ^4J(H,H) = 2.11 Hz, H_a), 7.83 (s, 2H, H_d), 1.49 (s, 18H, H_b).

^{13}C NMR (63 MHz, CD_2Cl_2): δ = 181.73, 151.91, 132.84, 132.65, 130.68, 128.73, 128.11, 127.21, 35.93, 31.75;

Elemental Analysis: 84.51% C, 7.07% H (calc. 83.69% C, 7.02% H, 9.29% O).

7.3.37 2,7-Di-*tert*-butyl-9,11-bis-(4-*tert*-butyl-phenyl)-cyclopenta[*e*]pyren-10-one (5-7)

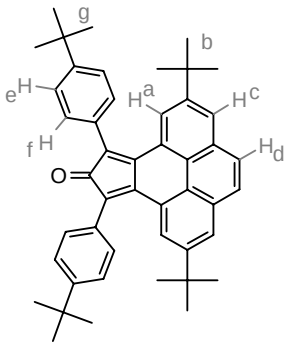

0.34 g 2,7-Di-*tert*-butylpyrene-4,5-dione (**5-5**, 1.0 mmol) and 0.35 g 1,3-bis-(4-*tert*-butyl-phenyl)propan-2-one (1.10 mmol) were suspended in 15 mL ethanol under an argon atmosphere. A solution prepared from 31 mg potassium hydroxide (0.55 mmol) in 1 mL methanol was added drop wise at room temperature. The mixture was heated to 80 ° C for 15 minutes, and then quenched by addition of 50 mL water. The product was extracted with dichloromethane, concentrated and the residue was purified by column chromatography (silica gel, eluent: low boiling petroleum ether,

dichloromethane = 3:1) to yield 0.49 g of the title compound as dark brown solid (78%, 0.78 mmol).

MS (FS, 8kV): m/z (%) = 630.2 (100%, M^+) (calc. for $C_{47}H_{50}O$ = 630.92 g mol^{-1})

^{1}H NMR (250 MHz, CD_2Cl_2): δ = 7.80 (d, ^4J(H,H) = 1.90 Hz, 2H, H_c), 7.68 (d, ^4J(H,H) = 1.90 Hz, 2H, H_a), 7.61 (s, 2H, H_d), 7.58 (d, 4H, ^3J(H,H) = 8.53 Hz, H_f), 7.38 (d, ^3J(H,H) = 8.53 Hz, H_e), 1.39 (s, 18H, H_g), 1.10 (s, 18H, H_b)

^{13}C NMR (63 MHz, CD_2Cl_2): δ = 201.63, 151.51, 150.06, 148.73, 132.34, 130.89, 129.89, 127.43, 127.36, 127.09, 126.90, 126.28, 125.03, 123.97, 35.01, 34.89, 31.41, 30.93.

7.3.38 4-Ethynyl-phenanthrene (5-21)

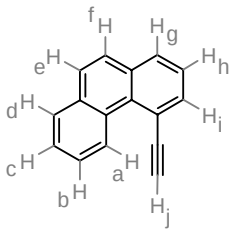

600 mg 4-Ethynyltrimethylsilyl-phenanthrene (**5-33**, 2.19 mmol) were dissolved under gentle heating in 60 mL methanol and degassed. Afterwards, 1.2 g potassium carbonate (8.70 mmol) was added and the mixture was stirred at room temperature over night. The reaction was quenched by adding water. The product was extracted using dichloromethane. After removing the solvent from the organic phase *in vacuo*, the residue was recrystallized with ethanol to afford 420 mg of the desired product as yellowish needles (95%, 2.1 mmol) (R_f = 0.67, hexane, ethyl acetate = 8:2).

MS (EI): m/z (%) = 51.0 (1.21), 61.8 (2.37), 63.0 (1.96), 73.7 (4.57), 75.1 (3.37), 86.6 (8.42), 87.8 (3.90), 88.3 (3.86), 95.9 (1.07), 97.8 (3.24), 99.4 (18.44), 100.4 (20.57), 101.3 (8.33), 109.3 (1.33), 148.9 (2.74), 149.9 (3. 19), 151.1 (1.40), 173.8 (4.92), 175.1 (2.21), 176.1 (1.37), 197.8 (4.30), 199.8 (38.48), 201.0 (3.50), 201.8 (100%), 203.2 (13.65, M^+) (calc. for $C_{16}H_{10}$ = 202.26 g mol^{-1})

^{1}H NMR (300 MHz, CD_2Cl_2): δ = 10.38 (m, 1H, H_a), 8.0-7.9 (m, 3H, H_d, H_b, H_e), 7.8-7.6 (m, 4H, H_c, H_f, H_g, H_i), 7.56 (t, 1H, ^3J(H,H) = 7.85 Hz, H_h), 3.80 (s, 1H, H_j)

^{13}C NMR (75 MHz, CD_2Cl_2): δ = 136.53, 133.51, 133.43, 130.83, 130.75, 130.33, 128.85, 128.35, 127.68, 127.51, 126.48, 126.37, 125.99, 118.43, 86.58(-C≡*C*H), 84.01

(-*C*≡CH)

Elemental Analysis: 95.30% C, 4.88% H (calc.: 95.02% C, 4.98% H)

7.3.39 4-Phenyl-[1,1';4',1'']terphenyl-2'yl)-phenanthrene (5-13a)

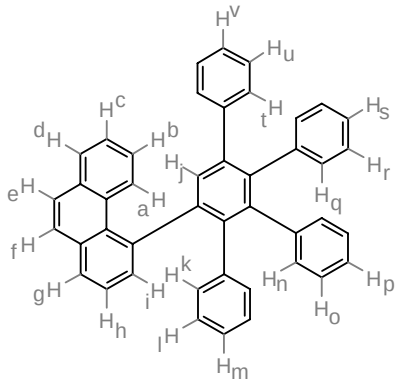

100 mg 2,3,4,5-Tetraphenyl-cyclopenta-2,4-dienone (**5-34a**, 260 µmol) and 53 mg 4-ethynyl-phenanthrene (**5-21**, 260 µmol) were dissolved in 1 mL *o*-xylene and degassed. The reaction was conducted in a sealed tube in a microwave oven (300 W, no ramp time) at 160 °C. After 10 minutes, the reaction was cooled to room temperature, the solvent was removed *in vacuo*, and the residue was purified utilizing preparative column chromatography (silica gel, eluent: low boiling petroleum ether, dichloromethane = 8:2, R_f = 0.18) to afford 122 mg of the title compound as a colorless powder (84%, 218 µmol).

MS (FD, 8kV): m/z (%) = 558.2 (100%, M^+) (calc. for $C_{44}H_{30}$ = 558.73 g mol^{-1})

^{1}H NMR (500 MHz, CD_2Cl_2, 303 K): δ = 8.28 (d, 1H, ^3J(H,H) = 8.60 Hz, H_a), 7.87 (dd, 1H, ^3J(H,H) = 7.89 Hz, ^4J(H,H) = 1.44 Hz, H_d), 7.77 (dd, 1H, ^3J(H,H) = 7.30 Hz, ^4J(H,H) = 2.01 Hz, H_g), 7.68 (s, 2H, H_e, H_f), 7.58 (s, 1H, H_j), 7.57 (t, 1H, ^3J(H,H) = 7.90 Hz, ^4J(H,H) = 1.04 Hz, H_c), 7.52-7.45 (m, 3H, H_h, H_i, H_b), 7.23-6.85 (m, 16H, H_n, H_o, H_p, H_q, H_r, H_s, H_t, H_u, H_v), 6.80 (bs, 1H, H_l), 6.69 (t, 1H, ^3J(H,H) = 7.36 Hz, ^4J(H,H) = 1.20 Hz, H_m), 6.52 (bs, 1H, $H_{l'}$), 6.45 (bs, 1H, $H_{k'}$)

^{13}C NMR (75 MHz, CD_2Cl_2): δ = 143.88, 143.09, 142.10, 141.95, 140.90, 140.62, 140.22, 140.08, 139.87, 139.55, 133.73, 133.57, 132.13, 132.07, 132.00, 131.83, 131.71, 131.21, 131.12, 130.29, 129.40, 128.95, 128.44, 127.89, 127.75, 127.57, 127.29, 126.95, 126.63, 126.59, 126.39, 126.06, 125.73, 125.70, 125.65, 125.51, 131.55, 131.50, 130.08, 127.86

Elemental Analysis: 94.96% C, 5.10% H (calc.: 94.59% C, 5.41% H)

7.3.40 Tetrabenzo[*bc,ef,hi,uv*]ovalene (5-4, 5-16a)

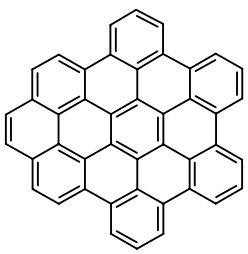

65.1 mg 4-Phenyl-[1,1';4',1'']terphenyl-2'yl)-phenanthrene (**5-13a**, 116 µmol) or 77.3 mg 9,10,11,12-tetraphenylbenzo[*e*]pyrene (**5-3**, 139 µmol) were dissolved in 25 mL dichloromethane. A stream of argon saturated with dichloromethane was bubbled into the solution through a Teflon tube. A solution of 679 mg iron(III) chloride

(5.17 mmol) in 1 mL nitromethane was quickly added. After a reaction time of 60 minutes, the reaction was stopped with methanol. The precipitate was filtered off and washed extensively with aqueous hydrochloride acid and methanol to afford 52 mg of the product as a orange solid (82%, 95.1 µmol).

MS (MALDI-TOF): m/z (%) = 546 (59%), 547 (26%), 548 (11%), 549 (4%) (calc. for $C_{44}H_{18}$ = 546.63 g mol^{-1}, isotope pattern: 546 (61%), 547 (30%), 548 (7%), 549 (1%))

UV/vis: λ / nm = 348, 363, 380, 414, 438, 465 (molar extinction coefficient could not be determined due to the vanishing solubility in organic solvents)

Elemental Analysis: 95.74% C, 3.18% H (calc.: 96.68% C, 3.32% H)

7.3.41 4-(4,4'',5',6'-Tetra-*t*-butyl-phenyl)-[1,1';4',1'']terphenyl-2'yl)-phenanthrene (5-13b)

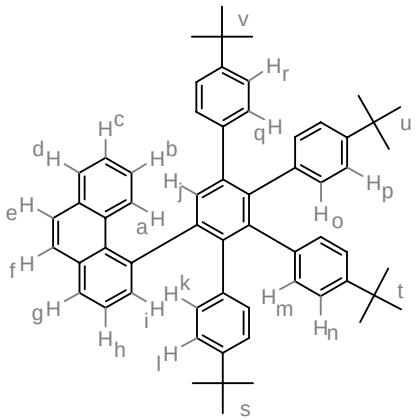

301 mg 2,3,4,5-Tetrakis(4-*t*-butyl-phenyl)-cyclopentadienone (**5-34b**, 494 µmol) and 100 mg 4-ethynyl-phenanthrene (**5-21**, 494 µmol) were dissolved in 1 mL *o*-xylene and degassed. The reaction was conducted in a sealed tube in a microwave oven (300 W, no ramp time) at 160 °C. After 10 minutes, the reaction was cooled to room temperature, the solvent was removed *in vacuo*, and the residue was purified utilizing preparative column chromatography (silica gel, eluent: low boiling petroleum ether, dichloromethane = 9:1, R_f = 0.3) to afford 324 mg of the title compound as a colorless powder (84%, 414 µmol).

MS (FD, 8kV): m/z (%) = 784.0 (100%, M^+) (calc. for $C_{60}H_{62}$ = 783.16 g mol^{-1})

UV/vis: λ / nm (ε / m^2·mol^{-1}) = 258 (3081), 282 (2077), 301 (1037)

^{1}H NMR (500 MHz, $C_2D_2Cl_4$, 353 K): δ = 8.13 (d, 1H, ^3J(H,H) = 8.57 Hz, H_a), 7.70 (d, 1H, ^3J(H,H) = 7.90 Hz, H_d), 7.62 (d, 1H, ^3J(H,H) = 7.79 Hz, H_g), 7.51 (d, 2H, ^3J(H,H) = 5.41 Hz, H_e, H_f), 7.50 (s, 1H, H_j), 7.46 (d, 1H, ^3J(H,H) = 7.23 Hz, H_i), 7.42 (t, 1H, ^3J(H,H) = 7.04 Hz, H_c), 7.38 (t, 1H, ^3J(H,H) = 7.36 Hz, H_h), 7.29 (t, 1H, ^3J(H,H) = 7.76 Hz, H_b), 7.04 (d, 2H, ^3J(H,H) = 8.48 Hz, H_r), 7.00 (d, 2H, ^3J(H,H) = 8.45 Hz, H_q), 6.88 (d, 2H, ^3J(H,H) = 7.95 Hz, H_p), 6.77 (d, 2H, ^3J(H,H) = 8.11 Hz, H_o), 6.74 (d, 2H, ^3J(H,H) = 8.00 Hz, H_n), 6.63 (d, 2H, ^3J(H,H) = 8.17 Hz, H_m), 6.42 (d, 2H, ^3J(H,H) = 7.62 H_z, H_l), 6.34 (d, 2H, ^3J(H,H) = 6.87 Hz, H_k), 1.18 (s, 9H, H_v), 1.13 (s, 9H, H_u), 1.04 (s, 9H, H_t), 0.91 (s, 9H, H_s)

^{13}C NMR (125 MHz, $C_2D_2Cl_4$, 353 K): δ = 149.05, 148.39, 147.91, 147.72, 143.29, 143.17, 141.40, 140.36, 140.28, 139.41, 139.14, 137.87, 137.63, 136.89, 133.44,

133.35, 131.74, 131.68, 131.46, 131.38, 130., 130.27, 129.87, 129.67, 128.45, 127.96, 127.88, 127.50, 127.18, 125.98, 125.32, 125.24, 124.33, 123.52, 123.12, 122.78, 34.41, 34.29, 34.16, 34.02, 31.53, 31.51, 31.43, 31.25.

Elemental Analysis: 91.88% C, 7.92% H (calc.: 92.02% C, 7.98% H)

7.3.42 8,11,14,17-Tetra(*t*-butyl)tetrabenzo[*bc,ef,hi,uv*]ovalene (5-16b)

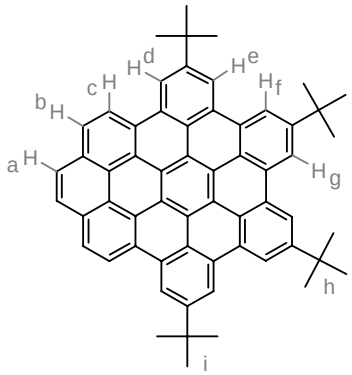

120 mg 4-(4,4'',5',6'-Tetra-*t*-butyl-phenyl)-[1,1';4',1'']terphenyl-2'yl)-phenanthrene (**5-13b**, 153 µmol) were dissolved in 100 mL dichloromethane. A stream of argon saturated with dichloromethane was bubbled into the solution through a Teflon tube. A solution of 820 mg iron(III) chloride (5.06 mmol) in 3 mL nitromethane was quickly added. After a reaction time of 35 minutes, the reaction was stopped with methanol. The precipitate was filtered off and washed extensively with aqueous hydrochloride acid and methanol. The crude material was recrystallized from toluene to afford 98 mg of the product as a orange, microcrystalline material (83%, 127 µmol).

MS (MALDI-TOF): m/z (%) = 770 (50%), 771 (34%), 772 (12%), 773 (4%) (calc. for $C_{60}H_{50}$ = 771.07 g mol^{-1}, isotope pattern: 770 (51%), 771 (34%), 772 (11%), 773 (2%))

UV/vis: λ / nm (ε / m^2·mol^{-1}) = 271 (755), 284 (550), 331 (727), 346 (1222), 361 (1887), 378 (2134), 390 (915), 413 (766), 436 (1125), 463 (40), 471 (22), 483 (24)

^{1}H NMR (500 MHz, THF, K): 9.50 (s, 2H, H_f), 9.47 (s, 2H, H_e), 9.44 (s, 2H, H_g), 9.41 (s, 2H, H_d), 9.32 (d, 2H, ^3J(H,H) = 8.89 Hz, H_c), 8.36 (d, 2H, ^3J(H,H) = 8.57 Hz, H_b), 8.18 (s, 2H, H_a), 1.96 (s, 18H, H_h), 1.92 (s, 18H, H_i)

^{13}C NMR: 153.51, 153.03, 135.28, 135.16, 134.78, 133.98, 133.87, 131.27, 131.25, 130.82, 130.29, 125.28, 125.19, 124.60, 124.11, 123.36, 123.26, 122.72, 40.00, 39.92, 35.93, 35.79

Elemental Analysis: 93.47% C, 6.29% H (calc.: 93.46% C, 6.54% H)

7.3.43 4-(4,4'',5',6'-Tetra-*n*-dodecyl-phenyl)-[1,1';4',1'']terphenyl-2'yl)-phenanthrene (5-13c)

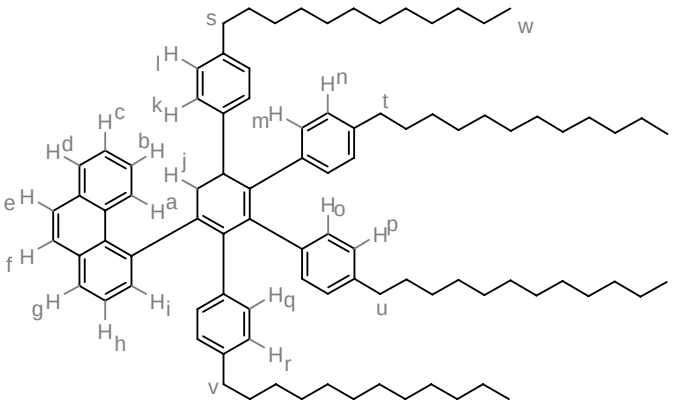

Method A:

100 mg 2''-Ethynyl-2,3,4,5-tetra(4-*n*-dodecylphenyl)-[1,1';2',1'']terphenyl (**5-15**, 0.08 mmol) and 1.1 mg platinum(II) chloride (4.1 µmol) were dissolved in 10 mL anhydrous toluene and stirred at 80 °C for 24 hours. After having removed the solvent *in vacuo*, the residue was purified utilizing preparative column chromatography (silica gel, eluent: hexane, ethyl acetate = 40:1, R_f =0.40-0.55) to yield 93 mg of the desired product as a colorless oil (93%, 0.08 mmol).

Method B:

575 mg 2,3,4,5-Tetrakis(4-*n*-dodecyl-phenyl)-cyclopentadienone (**5-34c**, 544 µmol) and 100 mg 4-ethynyl-phenanthrene (**5-21**, 494 µmol) were dissolved in 2 mL *o*-xylene and stirred at 160 °C for 3 hours. The solvent was removed in vacuo and the residue was purified with preparative column chromatography (silica gel, eluent: hexane, ethyl acetate = 40:1, R_f = 0.40-0.55) to afford the title compound as a colorless oil (95%, 469 µmol).

MS (FD, 8kV): m/z (%) =1231.3 (100%, M^+) (calc. for $C_{92}H_{126}$ = 1232.03 g mol^{-1})

^{1}H NMR (700 MHz, $C_2D_2Cl_4$, 353 K): δ = 8.16 (d, 1H, ^3J(H,H) = 8.58 Hz, H_a), 7.72 (d, 1H, ^3J(H,H) = 7.80 Hz, H_d), 7.63 (d, 1H, ^3J(H,H) = 7.65 Hz, H_g), 7.53 (2 x s, 2H, H_e, H_f), 7.50 (s, 1H, H_j), 7.43 (m, 2H, H_c, H_i), 7.37 (t, 1H, ^3J(H,H) = 7.46 Hz, H_h), 7.31 (t, 1H, ^3J(H,H) = 7.32 Hz, H_b), 7.00 (d, 2H, ^3J(H,H) = 7.81 Hz, H_l), 6.86 (d, 2H, ^3J(H,H) = 7.84 Hz, H_k), 6.79 (d, 2H, ^3J(H,H) = 7.58 Hz, H_n), 6.71 (d, 2H, ^3J(H,H) = 7.64 Hz, H_m), 6.66 (d, 2H, ^3J(H,H) = 7.79 Hz, H_p), 6.58 (d, 2H, ^3J(H,H) = 7.80 Hz, H_o), 6.37 (bd, 2H, ^3J(H,H) = 6.34 Hz, H_r), 6.27 (bd, 2H, ^3J(H,H) = 6.20 Hz, H_q), 2.47 (t, 2H, ^3J(H,H) = 7.52 Hz, H_s), 2.41 (t, 2H, ^3J(H,H) = 7.34 Hz, H_t), 2.31 (t, 2H, ^3J(H,H) = 7.38 Hz, H_u), 2.14 (t, 2H, ^3J(H,H) = 7.32 Hz, H_v), 1.5-1.0 (m, 80H, -CH_2-), 0.87 (m, 12H, H_w)

^{13}C NMR (175 MHz, $C_2D_2Cl_4$, 353 K): δ = 142.94, 142.75, 141.13, 140.32, 139.96, 139.79, 139.48, 139.08, 139.00, 137.77, 137.53, 136.90, 139.12, 133.08, 132.981, 131.51, 131.31, 131.00, 130.23, 130.13, 129.68, 129.23, 128.11, 127.52, 127.21, 127.17, 126.79, 126.61, 126.22, 125.85, 125.56, 124.86, 35.30, 35.24, 35.14, 34.960, 31.70, 30.98, 30.92, 30.88, 30.69, 29.44, 29.32, 29.26, 29.21, 29.11, 29.00, 28.66, 28.62, 28.52, 29.48, 29.39, 22.44, 13.80

7.3.44 8,11,14,17-Tetra-*n*-dodecyl-tetrabenzo[*bc,ef,hi,uv*]ovalene (5-16c)

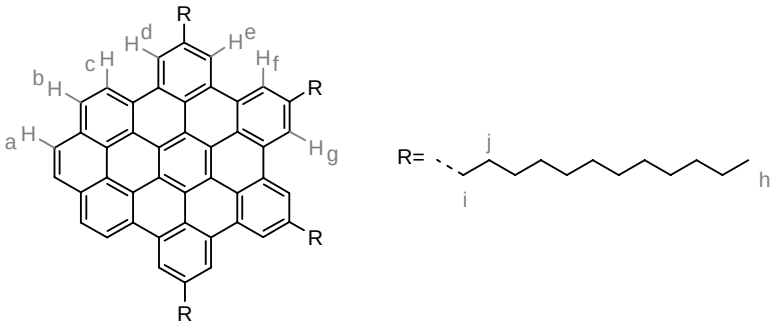

32 mg 4-(4,4'',5',6'-Tetra-*n*-dodecyl-phenyl)-[1,1';4',1'']terphenyl-2'yl)-phenanthrene (**5-13c**, 26 µmol) were dissolved in 25 mL dichloromethane. A stream of argon saturated with dichloromethane was bubbled into the solution through a Teflon tube. A solution of 140 mg iron(III) chloride (0.86 mmol) in 1 mL nitromethane was quickly added. After a reaction time of 25 minutes, the reaction was stopped with methanol. The precipitate was filtered off and washed extensively with aqueous hydrochloride acid and methanol. The crude material was reprecipitated from methanol and recrystallized from toluene to afford 25 mg of the product as an orange, microcrystalline material (79%, 20.5 µmol).

MS (MALDI-TOF): m/z (%) = 1219 (31%), 1220 (32%), 1221 (20%), 1222 (9%), 1223 (5%) (calc. for $C_{92}H_{114}$ = 1219.93 g mol^{-1}, isotope pattern: 1219 (36%), 1220 (37%), 1221 (19%), 1222 (6%), 1223 (2%))

UV/vis: λ / nm (ε / m^2·mol^{-1}) = 330 (1358), 347 (1726), 363 (2146), 380 (2048), 414 (885), 438 (974), 484 (82)

^{1}H NMR (700 MHz, THF, 60°C): δ = 8.79 (s, 2H, H_f), 8.55 (d, 2H, ^3J(H,H) = 8.19 Hz, H_c), 8.43 (m, 6H, H_d, H_e, H_g), 8.09 (d, 2H, ^3J(H,H) = 8.66 Hz, H_b), 8.00 (s, 2H, H_a), 3.09 (m, 8H, H_i), 2.06 (m, 8H, H_j), 1.8-1.2 (m, 36H, -CH_2-), 0.89 (t, 12H, ^3J(H,H) =6.72 Hz, H_h)

^{13}C NMR: could not be obtained due to the vanishing solubility in organic solvents even at elevated temperatures

DSC (°C): 148 (98)

Elemental Analysis: 90.61% C, 9.08% H (calc.: 90.58% C, 9.42% H)

7.3.45 2-(2-Methoxyphenyl)benzaldehyde (5-28)

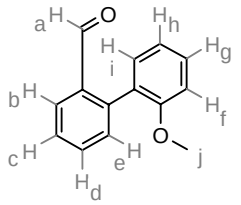

25 g 2-Formylphenylbronic acid (**5-27**, 166.8 mmol), 25.4 g 2-bromoanisol (**5-26**, 135.5 mmol), and 28.8 sodium carbonate (271.3 mmol) were dissolved in a mixture of 500 mL dimethoxyethane, 125 mL ethanol, and 125 mL water and degassed. 4.7 g Tetrakis(triphenylphosphino)-palladium (0) (1.62 mmol, 3 mol%) were added and the

mixture was refluxed for 16 hours. The product was extracted with dichloromethane, dried with magnesium sulfate and purified with preparative column chromatography after the solvent was removed (silica gel, eluent: hexane, ethyl acetate = 9:1, R_f = 0.32) to afford 21.1 g of the product as a colorless, crystalline solid (73%, 99.2 mmol).

MS (EI): m/z (%) = 212 (M^+, 55%), 181 (100%), 169 (15%), 139 (16), 115 (17) (calc. for $C_{14}H_{12}O_2$ = 212.25 g mol^{-1})

IR (KBr /cm^{-1}) = 3060, 3017, 2963, 2934, 2837, 2750, 1693, 1593, 1496, 1477, 1461, 1453, 1431, 1230, 762

^{1}H NMR (300 MHz, $CDCl_3$): δ = 9.71 (s, 1H, H_a), 7.99 (dd, 1H, ^3J(H,H) = 7.51 Hz, H_b), 7.63 (t, 1H, ^3J(H,H) = 7.63 Hz, H_d), 7.40 (m, 3H, H_e, H_g, H_h), 7.26 (dd, 1H, ^3J(H,H) = 7.33 Hz, ^4J(H,H) = 1.62 Hz, H_i), 7.08 (t, 1H, ^3J(H,H) = 7.52 Hz, H_c), 6.97 (d, 1H, ^3J(H,H) = 8.21 Hz, H_f), 3.73 (s, 3H, H_j)

^{13}C NMR (75 MHz, $CDCl_3$): δ = 193.01 (-*C*=O), 156.76, 142.20, 134.44, 134.16, 131.82, 131.65, 130.43, 128.18, 127.03, 121.76, 121.40, 111.01, 55.84 (-*C*H_3)

Elemental Analysis: 79.15% C, 5.81% H (calc.: 79.23% C, 5.70% H, 15.08% O).

7.3.46 2-Ethynyl-2'-methoxy-biphenyl (5-29)

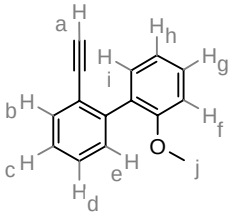

88.4 mL *n*-Butyl lithium (1.6 M in hexane, 141 mmol) were added to a solution of 162 mL freshly distilled di-*iso*-propylamine (153 mmol) in 25 mL anhydrous THF at 0 °C. After having stirred for 10 minutes, the solution was cooled to -78 °C and a solution of 71.3 mL trimethylsilyldiazomethane (2M in hexane, 142 mmol) was put in. After another 30 minutes at the same temperature, 25 g 2-(2-methoxyphenyl)benzaldehyde (**5-28**, 120 mmol), dissolved in 95 mL anhydrous THF, were carefully added drop wise. During the course of three hours, the reaction was brought to room temperature and stopped with water. The mixture was extracted with *t*-butyl methyl ether. The organic phase was dried with magnesium sulfate and the solvent was removed *in vacuo*. The residue was purified utilizing preparative column chromatography (silica gel, eluent: hexane, ethyl acetate = 9:1, R_f = 0.43) to afford 21.0 g of the desired compound as a crystalline solid (84%, 100 mmol).

MS (EI): m/z (%) = 208 (M^+, 100%), 193 (23%), 179 (22%), 165 (90%), 139 (12%), (calc. for $C_{15}H_{12}O$ = 208.26 g mol^{-1})

IR (KBr /cm^{-1}) = 3269, 3069, 3007, 2957, 2857, 2834, 2105, 1601, 1580, 1500, 1472, 1463, 1430, 1266, 1251, 1233, 760, 634

^{1}H NMR (300 MHz, CD_2Cl_2): δ = 7.59 (d, 1H, ^3J(H,H) = 7.58 Hz, H_e), 7.5-7.2 (m, 5H, H_b, H_c, H_d, H_g, H_i), 7.01 (m, 2H, H_h, H_f), 3.78 (s, 3H, H_j), 2.92 (s, 1H, H_a)

^{13}C NMR (75 MHz, CD_2Cl_2): δ = 156.81, 141.73, 133.03, 131.23, 130.36, 129.78, 129.11, 128.45, 126.93, 122.12, 120.39, 111.18, 83.11 (-*C*≡CH), 79.15 (-C≡*C*H), 55.63 (-*C*H_3)

Elemental Analysis: 86.41% C, 5.79% H (calc.: 86.51% C, 5.81% H, 7.68% O)

7.3.47 4-Methoxy-phenanthrene (5-30)

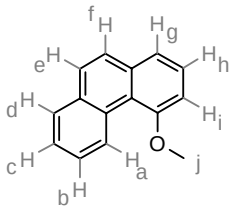

A mixture of 417 mg 2-Ethynyl-2'-methoxy-biphenyl (**5-29**, 2.00 mmol) and 26.6 mg platinum(II) chloride (0.10 mmol) in 10 mL toluene was stirred under argon for 24 hours. The solvent was removed *in vacuo* and the residue was purified using preparative column chromatography (silica gel, eluent: hexane, ethyl acetate = 9:1, R_f = 0.61) to obtain 317 mg of the desired product as a colorless solid (76%, 1.52 mmol).

MS (EI): m/z (%) = 208 (M^+, 100%), 193 (27%), 165 (55%) (calc. for $C_{15}H_{12}O$ = 208,26 g mol^{-1})

IR (KBr /cm^{-1}) = 3138, 3048, 2995, 2962, 2939, 2835, 1609, 1598, 1449, 1431, 1417, 1245, 823, 739, 713

^{1}H NMR (300 MHz, CD_2Cl_2): δ = 9.59 (dd, 1H, ^3J(H,H) = 8.61 Hz, ^4J(H,H) = 0.64 Hz, H_a), 7.80 (dd, 1H, ^3J(H,H) = 7.72 Hz, ^4J(H,H) = 1.56 Hz, H_d), 7.7-7.4 (m, 6H, H_b, H_c, H_e, H_f, H_g, H_h), 7.09 (d, 1H, ^3J(H,H) = 9.10 Hz, H_i), 4.07 (s, 3H, H_j)

^{13}C NMR (75 MHz, CD_2Cl_2): δ = 158.58 (*C*-OMe), 134.35, 132.41, 130.04, 128.25, 127.99, 127.76, 126.75, 126.17, 126.02, 125.52, 121.23, 120.57, 108.03, 55.41 (-*C*H_3)

Elemental Analysis: 86.65% C, 5.15% H (calc.: 86.51% C, 5.81% H, 7.68% O)

7.3.48 4-Hydroxy-phenanthrene (5-31)

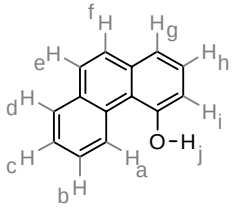

500 mg 4-Methoxy-phenathrene (**5-30**, 2.40 mmol) were dissolved in 15 mL dichloromethane and cooled to -78 °C. 0.45 mL Boron tribromide (1.20 g, 4.79 mmol) were added and the mixture was stirred over night at room temperature. The reaction was terminated by adding water. The organic phase was separated off and dried with magnesium sulfate. After having evaporated the solvent, the residue was purified using column chromatography (silica gel, eluent: hexane, ethyl acetate = 8:2, R_f = 0.2) to afford 403 mg of the desired compound as a colorless, crystalline solid (86%, 2.07 mmol).

MS (FD, 8kV): m/z (%) = 194.2 (M^+, 100%) (calc. for $C_{14}H_{10}O$=194.24 g mol^{-1})

^{1}H NMR (300 MHz, CD_2Cl_2): δ = 9.64 (dd, 1H, ^3J(H,H) = 8.26 Hz, ^4J(H,H) = 0.81 Hz, H_a), 7.90 (dd, 1H, ^3J(H,H) = 7.62 Hz, ^4J(H,H) = 1.51 Hz, H_d), 7.8-7.4 (m, 6H, H_b,

H_c, H_e, H_f, H_g, H_h), 7.03 (dd, 1H, ^3J(H,H) = 7.52 Hz, ^4J(H,H) = 1.29 Hz, H_i), 5.89 (s, 1H, H_j)

^{13}C NMR (75 MHz, CD_2Cl_2): δ = 154.76 (*C*-OH)), 135.28, 132.95, 130.60, 128.86, 128.57, 128.25, 127.38, 126.87, 126.82, 126.37, 121.96, 119.60, 113.67

Elemental Analysis: 86.43% C, 5.23% H (calc.: 86.57% C, 5.19% H, 8.24% O)

7.3.49 1,1,2,2,3,3,4,4,4-Nonafluoro-butane-1-sulfonic acid phenanthren-4-yl ester (5-32)

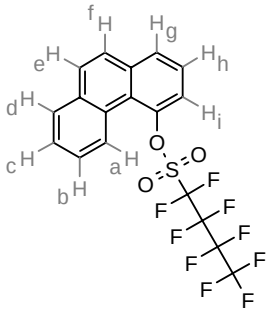

200 mg 4-Hydroxy-phenanthrene (**5-31**, 1.03 mmol) were dissolved in a mixture of 172 µL 1,1,2,2,3,3,4,4,4-Nonafluoro-butane-1-sulfonyl fluoride (1.24 mmol) and 6 mL dichloromethane and stirred over night. The reaction was stopped by adding water. The organic phase was separated, dried with magnesium sulfate and the solvent was evaporated *in vacuo*. The residue was purified using preparative column chromatography (silica gel, eluent: hexane, ethyl acetate = 8:2, R_f = 0.62) to obtain 457 mg of the desired material as a colorless oil (93%, 0.96 mmol).

MS (FD, 8kV): m/z (%) = 477.1 (M^+, 100%) (calc. for $C_{18}H_9F_9O_3S$=476.32 g mol^{-1})

^{1}H NMR (300 MHz, CD_2Cl_2): δ = 9.21 (dd, 1H, ^3J(H,H) = 8.21 Hz, ^4J(H,H) = 1.00 Hz, H_a), 7.95 (dd, 1H, ^3J(H,H) = 7.41 Hz, ^4J(H,H) = 1.56 Hz, H_d), 7.90 (dd, 1H, ^3J(H,H) = 7.71 Hz, ^4J(H,H) = 1.52 Hz, H_g), 7.8-7.5 (m, 6H, H_b, H_c, H_e, H_f, H_h, H_i)

^{13}C NMR (75 MHz, CD_2Cl_2): δ = 147.74, 135.64, 133.76, 129.76, 129.41, 129.35, 128.10, 127.76, 127.60, 126.67, 123.62, 121.07 (all Ar-*C*), 119.54, 115.11, 110.56, 106.97 (nonaflate-C, coupling due to fluorine nuclei)

7.3.50 4-Ethynyltrimethylsilyl-phenanthrene (5-33)

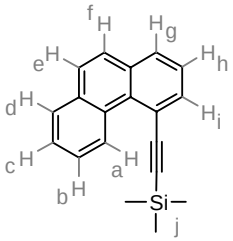

170 mg 1,1,2,2,3,3,4,4,4-Nonafluoro-butane-1-sulfonic acid phenanthren-4-yl ester (**5-32**, 0.36 mmol), 62 mg trimethylsilyl acetylene (0.18 mL, 0.63 mmol), 1.1 mg triphenylphosphine (4.2 µmol), and 0.8 mg copper(I) iodide (4.2 µmol) were dissolved in 5 mL triethyl amine and degassed with three freeze-vacuum-thaw cycles. Afterwards, 2.9 mg bis(triphenylphosphine)palladium(II) chloride (4.2 µmol) were added and the mixture was stirred under argon at 80 °C for 20 hours. The solvent was

removed *in vacuo* and the residue was purified using preparative column chromatography (silica gel, eluent: hexane, ethyl acetate = 8:2, R_f = 0.74). After a recrystallization with ethanol as solvent, 86 mg of the analytically clean product were obtained as a colorless solid (87%, 0.31 mmol).

MS (FS, 8kV): m/z (%) = 274.1 (100%, M^+) (calc. for $C_{19}H_{18}Si$ = 274.44 g mol^{-1})

^{1}H NMR (300 MHz, CD_2Cl_2): δ = 10.48 (m, 1H, H_a), 8.0-7.85 (m, 3H, H_b, H_d, H_e), 7.8-7.6 (m, 4H, H_c, H_f, H_g, H_i), 7.55 (t, 1H, ^3J(H,H) = 7.84 Hz, H_h), 0.44 (s, 9H, H_j)

^{13}C NMR (75 MHz, CD_2Cl_2): δ = 135.80, 133.46, 133.40, 130.92, 130.43, 130.13, 128.72, 128.25, 127.69, 127.395, 126.76, 125.97, 125.92, 119.48, 108.24 (*C*≡CSi), 101.23 (C≡*C*Si), -0.13 (-Si(*C*H_3)$_3$)

Elemental Analysis: 83.08% C, 6.57% H (calc.: 83.16% C, 6.61% H, 10.23% Si)

7.3.51 1,3-Bis(4-*t*-butyl-phenyl)-2-propanone

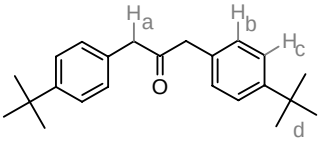

21 g Iron pentacarbonyl (0.11 mol) were added under argon to a concentrated sodium hydroxide solution (40 g in 40 mL water). Under vigorous stirring, 0.54 g benzyl triethylammonium chloride was put in as phase transfer catalyst (1.93 mmol). Afterwards, 50 g 4-*t*-butylbenzylbromide (0.22 mmol), dissolved in 300 mL dichloromethane, were added to the reaction flask and the resulting two-phasic mixture was brought to reflux for 15 hours. The reaction was cooled down to room temperature and 250 mL 2M aqueous hydrochloric acid was added to stop the reaction. The organic phase was separated, washed with diluted aqueous hydrochloric acid and water, dried with magnesium sulfate and the solvent was removed *in vacuo*. The crude product was recrystallized from ethanol to obtain 21 g of the desired product as colorless crystals (30%, 65.1 mmol).

Melting point: 84-85 °C

MS (FS, 8kV): *m/z* (%) = 321.6 (100%, M^+) (calc. for $C_{23}H_{30}O$ = 322.49 g mol^{-1})

^{1}H-NMR (700 MHz, CD_2Cl_2): δ = 7.32 (d, 4H, ^3J(H,H) = 8.09 Hz, H_b), 7.17 (d, 4H, ^3J(H,H) = 8.24 Hz, H_c), 2.88 (s, 4H, H_a), 1.31 (s, 18H, H_d)

^{13}C-NMR (175 MHz, CD_2Cl_2): δ = 148.77 (*C*=O), 139.10 (Ar-*C*), 128.00 (2-Ar-*C*), 125.26 (3-Ar-*C*), 37.27 (benzyl-*C*), 34.29 (*C*$(CH_3)_3$), 31.21 (C(*C*H_3)$_3$)

Elemental Analysis: 86.02% C, 9.87% H (calc.: 85.66% C, 9.38% H)

7.3.52 2,3,4,5-Tetrakis(4-*t*-butyl-phenyl)-cyclopentadienone (5-34b)

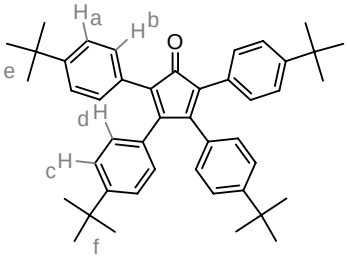

7 g 1,3-Bis(4-*t*-butyl-phenyl)-2-propanone (21.7 mmol) and 7 g 1,2-Bis-(4-*t*-butyl-phenyl)-ethane-1,2-dione (21.7 mmol) were dissolved under argon in 13 mL *t*-butanol and stirred at 85 °C. A mixture of 14 mL of a 0.8 M methanolic tetrabutyl ammonium hydroxide solution and 7 mL *t*-butanol were quickly added *via* a syringe. After 15 minutes, the reaction was quenched with 50 mL water. The product was extracted with dichloromethane and purified using preparative column chromatography (silica gel, eluent: low boiling petroleum ether, dichloromethane = 8:2, R_f = 0.44) to afford 8.3 g of the desired product as a violet crystalline compound (63%, 13.7 mmol).

Melting point: 236.1 °C

MS (FS, 8kV): *m/z* (%) = 608.3 (100%, M^+) (calc. for $C_{45}H_{52}O$ = 608.92 g mol^{-1})

^{1}H-NMR (300 MHz, CD_2Cl_2): δ = 7.31 (d, 4H, ^3J(H,H) = 8.77 Hz, H_b), 7.21 (d, 8H, ^3J(H,H) = 8.86 Hz, H_a, H_c), 6.89 (d, 4H, ^3J(H,H) = 8.35 Hz, H_d), 1.32 (s, 18H, H_e), 1.29 (s, 18H, H_f)

^{13}C-NMR (75 MHz, CD_2Cl_2): δ = 208.82 (-*C*=O), 154.23 (C_{quart}), 151.19 (C_{quart}), 149.95 (C_{quart}), 130.25 (C_{quart}), 129.33 (Ar-*C*H), 128.57 (Ar-*C*H), 128.02 (C_{quart}), 124.50 (Ar-*C*H), 124.26 (Ar-*C*H), 34.15 ($C(CH_3)_3$), 34.08 ($C(CH_3)_3$), 30.75 ($C(CH_3)_3$), 30.57 ($C(CH_3)_3$)

Elemental Analysis: 88.73% C, 8.65% H (calc.: 88.76% C, 8.61% H)

7.3.53 10-Phenanthren-4-yl-9,12-diphenyl-benzo[*e*]pyrene (5-35)

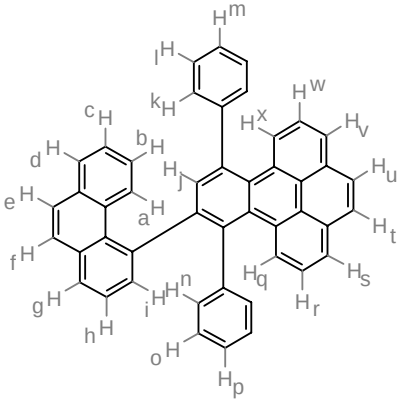

201 mg 9,11-Diphenyl-cyclopenta[*e*]pyren-10-one (**5-2**, 494 µmol) and 100 mg 4-Ethynyl-phenanthrene (**5-21**, 494 µmol) were dissolved in 1 mL *o*-xylene and degassed. The reaction was conducted in a sealed tube in a microwave oven (300 W, no ramp time) at 160 °C. After 30 minutes, the reaction was cooled to room temperature, the solvent was removed in vacuo, and the residue was purified utilizing preparative column chromatography (silica gel, eluent: low boiling petroleum ether, dichloromethane = 9:1, R_f = 0.53) to afford 207 mg of the title compound as a colorless powder (72%, 356 µmol).

MS (FD, 8kV): m/z (%) = 580.7 (100%, M^+) (calc. for $C_{46}H_{28}$ = 580.74 g mol^{-1})

^{1}H NMR (700 MHz, THF-d_8, 353 K): δ = 8.13 (d, 1H, ^3J(H,H) = 7.80 Hz, H_q), 8.11 (d, 1H, ^3J(H,H) = 8.70 Hz, H_a), 8.00 (d, 1H, ^3J(H,H) = 7.74 Hz, H_s), 7.97 (2d, 2H, H_t, H_u), 7.91 (d, 1H, ^3J(H,H) = 7.46 Hz, H_v), 7.89 (d, 1H, ^3J(H,H) = 8.07 Hz, H_x), 7.76 (d, 1H, ^3J(H,H) = 7.13 Hz, H_g), 7.73 (s, 1H, H_j), 7.70 (d, 1H, ^3J(H,H) = 7.60 Hz, H_d), 7.64 (d, 1H, ^3J(H,H) = 8.79 Hz, H_f), 7.59 (d, 1H, ^3J(H,H) = 8.89 Hz, H_e), 7.53-7.46 (m, 3H, H_r, H_k), 7.46-7.41 (m, 2H, H_h, H_i), 7.38-7.32 (m, 3H, H_l, H_m), 7.32-7.25 (m,

2H, H_c, H_w), 7.00 (t, 2H, ^3J(H,H) = 7.30 Hz, H_b, H_n), 6.91 (bt, 1H, H_o), 6.83 (dd, 1H, ^3J(H,H) = 7.24 Hz, H_p), 6.69 (bt, 1H, H_o), 6.57 (bd, 1H, H_n)

^{13}C NMR (175 MHz, THF-d_8, 323 K): δ = 149.46, 148.21, 146.72, 144.75, 143.66, 141.74, 137.79, 137.71, 137.41, 136.72, 136.26, 136.20, 135.79, 135.49, 135.39, 135.17, 134.92, 134.71, 134.65, 134.23, 133.86, 133.60, 133.52, 133.17, 132.56, 132.49, 132.30, 131.99, 131.85, 131.70, 131.50, 131.43, 131.35, 131.27, 131.02, 130.80, 130.33, 129.70, 129.65, 129.56, 129.47, 129.25, 129.06, 128.61, 128.43, 128.16.

Elemental Analysis: 95.13% C, 4.56% H (calc.: 95.14% C, 4.86% H)

7.3.54 Dibenzo[*hi,uv*]phenanthro-(3,4,5,6-bcdef)-ovalene (5-36)

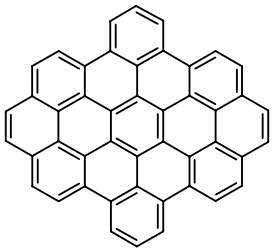

100 mg 10-Phenanthren-4-yl-9,12-diphenyl-benzo[*e*]pyrene (**5-35**, 172 µmol) were dissolved in 25 mL dichloromethane. A stream of argon saturated with dichloromethane was bubbled into the solution through a Teflon tube. A solution of 840 mg iron(III) chloride (5.17 mmol) in 1 mL nitromethane was quickly added. After a reaction time of 60 minutes, the reaction was stopped with methanol. The precipitate was filtered off and washed extensively with aqueous hydrochloride acid and methanol to afford 86 mg of the product as a orange-red solid (88%, 151 µmol).

MS (MALDI-TOF): m/z (%) = 570 (61%), 571 (28%), 572 (8%), 573 (3%) (calc. for $C_{46}H_{18}$ = 570.66 g mol^{-1}, isotope pattern: 570 (60%), 571 (31%), 572 (8%), 573 (1%))

UV/vis: λ / nm (oDCB) = 336, 352, 373, 393, (418), 446, 471, 480, 536 (molar extinction coefficient could not be determined due to the vanishing solubility in organic solvents)

Elemental Analysis: 96.96% C, 2.98% H (calc.: 96.82% C, 3.18% H)

7.3.55 2,7-Di-*t*-butyl-9,12-bis-(4-*t*-butyl-phenyl)-10-phenanthren-4-yl-benzo[*e*]pyrene (5-37)

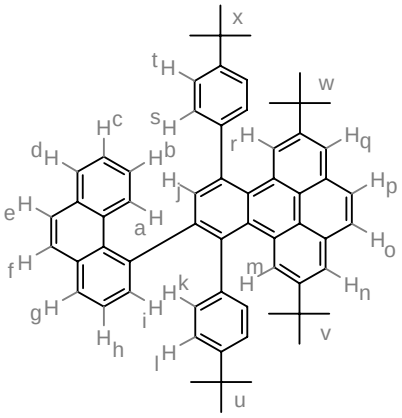

150 mg 2,7-Di-*t*-butyl-9,11-bis-(4-*t*-butyl-phenyl)-cyclopenta[*e*]pyren-10-one (238 µmol) and 53 mg 4-Ethynyl-phenanthrene (262 µmol) were dissolved in 3mL *o*-xylene and heated for 12 hours at 160 °C. Afterwards, the solvent was removed *in vacuo*, and the residue was purified by using preparative column chromatography (silica gel, eluent: low boiling petroleum ether, dichloromethane = 8:2, R_f = 0.68) to obtain 187 mg of the title compound as a colorless, microcrystalline powder (98%, 232 µmol).

MS (FD, 8kV): m/z (%) = 805.8 (100%, M^+) (calc. for $C_{62}H_{60}$ = 805.17 g mol^{-1})

UV/vis: λ / nm (ε / $m^2 \cdot mol^{-1}$) = 304 (1600), 320 (1703), 346 (926), 397 (29)

^{1}H NMR (500 MHz, CD_2Cl_2): δ = 8.35 (d, 1H, ^4J(H,H) = 1.77 Hz, H_m), 8.24 (d, 1H, ^4J(H,H) = 1.76 Hz, H_r), 8.13 (d, 1H, ^3J(H,H) = 8.65 Hz, H_a), 8.00 (d, 1H, ^4J(H,H) = 1.78 Hz, H_n), 7.94 (d, 1H, ^3J(H,H) = 8.96 Hz, H_f), 7.92 (d, 1H, ^3J(H,H) = 8.74 Hz, H_e), 7.91 (d, 1H, ^4J(H,H) = 1.77 Hz, H_q), 7.78 (d, 1H, ^3J(H,H) = 7.88 Hz, ^4J(H,H) = 1.42 Hz, H_g), 7.77 (s, 1H, H_j), 7.69 (d, 1H, ^3J(H,H) = 7.85 Hz, ^4J(H,H) = 1.24 Hz, H_d), 7.63 (d, 2H, ^3J(H,H) = 8.86 Hz, H_s), 7.55 (d, 2H, ^3J(H,H) = 8.81 Hz, H_t), 7.49 (t, 1H, ^3J(H,H) = 7.71 Hz, H_h), 7.43 (d, 1H, ^3J(H,H) = 7.25 Hz, ^4J(H,H) = 1.44 Hz, H_i), 7.32 (t, 1H, ^3J(H,H) = 7.96 Hz, ^4J(H,H) = 1.05 Hz, H_c), 7.06 (t, 1H, ^3J(H,H) = 8.56 Hz, ^4J(H,H) = 1.46 Hz, H_b), 6.86 (d, 1H, ^3J(H,H) = 8.13 Hz, ^4J(H,H) = 2.02 Hz, H_k), 6.75 (d, 1H, ^3J(H,H) = 8.13 Hz, ^4J(H,H) = 1.88 Hz, H_l), 6.54 (d, 1H, ^3J(H,H) = 8.15 Hz, ^4J(H,H) = 2.01 Hz, $H_{k'}$), 6.48 (d, 1H, ^3J(H,H) = 8.15 Hz, ^4J(H,H) = 1.89 Hz, $H_{l'}$), 1.35 (s, 9H, H_v), 1.17 (s, 9H, H_w), 1.05 (s, 9H, H_u), 1.00 (s, 9H, H_x)

^{13}C NMR (75 MHz, CD_2Cl_2): δ = 150.29, 148.86, 147.45, 147.29, 144.04, 142.95, 140.37, 140.01, 139.86, 137.44, 133.56, 133.51, 133.42, 132.51, 132.02, 131.33, 131.12, 130.88, 130.75, 130.60, 129.77, 129.60, 129.12, 128.46, 128.10, 127.69, 127.45, 127.41, 127.22, 126.66, 126.11, 126.08, 125.60, 125.56, 124.88, 124.78, 123.75, 123.47, 122.29, 122.24, 35.12, 35.0312, 34.83, 34.36, 31.59, 31.50, 31.16, 31.49

Elemental Analysis: 92.47% C, 7.65% H (calc.: 92.49% C, 7.51% H)

7.3.56 8,10,15,17-Tetra(*t*-butyl)-dibenzo[*hi,uv*]phenanthro-[3,4,5,6-*bcdef*]-ovalene (5-38)

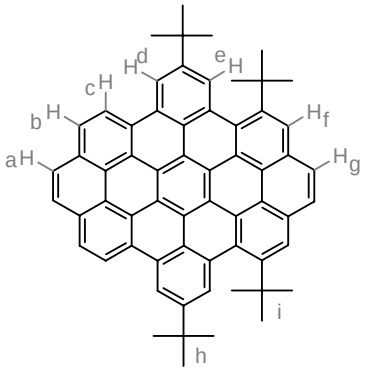

30 mg 2,7-Di-*t*-butyl-9,12-bis-(4-*t*-butyl-phenyl)-10-phenanthren-4-yl-benzo[*e*]pyrene (**5-37**, 37 µmol) were dissolved in 25 mL dichloromethane. A stream of argon saturated with dichloromethane was bubbled into the solution through a Teflon tube. A solution of 151 mg iron(III) chloride (0.93 mmol) in 1 mL nitromethane was quickly added. After a reaction time of 30 minutes, the reaction was stopped with methanol. The precipitate was filtered off and washed extensively with aqueous hydrochloride acid and methanol. The crude material was reprecipitated from methanol to afford 25 mg of the product as a orange-red, microcrystalline material (85%, 31.4 µmol).

MS (MALDI-TOF): m/z (%) = 794 (46%), 795 (33%), 796 (13%), 797 (8%) (calc. for $C_{62}H_{50}$ = 795,09 g mol^{-1}, isotope pattern: 794 (50%), 795 (35%), 796 (12%), 797 (3%)

UV/vis: λ / nm (ε / m^2·mol^{-1}) = 347 (785), 363 (1171), 376 (1538), 398 (2682), 420 (451), 445 (717), 473 (1322), 511 (24)

^{1}H NMR (700 MHz, THF, 330K): δ = 9.98 (d, 2H, ^3J(H,H) = 8.24 Hz, H_c), 9.82 (s, 2H, H_d), 9.35 (s, 2H, H_e), 9.32 (s, 2H, H_f), 9.00 (d, 2H, ^3J(H,H) = 8.43 Hz, H_b), 8.75 (s, 2H, H_a), 8.71 (s, 2H, H_g), 1.95 (s, 6H, H_i), 1.91 (s, 6H, H_h)

^{13}C NMR: could not be obtained due to the vanishing solubility in organic solvents even at elevated temperatures

Elemental Analysis: 93.66% C, 6.45% H (calc.: 93.66% C, 6.34% H)

7.3.57 9,11-Bis-(4-bromo-phenyl)-cyclopenta[*e*]pyren-10-one (5-39)

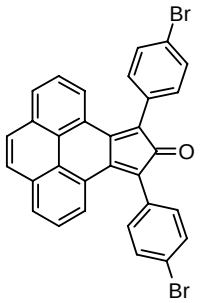

1.51 g Pyren-4,5-dione (**5-1**, 6.52 mmol) and 2.40 g 1,3-bis-(4-bromo-phenyl)-propan-2-one (6.52 mmol) were suspended in 90 mL ethanol and heated to 80°C.

Afterwards, a solution of 186 mg potassium hydroxide (3.31 mmol) in 0.9 mL methanol was added and the resulting solution was stirred for 25 minutes. The reaction was terminated with water. The mostly precipitated product was extracted with dichloromethane, which was dried afterwards with magnesium sulfate. After having removed the solvent, the material was purified using preparative column chromatography (neutral aluminum oxide, low boiling petroleum ether, dichloromethane = 3:1, R_f = 0.6) to afford 1.77 g of the thermally unstable title compound as a violet solid (47%, 3.14 mmol). The compound has to be quickly converted, because it is hardly stable in solution over longer periods of time.

MS (FD, 8kV): m/z (%) = 566.1 (100%, M^+)(calc. for $C_{31}H_{16}Br_2O$ = 564.28 g mol^{-1})

7.3.58 9,12-Bis-(4-bromo-phenyl)-10-phenanthren-4-yl-benzo[*e*]pyrene (5-40)

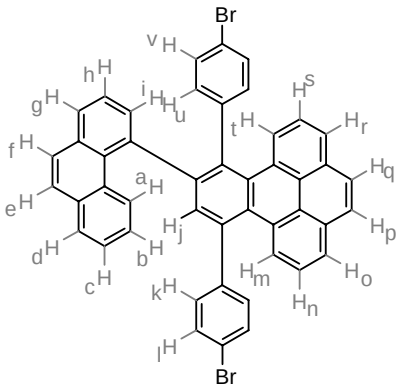

333 mg 9,11-Bis-(4-bromo-phenyl)-cyclopenta[*e*]pyren-10-one (**5-39**, 0.59 mmol) and 119 mg 4-Ethynyl-phenanthrene (**5-21**, 0.59 mmol) were dissolved in 2 mL o-xylene and heated to 160 °C for 5 hours. After having removed the solvent *in vacuo*, the residue was purified using preparative column chromatography (silica gel, low boiling petroleum ether, dichloromethane = 8:2, R_f = 0.34) to receive 327 mg of the desired polycyclic hydrocarbon as a colorless powder (75%, 0.44 mmol).

MS (FD, 8kV): m/z (%) = 739.1 (100%, M^+) (calc. for $C_{46}H_{26}Br_2$ = 738.53 g mol^{-1})

^{1}H NMR (500 MHz, $C_2D_2Cl_4$, 373 K): δ = 8.09 (d, 1H, ^3J(H,H) = 8.05 Hz, H_t), 8.00 (d, 1H, ^3J(H,H) = 7.65 Hz, H_r), 7.96 (d, 1H, ^3J(H,H) = 8.89 Hz, H_p), 7.93 (d, 1H, ^3J(H,H) = 8.92 Hz, H_q), 7.91 (d, 1H, ^3J(H,H) = 7.58 Hz, H_m), 7.83 (d, 1H, ^3J(H,H) = 8.63 Hz, H_a), 7.82 (d, 1H, ^3J(H,H) = 8.17 Hz, H_o), 7.77 (d, 1H, ^3J(H,H) = 7.71 Hz, ^4J(H,H) = 1.28 Hz, H_g), 7.74 (s, 1H, H_j), 7.67 (d, 1H, ^3J(H,H) = 7.85 Hz, H_d), 7.61 (d, 1H, ^3J(H,H) = 8.83 Hz, H_f), 7.56 (t, 1H, ^3J(H,H) = 7.78 Hz, H_s), 7.57 (d, 1H, ^3J(H,H) = 8.80 Hz, H_e), 7.50 (d, 2H, ^3J(H,H) = 8.27 Hz, H_l), 7.49 (t, 1H, ^3J(H,H) = 7.70 Hz, H_h), 7.44 (d, 1H, ^3J(H,H) = 7.18 Hz, ^4J(H,H) = 1.35 Hz, H_i), 7.37 (d, 2H, ^3J(H,H) = 8.04 Hz, H_k), 7.37 (t, 1H, ^3J(H,H) = 7.87 Hz, H_n), 7.26 (t, 1H, ^3J(H,H) = 7.79 Hz, H_b), 6.97 (t, 1H, ^3J(H,H) = 8.36 Hz, ^4J(H,H) = 1.12 Hz, H_c), 6.81 (bd, 2H, H_v), 6.57 (bd, 2H, H_u).

^{13}C NMR (125 MHz, $C_2D_2Cl_4$, 403 K): δ = 144.36, 144.11, 141.35, 139.69, 139.10, 136.97, 133.76, 133.64, 133.32, 132.57, 132.37, 131.44, 131.37, 131.14, 130.94, 130.69, 129.90, 129.77, 129.34, 128.47, 128.38, 127.82, 127.37, 127.32, 127.20, 127.05, 126.11, 125.95, 125.79, 125.44, 125.25, 124.76, 124.56, 121.69, 120.68.

Elemental Analysis: 74.70% C, 3.93% H (calc.: 74.81% C, 3.55% H)

7.3.59 9,12-Bis-(4-*n*-dodecyl-phenyl)-10-phenanthren-4-yl-benzo[*e*]pyrene (5-41)

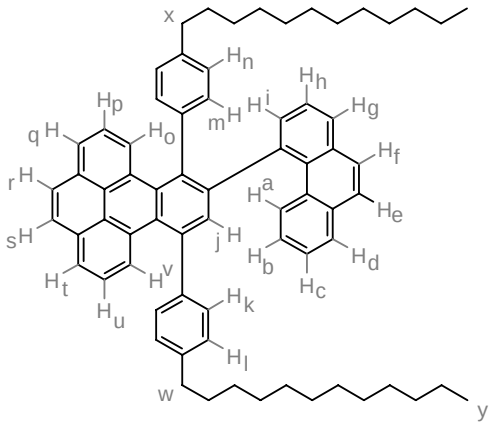

0.4 mL Dodeca-1-ene (300 mg, 1.8 mmol) were added to 4 mL of a 0.5 M solution 9-bora-bicyclo[3.3.1]nonane in THF and stirred at room temperature for 12 hours. A solution of 110 mg sodium hydroxide in 0.9 mL water was syringed to the reaction and allowed to react for an 20 minutes. Finally, 166 mg 9,12-Bis-(4-bromo-phenyl)-10-phenanthren-4-yl-benzo[*e*]pyrene (**5-40**, 0.22 mmol) and 8 mg dichloro[1,1'-bis(diphenyl-phosphino)ferrocene]palladium(II) (11 µmol) were added to the reaction, which was stirred for additional five hours. After having removed the solvent *in vacuo*, the residue was purified using preparative column chromatography (silica gel, eluent: low boiling petroleum ether, dichloromethane = 9:1, R_f = 0.51) to obtain 184 mg of the desired product as a colorless oil (91%, 201 µmol).

MS (FD, 8kV): m/z (%) = 916.8 (100%, M^+) (calc. for $C_{70}H_{76}$ = 917.39 g mol^{-1})

^{1}H NMR (500 MHz, $C_2D_2Cl_4$, 333 K): δ = 8.06 (d, 1H, ^3J(H,H) = 8.03 Hz, H_o), 7.96 (d, 1H, ^3J(H,H) = 8.68 Hz, H_d), 7.94 (d, 1H, ^3J(H,H) = 7.67 Hz, H_q), 7.92 (d, 1H, ^3J(H,H) = 8.98 Hz, H_s), 7.92 (d, 1H, ^3J(H,H) = 8.97 Hz, H_r), 7.86 (d, 1H, ^3J(H,H) = 8.20 Hz, H_t), 7.85 (d, 1H, ^3J(H,H) = 7.60 Hz, H_v), 7.72 (s, 1H, H_j), 7.70 (d, 1H, ^3J(H,H) = 7.04 Hz, ^4J(H,H) = 2.33 Hz, H_g), 7.63 (d, 1H, ^3J(H,H) = 7.90 Hz, ^4J(H,H) = 1.11 Hz, H_a), 7.56 (d, 1H, ^3J(H,H) = 8.88 Hz, H_f), 7.50 (d, 1H, ^3J(H, H) = 8.80 Hz, H_e), 7.45 (t, 1H, ^3J(H,H) = 7.84 Hz, H_p), 7.44 (t, 1H, ^3J(H,H) = 7.22 Hz, H_h), 7.41 (d, 1H, ^3J(H,H) = 7.17 Hz, H_i), 7.34 (bd, 2H, ^3J(H,H) = 6.44 Hz, H_k), 7.28 (t, 1H, ^3J(H,H) = 8.00 Hz, H_u), 7.25 (t, 1H, ^3J(H,H) = 6.91 Hz, H_b), 7.14 (d, 2H, ^3J(H,H) = 7.99 Hz, H_l), 6.97 (t, 1H, ^3J(H,H) = 8.55, ^4J(H,H) = 1.37 Hz, H_c), 6.73 (bd, 1H, H_n), 6.63 (bd, 1H H_m), 6.39 (bd, 1H $H_{n'}$), 6.29 (bd, 1H, $H_{m'}$), 2.59 (t, 2H, ^3J(H,H) = 7.63 Hz, H_x), 2.25 (t, 1H, ^3J(H,H) = 7.31 Hz, H_w), 1.7-1.0 (m, 40H, -CH_2-), 0.81 (2xt, 6H, ^3J(H,H) = 7.13 Hz, H_y)

^{13}C NMR (125 MHz, $C_2D_2Cl_4$, 373 K): δ = 144.03, 142.56, 142.14, 140.85, 140.50, 139.84, 139.55, 137.72, 133.42, 133.32, 133.12, 132.58, 131.77, 131.23, 131.09, 131.01, 130.79, 130.54, 129.92, 129.74, 129.60, 129.23, 128.52, 128.38, 128.11, 128.02, 127.74, 127.52, 127.47, 127.29, 127.26, 127.04, 125.91, 125.89, 125.60, 125.54, 125.30, 124.67, 124.52, 35.88, 35.49, 32.09, 32.07, 31.39, 31.20, 29.88, 29.84, 29.81, 29.69, 29.64, 29.47, 29.01, 22.80, 14.17.

7.3.60 8,17-Di-*n*-dodecyl-dibenzo[*hi,uv*]phenanthro-[3,4,5,6-*bcdef*]-ovalene (5-42)

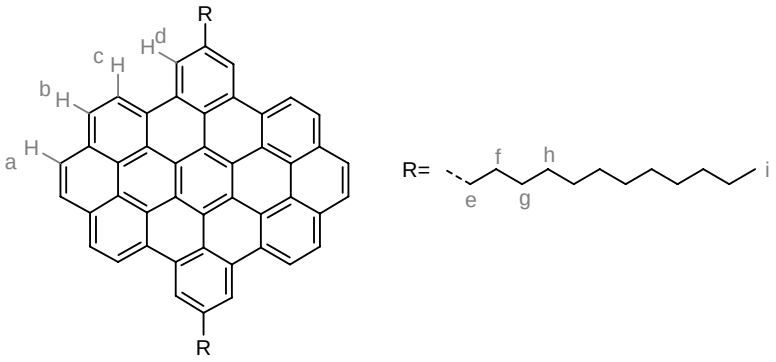

58.5 mg 9,12-Bis-(4-*n*-dodecyl-phenyl)-10-phenanthren-4-yl-benzo[*e*]pyrene (**5-41**, 63.7 µmol) were dissolved in 25 mL dichloromethane. A stream of argon saturated with dichloromethane was bubbled into the solution through a Teflon tube. A solution of 310 mg iron(III) chloride (1.91 mmol) in 0.5 mL nitromethane was quickly added. After a reaction time of 60 minutes, the reaction was stopped with methanol. The precipitate was filtered off and washed extensively with aqueous hydrochloride acid and methanol to afford 52 mg of the product as an orange-red solid (90%, 57.3 µmol).

MS (MALDI-TOF): m/z (%) = 906 (34%), 907 (33%), 908 (24%), 909 (9%) (calc. for $C_{70}H_{66}$ = 907.31 g mol^{-1}, isotope pattern: 906 (46%), 907 (36%), 908 (14%), 909 (4%))

^{1}H NMR (500 MHz, $C_2D_2Cl_4$, 410 K): δ = 9.11 (bd, 4H, ^{3}J(H,H)= 7.94 Hz, H_b), 8.89 (bs, 4H, H_a), 8.40 (bd, 4H, ^{3}J(H,H) = 8.91 Hz, H_c), 8.32 (bs, 4H, H_d), 3.32 (t, 4H, H_e), 2.17 (m, 4H, H_f), 1.76 (m, 4H, H_g), 1.66 (m, 4H, H_h), 1.6-1.2 (m, 32H, -CH_2-), 0.89 (t, 6H, ^{3}J(H,H) = 7.66 Hz, H_i).

^{13}C NMR: solubility too low to record spectrum with appropriate signal to noise ratio

DSC (°C): 226 (216)

Elemental Analysis: 92.58% C, 7.16% H (calc.: 92.67% C, 7.33% H)

7.3.61 4,4,5,5-Tetramethyl-2-phenanthren-4-yl-[1,3,2]dioxaborolane (5-43)

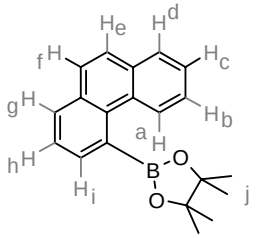

3.60 g 1,1,2,2,3,3,4,4,4-Nonafluoro-butane-1-sulfonic acid phenanthren-4-yl ester (**5-32**, 7.56 mmol), 3.00 g bis(pinacolato)diboron (11.8 mmol), and 4.46 g potassium acetate (45.4 mmol) were dissolved in 150 mL DMF and degassed carefully. After having added 875 mg tetrakis-(triphenylphosphino)-palladium(0) (757 µmol), the solution was stirred for 17 hours at 90°C. Water was added to quench the reaction. The product was extracted with ethyl acetate, the organic phase was dried with

magnesium sulfate and dried *in vacuo*. The residue was purified utilizing preparative column chromatography (flash silica gel, eluent: hexane, ethyl acetate (20:1), R_f = 0.24) to afford 1.90 g of the desired product (83%, 6.25 mmol) as an colorless crystalline material.

MS (FD, 8kV): m/z (%) = 304.8 (100%, M^+) (calc. for $C_{20}H_{21}BO_2$ = 304.20 g mol^{-1})

^{1}H-NMR (300 MHz, CD_2Cl_2): δ = 8.55 (d, 1H, ^3J(H,H) = 7.56 Hz, ^4J(H,H) = 1.96 Hz, H_a), 7.94 (t, 2H, ^3J(H,H) = 7.62 Hz, ^4J(H,H) = 1.70 Hz, H_c, H_h), 7.85 (d, 1H, ^3J(H,H) = 7.00 Hz, ^4J(H,H) = 1.41 Hz, H_f), 7.79 (d, 1H, ^3J(H,H) = 8.94 Hz, H_e), 7.75 (d, 1H, ^3J(H,H) = 8.91 Hz, H_i), 7.7-7.5 (m, 3H, H_b, H_d, H_g), 1.49 (s, 12H, H_j)

^{13}C-NMR (125 MHz, CD_2Cl_2, 306 K): δ = 133.99, 133.29, 133.16, 132.66, 131.20, 130.79, 128.67, 127.84, 127.27, 127.00, 126.93, 126.12, 125.63, 84.68, 24.97.

Elemental Analysis: 77.84% C, 7.06% H (calc.: 78.79% C, 6.96% H, 3.55% B, 10.52% O)

7.3.62 1,3,5-Tris-phenanthren-4-yl-benzene (5-44)

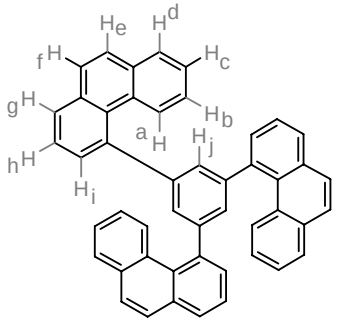

800 mg 4,4,5,5-Tetramethyl-2-phenanthren-4-yl-[1,3,2]dioxaborolane (**5-43**, 2.63 mmol), 138 mg 1,3,5-tribromobenzene (**5-63**, 0.44 mmol), and 830 mg barium hydroxide octahydrate (2.63 mmol) were dissolved in a mixture of 6 mL dimethoxyethane and 1 mL water and degassed. 25.3 mg Tetrakis-(triphenylphosphine)-palladium(0) (21.9 µmol) were added and the mixture was refluxed for 15 hours. The solvent was evaporated and the residue was purified using preparative column chromatography (silica gel, eluent: low boiling petroleum ether, dichloromethane (9:1), R_f = 0.17) to afford 10.1 mg of the title compound (15%, 16.8 µmol).

MS (FD, 8kV): m/z (%) = 607.1 (100%, M^+) (calc. for $C_{48}H_{30}$ = 606.77 g mol^{-1})

^{1}H NMR (500 MHz, oDCB, 453K): δ = 8.47 (db, 1H, H_a), 7.57 (t, 2H, ^3J(H,H) = 8.69 Hz, H_c, H_h), 7.47 (d, 1H, ^3J(H,H) = 9.37 Hz, H_f), 7.44 (d, 1H, ^3J(H,H) = 9.02 Hz, H_e), 7.40 (d, 1H, ^3J(H,H) = 7.16 Hz, H_i), 7.35-7.20 (m, 4H, H_b, H_d, H_g, H_j)

^{13}C NMR: δ = could not be obtained because of the vanishing solubility

Elemental Analysis: 94.41% C, 5.28% H (calc.: 95.02% C, 4.98% H).

7.3.63 Diphenanthro[3,4,5,6-*u,v,a,b,c*;3',4',5',6'-*e,f,g,h,i*]ovalene (5-45)

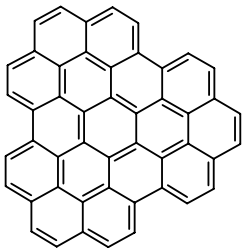

3.6 mg 1,3,5-Tris-phenanthren-4-yl-benzene (**5-44**, 5.93 µmol) were dissolved in 10 mL dichloromethane. A stream of argon saturated with dichloromethane was bubbled into the solution through a Teflon tube. A solution of 34.6 mg iron(III) chloride (214 µmol) in 0.2 mL nitromethane was quickly added. After a reaction time of 45 minutes, the reaction was stopped with methanol. The precipitate was filtered off and washed extensively with aqueous hydrochloride acid and methanol to afford 2.3 mg of the product as an orange, material (65%, 3.87 µmol).

MS (MALDI-TOF): m/z (%) = 594 (58%), 595 (30%), 596 (10%) (calc. for $C_{48}H_{18}$ = 594.68 g mol^{-1}, Isotope pattern: 594 (59%), 595 (31%), 596 (8%))

UV/vis: λ / nm (oDCB) = 350, 368, 391, 430, 484 (molar extinction coefficient could not be determined due to the vanishing solubility in organic solvents)

Elemental Analysis: 96.22% C, 3.86% H (calc.: 96.95% C, 3.05% H)

7.3.64 2-(Dihydroxyboryl)-N,N-diethyl-3-methoxybenzamide (5-48)

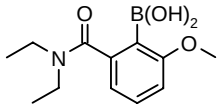

29.2 g N,N-Diethyl-3-methoxy-benzamide (**5-47**, 141 mmol) were dissolved in 280 mL anhydrous THF. A 1.7 M *tert*-butyl lithium solution in pentane was added drop-wise carefully at a temperature of -78 °C. After 1.5 hours of stirring, 63.6 mL trimethyl borate (568 mmol) were added. The mixture was stirred over night at room temperature before an aqueous saturated ammonium chloride solution was added. The product was extracted with dichloromethane, the solvent evaporated to yield 22.0 g of the desired product (62%, 87.6 mmol), which was directly converted in the Suzuki cross-coupling reaction.

7.3.65 6-Methoxy-2'-methyl-biphenyl-2-carboxylic acid diethylamide (5-49)

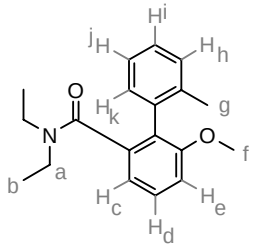

22.0 g 2-(Dihydroxyboryl)-N,N-diethyl-3-methoxybenzamid (**5-48**, 87.6 mmol), 13.7 g 2-iodotoluene (62.6 mmol) and 12.0 g sodium carbonate (113.0 mmol) were dissolved in a mixture of 220 mL 1,2-dimethoxyethane, 50 mL water and 50 mL ethanol and degassed.

1.9 g Tetrakis-(triphenylphosphino)-palladium(0) (1.64 mmol) were added and the mixture was refluxed for 24 hours. The reaction was quenched with aqueous ammonium chloride solution and extracted with dichloromethane. The organic phase was dried using magnesium sulfate and the solvent was evaporated. The residue was purified using preparative column chromatography (silica gel, eluent: hexane, ethyl acetate = 1:1, R_f = 0.51) and recrystallization from hexane to afford 15.1 g of the desired material as a colorless solid (81%, 50.8 mmol).

MS (FD, 8kV): m/z (%) = 297.7 (100%, M^+) (calc. for $C_{19}H_{23}NO_2$ = 297.40 g mol^{-1})

^{1}H NMR (500 MHz, $C_2D_2Cl_4$, 353 K): δ = 7.30 (t, 1H, ^3J(H,H) = 7.79 Hz, H_d), 7.13 (m, 3H, H_i, H_j, H_k), 7.06 (bd, 1H, H_k), 6.92 (d, 1H, ^3J(H,H) = 8.22 Hz, H_e), 6.86 (d, 1H, ^3J(H,H) = 7.11 Hz, H_c), 3.68 (s, 3H, H_f), 2.96 (bq, 4H, H_a), 2.07 (s, 3H, H_g), 0.89 (bt, 3H, H_b), 0.64 (bt, 3H, H_b).

^{13}C NMR (125 MHz, $C_2D_2Cl_4$): δ = 169.39, 157.09, 156.84, 139.45, 138.82, 138.64, 137.11, 136.20, 134.84, 131.69, 129.72, 129.59, 129.22, 128.91, 128.80, 127.62, 126.61, 125.44, 125.03, 118.78, 117.71, 111.18, 110.87, 56.07, 55.96, 42.90, 42.14, 37.85, 20.43, 19.81, 14.13, 13.88, 12.05.

Elemental Analysis: 76.80% C, 7.69% H, 4.33% N (calc.: 76.74% C, 7.80% H, 4.71% N, 10.76% O)

7.3.66 5-Methoxy-phenanthren-9-ol (5-50)

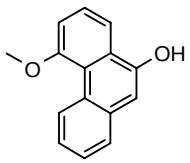

14 mL Di-*iso*-propylamine (10 mmol) were dissolved at 0 °C in 25 mL anhydrous THF. 6.24 mL of a 1.6 M *n*-butyl lithium hexane solution were added and the mixture was stirred for 10 minutes. 1.19 g 6-Methoxy-2'-methyl-biphenyl-2-carboxylic acid diethylamide (**5-49**, 4 mmol) were dissolved in 8 mL anhydrous THF and added to the reaction, which was stirred over night at room temperature. After having removed the solvent *in vacuo*, the residue was purified using preparative column chromatography (silica gel, eluent: hexane, ethyl acetate = 1:1, R_f = 0.34) to yield 843

mg of the desired compound as a colorless solid (94%, 3.76 mmol), which is unstable and was thus used without complete characterization.

MS (FD, 8kV): m/z (%) = 224.4 (100%, M^+) (calc. for $C_{15}H_{12}O_2$ = 224.26 g mol^{-1})

7.3.67 4-Methoxy-phenanthrene-9,10-dione (5-51)

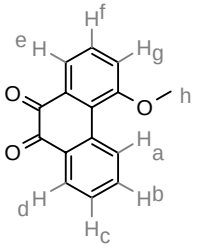

900 mg 5-Methoxy-phenanthren-9-ol (**5-50**, 4.01 mmol) and 130 mg N,N'-bis(salicylidene)ethylenediaminocobalt(II) (salcomine) were dissolved in 25 mL DMF and oxygen was bubbled for 5 hours through the solution. The mixture was extracted with ethyl acetate. The organic phase was washed with water, dried with magnesium sulfate and evaporated to yield 952 mg of desired product as a carmine solid (99%, 4.00 mmol).

MS (FD, 8kV): m/z (%) = 238.5 (100%, M^+) (calc. for $C_{15}H_{10}O_3$ = 297.40 g mol^{-1})

^{1}H NMR (300 MHz, CD_2Cl_2): δ = 8.87 (dd, 1H, ^3J(H,H) = 8.31 Hz, ^4J(H,H) = 0.67 Hz, H_a), 8.08 (dd, 1H, ^3J(H,H) = 7.72 Hz, ^4J(H,H) = 1.60 Hz, H_d), 7.76 (dd, 1H, , ^3J(H,H) = 7.52 Hz, ^4J(H,H) = 1.43 Hz, H_e), 7.66 (td, 1H, , ^3J(H,H) = 7.36 Hz, ^4J(H,H) = 1.68 Hz, H_f), 7.45-7.38 (m, 2H, H_b, H_c), 7.32 (dd, 1H, , ^3J(H,H) = 8.32 Hz, ^4J(H,H) = 1.33 Hz, H_g), 4,01 (s, 3H, H_h).

^{13}C NMR (75 MHz, CD_2Cl_2): δ = 182.22, 181.86, 158.58, 136.06, 133.05, 131.24, 130.46, 130.25, 130.14, 128.85, 124.61, 122.90, 120.07, 56.51.

Elemental Analysis: 75.48% C, 4.27% H (calc.: 75.62% C, 4.23% H, 20.15% O)

7.3.68 1,1,2,2,3,3,4,4,4-Nonafluoro-butane-1-sulfonic acid 9,10-di-*n*-dodecyl-phenanthren-4-yl ester (5-54)

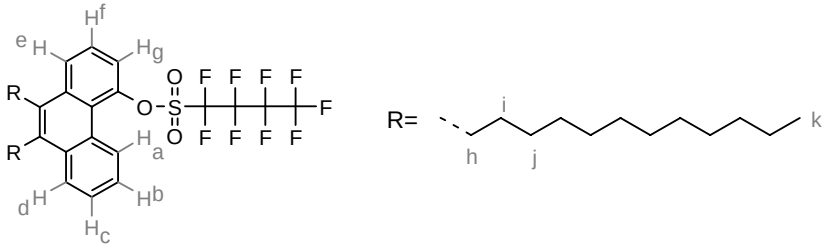

100 mg 4-Methoxy-phenanthrene-9,10-dione (**5-51**, 420 µmol) were dissolved in 20 mL anhydrous THF. 1 mL of a 1M solution of *n*-dodecylmagnesium bromide in diethyl ether (1 mmol) was slowly added and the resulting mixture was stirred for 1 hour. The solvent was evaporated and the oily residue dissolved in 5 mL acetic acid. 1 mL of an aqueous iodic acid solution (58%) was added and the reaction was heated to reflux for 24 hours. The product was extracted with dichloromethane, carefully neutralized with aqueous sodium carbonate, dried with magnesium sulfate and evaporated *in vacuo*. The residue was dissolved in triethyl amine and 300 mg 1,1,2,2,3,3,4,4,4-nonafluoro-butane-1-sulfonyl fluoride (1 mmol) were added to the

solution, which was stirred at 50 °C over night. The solvent was again removed *in vacuo* and the residue was purified using preparative column chromatography (flash silica gel, eluent: low boiling petroleum ether, dichloromethane = 9:1, R_f = 0.81) to yield 306 mg of the desired product as a colorless oil (90%, 377 µmol).

MS (FD, 8kV): m/z (%) = 814.6 (100%, M^+) (calc. for $C_{42}H_{57}F_9O_3S$ = 812.97 g mol^{-1})

^{1}H NMR (250 MHz, CD_2Cl_2): δ = 9.16 (d, 1H, ^3J(H,H) = 8.38 Hz, ^4J(H,H) = 1.09 Hz, H_a), 8.21 (d, 1H, ^3J(H,H) = 8.18 Hz, ^4J(H,H) = 1.09 Hz, H_d), 8.19 (d, 1H, ^3J(H,H) = 7.82 Hz, ^4J(H,H) = 1.73 Hz, H_e), 7.75-7.55 (m, 4H, H_b, H_c, H_f, H_g), 3.20-3.10 (m, 4H, H_h), 1.80-1.70 (m, 4H, H_i), 1.70-1.55 (m, 4H, H_j), 1.55-1.25 (m, 32H, -CH_2-), 0.95 (t, 6H, ^3J(H,H) = 6.88 Hz, H_k)

^{13}C NMR (63 MHz, CD_2Cl_2): δ = 147.74, 136.70, 135.12, 133.82, 133.06, 128.11, 127.20, 126.36, 126.03, 125.69, 125.13, 123.79, 120.13, 119.47 (C,F coupling), 115.64 (C,F coupling), 114.96 (C,F coupling), 110.46 (C,F coupling), 32.51, 31.10, 31.01, 30.90, 30.85, 30.38, 30.26, 30.12, 30.02, 29.95, 23.25, 14.40.

^{18}F NMR (471 MHz, CD_2Cl_2): δ = -80.61, -109.02, -120.50, -125.57 (fluorobenzene as standard)

7.3.69 2-(9,10-Di-*n*-dodecyl-phenanthren-4-yl)-4,4,5,5-tetramethyl-[1,3,2]dioxaborolane (5-55)

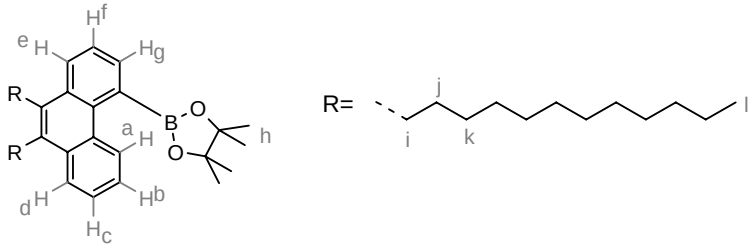

90 mg 1,1,2,2,3,3,4,4,4-Nonafluoro-butane-1-sulfonic acid 9,10-di-*n*-dodecyl-phenanthren-4-yl ester (**5-54**, 123 µmol), 47 mg bispinacolatodiborane (184 µmol), and 72.4 mg potassium acetate (738 µmol) were dissolved in 3 mL anhydrous DMF and degassed. 14.2 mg Tetrakis-(triphenylphosphino)-palladium(0) (12.3 µmol) were added and the resulting mixture was stirred over night at 90 °C. The product was extracted with ethyl acetate. The organic phase was extensively washed with water, dried over magnesium sulfate and evaporated. The residue was purified using preparative column chromatography (flash silica gel, eluent: hexane, ethyl acetate = 20:1, R_f = 0.33) to afford 57 mg of the title compound as a colorless oil (72%, 88.9 µmol).

MS (FD, 8kV): m/z (%) = 640.6 (100%, M^+) (calc. for $C_{44}H_{69}BO_2$ = 640.85 g mol^{-1})

^{1}H NMR (250 MHz, CD_2Cl_2): δ = 8.44 (d, 1H, ^3J(H,H) = 8.19 Hz, H_a), 8.23 (d, 1H, ^3J(H,H) = 8.36 Hz, H_d), 8.18 (d, 1H, ^3J(H,H) = 8.39 Hz, H_e), 7.84 (d, 1H, ^3J(H,H) = 6.81 Hz, H_g), 7.75-7.60 (m, 2H, H_b, H_c), 7.55 (t, 1H, ^3J(H,H) = 7.62 Hz, H_f), 3.30-3.10 (m, 4H, H_i), 1.90-1.70 (m, 4H, H_j), 1.70-1.60 (m, 4H, H_k), 1.49 (s, 12H, H_h), 1.55-1.30 (m, 32H, -CH_2-), 0.97 (t, 6H, ^3J(H,H) = 6.87 Hz, H_l)

^{13}C NMR (63 MHz, CD_2Cl_2): δ = 134.89, 134.64, 134.29, 132.57, 132.27, 132.15, 130.99, 128.20, 127.26, 126.88, 126.32, 124.85, 124.54, 84.71, 32.67, 31.53, 31.38, 31.07, 30.45, 30.24, 30.11, 30.01, 29.95, 25.17, 23.42, 14.62.

7.3.70 1,3,5-Tris-(9,10-bis-*n*-dodecyl-phenanthren-4-yl)-benzene and 1-Bromo-3,5-Bis-(9,10-bis-*n*-dodecyl-phenanthren-4-yl)-benzene (5-56)

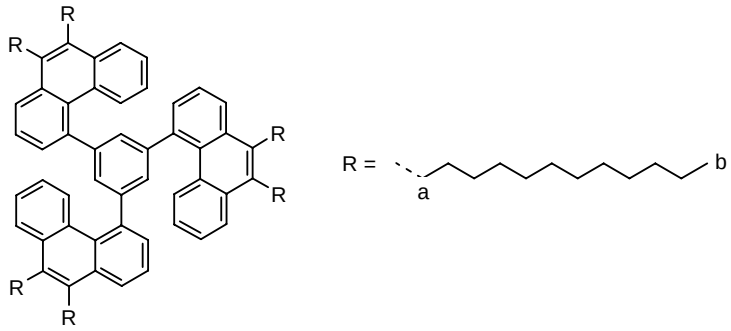

1.40 g 2-(9,10-Di-*n*-dodecyl-phenanthren-4-yl)-4,4,5,5-tetramethyl-[1,3,2]dioxaborolane (**5-55**, 2.18 mmol), 114 mg 1,3,5-tribromobenzene (**5-63**, 0.34 mmol), and 688 mg barium hydroxide octahydrate (2.18 mmol) were dissolved in a mixture of 6 mL dimethoxyethane and 1 mL water and degassed. 19.6 mg tetrakis-(triphenylphosphine)-palladium(0) (17.0 µmol) were added and the mixture was refluxed for 27 hours. The solvent was evaporated and the residue was purified using preparative column chromatography (flash silica gel, eluent: low boiling petroleum ether, dichloromethane (20:1), R_f = 0.48) to afford 44.0 mg of the title compound (8%, 27.2 µmol) and 217 mg of the double reacted compound 1-bromo-3,5-Bis-(9,10-bis-*n*-dodecyl-phenanthren-4-yl)-benzene as side product, both as colorless oils.

MS (MALDI-TOF, dithranol): m/z (%) = 1617.00 (M^+), 1640.00 ($M^+ + Na^+$) (calc. for $C_{120}H_{174}$ = 1616.72 g mol^{-1})

^{1}H NMR (250 MHz, CD_2Cl_2): substance formed stable atropisomers, which isomerize around 180°C in oDCB. However, oDCB covers most of the aromatic resonance, therefore, the resonances are given for the room temperature spectrum of the two atropisomers (ratio: 1:2) in CD_2Cl_2. (see chapter 5.4.3.)

8.81 (d, 0.6 H, ^3J(H,H) = 8.71 Hz), 8.39 (d, 0.82 H, ^3J(H,H) = 8.48 Hz), 8.21 (d, 0.41 H, ^3J(H,H) = 8.17 Hz), 8.05-7.85 (m), 7.76 (d, 0.41H, ^3J(H,H) = 8.49 Hz), 7.56-7.10 (m), (t, 0.83H, ^3J(H,H) = 7.55 Hz) (integration aromatic region = 24 H), 3.20-2.90 (m, 12H, H_a), 1.7-1.0 (m, 120H, -CH_2-), 0.79 (t, 18H, ^3J(H,H) = 6.72 Hz, H_b)

^{13}C NMR: could not be obtained resolved, see main text

7.3.71 5,6,11,12,17,18-Hexa-*n*-dodecyl-diphenanthro[3,4,5,6-*uvabc*;3',4',5',6'-*efghi*]ovalene (5-57)

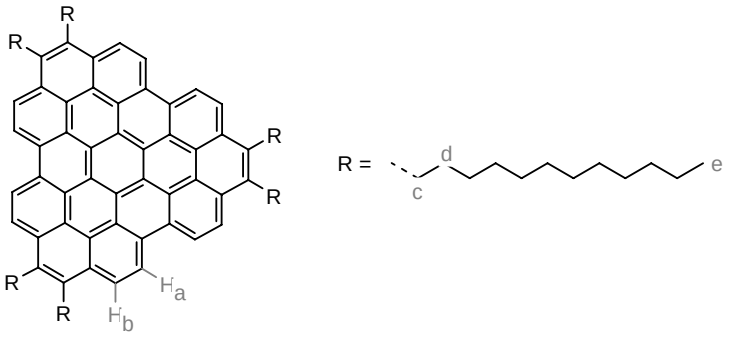

10.5 mg 1,3,5-Tris-(9,10-bis-*n*-dodecyl-phenanthren-4-yl)-benzene (6.52 µmol) were dissolved in 25 mL dichloromethane. A stream of argon saturated with dichloromethane was bubbled into the solution through a Teflon tube. A solution of 38.0 mg iron(III) chloride (235 µmol) in 0.1 mL nitromethane was quickly added. After a reaction time of 60 minutes, the reaction was stopped with methanol. The precipitate was filtered off and washed extensively with aqueous hydrochloride acid and methanol. Repetitive reprecipitation gave 8.72 mg of the desired product as an orange material (83%, 5.43 µmol).

MS (MALDI-TOF): m/z (%) = 1603 (30%), 1604 (34%), 1605 (22%), 1606 (10%), 1607 (4%) (calc. for $C_{120}H_{162}$ = 1604.63 g mol^{-1}, Isotope pattern: 1603 (26%), 1604 (35%), 1605 (24%), 1606 (11%), 1607 (3%))

UV/vis: λ / nm (ε / m^2·mol^{-1}) = 379 (1108), 397 (2509), 436 (903)

^{1}H NMR (500 MHz, THF, CS_2): 8.50 (bd, 6H, H_a), 8.20 (bd, 6H, H_b), 3.33 (bt, 12H, H_c), 2.09 (m, 12H, H_d), 2.0-1.2 (m, 108H, -CH_2-), 0.98 (bt, 18H, ^3J(H,H) = 6.71 Hz, H_e) (solubility of the compound is very low, NMR resonances are broad because of self-association phenomena)

^{13}C NMR: could not be obtained, because substance is hardly soluble

DSC (°C): 48 (22)

Elemental Analysis: 89.76% C, 10.04% H (calc. 89.82% C, 10.18% H)

7.3.72 1,3-Bis-(9,10-bis-*n*-dodecyl-phenanthren-4-yl)-5-(biphenyl-2-yl)-benzene (5-61)

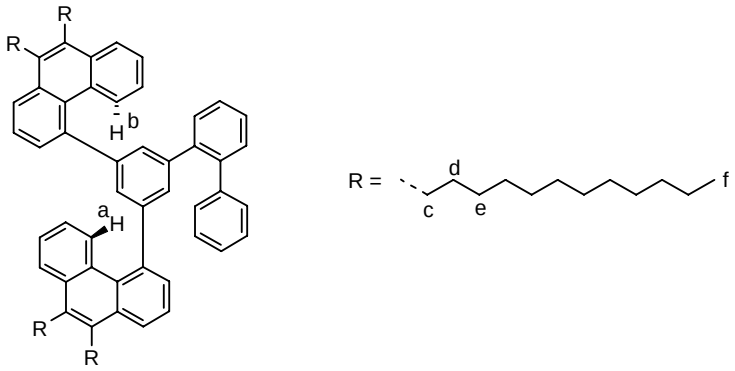

335 mg 2-Biphenylboronic acid (1.69 mmol), 200 mg 1-bromo-3,5-Bis-(9,10-bis-*n*-dodecyl-phenanthren-4-yl)-benzene (**5-60**, 169 µmol), and 688 mg barium hydroxide octahydrate (2.18 mmol) were dissolved in a mixture of 6 mL dimethoxyethane and 1 mL water and degassed. 19.6 mg Tetrakis-(triphenylphosphine)-palladium(0) (17.0 µmol) were added and the mixture was refluxed for 6 hours. The solvent was evaporated and the residue was purified using preparative column chromatography (silica gel, eluent: low boiling petroleum ether, dichloromethane (20:1), R_f = 0.48) to afford 149 mg of the title compound as a colorless oil (71%, 120 µmol).

MS (FS, 8kV): m/z (%) = 1256.0 (100%, M^+) (calc. for $C_{94}H_{126}$ = 1256.05 g mol^{-1})

^{1}H NMR (500 MHz, $C_2D_2Cl_4$): 8.31 (d, 1H, ^3J(H,H) = 7.83 Hz, H_a), 8.1-8.0 (m, 4H), 7.93 (d, 1H, ^3J(H,H) = 8.12 Hz, H_b), 7.50-6.9 (m, 20H), 3.07 (m, 8H, H_c), 1.68 (m, 8H, H_d), 1.54 (m, 8H, H_e), 1.35-1.15 (m, 64H, -CH_2-), 0.86 (t, 12H, ^3J(H,H) = 6.89 Hz, H_f)

^{13}C NMR: carbon resonances are broad and not very well resolved, because rotation around the central phenyl ring is limited

7.3.73 5,6,17,18-Tetra-*n*-dodecyl-dibenzo[*ef,hi*]phenanthro[3,4,5,6-*u,v,a,b,c*]ovalene (5-62)

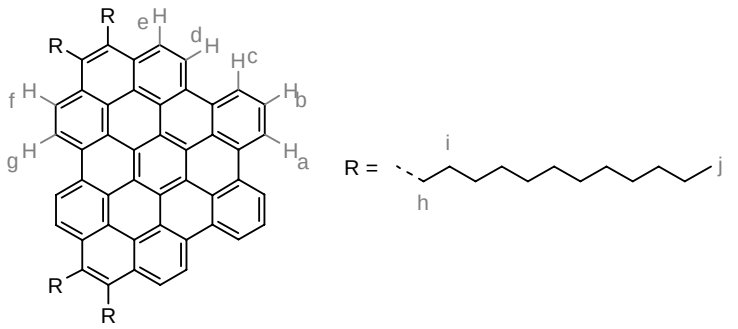

50.2 mg 1,3-Bis-(9,10-bis-*n*-dodecyl-phenanthren-4-yl)-5-(biphenyl-2-yl)-benzene (**5-61**, 39.9 µmol) were dissolved in 45 mL dichloromethane. A stream of argon saturated with dichloromethane was bubbled into the solution through a Teflon tube. A solution of 233 mg iron(III) chloride (1.44 mmol) in 0.5 mL nitromethane was quickly added. After a reaction time of 60 minutes, the reaction was stopped with methanol. The precipitate was filtered off and washed extensively with aqueous

hydrochloride acid and methanol. Repetitive reprecipitation into methanol gave 45.2 mg of the desired product as an orange-yellow material (91%, 36.3 µmol).

MS (MALDI-TOF): m/z (%) = 1243 (31%), 1244 (35%), 1245 (23%), 1246 (9%), 1247 (3%) (calc. for $C_{94}H_{114}$ = 1243.96 g mol^{-1}, Isotope pattern: 1243 (35%), 1244 (36%), 1245 (19%), 1246 (7%), 1247 (2%))

UV/vis: λ / nm (ε / m^2·mol^{-1}) = 332 (538), 353 (917), 372 (1329), 388 (2000), 422 (648), 448 (877), 469 (444), 490 (150)

^{1}H NMR (500 MHz, $C_2D_2Cl_4$, 413 K): 9.15 (db, 2H, H_a), 9.04 (tb, 2H, H_b), 8.93 (db, 2H, H_c), 8.47 (db, 2H, H_d), 8.15 (db, 2H, H_e), 8.09 (db, 2H, H_f), 7.87 (db, 2H, H_g), 3.69 (tb, 4H, H_h), 3.46 (tb, 4H, H_h), 2.15 (m, 4H, H_i), 2.03 (m, 4H, H_i), 2.0-1.1 (m, 72H, -CH_2-), 0.92 (tb, 12H, H_j) (^3J(H,H) couplings could not be resolved, resonances are broadened because of self-aggregation phenomena)

^{13}C NMR: could not be obtained, because substance is hardly soluble

DSC (°C): 173, 210 (144)

Elemental Analysis: 89.43% C, 10.27% H (calc. 90.76% C, 9.24% H)

7.3.74 [3,5-Bis-(4-*n*-dodecyl-benzyl)-phenyl]-trimethylsilane (5-65)

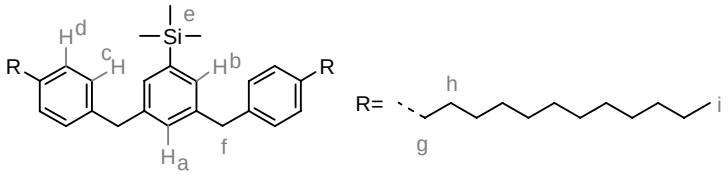

To a suspension of 450 mg magnesium (17.2 mmol) in 20 mL anhydrous diethyl ether, 5.75 g 4-*n*-dodecylbenzylbromide (17.0 mmol), dissolved in 20 mL diethyl ether, were added carefully in a drop-wise fashion. The Grignard solution was refluxed for 45 min, in order to complete the conversion. The reaction mixture was transferred to a solution of 1.74 g 1,3-dibromo-5-(trimethylsilyl)-benzene (**5-64**, 5.65 mmol) and 100 mg [1,3-bis(diphenyl-phosphino)propane] dichloronickel(II) (0.18 mmol) in 20 mL anhydrous diethyl ether. The reaction was kept under reflux for 20 hours, before quenching with 2M hydrochloric acid. The organic phase was separated, washed with water, dried with magnesium sulfate and evaporated. Repetitive recrystallization removed the major part of the dibenzyl side product. Finally, preparative column chromatography (silica gel, eluent: low boiling petroleum ether, dichloromethane = 20:1, R_f = 0.35) was applied to yield 1.1 g of the desired product as a colorless oil (29%, 1.65 mmol).

MS (FS, 8kV): m/z (%) = 668.8 (100%, M$^+$) (calc. for $C_{47}H_{74}Si$ = 667.20 g mol^{-1})

^{1}H NMR (700 MHz, CD_2Cl_2): δ = 7.14 (d, 2H, ^4J(H,H) = 1.26 Hz, H_b), 7.01 (d, 8H, ^4J(H,H) = H_c, H_d), 6.94 (t, 1H, ^4J(H,H) = 1.27 Hz, H_a), 3.81 (s, 4H, H_f), 2.49 (t, 4H, ^3J(H,H) = 7.56 Hz, H_g), 1.51 (pent., 4H, ^3J(H,H) = 7.35 Hz, H_h), 1.3-1.1 (m, 36H, -CH_2-), 0.82 (t, 6H, ^3J(H,H) = 7.00 Hz, H_i), 0.16 (s, 9H, H_e)

^{13}C NMR (175 MHz, CD_2Cl_2): δ = 141,29, 141,20, 141,12, 139,06 (alles Ar-C_{quart}), 132,00, 130,40, 128,93, 128,84 (alles Ar-*C*H), 41,97 (Ar-*C*H_2-Ar), 35,92 (α-*C*H_2), 32,38, 32,05, 30,12, 30,09, 30,06, 29,97, 29,80, 23,14 (alles -*C*H_2-), 14,31 (-*C*H_3), -5,35 (Ar-Si(*C*H_3)$_3$)

7.3.75 1,3-Bis-(4-*n*-dodecyl-benzyl)-5-iodo-benzene (5-66)

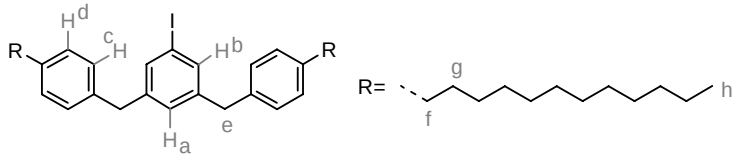

1.00 [3,5-Bis-(4-*n*-dodecyl-benzyl)-phenyl]-trimethylsilane (**5-65**, 1.50 mmol) were dissolved in 50 mL chloroform. 1.8 mL of a 1M iodomonochloride solution in dichloromethane was added slowly under light exclusion. After 30 minutes, the conversion was complete and the reaction was quenched with dilute aqueous sodium thiosulfate solution. The organic phase was separated, dried with magnesium sulfate and evaporated *in vacuo*. The residue was purified utilizing preparative column chromatography (silica gel, eluent: low oiling petroleum ether, R_f = 0.31) to obtain 944 mg of the title compound as colorless oil (87%, 1.31 mmol).

MS (FS, 8kV): m/z (%) = 721.2 (100%, M^+) (calc. for $C_{44}H_{65}I$ = 720.91 g mol^{-1})

^{1}H NMR (250 MHz, CD_2Cl_2): δ = 7,43 (d, 2H, ^4J(H,H) = 1.25 Hz, H_b), 7.2-7.0 (m, 9H, H_a, H_c, H_d), 3.89 (s, 4H, H_e), 2.59 (t, 4H, ^3J(H,H) = 7.58 Hz, H_f), 1.61 (m, 4H, H_g), 1.4-1.2 (m, 38H, -CH_2-), 0.91 (t, 6H, ^3J(H,H) = 6.32 Hz, H_h)

^{13}C NMR (63 MHz, CD_2Cl_2): δ = 144.45, 141.45, 137.97 (all Ar-C_{quart}), 135.81, 129.36, 128.99 (all Ar-*C*H), 128.94 (Ar-C_{quart}), 94.96 (*C*-I), 41.33 (benzyl-*C*), 35.90, 32.35, 32.02, 30.10, 30.07, 30.04, 29.94, 29.80, 23.12, 18.81 (all -*C*H_2-), 14.33 (-*C*H_3)

7.3.76 [3,5-Bis-(4-*n*-dodecyl-benzyl)-phenylethynyl]-trimethyl-silane (5-67)

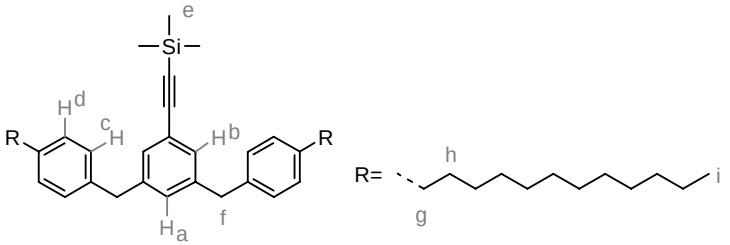

500 mg 1,3-Bis-(4-*n*-dodecyl-benzyl)-5-iodo-benzene (**5-66**, 0.69 mmol), 1.80 mg triphenylphosphine (6.91 µmol), and 1.34 mg (6.91 µmol) copper(I) iodide were dissolved in a mixture of 5 mL triethylamine and 2 mL THF and degassed. 88 mg Trimethylsilylacetylene (0.13 mL, 0.90 mmol) and 4.80 mg bis(triphenyl-phosphine)palladium(II) chloride (6.91 µmol) were added and the mixture was stirred at 55 °C for 1 hour. The solvents were removed *in vacuo* and the residue was purified using preparative column chromatography (silica gel, eluent: low boiling petroleum ether, dichloromethane = 9:1, R_f = 0.58) to obtain 440 mg of the desired product as a colorless oil (92%, 0.64 mmol).

MS (FS, 8kV): m/z (%) = 691.4 (100%, M^+), 1382.7 (43%, $M^{½+}$) (calc. for $C_{49}H_{74}Si$ = 691.22 g mol^{-1})

^{1}H NMR (250 MHz, CD_2Cl_2): δ = 7.25-7.10 (m, 11H, H_a, H_b, H_c, H_d), 3.95 (s, 4H, H_f), 2.68 (t, 4H, ^3J(H,H) = 7.58 Hz, H_g), 1.70 (m, 4H, H_h), 1.4-1.2 (m, 38H, -CH_2-), 1.01 (t, 6H, ^3J(H,H) = 6.95 Hz , H_i), 0.33 (s, 9H, H_e)

^{13}C NMR (63 MHz, CD_2Cl_2): δ = 142.22, 141.16, 138.17 (all Ar-C_{quart}), 130.31, 130.26, 128.94, 128.80 (all Ar-*C*H), 123.54 (Ar-C_{quart}), 105.54 (-*C*≡ C-Si(CH_3)$_3$), 93.91 (-C≡ *C*-Si(CH_3)$_3$), 41.48 (benzyl-*C*), 35.86, 33.26, 32.31, 31.97, 30.07, 30.04, 30.00, 29.91, 29.75, 23.07 (all -*C*H_2-), 14.30 (*C*H_3), 0.00 (-C≡ C-Si(*C*H_3)$_3$)

7.3.77 1,3-Bis-(4-*n*-dodecyl-benzyl)-5-ethynyl-benzol (5-68)

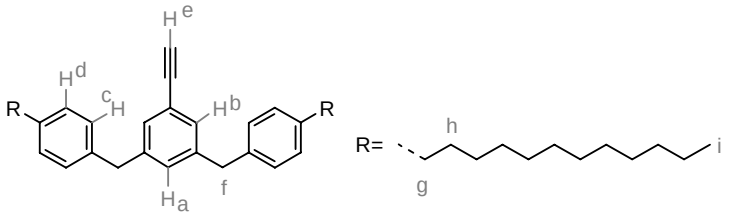

440 mg [3,5-Bis-(4-*n*-dodecyl-benzyl)-phenylethynyl]-trimethyl-silane (**5-67**, 0.64 mmol) were dissolved in 60 mL THF. A solution of 301 mg tetra-*n*-butyl ammonium fluoride trihydrate (0.96 mmol) in 5 mL THF was added. After 10 minutes, the reaction was stopped with water. The product was extracted with dichloromethane. The organic phase was dried with magnesium sulfate and evaporated *in vacuo*. The residue was filtered with low boiling petroleum ether and dichloromethane (1:1) through a pad of silica gel to obtain the title compound as colorless oil (96%, 0.62 mmol).

MS (FS, 8kV): m/z (%) = 309.2 (7%, M^{2+}), 618.8 (100%, M^+) (calc. for $C_{46}H_{66}$ = 619.04 g mol^{-1})

^{1}H NMR (250 MHz, CD_2Cl_2): δ = 7.24 (d, 2H, ^4J(H,H) = 1.25 Hz, H_b), 7.2-7.1 (m, 9H, H_a, H_c, H_d), 3.95 (s, 4H, H_f), 3.10 (s, 1H, H_e), 2.66 (t, 4H, ^3J(H,H) = 7.58 Hz, H_g), 1.70 (m, 4H, H_h), 1.5-1.3 (m, 38H, -CH_2-), 1.00 (t, 6H, ^3J(H,H) = 6.93 Hz , H_i)

^{13}C NMR (63 MHz, CD_2Cl_2): δ = 142.58, 141.45, 138.30 (all Ar-C_{quart}), 130.77, 130.72, 129.18, 129.06 (all Ar-*C*H), 122.71 (Ar-C_{quart}), 84.27 (-*C*≡C-H), 77.25 (-C≡ *C*-Si(CH_3)$_3$), 41.69 (benzyl-*C*), 36.10, 32.54, 32.19, 30.31, 30.27, 30.24, 30.15, 29.99, 23.30 (all -*C*H_2-), 14.52 (-*C*H_3)

7.3.78 Bis(3,5-(4'-*n*-dodecyl-benzyl)-phenyl)-acetylene (5-69)

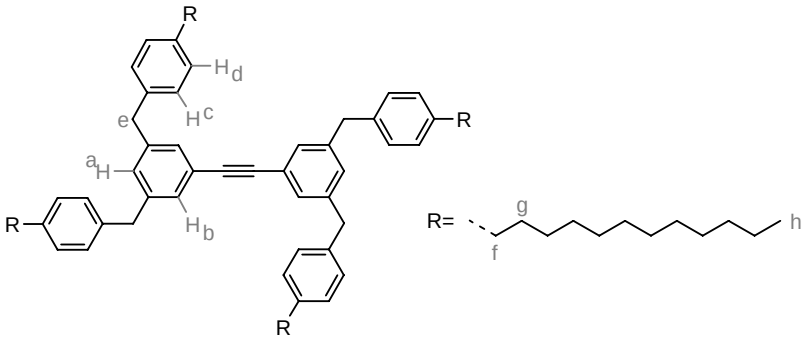

443 mg 1,3-Bis-(4-*n*-dodecyl-benzyl)-5-iodo-benzene (**5-66**, 0.61 mmol), 380 mg 1,3-bis-(4-*n*-dodecyl-benzyl)-5-ethynyl-benzene (**5-68**, 0.61 mmol), 1.70 mg (6.17 µmol) triphenylphosphine, and 1.20 mg (6.17 µmol) copper(I)iodide were dissolved in a mixture of 2 mL THF and 5 mL triethyl amine and degassed with five consecutive freeze-pump-thaw cycles. 4.52 mg Bis(triphenylphosphine)palladium(II)-chloride (6.17 µmol) were added and the mixture was warmed to 55 °C for one hour.

The solvent was evaporated and the residue was purified utilizing preparative column chromatography (flash silica gel, eluent: low boiling petroleum ether, dichloromethane = 9:1, R_f = 0.31) to obtain 622 mg of the desired compound as a colorless oil (84%, 0.51 mmol).

MS (FS, 8kV): m/z (%) = 1212.7 (100%, M^+), 2424.3 (5%, $M^{½+}$) (calc. for $C_{90}H_{130}$ = 1212.04 g mol^{-1})

^{1}H NMR (250 MHz, CD_2Cl_2): δ = 7.20 (d, 4H, ^4J(H,H) = 1.58 Hz, H_b), 7.18-7.05 (m, 18H, H_a, H_c, H_d), 3.92 (s, 8H, H_e), 2.62 (t, 8H, ^3J(H,H) = 7.28 Hz, H_f), 1.64 (m, 8H, H_g), 1.5-1.3 (m, 76H, -CH_2-), 0.95 (t, 12H, ^3J(H,H) = 6.00 Hz , H_h)

^{13}C NMR (63 MHz, CD_2Cl_2): δ = 142.51, 141.40, 138.40 (all Ar-C_{quart}), 130.14, 130.10, 129.11, 128.97 (all Ar-*C*H), 123.74 (Ar-C_{quart}), 89.66 (-*C*≡ *C*-), 41.68 (benzyl-*C*), 36.01, 32.45, 32.11, 30.20, 30.17, 30.14, 30.04, 29.91, 29.89, 23.20 (all -*C*H_2-), 14.41 (-*C*H_3)

7.3.79 Hexa-(3,5-bis-(4-*n*-dodecylbenzyl))phenylbenzene (5-70)

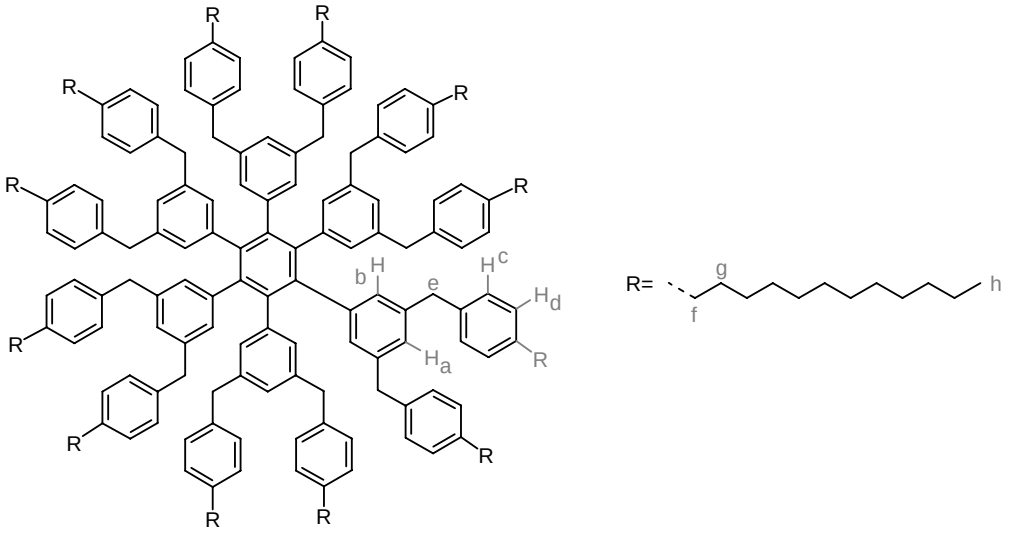

100 mg Bis(3,5-(4'-*n*-dodecyl-benzyl)-phenyl)-acetylene (**5-69**, 0.08 mmol) were dissolved in 25 mL anhydrous 1,4-dioxane and five consecutive freeze-pump-thaw cycles were conducted. 6 mg Dicobaltoctacarbonyl (0.02 mmol) was added and the reaction mixture was kept under reflux for 15 hours. The solvent was evaporated *in vacuo* and the residue was purified using preparative column chromatography (silica gel, eluent: low boiling petroleum ether, dichloromethane = 8:2, R_f = 0,88) to afford 87 mg of the desired product as a colorless oil (86%, 23.9 µmol).

MS (MALDI-TOF): m/z (%) = 3745 (100%, $M^+ + Ag^+$) 3768 (8%, $M^+ + Cs^+$) (calc. for $C_{270}H_{390}$ = 3636.12 g mol^{-1})

^{1}H NMR (700 MHz, CD_2Cl_2): δ = 6.87 (d, 24H, ^3J(H,H) = 7.21 Hz, H_d), 6.60 (d, 24H, ^3J(H,H) = 7.28 Hz, H_c), 6.54 (s, 6H, H_a), 6.42 (s, 12H, H_b), 3.47 (s, 24H, H_e), 2.48 (m, 24H, H_f), 1.52 (m, 24H, H_g), 1.4-1.1 (m, 216H, -CH_2-), 0.89 (t, 36H, ^3J(H,H) = 6.44 Hz , H_h)

^{13}C NMR (175 MHz, CD_2Cl_2): δ = 141.18, 140.45, 139.90, 138.92 (all Ar-C_{quart}), 128.95, 128.83, 128.50, 128.41 (all Ar-*C*H), 41.43 (benzyl-*C*), 36.94 (α-*C*H_2-), 32.35, 32.05, 30.14, 30.10, 30.01, 29.94, 29.80, 23.11 (all -*C*H_2-), 14.30 (-*C*H_3)

7.3.80 Tetra-(4,4',4'',4'''-*n*-dodecyl-)phenylbenzene (5-73)

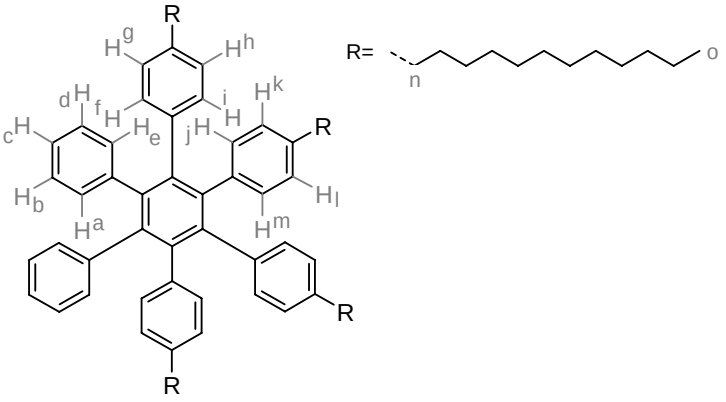

200 mg 2,3,4,5-Tetrakis(4-*n*-dodecyl-phenyl)-cyclopentadienone (**5-34c**, 189 µmol) and 37 mg diphenyl acetylene (**5-72**, 208 µmol) were heated over night in 1 mL diphenylether to 280 °C. The solvent was removed using high vacuum and the residue was purified utilizing preparative column chromatography (silica gel, eluent: low boiling petroleum ether, dichloromethane = 9:1, R_f = 0.63) to afford 212 mg of the desired product as a colorless oil (93%, 175 µmol).

MS (FD, 8kV): m/z (%) = 1208.2 (100%, M^+) (calc. for $C_{90}H_{126}$ = 1208.01 g mol^{-1})

^{1}H NMR (300 MHz, CD_2Cl_2, 303K): δ = 6.75 (m, 10H, H_a, H_b, H_c, H_d, H_e), 6.61 (m, 8H, H_f, H_g, H_h, H_i), 6.55 (m, 8H, H_j, H_k, H_l, H_m), 2.26 (t, 8H, ^3J(H,H) = 7.53 Hz, H_n), 1.5-1.0 (m, 40H, -CH_2), 0.80 (t, 12H, ^3J(H,H) = 6.90 Hz, H_o)

^{13}C NMR (75 MHz, CD_2Cl_2, 383K): δ = 141.50, 140.98, 140.79, 140.48, 139.92, 139.87, 138.58, 138.52, 131.88, 131.64, 131.63, 130.11, 126.89, 126.85, 126.78, 125.34, 123.60, 119.19, 128.78, 35.68, 35.61, 32.34, 31.70, 31.59, 30.12, 30.09, 29.92, 29.89, 29.78, 29.31, 29.20, 23.09, 14.27, 30.13, 30.06

7.3.81 2,5,8,11-Tetra-*n*-dodecyl-hexa-*peri*-hexabenzocoronene (5-74)

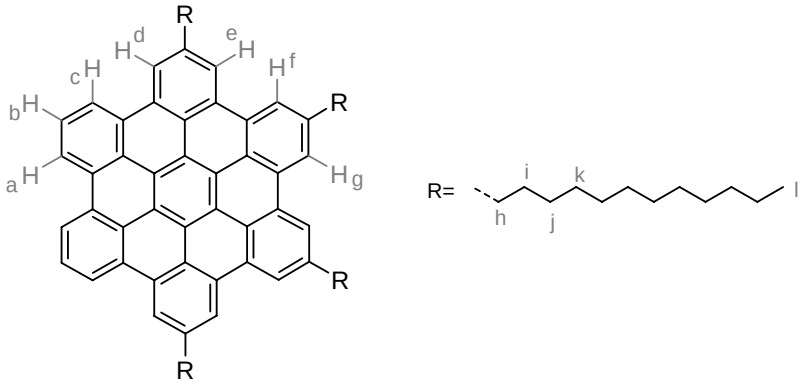

50 mg Tetra-(4,4',4'',4'''-*n*-dodecyl-)phenylbenzene (**5-73**, 41.4 µmol) were dissolved in 25 mL dichloromethane. A stream of argon saturated with dichloromethane was bubbled into the solution through a Teflon tube. A solution of 113 mg iron(III) chloride (695 µmol) in 0.5 mL nitromethane was quickly added. After a reaction time of 45 minutes, the reaction was stopped with methanol. The precipitate was collected and washed extensively with aqueous hydrochloride acid

and methanol. The crude product was recrystallized from toluene to afford 46 mg of the product as a yellow, waxy solid (93%, 38.5 µmol).

MS (MALDI-TOF): m/z (%) = 1195 (33%), 1196 (33%), 1197 (21%), 1198 (8%), 1199 (4%) (calc. for $C_{90}H_{114}$ = 1195.91 g mol^{-1}, isotope pattern: 1195 (36%), 1196 (37%), 1197 (19%), 1198 (6%), 1199 (2%))

^{1}H NMR (500 MHz, $C_2D_2Cl_4$, 383K): δ = 8.77 (d, 2H, ^3J(H,H) = 8.39 Hz, H_a), 8.75 (d, 2H, ^3J(H,H) = 8.34 Hz, H_c), 8.7-8.5 (m, 8H, H_d, H_e, H_f, H_g), 7.87 (t, 2H, ^3J(H,H) = 7.56 Hz, H_b), 3.15 (m, 8H, H_h), 2.05 (tt, 8H, ^3J(H,H) = 6.95 Hz, H_i), 1.66 (m, 8H, H_j), 1.55 (m, 8H, H_k), 1.5-1.2 (m, 56H, -CH_2-), 0.87 (t, 12H, ^3J(H,H) = 6.56Hz, H_l)

^{13}C NMR (125 MHz, $C_2D_2Cl_4$, 383K): δ = 140.96, 130.29, 130.41, 130.25, 130.19, 130.15, 126.31, 125.34, 123.68, 123.58, 123.04, 123.01, 121.96, 121.83, 121.69, 121.60, 120.35, 120.18, 37.35, 37.32, 32.08, 30.06, 30.02, 29.97, 29.93, 29.84, 29.47, 22.77, 14.11

UV/vis: λ / nm (ε / m^2·mol^{-1}) = 342 (856), 361 (2043), 392 (663), 441 (27), 448 (25), 466 (9)

DSC (°C): 147 (123)

Elemental Analysis: 90.21% C, 9.49% H (calc.: 90.39% C, 9.61% H)

7.3.82 4-Trimethylsilylethynyl-fluoren-9-one

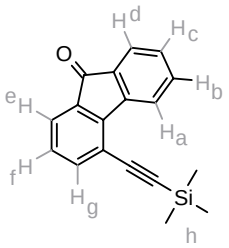

2.84 g 4-Iodofluoren-9-one (**5-76**, 9.28 mmol), 2.28 g trimethylsilyl acetylene (23.2 mmol), 49 mg triphenylphosphine (0.19 mmol), and 36 mg copper (I) iodide (0.19 mmol) were dissolved in a mixture of 10 mL THF and 100 mL triethylamine and degassed carefully. 134 mg (0.19 mmol, 2 mol%) Bis(triphenylphosphine)palladium(II)chloride were added and the mixture was stirred at 55 °C over night. After having removed the solvent *in vacuo*, the residue was purified by using preparative column chromatography (silica gel, eluent: low boiling petroleum ether: dichloromethane = 1:1, R_f = 0.50) to afford 1.82 g of the desired product as yellow crystals (71%, 6.58 mmol).

MS (FD, 8kV): m/z (%) = 276.6 (100%, M$^+$) (berechnet für $C_{18}H_{16}OSi$ = 276.41 g mol^{-1})

^{1}H-NMR (300 MHz, CD_2Cl_2): δ = 8.33 (d, 1H, ^3J(H,H) = 7.57 Hz, H_a), 7.66 (d, 1H, ^3J(H,H) = 7.66 Hz, H_e), 7.60 (dd, 1H, ^3J(H,H) = 7.32 Hz, ^4J(H,H) = 1.10 Hz, H_g), 7.54 (td, 1H, ^3J(H,H) = 7.59 Hz, ^4J(H,H) = 1.23 Hz, H_f), 7.54 (dd, 1H, ^3J(H,H) = 7.81 Hz, ^4J(H,H) = 1.12 Hz, H_d), 7.35 (t, 1H, ^3J(H,H) = 7.43 Hz, H_b), 7.26 (t, 1H, ^3J(H,H) = 7.41 Hz, H_c), 0.35 (s, 9H, H_h)

^{13}C-NMR (75 MHz, CD_2Cl_2): δ = 192.94, 144.63, 144.43, 138.98, 135.05, 134.80, 134.45, 129.78, 129.05, 124.29, 123.43, 117.63, 102.63, 101.22, -0.20.

Elementaranalyse: 80.09% C, 5.90% H (berechnet: 78.22% C, 5.83% H, 5.76% O, 10.16% Si)

7.3.83 4-Ethynyl-fluoren-9-one (5-77)

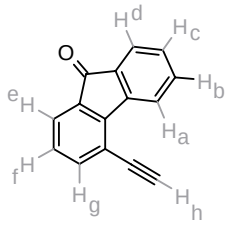

1.7 g 4-Trimethylsilylethynyl-fluoren-9-one (8.32 mmol) and 1 g potassium carbonate were dissolved in a mixture of 5 mL dichloromethane and 45 mL methanol and stirred at room temperature for 14 hours. After having removed the solvent, the residue was purified by filtering through a short pad of silica gel with a solvent mixture of low boiling petroleum ether and dichloromethane (1:1) to obtain 1.56 g of the desired compound as a yellow crystalline material (92%, 7.64 mmol).

MS (FD, 8kV): m/z (%) = 204.3 (100%, M^+) (berechnet für $C_{15}H_8O$ = 204.23 g mol^{-1})

^{1}H-NMR (250 MHz, CD_2Cl_2): δ = 8.31 (dt, 1H, ^3J(H,H) = 7.58 Hz, ^4J(H,H) = 0.76 Hz, H_a), 7.66 (dd, 1H, ^3J(H,H) = 7.37 Hz, ^4J(H,H) = 1.92 Hz, H_e), 7.63 (dd, 1H, ^3J(H,H) = 7.36 Hz, ^4J(H,H) = 1.12 Hz, H_g), 7.57 (dd, 1H, ^3J(H,H) = 7.81 Hz, ^4J(H,H) = 1.12 Hz, H_e), 7.54 (td, 1H, ^3J(H,H) = 7.57 Hz, ^4J(H,H) = 1.25 Hz, H_b), 7.36 (td, 1H, ^3J(H,H) = 7.45 Hz, ^4J(H,H) = 0.93 Hz, H_f), 7.28 (t, 1H, ^3J(H,H) = 7.42 Hz, H_f), 3.58 (s, 1H, H_h)

^{13}C-NMR (65 MHz, CD_2Cl_2): δ = 192.84, 144.98, 144.17, 139.38, 135.24, 134.84, 134.37, 129.91, 129.12, 124.64, 124.34, 123.41, 12.49, 83.33, 81.33.

Elementaranalyse: 90.26% C, 4.69% H (berechnet: 88.22% C, 3.95% H, 7.83% O)

7.3.84 4-(2,3,4,5-Tetra(4-*n*-dodecylphenyl)phenyl)-fluoren-9-one (5-78)

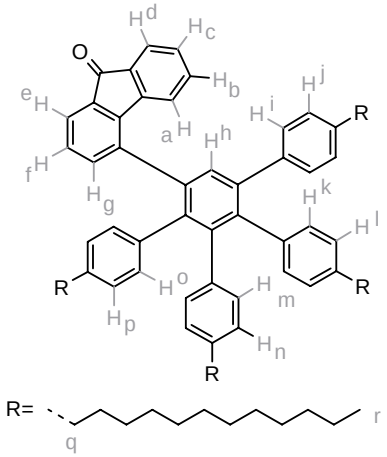

100 mg 4-Ethynyl-fluoren-9-one (**5-77**, 490 µmol) and 518 mg 2,3,4,5-Tetrakis-(4-*n*-dodecyl-phenyl)-cyclopenta-2,4-dienone (490 µmol) were dissolved in 1 mL *o*-xylene and filled in a tube and closed with a metal seal. The reaction was performed at 160 °C and completed after 1 hour. After having removed the solvent *in vacuo*,

preparative column chromatography was applied to purify the crude material to obtain 563 mg of the desired product as a yellow oil (93%, 456 µmol).

MS (FD, 8kV): m/z (%) = 1234.5 (100%, M^+) (berechnet für $C_{91}H_{124}O$ = 1234.00 g mol^{-1})

^{1}H-NMR (300 MHz, CD_2Cl_2): δ = 7.62 (d, 1H, ^3J(H,H) = 7.19 Hz, H_a), 7.60 (s, 1H, H_h), 7.47 (dd, 1H, ^3J(H,H) =7.20, ^4J(H,H) = 1.25 Hz, H_e), 7.37 (td, 1H, ^3J(H,H) = 7.55 Hz, ^4J(H,H) = 1.27 Hz, H_f), 7.26 (td, 1H, ^3J(H,H) = 7.44 Hz, ^4J(H,H) = 0.71 Hz, H_b), 7.19 (dd, 1H, ^3J(H,H) = 7.74 Hz, ^4J(H,H) = 1.25 Hz, H_d), 7.15-6.50 (m, 18H, H_c, H_g, H_i, H_j, H_k, H_l, H_m, H_n, H_o, H_p), 2.60 -2.30 (m, 8H, H_q), 1.70-1.00 (m, 80H, -CH_2-), 0.95-0.85 (m, 12H, H_r).

^{13}C-NMR (75 MHz, CD_2Cl_2): δ = 193.88, 145.33, 143.08, 142.18, 141.46, 141.35, 140.90, 140.71, 140.63, 140.28, 140.23, 139.35, 138.36, 138.08, 138.01, 137.87, 137.81, 137.19, 134.94, 134.87, 134.56, 131.88, 131.72, 130.66, 130.13, 128.96, 128.29, 127.99, 127.38, 127.21, 127.04, 124.13, 123.53, 122.67, 35.89, 35.78, 35.74, 35.63, 32.40, 31.81, 31.75, 31.49, 30.21, 30.16, 30.10, 30.02, 29.99, 29.95, 29.85, 29.71, 29.34, 29.28, 23.15, 14.34.

7.3.85 4-(2,3,4,5-Tetra(4-*n*-dodecylphenyl)phenyl)-fluoren-9-one (5-79)

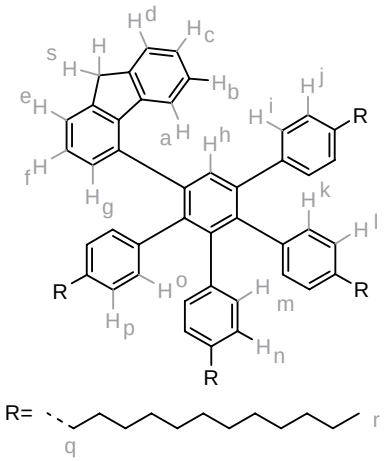

100 mg 4-(2,3,4,5-Tetra(4-*n*-dodecylphenyl)phenyl)-fluoren-9-one (**5-78**, 81.0 µmol) were dissolved in 5 mL THF. 2-3 mL Concentrated aqueous hydrochloric acid was added until the mixture became cloudy. Finally, 50 mg palladium on charcoal was added and the atmosphere in the reaction flask was exchanged with hydrogen. The mixture was stirred for 1 hour at 50 °C. The product was extracted with dichloromethane, dried over magnesium sulfate and evaporated *in vacuo* to afford 94 mg of the desired product as an colorless oil (95%, 77.0 µmol).

MS (FD, 8kV): m/z (%) = 1220.3 (100%, M^+), 1346.1 (5%, $(M-I)^+$) (berechnet für $C_{91}H_{126}$ = 1220.02 g mol^{-1})

^{1}H-NMR (300 MHz, CD_2Cl_2): δ = 7.51 (d, 1H, ^3J(H,H) = 7.09 Hz, H_a), 7.43 (s, 1H, H_h), 7.36 (d, 1H, ^3J(H,H) =7.12, H_e), 7.3-6.3 (m, 21H, H_f, H_b, H_d, H_c, H_g, H_i, H_j, H_k, H_l, H_m, H_n, H_o, H_p), 3.86 (s, 2H, H_s), 2.50 -2.20 (m, 8H, H_q), 1.70-1.00 (m, 80H, -CH_2-), 0.95-0.85 (m, 12H, H_r).

^{13}C-NMR (75 MHz, CD_2Cl_2): δ = 144.16, 143.74, 142.86, 142.39, 141.22, 141.01, 140.51, 140.44, 140.23, 140.18, 140.04, 139.73, 139.58, 138.33, 138.12, 137.79,

137.60, 131.95, 131.82, 131.73, 131.64, 131.16, 130.14, 129.68, 127.87, 127.30, 126.87, 126.76, 126.60, 125.87, 125.11, 123.48, 123.17, 37.23, 35.85, 35.76, 35.59, 32.38, 31.80, 31., 31.47, 30.14, 30.01, 29.93, 29.83, 29.69, 29.32, 23.13, 14.33.

7.3.86 8,11,14,17-Tetra-*n*-dodecyl-3H-cyclopenta[*cde*]hexa-*peri*-hexabenzocoronene (5-80)

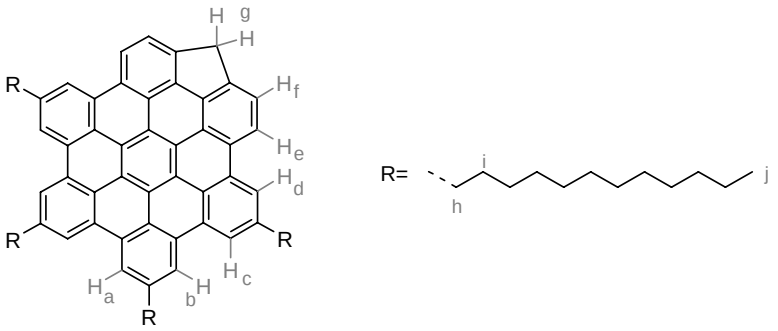

54.8 mg 4-(2,3,4,5-Tetra(4-*n*-dodecylphenyl)phenyl)-fluoren-9-one (**5-79**, 44.9 µmol) were dissolved in 50 mL dichloromethane. A stream of argon saturated with dichloromethane was bubbled into the solution through a Teflon tube. A solution of 262 mg iron(III) chloride (1.62 mmol) in 1 mL nitromethane was quickly added. After a reaction time of 60 minutes, the reaction was stopped with methanol. The precipitate was filtered off and washed extensively with methanol. The crude material was recrystallized from toluene to afford 47 mg of the product as a yellow, microcrystalline material (87%, 38.9 µmol).

MS (MALDI-TOF): m/z (%) = 1207 (34%), 1208 (36%), 1209 (17%), 1210 (10%), 1211 (4%) (calc. for $C_{91}H_{114}$ = 1207.92 g mol^{-1}, isotope pattern: 1207 (36%), 1208 (37%), 1209 (19%), 1210 (6%), 1211 (2%))

^{1}H NMR (500 MHz, THF, 328 K): δ = 8.59 (s, 2H, H_a), 8.54 (s, 2H, H_b), 8.43 (s, 2H, H_c), 8.20 (s, 2H, H_d), 8.09 (d, 2H, ^{3}J(H,H) = 7.08 Hz, H_e), 7.52 (d, 2H, ^{3}J(H,H) = 7.47 Hz, H_f), 4.45 (s, 2H, H_g), 3.62 (t, 8H, ^{3}J(H,H) = 6.66Hz, H_h), 1.78 (m, 8H, H_i), 1.5-1.2 (m, 72H, -CH_2-), 0.87 (t, 12H, ^{3}J(H,H) = 6.56Hz, H_j).

^{13}C NMR: could not be obtained, because of vanishing solubility

UV/vis: λ / nm (ε / m^2·mol^{-1}) = 345 (877), 360 (2047), 392 (496), 466 (27)

DSC (°C): 139 (19, 101)

Elemental Analysis: 90.41% C, 9.53% H (calc.: 90.49% C, 9.51% H)

7.3.87 8,11,14,17-Tetra-*n*-dodecyl-cyclopenta[*cde*]hexa-*peri*-hexabenzocoronene-3-one (5-81)

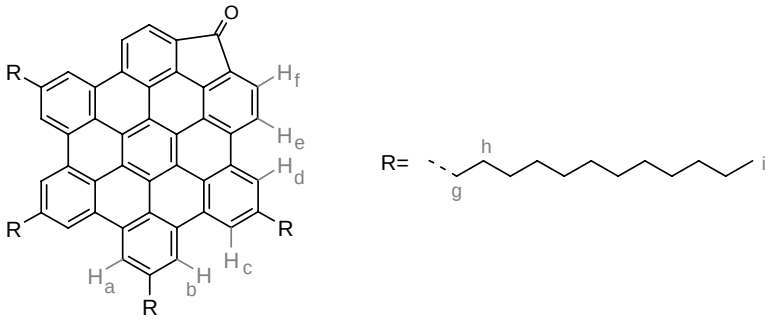

10.0 mg 8,11,14,17-Tetra-*n*-dodecyl-3H-cyclopenta[*cde*]hexa-peri-hexabenzocoronene (8.28 µmol) were dissolved under gentle heating in 10 mL THF. 1 mL of a 1.0 M solution of lithium bis(trimethylsilyl)amide in THF was added dropwise at room temperature, while dry oxygen was bubbled into the solution. The bubbling was continued for an additional hour, before 20 mL methanol was added. The red precipitate was filtered off and washed extensively with methanol to afford 8.25 mg of the product as a red solid (82%, 6.75 µmol).

MS (MALDI-TOF): m/z (%) = 1221 (32%), 1222 (31%), 1223 (20%), 1224 (10%), 1225 (4%) (calc. for $C_{91}H_{112}O$ = 1221.91 g mol^{-1}, isotope pattern: 1221 (36%), 1222 (37%), 1223 (19%), 1224 (6%), 1225 (2%))

^{1}H NMR (500 MHz, $C_2D_2Cl_4$, 413 K): δ = 8.44 (s, 2H, H_a), 8.33 (s, 2H, H_b) 8.25 (s, 2H, H_c) 7.90 (s, 2H, H_d) 7.77 (d, 2H, ^3J(H,H) = 8.06 Hz, H_e) 7.41 (d, 2H, ^3J(H,H) = 8.09 Hz, H_f), 3.17 (tb, 4H, H_g), 2.98 (tb, 4H, H_g), 2.10 (m, 4H, H_h), 1.97 (m, 4H, H_h), 1.80-1.20 (m, 72H, -CH_2-), 0.98 (tb, 12H, H_i).

^{13}C NMR: could not be obtained, because of vanishing solubility

UV/vis: λ / nm (ε / m^2·mol^{-1}) = 327 (1553), 353 (2054), 363 (1924), 383 (1133), 445 (177), 517 (77)

DSC (°C): 73 (22)

Elemental Analysis: 89.31% C, 9.16% H (calc.: 89.45% C, 9.24% H, 1.31% O)

7.3.88 2-Bromo-7-(2-decyl-tetradecyl)-pyrene (5-97)

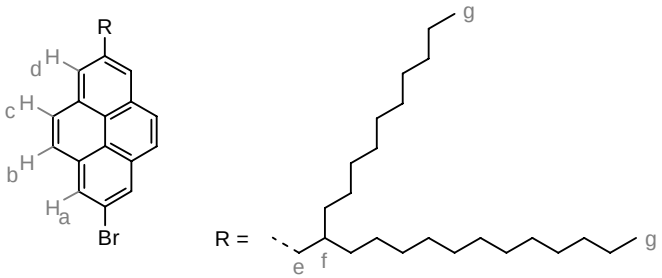

400 mg 2,7-Dibromopyrene (**5-95**, 1.11 mmol) were dissolved in 120 mL anhydrous THF and degassed. 40 mg Dichloro[1,1'bis(diphenylphosphino)ferrocene]-palladium(II) (54.7 µmol) were added and the mixture was warmed to 45 °C. A freshly prepared 1M 2-decyltetradecylmagnesium bromide THF solution was added hot in small quantities under TLC control (silica gel, eluent: hexane, R_f = 0.77) to

follow the conversion. The reaction was immediately quenched to avoid side product formation. After having evaporated the solvent, the residue was purified using preparative column chromatography to afford 520 mg of the title compound as a colorless oil (77%, 842 µmol).

MS (FD, 8kV): m/z (%) = 619.1 (100%, M^+) (calc. for $C_{40}H_{57}Br$ = 617.80 g mol^{-1})

^{1}H NMR (250 MHz, CD_2Cl_2): δ = 8.27 (s, 2H, H_a), 8.08 (d, 2H, ^3J(H,H) = 9.05 Hz, H_c), 8.03 (s, 2H, H_d), 7.97 (d, 2H, ^3J(H,H) = 8.99 Hz, H_b), 2.97 (d, 2H, ^3J(H,H) = 7.04 Hz, H_e), 1.88 (m, 1H, H_f), 1.40-1.10 (m, 40H, -CH_2-), 0.87 (t, 6H, ^3J(H,H) = 7.14 Hz, H_g)

^{13}C NMR (63 MHz, CD_2Cl_2): δ = 141.05, 133.04, 131.35, 129.05, 127.39, 127.33, 126.63, 123.70, 123.25, 120.04, 41.84, 41.03, 34.02, 32.77, 32.71, 30.83, 30.51, 30.21, 27.39, 23.52, 14.76.

7.3.89 Bis(7,7'-di-(2-decyl-tetradecyl)-2-pyrenyl)-acetylene (5-98)

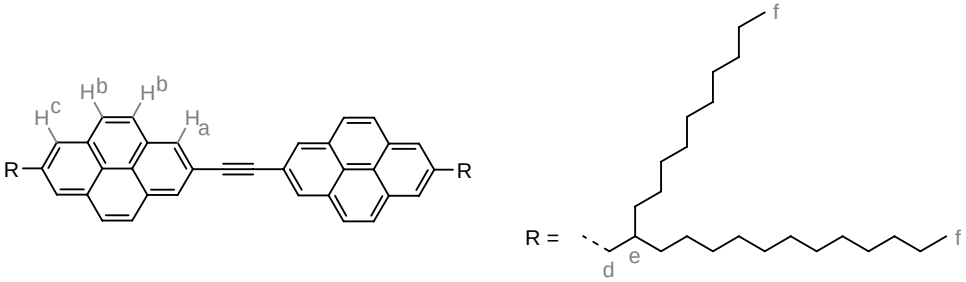

136 mg 2-Bromo-7-(2-decyl-tetradecyl)-pyrene (**5-97**, 220 µmol), 4.20 mg copper(I) iodide (22.1 µmol) and 7.60 mg tetrakis-(triphenylphosphino)-palladium(0) (6.55 µmol) were dried in high vacuum in a Schlenk flask. Afterwards, 2 mL anhydrous, freshly distilled and degassed toluene, 0.20 mL degassed DBU (1.34 mmol), 16 µL degassed trimethylsilyl acetylene (110 µmol) and 1.0 µL degassed water were added step-wise and the resulting mixture was stirred at 80 °C over night. After having removed the solvent *in vacuo*, the residue was purified using preparative column chromatography (flash silica gel, eluent: low boiling petroleum ether, dichloromethane = 15:1, R_f = 0.21-0.34) to afford 117 mg of the desired compound as a highly fluorescent, colorless oil (96%, 106 µmol).

MS (FD, 8kV): m/z (%) = 550.1 (17%, M^{2+}), 1100.5 (100%, M^+) (calc. for $C_{82}H_{114}$ = 1099.82 g mol^{-1})

^{1}H NMR (250 MHz, CD_2Cl_2): δ = 8.43 (s, 2H, H_a), 8.07 (s, 4H, H_b), 8.02 (s, 2H, H_c), 3.01 (d, 4H, ^3J(H,H) = 6.84 Hz, H_d), 1.95 (m, 2H, H_e), 1.50-1.10 (m, 80H, -CH_2-), 0.95 (t, 12H, ^3J(H,H) = 6.48 Hz, H_f)

^{13}C NMR (63 MHz, CD_2Cl_2): δ = 141.32, 131.75, 131.51, 128.56, 128.19, 127.35, 127.00, 124.81, 123.33, 120.88, 90.95, 41.76, 40.91, 33.88, 32.58, 30.63, 30.31, 30.01, 27.21, 23.34, 14.54.

UV/vis: λ / nm (ε / $m^2 \cdot mol^{-1}$) = 308 (3417), 323 (3408), 340 (4088)

DSC (°C): 43 (20), 85 (57)

7.3.90 Hexa(7-(2-decyltetradecyl)-pyren-2-yl)benzene (5-99)

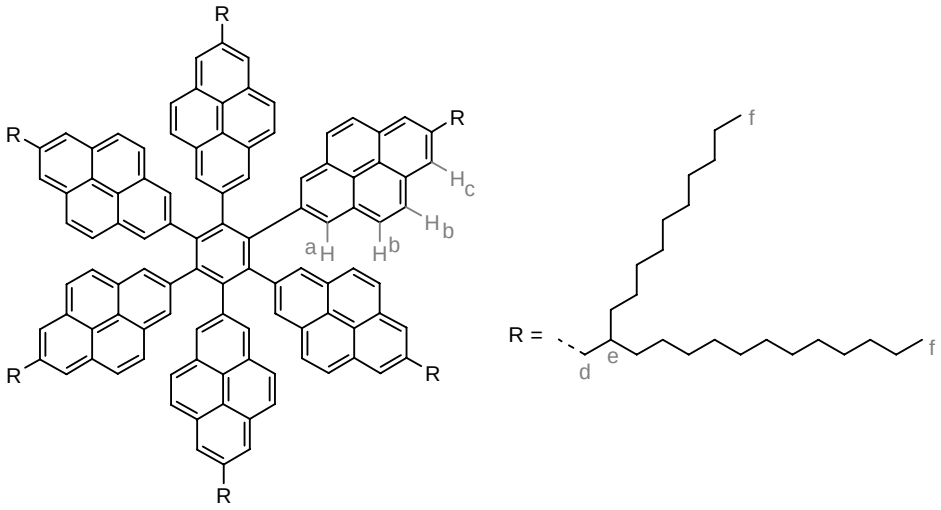

81 mg Bis(7,7'-di-(2-decyl-tetradecyl)-2-pyrenyl)-acetylene (**5-98**, 73.6 µmol) were dissolved in 20 mL anhydrous 1,4-dioxane and degassed. 2.52 mg Dicobaltoctacarbonyl (7.36 µmol) were added and the resulting mixture was refluxed for 24 hours. The solvent was evaporated and the residue was purified using preparative column chromatography (silica gel, eluent: low boiling petroleum ether, dichloromethane = 9:1, R_f = 0.2-0.4) to afford 67 mg of the title compound as a colorless oil (83%, 20.3 µmol).

MS (FD, 8kV): m/z (%) = 1649.3 (100%, M^{2+}), 3300.3 (85%, M^+) (calc. for $C_{246}H_{342}$ = 3299.47 g mol^{-1})

^{1}H NMR (250 MHz, CD_2Cl_2): δ = 8.10 (s, 12H, H_a), 7.58 (s, 24H, H_b), 7.56 (s, 12H, H_c), 2.70 (d, 12H, ^3J(H,H) = 6.38 Hz, H_d), 2.13 (m, 6H, H_e), 1.60-1.00 (m, 240H, -CH_2-), 0.95-0.80 (m, 36H, H_f)

^{13}C NMR (63 MHz, CD_2Cl_2): δ = 142.47, 139.99, 138.67, 131.13, 129.81, 128.69, 127.20, 125.99, 122.91, 122.64, 41.26, 40.69, 33.50, 32.55, 32.51, 30.50, 30.25, 30.20, 29.98, 29.92, 26.97, 23.29, 14.51.

UV/vis: λ / nm (ε / $m^2 \cdot mol^{-1}$) = 332 (5409), 348 (5389)

7.3.91 1,3-Diiodo-5-(trimethylsilyl)-benzene (5-102)

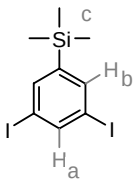

10.5 g 1,3-Dibromo-5-(trimethylsilyl)-benzene (**5-64**, 34 mmol) were dissolved in 350 mL anhydrous diethyl ether and carefully degassed. The solution was cooled down to -78 °C and 80 mL *t*-butyl lithium (1.7 M in pentane, 136 mmol) was slowly added. After 30 min, the reaction mixture was stirred for one hour at room temperature, before the solution was again brought to -78°C. A solution of 36 g iodine (142 mmol) in 200 mL diethyl ether was added and the reaction was stirred over night at room temperature. The organic phase was washed with water, aqueous

sodium bisulfite and ammonium chloride, dried with magnesium sulfate. After removing the solvent in vacuo, the residue was filtered over a short silica pad with hexane to afford 11.2 g of the desired product (82%, 28 mmol) as a colorless, crystalline material.

MS (FS, 8kV): m/z (%) = 402.1 (100%, M^+) (calc. for $C_9H_{12}I_2Si$ = 402.09 g mol^{-1})

^{1}H NMR (300 MHz, CD_2Cl_2): δ = 8.05 (t, 1H, ^4J(H,H) = 1.71 Hz, H_a), 7.77 (d, 2H, ^4J(H,H) = 1.53 Hz, H_b), 0.25 (s, 9H, H_c).

^{13}C NMR (75 MHz, CD_2Cl_2): δ = 147.4 (Ar-*C*-Si(CH_3)$_3$), 145.5 (2-Ar-*C*H), 141.3 (4-Ar-*C*H), 96.0 (Ar-*C*I), -1.4 (Si(*C*H_3)$_3$).

Elemental Analyis: 27.56% C, 3.05% H (calc. 26.88% C, 3.01% H).

7.3.92 3-Bromo-5-(trimethylsilyl)-phenylboronic acid (5-103)

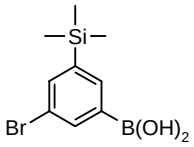

10 g 1,3-Dibromo-5-(trimethylsilyl)-benzene (**5-64**, 32.4 mmol) were dissolved in anhydrous 150 mL diethyl ether, degassed, and cooled to -78 °C. 20.3 mL *n*-Buthyl lithium (1.6 M in hexane, 32.4 mmol) were added drop-wise to the mixture. The resulting solution was allowed to stir at room temperature for an additional hour. Again at -78 °C, 15 mL tri-*iso*-propyl borate (64.9 mmol) was quickly added and the mixture was stirred at room temperature over night. The reaction was stopped by adding 10% aqueous hydrochloride solution. The organic phase was separated, washed with water and dried with magnesium sulfate. After removing the solvent *in vacuo*, 8.6 g product (97%, 31.5 mmol) were obtained as a colorless, amorphous solid, which was used without further purification.

MS (FS, 8kV): m/z (%) = 273.1 (7%, M^+), 382.1 (30%, trimer-M^{2+}), 766.2 (100%, trimer-M^+) (calc. for $C_9H_{14}BBrO_2Si$ = 273.01)

NMR: difficult, many signals arising due to oligomerisation

Elemental Analysis: 41.95% C, 5.06% H (calc. 39.60% C, 5.17% H)

7.3.93 5,3''-Dibromo-3,5',5''-tris-trimethylsilyl-[1,1';3',1'']terphenyl (5-104)

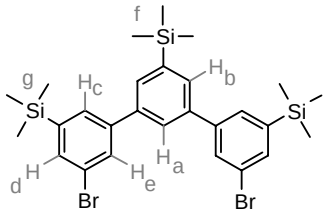

4 g 3-Bromo-5-trimethylsilyl)-phenylboronic acid (**5-103**, 14.65 mmol), 2.94 g 1,3-diiodo-5-(trimethylsilyl)-benzene (**5-102**, 7.31 mmol), and 32 g potassium carbonate were dissolved in a mixture of 240 mL toluene, 120 mL water, and 18 mL ethanol and carefully degassed. 426 mg Tetrakis-(triphenylphosphino)-palladium(0) (0.37 mmol, 2.5 mol% per iodo functionality) were added and the mixture was stirred at

room temperature for 48 hours. The organic phase was separated, washed with water, dried with magnesium sulfate. After the removal of the solvent, the residue was purified using preparative column chromatography (silica gel, eluent: hexane, R_f = 0.50) to afford 3.6 g of the desired product (81%, 6 mmol) as an colorless solid.

MS (FS, 8kV): m/z (%) = 602.4 (100%, M^+) (calc. for $C_{27}H_{36}Br_2Si_3$ = 604,65 g mol^{-1})

^{1}H NMR (300 MHz, CD_2Cl_2): δ = 7.77 (dd, 2H, ^4J(H,H) = 1.92 Hz, H_e), 7.69 (s, 3H, $H_{a,b}$), 7.67 (dd, 2H, ^4J(H,H) = 1.52 Hz, H_d), 7.65 (dd, 2H, ^4J(H,H) = 1.92 Hz, H_c), 0.36 (s, 9H, H_f), 0.32 (s, 18H, H_g).

^{13}C NMR (75 MHz, CD_2Cl_2): δ = 144.79, 143.31, 142.71, 140.46, 135.22, 132.04, 131.24, 130.92, 127.18, 123.43, -1.21 (Si(CH_3)$_3$).

Elemental Analysis: 53.95% C, 5.91% H (calc. 53.63% C, 6.00% H).

7.3.94 5,5',5'',5''',5'''',5'''''-Hexatrimethylsilyl-hexa-*m*-phenylene (5-105)

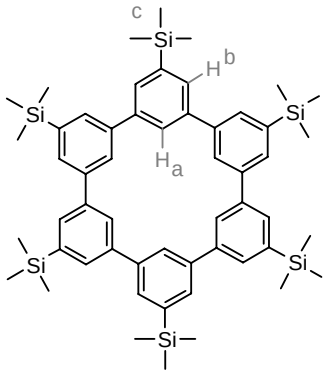

218 mg [2,2']-Bipyridine (1.40 mmol), 152 mg cyclooctadiene (1.40 mmol, 173 µL), and 386 mg bis-(1,5-cyclooctadiene-)nickel(0) (1.40 mmol) were placed in a well dried Schlenk flask, dissolved in 30 mL anhydrous DMF, and stirred for 30 min at 80°C in the absence of light. A solution of 423 mg 5,3"-dibromo-3,5',5"-tris-trimethylsilyl-[1,1';3',1"]terphenyl (0.70 mmol) in 150 mL dry and degassed toluene was added quickly and the resulting mixture was stirred for three days at 80 °C. The reaction was stopped by adding 10% aqueous hydrochloride acid. The organic phase was separated, washed with water, dried with magnesium sulfate. After having removed the solvent *in vacuo*, the residue was purified using preparative column chromatography (silica gel, eluent: low boiling petrol ether, dichlormethane (20:1), R_f = 0.29) to obtain 180 mg (58%, 0.20 mmol) of the desired product as a colorless, crystalline solid.

MS (FS, 8kV): m/z (%) = 888.2 (100%, M^+) (calc. for $C_{54}H_{72}Si_6$ = 889.69 g mol^{-1})

^{1}H NMR (700 MHz, CD_2Cl_2): δ = 8.28 (s, 6H, H_a), 7.92 (s, 12H, H_b), 0.43 (s, 54H, H_c).

^{13}C NMR (175 MHz, CD_2Cl_2): δ = 142.62 (1-Ar-*C*, 3-Ar-*C*), 141.30 (4-Ar-*C*H, 6-Ar-*C*H), 130.89 (2-Ar-*C*H), 128.46 (5-Ar-*C*), -0.88 (Ar-Si(CH_3)$_3$).

Elemental Analysis: 73.15% C, 8.17% H (calc. 72.90% C, 8.16% H).

7.3.95 5,5',5'',5''',5'''',5''''',5'''''-Hexa-iodo-hexa-*m*-phenylene (5-106)

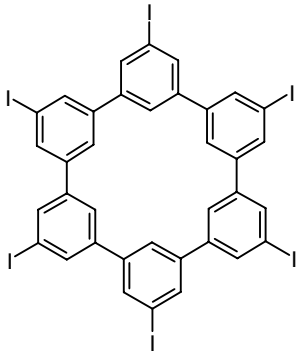

110 mg 5,5',5'',5''',5'''',5''''',5'''''-Hexatrimethylsilyl-hexa-*m*-phenylene (**5-105**, 120 µmol) were dissolved in 20 mL chloroform and degassed. 1.5 mL of a 1M solution of iodomonochloride (1.50 mmol) in dichloromethane were added in the absence of light. The resulting mixture was stirred at room temperature for seven hours, before it was stopped with 5 mL of a concentrated, aqueous sodium thiosulfate solution. The precipitate was filtered off, washed extensively with chloroform, THF, water, and dried *in vacuo* to afford 122 mg of the desired product (84%, 100 µmol) as a hardly soluble colorless material. The compound was used without further purification.

MS (FD, 8kV): m/z (%) = 606.3 (25%, M^{2+}), 1212.2 (100%, M^{+}) (calc. for $C_{36}H_{18}I_6$= 1211.97 g mol^{-1})

7.3.96 5,5',5'',5''',5'''',5''''',5'''''-Hexa-ethynyltri-*iso*-propylsilyl-cyclohexa-*m*-phenylene (5-107)

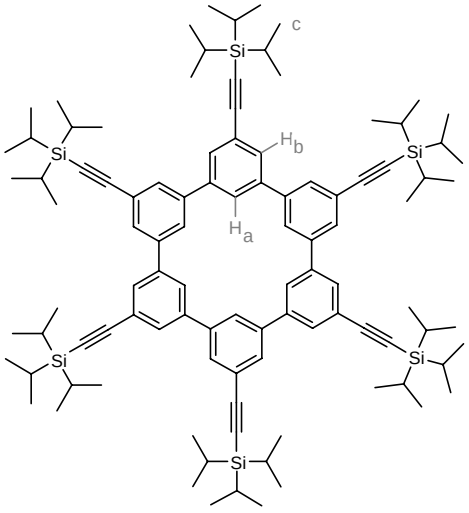

50 mg 5,5',5'',5''',5'''',5''''',5'''''-Hexa-iodo-hexa-*m*-phenylen (**5-106**, 41.0 µmol), 90 mg tri-*iso*-propylsilylacetylene (0.49 mmol), 1.6 mg (6.2 µmol) triphenylphosphine, and 1.2 mg (6.20 µmol) copper (I) iodide were dissolved in 8 mL piperidine and degassed with three freeze-vacuum-thaw cycles. Finally, 7.1 mg tetrakis-(triphenylphosphino)-palladium(0) (6.2 µmol, 1.1 mol% per iodide) were added to the mixture, which was then stirred for 3 days at 80°C under an argon atmosphere. The solvent was removed *in vacuo* and the residue was purified using preparative column chromatography (silica gel, eluent: hexane, R_f = 0.41-0.22) to obtain 35 mg of the desired product (55%, 23 µmol) as colorless crystals.

MS (FD, 8kV): m/z (%) =1538.9 (100%, M^+)(calc. for $C_{120}H_{144}Si_6$ = 1538.80 g mol^{-1})

^{1}H NMR (300 MHz, CD_2Cl_2): δ = 8.14 (s, 6H, H_a), 7.79 (d, 12H, ^4J(H,H) = 1.50 Hz, H_b), 1.10 (s, 21H, H_c).

^{13}C NMR (75 MHz, CD_2Cl_2): δ = 140.90 (1-Ar-*C*, 3-Ar-*C*), 129.79 (4-Ar-*C*H, 6-Ar-*C*H), 127.17 (2-Ar-*C*H), 125.42 (5-Ar-*C*-), 106.92 (Ar-*C*≡C-TIPS), 92.20 (Ar-C≡*C*-TIPS), 18.88 (TIPS-*C*H_3), 11.78 (TIPS-*C*H).

Elemental Analysis: 79.13% C, 9.66% H (calc.: 79.62% C, 9.43% H, 10.95% Si).

7.3.97 5,5',5'',5''',5'''',5'''''-Hexa-ethynyl-cyclohexa-*m*-phenylene (5-108)

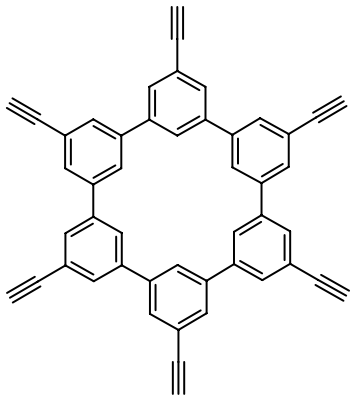

50 mg 5,5',5'',5''',5'''',5'''''-Hexa-ethynyltri-*iso*-propylsilyl-cyclohexa-*m*-phenylene (**5-107**, 33.0 µmol) were dissolved in 5 mL of dry THF and degassed with five consecutive freeze-pump-thaw cycles. Afterwards a solution of 62 mg tetra-*n*-butylammoniumfluorid trihydrate (195 µmol) in 1 mL anhydrous THF was added and the reaction mixture was stirred at room temperature for 40 min. The reaction was stopped by adding a small amount of water before the solvent was removed *in vacuo*. The residue was extensively washed with water, methanol and dichloromethane to obtain 15 mg (76%, 25 µmol) of the desired, hardly soluble, colorless solid. The material was used without further purification steps.

7.3.98 5,5',5'',5''',5'''',5''''',5'''''-Hexa-((2,3,4,5-tetraphenyl)phenyl)-cyclohexa-*m*-phenylene (5-109)

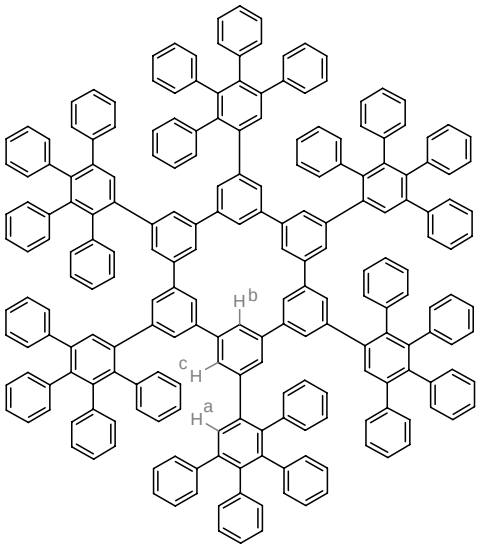

3.5 mg 5,5',5'',5''',5'''',5''''',5'''''-Hexa-ethynyl-cyclohexa-*m*-phenylene (**5-108**, 5.80 µmol) and 76 mg 2,3,4,5-tetraphenyl-cyclopenta-2,4-dienone (**5-34a**, 0.19 mmol) were dissolved in 1 mL *o*-xylene and degassed. The reaction was conducted within 10 min in a microwave furnace (300W, 250 °C). The mixture was given into pentane and the precipitate was filtered off and further purified with preparative column chromatography (silica gel, eluent: low boiling petrol ether, dichloromethane (3:1), finally THF). The oily solid was reprecipitated from THF into methanol to obtain 13.5 mg of the desired product (85%, 4.93 µmol) as a colorless solid.

MS (FD, 8kV): m/z (%) = 1372.0 (35%, M^{2+}), 2741.3 (100%, M^{+}) (calc. for $C_{216}H_{144}$ = 2739.56 g mol^{-1})

^{1}H NMR (700 MHz, CD_2Cl_2): δ = 7.96 (s, 6H, H_a), 7.51 (s, 6H, H_b), 7.25-7.15 (m, 30H), 7.08 (s, 12H, H_c), 7.00-6.75 (m, 72H), 6.71 (t, 12H, ^{3}J(H,H) = 7.65 Hz), 6.30-6.20 (m, 6H).

^{13}C NMR (125 MHz, CD_2Cl_2): δ = 143.06, 142.24, 142.13, 141.25, 140.87, 140.54, 140.40, 140.28, 139.80, 139.43, 132.04, 131.91, 131.81, 130.28, 128.05, 127.56, 127.22, 126.93, 126.73, 126.11, 125.96, 125.76, 125.71, 124.40.

Elemental Analysis: 94.86% C, 5.23% H (calc.: 94.79% C, 5.30% H)

7.3.99 5,5',5'',5''',5'''',5''''',5'''''-Hexa-phenylethynyl-cyclohexa-*m*-phenylene (5-113)

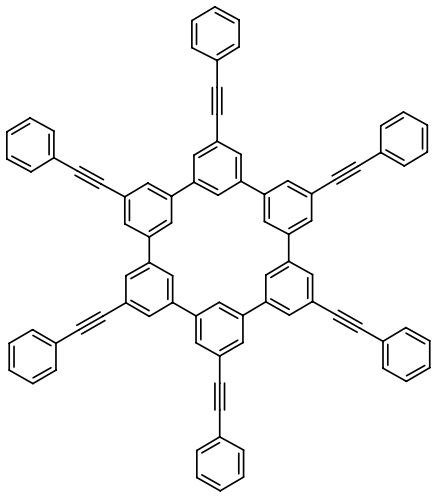

50 mg 5,5',5'',5''',5'''',5''''',5'''''-Hexa-iodo-hexa-*m*-phenylene (**5-106**, 41.0 µmol), 50 mg phenyl acetylene (0.49 mmol), 1.6 mg triphenylphosphine (6.2 µmol), and 1.2 mg (6.2 µmol) copper (I) iodide were dissolved in 8 mL piperidine and degassed with five freeze-pump-thaw cycles. After having added 7.1 mg tetrakis-(triphenylphosphino)-palladium (0) (6.20 µmol, 1.1 mol% per iodide), the mixture was stirred for two days at 80 °C. The reaction mixture was cooled down to room temperature and the precipitate was collected, carefully washed with methanol, THF, and dichloromethane, and dried in vacuum to afford 39 mg of the desired product (90%, 37 µmol) as an hardly soluble, colorless solid. The substance was used without further purification.

MS (FD, 8kV): m/z (%) = 528.2 (100%, M^{2+}) 1055.2 (75%, M^{+}) (calc. for $C_{84}H_{48}$ = 1057.32 g mol^{-1}).

7.3.100 5,5',5'',5''',5'''',5''''',5'''''-Hexa-((2,3,4,5,6-pentaphenyl)phenyl)-cyclohexa-*m*-phenylene (5-114)

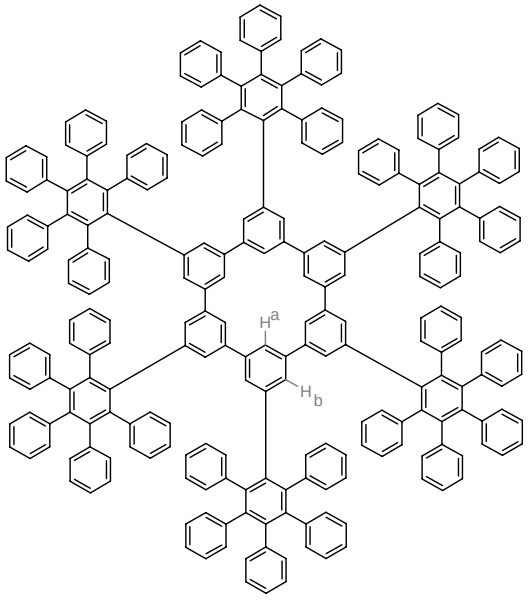

17.7 mg 5,5',5'',5''',5'''',5''''',5'''''-Hexa-phenylethynyl-cyclohexa-*m*-phenylene (**5-113**, 16.7 µmol) and 192 mg 2,3,4,5-tetraphenyl-cyclopenta-2,4-dienone (**5-34a**, 500 µmol) were dissolved in 1 mL diphenylether and degassed. The reaction was performed in a microwave oven and was completed after 7 hours (240 °C, 300 W). The solvent was removed *in vacuo* and the residue was purified using preparative column chromatography (silica gel, eluent: low boiling petrol ether, dichloromethane (3:1)). After reprecipitation into methanol, one obtained 47 mg product (88%, 14.7 µmol) as a colorless, crystalline powder.

MS (FD, 8kV): m/z (%) = 3194.4 (100%, M^+) (calc. for $C_{252}H_{168}$ = 3196.15 g mol^{-1})

^{1}H NMR (500 MHz, CD_2Cl_2): δ = 7.16 (s, 6H, H_a), 7.0-6.8 (m, 150H, *H*), 6.66 (s, 12H, H_b)

^{13}C NMR (125 MHz, $C_2D_2Cl_4$, 353 K): δ = 141.33, 141.28, 141.23, 141.18, 141.13, 140.98, 140.94, 140.83, 140.64, 140.54, 138.81, 132.52, 132.46, 132.41, 132.29, 132.23, 131.19, 131.15, 131.02, 128.86, 128.80, 127.61, 127.55, 126.47, 126.28, 125.13, 125.07, 125.01.

7.3.101 5,5',5'',5''',5'''',5'''''-Hexa-tradec-1-yne-hexa-*m*-phenylene (5-115)

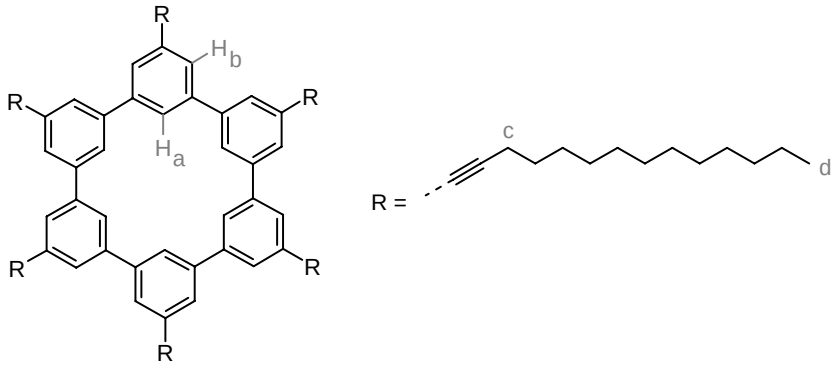

50 mg 5,5',5'',5''',5'''',5''''',5'''''-Hexa-iodo-hexa-*m*-phenylene (**5-106**, 41.0 µmol), 96 mg tetradec-1-yne (0.49 mmol), 1.6 mg triphenylphosphine (6.20 µmol), and 1.2 mg (6.20 µmol) copper (I) iodide were dissolved in 8 mL piperidine and degassed with three freeze-vacuum-thaw cycles. Afterwards, 7.1 mg tetrakis-(triphenylphosphino)-palladium(0) (6.2 µmol, 1.1 mol% per iodide) were added under an argon atmosphere and the mixture was stirred over night at 55 °C. The solvent was removed *in vacuo* and the residue was purified using preparative column chromatography (silica gel, eluent: low boiling petrol ether, dichloromethane (1:1), R_f = 0.67) to afford 34 mg of the desired product (51%, 21.1 µmol) as a colorless oil.

MS (FD, 8kV): m/z (%) = 806.0 (30%, M^{2+}), 1610.9 (100%, M^+) (calc. for $C_{120}H_{168}$ = 1610.68 g mol^{-1})

^{1}H NMR (300 MHz, CD2Cl2): δ = 8.05 (s, 6H, H_a), 7.68 (s, 12H, H_b), 2.48 (t, 12H, ^3J(H,H) = 6.78 Hz, H_c), 1.8-1.1 (m, 120H, -CH_2-), 0.88 (t, 18H, ^3J(H,H) = 6.78 Hz, H_d).

^{13}C NMR (125 MHz, CD_2Cl_2): δ = 140.59 (1-Ar-*C*, 3-Ar-*C*), 129.06 (4-Ar-*C*H, 6-Ar-*C*H), 125.99 (2-Ar-*C*H), 125.69 (5-Ar-*C*-), 91.67 (Ar-C≡*C*-CH_2-), 80.65 (Ar-*C*≡C-CH_2-), 32.36, 30.13, 30.10, 30.02, 29.80, 29.67, 29.49, 29.30, 23.12 (all -*C*H_2-), 19.86, 14.29 (-*C*H_3).

DSC (°C): 45 (-7)

7.3.102 3,3''-Diiodo-5,5',5''-tris-trimethylsilyl-[1,1';3',1'']-terphenyl (5-121)

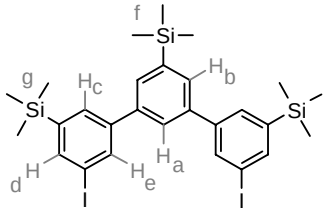

1.0 g 3,3''-Dibromo-5,5',5''-tris-trimethylsilyl-[1,1';3',1'']-terphenyl (**5-104**, 1.65 mmol) were dissolved in 40 mL of anhydrous diethyl ether and cooled to -78 °C. 3.1 mL of a 1.6 M solution of *n*-butyl lithium in hexane (4.96 mmol) were added drop wise over the course of 30 minutes. The mixture was allowed to stir at the same temperature for additional 30 minutes and afterwards 60 minutes at room temperature. Finally, the reaction mixture was cooled again to -78 °C and 1.3 g iodine (5.12 mmol), dissolved in 20 mL diethyl ether, were added. The reaction solution was warmed to room temperature over night, before saturated aqueous ammonium chloride was added carefully. The organic phase was separated and washed with sodium sulfite and water, dried with magnesium sulfate and evaporated *in vacuo*. The residue was purified with preparative column chromatography (silica gel, eluent: hexane, R_f = 0.55) to yield 989 mg product (86%, 1.42 mmol) as a colorless material.

MS (FS, 8kV): m/z (%) = 698.0 (100%, M^+) (calc. for $C_{27}H_{36}I_2Si_3$ = 698.65 g mol^{-1})

^{1}H NMR (700 MHz, CD_2Cl_2): δ = 7.89 (s, 2H, H_d), 7.86 (s, 2H, H_e), 7.70 (s, 2H, H_c), 7.67 (d, 2H, ^4J(H,H) = 1.75 Hz, H_b), 7.65 (d, 1H, ^4J(H,H) = 1.75 Hz, H_a), 0.36 (s, 9H, H_f), 0.32 (s, 18H, H_g).

^{13}C NMR (175 MHz, CD_2Cl_2): δ = 145.09, 143.49, 142.74, 141.38, 140.51, 136.97, 132.04, 131.88, 127.23 (all Ar-C), 96.04 (Ar-I), -0.99 (5'-Ar-Si$(CH_3)_3$), -1.16 (5-Ar-Si$(CH_3)_3$, 5''-Ar-Si$(CH_3)_3$).

Elemental Analysis: 46.47% C, 5.13% H (calc.: 46.42% C, 5.19% H).

7.3.103 5,3''''-Dibromo-3,5',5'',5''',5''''-pentakis-trimethylsilyl-[1,1';3',1'';3'',1''';3''',1'''']quinquephenyl (5-122)

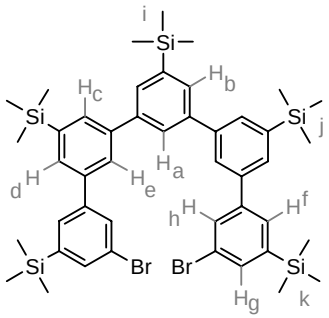

430 mg 3-Bromo-5-(trimethylsilyl)-phenylboronic acid (**5-103**, 1.57 mmol), 500 mg 3,3''-dibromo-5,5',5''-tris-trimethylsilyl-[1,1';3',1'']-terphenyl (**5-104**, 0.72 mmol), and 3.2 g potassium carbonate were dissolved in a mixture of 24 mL toluene, 12 mL water, and 1.8 mL ethanol and degassed. Afterwards, 43 mg tetrakis-

(triphenylphosphino)-palladium(0) (0.04 mmol, 2.5 mol% per iodide) were added under a stream of argon. The mixture was stirred at room temperature for 2 days. After having removed the solvents, the residue was purified using preparative column chromatography (silica gel, eluent: low boiling petrol ether, R_f = 0.78) to afford 552 mg product (85%, 0.61 mmol) as a colorless oil.

MS (FS, 8kV): m/z (%) = 902.6 (100%, M^+) (calc. for $C_{45}H_{60}Br_2Si_5$ = 901.22 g mol^{-1})

^{1}H NMR (500 MHz, CD_2Cl_2): δ = 7.87 (d, 1H, ^4J(H,H) = 1.80 Hz, H_a), 7.82-7.70 (m, 12H, H_c, H_e, H_b, H_h, H_d, H_f), 7,65 (dd, 2H, ^4J(H,H) = 1.95 Hz, H_g), 0,39 (s, 9H, H_i), 0,38 (s, 18H, H_j), 0,33 (s, 18H, H_k). (H,H-COSY and NOESY spectra used to assign protons)

^{13}C NMR (75 MHz, CD_2Cl_2): δ = 144.79, 143.48, 142.61, 142.51, 141.88, 141.72, 140.44, 135.18, 132.33, 131.97, 131.69, 131.29, 130.95, 127.55, 127.40, 123.46, (all Ar-*C*) -1.01, -1.18 (both Ar-Si(CH_3)$_3$)

7.3.104 3’’’’-Brom-5-(4,4,5,5-tetramethyl-1,3,2-dioxaborolan-2-yl)-3,5’,5’’,5’’’,5’’’’-pentakis-trimethylsilanyl-[1,1’;3’,1’’;3’’,1’’’;3’’’,1’’’’]quinquephenyl (5-123)

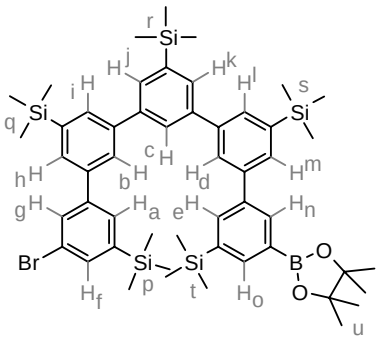

1g 5,3’’’’-Dibromo-3,5’,5’’,5’’’,5’’’’-pentakis-trimethylsilyl-[1,1’;3’,1’’;3’’,1’’’;3’’’,1’’’’]quinquephenyl (**5-104**, 1.11 mmol), 282 mg bis(pinacolato)diboron (1.11 mmol), 218 mg potassium acetate (2.22 mmol) were dissolved in 100 mL anhydrous toluene and degassed. Afterwards, 57 mg dichloro[1,1’bis(diphenylphosphino)ferrocene]palladium(II) (78 µmol) were added and the mixture was stirred at 80 °C over night. After having removed the solvent *in vacuo*, the residue was purified utilizing preparative column chromatography (silica gel, hexane, ethyl acetate = 8:2, R_f = 0.51) to afford 463 mg of the title compound as a colorless, viscous oil (44%, 488 µmol).

MS (FD, 8kV): m/z (%) = 947.5 (70%, M^+), 1899.5 (100%, $M^{½+}$) (calc. for $C_{51}H_{73}BBrO_2Si_5$ = 948.29 g mol^{-1})

^{1}H NMR (300 MHz, CD_2Cl_2): δ = 7.84 (dd, 1H, ^4J(H,H) = 1.11 Hz, H_a), 7.77 (dd, 1H, ^4J(H,H) = 1.16 Hz, H_f), 7.70 (m, 2H, H_b, H_g), 7.66 (dd, 1H, ^4J(H,H) = 1.74 Hz, H_c), 7.64-7.58 (m, 6H, H_d, H_e, H_h, H_i, H_j, H_l), 7.57 (dd, 1H, ^4J(H,H) = 1.40 Hz, H_k), 5.52 (m, 2H, H_m, H_n), 7.47 (dd, 1H, ^4J(H,H) = 1.74 Hz, H_o), 1,18 (s, 12H, H_u), 0.20 (s, 9H, H_p), 0.20 (s, 9H, H_q), 0.19 (s, 9H, H_r), 0.16 (s, 9H, H_s), 0.14 (s, 9H, H_t)

^{13}C NMR (75 MHz, CD_2Cl_2): δ = 153.53, 145.78, 144.52, 143.59, 143.42, 143.22, 143.01, 142.97, 142.71, 142.67, 141.71, 141.44, 140.04, 136.68, 136.17, 135.54, 133.36, 133.06, 132.86, 132.81, 132.73, 132.66, 132.32, 131.96, 128.63, 128.56,

128.42, 124.46 (all Ar-*C*), 85.25(BO*C*(CH_3)$_2$), 26.05 (BOC(*C*H_3)$_2$), 0.04, 0.00, -0.17 (Si(*C*H_3)$_3$).

7.3.105 5,5',5'',5''',5'''',5''''',5''''''',5'''''''',5''''''''',5'''''''''-Decatrimethylsilyl-cyclodeca-*m*-phenylene (5-127)

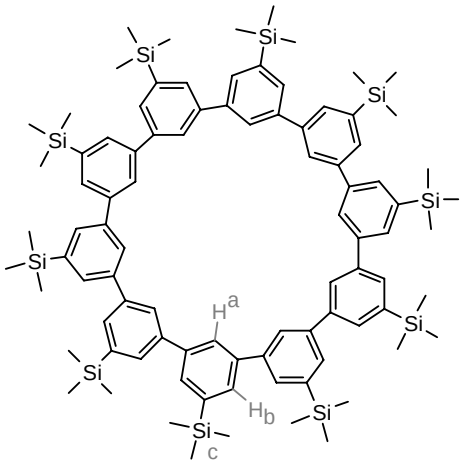

100 mg 3''''-Brom-5-(4,4,5,5-tetramethyl-1,3,2-dioxaborolan-2-yl)-3,5',5'',5''',5''''-pentakis-trimethylsilanyl-[1,1';3',1'';3'',1''';3''',1'''']quinquephenyl (**5-123**, 0.11 mmol), 440 mg potassium carbonate (3.18 mmol) were dissolved in a mixture of 25 mL toluene, 10 mL water, and 1 mL ethanol and degassed. 12.2 mg Tetrakis-(triphenylphophino)-palladium(0) (10.7µmol) were added and the resulting mixture was stirred for three days at 80 °C. The phases were separated and the aqueous phase was repetitively extracted with toluene. The combined organic phases were dried with magnesium sulfate and the solvent was removed. The residue was purified using preparative column chromatography (silica gel, eluent: low boiling petroleum ether, dichloromethane = 20:1, R_f = 0.37) to yield 17 mg of the title compound as colorless crystals (44%, 23.0 µmol).

MS (FD, 8kV): m/z (%) = 1484.9 (100%, M^+) (calc. for $C_{90}H_{120}Si_{10}$ = 1482.82 g mol^{-1})

^{1}H NMR (300 MHz, CD_2Cl_2): δ = 7.65 (t, 10H, ^4J(H,H) = 1.60 Hz, H_a), 7.60 (d, 20H, ^4J(H,H) = 1.68 Hz, H_b), 0.20 (s, 90H, H_c)

^{13}C NMR (75 MHz, CD_2Cl_2): δ = 142.21 (4-Ar-*C*, 6-Ar-*C*), 141.84 (2-Ar-*C*), 131.92 (1-Ar-*C*, 3-Ar-*C*), 127.54 (5-Ar-*C*)), -1.05 (Si(*C*H_3)$_3$).

Elemental Analysis: 72.63% C, 8.15% H (calc.: 72.90% C, 8.16% H)

8 Appendix: Single Crystal Structures

8.1 8,11,14,17-Tetra(t-butyl)tetrabenzo[bc,ef,hi,uv]ovalene (5-16b) (crystallized with TCNQ)

Atom	x/a	y/b	z/c	U(iso)
O(81)	0.7145(4)	0.22805(8)	0.7882(2)	0.113
N(1)	0.9331(2)	0.10191(8)	-0.31719(13)	0.0441
N(2)	0.9741(2)	0.09275(6)	-0.05667(12)	0.0322
N(3)	0.9523(3)	-0.15050(7)	-0.34119(14)	0.048
N(4)	0.9577(2)	-0.16100(7)	-0.08845(14)	0.0446
C(1)	0.6782(2)	0.07332(6)	0.07683(11)	0.0194
C(2)	0.6902(2)	0.05350(6)	0.15420(12)	0.022
C(3)	0.6954(2)	0.00998(6)	0.15574(13)	0.0218
C(4)	0.6852(2)	-0.01277(6)	0.08471(13)	0.0241
C(5)	0.6703(2)	0.00786(8)	0.01042(14)	0.032
C(6)	0.6677(2)	0.05144(7)	0.00576(13)	0.027
C(7)	0.6822(3)	0.11655(9)	0.07602(15)	0.0391
C(8)	0.6739(2)	0.13715(7)	0.00333(14)	0.0309
C(10)	0.7057(3)	0.20254(7)	0.07088(14)	0.0353
C(12)	0.6889(3)	0.14053(8)	0.14520(15)	0.0361
C(13)	0.6973(2)	0.07641(6)	0.22584(13)	0.0233
C(14)	0.6929(3)	0.12045(7)	0.22286(15)	0.0345
C(16)	0.6803(2)	0.12133(6)	0.36373(12)	0.0236
C(18)	0.7052(3)	0.05650(8)	0.29995(14)	0.0362
C(19)	0.7123(3)	-0.01018(9)	0.23223(16)	0.0418
C(20)	0.7156(2)	0.01308(6)	0.30497(12)	0.0197
C(22)	0.7539(2)	-0.04977(8)	0.38142(13)	0.0268
C(24)	0.7190(3)	-0.05292(9)	0.23584(15)	0.0427
C(25)	0.6935(2)	-0.05597(7)	0.08864(12)	0.0232
C(26)	0.71271(19)	-0.07631(6)	0.16360(13)	0.0218
C(28)	0.7245(2)	-0.14166(7)	0.09603(13)	0.0256
C(30)	0.6847(3)	-0.07958(7)	0.01695(14)	0.0353
C(31)	0.6601(2)	-0.01451(7)	-0.06201(13)	0.0267
C(32)	0.6635(2)	-0.05796(6)	-0.05994(12)	0.0206
C(35)	0.6300(2)	-0.01734(7)	-0.21059(13)	0.0267
C(36)	0.6446(2)	0.00479(8)	-0.13811(12)	0.0274
C(37)	0.6533(3)	0.07175(7)	-0.06996(16)	0.034
C(38)	0.6401(2)	0.04818(7)	-0.14193(13)	0.0294
C(39)	0.6261(2)	0.06814(7)	-0.21565(13)	0.0288
C(42)	0.6551(2)	0.11461(7)	-0.07189(16)	0.034
C(45)	0.7316(3)	0.24927(6)	0.07084(15)	0.0314
C(49)	0.6749(3)	0.14740(8)	0.43923(15)	0.0418
C(53)	0.7931(3)	-0.07082(7)	0.46503(13)	0.0309
C(57)	0.7528(3)	-0.18762(6)	0.10545(13)	0.0304
C(61)	0.96391(19)	0.01365(7)	-0.19466(13)	0.0229
C(64)	0.9713(2)	-0.07189(7)	-0.20037(13)	0.0266
C(67)	0.9604(2)	0.05523(8)	-0.19123(14)	0.0333
C(68)	0.9439(2)	0.08073(7)	-0.26120(12)	0.0261
C(69)	0.97011(19)	0.07637(6)	-0.11655(13)	0.0178
C(70)	0.9716(2)	-0.11308(7)	-0.20536(14)	0.0291
C(71)	0.9626(3)	-0.13390(7)	-0.28085(15)	0.0335
C(72)	0.9671(2)	-0.13906(7)	-0.13993(13)	0.0246
C(9)	0.6900(2)	0.17973(7)	-0.00039(13)	0.0264
C(11)	0.7041(2)	0.18159(6)	0.14373(12)	0.0181
C(15)	0.6816(2)	0.14122(8)	0.29142(14)	0.0358
C(17)	0.6934(2)	0.07966(6)	0.36831(13)	0.0235
C(21)	0.7450(2)	-0.00763(8)	0.37911(14)	0.0312
C(23)	0.7420(2)	-0.07226(7)	0.31113(12)	0.0233
C(27)	0.7299(2)	-0.11853(8)	0.16389(14)	0.0317
C(29)	0.6999(2)	-0.12098(6)	0.02225(12)	0.0176
C(33)	0.6521(2)	-0.08106(8)	-0.13436(16)	0.0385
C(34)	0.6336(2)	-0.06053(8)	-0.20772(15)	0.0329
C(40)	0.6247(2)	0.11043(7)	-0.21808(13)	0.0304
C(41)	0.6396(2)	0.13275(8)	-0.15084(15)	0.0343
C(43)	0.6123(2)	0.04418(8)	-0.28768(12)	0.031
C(44)	0.6142(2)	0.00341(6)	-0.28379(14)	0.0235
C(62)	0.9759(2)	-0.00966(7)	-0.12181(13)	0.0232
C(63)	0.9821(2)	-0.05106(8)	-0.12573(13)	0.032
C(65)	0.9674(2)	-0.04786(7)	-0.27340(12)	0.0237

C(66)	0.9639(3)	-0.00636(9)	-0.27033(15)	0.0401
H(91)	0.6896(2)	0.19273(7)	-0.05010(13)	0.035
H(111)	0.7131(2)	0.19656(6)	0.19214(12)	0.0254
H(151)	0.6743(2)	0.16991(8)	0.28962(14)	0.0485
H(171)	0.6941(2)	0.06633(6)	0.41772(13)	0.0308
H(211)	0.7589(2)	0.00719(8)	0.42797(14)	0.0423
H(231)	0.7489(2)	-0.10094(7)	0.31406(12)	0.0323
H(271)	0.7472(2)	-0.13202(8)	0.21430(14)	0.0434
H(291)	0.6930(2)	-0.13608(6)	-0.02585(12)	0.0232
H(331)	0.6577(2)	-0.10977(8)	-0.13273(16)	0.0519
H(341)	0.6229(2)	-0.07555(8)	-0.25619(15)	0.0441
H(401)	0.6128(2)	0.12373(7)	-0.26851(13)	0.0406
H(411)	0.6402(2)	0.16143(8)	-0.15514(15)	0.0434
H(431)	0.6015(2)	0.05717(8)	-0.33836(12)	0.041
H(441)	0.6051(2)	-0.01170(6)	-0.33206(14)	0.0311
H(621)	0.9796(2)	0.00347(7)	-0.07186(13)	0.0304
H(631)	0.9933(2)	-0.06638(8)	-0.07759(13)	0.0431
H(651)	0.9673(2)	-0.06115(7)	-0.32277(12)	0.0307
H(661)	0.9620(3)	0.00917(9)	-0.31742(15)	0.0544
C(461)	0.8667(10)	0.2553(3)	0.0295(6)	0.0625
H(4611)	0.8498(10)	0.2418(3)	-0.0209(6)	0.092
H(4612)	0.8808(10)	0.2833(3)	0.0220(6)	0.092
H(4613)	0.9462(10)	0.2441(3)	0.0639(6)	0.092
C(462)	0.8818(5)	0.25769(13)	0.1283(3)	0.0657
H(4621)	0.9505(5)	0.24580(13)	0.1051(3)	0.0825
H(4622)	0.8971(5)	0.28604(13)	0.1338(3)	0.0825
H(4623)	0.8859(5)	0.24610(13)	0.1798(3)	0.0825
C(471)	0.7536(9)	0.2694(2)	0.1471(5)	0.051
H(4711)	0.6759(9)	0.2656(2)	0.1699(5)	0.0718
H(4712)	0.7673(9)	0.2975(2)	0.1400(5)	0.0718
H(4713)	0.8327(9)	0.2583(2)	0.1819(5)	0.0718
C(472)	0.6246(5)	0.27040(15)	0.1154(3)	0.0623
H(4721)	0.5339(5)	0.26651(15)	0.0844(3)	0.0924
H(4722)	0.6437(5)	0.29856(15)	0.1210(3)	0.0924
H(4723)	0.6325(5)	0.25862(15)	0.1670(3)	0.0924
C(481)	0.6107(11)	0.2681(3)	0.0027(6)	0.076
H(4811)	0.6035(11)	0.2528(3)	-0.0453(6)	0.0994
H(4812)	0.6323(11)	0.2954(3)	-0.0068(6)	0.0994
H(4813)	0.5257(11)	0.2671(3)	0.0190(6)	0.0994
C(482)	0.7265(6)	0.26592(15)	-0.0124(3)	0.0629
H(4821)	0.7925(6)	0.25214(15)	-0.0351(3)	0.0782
H(4822)	0.7474(6)	0.29402(15)	-0.0088(3)	0.0782
H(4823)	0.6375(6)	0.26203(15)	-0.0456(3)	0.0782
C(50)	0.8086(3)	0.17146(8)	0.46754(17)	0.0469
H(501)	0.8030(3)	0.18718(8)	0.51331(17)	0.0634
H(502)	0.8840(3)	0.15327(8)	0.48109(17)	0.0634
H(503)	0.8215(3)	0.18886(8)	0.42551(17)	0.0634
C(51)	0.5509(4)	0.17619(10)	0.4196(2)	0.065
H(511)	0.5475(4)	0.19202(10)	0.4656(2)	0.0831
H(512)	0.5603(4)	0.19351(10)	0.3767(2)	0.0831
H(513)	0.4686(4)	0.16092(10)	0.4042(2)	0.0831
C(52)	0.6578(3)	0.12031(8)	0.51121(14)	0.0383
H(521)	0.6543(3)	0.13698(8)	0.55606(14)	0.0528
H(522)	0.7339(3)	0.10236(8)	0.52496(14)	0.0528
H(523)	0.5753(3)	0.10509(8)	0.49652(14)	0.0528
C(54)	0.7110(3)	-0.05141(8)	0.52333(14)	0.042
H(541)	0.7347(3)	-0.06435(8)	0.57425(14)	0.0548
H(542)	0.7327(3)	-0.02342(8)	0.52940(14)	0.0548
H(543)	0.6153(3)	-0.05453(8)	0.50154(14)	0.0548
C(55)	0.7555(3)	-0.11673(7)	0.45894(15)	0.0482
H(551)	0.7804(3)	-0.12882(7)	0.51065(15)	0.0605
H(552)	0.8037(3)	-0.12964(7)	0.42378(15)	0.0605
H(553)	0.6594(3)	-0.11968(7)	0.43844(15)	0.0605
C(56)	0.9487(3)	-0.06608(8)	0.49817(15)	0.0388
H(561)	0.9745(3)	-0.07888(8)	0.54915(15)	0.0458
H(562)	0.9968(3)	-0.07824(8)	0.46207(15)	0.0458
H(563)	0.9710(3)	-0.03810(8)	0.50361(15)	0.0458
C(58)	0.6599(4)	-0.20711(9)	0.15446(19)	0.0607
H(581)	0.6786(4)	-0.23530(9)	0.15988(19)	0.0815
H(582)	0.6764(4)	-0.19498(9)	0.20619(19)	0.0815
H(583)	0.5666(4)	-0.20312(9)	0.12791(19)	0.0815
C(59)	0.7227(3)	-0.20739(7)	0.01803(14)	0.0336
H(591)	0.7397(3)	-0.23569(7)	0.02257(14)	0.0466
H(592)	0.7809(3)	-0.19544(7)	-0.01259(14)	0.0466
H(593)	0.6294(3)	-0.20282(7)	-0.00796(14)	0.0466
C(60)	0.9067(3)	-0.19316(11)	0.1427(2)	0.0681
H(601)	0.9273(3)	-0.22121(11)	0.1493(2)	0.0859

H(602)	0.9590(3)	-0.18153(11)	0.1083(2)	0.0859
H(603)	0.9290(3)	-0.18011(11)	0.1936(2)	0.0859
C(81)	0.7263(7)	0.20831(17)	0.7178(4)	0.147
H(811)	0.7797(7)	0.18437(17)	0.7294(4)	0.1857
H(812)	0.6378(7)	0.20166(17)	0.6865(4)	0.1857
C(82)	0.7948(7)	0.23872(16)	0.6745(3)	0.1239
H(821)	0.8830(7)	0.22905(16)	0.6712(3)	0.1639
H(822)	0.7411(7)	0.24337(16)	0.6219(3)	0.1639
C(83)	0.8105(7)	0.2768(2)	0.7226(4)	0.1368
H(831)	0.9025(7)	0.2809(2)	0.7515(4)	0.1634
H(832)	0.7812(7)	0.2996(2)	0.6893(4)	0.1634
C(84)	0.7180(5)	0.26973(13)	0.7779(2)	0.0977
H(841)	0.7521(5)	0.28288(13)	0.8278(2)	0.1218
H(842)	0.6282(5)	0.27944(13)	0.7549(2)	0.1218

Atom	u(11)	u(22)	u(33)	u(23)	u(13)	u(12)
O(81)	0.208(4)	0.0517(17)	0.106(2)	0.0065(17)	0.090(2)	0.020(2)
N(1)	0.0333(12)	0.0686(17)	0.0291(11)	0.0034(12)	0.0042(9)	0.0061(11)
N(2)	0.0439(12)	0.0270(11)	0.0256(10)	-0.0106(9)	0.0074(9)	0.0003(9)
N(3)	0.0622(16)	0.0457(14)	0.0396(13)	-0.0154(11)	0.0189(11)	-0.0140(11)
N(4)	0.0546(15)	0.0423(14)	0.0408(13)	-0.0109(11)	0.0193(11)	-0.0072(11)
C(1)	0.0172(10)	0.0247(11)	0.0132(10)	0.0077(8)	-0.0034(8)	-0.0052(8)
C(2)	0.0273(11)	0.0219(11)	0.0153(10)	0.0016(9)	0.0013(8)	0.0064(9)
C(3)	0.0104(9)	0.0230(11)	0.0304(12)	-0.0020(9)	0.0010(8)	-0.0016(8)
C(4)	0.0218(11)	0.0185(11)	0.0340(13)	0.0027(9)	0.0105(9)	0.0037(9)
C(5)	0.0294(12)	0.0361(15)	0.0268(12)	-0.0051(11)	-0.0014(10)	0.0006(11)
C(6)	0.0210(11)	0.0302(13)	0.0269(12)	0.0009(10)	-0.0008(9)	0.0038(9)
C(7)	0.0348(14)	0.0550(17)	0.0245(13)	0.0119(12)	0.0004(11)	0.0069(12)
C(8)	0.0261(11)	0.0270(12)	0.0340(13)	-0.0075(11)	-0.0054(10)	0.0020(10)
C(10)	0.0534(16)	0.0307(13)	0.0208(12)	0.0057(10)	0.0063(11)	0.0061(12)
C(12)	0.0364(14)	0.0415(15)	0.0310(13)	0.0060(12)	0.0084(11)	0.0026(11)
C(13)	0.0271(11)	0.0183(11)	0.0244(11)	-0.0077(9)	0.0054(9)	0.0072(9)
C(14)	0.0384(14)	0.0280(13)	0.0351(14)	0.0049(11)	0.0040(11)	-0.0077(10)
C(16)	0.0302(12)	0.0200(11)	0.0210(11)	-0.0099(9)	0.0062(9)	-0.0100(9)
C(18)	0.0411(15)	0.0344(15)	0.0265(12)	-0.0068(11)	-0.0067(11)	0.0020(11)
C(19)	0.0431(15)	0.0457(17)	0.0356(15)	-0.0100(13)	0.0064(12)	-0.0093(13)
C(20)	0.0246(11)	0.0179(10)	0.0189(10)	0.0022(8)	0.0099(9)	0.0081(8)
C(22)	0.0179(10)	0.0457(14)	0.0222(11)	0.0069(10)	0.0161(9)	0.0009(10)
C(24)	0.0441(16)	0.0447(17)	0.0347(15)	-0.0092(13)	-0.0008(12)	0.0019(12)
C(25)	0.0244(11)	0.0251(12)	0.0191(11)	0.0091(9)	0.0027(9)	0.0094(9)
C(26)	0.0066(9)	0.0174(10)	0.0365(13)	-0.0029(9)	-0.0060(8)	0.0008(7)
C(28)	0.0235(11)	0.0229(11)	0.0245(11)	-0.0103(9)	-0.0075(9)	0.0036(9)
C(30)	0.0419(14)	0.0320(14)	0.0272(13)	-0.0101(11)	-0.0026(11)	0.0110(11)
C(31)	0.0247(11)	0.0269(12)	0.0258(12)	-0.0085(10)	0.0001(9)	-0.0096(10)
C(32)	0.0174(10)	0.0302(12)	0.0131(9)	-0.0104(9)	0.0006(8)	0.0010(9)
C(35)	0.0246(11)	0.0341(13)	0.0176(11)	0.0042(10)	-0.0031(9)	0.0046(10)
C(36)	0.0201(11)	0.0441(15)	0.0129(11)	-0.0003(10)	-0.0069(8)	-0.0014(10)
C(37)	0.0358(14)	0.0195(12)	0.0436(15)	0.0075(11)	0.0020(11)	0.0021(10)
C(38)	0.0345(13)	0.0266(12)	0.0222(12)	-0.0112(10)	-0.0044(10)	-0.0020(10)
C(39)	0.0330(13)	0.0338(13)	0.0216(11)	0.0024(10)	0.0101(9)	0.0141(10)
C(42)	0.0311(13)	0.0244(12)	0.0496(16)	0.0032(11)	0.0159(12)	-0.0011(10)
C(45)	0.0454(14)	0.0073(10)	0.0373(15)	0.0007(9)	-0.0001(11)	-0.0108(10)
C(49)	0.0557(17)	0.0374(14)	0.0292(13)	-0.0214(12)	0.0027(12)	-0.0030(12)
C(53)	0.0437(14)	0.0355(13)	0.0144(10)	-0.0031(10)	0.0084(9)	-0.0019(11)
C(57)	0.0627(16)	0.0056(10)	0.0209(11)	-0.0083(8)	0.0049(11)	0.0048(10)
C(61)	0.0091(9)	0.0221(11)	0.0317(12)	0.0074(9)	-0.0079(8)	-0.0032(8)
C(64)	0.0279(12)	0.0237(12)	0.0245(11)	0.0167(10)	-0.0017(9)	-0.0008(9)
C(67)	0.0191(12)	0.0448(16)	0.0313(13)	-0.0003(11)	-0.0040(9)	-0.0046(10)
C(68)	0.0316(12)	0.0353(13)	0.0084(10)	-0.0038(9)	-0.0017(9)	-0.0047(10)
C(69)	0.0162(9)	0.0076(9)	0.0313(12)	0.0029(8)	0.0087(8)	0.0032(7)
C(70)	0.0158(10)	0.0378(14)	0.0314(13)	0.0120(11)	0.0003(9)	0.0018(9)
C(71)	0.0408(14)	0.0247(12)	0.0318(14)	0.0116(11)	0.0014(11)	0.0051(10)
C(72)	0.0286(12)	0.0292(12)	0.0205(11)	-0.0062(10)	0.0149(9)	0.0018(10)
C(9)	0.0286(12)	0.0241(12)	0.0241(11)	-0.0045(9)	0.0011(9)	-0.0020(9)
C(11)	0.0171(10)	0.0141(10)	0.0243(11)	-0.0123(8)	0.0072(8)	-0.0057(8)
C(15)	0.0254(12)	0.0511(16)	0.0325(13)	-0.0080(12)	0.0101(10)	0.0015(11)
C(17)	0.0192(10)	0.0247(12)	0.0251(11)	0.0046(9)	0.0018(8)	-0.0071(9)
C(21)	0.0214(11)	0.0454(16)	0.0270(12)	0.0013(11)	0.0060(9)	-0.0026(10)
C(23)	0.0249(11)	0.0272(12)	0.0165(11)	0.0004(9)	0.0018(9)	-0.0009(9)
C(27)	0.0222(11)	0.0479(15)	0.0256(13)	0.0061(11)	0.0067(10)	-0.0124(10)
C(29)	0.0153(9)	0.0165(10)	0.0186(10)	-0.0028(8)	-0.0017(8)	-0.0030(8)
C(33)	0.0208(12)	0.0417(15)	0.0521(17)	0.0033(12)	0.0062(11)	-0.0120(10)

C(34)	0.0291(12)	0.0366(14)	0.0337(13)	-0.0049(11)	0.0084(10)	0.0153(10)
C(40)	0.0390(14)	0.0338(14)	0.0170(11)	0.0121(10)	0.0034(10)	0.0125(11)
C(41)	0.0295(13)	0.0305(13)	0.0385(14)	0.0100(11)	-0.0018(10)	0.0101(10)
C(43)	0.0073(9)	0.0738(18)	0.0107(10)	0.0040(11)	-0.0004(8)	-0.0041(10)
C(44)	0.0123(9)	0.0201(11)	0.0364(13)	-0.0078(10)	0.0017(9)	-0.0096(8)
C(62)	0.0157(10)	0.0363(13)	0.0169(10)	-0.0033(10)	0.0023(8)	-0.0017(9)
C(63)	0.0191(11)	0.0596(17)	0.0174(11)	0.0011(11)	0.0043(9)	-0.0061(11)
C(65)	0.0303(12)	0.0240(11)	0.0134(11)	-0.0094(9)	-0.0024(9)	0.0000(9)
C(66)	0.0356(14)	0.0559(18)	0.0283(13)	-0.0233(13)	0.0063(11)	-0.0103(12)
C(461)	0.059(6)	0.054(5)	0.089(7)	0.008(5)	0.048(6)	0.011(5)
C(462)	0.075(4)	0.026(2)	0.088(4)	-0.011(2)	0.004(3)	-0.008(2)
C(471)	0.043(5)	0.038(4)	0.064(6)	-0.005(4)	-0.006(4)	0.020(4)
C(472)	0.063(3)	0.055(3)	0.086(4)	0.020(3)	0.054(3)	0.014(2)
C(481)	0.050(6)	0.071(7)	0.081(7)	0.011(6)	-0.041(5)	-0.004(5)
C(482)	0.073(4)	0.048(3)	0.061(3)	-0.006(3)	0.001(3)	-0.016(3)
C(50)	0.068(2)	0.0311(14)	0.0453(16)	-0.0023(12)	0.0203(14)	-0.0191(13)
C(51)	0.071(2)	0.057(2)	0.064(2)	-0.0072(17)	0.0073(17)	0.0196(17)
C(52)	0.0580(17)	0.0317(13)	0.0276(13)	0.0002(11)	0.0150(12)	0.0019(12)
C(54)	0.0588(17)	0.0500(16)	0.0198(12)	0.0200(12)	0.0138(11)	0.0183(13)
C(55)	0.095(2)	0.0166(12)	0.0292(14)	0.0091(10)	0.0052(14)	-0.0013(13)
C(56)	0.0437(15)	0.0299(13)	0.0336(14)	0.0067(11)	-0.0107(11)	0.0071(11)
C(58)	0.088(2)	0.0516(19)	0.0463(17)	0.0218(15)	0.0238(17)	0.0028(18)
C(59)	0.0599(16)	0.0144(10)	0.0334(13)	-0.0119(10)	0.0249(12)	-0.0067(11)
C(60)	0.0425(18)	0.060(2)	0.092(3)	0.0029(19)	-0.0062(17)	0.0207(15)
C(81)	0.176(6)	0.095(4)	0.150(5)	0.014(4)	-0.007(5)	-0.021(4)
C(82)	0.176(6)	0.086(4)	0.111(4)	0.055(3)	0.034(4)	0.025(4)
C(83)	0.141(5)	0.126(5)	0.115(4)	0.021(4)	-0.032(4)	-0.030(4)
C(84)	0.141(4)	0.075(3)	0.073(3)	0.012(2)	0.015(3)	0.088(3)

	angle /°
C(81) - O(81) - C(84)	110.1(4)
C(2) - C(1) - C(6)	122.1(2)
C(2) - C(1) - C(7)	117.5(2)
C(6) - C(1) - C(7)	120.39(19)
C(1) - C(2) - C(3)	117.49(19)
C(1) - C(2) - C(13)	121.19(19)
C(3) - C(2) - C(13)	121.32(19)
C(2) - C(3) - C(4)	121.4(2)
C(2) - C(3) - C(19)	118.3(2)
C(4) - C(3) - C(19)	120.3(2)
C(3) - C(4) - C(5)	119.1(2)
C(3) - C(4) - C(25)	119.9(2)
C(5) - C(4) - C(25)	121.0(2)
C(4) - C(5) - C(6)	121.7(2)
C(4) - C(5) - C(31)	120.0(2)
C(6) - C(5) - C(31)	118.2(2)
C(1) - C(6) - C(5)	118.2(2)
C(1) - C(6) - C(37)	120.9(2)
C(5) - C(6) - C(37)	120.9(2)
C(1) - C(7) - C(8)	119.8(2)
C(1) - C(7) - C(12)	123.3(2)
C(8) - C(7) - C(12)	116.8(2)
C(7) - C(8) - C(42)	120.1(2)
C(7) - C(8) - C(9)	122.4(2)
C(42) - C(8) - C(9)	117.4(2)
C(45) - C(10) - C(9)	120.9(2)
C(45) - C(10) - C(11)	120.8(2)
C(9) - C(10) - C(11)	118.2(2)
C(7) - C(12) - C(14)	119.1(2)
C(7) - C(12) - C(11)	121.8(2)
C(14) - C(12) - C(11)	118.8(2)
C(2) - C(13) - C(14)	120.3(2)
C(2) - C(13) - C(18)	120.2(2)
C(14) - C(13) - C(18)	119.5(2)
C(12) - C(14) - C(13)	118.4(2)
C(12) - C(14) - C(15)	123.1(2)
C(13) - C(14) - C(15)	118.3(2)
C(49) - C(16) - C(15)	118.5(2)
C(49) - C(16) - C(17)	121.5(2)
C(15) - C(16) - C(17)	119.8(2)
C(13) - C(18) - C(20)	120.4(2)
C(13) - C(18) - C(17)	119.1(2)

C(20) - C(18) - C(17)	120.3(2)
C(3) - C(19) - C(20)	120.3(2)
C(3) - C(19) - C(24)	119.7(2)
C(20) - C(19) - C(24)	119.9(2)
C(18) - C(20) - C(19)	119.2(2)
C(18) - C(20) - C(21)	122.3(2)
C(19) - C(20) - C(21)	118.1(2)
C(53) - C(22) - C(21)	118.2(2)
C(53) - C(22) - C(23)	120.5(2)
C(21) - C(22) - C(23)	121.0(2)
C(19) - C(24) - C(26)	120.3(2)
C(19) - C(24) - C(23)	119.3(2)
C(26) - C(24) - C(23)	120.3(2)
C(4) - C(25) - C(26)	120.6(2)
C(4) - C(25) - C(30)	120.63(19)
C(26) - C(25) - C(30)	118.8(2)
C(24) - C(26) - C(25)	119.2(2)
C(24) - C(26) - C(27)	123.1(2)
C(25) - C(26) - C(27)	117.7(2)
C(57) - C(28) - C(27)	119.0(2)
C(57) - C(28) - C(29)	124.18(18)
C(27) - C(28) - C(29)	116.8(2)
C(25) - C(30) - C(32)	117.8(2)
C(25) - C(30) - C(29)	119.9(2)
C(32) - C(30) - C(29)	122.3(2)
C(5) - C(31) - C(32)	120.0(2)
C(5) - C(31) - C(36)	122.2(2)
C(32) - C(31) - C(36)	117.8(2)
C(30) - C(32) - C(31)	120.41(18)
C(30) - C(32) - C(33)	119.4(2)
C(31) - C(32) - C(33)	120.2(2)
C(36) - C(35) - C(34)	119.3(2)
C(36) - C(35) - C(44)	119.7(2)
C(34) - C(35) - C(44)	121.0(2)
C(31) - C(36) - C(35)	122.4(2)
C(31) - C(36) - C(38)	119.0(2)
C(35) - C(36) - C(38)	118.7(2)
C(6) - C(37) - C(38)	119.3(2)
C(6) - C(37) - C(42)	119.3(2)
C(38) - C(37) - C(42)	121.4(2)
C(36) - C(38) - C(37)	120.4(2)
C(36) - C(38) - C(39)	120.5(2)
C(37) - C(38) - C(39)	119.1(2)
C(38) - C(39) - C(40)	119.7(2)
C(38) - C(39) - C(43)	118.6(2)
C(40) - C(39) - C(43)	121.6(2)
C(8) - C(42) - C(37)	119.3(2)
C(8) - C(42) - C(41)	124.9(2)
C(37) - C(42) - C(41)	115.8(2)
C(10) - C(45) - C(461)	105.5(4)
C(10) - C(45) - C(462)	107.4(2)
C(461)- C(45) - C(462)	60.7(4)
C(10) - C(45) - C(471)	116.6(4)
C(461)- C(45) - C(471)	110.8(6)
C(462)- C(45) - C(471)	55.8(4)
C(10) - C(45) - C(472)	107.5(2)
C(461)- C(45) - C(472)	146.8(4)
C(462)- C(45) - C(472)	105.2(3)
C(471)- C(45) - C(472)	49.5(4)
C(10) - C(45) - C(481)	106.5(4)
C(461)- C(45) - C(481)	101.3(6)
C(462)- C(45) - C(481)	144.9(4)
C(471)- C(45) - C(481)	114.7(6)
C(472)- C(45) - C(481)	72.7(5)
C(10) - C(45) - C(482)	112.8(3)
C(461)- C(45) - C(482)	54.6(4)
C(462)- C(45) - C(482)	109.8(3)
C(471)- C(45) - C(482)	130.6(4)
C(472)- C(45) - C(482)	113.6(3)
C(481)- C(45) - C(482)	46.8(5)
C(16) - C(49) - C(50)	110.9(2)
C(16) - C(49) - C(51)	109.6(2)
C(50) - C(49) - C(51)	110.5(2)
C(16) - C(49) - C(52)	111.3(2)
C(50) - C(49) - C(52)	106.8(2)
C(51) - C(49) - C(52)	107.6(2)
C(22) - C(53) - C(54)	109.91(19)

C(22) - C(53) - C(55)	111.42(19)
C(54) - C(53) - C(55)	106.8(2)
C(22) - C(53) - C(56)	108.60(18)
C(54) - C(53) - C(56)	110.7(2)
C(55) - C(53) - C(56)	109.4(2)
C(28) - C(57) - C(58)	110.6(2)
C(28) - C(57) - C(59)	108.22(17)
C(58) - C(57) - C(59)	109.2(2)
C(28) - C(57) - C(60)	107.6(2)
C(58) - C(57) - C(60)	113.4(2)
C(59) - C(57) - C(60)	107.6(2)
C(67) - C(61) - C(62)	119.6(2)
C(67) - C(61) - C(66)	119.8(2)
C(62) - C(61) - C(66)	120.5(2)
C(70) - C(64) - C(63)	122.3(2)
C(70) - C(64) - C(65)	119.0(2)
C(63) - C(64) - C(65)	118.5(2)
C(61) - C(67) - C(68)	123.2(2)
C(61) - C(67) - C(69)	121.7(2)
C(68) - C(67) - C(69)	115.1(2)
N(1) - C(68) - C(67)	178.5(2)
N(2) - C(69) - C(67)	177.9(2)
C(64) - C(70) - C(71)	122.0(2)
C(64) - C(70) - C(72)	123.7(2)
C(71) - C(70) - C(72)	114.1(2)
N(3) - C(71) - C(70)	178.5(3)
N(4) - C(72) - C(70)	176.8(2)
C(8) - C(9) - C(10)	118.9(2)
C(10) - C(11) - C(12)	121.4(2)
C(14) - C(15) - C(16)	122.1(2)
C(16) - C(17) - C(18)	120.9(2)
C(20) - C(21) - C(22)	120.6(2)
C(22) - C(23) - C(24)	120.6(2)
C(26) - C(27) - C(28)	124.4(2)
C(28) - C(29) - C(30)	122.4(2)
C(32) - C(33) - C(34)	119.5(2)
C(35) - C(34) - C(33)	120.8(2)
C(39) - C(40) - C(41)	121.6(2)
C(42) - C(41) - C(40)	122.4(2)
C(39) - C(43) - C(44)	120.5(2)
C(35) - C(44) - C(43)	121.9(2)
C(61) - C(62) - C(63)	119.0(2)
C(64) - C(63) - C(62)	121.8(2)
C(64) - C(65) - C(66)	120.2(2)
C(61) - C(66) - C(65)	119.6(2)
C(45) - C(461)- C(462)	58.4(4)
C(45) - C(461)- C(482)	57.4(4)
C(462)- C(461)- C(482)	110.2(5)
C(45) - C(462)- C(461)	61.0(4)
C(45) - C(462)- C(471)	55.4(4)
C(461)- C(462)- C(471)	110.7(5)
C(45) - C(471)- C(462)	68.8(4)
C(45) - C(471)- C(472)	72.1(5)
C(462)- C(471)- C(472)	140.6(7)
C(45) - C(472)- C(471)	58.4(4)
C(45) - C(481)- C(482)	62.8(5)
C(45) - C(482)- C(461)	68.0(4)
C(45) - C(482)- C(481)	70.4(5)
C(461)- C(482)- C(481)	138.1(7)
O(81) - C(81) - C(82)	104.3(5)
C(81) - C(82) - C(83)	107.3(5)
C(82) - C(83) - C(84)	102.3(5)
O(81) - C(84) - C(83)	106.0(4)

	distance / Å
O(81) - C(81)	1.396(6)
O(81) - C(84)	1.389(5)
N(1) - C(68)	1.170(3)
N(2) - C(69)	1.149(3)
N(3) - C(71)	1.151(3)
N(4) - C(72)	1.159(3)
C(1) - C(2)	1.455(3)
C(1) - C(6)	1.396(3)

C(1) - C(7)	1.428(3)
C(2) - C(3)	1.438(3)
C(2) - C(13)	1.426(3)
C(3) - C(4)	1.411(3)
C(3) - C(19)	1.442(3)
C(4) - C(5)	1.418(3)
C(4) - C(25)	1.430(3)
C(5) - C(6)	1.441(3)
C(5) - C(31)	1.424(3)
C(6) - C(37)	1.435(3)
C(7) - C(8)	1.401(3)
C(7) - C(12)	1.411(4)
C(8) - C(42)	1.460(3)
C(8) - C(9)	1.418(3)
C(10) - C(45)	1.565(3)
C(10) - C(9)	1.410(3)
C(10) - C(11)	1.426(3)
C(12) - C(14)	1.475(3)
C(12) - C(11)	1.365(3)
C(13) - C(14)	1.456(3)
C(13) - C(18)	1.412(3)
C(14) - C(15)	1.383(3)
C(16) - C(49)	1.561(3)
C(16) - C(15)	1.401(3)
C(16) - C(17)	1.383(3)
C(18) - C(20)	1.439(3)
C(18) - C(17)	1.422(3)
C(19) - C(20)	1.454(3)
C(19) - C(24)	1.414(4)
C(20) - C(21)	1.411(3)
C(22) - C(53)	1.557(3)
C(22) - C(21)	1.395(3)
C(22) - C(23)	1.393(3)
C(24) - C(26)	1.444(3)
C(24) - C(23)	1.408(3)
C(25) - C(26)	1.420(3)
C(25) - C(30)	1.437(3)
C(26) - C(27)	1.404(3)
C(28) - C(57)	1.546(3)
C(28) - C(27)	1.379(3)
C(28) - C(29)	1.405(3)
C(30) - C(32)	1.468(3)
C(30) - C(29)	1.376(3)
C(31) - C(32)	1.435(3)
C(31) - C(36)	1.424(3)
C(32) - C(33)	1.464(3)
C(35) - C(36)	1.416(3)
C(35) - C(34)	1.427(3)
C(35) - C(44)	1.403(3)
C(36) - C(38)	1.435(3)
C(37) - C(38)	1.436(3)
C(37) - C(42)	1.416(3)
C(38) - C(39)	1.400(3)
C(39) - C(40)	1.397(3)
C(39) - C(43)	1.443(3)
C(42) - C(41)	1.451(3)
C(45) - C(461)	1.666(8)
C(45) - C(462)	1.623(5)
C(45) - C(471)	1.433(8)
C(45) - C(472)	1.602(5)
C(45) - C(481)	1.603(8)
C(45) - C(482)	1.514(5)
C(49) - C(50)	1.536(4)
C(49) - C(51)	1.537(4)
C(49) - C(52)	1.560(4)
C(53) - C(54)	1.561(3)
C(53) - C(55)	1.560(3)
C(53) - C(56)	1.538(3)
C(57) - C(58)	1.523(4)
C(57) - C(59)	1.595(3)
C(57) - C(60)	1.537(4)
C(61) - C(67)	1.375(3)
C(61) - C(62)	1.445(3)
C(61) - C(66)	1.451(3)
C(64) - C(70)	1.363(3)
C(64) - C(63)	1.431(3)
C(64) - C(65)	1.471(3)
C(67) - C(68)	1.441(3)
C(67) - C(69)	1.438(3)
C(70) - C(71)	1.446(3)
C(70) - C(72)	1.417(3)
C(33) - C(34)	1.400(3)
C(40) - C(41)	1.344(3)

C(43) - C(44)	1.348(3)
C(62) - C(63)	1.371(3)
C(65) - C(66)	1.372(3)
C(461)- C(462)	1.661(11)
C(461)- C(482)	1.465(11)
C(462)- C(471)	1.440(10)
C(471)- C(472)	1.280(9)
C(481)- C(482)	1.241(12)
C(81) - C(82)	1.499(7)
C(82) - C(83)	1.493(7)
C(83) - C(84)	1.478(7)

8.2 4,4,5,5-Tetramethyl-2-phenanthren-4-yl-[1,3,2]dioxaborolane (5-43)

Atom	x/a	y/b	z/c	U(iso)
O(1)	0.4576(4)	0.6743(3)	0.1720(3)	0.0399
O(2)	0.6323(4)	0.7949(3)	0.1576(3)	0.0411
B(1)	0.5985(6)	0.6918(4)	0.1583(4)	0.0225
C(1)	0.7018(5)	0.5994(4)	0.1328(4)	0.0255
C(5)	0.9079(5)	0.4816(4)	0.1434(5)	0.036
C(6)	0.8237(5)	0.5613(4)	0.1861(4)	0.0268
C(7)	0.8641(5)	0.5958(4)	0.2827(4)	0.0292
C(8)	0.9924(6)	0.5572(5)	0.3281(5)	0.042
C(15)	0.3930(6)	0.7761(5)	0.1915(6)	0.0694
C(16)	0.4959(6)	0.8520(5)	0.1593(6)	0.0678
C(2)	0.6679(6)	0.5566(4)	0.0438(4)	0.0334
C(3)	0.7491(6)	0.4772(4)	0.0032(4)	0.0389
C(4)	0.8678(6)	0.4412(5)	0.0530(5)	0.0433
C(9)	1.0758(6)	0.4808(5)	0.2801(6)	0.0524
C(10)	1.0339(6)	0.4429(5)	0.1934(5)	0.0501
C(11)	0.7809(6)	0.6623(4)	0.3377(4)	0.0347
C(12)	0.8201(6)	0.6950(5)	0.4287(4)	0.0442
C(13)	0.9496(7)	0.6595(5)	0.4690(5)	0.0509
C(14)	1.0331(7)	0.5931(6)	0.4203(5)	0.0553
H(21)	0.5866(6)	0.5828(4)	0.0089(4)	0.0363
H(31)	0.7227(6)	0.4480(4)	-0.0574(4)	0.0464
H(41)	0.9253(6)	0.3882(5)	0.0262(5)	0.046
H(91)	1.1616(6)	0.4554(5)	0.3102(6)	0.0587
H(101)	1.0885(6)	0.3892(5)	0.1651(5)	0.0517
H(111)	0.6940(6)	0.6879(4)	0.3094(4)	0.0382
H(121)	0.7593(6)	0.7387(5)	0.4641(4)	0.0516
H(131)	0.9810(7)	0.6828(5)	0.5308(5)	0.0549
H(141)	1.1199(7)	0.5687(6)	0.4495(5)	0.0624
C(17)	0.2404(6)	0.7746(5)	0.1706(5)	0.06
H(171)	0.2022(6)	0.8416(5)	0.1844(5)	0.0656
H(172)	0.2217(6)	0.7585(5)	0.1050(5)	0.0656
H(173)	0.1972(6)	0.7231(5)	0.2093(5)	0.0656
C(18)	0.4123(12)	0.7947(9)	0.3095(5)	0.1485
H(181)	0.3708(12)	0.8597(9)	0.3266(5)	0.1171
H(182)	0.5101(12)	0.7940(9)	0.3300(5)	0.1171
H(183)	0.3638(12)	0.7390(9)	0.3395(5)	0.1171
C(19)	0.4335(12)	0.8543(10)	0.0416(5)	0.1565
H(191)	0.3459(12)	0.8918(10)	0.0367(5)	0.1257
H(192)	0.5025(12)	0.8887(10)	0.0048(5)	0.1257
H(193)	0.4192(12)	0.7850(10)	0.0183(5)	0.1257
C(20)	0.5152(7)	0.9574(5)	0.1876(6)	0.0778
H(201)	0.4256(7)	0.9922(5)	0.1862(6)	0.0664
H(202)	0.5780(7)	0.9929(5)	0.1469(6)	0.0664
H(203)	0.5548(7)	0.9572(5)	0.2511(6)	0.0664

Atom	u(11)	u(22)	u(33)	u(23)	u(13)	u(12)
O(1)	0.0219(19)	0.028(2)	0.070(3)	-0.0063(19)	0.0045(18)	0.0017(16)
O(2)	0.027(2)	0.0246(19)	0.072(3)	0.004(2)	0.0096(19)	0.0040(17)
B(1)	0.021(3)	0.030(3)	0.017(3)	-0.001(2)	0.000(2)	-0.004(2)
C(1)	0.024(3)	0.019(3)	0.034(3)	0.005(2)	0.006(2)	-0.001(2)
C(5)	0.024(3)	0.028(3)	0.057(4)	0.011(3)	0.017(3)	0.005(2)
C(6)	0.019(3)	0.028(3)	0.034(3)	0.011(2)	0.006(2)	0.001(2)
C(7)	0.023(3)	0.026(3)	0.038(4)	0.012(3)	-0.003(3)	-0.006(2)
C(8)	0.022(3)	0.046(3)	0.058(4)	0.020(3)	-0.005(3)	-0.007(3)

C(15)	0.029(4)	0.030(4)	0.149(8)	-0.014(4)	0.004(4)	0.012(3)
C(16)	0.030(3)	0.026(3)	0.148(8)	0.002(4)	0.020(4)	0.015(3)
C(2)	0.038(3)	0.027(3)	0.035(3)	-0.003(3)	-0.001(3)	0.001(3)
C(3)	0.047(4)	0.034(3)	0.037(3)	-0.001(3)	0.016(3)	-0.005(3)
C(4)	0.044(4)	0.032(3)	0.057(4)	-0.001(3)	0.030(3)	0.001(3)
C(9)	0.025(3)	0.060(4)	0.073(5)	0.028(4)	0.008(3)	0.012(3)
C(10)	0.034(4)	0.047(4)	0.070(5)	0.016(4)	0.021(4)	0.014(3)
C(11)	0.030(3)	0.030(3)	0.043(4)	0.001(3)	-0.010(3)	0.002(2)
C(12)	0.047(4)	0.038(3)	0.046(4)	-0.006(3)	-0.011(3)	-0.009(3)
C(13)	0.053(4)	0.054(4)	0.044(4)	0.009(3)	-0.020(3)	-0.022(4)
C(14)	0.034(4)	0.068(5)	0.063(5)	0.025(4)	-0.016(3)	-0.005(3)
C(17)	0.027(3)	0.055(4)	0.099(6)	-0.003(4)	0.011(3)	0.010(3)
C(18)	0.216(12)	0.197(11)	0.034(5)	0.003(6)	0.019(6)	0.168(10)
C(19)	0.213(12)	0.216(12)	0.042(5)	0.052(6)	0.026(6)	0.169(11)
C(20)	0.041(4)	0.034(4)	0.158(8)	-0.016(4)	0.003(5)	0.010(3)

center	angle /°
B(1) - O(1) - C(15)	107.0(4)
B(1) - O(2) - C(16)	106.1(4)
O(1) - B(1) - O(2)	112.9(4)
O(1) - B(1) - C(1)	121.2(4)
O(2) - B(1) - C(1)	125.4(4)
B(1) - C(1) - C(6)	128.6(5)
B(1) - C(1) - C(2)	112.1(4)
C(6) - C(1) - C(2)	119.2(5)
C(6) - C(5) - C(4)	120.2(5)
C(6) - C(5) - C(10)	119.8(6)
C(4) - C(5) - C(10)	120.0(6)
C(1) - C(6) - C(5)	117.9(5)
C(1) - C(6) - C(7)	123.8(5)
C(5) - C(6) - C(7)	118.2(5)
C(6) - C(7) - C(8)	119.6(5)
C(6) - C(7) - C(11)	124.1(5)
C(8) - C(7) - C(11)	116.2(5)
C(7) - C(8) - C(9)	119.5(6)
C(7) - C(8) - C(14)	119.3(6)
C(9) - C(8) - C(14)	121.2(6)
O(1) - C(15) - C(16)	104.4(5)
O(1) - C(15) - C(17)	111.3(5)
C(16) - C(15) - C(17)	127.6(7)
O(1) - C(15) - C(18)	106.2(6)
C(16) - C(15) - C(18)	99.4(7)
C(17) - C(15) - C(18)	105.6(7)
O(2) - C(16) - C(15)	105.3(5)
O(2) - C(16) - C(19)	104.8(6)
C(15) - C(16) - C(19)	95.9(7)
O(2) - C(16) - C(20)	111.9(5)
C(15) - C(16) - C(20)	128.9(7)
C(19) - C(16) - C(20)	106.6(7)
C(1) - C(2) - C(3)	122.6(5)
C(2) - C(3) - C(4)	118.7(6)
C(5) - C(4) - C(3)	121.3(5)
C(8) - C(9) - C(10)	121.3(6)
C(5) - C(10) - C(9)	121.3(6)
C(7) - C(11) - C(12)	123.8(5)
C(11) - C(12) - C(13)	118.2(6)
C(12) - C(13) - C(14)	120.8(6)
C(8) - C(14) - C(13)	121.5(6)

	distance /Å
O(1) - B(1)	1.361(6)
O(1) - C(15)	1.463(7)
O(2) - B(1)	1.353(7)
O(2) - C(16)	1.473(6)
B(1) - C(1)	1.575(7)
C(1) - C(6)	1.425(7)
C(1) - C(2)	1.384(7)
C(5) - C(6)	1.432(7)

C(5) - C(4)	1.403(8)
C(5) - C(10)	1.437(8)
C(6) - C(7)	1.457(7)
C(7) - C(8)	1.426(7)
C(7) - C(11)	1.403(8)
C(8) - C(9)	1.433(9)
C(8) - C(14)	1.407(9)
C(15) - C(16)	1.450(9)
C(15) - C(17)	1.450(8)
C(15) - C(18)	1.671(11)
C(16) - C(19)	1.725(11)
C(16) - C(20)	1.411(9)
C(2) - C(3)	1.401(7)
C(3) - C(4)	1.369(8)
C(9) - C(10)	1.349(9)
C(11) - C(12)	1.375(8)
C(12) - C(13)	1.395(8)
C(13) - C(14)	1.355(9)

8.3 1-bromo-3,5-Bis-(9,10-bis-n-dodecyl-phenanthren-4-yl)-benzene (5-60)

Atom	x/a	y/b	z/c	U(iso)
Br(1)	0.10435(10)	0.23091(4)	-0.16058(5)	0.0432
C(1)	0.0978(7)	0.3243(3)	-0.2076(5)	0.0302
C(2)	0.0992(8)	0.3790(3)	-0.1466(5)	0.0305
C(3)	0.0871(7)	0.4487(3)	-0.1781(4)	0.0243
C(4)	0.0810(6)	0.4586(3)	-0.2672(4)	0.0174
C(5)	0.0818(6)	0.4037(3)	-0.3266(4)	0.0249
C(6)	0.0891(7)	0.3360(3)	-0.2931(4)	0.0251
C(7)	0.0949(7)	0.4167(3)	-0.4197(3)	0.0205
C(8)	0.2390(8)	0.4540(3)	-0.4463(4)	0.0237
C(9)	0.2835(8)	0.4594(3)	-0.5308(4)	0.0311
C(10)	0.1903(7)	0.4270(3)	-0.5949(4)	0.0243
C(11)	0.0381(8)	0.3904(3)	-0.5725(4)	0.025
C(12)	-0.0143(8)	0.3899(3)	-0.4863(4)	0.0245
C(13)	-0.1868(7)	0.3608(3)	-0.4720(4)	0.0204
C(14)	-0.2708(8)	0.3683(3)	-0.3938(4)	0.0292
C(15)	-0.4351(8)	0.3438(3)	-0.3836(5)	0.0334
C(16)	-0.5194(8)	0.3116(3)	-0.4511(5)	0.0344
C(17)	-0.4444(8)	0.3038(3)	-0.5273(5)	0.0337
C(18)	-0.2755(7)	0.3298(3)	-0.5421(4)	0.0289
C(19)	-0.2085(7)	0.3269(3)	-0.6262(4)	0.0288
C(20)	-0.0569(8)	0.3576(3)	-0.6411(4)	0.0273
C(21)	0.0985(7)	0.5094(3)	-0.1179(4)	0.0249
C(22)	0.2434(8)	0.5140(3)	-0.0659(4)	0.0318
C(23)	0.2853(7)	0.5755(3)	-0.0213(4)	0.0362
C(24)	0.1875(7)	0.6332(3)	-0.0283(4)	0.0304
C(25)	0.0357(8)	0.6305(3)	-0.0807(4)	0.0268
C(26)	-0.0162(7)	0.5678(3)	-0.1197(4)	0.0224
C(27)	-0.1879(7)	0.5635(3)	-0.1612(4)	0.026
C(28)	-0.2710(7)	0.5015(3)	-0.1852(4)	0.0256
C(29)	-0.4313(8)	0.5012(3)	-0.2208(4)	0.0275
C(30)	-0.5161(8)	0.5651(3)	-0.2384(4)	0.0321
C(31)	-0.4416(8)	0.6262(3)	-0.2132(4)	0.0338
C(32)	-0.2766(7)	0.6284(3)	-0.1724(4)	0.0269
C(33)	-0.2117(8)	0.6921(3)	-0.1383(4)	0.0339
C(34)	-0.0645(8)	0.6923(4)	-0.0900(4)	0.0371
H(21)	0.1067(8)	0.3701(3)	-0.0858(5)	0.0359
H(41)	0.0770(6)	0.5054(3)	-0.2887(4)	0.021
H(61)	0.0868(7)	0.2970(3)	-0.3318(4)	0.0273
H(81)	0.3083(8)	0.4762(3)	-0.4030(4)	0.0277
H(91)	0.3800(8)	0.4866(3)	-0.5459(4)	0.0342
H(101)	0.2267(7)	0.4276(3)	-0.6535(4)	0.0312
H(141)	-0.2124(8)	0.3915(3)	-0.3473(4)	0.0319
H(151)	-0.4890(8)	0.3501(3)	-0.3294(5)	0.0421
H(161)	-0.6301(8)	0.2928(3)	-0.4430(5)	0.0394
H(171)	-0.5059(8)	0.2816(3)	-0.5735(5)	0.0361
H(191)	-0.2709(7)	0.3041(3)	-0.6716(4)	0.0343
H(201)	-0.0126(8)	0.3561(3)	-0.6981(4)	0.0309
H(221)	0.3162(8)	0.4742(3)	-0.0606(4)	0.0393
H(231)	0.3846(7)	0.5764(3)	0.0150(4)	0.0427
H(241)	0.2196(7)	0.6756(3)	0.0004(4)	0.0432
H(281)	-0.2127(7)	0.4582(3)	-0.1766(4)	0.0354

H(291)	-0.4881(8)	0.4578(3)	-0.2318(4)	0.0383
H(301)	-0.6222(8)	0.5652(3)	-0.2692(4)	0.0412
H(311)	-0.4990(8)	0.6694(3)	-0.2241(4)	0.0409
H(331)	-0.2689(8)	0.7350(3)	-0.1515(4)	0.0442
H(341)	-0.0289(8)	0.7344(4)	-0.0617(4)	0.0472

Atom	u(11)	u(22)	u(33)	u(23)	u(13)	u(12)
Br(1)	0.0508(4)	0.0341(3)	0.0444(4)	0.0134(5)	-0.0052(3)	0.0056(5)
C(1)	0.019(4)	0.031(4)	0.040(4)	0.011(3)	-0.006(3)	0.001(3)
C(2)	0.019(3)	0.046(4)	0.027(4)	0.002(3)	0.001(3)	0.000(3)
C(3)	0.011(3)	0.032(3)	0.030(5)	0.008(3)	-0.004(3)	-0.003(3)
C(4)	0.008(3)	0.030(3)	0.014(3)	0.001(3)	-0.003(2)	0.002(2)
C(5)	0.012(3)	0.026(3)	0.036(4)	0.009(3)	0.004(3)	0.002(3)
C(6)	0.022(3)	0.021(3)	0.032(4)	-0.008(3)	0.001(3)	0.003(3)
C(7)	0.023(4)	0.016(3)	0.023(3)	0.002(2)	-0.001(3)	0.001(2)
C(8)	0.028(4)	0.023(4)	0.020(4)	-0.008(3)	-0.009(3)	0.005(3)
C(9)	0.023(4)	0.031(4)	0.039(4)	-0.001(3)	-0.007(3)	0.000(3)
C(10)	0.028(4)	0.018(3)	0.027(3)	0.004(3)	-0.005(3)	0.008(3)
C(11)	0.028(4)	0.016(3)	0.030(4)	-0.002(3)	-0.011(3)	0.011(3)
C(12)	0.027(4)	0.011(3)	0.035(4)	-0.001(3)	0.004(3)	-0.006(3)
C(13)	0.021(3)	0.015(3)	0.026(4)	0.004(3)	-0.005(3)	0.002(2)
C(14)	0.029(4)	0.019(3)	0.040(4)	0.004(3)	-0.001(3)	-0.001(3)
C(15)	0.022(4)	0.021(3)	0.058(5)	0.011(3)	0.003(3)	0.001(3)
C(16)	0.015(3)	0.013(3)	0.074(5)	-0.005(3)	-0.005(4)	-0.005(3)
C(17)	0.016(4)	0.016(3)	0.069(5)	-0.007(3)	-0.014(3)	0.004(3)
C(18)	0.022(4)	0.023(3)	0.042(5)	0.001(3)	-0.015(3)	0.008(3)
C(19)	0.029(4)	0.025(3)	0.032(4)	-0.003(3)	-0.020(3)	0.003(3)
C(20)	0.031(4)	0.025(3)	0.025(4)	0.009(3)	-0.010(3)	0.012(3)
C(21)	0.021(4)	0.032(3)	0.021(3)	0.001(3)	-0.004(3)	-0.014(3)
C(22)	0.032(4)	0.038(4)	0.026(4)	0.004(3)	0.006(3)	0.004(3)
C(23)	0.016(4)	0.060(5)	0.033(4)	0.006(3)	-0.008(3)	0.005(3)
C(24)	0.026(4)	0.049(4)	0.016(3)	-0.009(3)	0.001(3)	-0.005(3)
C(25)	0.023(3)	0.038(4)	0.019(4)	-0.011(3)	0.004(3)	0.001(3)
C(26)	0.018(3)	0.031(3)	0.018(3)	-0.009(3)	0.004(3)	0.006(3)
C(27)	0.017(3)	0.033(3)	0.028(3)	0.001(3)	0.007(3)	0.000(3)
C(28)	0.025(4)	0.027(3)	0.025(3)	-0.005(3)	-0.005(3)	0.005(3)
C(29)	0.026(4)	0.027(4)	0.030(4)	-0.007(3)	0.007(3)	-0.002(3)
C(30)	0.021(3)	0.039(4)	0.036(4)	-0.006(3)	-0.006(3)	0.005(3)
C(31)	0.019(4)	0.045(4)	0.037(4)	-0.004(3)	0.002(3)	0.012(3)
C(32)	0.014(4)	0.031(3)	0.036(4)	-0.004(3)	0.001(3)	0.003(3)
C(33)	0.031(4)	0.036(4)	0.035(4)	-0.005(3)	0.003(3)	0.000(3)
C(34)	0.037(4)	0.046(4)	0.028(4)	-0.010(3)	0.001(3)	-0.003(3)

	Angle /°
Br(1) - C(1) - C(2)	115.8(5)
Br(1) - C(1) - C(6)	121.8(5)
C(2) - C(1) - C(6)	122.4(6)
C(1) - C(2) - C(3)	117.8(6)
C(2) - C(3) - C(4)	117.9(6)
C(2) - C(3) - C(21)	120.8(5)
C(4) - C(3) - C(21)	121.0(5)
C(3) - C(4) - C(5)	123.4(6)
C(4) - C(5) - C(6)	117.0(5)
C(4) - C(5) - C(7)	121.3(5)
C(6) - C(5) - C(7)	121.3(5)
C(1) - C(6) - C(5)	121.5(6)
C(5) - C(7) - C(8)	116.4(5)
C(5) - C(7) - C(12)	126.5(5)
C(8) - C(7) - C(12)	116.8(5)
C(7) - C(8) - C(9)	122.8(5)
C(8) - C(9) - C(10)	120.9(6)
C(9) - C(10) - C(11)	119.0(6)
C(10) - C(11) - C(12)	119.6(5)
C(10) - C(11) - C(20)	117.6(5)
C(12) - C(11) - C(20)	122.7(6)
C(7) - C(12) - C(11)	119.9(6)
C(7) - C(12) - C(13)	124.7(6)
C(11) - C(12) - C(13)	115.4(5)

C(12) - C(13) - C(14)	122.7(5)
C(12) - C(13) - C(18)	119.0(5)
C(14) - C(13) - C(18)	118.1(6)
C(13) - C(14) - C(15)	121.5(6)
C(14) - C(15) - C(16)	120.3(6)
C(15) - C(16) - C(17)	120.2(6)
C(16) - C(17) - C(18)	121.8(6)
C(13) - C(18) - C(17)	118.0(6)
C(13) - C(18) - C(19)	122.3(6)
C(17) - C(18) - C(19)	119.6(5)
C(18) - C(19) - C(20)	119.0(6)
C(11) - C(20) - C(19)	121.0(6)
C(3) - C(21) - C(22)	116.7(5)
C(3) - C(21) - C(26)	124.2(6)
C(22) - C(21) - C(26)	118.3(6)
C(21) - C(22) - C(23)	121.5(6)
C(22) - C(23) - C(24)	121.1(6)
C(23) - C(24) - C(25)	119.2(6)
C(24) - C(25) - C(26)	120.6(6)
C(24) - C(25) - C(34)	118.9(5)
C(26) - C(25) - C(34)	120.5(6)
C(21) - C(26) - C(25)	118.5(6)
C(21) - C(26) - C(27)	122.2(5)
C(25) - C(26) - C(27)	119.3(5)
C(26) - C(27) - C(28)	125.3(5)
C(26) - C(27) - C(32)	116.2(5)
C(28) - C(27) - C(32)	118.3(5)
C(27) - C(28) - C(29)	122.3(6)
C(28) - C(29) - C(30)	120.2(6)
C(29) - C(30) - C(31)	118.9(6)
C(30) - C(31) - C(32)	122.3(6)
C(27) - C(32) - C(31)	117.7(5)
C(27) - C(32) - C(33)	121.7(6)
C(31) - C(32) - C(33)	120.4(5)
C(32) - C(33) - C(34)	120.1(6)
C(25) - C(34) - C(33)	121.1(6)

	distance /Å
Br(1) - C(1)	1.915(6)
C(1) - C(2)	1.400(8)
C(1) - C(6)	1.333(8)
C(2) - C(3)	1.412(8)
C(3) - C(4)	1.382(8)
C(3) - C(21)	1.481(8)
C(4) - C(5)	1.386(8)
C(5) - C(6)	1.386(7)
C(5) - C(7)	1.458(7)
C(7) - C(8)	1.402(8)
C(7) - C(12)	1.418(8)
C(8) - C(9)	1.356(8)
C(9) - C(10)	1.363(8)
C(10) - C(11)	1.431(8)
C(11) - C(12)	1.395(8)
C(11) - C(20)	1.423(8)
C(12) - C(13)	1.483(8)
C(13) - C(14)	1.389(8)
C(13) - C(18)	1.401(8)
C(14) - C(15)	1.383(8)
C(15) - C(16)	1.365(9)
C(16) - C(17)	1.328(9)
C(17) - C(18)	1.439(8)
C(18) - C(19)	1.405(8)
C(19) - C(20)	1.349(8)
C(21) - C(22)	1.381(8)
C(21) - C(26)	1.429(8)
C(22) - C(23)	1.391(8)
C(23) - C(24)	1.341(8)
C(24) - C(25)	1.427(9)
C(25) - C(26)	1.391(7)
C(25) - C(34)	1.418(8)
C(26) - C(27)	1.484(8)
C(27) - C(28)	1.393(7)

C(27) - C(32)	1.425(8)
C(28) - C(29)	1.363(8)
C(29) - C(30)	1.409(8)
C(30) - C(31)	1.354(8)
C(31) - C(32)	1.430(8)
C(32) - C(33)	1.410(8)
C(33) - C(34)	1.362(8)

8.4 4,5,9,10-Tetrahydro-pyrene (5-94)

Atom	x/a	y/b	z/c	U(iso)
C(1)	0.5634(4)	0.9082(4)	0.14547(11)	0.0184
C(2)	0.5817(4)	0.8813(4)	0.18843(11)	0.0212
C(6)	0.4184(5)	0.9828(3)	0.13011(11)	0.0208
C(7)	0.6989(5)	0.8592(3)	0.11643(11)	0.0207
C(8)	0.6637(5)	0.8482(4)	0.07373(11)	0.0222
C(12)	0.8600(5)	0.8284(4)	0.13210(11)	0.0217
C(3)	0.4590(5)	0.9340(4)	0.21569(12)	0.0257
C(4)	0.3158(5)	1.0108(4)	0.20054(13)	0.0281
C(5)	0.2971(5)	1.0325(4)	0.15839(12)	0.025
C(9)	0.7936(5)	0.8049(4)	0.04675(12)	0.023
C(10)	0.9556(5)	0.7766(4)	0.06173(13)	0.025
C(11)	0.9865(5)	0.7877(4)	0.10378(12)	0.0239
H(31)	0.4725(5)	0.9189(4)	0.24490(12)	0.0296
H(41)	0.2320(5)	1.0463(4)	0.21948(13)	0.031
H(51)	0.1984(5)	1.0821(4)	0.14809(12)	0.0297
H(91)	0.7701(5)	0.7953(4)	0.01776(12)	0.0241
H(101)	1.0441(5)	0.7506(4)	0.04303(13)	0.0256
H(111)	1.0962(5)	0.7675(4)	0.11420(12)	0.0304
C(13)	0.8907(4)	0.8449(4)	0.17824(11)	0.0206
H(131)	0.9145(4)	0.9525(4)	0.18416(11)	0.0254
H(132)	0.9843(4)	0.7816(4)	0.18597(11)	0.0254
C(14)	0.7382(5)	0.7950(4)	0.20339(11)	0.0227
H(141)	0.7574(5)	0.8179(4)	0.23205(11)	0.0245
H(142)	0.7217(5)	0.6846(4)	0.20001(11)	0.0245
C(15)	0.4055(5)	1.0127(4)	0.08367(11)	0.0244
H(151)	0.4619(5)	1.1085(4)	0.07717(11)	0.0269
H(152)	0.2903(5)	1.0215(4)	0.07614(11)	0.0269
C(16)	0.4878(5)	0.8792(4)	0.05865(11)	0.0257
H(161)	0.4908(5)	0.9071(4)	0.02991(11)	0.0309
H(162)	0.4228(5)	0.7860(4)	0.06212(11)	0.0309
C(21)	0.0859(4)	1.3898(4)	0.13508(12)	0.0213
C(22)	0.1112(5)	1.4483(4)	0.17568(11)	0.0212
C(26)	-0.0602(4)	1.3037(3)	0.12525(12)	0.022
C(27)	0.2160(5)	1.4126(3)	0.10318(13)	0.0222
C(28)	0.1750(5)	1.3921(4)	0.06061(11)	0.023
C(32)	0.3804(5)	1.4496(4)	0.11511(12)	0.0221
C(23)	-0.0073(5)	1.4183(4)	0.20620(12)	0.0275
C(24)	-0.1514(5)	1.3295(4)	0.19699(13)	0.0311
C(25)	-0.1769(5)	1.2750(4)	0.15662(12)	0.0269
C(29)	0.3005(6)	1.4085(4)	0.03095(13)	0.029
C(30)	0.4647(5)	1.4463(4)	0.04267(13)	0.0294
C(31)	0.5039(5)	1.4656(4)	0.08437(12)	0.0268
H(231)	0.0083(5)	1.4597(4)	0.23350(12)	0.0347
H(241)	-0.2300(5)	1.3057(4)	0.21843(13)	0.0385
H(251)	-0.2762(5)	1.2175(4)	0.15026(12)	0.03
H(291)	0.2741(6)	1.3943(4)	0.00225(13)	0.0311
H(301)	0.5498(5)	1.4580(4)	0.02207(13)	0.033
H(311)	0.6158(5)	1.4901(4)	0.09241(12)	0.0303
C(33)	0.4168(5)	1.4672(4)	0.16083(12)	0.0257
H(331)	0.5130(5)	1.5326(4)	0.16411(12)	0.0285
H(332)	0.4387(5)	1.3662(4)	0.17251(12)	0.0285
C(34)	0.2707(5)	1.5414(4)	0.18378(11)	0.0243
H(341)	0.2549(5)	1.6458(4)	0.17362(11)	0.0301
H(342)	0.2926(5)	1.5447(4)	0.21294(11)	0.0301
C(35)	-0.0820(5)	1.2414(4)	0.08169(12)	0.0272
H(351)	-0.1983(5)	1.2269(4)	0.07606(12)	0.0307
H(352)	-0.0256(5)	1.1428(4)	0.07956(12)	0.0307
C(36)	-0.0064(5)	1.3543(4)	0.04982(11)	0.0245
H(361)	-0.0699(5)	1.4494(4)	0.04966(11)	0.0288
H(362)	-0.0100(5)	1.3074(4)	0.02288(11)	0.0288

Atom	u(11)	u(22)	u(33)	u(23)	u(13)	u(12)
C(1)	0.0125(15)	0.0134(13)	0.029(2)	-0.0017(13)	0.0033(15)	-0.0041(12)
C(2)	0.0188(18)	0.0210(15)	0.0239(18)	0.0023(13)	-0.0021(16)	-0.0075(13)
C(6)	0.0206(17)	0.0125(13)	0.029(2)	0.0016(13)	-0.0053(16)	-0.0029(13)
C(7)	0.0213(17)	0.0096(12)	0.031(2)	0.0006(12)	0.0019(16)	-0.0028(13)
C(8)	0.0260(18)	0.0128(13)	0.028(2)	0.0024(12)	0.0015(16)	0.0001(14)
C(12)	0.0241(18)	0.0128(13)	0.028(2)	0.0022(12)	0.0007(16)	-0.0012(13)
C(3)	0.027(2)	0.0246(16)	0.0252(18)	-0.0014(13)	-0.0026(16)	-0.0082(14)
C(4)	0.0214(18)	0.0221(16)	0.041(2)	-0.0053(14)	0.0120(18)	-0.0050(14)
C(5)	0.0213(17)	0.0168(14)	0.037(2)	-0.0047(14)	0.0020(16)	-0.0001(15)
C(9)	0.0284(19)	0.0155(13)	0.0252(18)	0.0006(14)	0.0027(16)	0.0005(14)
C(10)	0.0224(18)	0.0156(13)	0.037(2)	-0.0031(14)	0.0103(17)	-0.0002(14)
C(11)	0.0211(17)	0.0141(13)	0.036(2)	-0.0003(14)	0.0008(18)	0.0042(14)
C(13)	0.0093(14)	0.0194(14)	0.033(2)	0.0010(13)	-0.0010(15)	0.0036(13)
C(14)	0.0253(18)	0.0242(15)	0.0187(18)	0.0012(14)	-0.0042(16)	-0.0056(15)
C(15)	0.026(2)	0.0164(14)	0.031(2)	0.0032(13)	-0.0085(18)	0.0010(13)
C(16)	0.037(2)	0.0203(15)	0.0197(17)	0.0010(13)	-0.0068(17)	0.0031(16)
C(21)	0.0192(17)	0.0134(13)	0.031(2)	0.0006(12)	-0.0027(17)	0.0036(13)
C(22)	0.0214(16)	0.0160(13)	0.0263(19)	0.0013(13)	-0.0029(16)	0.0089(14)
C(26)	0.0177(16)	0.0137(13)	0.035(2)	0.0025(14)	-0.0019(15)	0.0051(13)
C(27)	0.0258(17)	0.0084(12)	0.032(2)	0.0014(13)	0.0017(17)	0.0043(13)
C(28)	0.033(2)	0.0107(13)	0.0256(18)	0.0006(12)	0.0012(18)	0.0018(14)
C(32)	0.0203(17)	0.0111(12)	0.035(2)	0.0006(13)	-0.0017(17)	0.0040(13)
C(23)	0.0300(19)	0.0254(16)	0.027(2)	0.0011(14)	-0.0018(18)	0.0075(17)
C(24)	0.0191(18)	0.0332(19)	0.041(2)	0.0103(17)	0.0103(17)	0.0120(16)
C(25)	0.0194(18)	0.0204(15)	0.041(2)	0.0036(14)	-0.0013(18)	0.0056(15)
C(29)	0.046(2)	0.0149(14)	0.027(2)	0.0032(13)	0.0000(19)	0.0075(16)
C(30)	0.031(2)	0.0157(14)	0.041(2)	0.0035(15)	0.0140(19)	0.0032(14)
C(31)	0.0213(17)	0.0120(13)	0.047(2)	0.0034(14)	0.0015(18)	0.0014(14)
C(33)	0.0219(17)	0.0180(13)	0.037(2)	0.0028(15)	0.0000(17)	-0.0020(15)
C(34)	0.0251(18)	0.0231(15)	0.0246(18)	-0.0015(14)	-0.0097(15)	0.0011(15)
C(35)	0.0248(19)	0.0169(14)	0.040(2)	-0.0016(14)	-0.0069(19)	0.0012(14)
C(36)	0.0248(17)	0.0178(14)	0.0311(19)	-0.0069(14)	-0.0081(18)	0.0043(15)

	angle /°
C(2) - C(1) - C(6)	120.2(3)
C(2) - C(1) - C(7)	119.6(3)
C(6) - C(1) - C(7)	120.3(3)
C(1) - C(2) - C(3)	119.5(3)
C(1) - C(2) - C(14)	118.2(3)
C(3) - C(2) - C(14)	122.3(3)
C(1) - C(6) - C(5)	118.6(3)
C(1) - C(6) - C(15)	118.4(3)
C(5) - C(6) - C(15)	122.9(3)
C(1) - C(7) - C(8)	119.1(3)
C(1) - C(7) - C(12)	119.5(3)
C(8) - C(7) - C(12)	121.4(3)
C(7) - C(8) - C(9)	118.3(3)
C(7) - C(8) - C(16)	119.3(3)
C(9) - C(8) - C(16)	122.4(3)
C(7) - C(12) - C(11)	118.2(3)
C(7) - C(12) - C(13)	118.9(3)
C(11) - C(12) - C(13)	122.9(3)
C(2) - C(3) - C(4)	120.4(4)
C(3) - C(4) - C(5)	119.5(4)
C(6) - C(5) - C(4)	121.8(3)
C(8) - C(9) - C(10)	121.1(4)
C(9) - C(10) - C(11)	119.4(4)
C(12) - C(11) - C(10)	121.7(3)
C(12) - C(13) - C(14)	111.4(3)
C(2) - C(14) - C(13)	110.8(3)
C(6) - C(15) - C(16)	111.2(3)
C(8) - C(16) - C(15)	111.0(3)
C(22) - C(21) - C(26)	120.5(3)
C(22) - C(21) - C(27)	119.7(3)
C(26) - C(21) - C(27)	119.7(3)
C(21) - C(22) - C(23)	119.4(3)
C(21) - C(22) - C(34)	117.5(3)
C(23) - C(22) - C(34)	123.1(3)
C(21) - C(26) - C(25)	118.8(3)
C(21) - C(26) - C(35)	119.0(3)

C(25) - C(26) - C(35)	122.2(3)
C(21) - C(27) - C(28)	119.5(3)
C(21) - C(27) - C(32)	120.0(4)
C(28) - C(27) - C(32)	120.5(4)
C(27) - C(28) - C(29)	118.9(4)
C(27) - C(28) - C(36)	117.7(3)
C(29) - C(28) - C(36)	123.4(4)
C(27) - C(32) - C(31)	119.2(4)
C(27) - C(32) - C(33)	118.0(3)
C(31) - C(32) - C(33)	122.8(3)
C(22) - C(23) - C(24)	120.5(4)
C(23) - C(24) - C(25)	119.6(4)
C(26) - C(25) - C(24)	121.2(3)
C(28) - C(29) - C(30)	120.9(4)
C(29) - C(30) - C(31)	119.9(4)
C(32) - C(31) - C(30)	120.7(4)
C(32) - C(33) - C(34)	111.5(3)
C(22) - C(34) - C(33)	110.1(3)
C(26) - C(35) - C(36)	110.8(3)
C(28) - C(36) - C(35)	110.8(3)

	distance / Å
C(1) - C(2)	1.402(5)
C(1) - C(6)	1.405(5)
C(1) - C(7)	1.483(5)
C(2) - C(3)	1.384(5)
C(2) - C(14)	1.520(5)
C(6) - C(5)	1.388(5)
C(6) - C(15)	1.511(5)
C(7) - C(8)	1.398(5)
C(7) - C(12)	1.402(5)
C(8) - C(9)	1.396(5)
C(8) - C(16)	1.504(5)
C(12) - C(11)	1.397(5)
C(12) - C(13)	1.503(5)
C(3) - C(4)	1.399(5)
C(4) - C(5)	1.370(6)
C(9) - C(10)	1.396(5)
C(10) - C(11)	1.371(6)
C(13) - C(14)	1.517(5)
C(15) - C(16)	1.532(5)
C(21) - C(22)	1.405(5)
C(21) - C(26)	1.407(5)
C(21) - C(27)	1.467(5)
C(22) - C(23)	1.381(5)
C(22) - C(34)	1.517(5)
C(26) - C(25)	1.389(5)
C(26) - C(35)	1.501(5)
C(27) - C(28)	1.412(5)
C(27) - C(32)	1.398(5)
C(28) - C(29)	1.385(6)
C(28) - C(36)	1.518(5)
C(32) - C(31)	1.397(5)
C(32) - C(33)	1.499(5)
C(23) - C(24)	1.403(6)
C(24) - C(25)	1.387(6)
C(29) - C(30)	1.397(6)
C(30) - C(31)	1.380(6)
C(33) - C(34)	1.512(5)
C(35) - C(36)	1.522(5)

8.5 2,7-Dibromopyrene (5-95)

Atom	x/a	y/b	z/c	U(iso)
Br(1)	0.35018(5)	0.5	0.01127(13)	0.0222
C(4)	0.0452(4)	0.5	0.4311(10)	0.0175
C(5)	0.0429(3)	0.2738(3)	0.4346(8)	0.0203

C(1)	0.2239(4)	0.5	0.1753(10)	0.0182
C(3)	0.0909(3)	0.3870(3)	0.3662(7)	0.017
C(2)	0.1805(3)	0.3876(3)	0.2351(8)	0.0199
H(51)	0.0718(3)	0.1978(3)	0.3864(8)	0.0277
H(21)	0.2110(3)	0.3125(3)	0.1875(8)	0.0252

Atom	u(11)	u(22)	u(33)	u(23)	u(13)	u(12)
Br(1)	0.0186(2)	0.0284(3)	0.0218(2)	0	0.00941(16)	0
C(4)	0.017(2)	0.017(2)	0.018(2)	0	0.0038(17)	0
C(5)	0.0184(15)	0.0173(16)	0.0221(15)	-0.0011(13)	0.0018(13)	-0.0001(12)
C(1)	0.0134(19)	0.028(3)	0.0132(19)	0	0.0037(16)	0
C(3)	0.0143(13)	0.0164(16)	0.0185(14)	-0.0005(12)	0.0024(11)	0.0008(12)
C(2)	0.0176(14)	0.0209(15)	0.0177(14)	-0.0009(13)	0.0005(12)	0.0015(13)

	angle /°
C(4) - C(4) - C(3)	119.9(2)
C(4) - C(4) - C(3)	119.9(2)
C(3) - C(4) - C(3)	120.1(4)
C(5) - C(5) - C(3)	121.10(19)
C(5) - C(5) - H(51)	119.677(5)
C(3) - C(5) - H(51)	119.22(19)
Br(1) - C(1) - C(2)	118.6(2)
Br(1) - C(1) - C(2)	118.6(2)
C(2) - C(1) - C(2)	122.8(4)
C(4) - C(3) - C(5)	118.9(3)
C(4) - C(3) - C(2)	119.7(3)
C(5) - C(3) - C(2)	121.4(3)
C(1) - C(2) - C(3)	118.8(3)
C(1) - C(2) - H(21)	120.7(2)
C(3) - C(2) - H(21)	120.5(2)

	distance /Å
Br(1) - C(1)	1.907(5)
C(4) - C(4)	1.428(9)
C(4) - C(3)	1.417(4)
C(4) - C(3)	1.417(4)
C(5) - C(5)	1.357(7)
C(5) - C(3)	1.438(5)
C(5) - H(51)	0.95
C(1) - C(2)	1.391(4)
C(1) - C(2)	1.391(4)
C(3) - C(2)	1.399(5)
C(2) - H(21)	0.95

8.6 5,5',5'',5''',5'''',5'''''-Hexatrimethylsilyl-hexa-m-phenylene (5-105)

Atom	x/a	y/b	z/c	U(iso)	Occ
Si(1)	-0.15915(6)	0	0.27609(3)	0.0168	
Si(2)	0.12921(4)	0.29368(2)	0.144659(18)	0.0171	
C(1)	-0.1015(2)	0	0.20918(9)	0.0145	
C(3)	-0.03024(14)	0.05768(8)	0.13524(6)	0.0138	
C(5)	-0.00411(14)	0.11777(8)	0.10828(6)	0.0138	
C(7)	0.06521(15)	0.22650(8)	0.10791(6)	0.0155	
C(9)	0.00685(15)	0.17603(8)	0.02813(6)	0.0142	
C(2)	-0.07706(15)	0.05677(8)	0.18418(6)	0.0149	
C(4)	-0.0075(2)	0.000000(7)	0.11151(9)	0.0149	
C(6)	0.03745(15)	0.17039(8)	0.13358(6)	0.0157	
C(8)	0.04842(15)	0.22824(8)	0.05501(6)	0.0162	
C(10)	-0.01979(15)	0.12160(8)	0.05541(6)	0.0147	
H(21)	-0.09265(15)	0.09560(8)	0.20085(6)	0.0207	
H(41)	0.0248(2)	0.000000(7)	0.07835(9)	0.0206	

H(61)	0.04791(15)	0.16837(8)	0.16945(6)	0.0218	
H(81)	0.06530(15)	0.26586(8)	0.03685(6)	0.0225	
H(101)	-0.04948(15)	0.08620(8)	0.03771(6)	0.0204	
C(11)	-0.0361(3)	0.000000(7)	0.32046(11)	0.0309	
H(111)	-0.0617(3)	0.000000(7)	0.35479(11)	0.0413	
H(112)	0.0085(3)	-0.036403(7)	0.31424(11)	0.0413	
C(12)	-0.24811(18)	-0.07151(9)	0.28614(8)	0.0287	
H(121)	-0.31044(18)	-0.07047(9)	0.26343(8)	0.0396	
H(122)	-0.27465(18)	-0.07224(9)	0.32032(8)	0.0396	
H(123)	-0.20446(18)	-0.10825(9)	0.27977(8)	0.0396	
C(13)	0.25912(18)	0.26399(10)	0.17614(9)	0.0317	
H(131)	0.31141(18)	0.25039(10)	0.15102(9)	0.0422	
H(132)	0.29180(18)	0.29683(10)	0.19588(9)	0.0422	
H(133)	0.24037(18)	0.22957(10)	0.19774(9)	0.0422	
C(14)	0.0276(2)	0.32039(10)	0.19429(8)	0.0324	
H(141)	-0.0387(2)	0.33561(10)	0.17815(8)	0.0416	
H(142)	0.0604(2)	0.35320(10)	0.21401(8)	0.0416	
H(143)	0.0089(2)	0.28594(10)	0.21587(8)	0.0416	
C(15)	0.1655(2)	0.36061(10)	0.10167(8)	0.0325	
H(151)	0.2177(2)	0.34651(10)	0.07667(8)	0.0444	
H(152)	0.1984(2)	0.39377(10)	0.12099(8)	0.0444	
H(153)	0.0992(2)	0.37555(10)	0.08534(8)	0.0444	
C(21)	0.3256(3)	0.14441(17)	0.05250(15)	0.0752	
H(211)	0.3844(3)	0.16914(17)	0.06680(15)	0.0983	
H(212)	0.3017(3)	0.16279(17)	0.02128(15)	0.0983	
H(213)	0.2640(3)	0.14286(17)	0.07559(15)	0.0983	
C(22)	0.3647(7)	0.0827(3)	0.0433(3)	0.0708	0.5
H(221)	0.4267(7)	0.0852(3)	0.0205(3)	0.1077	0.5
H(222)	0.3890(7)	0.0652(3)	0.0748(3)	0.1077	0.5
C(23)	0.2748(7)	0.0351(3)	0.0171(3)	0.0788	0.5
H(231)	0.2713(7)	0.0376(3)	-0.0190(3)	0.1077	0.5
H(232)	0.2016(7)	0.0412(3)	0.0309(3)	0.1077	0.5
C(24)	0.2816(7)	0.0793(3)	0.0489(3)	0.0708	0.5
H(241)	0.2482(7)	0.0720(3)	0.0813(3)	0.1077	0.5
H(242)	0.2246(7)	0.0805(3)	0.0235(3)	0.1077	0.5
C(25)	0.3256(7)	0.0306(3)	0.0405(3)	0.0788	0.5
H(251)	0.3641(7)	0.0200(3)	0.0711(3)	0.1077	0.5
H(252)	0.3788(7)	0.0426(3)	0.0152(3)	0.1077	0.5

Atom	**u(11)**	**u(22)**	**u(33)**	**u(23)**	**u(13)**	**u(12)**
Si(1)	0.0227(4)	0.0150(3)	0.0128(3)	0	0.0057(3)	0
Si(2)	0.0223(2)	0.01242(19)0	.01647(19)	-0.0016(2)	-0.0028(2)	-0.0033(2)
C(1)	0.0145(12)	0.0175(11)	0.0116(10)	0	0.0028(9)	0
C(3)	0.0163(8)	0.0126(7)	0.0124(7)	0.0013(6)	-0.0013(6)	0.0000(6)
C(5)	0.0159(8)	0.0128(7)	0.0125(7)	0.0009(6)	0.0015(6)	0.0013(6)
C(7)	0.0182(8)	0.0133(7)	0.0149(7)	-0.0024(6)	-0.0024(6)	-0.0001(6)
C(9)	0.0166(8)	0.0137(7)	0.0122(7)	-0.0003(6)	-0.0012(6)	0.0010(6)
C(2)	0.0182(8)	0.0135(7)	0.0131(7)	-0.0018(6)	0.0009(6)	0.0009(7)
C(4)	0.0176(12)	0.0157(11)	0.0114(10)	0	0.0018(9)	0
C(6)	0.0210(8)	0.0142(8)	0.0120(7)	-0.0021(6)	-0.0005(6)	0.0009(7)
C(8)	0.0224(9)	0.0119(7)	0.0144(7)	0.0015(6)	0.0020(7)	-0.0013(7)
C(10)	0.0193(8)	0.0124(7)	0.0125(7)	-0.0026(6)	0.0001(6)	-0.0008(7)
C(11)	0.0415(18)	0.0301(15)	0.0212(13)	0	0.0074(13)	0
C(12)	0.0325(11)	0.0250(10)	0.0288(10)	0.0007(8)	0.0123(9)	-0.0073(9)
C(13)	0.0291(11)	0.0267(11)	0.0392(12)	-0.0045(9)	-0.0147(9)	-0.0017(9)
C(14)	0.0390(13)	0.0258(10)	0.0324(11)	-0.0142(9)	0.0064(10)	-0.0079(10)
C(15)	0.0453(13)	0.0219(9)	0.0301(10)	0.0054(8)	-0.0050(10)	-0.0122(9)
C(21)	0.067(2)	0.076(2)	0.082(2)	-0.015(2)	0.0008(19)	-0.017(2)
C(22)	0.0708(11)	0.0708(11)	0.0708(11)	0.0002(11)	0.0002(11)	0.0002(11)
C(23)	0.0788(12)	0.0788(12)	0.0788(12)	-0.0106(12)	-0.0106(12)	-0.0106(12)
C(24)	0.0708(11)	0.0708(11)	0.0708(11)	0.0002(11)	0.0002(11)	0.0002(11)
C(25)	0.0788(12)	0.0788(12)	0.0788(12)	-0.0106(12)	-0.0106(12)	-0.0106(12)

	angle /°
C(1) - Si(1) - C(11)	107.23(13)
C(1) - Si(1) - C(12)	109.72(8)
C(11) - Si(1) - C(12)	110.76(9)
C(1) - Si(1) - C(12)	109.72(8)
C(11) - Si(1) - C(12)	110.76(9)
C(12) - Si(1) - C(12)	108.63(14)
C(7) - Si(2) - C(13)	107.85(9)

C(7) - Si(2) - C(14)	109.06(9)
C(13) - Si(2) - C(14)	109.26(11)
C(7) - Si(2) - C(15)	111.11(9)
C(13) - Si(2) - C(15)	109.55(11)
C(14) - Si(2) - C(15)	109.96(11)
Si(1) - C(1) - C(2)	120.75(11)
Si(1) - C(1) - C(2)	120.75(11)
C(2) - C(1) - C(2)	118.4(2)
C(5) - C(3) - C(2)	122.01(15)
C(5) - C(3) - C(4)	119.75(15)
C(2) - C(3) - C(4)	118.24(16)
C(3) - C(5) - C(6)	122.29(15)
C(3) - C(5) - C(10)	119.44(15)
C(6) - C(5) - C(10)	118.26(15)
Si(2) - C(7) - C(6)	119.35(13)
Si(2) - C(7) - C(8)	123.02(13)
C(6) - C(7) - C(8)	117.56(16)
C(9) - C(9) - C(8)	122.57(11)
C(9) - C(9) - C(10)	119.04(11)
C(8) - C(9) - C(10)	118.37(15)
C(1) - C(2) - C(3)	121.57(17)
C(3) - C(4) - C(3)	121.9(2)
C(5) - C(6) - C(7)	122.29(15)
C(7) - C(8) - C(9)	121.79(16)
C(5) - C(10) - C(9)	121.71(16)
C(22) - C(21) - C(24)	40.4(4)
C(21) - C(22) - C(23)	115.7(6)
C(21) - C(22) - C(24)	73.5(7)
C(23) - C(22) - C(24)	50.8(6)
C(21) - C(22) - C(25)	137.6(8)
C(23) - C(22) - C(25)	31.5(5)
C(24) - C(22) - C(25)	64.1(7)
C(22) - C(23) - C(23)	128.4(4)
C(22) - C(23) - C(24)	38.0(5)
C(23) - C(23) - C(24)	138.2(5)
C(22) - C(23) - C(25)	46.4(7)
C(23) - C(23) - C(25)	83.6(8)
C(24) - C(23) - C(25)	64.5(8)
C(22) - C(23) - C(25)	97.3(5)
C(23) - C(23) - C(25)	31.7(3)
C(24) - C(23) - C(25)	111.3(7)
C(25) - C(23) - C(25)	51.9(8)
C(21) - C(24) - C(22)	66.1(6)
C(21) - C(24) - C(23)	139.6(8)
C(22) - C(24) - C(23)	91.2(8)
C(21) - C(24) - C(25)	132.4(8)
C(22) - C(24) - C(25)	66.3(7)
C(23) - C(24) - C(25)	41.5(5)
C(22) - C(25) - C(23)	102.2(10)
C(22) - C(25) - C(23)	161.6(9)
C(23) - C(25) - C(23)	64.7(8)
C(22) - C(25) - C(24)	49.7(5)
C(23) - C(25) - C(24)	74.1(9)
C(23) - C(25) - C(24)	130.7(8)
C(22) - C(25) - C(25)	157.0(6)
C(23) - C(25) - C(25)	96.4(8)
C(23) - C(25) - C(25)	31.7(3)
C(24) - C(25) - C(25)	151.2(6)

	distance /Å
Si(1) - C(1)	1.883(2)
Si(1) - C(11)	1.867(3)
Si(1) - C(12)	1.8658(19)
Si(1) - C(12)	1.8658(19)
Si(2) - C(7)	1.8796(17)
Si(2) - C(13)	1.859(2)
Si(2) - C(14)	1.863(2)
Si(2) - C(15)	1.862(2)
C(1) - C(2)	1.400(2)
C(1) - C(2)	1.400(2)
C(3) - C(5)	1.489(2)
C(3) - C(2)	1.399(2)

C(3) - C(4)	1.398(2)
C(5) - C(6)	1.388(2)
C(5) - C(10)	1.401(2)
C(7) - C(6)	1.406(2)
C(7) - C(8)	1.402(2)
C(9) - C(9)	1.484(3)
C(9) - C(8)	1.402(2)
C(9) - C(10)	1.394(2)
C(21) - C(22)	1.409(8)
C(21) - C(24)	1.478(8)
C(22) - C(23)	1.620(10)
C(22) - C(24)	0.999(9)
C(22) - C(25)	1.200(9)
C(23) - C(23)	1.489(14)
C(23) - C(24)	1.256(10)
C(23) - C(25)	0.865(9)
C(23) - C(25)	1.636(8)
C(24) - C(25)	1.179(9)
C(25) - C(25)	1.296(15)

8.7 5,5',5'',5''',5'''',5'''''-Hexa-ethynyltri-iso-propylsilyl-cyclohexa-m-phenylene (5-107)

Atom	x/a	y/b	z/c	U(iso)
Si(1)	0.37150(9)	0.99935(7)	0.13516(6)	0.0296
Si(2)	1.03330(8)	0.75695(7)	0.09330(6)	0.0284
Si(3)	0.94898(9)	0.12468(7)	0.27904(6)	0.0354
C(1)	0.4001(3)	0.7062(2)	-0.00696(19)	0.0192
C(3)	0.5456(2)	0.68482(19)	0.04626(18)	0.014
C(5)	0.4422(3)	0.7941(2)	0.0550(2)	0.0215
C(7)	0.6321(3)	0.6385(2)	0.06077(17)	0.0166
C(9)	0.7193(2)	0.5136(2)	0.07377(19)	0.0181
C(11)	0.7932(3)	0.6291(2)	0.0784(2)	0.0228
C(13)	0.7196(2)	0.4280(2)	0.0777(2)	0.0206
C(15)	0.6629(3)	0.3206(2)	0.0462(2)	0.0217
C(17)	0.7755(3)	0.2937(2)	0.1287(2)	0.0255
C(19)	0.4205(3)	0.8604(2)	0.0799(2)	0.0241
C(20)	0.4022(3)	0.9162(2)	0.1004(2)	0.0264
C(30)	0.8735(3)	0.6661(2)	0.0854(2)	0.0247
C(31)	0.9403(3)	0.6961(2)	0.0884(2)	0.0302
C(41)	0.8315(3)	0.2384(2)	0.1781(2)	0.0273
C(42)	0.8791(3)	0.1951(2)	0.2179(2)	0.0299
C(2)	0.4844(2)	0.6658(2)	0.00778(19)	0.0181
C(4)	0.5239(3)	0.7501(2)	0.0703(2)	0.0217
C(6)	0.3820(3)	0.7711(2)	0.0177(2)	0.0241
C(8)	0.6366(2)	0.5591(2)	0.0638(2)	0.0201
C(10)	0.7946(2)	0.5490(2)	0.08084(18)	0.0203
C(12)	0.7097(3)	0.6722(2)	0.06874(19)	0.0205
C(14)	0.6657(3)	0.4005(2)	0.03957(19)	0.0197
C(16)	0.7186(3)	0.2664(2)	0.0910(2)	0.0247
C(18)	0.7759(3)	0.3740(2)	0.1229(2)	0.0249
C(21)	0.2643(3)	0.9748(2)	0.1855(2)	0.0344
C(24)	0.3589(4)	1.0914(2)	0.0659(2)	0.0424
C(27)	0.4634(3)	1.0020(3)	0.1921(3)	0.0502
C(32)	0.9830(3)	0.8285(2)	0.1370(3)	0.0393
C(35)	1.0748(3)	0.8031(3)	0.0064(2)	0.0474
C(38)	1.1216(3)	0.6890(2)	0.1437(2)	0.0284
C(43)	1.0555(3)	0.1711(3)	0.2849(2)	0.0416
C(46)	0.8845(4)	0.1002(3)	0.3601(3)	0.0523
C(49)	0.9732(4)	0.0385(3)	0.2451(3)	0.058
H(21)	0.4994(2)	0.6227(2)	-0.00954(19)	0.0187
H(41)	0.5640(3)	0.7640(2)	0.0977(2)	0.0266
H(61)	0.3260(3)	0.7997(2)	0.0091(2)	0.0263
H(81)	0.5837(2)	0.5350(2)	0.0590(2)	0.0209
H(101)	0.8498(2)	0.5188(2)	0.08704(18)	0.0219
H(121)	0.7068(3)	0.7263(2)	0.06696(19)	0.029
H(141)	0.6293(3)	0.4371(2)	0.00817(19)	0.0199
H(161)	0.7180(3)	0.2117(2)	0.0955(2)	0.0247
H(181)	0.8152(3)	0.3920(2)	0.1483(2)	0.0253
H(211)	0.2500(3)	1.0161(2)	0.2050(2)	0.0442
H(241)	0.4185(4)	1.1053(2)	0.0524(2)	0.0489
H(271)	0.4788(3)	0.9500(3)	0.2184(3)	0.0734
H(321)	1.0275(3)	0.8642(2)	0.1367(3)	0.0476
H(351)	1.1161(3)	0.7642(3)	-0.0024(2)	0.0656

H(381)	1.0916(3)	0.6609(2)	0.1836(2)	0.0407
H(431)	1.0811(3)	0.1396(3)	0.3247(2)	0.0576
H(461)	0.9261(4)	0.0738(3)	0.3926(3)	0.0676
H(491)	1.0126(4)	0.0566(3)	0.2078(3)	0.057
C(22)	0.2737(3)	0.8976(3)	0.2402(2)	0.0447
H(221)	0.3220(3)	0.9001(3)	0.2665(2)	0.0511
H(222)	0.2204(3)	0.8883(3)	0.2672(2)	0.0511
H(223)	0.2859(3)	0.8560(3)	0.2208(2)	0.0511
C(23)	0.1843(3)	0.9715(3)	0.1440(3)	0.0518
H(231)	0.1774(3)	1.0202(3)	0.1103(3)	0.0622
H(232)	0.1308(3)	0.9624(3)	0.1708(3)	0.0622
H(233)	0.1963(3)	0.9300(3)	0.1244(3)	0.0622
C(25)	0.3068(5)	1.1588(3)	0.0873(3)	0.0732
H(251)	0.3017(5)	1.2051(3)	0.0510(3)	0.0739
H(252)	0.3372(5)	1.1696(3)	0.1216(3)	0.0739
H(253)	0.2488(5)	1.1419(3)	0.1033(3)	0.0739
C(26)	0.3207(4)	1.0824(3)	0.0020(3)	0.0552
H(261)	0.3178(4)	1.1316(3)	-0.0315(3)	0.0559
H(262)	0.2621(4)	1.0644(3)	0.0134(3)	0.0559
H(263)	0.3562(4)	1.0451(3)	-0.0140(3)	0.0559
C(28)	0.5525(5)	1.0290(6)	0.1519(4)	0.1136
H(281)	0.5669(5)	0.9973(6)	0.1232(4)	0.065
H(282)	0.5453(5)	1.0826(6)	0.1265(4)	0.065
H(283)	0.5994(5)	1.0232(6)	0.1816(4)	0.065
C(29)	0.4382(5)	1.0509(3)	0.2390(3)	0.0723
H(291)	0.3841(5)	1.0311(3)	0.2612(3)	0.08
H(292)	0.4285(5)	1.1050(3)	0.2153(3)	0.08
H(293)	0.4827(5)	1.0456(3)	0.2705(3)	0.08
C(33)	0.9580(3)	0.7875(3)	0.2093(3)	0.058
H(331)	0.9333(3)	0.8253(3)	0.2300(3)	0.0592
H(332)	1.0096(3)	0.7615(3)	0.2316(3)	0.0592
H(333)	0.9150(3)	0.7501(3)	0.2110(3)	0.0592
C(34)	0.9010(4)	0.8751(4)	0.1005(3)	0.0822
H(341)	0.8769(4)	0.9111(4)	0.1232(3)	0.0789
H(342)	0.9191(4)	0.9033(4)	0.0566(3)	0.0789
H(343)	0.8568(4)	0.8398(4)	0.0992(3)	0.0789
C(36)	1.1285(4)	0.8779(3)	-0.0012(3)	0.0586
H(361)	1.1483(4)	0.8984(3)	-0.0461(3)	0.0661
H(362)	1.1787(4)	0.8645(3)	0.0262(3)	0.0661
H(363)	1.0907(4)	0.9164(3)	0.0115(3)	0.0661
C(37)	1.0029(4)	0.8228(4)	-0.0462(3)	0.0738
H(371)	1.0284(4)	0.8462(4)	-0.0891(3)	0.0911
H(372)	0.9576(4)	0.8578(4)	-0.0359(3)	0.0911
H(373)	0.9775(4)	0.7749(4)	-0.0454(3)	0.0911
C(39)	1.1938(3)	0.7308(3)	0.1656(3)	0.0555
H(391)	1.1663(3)	0.7673(3)	0.1866(3)	0.0596
H(392)	1.2289(3)	0.7581(3)	0.1281(3)	0.0596
H(393)	1.2310(3)	0.6934(3)	0.1958(3)	0.0596
C(40)	1.1630(3)	0.6286(3)	0.1102(3)	0.0601
H(401)	1.1163(3)	0.6035(3)	0.0973(3)	0.0645
H(402)	1.1978(3)	0.6549(3)	0.0722(3)	0.0645
H(403)	1.1999(3)	0.5903(3)	0.1399(3)	0.0645
C(44)	1.0419(4)	0.2561(3)	0.2868(3)	0.0697
H(441)	0.9990(4)	0.2562(3)	0.3215(3)	0.0791
H(442)	1.0963(4)	0.2747(3)	0.2958(3)	0.0791
H(443)	1.0203(4)	0.2895(3)	0.2462(3)	0.0791
C(45)	1.1253(4)	0.1693(4)	0.2300(4)	0.0802
H(451)	1.1341(4)	0.1165(4)	0.2281(4)	0.0923
H(452)	1.1803(4)	0.1872(4)	0.2385(4)	0.0923
H(453)	1.1043(4)	0.2020(4)	0.1889(4)	0.0923
C(47)	0.8453(4)	0.1737(4)	0.3781(3)	0.0693
H(471)	0.8136(4)	0.1596(4)	0.4197(3)	0.0779
H(472)	0.8925(4)	0.2060(4)	0.3798(3)	0.0779
H(473)	0.8058(4)	0.2018(4)	0.3446(3)	0.0779
C(48)	0.8103(4)	0.0442(3)	0.3654(3)	0.0728
H(481)	0.7799(4)	0.0332(3)	0.4075(3)	0.0873
H(482)	0.8354(4)	-0.0035(3)	0.3588(3)	0.0873
H(483)	0.7694(4)	0.0684(3)	0.3318(3)	0.0873
C(50)	1.0223(5)	-0.0318(3)	0.2957(3)	0.0792
H(501)	1.0730(5)	-0.0145(3)	0.3114(3)	0.0721
H(502)	1.0406(5)	-0.0728(3)	0.2766(3)	0.0721
H(503)	0.9808(5)	-0.0510(3)	0.3316(3)	0.0721
C(51)	0.8945(6)	0.0116(3)	0.2186(3)	0.1003
H(511)	0.8676(6)	0.0547(3)	0.1862(3)	0.0889
H(512)	0.9125(6)	-0.0293(3)	0.1993(3)	0.0889
H(513)	0.8527(6)	-0.0075(3)	0.2542(3)	0.0889
C(201)	0.0309(5)	0.4978(7)	0.0242(5)	0.1305

H(2011)	0.0065(5)	0.5293(7)	0.0510(5)	0.12
H(2012)	0.0845(5)	0.5193(7)	0.0023(5)	0.12
C(202)	0.0490(6)	0.4113(6)	0.0713(5)	0.1099
H(2021)	-0.0004(6)	0.3963(6)	0.1016(5)	0.12
H(2022)	0.0578(6)	0.3760(6)	0.0452(5)	0.12
C(203)	0.1304(5)	0.4050(6)	0.1083(5)	0.1333
H(2031)	0.1373(5)	0.3517(6)	0.1347(5)	0.12
H(2032)	0.1236(5)	0.4384(6)	0.1362(5)	0.12
H(2033)	0.1818(5)	0.4182(6)	0.0798(5)	0.12
Si(11)	1.44923(9)	0.38691(7)	0.25200(7)	0.0346
Si(12)	1.03787(8)	0.49370(6)	0.64063(6)	0.0203
Si(13)	0.42345(8)	0.24718(8)	0.63952(7)	0.0356
C(101)	1.2261(2)	0.0718(2)	0.42369(18)	0.0157
C(103)	1.1464(3)	0.1754(2)	0.46345(19)	0.0174
C(105)	1.2716(3)	0.2074(2)	0.3825(2)	0.0283
C(107)	1.0723(2)	0.1972(2)	0.50597(19)	0.0158
C(109)	0.9217(2)	0.1782(2)	0.55620(19)	0.016
C(111)	1.0105(3)	0.2788(2)	0.57433(19)	0.0191
C(113)	0.8385(2)	0.1335(2)	0.56624(17)	0.0158
C(115)	0.7655(3)	0.0118(2)	0.57727(18)	0.0192
C(117)	0.6771(3)	0.1282(2)	0.5867(2)	0.0226
C(119)	1.3266(3)	0.2668(2)	0.3404(2)	0.0271
C(120)	1.3744(3)	0.3154(2)	0.3073(2)	0.0301
C(130)	1.0197(3)	0.3439(2)	0.6012(2)	0.02
C(131)	1.0270(2)	0.4003(2)	0.6199(2)	0.0198
C(141)	0.5928(3)	0.1663(2)	0.5985(2)	0.0265
C(142)	0.5252(3)	0.1984(2)	0.6119(2)	0.0317
C(102)	1.1593(2)	0.0953(2)	0.46448(18)	0.0128
C(104)	1.2017(2)	0.2294(2)	0.42322(18)	0.0163
C(106)	1.2812(2)	0.1296(2)	0.38273(19)	0.0192
C(108)	0.9924(3)	0.1596(2)	0.51614(18)	0.0182
C(110)	0.9322(3)	0.2379(2)	0.58564(19)	0.0178
C(112)	1.0806(2)	0.2574(2)	0.53582(19)	0.0163
C(114)	0.8420(3)	0.0554(2)	0.56709(19)	0.0176
C(116)	0.6829(3)	0.0498(2)	0.58673(18)	0.018
C(118)	0.7550(2)	0.1708(2)	0.57532(19)	0.0211
C(121)	1.3902(4)	0.4881(3)	0.2366(3)	0.0584
C(124)	1.4597(3)	0.3583(3)	0.1724(3)	0.0498
C(127)	1.5613(3)	0.3750(3)	0.2925(3)	0.0424
C(132)	1.1123(3)	0.5545(2)	0.5728(2)	0.0277
C(135)	1.0798(3)	0.4670(2)	0.7281(2)	0.0259
C(138)	0.9211(3)	0.5441(3)	0.6384(2)	0.0323
C(143)	0.4476(5)	0.2687(7)	0.7167(5)	0.1582
C(146)	0.3863(4)	0.3326(4)	0.5693(4)	0.0834
C(149)	0.3382(5)	0.1739(4)	0.6578(6)	0.1378
H(1021)	1.1234(2)	0.0569(2)	0.49368(18)	0.0142
H(1041)	1.1929(2)	0.2833(2)	0.42180(18)	0.016
H(1061)	1.3265(2)	0.1144(2)	0.35497(19)	0.0215
H(1081)	0.9851(3)	0.1201(2)	0.49503(18)	0.0218
H(1101)	0.8856(3)	0.2510(2)	0.61349(19)	0.0166
H(1121)	1.1344(2)	0.2844(2)	0.52916(19)	0.0147
H(1141)	0.8984(3)	0.0304(2)	0.56089(19)	0.0197
H(1161)	0.6300(3)	0.0215(2)	0.59321(18)	0.0188
H(1181)	0.7510(2)	0.2254(2)	0.57201(19)	0.0283
H(1211)	1.3303(4)	0.4843(3)	0.2260(3)	0.0658
H(1241)	1.4986(3)	0.3935(3)	0.1429(3)	0.0643
H(1271)	1.5856(3)	0.3236(3)	0.2947(3)	0.0577
H(1321)	1.0799(3)	0.5609(2)	0.5341(2)	0.0343
H(1351)	1.0368(3)	0.4334(2)	0.7547(2)	0.0374
H(1381)	0.9251(3)	0.5973(3)	0.6381(2)	0.0319
H(1431)	0.4709(5)	0.3063(7)	0.6954(5)	0.05
H(1461)	0.3337(4)	0.3569(4)	0.5833(4)	0.0928
H(1491)	0.3471(5)	0.1603(4)	0.7049(6)	0.05
C(122)	1.3830(4)	0.5157(3)	0.2994(3)	0.0725
H(1221)	1.3582(4)	0.4752(3)	0.3346(3)	0.0823
H(1222)	1.4407(4)	0.5255(3)	0.3104(3)	0.0823
H(1223)	1.3455(4)	0.5624(3)	0.2923(3)	0.0823
C(123)	1.4269(4)	0.5500(3)	0.1765(3)	0.0803
H(1231)	1.4293(4)	0.5298(3)	0.1396(3)	0.0853
H(1232)	1.4856(4)	0.5605(3)	0.1852(3)	0.0853
H(1233)	1.3903(4)	0.5974(3)	0.1672(3)	0.0853
C(125)	1.5007(4)	0.2755(3)	0.1837(3)	0.0696
H(1251)	1.5567(4)	0.2709(3)	0.2037(3)	0.0765
H(1252)	1.5089(4)	0.2640(3)	0.1426(3)	0.0765
H(1253)	1.4615(4)	0.2394(3)	0.2121(3)	0.0765
C(126)	1.3691(4)	0.3683(4)	0.1400(3)	0.0739
H(1261)	1.3449(4)	0.4207(4)	0.1332(3)	0.0932

H(1262)	1.3768(4)	0.3573(4)	0.0987(3)	0.0932
H(1263)	1.3294(4)	0.3326(4)	0.1682(3)	0.0932
C(128)	1.5570(4)	0.3746(4)	0.3647(3)	0.0762
H(1281)	1.5152(4)	0.3373(4)	0.3878(3)	0.0933
H(1282)	1.6137(4)	0.3603(4)	0.3838(3)	0.0933
H(1283)	1.5372(4)	0.4254(4)	0.3676(3)	0.0933
C(129)	1.6282(4)	0.4308(4)	0.2523(3)	0.0741
H(1291)	1.6295(4)	0.4283(4)	0.2080(3)	0.0867
H(1292)	1.6862(4)	0.4176(4)	0.2694(3)	0.0867
H(1293)	1.6097(4)	0.4826(4)	0.2533(3)	0.0867
C(133)	1.1273(3)	0.6358(3)	0.5809(3)	0.046
H(1331)	1.1650(3)	0.6641(3)	0.5455(3)	0.0576
H(1332)	1.1547(3)	0.6292(3)	0.6217(3)	0.0576
H(1333)	1.0714(3)	0.6644(3)	0.5806(3)	0.0576
C(134)	1.2035(3)	0.5130(3)	0.5627(2)	0.0407
H(1341)	1.2369(3)	0.5471(3)	0.5277(2)	0.0517
H(1342)	1.2352(3)	0.5011(3)	0.6024(2)	0.0517
H(1343)	1.1950(3)	0.4657(3)	0.5522(2)	0.0517
C(136)	1.0807(4)	0.5362(3)	0.7572(3)	0.0515
H(1361)	1.0233(4)	0.5627(3)	0.7545(3)	0.0533
H(1362)	1.0967(4)	0.5175(3)	0.8022(3)	0.0533
H(1363)	1.1235(4)	0.5715(3)	0.7326(3)	0.0533
C(137)	1.1717(3)	0.4214(3)	0.7336(2)	0.0387
H(1371)	1.1697(3)	0.3783(3)	0.7158(2)	0.0432
H(1372)	1.1879(3)	0.4024(3)	0.7785(2)	0.0432
H(1373)	1.2146(3)	0.4565(3)	0.7089(2)	0.0432
C(139)	0.8754(3)	0.5447(2)	0.5750(2)	0.0366
H(1391)	0.9135(3)	0.5687(2)	0.5382(2)	0.0344
H(1392)	0.8192(3)	0.5733(2)	0.5714(2)	0.0344
H(1393)	0.8670(3)	0.4920(2)	0.5757(2)	0.0344
C(140)	0.8634(3)	0.5095(3)	0.6986(3)	0.0556
H(1401)	0.8930(3)	0.5112(3)	0.7366(3)	0.0624
H(1402)	0.8070(3)	0.5376(3)	0.6967(3)	0.0624
H(1403)	0.8548(3)	0.4562(3)	0.7010(3)	0.0624
C(144)	0.5302(5)	0.2595(4)	0.7427(4)	0.1038
H(1441)	0.5665(5)	0.2255(4)	0.7235(4)	0.1066
H(1442)	0.5192(5)	0.2340(4)	0.7884(4)	0.1066
H(1443)	0.5600(5)	0.3065(4)	0.7377(4)	0.1066
C(145)	0.3856(5)	0.3302(5)	0.7361(4)	0.1119
H(1451)	0.4065(5)	0.3433(5)	0.7729(4)	0.1089
H(1452)	0.3756(5)	0.3770(5)	0.7008(4)	0.1089
H(1453)	0.3313(5)	0.3042(5)	0.7485(4)	0.1089
C(147)	0.4523(7)	0.3946(4)	0.5491(5)	0.1453
H(1471)	0.4649(7)	0.4121(4)	0.5859(5)	0.1587
H(1472)	0.5053(7)	0.3715(4)	0.5343(5)	0.1587
H(1473)	0.4310(7)	0.4381(4)	0.5143(5)	0.1587
C(148)	0.3620(5)	0.3088(6)	0.5097(4)	0.1401
H(1481)	0.3177(5)	0.2709(6)	0.5235(4)	0.1373
H(1482)	0.4145(5)	0.2853(6)	0.4946(4)	0.1373
H(1483)	0.3402(5)	0.3519(6)	0.4747(4)	0.1373
C(150)	0.2443(4)	0.2043(4)	0.6769(4)	0.0829
H(1501)	0.2056(4)	0.1618(4)	0.6894(4)	0.095
H(1502)	0.2443(4)	0.2284(4)	0.7114(4)	0.095
H(1503)	0.2241(4)	0.2419(4)	0.6377(4)	0.095
C(151)	0.3544(5)	0.0971(5)	0.6738(8)	0.2178
H(1511)	0.4156(5)	0.0860(5)	0.6641(8)	0.1721
H(1512)	0.3400(5)	0.0705(5)	0.7188(8)	0.1721
H(1513)	0.3181(5)	0.0798(5)	0.6460(8)	0.1721
C(211)	0.4999(4)	0.0438(4)	0.4815(4)	0.0759
H(2111)	0.5187(4)	0.0696(4)	0.5115(4)	0.0942
H(2112)	0.4408(4)	0.0624(4)	0.4688(4)	0.0942
C(212)	0.5625(6)	0.0631(5)	0.4253(5)	0.1214
H(2121)	0.6194(6)	0.0373(5)	0.4367(5)	0.1268
H(2122)	0.5383(6)	0.0445(5)	0.3925(5)	0.1268
C(213)	0.5681(5)	0.1504(6)	0.3916(6)	0.1886
H(2131)	0.6072(5)	0.1602(6)	0.3535(6)	0.1692
H(2132)	0.5926(5)	0.1694(6)	0.4241(6)	0.1692
H(2133)	0.5115(5)	0.1766(6)	0.3799(6)	0.1692

Atom	u(11)	u(22)	u(33)	u(23)	u(13)	u(12)
Si(1)	0.0363(8)	0.0216(6)	0.0363(8)	-0.0175(6)	-0.0043(6)	0.0040(5)
Si(2)	0.0224(7)	0.0288(6)	0.0367(8)	-0.0126(6)	-0.0037(6)	-0.0045(5)

Si(3)	0.0523(9)	0.0247(6)	0.0301(8)	-0.0100(6)	-0.0202(7)	0.0151(6)
C(1)	0.015(2)	0.0180(19)	0.023(2)	-0.0058(18)	0.0068(18)	0.0000(17)
C(3)	0.0073(19)	0.0166(18)	0.018(2)	-0.0036(17)	-0.0066(17)	0.0013(15)
C(5)	0.023(2)	0.0166(19)	0.026(2)	-0.0067(18)	0.0017(19)	-0.0044(17)
C(7)	0.027(2)	0.0197(18)	0.0032(18)	-0.0028(16)	-0.0047(17)	-0.0029(17)
C(9)	0.017(2)	0.0162(18)	0.023(2)	-0.0076(18)	-0.0058(18)	-0.0026(16)
C(11)	0.025(2)	0.020(2)	0.021(2)	-0.0022(19)	-0.0028(19)	-0.0066(18)
C(13)	0.013(2)	0.0162(18)	0.033(2)	-0.0079(19)	0.0025(19)	-0.0046(16)
C(15)	0.022(2)	0.0177(19)	0.028(2)	-0.0120(19)	-0.005(2)	0.0022(17)
C(17)	0.016(2)	0.032(2)	0.028(3)	-0.009(2)	-0.003(2)	-0.0007(18)
C(19)	0.025(2)	0.025(2)	0.027(2)	-0.012(2)	-0.012(2)	-0.0022(18)
C(20)	0.027(2)	0.020(2)	0.039(3)	-0.020(2)	-0.008(2)	0.0009(18)
C(30)	0.024(2)	0.0187(19)	0.033(3)	-0.008(2)	-0.004(2)	-0.0060(19)
C(31)	0.021(2)	0.028(2)	0.045(3)	-0.016(2)	0.000(2)	-0.0046(19)
C(41)	0.032(2)	0.023(2)	0.033(3)	-0.015(2)	-0.011(2)	-0.0022(19)
C(42)	0.038(3)	0.016(2)	0.038(3)	-0.009(2)	-0.020(2)	0.007(2)
C(2)	0.022(2)	0.0145(18)	0.020(2)	-0.0087(17)	-0.0071(19)	0.0038(16)
C(4)	0.023(2)	0.0141(18)	0.030(2)	-0.0099(18)	-0.007(2)	0.0007(17)
C(6)	0.017(2)	0.019(2)	0.037(3)	-0.011(2)	0.000(2)	0.0047(17)
C(8)	0.007(2)	0.0226(19)	0.031(2)	-0.0101(19)	0.0003(18)	0.0031(16)
C(10)	0.012(2)	0.028(2)	0.017(2)	-0.0021(19)	-0.0036(18)	0.0073(17)
C(12)	0.029(2)	0.0152(18)	0.020(2)	-0.0076(18)	-0.0070(19)	-0.0007(18)
C(14)	0.019(2)	0.0178(19)	0.020(2)	-0.0015(18)	-0.0049(19)	0.0020(17)
C(16)	0.022(2)	0.0129(19)	0.039(3)	-0.008(2)	-0.009(2)	0.0096(17)
C(18)	0.020(2)	0.021(2)	0.033(3)	-0.009(2)	-0.010(2)	0.0094(18)
C(21)	0.026(3)	0.032(2)	0.048(3)	-0.019(2)	-0.007(2)	0.012(2)
C(24)	0.064(4)	0.023(2)	0.045(3)	-0.016(2)	0.003(3)	-0.010(2)
C(27)	0.044(3)	0.047(3)	0.070(4)	-0.030(3)	-0.009(3)	-0.011(3)
C(32)	0.028(3)	0.029(2)	0.073(4)	-0.031(3)	-0.003(3)	-0.007(2)
C(35)	0.049(3)	0.055(3)	0.039(3)	-0.015(3)	-0.010(3)	0.005(3)
C(38)	0.019(2)	0.032(2)	0.033(3)	-0.006(2)	-0.004(2)	-0.0104(19)
C(43)	0.030(3)	0.052(3)	0.038(3)	-0.007(3)	-0.016(3)	0.011(2)
C(46)	0.060(4)	0.044(3)	0.052(3)	-0.010(3)	-0.030(3)	0.009(3)
C(49)	0.110(5)	0.025(3)	0.038(3)	-0.008(2)	-0.031(3)	0.021(3)
C(22)	0.039(3)	0.048(3)	0.041(3)	-0.006(3)	0.002(3)	0.008(2)
C(23)	0.033(3)	0.053(3)	0.066(4)	-0.014(3)	-0.010(3)	0.008(2)
C(25)	0.145(6)	0.032(3)	0.035(3)	-0.005(3)	-0.005(4)	0.026(3)
C(26)	0.096(5)	0.022(2)	0.043(3)	-0.005(2)	-0.009(3)	0.012(3)
C(28)	0.075(5)	0.188(9)	0.101(6)	-0.069(6)	-0.010(5)	-0.042(6)
C(29)	0.118(6)	0.046(3)	0.069(4)	-0.035(3)	-0.037(4)	-0.005(3)
C(33)	0.049(4)	0.046(3)	0.084(5)	-0.028(3)	0.023(3)	-0.010(3)
C(34)	0.071(4)	0.075(4)	0.116(6)	-0.056(4)	-0.038(4)	0.044(4)
C(36)	0.059(4)	0.051(3)	0.058(4)	-0.004(3)	0.003(3)	-0.007(3)
C(37)	0.087(5)	0.091(5)	0.038(3)	-0.004(3)	-0.018(3)	-0.024(4)
C(39)	0.038(3)	0.066(4)	0.054(4)	-0.001(3)	-0.013(3)	-0.004(3)
C(40)	0.046(3)	0.046(3)	0.091(5)	-0.027(3)	-0.020(3)	0.023(3)
C(44)	0.049(4)	0.081(4)	0.097(5)	-0.053(4)	-0.005(3)	-0.008(3)
C(45)	0.063(4)	0.070(4)	0.114(6)	-0.041(4)	0.016(4)	-0.001(3)
C(47)	0.075(4)	0.083(4)	0.062(4)	-0.042(4)	-0.002(4)	0.005(4)
C(48)	0.073(4)	0.065(4)	0.070(4)	0.002(4)	-0.011(4)	-0.018(3)
C(50)	0.133(6)	0.039(3)	0.066(4)	-0.018(3)	-0.040(4)	0.044(4)
C(51)	0.189(8)	0.028(3)	0.096(5)	-0.029(3)	-0.079(6)	0.019(4)
C(201)	0.078(6)	0.202(10)	0.175(11)	-0.158(9)	0.068(6)	-0.040(7)
C(202)	0.126(8)	0.105(6)	0.116(7)	-0.056(6)	-0.005(6)	-0.019(5)
C(203)	0.095(7)	0.160(8)	0.143(8)	-0.051(7)	0.014(7)	0.019(6)
Si(11)	0.0330(8)	0.0308(7)	0.0391(8)	-0.0092(6)	0.0097(7)	-0.0089(6)
Si(12)	0.0208(7)	0.0158(5)	0.0286(7)	-0.0131(5)	-0.0046(6)	0.0013(5)
Si(13)	0.0207(7)	0.0456(7)	0.0444(8)	-0.0229(7)	-0.0051(6)	0.0187(6)
C(101)	0.011(2)	0.0186(18)	0.021(2)	-0.0106(17)	-0.0032(18)	0.0013(16)
C(103)	0.018(2)	0.0150(18)	0.022(2)	-0.0086(17)	-0.0019(18)	-0.0005(16)
C(105)	0.031(3)	0.032(2)	0.026(2)	-0.015(2)	-0.004(2)	0.000(2)
C(107)	0.016(2)	0.0111(17)	0.018(2)	-0.0018(16)	0.0011(18)	0.0018(16)
C(109)	0.0095(19)	0.0164(18)	0.024(2)	-0.0102(18)	0.0002(17)	0.0019(15)
C(111)	0.022(2)	0.0120(18)	0.022(2)	-0.0006(18)	-0.0038(19)	-0.0046(17)
C(113)	0.018(2)	0.0232(19)	0.009(2)	-0.0090(17)	0.0000(17)	0.0028(16)
C(115)	0.020(2)	0.0217(19)	0.015(2)	-0.0035(18)	-0.0007(18)	-0.0014(18)
C(117)	0.021(2)	0.026(2)	0.024(2)	-0.0127(19)	-0.0051(19)	0.0063(18)
C(119)	0.031(3)	0.019(2)	0.033(3)	-0.013(2)	0.000(2)	0.006(2)
C(120)	0.031(3)	0.023(2)	0.035(3)	-0.006(2)	0.007(2)	-0.011(2)
C(130)	0.018(2)	0.0152(19)	0.024(2)	-0.0014(18)	-0.0068(19)	0.0013(16)
C(131)	0.014(2)	0.0201(19)	0.030(2)	-0.0152(19)	-0.0028(19)	-0.0034(17)
C(141)	0.021(2)	0.033(2)	0.029(2)	-0.016(2)	0.002(2)	-0.0019(19)
C(142)	0.010(2)	0.044(2)	0.043(3)	-0.018(2)	-0.004(2)	0.0147(19)
C(102)	0.0081(19)	0.0146(18)	0.014(2)	-0.0013(16)	0.0028(16)	-0.0028(15)
C(104)	0.014(2)	0.0124(18)	0.021(2)	-0.0016(17)	0.0005(18)	-0.0063(16)
C(106)	0.012(2)	0.027(2)	0.018(2)	-0.0078(19)	0.0073(17)	-0.0020(17)

C(108)	0.022(2)	0.0126(17)	0.022(2)	-0.0082(17)	-0.0039(19)	0.0060(17)
C(110)	0.019(2)	0.0161(18)	0.019(2)	-0.0079(17)	-0.0039(18)	0.0052(16)
C(112)	0.012(2)	0.0141(18)	0.025(2)	-0.0061(17)	-0.0045(18)	-0.0038(15)
C(114)	0.016(2)	0.0195(19)	0.018(2)	-0.0073(18)	0.0017(18)	0.0028(17)
C(116)	0.011(2)	0.023(2)	0.023(2)	-0.0106(18)	0.0025(18)	-0.0026(16)
C(118)	0.019(2)	0.0249(19)	0.020(2)	-0.0093(18)	-0.0029(19)	0.0047(17)
C(121)	0.039(3)	0.044(3)	0.086(5)	-0.012(3)	0.012(3)	0.000(3)
C(124)	0.047(3)	0.063(3)	0.040(3)	-0.014(3)	0.016(3)	-0.025(3)
C(127)	0.028(3)	0.042(3)	0.054(4)	-0.010(3)	0.011(3)	-0.011(2)
C(132)	0.022(2)	0.031(2)	0.033(3)	-0.010(2)	-0.012(2)	-0.003(2)
C(135)	0.035(3)	0.028(2)	0.016(2)	-0.010(2)	-0.007(2)	0.0011(19)
C(138)	0.037(3)	0.025(2)	0.038(3)	-0.016(2)	-0.007(2)	0.012(2)
C(143)	0.054(5)	0.294(15)	0.144(9)	-0.099(10)	-0.029(6)	0.054(7)
C(146)	0.072(5)	0.065(4)	0.095(5)	-0.006(4)	0.008(4)	0.040(4)
C(149)	0.071(5)	0.062(5)	0.237(11)	0.004(6)	0.079(6)	0.013(4)
C(122)	0.057(4)	0.046(3)	0.125(6)	-0.041(4)	-0.006(4)	-0.001(3)
C(123)	0.048(4)	0.044(3)	0.115(5)	0.023(4)	0.024(4)	0.000(3)
C(125)	0.088(5)	0.052(3)	0.074(4)	-0.027(3)	0.034(4)	-0.032(3)
C(126)	0.062(4)	0.116(5)	0.051(4)	-0.031(4)	-0.002(3)	-0.023(4)
C(128)	0.049(4)	0.116(5)	0.064(5)	-0.027(4)	0.002(3)	-0.008(4)
C(129)	0.044(4)	0.092(5)	0.076(5)	-0.009(4)	0.006(3)	-0.011(3)
C(133)	0.049(3)	0.029(2)	0.061(4)	-0.011(3)	-0.013(3)	-0.009(2)
C(134)	0.033(3)	0.045(3)	0.039(3)	-0.004(3)	-0.002(2)	0.001(2)
C(136)	0.069(4)	0.039(3)	0.058(3)	-0.030(3)	-0.035(3)	0.016(3)
C(137)	0.020(2)	0.048(3)	0.046(3)	-0.010(3)	-0.014(2)	0.010(2)
C(139)	0.029(3)	0.030(2)	0.051(3)	-0.016(2)	0.001(2)	0.012(2)
C(140)	0.025(3)	0.091(4)	0.050(3)	-0.027(3)	0.012(3)	0.014(3)
C(144)	0.117(6)	0.095(5)	0.134(7)	-0.089(5)	-0.076(5)	0.062(5)
C(145)	0.074(5)	0.190(8)	0.112(6)	-0.119(6)	-0.037(4)	0.076(5)
C(147)	0.180(10)	0.042(4)	0.189(10)	-0.003(5)	0.043(8)	-0.010(5)
C(148)	0.059(5)	0.286(13)	0.054(5)	-0.025(7)	-0.018(4)	0.039(7)
C(150)	0.033(3)	0.087(5)	0.124(6)	-0.030(5)	0.023(4)	-0.003(3)
C(151)	0.068(6)	0.084(6)	0.53(3)	-0.130(11)	-0.026(9)	-0.020(5)
C(211)	0.047(4)	0.106(5)	0.088(6)	-0.048(5)	-0.045(4)	0.023(4)
C(212)	0.107(7)	0.103(6)	0.128(8)	0.002(6)	-0.024(6)	0.029(6)
C(213)	0.074(6)	0.143(8)	0.268(14)	0.063(9)	-0.028(8)	0.027(6)

	angle /°
C(20) - Si(1) - C(21)	106.71(19)
C(20) - Si(1) - C(24)	108.8(2)
C(21) - Si(1) - C(24)	112.2(2)
C(20) - Si(1) - C(27)	106.8(2)
C(21) - Si(1) - C(27)	109.1(2)
C(24) - Si(1) - C(27)	112.9(2)
C(31) - Si(2) - C(32)	104.79(19)
C(31) - Si(2) - C(35)	106.6(2)
C(32) - Si(2) - C(35)	114.7(2)
C(31) - Si(2) - C(38)	107.23(19)
C(32) - Si(2) - C(38)	111.3(2)
C(35) - Si(2) - C(38)	111.6(2)
C(42) - Si(3) - C(43)	109.0(2)
C(42) - Si(3) - C(46)	107.5(2)
C(43) - Si(3) - C(46)	110.9(2)
C(42) - Si(3) - C(49)	105.1(2)
C(43) - Si(3) - C(49)	110.1(3)
C(46) - Si(3) - C(49)	114.0(3)
C(15) - C(1) - C(2)	120.1(3)
C(15) - C(1) - C(6)	123.9(4)
C(2) - C(1) - C(6)	116.0(4)
C(7) - C(3) - C(2)	120.8(3)
C(7) - C(3) - C(4)	121.3(3)
C(2) - C(3) - C(4)	117.9(3)
C(19) - C(5) - C(4)	120.0(4)
C(19) - C(5) - C(6)	120.6(4)
C(4) - C(5) - C(6)	119.4(3)
C(3) - C(7) - C(8)	119.1(3)
C(3) - C(7) - C(12)	122.4(3)
C(8) - C(7) - C(12)	118.5(3)
C(13) - C(9) - C(8)	118.4(3)
C(13) - C(9) - C(10)	122.5(3)
C(8) - C(9) - C(10)	119.1(3)
C(30) - C(11) - C(10)	121.6(4)

C(30) - C(11) - C(12)	121.1(3)
C(10) - C(11) - C(12)	117.3(4)
C(9) - C(13) - C(14)	122.1(3)
C(9) - C(13) - C(18)	118.6(3)
C(14) - C(13) - C(18)	119.3(4)
C(1) - C(15) - C(14)	119.5(3)
C(1) - C(15) - C(16)	121.0(3)
C(14) - C(15) - C(16)	119.5(4)
C(41) - C(17) - C(16)	120.8(4)
C(41) - C(17) - C(18)	118.6(4)
C(16) - C(17) - C(18)	120.5(4)
C(5) - C(19) - C(20)	179.5(4)
Si(1) - C(20) - C(19)	177.5(4)
C(11) - C(30) - C(31)	177.1(5)
Si(2) - C(31) - C(30)	170.8(4)
C(17) - C(41) - C(42)	177.9(5)
Si(3) - C(42) - C(41)	177.3(4)
C(1) - C(2) - C(3)	123.8(3)
C(3) - C(4) - C(5)	120.4(4)
C(1) - C(6) - C(5)	122.4(4)
C(7) - C(8) - C(9)	120.9(4)
C(9) - C(10) - C(11)	122.0(3)
C(7) - C(12) - C(11)	122.2(3)
C(13) - C(14) - C(15)	121.7(4)
C(15) - C(16) - C(17)	119.4(3)
C(13) - C(18) - C(17)	119.6(4)
Si(1) - C(21) - C(22)	112.1(3)
Si(1) - C(21) - C(23)	113.7(3)
C(22) - C(21) - C(23)	108.6(4)
Si(1) - C(24) - C(25)	112.6(3)
Si(1) - C(24) - C(26)	115.7(3)
C(25) - C(24) - C(26)	110.6(4)
Si(1) - C(27) - C(28)	111.2(4)
Si(1) - C(27) - C(29)	114.0(4)
C(28) - C(27) - C(29)	110.9(5)
Si(2) - C(32) - C(33)	111.8(3)
Si(2) - C(32) - C(34)	110.7(4)
C(33) - C(32) - C(34)	110.8(4)
Si(2) - C(35) - C(36)	113.0(4)
Si(2) - C(35) - C(37)	115.3(4)
C(36) - C(35) - C(37)	109.2(4)
Si(2) - C(38) - C(39)	114.4(3)
Si(2) - C(38) - C(40)	112.8(3)
C(39) - C(38) - C(40)	110.8(4)
Si(3) - C(43) - C(44)	113.6(4)
Si(3) - C(43) - C(45)	114.4(4)
C(44) - C(43) - C(45)	107.6(5)
Si(3) - C(46) - C(47)	112.8(4)
Si(3) - C(46) - C(48)	114.3(4)
C(47) - C(46) - C(48)	108.9(5)
Si(3) - C(49) - C(50)	111.7(3)
Si(3) - C(49) - C(51)	115.4(4)
C(50) - C(49) - C(51)	110.9(5)
C(201)- C(201)- C(202)	113.2(11)
C(201)- C(202)- C(203)	111.5(7)
C(120)- Si(11)- C(121)	107.1(2)
C(120)- Si(11)- C(124)	105.0(2)
C(121)- Si(11)- C(124)	109.8(3)
C(120)- Si(11)- C(127)	107.9(2)
C(121)- Si(11)- C(127)	115.2(2)
C(124)- Si(11)- C(127)	111.3(2)
C(131)- Si(12)- C(132)	105.58(18)
C(131)- Si(12)- C(135)	107.51(18)
C(132)- Si(12)- C(135)	116.6(2)
C(131)- Si(12)- C(138)	107.14(18)
C(132)- Si(12)- C(138)	110.1(2)
C(135)- Si(12)- C(138)	109.49(19)
C(142)- Si(13)- C(143)	108.2(3)
C(142)- Si(13)- C(146)	108.6(3)
C(143)- Si(13)- C(146)	116.7(4)
C(142)- Si(13)- C(149)	105.4(3)
C(143)- Si(13)- C(149)	108.8(5)
C(146)- Si(13)- C(149)	108.5(4)
C(115)- C(101)- C(102)	119.6(3)
C(115)- C(101)- C(106)	122.0(3)
C(102)- C(101)- C(106)	118.4(3)
C(107)- C(103)- C(102)	118.3(3)

C(107)- C(103)- C(104)	122.9(3)
C(102)- C(103)- C(104)	118.8(3)
C(119)- C(105)- C(104)	119.5(3)
C(119)- C(105)- C(106)	122.2(4)
C(104)- C(105)- C(106)	118.2(4)
C(103)- C(107)- C(108)	120.8(3)
C(103)- C(107)- C(112)	121.2(3)
C(108)- C(107)- C(112)	118.0(3)
C(113)- C(109)- C(108)	119.0(3)
C(113)- C(109)- C(110)	122.6(3)
C(108)- C(109)- C(110)	118.4(3)
C(130)- C(111)- C(110)	121.1(4)
C(130)- C(111)- C(112)	119.4(3)
C(110)- C(111)- C(112)	119.5(3)
C(109)- C(113)- C(114)	121.0(3)
C(109)- C(113)- C(118)	120.0(3)
C(114)- C(113)- C(118)	119.0(4)
C(101)- C(115)- C(114)	119.4(3)
C(101)- C(115)- C(116)	122.5(3)
C(114)- C(115)- C(116)	118.1(3)
C(141)- C(117)- C(116)	121.1(4)
C(141)- C(117)- C(118)	119.4(3)
C(116)- C(117)- C(118)	119.5(3)
C(105)- C(119)- C(120)	177.6(5)
Si(11)- C(120)- C(119)	176.2(4)
C(111)- C(130)- C(131)	176.5(4)
Si(12)- C(131)- C(130)	174.5(4)
C(117)- C(141)- C(142)	175.8(4)
Si(13)- C(142)- C(141)	175.2(4)
C(101)- C(102)- C(103)	120.8(3)
C(103)- C(104)- C(105)	121.9(3)
C(101)- C(106)- C(105)	121.8(4)
C(107)- C(108)- C(109)	122.2(3)
C(109)- C(110)- C(111)	120.7(4)
C(107)- C(112)- C(111)	121.1(3)
C(113)- C(114)- C(115)	122.2(3)
C(115)- C(116)- C(117)	121.2(4)
C(113)- C(118)- C(117)	120.1(3)
Si(11)- C(121)- C(122)	112.0(4)
Si(11)- C(121)- C(123)	114.2(4)
C(122)- C(121)- C(123)	112.6(5)
Si(11)- C(124)- C(125)	111.3(4)
Si(11)- C(124)- C(126)	110.9(4)
C(125)- C(124)- C(126)	111.6(5)
Si(11)- C(127)- C(128)	115.5(4)
Si(11)- C(127)- C(129)	113.1(4)
C(128)- C(127)- C(129)	111.5(5)
Si(12)- C(132)- C(133)	113.0(3)
Si(12)- C(132)- C(134)	114.3(3)
C(133)- C(132)- C(134)	109.5(4)
Si(12)- C(135)- C(136)	114.8(3)
Si(12)- C(135)- C(137)	111.5(3)
C(136)- C(135)- C(137)	111.1(4)
Si(12)- C(138)- C(139)	110.2(3)
Si(12)- C(138)- C(140)	113.7(3)
C(139)- C(138)- C(140)	111.2(4)
Si(13)- C(143)- C(144)	124.5(6)
Si(13)- C(143)- C(145)	116.4(5)
C(144)- C(143)- C(145)	114.1(7)
Si(13)- C(146)- C(147)	112.9(6)
Si(13)- C(146)- C(148)	113.1(5)
C(147)- C(146)- C(148)	109.9(7)
Si(13)- C(149)- C(150)	114.5(5)
Si(13)- C(149)- C(151)	125.2(6)
C(150)- C(149)- C(151)	117.3(7)
C(211)- C(211)- C(212)	114.1(8)
C(211)- C(212)- C(213)	114.4(8)

	distance / Å
Si(1) - C(20)	1.855(4)
Si(1) - C(21)	1.882(5)
Si(1) - C(24)	1.855(5)

Si(1) - C(27)	1.894(5)
Si(2) - C(31)	1.847(5)
Si(2) - C(32)	1.878(4)
Si(2) - C(35)	1.869(5)
Si(2) - C(38)	1.883(4)
Si(3) - C(42)	1.835(4)
Si(3) - C(43)	1.874(5)
Si(3) - C(46)	1.870(6)
Si(3) - C(49)	1.880(5)
C(1) - C(15)	1.481(5)
C(1) - C(2)	1.417(5)
C(1) - C(6)	1.404(5)
C(3) - C(7)	1.487(5)
C(3) - C(2)	1.381(5)
C(3) - C(4)	1.410(5)
C(5) - C(19)	1.438(5)
C(5) - C(4)	1.410(5)
C(5) - C(6)	1.388(5)
C(7) - C(8)	1.392(5)
C(7) - C(12)	1.385(5)
C(9) - C(13)	1.500(5)
C(9) - C(8)	1.426(5)
C(9) - C(10)	1.365(5)
C(11) - C(30)	1.447(6)
C(11) - C(10)	1.410(5)
C(11) - C(12)	1.417(5)
C(13) - C(14)	1.379(5)
C(13) - C(18)	1.411(5)
C(15) - C(14)	1.390(5)
C(15) - C(16)	1.404(5)
C(17) - C(41)	1.466(6)
C(17) - C(16)	1.400(5)
C(17) - C(18)	1.397(5)
C(19) - C(20)	1.206(5)
C(30) - C(31)	1.180(5)
C(41) - C(42)	1.194(5)
C(21) - C(22)	1.517(6)
C(21) - C(23)	1.541(6)
C(24) - C(25)	1.551(7)
C(24) - C(26)	1.552(7)
C(27) - C(28)	1.569(8)
C(27) - C(29)	1.517(7)
C(32) - C(33)	1.525(7)
C(32) - C(34)	1.547(7)
C(35) - C(36)	1.564(7)
C(35) - C(37)	1.545(7)
C(38) - C(39)	1.518(6)
C(38) - C(40)	1.533(6)
C(43) - C(44)	1.524(7)
C(43) - C(45)	1.525(7)
C(46) - C(47)	1.537(7)
C(46) - C(48)	1.521(7)
C(49) - C(50)	1.560(7)
C(49) - C(51)	1.499(8)
C(201)- C(201)	1.404(16)
C(201)- C(202)	1.583(13)
C(202)- C(203)	1.468(10)
Si(11)- C(120)	1.849(5)
Si(11)- C(121)	1.898(5)
Si(11)- C(124)	1.891(5)
Si(11)- C(127)	1.901(5)
Si(12)- C(131)	1.857(4)
Si(12)- C(132)	1.884(5)
Si(12)- C(135)	1.903(4)
Si(12)- C(138)	1.911(4)
Si(13)- C(142)	1.856(4)
Si(13)- C(143)	1.842(8)
Si(13)- C(146)	1.866(6)
Si(13)- C(149)	1.833(8)
C(101)- C(115)	1.489(5)
C(101)- C(102)	1.408(5)
C(101)- C(106)	1.415(5)
C(103)- C(107)	1.492(5)
C(103)- C(102)	1.418(5)
C(103)- C(104)	1.373(5)
C(105)- C(119)	1.441(6)
C(105)- C(104)	1.427(5)

C(105)- C(106)	1.379(5)
C(107)- C(108)	1.388(5)
C(107)- C(112)	1.408(5)
C(109)- C(113)	1.498(5)
C(109)- C(108)	1.403(5)
C(109)- C(110)	1.400(5)
C(111)- C(130)	1.449(5)
C(111)- C(110)	1.395(5)
C(111)- C(112)	1.395(5)
C(113)- C(114)	1.381(5)
C(113)- C(118)	1.407(5)
C(115)- C(114)	1.399(5)
C(115)- C(116)	1.404(5)
C(117)- C(141)	1.439(5)
C(117)- C(116)	1.390(5)
C(117)- C(118)	1.408(6)
C(119)- C(120)	1.191(6)
C(130)- C(131)	1.196(5)
C(141)- C(142)	1.191(5)
C(121)- C(122)	1.541(8)
C(121)- C(123)	1.521(8)
C(124)- C(125)	1.514(7)
C(124)- C(126)	1.534(7)
C(127)- C(128)	1.522(7)
C(127)- C(129)	1.501(7)
C(132)- C(133)	1.538(6)
C(132)- C(134)	1.545(6)
C(135)- C(136)	1.529(5)
C(135)- C(137)	1.545(5)
C(138)- C(139)	1.537(6)
C(138)- C(140)	1.495(7)
C(143)- C(144)	1.364(8)
C(143)- C(145)	1.522(9)
C(146)- C(147)	1.483(10)
C(146)- C(148)	1.513(9)
C(149)- C(150)	1.549(8)
C(149)- C(151)	1.315(9)
C(211)- C(211)	1.525(13)
C(211)- C(212)	1.445(10)
C(212)- C(213)	1.512(11)

8.8 5,5',5'',5''',5'''',5'''''-Hexa-((2,3,4,5,6-pentaphenyl)phenyl)-cyclohexa-m-phenylene (5-114)

Atom	x/a	y/b	z/c	U(iso)	Occ
C(1)	0.06687(7)	0.09641(7)	0.23856(10)	0.0231	
C(3)	0.12941(7)	0.12660(7)	0.21003(10)	0.0214	
C(5)	0.09821(7)	0.06354(7)	0.24062(10)	0.0218	
C(7)	0.09658(7)	0.02840(6)	0.24864(10)	0.0201	
C(9)	0.12575(7)	-0.00084(6)	0.28054(10)	0.0202	
C(11)	0.06590(7)	-0.03204(7)	0.24982(11)	0.024	
C(13)	0.16215(7)	0.15950(7)	0.20428(10)	0.0194	
C(14)	0.17865(7)	0.18495(6)	0.24051(10)	0.0192	
C(15)	0.21460(7)	0.21313(7)	0.23496(11)	0.0246	
C(16)	0.22990(7)	0.21547(7)	0.17923(11)	0.024	
C(17)	0.21506(7)	0.19021(7)	0.13541(11)	0.0221	
C(18)	0.18450(7)	0.16011(7)	0.14177(11)	0.0214	
C(19)	0.15741(7)	-0.00195(6)	0.30408(11)	0.0216	
C(20)	0.17757(7)	0.02068(7)	0.35762(11)	0.0229	
C(21)	0.20822(7)	0.02233(7)	0.37250(11)	0.0224	
C(22)	0.22406(7)	0.00325(7)	0.33706(11)	0.0238	
C(23)	0.20743(7)	-0.01282(7)	0.28953(11)	0.0232	
C(24)	0.17187(7)	-0.01733(7)	0.26754(11)	0.022	
C(25)	0.15700(6)	0.18073(6)	0.29598(11)	0.0221	
C(31)	0.23436(7)	0.23805(7)	0.28607(11)	0.0258	
C(37)	0.26766(7)	0.24938(7)	0.16742(11)	0.0257	
C(43)	0.23288(7)	0.19114(7)	0.08201(11)	0.0257	
C(49)	0.16628(7)	0.13006(7)	0.09820(11)	0.0251	
C(55)	0.15872(7)	0.03545(7)	0.39877(11)	0.0271	
C(61)	0.22725(7)	0.04303(7)	0.42961(11)	0.0277	
C(67)	0.25709(7)	0.00895(7)	0.35710(11)	0.028	
C(73)	0.21881(7)	-0.03182(7)	0.25112(11)	0.0272	
C(79)	0.15409(7)	-0.03718(7)	0.21167(12)	0.0299	
C(2)	0.09739(7)	0.12599(7)	0.22132(10)	0.0209	

C(4)	0.12703(7)	0.09456(6)	0.22494(10)	0.0196
C(6)	0.06903(6)	0.06709(6)	0.24762(10)	0.0176
C(8)	0.12817(7)	0.03094(7)	0.26895(10)	0.0209
C(10)	0.09459(7)	-0.03303(7)	0.27760(11)	0.0226
C(12)	0.06613(7)	-0.00180(7)	0.24610(10)	0.0207
C(26)	0.14468(7)	0.20499(7)	0.30426(11)	0.0237
C(27)	0.12273(7)	0.20012(7)	0.34723(11)	0.0265
C(28)	0.11447(7)	0.17431(7)	0.39012(11)	0.024
C(29)	0.12362(7)	0.15102(7)	0.38734(11)	0.0256
C(30)	0.15055(7)	0.15734(7)	0.33640(11)	0.0226
C(32)	0.24384(7)	0.22558(8)	0.33847(11)	0.0267
C(33)	0.26226(7)	0.24940(8)	0.38597(12)	0.0281
C(34)	0.27478(7)	0.28563(8)	0.37617(12)	0.0292
C(35)	0.26684(7)	0.29954(8)	0.32641(12)	0.0283
C(36)	0.24310(7)	0.27400(7)	0.28006(12)	0.0262
C(38)	0.29965(7)	0.25760(7)	0.19541(11)	0.0252
C(39)	0.33139(8)	0.28700(7)	0.18003(12)	0.0305
C(40)	0.33056(8)	0.31377(8)	0.14533(11)	0.0285
C(41)	0.29942(7)	0.30474(8)	0.11119(11)	0.0282
C(42)	0.26714(7)	0.27187(7)	0.12181(11)	0.026
C(44)	0.26448(7)	0.19034(7)	0.08697(12)	0.0256
C(45)	0.28302(8)	0.19098(7)	0.03457(12)	0.0313
C(46)	0.26904(8)	0.19054(7)	-0.02717(12)	0.0286
C(47)	0.24007(7)	0.19690(7)	-0.02700(12)	0.0271
C(48)	0.22098(7)	0.19262(7)	0.02602(11)	0.0262
C(50)	0.13452(7)	0.12502(7)	0.07301(11)	0.0252
C(51)	0.12178(7)	0.09619(7)	0.02922(12)	0.0278
C(52)	0.13070(8)	0.06981(8)	0.01735(12)	0.0275
C(53)	0.16250(7)	0.08191(7)	0.04595(11)	0.0265
C(54)	0.18001(7)	0.10802(7)	0.08354(11)	0.0259
C(56)	0.17548(7)	0.07184(7)	0.40917(12)	0.0278
C(57)	0.15945(8)	0.08604(8)	0.44575(12)	0.0303
C(58)	0.12771(8)	0.06533(8)	0.47138(13)	0.0307
C(59)	0.11021(8)	0.02881(7)	0.46149(11)	0.0267
C(60)	0.12548(7)	0.01365(7)	0.42540(11)	0.0267
C(62)	0.25685(7)	0.07440(7)	0.41744(13)	0.0299
C(63)	0.27728(8)	0.09652(8)	0.46462(12)	0.0304
C(64)	0.26330(8)	0.07994(8)	0.52722(13)	0.03
C(65)	0.23159(8)	0.04793(8)	0.53812(12)	0.0289
C(66)	0.21422(7)	0.02900(8)	0.48603(12)	0.0283
C(68)	0.28836(8)	0.03082(8)	0.32196(12)	0.0311
C(69)	0.31762(8)	0.03245(8)	0.33848(13)	0.0313
C(70)	0.31826(8)	0.01337(7)	0.38901(12)	0.0307
C(71)	0.29204(8)	-0.00383(8)	0.42443(13)	0.0309
C(72)	0.25925(8)	-0.00963(7)	0.40487(12)	0.0281
C(74)	0.21479(8)	-0.06423(8)	0.26985(13)	0.0326
C(75)	0.22584(8)	-0.08237(8)	0.23218(13)	0.0345
C(76)	0.24112(8)	-0.06830(8)	0.17593(13)	0.0324
C(77)	0.24585(8)	-0.03508(8)	0.15648(13)	0.0318
C(78)	0.23433(7)	-0.01698(8)	0.19398(12)	0.0319
C(80)	0.14267(8)	-0.07325(8)	0.20910(12)	0.0313
C(81)	0.12174(8)	-0.09423(8)	0.16324(13)	0.034
C(82)	0.11794(8)	-0.07766(8)	0.11158(13)	0.0325
C(83)	0.13120(7)	-0.04157(8)	0.11082(13)	0.0307
C(84)	0.14792(7)	-0.02163(8)	0.16223(12)	0.0288
H(21)	0.09696(7)	0.14743(7)	0.21678(10)	0.0286
H(41)	0.14862(7)	0.09423(6)	0.22330(10)	0.0247
H(61)	0.04790(6)	0.04655(6)	0.26014(10)	0.0234
H(81)	0.14932(7)	0.05297(7)	0.27439(10)	0.026
H(101)	0.09253(7)	-0.05428(7)	0.29313(11)	0.0286
H(121)	0.04456(7)	-0.00161(7)	0.24175(10)	0.0286
H(261)	0.15250(7)	0.22475(7)	0.27802(11)	0.0312
H(271)	0.11228(7)	0.21468(7)	0.34935(11)	0.0338
H(281)	0.10099(7)	0.17398(7)	0.42410(11)	0.0312
H(291)	0.11472(7)	0.13136(7)	0.41407(11)	0.0312
H(301)	0.16217(7)	0.14385(7)	0.33515(11)	0.0299
H(321)	0.23776(7)	0.20147(8)	0.34172(11)	0.0351
H(331)	0.26631(7)	0.24120(8)	0.42323(12)	0.0369
H(341)	0.28950(7)	0.30171(8)	0.40644(12)	0.0382
H(351)	0.27618(7)	0.32430(8)	0.32183(12)	0.0364
H(361)	0.23412(7)	0.28135(7)	0.24747(12)	0.0325
H(381)	0.29958(7)	0.24235(7)	0.22612(11)	0.0351
H(391)	0.35326(8)	0.28920(7)	0.19238(12)	0.0382
H(401)	0.35021(8)	0.33719(8)	0.14473(11)	0.0377
H(411)	0.29993(7)	0.32050(8)	0.08106(11)	0.0364
H(421)	0.24627(7)	0.26562(7)	0.09931(11)	0.0351
H(441)	0.27332(7)	0.18924(7)	0.12565(12)	0.0351

H(451)	0.30524(8)	0.19208(7)	0.03853(12)	0.039	
H(461)	0.27830(8)	0.18614(7)	-0.06290(12)	0.039	
H(471)	0.23362(7)	0.20404(7)	-0.06311(12)	0.0364	
H(481)	0.19841(7)	0.19081(7)	0.02288(11)	0.0338	
H(501)	0.12311(7)	0.13808(7)	0.08286(11)	0.0351	
H(511)	0.10386(7)	0.09496(7)	0.00324(12)	0.0377	
H(521)	0.11773(8)	0.04868(8)	-0.00544(12)	0.0364	
H(531)	0.17384(7)	0.06864(7)	0.03735(11)	0.0351	
H(541)	0.20182(7)	0.11224(7)	0.10036(11)	0.0338	
H(561)	0.19792(7)	0.08707(7)	0.39147(12)	0.0351	
H(571)	0.17116(8)	0.11087(8)	0.45240(12)	0.0377	
H(581)	0.11726(8)	0.07552(8)	0.49590(13)	0.0382	
H(591)	0.08778(8)	0.01412(7)	0.47968(11)	0.0351	
H(601)	0.11352(7)	-0.01122(7)	0.41906(11)	0.0351	
H(621)	0.26370(7)	0.08134(7)	0.37671(13)	0.0377	
H(631)	0.29752(8)	0.11922(8)	0.45870(12)	0.039	
H(641)	0.27721(8)	0.09238(8)	0.56131(13)	0.0403	
H(651)	0.22278(8)	0.03990(8)	0.57769(12)	0.0377	
H(661)	0.19341(7)	0.00650(8)	0.48960(12)	0.0364	
H(681)	0.28755(8)	0.04361(8)	0.28783(12)	0.039	
H(691)	0.33874(8)	0.04658(8)	0.31626(13)	0.0416	
H(701)	0.33956(8)	0.01322(7)	0.39721(12)	0.0403	
H(711)	0.29491(8)	-0.01211(8)	0.46254(13)	0.039	
H(721)	0.23825(8)	-0.02686(7)	0.42440(12)	0.0364	
H(741)	0.20441(8)	-0.07391(8)	0.30794(13)	0.0429	
H(751)	0.22309(8)	-0.10444(8)	0.24473(13)	0.0455	
H(761)	0.24870(8)	-0.08082(8)	0.15058(13)	0.0434	
H(771)	0.25624(8)	-0.02549(8)	0.11836(13)	0.0416	
H(781)	0.23703(7)	0.00510(8)	0.18161(12)	0.0403	
H(801)	0.14962(8)	-0.08358(8)	0.24011(12)	0.0403	
H(811)	0.10999(8)	-0.11930(8)	0.16626(13)	0.0429	
H(821)	0.10642(8)	-0.09143(8)	0.07684(13)	0.0416	
H(831)	0.12866(7)	-0.03051(8)	0.07569(13)	0.0403	
H(841)	0.15540(7)	0.00290(8)	0.16289(12)	0.039	
Cl(301)	0.27596(4)	0.12340(5)	0.27664(6)	0.0676	0.6667
Cl(302)	0.21249(5)	0.07626(6)	0.20457(9)	0.0978	0.6667
Cl(303)	0.22504(6)	0.14087(6)	0.24112(9)	0.1078	0.6667
Cl(310)	0.05797(4)	0.22409(4)	0.41350(7)	0.1045	
Cl(311)	0.08026(3)	0.24715(3)	0.54158(6)	0.0926	
Cl(320)	0.26350(4)	0.03923(3)	0.05799(6)	0.0946	
Cl(321)	0.28304(3)	0.10524(3)	0.11082(5)	0.0719	
Cl(330)	0.21871(3)	0.33558(4)	0.02859(5)	0.0866	
Cl(331)	0.22152(4)	0.31855(4)	0.16184(7)	0.1095	
Cl(340)	0.15955(4)	0.21857(4)	0.09014(6)	0.1002	
Cl(341)	0.12529(3)	0.24557(4)	0.03223(5)	0.0894	
Cl(350)	0.02792(11)	0.04466(10)	0.39694(14)	0.0813	0.3333
Cl(351)	0.04565(9)	0.01622(11)	0.39973(14)	0.0795	0.3333
Cl(360)	0.02617(10)	0.04260(8)	0.09710(14)	0.068	0.3333
Cl(361)	0.04223(9)	0.01535(11)	0.08770(14)	0.0786	0.3333
C(350)	0	0	0.3793(13)	0.107	0.3333
C(360)	0	0	0.0963(15)	0.136	0.3333
C(301)	0.22984(15)	0.10689(15)	0.2615(3)	0.1158	
H(3011)	0.21733(15)	0.09538(15)	0.2973(3)	0.1495	
C(310)	0.08701(16)	0.23668(16)	0.4704(2)	0.1239	
H(3101)	0.10777(16)	0.25701(16)	0.4562(2)	0.1573	
H(3102)	0.09164(16)	0.21775(16)	0.4756(2)	0.1573	
C(320)	0.28441(15)	0.06766(14)	0.1239(2)	0.119	
H(3201)	0.30821(15)	0.07278(14)	0.1277(2)	0.1547	
H(3202)	0.27169(15)	0.05631(14)	0.1596(2)	0.1547	
C(330)	0.24495(15)	0.33265(15)	0.0959(2)	0.1141	
H(3301)	0.26474(15)	0.35555(15)	0.1026(2)	0.1456	
H(3302)	0.25298(15)	0.31668(15)	0.0857(2)	0.1456	
C(340)	0.16240(16)	0.25404(16)	0.0703(3)	0.1311	
H(3401)	0.16487(16)	0.26798(16)	0.1049(3)	0.1703	
H(3402)	0.18242(16)	0.26657(16)	0.0447(3)	0.1703	
C(101)	0.17592(12)	0.34077(11)	0.30537(15)	0.071	
H(1011)	0.20013(12)	0.35163(11)	0.31676(15)	0.1105	
H(1012)	0.17029(12)	0.35853(11)	0.29508(15)	0.1105	
C(102)	0.17470(12)	0.32496(11)	0.2547(2)	0.0742	
H(1021)	0.19056(12)	0.34197(11)	0.2266(2)	0.117	
H(1022)	0.15126(12)	0.31424(11)	0.2392(2)	0.117	
C(103)	0.18526(12)	0.29667(11)	0.26408(19)	0.0826	
H(1031)	0.18408(12)	0.28533(11)	0.22679(19)	0.1209	
H(1032)	0.20870(12)	0.30739(11)	0.27952(19)	0.1209	
H(1033)	0.16939(12)	0.27966(11)	0.29218(19)	0.1209	

Atom	u(11)	u(22)	u(33)	u(23)	u(13)	u(12)
C(1)	0.0251(14)	0.0223(13)	0.0211(11)	-0.0007(11)	0.0026(11)	0.0114(11)
C(3)	0.0211(13)	0.0237(14)	0.0216(11)	-0.0014(11)	0.0005(11)	0.0128(12)
C(5)	0.0237(14)	0.0180(12)	0.0220(10)	0.0011(11)	0.0015(11)	0.0091(11)
C(7)	0.0208(12)	0.0162(12)	0.0207(10)	-0.0021(10)	-0.0024(10)	0.0075(10)
C(9)	0.0227(13)	0.0159(12)	0.0202(10)	0.0000(10)	0.0002(11)	0.0082(11)
C(11)	0.0275(14)	0.0225(14)	0.0217(10)	-0.0009(11)	0.0003(11)	0.0124(12)
C(13)	0.0198(13)	0.0212(13)	0.0171(10)	0.0012(10)	-0.0017(10)	0.0102(11)
C(14)	0.0177(12)	0.0182(12)	0.0207(10)	0.0010(10)	-0.0004(11)	0.0083(10)
C(15)	0.0234(14)	0.0264(14)	0.0234(11)	0.0028(12)	0.0000(12)	0.0121(12)
C(16)	0.0240(14)	0.0231(14)	0.0248(11)	0.0004(11)	0.0001(12)	0.0116(12)
C(17)	0.0186(13)	0.0227(13)	0.0234(11)	-0.0020(11)	-0.0001(11)	0.0092(11)
C(18)	0.0191(13)	0.0228(13)	0.0216(10)	-0.0013(10)	-0.0031(11)	0.0101(11)
C(19)	0.0186(13)	0.0209(13)	0.0218(10)	-0.0027(11)	-0.0019(11)	0.0072(11)
C(20)	0.0228(14)	0.0258(14)	0.0224(11)	-0.0018(11)	-0.0019(11)	0.0140(11)
C(21)	0.0243(14)	0.0214(13)	0.0218(10)	-0.0007(11)	0.0005(11)	0.0117(11)
C(22)	0.0257(14)	0.0249(14)	0.0212(11)	-0.0009(11)	-0.0015(11)	0.0129(12)
C(23)	0.0242(13)	0.0246(13)	0.0194(10)	0.0019(11)	-0.0008(11)	0.0112(11)
C(24)	0.0260(14)	0.0218(13)	0.0196(10)	-0.0005(10)	-0.0008(11)	0.0130(11)
C(25)	0.0196(12)	0.0206(13)	0.0247(11)	0.0007(11)	-0.0013(11)	0.0091(11)
C(31)	0.0277(15)	0.0252(14)	0.0261(12)	0.0016(12)	0.0010(12)	0.0144(12)
C(37)	0.0301(15)	0.0243(14)	0.0270(12)	-0.0003(11)	-0.0019(12)	0.0169(12)
C(43)	0.0247(14)	0.0264(14)	0.0259(11)	0.0010(12)	-0.0001(12)	0.0126(12)
C(49)	0.0267(14)	0.0275(14)	0.0259(12)	-0.0028(12)	-0.0024(11)	0.0171(12)
C(55)	0.0275(15)	0.0273(14)	0.0265(12)	0.0006(12)	-0.0014(12)	0.0138(12)
C(61)	0.0256(14)	0.0295(15)	0.0263(12)	-0.0018(12)	-0.0002(12)	0.0125(12)
C(67)	0.0239(14)	0.0330(16)	0.0273(12)	-0.0034(12)	-0.0019(12)	0.0145(13)
C(73)	0.0282(14)	0.0280(15)	0.0267(11)	-0.0010(12)	-0.0034(12)	0.0150(13)
C(79)	0.0252(14)	0.0293(15)	0.0327(13)	-0.0005(13)	0.0001(13)	0.0118(12)
C(2)	0.0195(13)	0.0225(13)	0.0218(11)	0.0019(11)	0.0009(11)	0.0112(11)
C(4)	0.0215(13)	0.0195(13)	0.0188(10)	-0.0011(11)	-0.0012(11)	0.0108(11)
C(6)	0.0167(12)	0.0174(13)	0.0175(10)	0.0026(10)	-0.0019(10)	0.0077(11)
C(8)	0.0210(13)	0.0227(14)	0.0191(10)	-0.0007(11)	-0.0020(11)	0.0109(11)
C(10)	0.0194(13)	0.0231(14)	0.0218(11)	-0.0018(11)	-0.0008(11)	0.0079(11)
C(12)	0.0183(13)	0.0187(13)	0.0230(11)	-0.0004(11)	0.0009(11)	0.0076(11)
C(26)	0.0261(14)	0.0210(13)	0.0250(12)	0.0022(11)	0.0011(12)	0.0126(12)
C(27)	0.0303(16)	0.0283(15)	0.0251(12)	0.0011(12)	0.0006(13)	0.0178(13)
C(28)	0.0229(14)	0.0250(14)	0.0260(12)	0.0006(12)	0.0001(12)	0.0133(12)
C(29)	0.0238(14)	0.0254(14)	0.0264(12)	0.0024(12)	0.0005(12)	0.0113(12)
C(30)	0.0223(14)	0.0204(13)	0.0250(11)	-0.0018(11)	-0.0011(12)	0.0107(12)
C(32)	0.0258(15)	0.0263(15)	0.0266(12)	0.0018(12)	0.0028(12)	0.0118(12)
C(33)	0.0263(15)	0.0282(15)	0.0290(13)	0.0027(13)	-0.0009(12)	0.0129(13)
C(34)	0.0278(15)	0.0311(16)	0.0289(13)	0.0008(13)	-0.0008(13)	0.0149(13)
C(35)	0.0252(15)	0.0311(16)	0.0278(13)	-0.0022(13)	-0.0047(12)	0.0135(13)
C(36)	0.0233(14)	0.0279(15)	0.0247(12)	0.0005(12)	0.0012(12)	0.0106(12)
C(38)	0.0232(15)	0.0244(14)	0.0267(12)	-0.0013(12)	0.0008(12)	0.0109(12)
C(39)	0.0302(16)	0.0278(16)	0.0317(14)	-0.0005(13)	-0.0003(13)	0.0132(14)
C(40)	0.0265(15)	0.0330(16)	0.0281(13)	-0.0020(13)	-0.0017(13)	0.0165(13)
C(41)	0.0284(16)	0.0279(16)	0.0279(13)	0.0013(13)	0.0004(12)	0.0138(14)
C(42)	0.0249(14)	0.0257(15)	0.0265(12)	0.0005(12)	0.0002(12)	0.0120(13)
C(44)	0.0226(14)	0.0268(15)	0.0258(12)	-0.0003(12)	0.0010(11)	0.0112(12)
C(45)	0.0325(17)	0.0331(17)	0.0277(13)	0.0007(14)	0.0001(13)	0.0159(14)
C(46)	0.0289(16)	0.0312(16)	0.0291(13)	-0.0016(13)	0.0005(13)	0.0175(14)
C(47)	0.0255(15)	0.0256(15)	0.0304(13)	0.0022(12)	0.0009(13)	0.0130(13)
C(48)	0.0297(15)	0.0251(14)	0.0254(12)	-0.0002(12)	0.0017(12)	0.0148(13)
C(50)	0.0262(15)	0.0236(14)	0.0278(12)	-0.0021(12)	-0.0001(12)	0.0139(12)
C(51)	0.0285(16)	0.0293(15)	0.0269(12)	-0.0042(13)	-0.0028(13)	0.0154(13)
C(52)	0.0256(15)	0.0287(15)	0.0281(12)	0.0023(12)	0.0011(12)	0.0136(13)
C(53)	0.0238(15)	0.0263(15)	0.0283(12)	-0.0008(12)	0.0005(12)	0.0116(12)
C(54)	0.0263(15)	0.0252(14)	0.0275(12)	-0.0016(12)	0.0015(12)	0.0137(13)
C(56)	0.0283(15)	0.0273(15)	0.0280(12)	-0.0011(12)	-0.0011(12)	0.0140(13)
C(57)	0.0319(16)	0.0302(16)	0.0292(13)	-0.0028(13)	-0.0027(13)	0.0159(14)
C(58)	0.0310(16)	0.0305(16)	0.0332(14)	-0.0005(13)	-0.0044(14)	0.0174(14)
C(59)	0.0302(16)	0.0257(15)	0.0250(12)	-0.0011(12)	0.0002(12)	0.0146(13)
C(60)	0.0260(14)	0.0276(15)	0.0276(12)	-0.0002(12)	-0.0014(12)	0.0143(13)
C(62)	0.0280(15)	0.0302(16)	0.0298(13)	0.0020(13)	0.0004(13)	0.0134(13)
C(63)	0.0290(16)	0.0295(16)	0.0320(13)	-0.0012(13)	0.0012(14)	0.0141(13)
C(64)	0.0317(17)	0.0332(17)	0.0290(14)	0.0023(14)	0.0006(13)	0.0190(14)
C(65)	0.0297(16)	0.0306(16)	0.0290(13)	-0.0032(13)	-0.0021(13)	0.0170(14)
C(66)	0.0259(15)	0.0312(16)	0.0279(13)	-0.0004(13)	-0.0004(12)	0.0145(13)
C(68)	0.0302(16)	0.0331(16)	0.0307(13)	0.0024(14)	0.0009(14)	0.0164(14)
C(69)	0.0319(17)	0.0275(16)	0.0337(14)	0.0006(13)	-0.0014(14)	0.0143(14)

C(70)	0.0271(16)	0.0307(16)	0.0315(14)	-0.0001(13)	-0.0006(13)	0.0123(14)
C(71)	0.0296(16)	0.0346(17)	0.0293(13)	-0.0018(13)	0.0007(13)	0.0167(14)
C(72)	0.0312(16)	0.0271(16)	0.0290(13)	-0.0004(13)	-0.0009(13)	0.0168(14)
C(74)	0.0345(17)	0.0299(16)	0.0342(14)	0.0009(13)	0.0042(14)	0.0168(14)
C(75)	0.0343(18)	0.0313(17)	0.0362(15)	0.0021(14)	0.0036(14)	0.0152(15)
C(76)	0.0343(18)	0.0326(17)	0.0317(14)	0.0004(14)	0.0021(14)	0.0178(15)
C(77)	0.0354(17)	0.0295(17)	0.0315(14)	0.0005(14)	0.0010(14)	0.0171(14)
C(78)	0.0322(16)	0.0337(17)	0.0333(14)	0.0015(13)	0.0036(14)	0.0191(14)
C(80)	0.0317(17)	0.0323(17)	0.0303(13)	0.0002(13)	0.0041(13)	0.0162(14)
C(81)	0.0359(18)	0.0341(17)	0.0356(15)	0.0001(14)	-0.0016(14)	0.0201(15)
C(82)	0.0304(16)	0.0371(18)	0.0334(15)	0.0001(14)	-0.0030(14)	0.0194(15)
C(83)	0.0300(16)	0.0320(17)	0.0296(13)	-0.0010(13)	-0.0019(13)	0.0150(14)
C(84)	0.0281(16)	0.0313(16)	0.0271(13)	-0.0011(13)	0.0013(13)	0.0148(13)
Cl(301)	0.0676(10)	0.1140(14)	0.0524(7)	0.0008(9)	-0.0007(7)	0.0687(10)
Cl(302)	0.0737(12)	0.1397(19)	0.1002(14)	-0.0012(14)	0.0003(11)	0.0685(13)
Cl(303)	0.154(2)	0.0945(15)	0.0871(13)	0.0016(12)	-0.0032(13)	0.0711(16)
Cl(310)	0.0814(9)	0.1113(11)	0.1440(13)	-0.0005(10)	-0.0027(9)	0.0657(9)
Cl(311)	0.1074(10)	0.0665(7)	0.1299(12)	0.0018(7)	-0.0011(9)	0.0631(8)
Cl(320)	0.1259(11)	0.0780(8)	0.0901(8)	0.0027(7)	-0.0006(8)	0.0586(9)
Cl(321)	0.1183(10)	0.0544(6)	0.0718(6)	0.0015(5)	0.0021(6)	0.0647(7)
Cl(330)	0.0744(8)	0.1436(12)	0.0643(6)	-0.0022(7)	-0.0021(6)	0.0714(8)
Cl(331)	0.0910(10)	0.1333(13)	0.1199(12)	0.0017(10)	0.0036(9)	0.0678(10)
Cl(340)	0.0937(10)	0.1364(13)	0.0853(8)	-0.0012(9)	-0.0025(7)	0.0687(10)
Cl(341)	0.0752(8)	0.1249(11)	0.0849(8)	-0.0014(8)	0.0001(7)	0.0625(8)
Cl(350)	0.123(3)	0.087(3)	0.0578(18)	0.0026(18)	-0.002(2)	0.071(3)
Cl(351)	0.077(2)	0.123(3)	0.0622(18)	-0.003(2)	-0.0058(18)	0.068(3)
Cl(360)	0.098(3)	0.0651(19)	0.075(2)	-0.0021(17)	-0.0034(19)	0.066(2)
Cl(361)	0.077(2)	0.131(3)	0.0636(18)	0.003(2)	0.0005(17)	0.079(3)
C(350)	0.103(14)	0.103(14)	0.12(2)	0	0	0.051(7)
C(360)	0.130(18)	0.130(18)	0.15(3)	0	0	0.065(9)
C(301)	0.122(5)	0.117(5)	0.110(4)	-0.006(4)	0.003(4)	0.061(4)
C(310)	0.139(6)	0.133(5)	0.110(5)	0.011(4)	0.015(4)	0.076(5)
C(320)	0.122(5)	0.121(5)	0.110(4)	0.005(4)	0.006(4)	0.058(4)
C(330)	0.128(5)	0.111(5)	0.111(4)	-0.007(4)	-0.006(4)	0.065(4)
C(340)	0.141(6)	0.126(6)	0.128(5)	0.003(4)	0.002(4)	0.068(5)
C(101)	0.101(4)	0.067(3)	0.058(2)	-0.006(2)	-0.004(3)	0.051(3)
C(102)	0.094(4)	0.062(3)	0.078(3)	0.005(2)	0.003(3)	0.047(3)
C(103)	0.096(4)	0.071(3)	0.084(3)	-0.005(3)	0.002(3)	0.044(3)

	angle /°
C(11) - C(1) - C(2)	120.6(2)
C(11) - C(1) - C(6)	123.1(2)
C(2) - C(1) - C(6)	116.2(2)
C(13) - C(3) - C(2)	121.1(2)
C(13) - C(3) - C(4)	124.3(2)
C(2) - C(3) - C(4)	111.4(2)
C(7) - C(5) - C(4)	126.5(2)
C(7) - C(5) - C(6)	121.9(2)
C(4) - C(5) - C(6)	111.6(2)
C(5) - C(7) - C(8)	114.4(2)
C(5) - C(7) - C(12)	121.3(2)
C(8) - C(7) - C(12)	123.4(2)
C(19) - C(9) - C(8)	119.6(2)
C(19) - C(9) - C(10)	115.9(2)
C(8) - C(9) - C(10)	124.2(2)
C(1) - C(11) - C(10)	121.3(2)
C(1) - C(11) - C(12)	117.2(2)
C(10) - C(11) - C(12)	119.6(2)
C(3) - C(13) - C(14)	131.8(2)
C(3) - C(13) - C(18)	111.52(19)
C(14) - C(13) - C(18)	115.9(2)
C(13) - C(14) - C(15)	126.7(2)
C(13) - C(14) - C(25)	111.3(2)
C(15) - C(14) - C(25)	121.7(2)
C(14) - C(15) - C(16)	114.9(2)
C(14) - C(15) - C(31)	122.7(2)
C(16) - C(15) - C(31)	122.4(2)
C(15) - C(16) - C(17)	124.0(3)
C(15) - C(16) - C(37)	116.9(2)
C(17) - C(16) - C(37)	119.1(2)
C(16) - C(17) - C(18)	124.0(2)
C(16) - C(17) - C(43)	122.9(2)

C(18) - C(17) - C(43)	112.6(2)
C(13) - C(18) - C(17)	112.9(2)
C(13) - C(18) - C(49)	117.7(2)
C(17) - C(18) - C(49)	128.9(2)
C(9) - C(19) - C(20)	119.7(2)
C(9) - C(19) - C(24)	117.5(2)
C(20) - C(19) - C(24)	121.1(2)
C(19) - C(20) - C(21)	117.8(2)
C(19) - C(20) - C(55)	118.1(2)
C(21) - C(20) - C(55)	123.3(2)
C(20) - C(21) - C(22)	123.4(2)
C(20) - C(21) - C(61)	117.7(2)
C(22) - C(21) - C(61)	118.8(2)
C(21) - C(22) - C(23)	115.7(2)
C(21) - C(22) - C(67)	116.2(2)
C(23) - C(22) - C(67)	127.6(3)
C(22) - C(23) - C(24)	126.3(2)
C(22) - C(23) - C(73)	122.7(3)
C(24) - C(23) - C(73)	110.8(2)
C(19) - C(24) - C(23)	115.2(2)
C(19) - C(24) - C(79)	122.4(2)
C(23) - C(24) - C(79)	122.4(2)
C(14) - C(25) - C(26)	117.6(2)
C(14) - C(25) - C(30)	122.9(2)
C(26) - C(25) - C(30)	119.4(2)
C(15) - C(31) - C(32)	120.4(2)
C(15) - C(31) - C(36)	117.8(2)
C(32) - C(31) - C(36)	121.8(2)
C(16) - C(37) - C(38)	127.0(2)
C(16) - C(37) - C(42)	113.2(2)
C(38) - C(37) - C(42)	119.8(3)
C(17) - C(43) - C(44)	118.1(2)
C(17) - C(43) - C(48)	123.4(2)
C(44) - C(43) - C(48)	118.5(2)
C(18) - C(49) - C(50)	116.3(2)
C(18) - C(49) - C(54)	121.9(2)
C(50) - C(49) - C(54)	121.8(2)
C(20) - C(55) - C(56)	118.7(2)
C(20) - C(55) - C(60)	122.8(2)
C(56) - C(55) - C(60)	118.5(2)
C(21) - C(61) - C(62)	113.1(2)
C(21) - C(61) - C(66)	120.1(2)
C(62) - C(61) - C(66)	126.8(3)
C(22) - C(67) - C(68)	119.6(2)
C(22) - C(67) - C(72)	120.6(3)
C(68) - C(67) - C(72)	119.3(3)
C(23) - C(73) - C(74)	120.2(2)
C(23) - C(73) - C(78)	119.0(2)
C(74) - C(73) - C(78)	120.8(2)
C(24) - C(79) - C(80)	118.7(2)
C(24) - C(79) - C(84)	123.0(2)
C(80) - C(79) - C(84)	118.3(3)
C(1) - C(2) - C(3)	123.9(2)
C(3) - C(4) - C(5)	129.2(2)
C(1) - C(6) - C(5)	127.1(2)
C(7) - C(8) - C(9)	114.1(2)
C(9) - C(10) - C(11)	115.1(2)
C(7) - C(12) - C(11)	119.7(3)
C(25) - C(26) - C(27)	120.0(3)
C(26) - C(27) - C(28)	120.8(3)
C(27) - C(28) - C(29)	124.4(3)
C(28) - C(29) - C(30)	114.1(2)
C(25) - C(30) - C(29)	119.7(2)
C(31) - C(32) - C(33)	119.4(3)
C(32) - C(33) - C(34)	118.0(3)
C(33) - C(34) - C(35)	125.0(3)
C(34) - C(35) - C(36)	117.0(3)
C(31) - C(36) - C(35)	117.6(2)
C(37) - C(38) - C(39)	122.5(3)
C(38) - C(39) - C(40)	118.3(3)
C(39) - C(40) - C(41)	118.3(3)
C(40) - C(41) - C(42)	120.7(3)
C(37) - C(42) - C(41)	117.4(2)
C(43) - C(44) - C(45)	119.9(3)
C(44) - C(45) - C(46)	121.8(3)
C(45) - C(46) - C(47)	113.1(2)
C(46) - C(47) - C(48)	120.3(3)

C(43) - C(48) - C(47)	123.8(3)
C(49) - C(50) - C(51)	108.6(2)
C(50) - C(51) - C(52)	133.2(3)
C(51) - C(52) - C(53)	103.8(3)
C(52) - C(53) - C(54)	132.1(3)
C(49) - C(54) - C(53)	118.8(3)
C(55) - C(56) - C(57)	120.3(3)
C(56) - C(57) - C(58)	121.4(3)
C(57) - C(58) - C(59)	119.5(3)
C(58) - C(59) - C(60)	120.7(3)
C(55) - C(60) - C(59)	119.6(3)
C(61) - C(62) - C(63)	120.3(3)
C(62) - C(63) - C(64)	112.4(3)
C(63) - C(64) - C(65)	125.5(3)
C(64) - C(65) - C(66)	114.6(3)
C(61) - C(66) - C(65)	120.1(3)
C(67) - C(68) - C(69)	117.7(3)
C(68) - C(69) - C(70)	120.3(3)
C(69) - C(70) - C(71)	124.1(3)
C(70) - C(71) - C(72)	117.0(3)
C(67) - C(72) - C(71)	120.2(3)
C(73) - C(74) - C(75)	119.6(3)
C(74) - C(75) - C(76)	120.5(3)
C(75) - C(76) - C(77)	120.6(3)
C(76) - C(77) - C(78)	119.0(3)
C(73) - C(78) - C(77)	119.4(3)
C(79) - C(80) - C(81)	121.9(3)
C(80) - C(81) - C(82)	118.1(3)
C(81) - C(82) - C(83)	120.4(3)
C(82) - C(83) - C(84)	119.4(3)
C(79) - C(84) - C(83)	120.5(3)
Cl(351- Cl(350- Cl(351)	122.4(3)
Cl(351- Cl(350- C(350)	61.9(2)
Cl(351- Cl(350- C(350)	63.2(2)
Cl(350- Cl(351- Cl(350)	117.4(3)
Cl(350- Cl(351- C(350)	58.72(19)
Cl(350- Cl(351- C(350)	59.83(19)
Cl(361- Cl(360- Cl(361)	117.9(3)
Cl(361- Cl(360- C(360)	59.2(2)
Cl(361- Cl(360- C(360)	60.7(2)
Cl(360- Cl(361- Cl(360)	118.9(3)
Cl(360- Cl(361- C(360)	59.03(18)
Cl(360- Cl(361- C(360)	60.5(2)
Cl(350- C(350)- Cl(350)	115.2(6)
Cl(350- C(350)- Cl(350)	115.2(6)
Cl(350- C(350)- Cl(350)	115.2(6)
Cl(350- C(350)- Cl(351)	59.3(3)
Cl(350- C(350)- Cl(351)	152.6(18)
Cl(350- C(350)- Cl(351)	57.0(3)
Cl(350- C(350)- Cl(351)	57.0(3)
Cl(350- C(350)- Cl(351)	59.3(3)
Cl(350- C(350)- Cl(351)	152.6(18)
Cl(351- C(350)- Cl(351)	114.0(7)
Cl(350- C(350)- Cl(351)	152.6(18)
Cl(350- C(350)- Cl(351)	57.0(3)
Cl(350- C(350)- Cl(351)	59.3(3)
Cl(351- C(350)- Cl(351)	114.0(7)
Cl(351- C(350)- Cl(351)	114.0(7)
Cl(360- C(360)- Cl(360)	119.99(4)
Cl(360- C(360)- Cl(360)	119.99(4)
Cl(360- C(360)- Cl(360)	119.99(4)
Cl(360- C(360)- Cl(361)	61.75(17)
Cl(360- C(360)- Cl(361)	174(2)
Cl(360- C(360)- Cl(361)	58.88(17)
Cl(360- C(360)- Cl(361)	58.88(17)
Cl(360- C(360)- Cl(361)	61.75(17)
Cl(360- C(360)- Cl(361)	174(2)
Cl(361- C(360)- Cl(361)	118.6(5)
Cl(360- C(360)- Cl(361)	174(2)
Cl(360- C(360)- Cl(361)	58.88(17)
Cl(360- C(360)- Cl(361)	61.75(17)
Cl(361- C(360)- Cl(361)	118.6(5)
Cl(361- C(360)- Cl(361)	118.6(5)
Cl(301- C(301)- Cl(302)	114.7(3)
Cl(301- C(301)- Cl(303)	108.0(3)
Cl(302- C(301)- Cl(303)	107.0(3)
Cl(310- C(310)- Cl(311)	125.4(4)

Cl(320- C(320)- Cl(321)	105.8(3)
Cl(330- C(330)- Cl(331)	114.6(3)
Cl(340- C(340)- Cl(341)	109.4(4)
C(101)- C(101)- C(102)	129.4(5)
C(101)- C(102)- C(103)	111.1(4)

	distance / Å
C(1) - C(11)	1.574(4)
C(1) - C(2)	1.366(4)
C(1) - C(6)	1.344(4)
C(3) - C(13)	1.437(3)
C(3) - C(2)	1.406(3)
C(3) - C(4)	1.388(3)
C(5) - C(7)	1.509(3)
C(5) - C(4)	1.353(3)
C(5) - C(6)	1.366(3)
C(7) - C(8)	1.400(4)
C(7) - C(12)	1.324(3)
C(9) - C(19)	1.499(3)
C(9) - C(8)	1.360(3)
C(9) - C(10)	1.384(3)
C(11) - C(10)	1.414(4)
C(11) - C(12)	1.316(4)
C(13) - C(14)	1.262(3)
C(13) - C(18)	1.685(3)
C(14) - C(15)	1.434(3)
C(14) - C(25)	1.503(3)
C(15) - C(16)	1.381(3)
C(15) - C(31)	1.505(4)
C(16) - C(17)	1.364(3)
C(16) - C(37)	1.592(4)
C(17) - C(18)	1.330(3)
C(17) - C(43)	1.404(3)
C(18) - C(49)	1.496(3)
C(19) - C(20)	1.511(3)
C(19) - C(24)	1.387(3)
C(20) - C(21)	1.343(3)
C(20) - C(55)	1.565(3)
C(21) - C(22)	1.536(3)
C(21) - C(61)	1.534(3)
C(22) - C(23)	1.271(3)
C(22) - C(67)	1.406(3)
C(23) - C(24)	1.542(3)
C(23) - C(73)	1.438(3)
C(24) - C(79)	1.486(3)
C(25) - C(26)	1.418(4)
C(25) - C(30)	1.278(3)
C(31) - C(32)	1.427(4)
C(31) - C(36)	1.422(4)
C(37) - C(38)	1.399(4)
C(37) - C(42)	1.415(4)
C(43) - C(44)	1.400(4)
C(43) - C(48)	1.357(4)
C(49) - C(50)	1.405(4)
C(49) - C(54)	1.401(4)
C(55) - C(56)	1.395(4)
C(55) - C(60)	1.405(4)
C(61) - C(62)	1.358(4)
C(61) - C(66)	1.381(4)
C(67) - C(68)	1.440(4)
C(67) - C(72)	1.363(4)
C(73) - C(74)	1.398(4)
C(73) - C(78)	1.427(4)
C(79) - C(80)	1.394(4)
C(79) - C(84)	1.383(4)
C(26) - C(27)	1.289(3)
C(27) - C(28)	1.376(3)
C(28) - C(29)	1.265(3)
C(29) - C(30)	1.550(4)
C(32) - C(33)	1.412(4)
C(33) - C(34)	1.407(4)
C(34) - C(35)	1.382(4)

C(35) - C(36)	1.487(4)
C(38) - C(39)	1.379(4)
C(39) - C(40)	1.413(4)
C(40) - C(41)	1.427(4)
C(41) - C(42)	1.440(3)
C(44) - C(45)	1.406(3)
C(45) - C(46)	1.492(3)
C(46) - C(47)	1.422(3)
C(47) - C(48)	1.396(3)
C(50) - C(51)	1.460(4)
C(51) - C(52)	1.411(4)
C(52) - C(53)	1.368(3)
C(53) - C(54)	1.305(3)
C(56) - C(57)	1.400(4)
C(57) - C(58)	1.343(4)
C(58) - C(59)	1.397(4)
C(59) - C(60)	1.400(4)
C(62) - C(63)	1.399(4)
C(63) - C(64)	1.540(4)
C(64) - C(65)	1.410(4)
C(65) - C(66)	1.400(3)
C(68) - C(69)	1.295(4)
C(69) - C(70)	1.402(4)
C(70) - C(71)	1.276(4)
C(71) - C(72)	1.391(4)
C(74) - C(75)	1.391(4)
C(75) - C(76)	1.401(4)
C(76) - C(77)	1.424(4)
C(77) - C(78)	1.400(4)
C(80) - C(81)	1.366(4)
C(81) - C(82)	1.406(4)
C(82) - C(83)	1.379(4)
C(83) - C(84)	1.396(4)
Cl(301- C(301)	1.797(6)
Cl(302- C(301)	1.713(5)
Cl(303- C(301)	1.660(6)
Cl(310- C(310)	1.673(6)
Cl(311- C(310)	1.705(5)
Cl(320- C(320)	1.834(5)
Cl(321- C(320)	1.695(5)
Cl(330- C(330)	1.921(5)
Cl(331- C(330)	1.710(5)
Cl(340- C(340)	1.552(6)
Cl(341- C(340)	1.693(6)
Cl(350- Cl(351)	1.760(4)
Cl(350- Cl(351)	1.695(5)
Cl(350- C(350)	1.749(7)
Cl(351- C(350)	1.805(8)
Cl(360- Cl(361)	1.667(4)
Cl(360- Cl(361)	1.597(5)
Cl(360- C(360)	1.623(3)
Cl(361- C(360)	1.626(5)
C(101)- C(101)	1.442(7)
C(101)- C(102)	1.304(5)
C(102)- C(103)	1.532(5)

8.9 5,5',5'',5''',5'''',5''''',5''''''',5'''''''',5''''''''',5'''''''''-Decatrimethylsilyl-cyclodeca-m-phenylene (5-127)

Atom	x/a	y/b	z/c	U(iso)
C(14)	-0.0213(12)	0.8964(6)	-0.1270(4)	0.018(2)
C(15)	-0.1389(12)	0.8462(6)	-0.1078(4)	0.020(2)
C(35)	0.1067(13)	0.8004(7)	-0.1272(4)	0.023(3)
C(36)	0.0995(13)	0.8737(7)	-0.1360(4)	0.023(2)
C(40)	0.7139(12)	0.7718(6)	0.6227(4)	0.019(2)
C(41)	0.7213(12)	0.7352(6)	0.6612(4)	0.021(2)
C(42)	0.6504(12)	0.7493(6)	0.6981(4)	0.018(2)
C(43)	0.5722(12)	0.8021(6)	0.6956(4)	0.021(2)
C(44)	0.5673(12)	0.8419(6)	0.6575(4)	0.021(2)
C(45)	0.6371(12)	0.8256(6)	0.6215(4)	0.018(2)
C(46)	0.4917(12)	0.9018(6)	0.6564(4)	0.022(2)
C(47)	0.5611(13)	0.9681(7)	0.6388(4)	0.022(2)
C(48)	0.4998(13)	1.0289(7)	0.6400(4)	0.024(3)
C(51)	0.4088(12)	0.7753(6)	0.4008(4)	0.021(2)

C(52)	0.4843(12)	0.7223(7)	0.4199(4)	0.021(2)
C(53)	0.5827(12)	0.7427(6)	0.4521(4)	0.019(2)
C(54)	0.6521(13)	0.6940(7)	0.4696(4)	0.023(2)
C(55)	0.7504(12)	0.7153(6)	0.5076(4)	0.021(2)
C(56)	0.6970(13)	0.7398(7)	0.5446(4)	0.022(2)
C(57)	0.7778(13)	0.7518(7)	0.5819(4)	0.022(2)
C(58)	0.6217(13)	0.6210(7)	0.4533(4)	0.024(3)
C(59)	0.5207(13)	0.5976(7)	0.4209(4)	0.024(3)
C(60)	0.4512(13)	0.6478(7)	0.4045(4)	0.026(3)
C(61)	0.2632(13)	0.7518(7)	0.3906(4)	0.023(2)
C(65)	0.3627(12)	1.0176(6)	0.6569(4)	0.020(2)
C(66)	0.2881(12)	0.9495(6)	0.6743(4)	0.018(2)
Si(67)	0.6538(4)	0.6989(2)	0.75018(12)	0.0272(8)
C(68)	0.4753(18)	0.6365(9)	0.7595(6)	0.047(4)
C(206)	0.7013(17)	0.7663(9)	0.7957(5)	0.043(4)
C(207)	0.3565(13)	0.8922(7)	0.6736(4)	0.024(3)
C(215)	0.9193(15)	0.7448(8)	0.5813(5)	0.033(3)
C(218)	0.8909(14)	0.7066(7)	0.5067(4)	0.031(3)
C(219)	0.7931(18)	0.6463(10)	0.7479(6)	0.050(4)
C(233)	0.9762(15)	0.7250(8)	0.5436(5)	0.034(3)
Si(71)	1.1715(6)	0.7225(3)	0.54049(17)	0.0515(12)
C(212)	1.186(2)	0.6423(11)	0.5053(6)	0.060(5)
Si(61)	0.1063(4)	0.9389(2)	0.69785(13)	0.0320(8)
Si(53)	0.4570(5)	0.4983(3)	0.40494(16)	0.0462(11)
C(405)	1.2405(19)	0.7173(10)	0.5963(6)	0.056(5)
C(317)	0.264(2)	0.4644(12)	0.4255(7)	0.073(6)
C(319)	0.454(2)	0.4866(13)	0.3466(8)	0.081(7)
C(320)	0.565(2)	0.4442(12)	0.4326(7)	0.071(6)
C(502)	0.0335(19)	0.8414(10)	0.7194(6)	0.055(5)
C(504)	-0.0180(19)	0.9545(10)	0.6544(6)	0.055(4)
C(507)	0.123(2)	1.0081(12)	0.7430(7)	0.067(5)
C(224)	1.274(3)	0.8099(14)	0.5140(8)	0.084(7)
C(49)	0.5822(12)	1.1036(6)	0.6272(4)	0.019(2)
C(50)	0.5150(12)	1.1537(6)	0.6075(4)	0.019(2)
C(62)	0.8047(12)	1.1987(7)	0.6272(4)	0.020(2)
C(63)	0.7253(13)	1.1271(7)	0.6358(4)	0.025(3)
Si(64)	1.0023(4)	1.2267(2)	0.64079(13)	0.0323(8)
C(217)	1.0792(17)	1.3264(9)	0.6305(5)	0.045(4)
C(222)	1.094(2)	1.1723(12)	0.6072(7)	0.070(6)
C(228)	1.020(2)	1.2076(11)	0.7007(7)	0.064(5)
C(1)	0.4414(12)	1.2278(6)	-0.1228(4)	0.018(2)
C(2)	0.4872(12)	1.2649(6)	-0.1614(4)	0.019(2)
C(3)	0.4013(11)	1.2520(6)	-0.1981(4)	0.016(2)
Si(4)	0.4548(4)	1.3009(2)	-0.25029(12)	0.0265(8)
C(5)	0.3364(18)	1.3639(10)	-0.2590(6)	0.049(4)
C(7)	0.6478(17)	1.3544(9)	-0.2482(5)	0.045(4)
C(8)	0.2718(12)	1.1974(6)	-0.1963(4)	0.020(2)
C(9)	0.2260(13)	1.1581(7)	-0.1575(4)	0.024(3)
C(10)	0.3123(13)	1.1748(6)	-0.1210(4)	0.021(2)
C(11)	0.0922(13)	1.0989(7)	-0.1566(4)	0.023(2)
C(12)	0.0930(13)	1.0312(7)	-0.1387(4)	0.024(3)
C(13)	-0.0291(12)	0.9712(7)	-0.1403(4)	0.022(2)
C(16)	-0.1345(12)	0.7757(6)	-0.0991(4)	0.018(2)
C(17)	-0.2607(13)	0.7222(7)	-0.0805(4)	0.022(2)
C(18)	-0.3411(12)	0.7427(6)	-0.0471(4)	0.017(2)
C(19)	-0.4595(12)	0.6940(7)	-0.0305(4)	0.022(2)
C(20)	-0.5359(12)	0.7149(6)	0.0073(4)	0.020(2)
C(21)	-0.4583(13)	0.7392(7)	0.0438(4)	0.024(3)
C(22)	0.5254(13)	1.2478(7)	-0.0828(4)	0.023(2)
C(23)	0.6752(14)	1.2552(7)	-0.0817(4)	0.029(3)
C(24)	-0.7523(15)	0.7245(8)	0.0437(5)	0.032(3)
C(25)	-0.6835(14)	0.7058(7)	0.0069(4)	0.027(3)
Si(26)	-0.9483(5)	0.7223(3)	0.04050(16)	0.0456(11)
C(27)	-1.0403(19)	0.6421(10)	0.0056(6)	0.053(4)
C(28)	-0.5029(13)	0.6206(7)	-0.0469(4)	0.025(3)
C(29)	-0.4214(13)	0.5984(7)	-0.0789(4)	0.024(3)
C(30)	-0.3033(13)	0.6472(7)	-0.0960(4)	0.027(3)
Si(31)	-0.4584(5)	0.4984(3)	-0.09524(15)	0.0403(10)
C(32)	-0.623(2)	0.4429(11)	-0.0682(7)	0.063(5)
C(33)	-0.302(2)	0.4635(11)	-0.0752(7)	0.064(5)
C(34)	-0.0095(13)	0.7524(7)	-0.1094(4)	0.022(2)
C(37)	-0.1555(13)	0.9822(7)	-0.1569(4)	0.024(3)
C(38)	-0.1602(12)	1.0502(6)	-0.1743(4)	0.020(2)
C(39)	-0.0355(13)	1.1087(7)	-0.1743(4)	0.023(2)
C(213)	-0.965(3)	0.8073(14)	0.0121(8)	0.085(7)
C(214)	-0.464(3)	0.4872(14)	-0.1538(8)	0.082(7)
C(221)	-1.022(2)	0.7148(11)	0.0966(6)	0.059(5)

Si(51)	-0.3332(4)	1.0612(2)	-0.19778(13)	0.0309(8)
C(304)	0.4337(16)	1.2337(9)	-0.2958(5)	0.041(4)
C(308)	-0.3070(19)	1.1586(10)	-0.2196(6)	0.053(4)
C(309)	-0.471(2)	1.0470(10)	-0.1542(6)	0.056(5)
C(310)	-0.386(2)	0.9923(12)	-0.2422(7)	0.066(5)
Si(201)	0.2757(5)	0.7733(2)	-0.14072(14)	0.0383(10)
C(201)	0.2517(19)	0.6735(10)	-0.1301(6)	0.054(4)
C(202)	0.423(2)	0.8273(11)	-0.1081(7)	0.065(5)
C(23)	0.309(2)	0.7898(12)	-0.2009(7)	0.069(6)

	degree /°
C(15) - C(14) - C(36)	119.1(10)
C(15) - C(14) - C(13)	121.3(10)
C(36) - C(14) - C(13)	119.4(10)
C(14) - C(15) - C(16)	120.7(11)
C(36) - C(35) - C(34)	118.6(11)
C(36) - C(35) - Si(201)	118.8(9)
C(34) - C(35) - Si(201)	122.6(10)
C(14) - C(36) - C(35)	121.2(11)
C(41) - C(40) - C(45)	119.2(11)
C(41) - C(40) - C(57)	121.6(11)
C(45) - C(40) - C(57)	119.1(10)
C(40) - C(41) - C(42)	121.3(11)
C(41) - C(42) - C(43)	118.2(10)
C(41) - C(42) - Si(67)	122.4(9)
C(43) - C(42) - Si(67)	119.4(9)
C(42) - C(43) - C(44)	121.6(11)
C(43) - C(44) - C(45)	118.5(11)
C(43) - C(44) - C(46)	120.7(11)
C(45) - C(44) - C(46)	120.8(11)
C(40) - C(45) - C(44)	121.2(11)
C(44) - C(46) - C(47)	118.2(10)
C(44) - C(46) - C(207)	121.7(11)
C(47) - C(46) - C(207)	120.0(11)
C(46) - C(47) - C(48)	120.9(11)
C(47) - C(48) - C(65)	117.9(11)
C(47) - C(48) - C(49)	121.4(11)
C(65) - C(48) - C(49)	120.5(11)
C(52) - C(51) - C(61)	120.2(10)
C(52) - C(51) - C(50)	119.1(10)
C(61) - C(51) - C(50)	120.7(11)
C(51) - C(52) - C(53)	122.0(11)
C(51) - C(52) - C(60)	119.4(10)
C(53) - C(52) - C(60)	118.6(11)
C(52) - C(53) - C(54)	121.9(11)
C(53) - C(54) - C(55)	121.2(11)
C(53) - C(54) - C(58)	119.0(11)
C(55) - C(54) - C(58)	119.6(11)
C(54) - C(55) - C(56)	118.0(11)
C(54) - C(55) - C(218)	121.3(11)
C(56) - C(55) - C(218)	120.6(11)
C(55) - C(56) - C(57)	120.1(11)
C(40) - C(57) - C(56)	119.5(11)
C(40) - C(57) - C(215)	120.7(11)
C(56) - C(57) - C(215)	119.8(11)
C(54) - C(58) - C(59)	120.9(11)
C(58) - C(59) - C(60)	118.4(12)
C(58) - C(59) - Si(53)	121.8(10)
C(60) - C(59) - Si(53)	119.1(9)
C(52) - C(60) - C(59)	121.0(11)
C(51) - C(61) - C(62)	119.4(11)
C(48) - C(65) - C(66)	122.0(11)
C(65) - C(66) - C(207)	117.3(10)
C(65) - C(66) - Si(61)	119.8(9)
C(207)- C(66) - Si(61)	122.9(9)
C(42) - Si(67)- C(68)	108.7(6)
C(42) - Si(67)- C(206)	109.8(6)
C(68) - Si(67)- C(206)	109.8(8)
C(42) - Si(67)- C(219)	110.1(7)
C(68) - Si(67)- C(219)	111.0(8)
C(206)- Si(67)- C(219)	107.5(7)

C(46) - C(207)- C(66)	121.7(11)
C(57) - C(215)- C(233)	120.2(13)
C(55) - C(218)- C(233)	118.8(12)
C(215)- C(233)- C(218)	120.2(13)
C(215)- C(233)- Si(71)	121.2(11)
C(218)- C(233)- Si(71)	118.6(11)
C(233)- Si(71)- C(212)	109.1(8)
C(233)- Si(71)- C(405)	109.0(8)
C(212)- Si(71)- C(405)	112.9(9)
C(233)- Si(71)- C(224)	107.8(9)
C(212)- Si(71)- C(224)	108.2(10)
C(405)- Si(71)- C(224)	109.7(10)
C(66) - Si(61)- C(502)	110.2(7)
C(66) - Si(61)- C(504)	109.1(7)
C(502)- Si(61)- C(504)	108.0(8)
C(66) - Si(61)- C(507)	107.8(7)
C(502)- Si(61)- C(507)	110.1(9)
C(504)- Si(61)- C(507)	111.6(9)
C(59) - Si(53)- C(317)	106.6(8)
C(59) - Si(53)- C(319)	111.7(9)
C(317)- Si(53)- C(319)	107.8(10)
C(59) - Si(53)- C(320)	109.7(8)
C(317)- Si(53)- C(320)	107.7(10)
C(319)- Si(53)- C(320)	112.9(11)
C(48) - C(49) - C(50)	121.3(10)
C(48) - C(49) - C(63)	120.4(11)
C(50) - C(49) - C(63)	118.2(10)
C(51) - C(50) - C(49)	120.2(10)
C(61) - C(62) - C(63)	119.0(11)
C(61) - C(62) - Si(64)	121.5(9)
C(63) - C(62) - Si(64)	119.5(9)
C(49) - C(63) - C(62)	122.3(11)
C(62) - Si(64)- C(217)	110.8(6)
C(62) - Si(64)- C(222)	108.7(8)
C(217)- Si(64)- C(222)	109.6(9)
C(62) - Si(64)- C(228)	107.1(7)
C(217)- Si(64)- C(228)	109.1(8)
C(222)- Si(64)- C(228)	111.4(9)
C(2) - C(1) - C(10)	120.3(11)
C(2) - C(1) - C(22)	120.5(10)
C(10) - C(1) - C(22)	119.1(10)
C(1) - C(2) - C(3)	120.9(10)
C(2) - C(3) - Si(4)	123.0(8)
C(2) - C(3) - C(8)	118.3(10)
Si(4) - C(3) - C(8)	118.7(8)
C(3) - Si(4) - C(5)	107.5(7)
C(3) - Si(4) - C(7)	110.3(6)
C(5) - Si(4) - C(7)	110.8(8)
C(3) - Si(4) - C(304)	110.6(6)
C(5) - Si(4) - C(304)	109.8(7)
C(7) - Si(4) - C(304)	107.8(7)
C(3) - C(8) - C(9)	121.1(11)
C(8) - C(9) - C(10)	118.7(11)
C(8) - C(9) - C(11)	120.4(11)
C(10) - C(9) - C(11)	120.9(11)
C(1) - C(10) - C(9)	120.6(11)
C(9) - C(11) - C(12)	119.0(11)
C(9) - C(11) - C(39)	121.7(11)
C(12) - C(11) - C(39)	119.2(11)
C(11) - C(12) - C(13)	121.1(11)
C(14) - C(13) - C(12)	120.6(11)
C(14) - C(13) - C(37)	120.4(11)
C(12) - C(13) - C(37)	118.9(11)
C(15) - C(16) - C(17)	120.5(10)
C(15) - C(16) - C(34)	119.6(10)
C(17) - C(16) - C(34)	119.8(10)
C(16) - C(17) - C(18)	121.3(11)
C(16) - C(17) - C(30)	120.5(11)
C(18) - C(17) - C(30)	118.1(11)
C(17) - C(18) - C(19)	121.5(11)
C(18) - C(19) - C(20)	120.6(11)
C(18) - C(19) - C(28)	120.0(11)
C(20) - C(19) - C(28)	119.2(10)
C(19) - C(20) - C(21)	117.9(11)
C(19) - C(20) - C(25)	121.8(11)
C(21) - C(20) - C(25)	120.2(11)
C(20) - C(21) - C(22)	121.4(11)

C(1) - C(22) - C(21)	120.5(11)
C(1) - C(22) - C(23)	121.8(11)
C(21) - C(22) - C(23)	117.7(11)
C(22) - C(23) - C(24)	120.6(12)
C(23) - C(24) - C(25)	119.6(13)
C(23) - C(24) - Si(26)	121.0(11)
C(25) - C(24) - Si(26)	119.4(10)
C(20) - C(25) - C(24)	120.1(12)
C(24) - Si(26)- C(27)	108.3(7)
C(24) - Si(26)- C(213)	108.4(9)
C(27) - Si(26)- C(213)	106.6(10)
C(24) - Si(26)- C(221)	108.5(8)
C(27) - Si(26)- C(221)	112.2(8)
C(213)- Si(26)- C(221)	112.7(10)
C(19) - C(28) - C(29)	119.3(11)
C(28) - C(29) - C(30)	121.0(12)
C(28) - C(29) - Si(31)	120.5(9)
C(30) - C(29) - Si(31)	118.2(10)
C(17) - C(30) - C(29)	120.1(12)
C(29) - Si(31)- C(32)	110.6(8)
C(29) - Si(31)- C(33)	107.0(7)
C(32) - Si(31)- C(33)	107.8(9)
C(29) - Si(31)- C(214)	111.7(9)
C(32) - Si(31)- C(214)	112.7(10)
C(33) - Si(31)- C(214)	106.7(10)
C(35) - C(34) - C(16)	120.7(11)
C(13) - C(37) - C(38)	121.1(11)
C(37) - C(38) - C(39)	119.2(11)
C(37) - C(38) - Si(51)	119.2(9)
C(39) - C(38) - Si(51)	121.5(9)
C(11) - C(39) - C(38)	120.3(11)
C(38) - Si(51)- C(308)	109.9(7)
C(38) - Si(51)- C(309)	109.3(7)
C(308)- Si(51)- C(309)	107.9(8)
C(38) - Si(51)- C(310)	107.5(7)
C(308)- Si(51)- C(310)	110.3(9)
C(309)- Si(51)- C(310)	111.9(9)
C(35) - Si(201- C(201)	110.0(7)
C(35) - Si(201- C(202)	109.8(8)
C(201)- Si(201- C(202)	109.7(9)
C(35) - Si(201- C(23)	107.2(8)
C(201)- Si(201- C(23)	108.2(9)
C(202)- Si(201- C(23)	112.0(9)

	distance /Å
C(14) - C(15)	1.412(15)
C(14) - C(36)	1.376(16)
C(14) - C(13)	1.487(16)
C(15) - C(16)	1.366(15)
C(35) - C(36)	1.424(16)
C(35) - C(34)	1.367(16)
C(35) - Si(201)	1.886(13)
C(40) - C(41)	1.389(15)
C(40) - C(45)	1.404(16)
C(40) - C(57)	1.497(16)
C(41) - C(42)	1.395(16)
C(42) - C(43)	1.399(16)
C(42) - Si(67)	1.880(12)
C(43) - C(44)	1.406(16)
C(44) - C(45)	1.380(16)
C(44) - C(46)	1.495(16)
C(46) - C(47)	1.370(16)
C(46) - C(207)	1.384(16)
C(47) - C(48)	1.419(17)
C(48) - C(65)	1.395(16)
C(48) - C(49)	1.481(16)
C(51) - C(52)	1.505(16)
C(51) - C(61)	1.403(16)
C(51) - C(50)	1.372(16)
C(52) - C(53)	1.363(16)
C(52) - C(60)	1.434(16)
C(53) - C(54)	1.382(16)

C(54) - C(55)	1.501(16)
C(54) - C(58)	1.417(17)
C(55) - C(56)	1.383(16)
C(55) - C(218)	1.415(17)
C(56) - C(57)	1.383(16)
C(57) - C(215)	1.413(17)
C(58) - C(59)	1.391(17)
C(59) - C(60)	1.391(17)
C(59) - Si(53)	1.873(13)
C(61) - C(62)	1.389(16)
C(65) - C(66)	1.407(15)
C(66) - C(207)	1.403(16)
C(66) - Si(61)	1.874(12)
Si(67)- C(68)	1.847(17)
Si(67)- C(206)	1.868(17)
Si(67)- C(219)	1.871(18)
C(215)- C(233)	1.382(19)
C(218)- C(233)	1.400(19)
C(233)- Si(71)	1.911(15)
Si(71)- C(212)	1.89(2)
Si(71)- C(405)	1.865(19)
Si(71)- C(224)	1.88(3)
Si(61)- C(502)	1.910(19)
Si(61)- C(504)	1.882(19)
Si(61)- C(507)	1.88(2)
Si(53)- C(317)	1.93(2)
Si(53)- C(319)	1.82(2)
Si(53)- C(320)	1.85(2)
C(49) - C(50)	1.416(15)
C(49) - C(63)	1.371(16)
C(62) - C(63)	1.394(16)
C(62) - Si(64)	1.899(12)
Si(64)- C(217)	1.857(17)
Si(64)- C(222)	1.84(2)
Si(64)- C(228)	1.91(2)
C(1) - C(2)	1.401(15)
C(1) - C(10)	1.386(15)
C(1) - C(22)	1.475(16)
C(2) - C(3)	1.394(15)
C(3) - Si(4)	1.869(11)
C(3) - C(8)	1.403(15)
Si(4) - C(5)	1.871(18)
Si(4) - C(7)	1.884(17)
Si(4) - C(304)	1.864(16)
C(8) - C(9)	1.423(16)
C(9) - C(10)	1.392(17)
C(9) - C(11)	1.476(16)
C(11) - C(12)	1.391(16)
C(11) - C(39)	1.410(16)
C(12) - C(13)	1.410(16)
C(13) - C(37)	1.395(16)
C(16) - C(17)	1.488(15)
C(16) - C(34)	1.428(16)
C(17) - C(18)	1.407(16)
C(17) - C(30)	1.444(17)
C(18) - C(19)	1.373(15)
C(19) - C(20)	1.490(16)
C(19) - C(28)	1.426(16)
C(20) - C(21)	1.371(16)
C(20) - C(25)	1.399(16)
C(21) - C(22)	1.422(17)
C(22) - C(23)	1.425(17)
C(23) - C(24)	1.393(19)
C(24) - C(25)	1.409(18)
C(24) - Si(26)	1.895(14)
Si(26)- C(27)	1.878(19)
Si(26)- C(213)	1.87(3)
Si(26)- C(221)	1.87(2)
C(28) - C(29)	1.398(17)
C(29) - C(30)	1.378(17)
C(29) - Si(31)	1.887(13)
Si(31)- C(32)	1.87(2)
Si(31)- C(33)	1.91(2)
Si(31)- C(214)	1.83(3)
C(37) - C(38)	1.399(16)
C(38) - C(39)	1.409(16)
C(38) - Si(51)	1.890(12)

Si(51)- C(308)	1.908(19)
Si(51)- C(309)	1.873(19)
Si(51)- C(310)	1.87(2)
Si(201- C(201)	1.859(19)
Si(201- C(202)	1.83(2)
Si(201- C(23)	1.91(2)